# SEDIMENTATION IN QUIESCENT AND SHEARED SUSPENSIONS

Thesis by

Edward Douglas Lynch

In Partial Fulfillment of the Requirements

for the Degree of

Doctor of Philosophy

California Institute of Technology

Pasadena, California

1985

(Submitted May 21, 1985)

## ACKNOWLEDGEMENTS

I wish to thank all those who have aided me in my research and have made my stay at Caltech more enjoyable; in particular, I want to acknowledge the help of several individuals. First, I am grateful to George Griffith for building the Couette device used in the shear flow experiments, to Tom Remmers for conducting much of the experimental work, and especially to Rita Mendelson for typing much of this thesis under the pressure of a deadline. I wish to thank the Chevron Oil Company, the Atlantic Richfield Company, and the Stauffer Chemical Company for their financial support. I consider myself fortunate to have such fine friends, and I want to mention specially Ron Lagnado, Diane Hood, Dan Zirin, Tony Geller, Chris Chow, Laura Sylvester, Ardith El-Kareh, Ed Ascoli, Hong-Man Chan, Eliana Makhlouf, and Julia Lester. Finally, I will always be indebted to my adviser Eric Herbolzheimer for his guidance, support, and warm friendship over the past six years.

## ABSTRACT

This thesis explores how the average sedimentation velocity $u_0$ of a monodisperse suspension of spheres depends on the volume fraction of solids c and on the application of shear to the suspension and considers how changes in the sedimentation velocity reflect changes in the microscale distribution of particles in the suspension. For dilute, quiescent, monodisperse suspensions of spheres with radius a greater than $2\mu$m, previous experimental measurements of $u_0$ are well-correlated by the result

$$u_0 = u_s(1 - c^{1/3})$$

where $u_s$ is the Stokes settling velocity of the spheres (cf. Barnea, E. and Mizrahi, J., Chem. Eng. J. 5, 171-189 (1973)). Although none of the previous theoretical predictions are in even rough accord with this result, this type of behavior is shown to be consistent with that of a suspension having a pair-probability function changing over a length scale of $O(ac^{-1/3})$, which is comparable to the average interparticle spacing. A molecular-dynamics-type simulation is employed to show that multiparticle hydrodynamic interactions can create this type of microscale "structure" in a sedimenting suspension. This thesis also presents the first results for the influence of bulk flow on non-flocculating sedimenting suspensions. In a uniaxial extensional flow, a dilute suspension which is being sheared sufficiently rapidly for the effect of the shear to dominate the effect of multiparticle hydrodynamic interactions is shown to settle with velocity

$$u_0 = u_s(1 - 4.52c) + o(c).$$

This increase in $u_0$ results because the pair-probability function now changes over a length scale of O(a), not of $O(ac^{-1/3})$. Experimental measurements presented here of the sedimentation velocity as a function of particle volume fraction and dimensionless shear rate in the simple shear flow created by a Couette device agree remarkably well with this result.

# TABLE OF CONTENTS

# INTRODUCTION

Flows of suspensions of solid particles in liquids occur in a vast range of problems in both technology and nature. One possible approach for characterizing the flows of suspensions is the method of averaged equations. Suspension flows have two important length scales: a macroscopic length scale L over which the overall suspension flow changes and a microscopic length scale l over which the flow about the particles changes. Because L is usually much greater than l, the equations governing the motion of the particles and the fluid may be averaged over a volume comparable to $l^3$ to yield equations governing the locally averaged velocity, temperature, and pressure of the suspension (Anderson and Jackson 1967). However, the averaged momentum equation together with the suspension and particle continuity equations and a balance describing the forces on an average suspension particle do not constitute a complete set of equations for describing the isothermal behavior of the suspension because the averaging process introduces terms depending upon the flow about the particles.

To make the suspension flow equations complete, constitutive relations must be posed for these terms. In particular, constitutive relations must be specified for both the average stress in the suspension (the so-called viscosity problem) and the average hydrodynamic force on a particle in the suspension (the so-called sedimentation velocity problem). When the equations are averaged, information about the details of the flow about the particles is lost; therefore, the averaging process cannot serve as a basis for developing constitutive relations.

In neutrally buoyant suspensions the average fluid and average particle velocities are identical, and the suspension can be treated as an effective fluid with the principal effect of the particles being to alter the rheological properties from those of the pure fluid. However, in many applications the particles settle relative to the fluid and this relative motion can often affect immensely the flow of the suspension. For example, inhomogenities in the concentration or the properties of the bulk suspension flow of the suspension can in non-neutrally buoyant suspensions

drive large-scale convective flows.

This thesis explores two approaches for developing constitutive relations for non-neutrally buoyant suspensions. In the first approach the suspension properties are measured experimentally in terms of the relevant physical parameters of the problem (e.g., the volume fraction of particles in the suspension, the shear rate and flow type describing the bulk flow of the suspension, and the properties of the fluid and the solid). In the second approach constitutive relations are developed by understanding in detail the flow about the particles on the microscale. Because the flow about the particles depends upon on how the particles are arranged relative to one another, determining the microscale distribution of particles is important in characterizing the suspension properties. One method of describing the microscale distribution of particles is in terms of the pair-probability function $P(\underline{r})$ (i.e., the probability of a particle being at position $\underline{x}_0+\underline{r}$ given another particle at position $\underline{x}_0$), which may be determined either through experimentation or by gaining a detailed theoretical understanding of the forces on the particles.

Since the problem of understanding how the microscale structure affects constitutive relations for suspensions is very difficult, this thesis represents only a first step toward solving this problem. Because the viscosity problem has previously received far more attention than the sedimentation velocity problem (see the review in Jeffrey and Acrivos (1976)) and because the sedimentation velocity is a far more incisive probe into the microscale structure than the rheological properties (because the structure begins to affect the settling velocity in the first correction term to the Stokes velocity and the rheological properties in the second correction term to the pure fluid viscosity), this thesis considers only the problem of developing constitutive relations for the sedimentation velocity. Furthermore, to simplify the analysis and to reduce the number of variable parameters, the suspensions treated here are assumed to be monodisperse and to consist of an incompressible, Newtonian suspending fluid and of particles which are rigid spheres small enough so that an appropriately defined particle Reynolds number is much less than one.

Each chapter of this thesis treats a different aspect of the problem of developing

constitutive relations for the sedimentation velocity of a monodisperse suspension of spheres. Chapter I summarizes the previous theoretical and experimental results for the sedimentation velocity of quiescent suspensions and discusses how the current discrepancy between the existing theoretical and experimental results may be explained by supposing that suspensions have a pair-probability function which varies over a length scale of O(a) for "small" particles and of $O(ac^{-1/3})$ for "large" particles. A molecular-dynamics-type simulation is then used to demonstrate that multiparticle hydrodynamic interactions can give rise to such a pair-probability function in the case of "large" particles. Chapter II explains the method of the simulation in a manner which should make apparent how the technique could be applied to other problems in suspension mechanics. The calculation of the velocities of the particles in the simulation is explained in detail, and results of the simulation for small numbers of particles are compared to previous results from the literature. Finally Chapter III considers theoretically and experimentally how the shear rate and flow type of the bulk suspension flow affect the microscale arrangement of particles and the sedimentation velocity.

## REFERENCES

Anderson, T.B. and Jackson R. 1967 A fluid mechanical description of fluidized beds. Ind. Eng. Chem. Fund. 6, 527-539.

Jeffrey, D.J. and Acrivos, A. 1976 The rheological properties of suspensions of rigid particles. Amer. Inst. Chem. Eng. J. 22, 417-432.

# CHAPTER I

Sedimentation in Quiescent Suspensions

(Chapter I consists of a paper

by Edward D. Lynch and Eric Herbolzheimer)

# Sedimentation in Quiescent Suspensions

Edward D. Lynch
and
Eric Herbolzheimer

California Institute of Technology
Department of Chemical Engineering
Pasadena, California 91125

## Abstract

Previous experimental work (Barnea and Mizrahi 1973) has shown that for dilute, quiescent, monodisperse suspensions of spheres with radius a greater than approximately 2μm, the average sedimentation velocity of the spheres, $u_o$, is equal to $u_s$ $(1 - c^{1/3})$, in which c is the volume fraction of particles and $u_s$ is their Stokes settling velocity. This result is inconsistent with the theoretical predictions both of Hasimoto (1959), who showed that if the spheres are positioned at the lattice points of a simple cubic array, $u_o = u_s$ $(1 - 1.76c^{1/3} + O(c))$, and of Batchelor (1972), who showed that if the spheres are randomly distributed, $u_o = u_s$ $(1 - 6.55c + o(c))$. However, the observed $O(c^{1/3})$ correction factor to the Stokes velocity can be shown to be consistent with Batchelor's analysis provided the pair-probability function varies over a length scale of $O(ac^{-1/3})$, which is comparable to the average spacing between the particles in the suspension. In this paper we employ a molecular-dynamics-type simulation to show that multiparticle hydrodynamic interactions can create this type of microscale "structure" in a settling suspension.

## 1. Introduction

The theoretical analysis of the bulk flow of a suspension of solid particles dispersed in a liquid requires constitutive relations for both the rheological properties of the suspension and also the sedimentation velocity of the suspension, the physical problem considered in this paper. In general, these constitutive relations depend on the properties of the fluid and particles, on the volume fraction of solids in the suspension, and on the local characteristics of the bulk flow of the suspension. However, since significant disagreement still exists between experimental results and theoretical predictions for the sedimentation velocity of uniform, quiescent suspensions (i.e., suspensions in which no overall bulk flow occurs) of rigid, identical spheres dispersed in an incompressible, Newtonian fluid, we shall restrict our attention to this simplified set of conditions and investigate the dependence of $u_o$, the sedimentation velocity, on c, the volume fraction of particles, in the dilute limit.

To begin, if the suspension is sufficiently dilute, to a first approximation the particles do not interact, and we can consider each particle to be settling in an infinite fluid which is at rest far from the particle. For spherical particles with radius small enough so that the particle Reynolds number, $\frac{u_s a}{\nu}$, is much less than unity, the sedimentation velocity is given by the well-known Stokes law

$$u_s = \frac{2}{9} \frac{a^2(\rho_s - \rho)g}{\mu} \tag{1}$$

where $u_s$ is the Stokes velocity, g is the gravitational acceleration, a and $\rho_s$ are the radius and density of the particles, respectively, and $\rho$, $\mu$, and $\nu$ are the fluid density, viscosity, and kinematic viscosity, respectively.

As the concentration of particles increases, however, the flow of fluid around any given particle is significantly disturbed by the other spheres via two major mechanisms. First, when a particle settles, it creates in the surrounding fluid a velocity field with a component directed downward; therefore, any given particle is in the downdraft of the other particles, which tends to increase its settling velocity. This effect is more than offset, however, by the upward flow of pure fluid which must develop in order to maintain overall continuity and which tends to slow the settling of all the particles in the suspension. When taken together, these two effects substantially hinder the average sedimentation velocity of the suspension even at low particle concentrations; e.g., at a particle concentration of only 1% by volume, the measured sedimentation velocity is already reduced to about 80% of the Stokes velocity (Barnea and Mizrahi 1973).

Four different models have previously been employed to predict the effect of particle interactions on the settling velocity of quiescent suspensions. A common feature all of these methods share for the problem of the sedimentation of a quiescent, monodisperse suspension of spheres is that they make some a priori assumption regarding the relative positions of the particles in the suspension.

In the first of these methods, the cell model, the suspension is conceived of as cells containing one particle surrounded by fluid and having a ratio of particle volume to cell volume equal to the volume fraction of solids in the suspension. The velocity field in the fluid cell and the settling velocity of

the particle are calculated by solving the Stokes equations subject to some ad hoc boundary condition (e.g., zero vorticity) at the outside surface of the cell. Unfortunately no procedure exists for determining the proper boundary condition at this surface. Furthermore, the requirement that each cell can include only one particle has implicitly restricted the analysis to suspensions in which the particles are well-spaced from each other. In essence, the cell model makes the rather strenuous and unphysical assumption that the particle interactions can be accounted for by having the particle settle in a fluid volume with dimensions of $O(ac^{-1/3})$ rather than in an infinite fluid. All cell models yield results of the form

$$u_o = u_s (1 - \beta_{CM} c^{1/3}) \tag{2}$$

where the coefficient $\beta_{CM}$ depends upon the assumed shape of the cell and on the conditions imposed at the outer cell boundary and lies in the range 1.5 to 2.1 (see the discussion in Happel and Brenner (1965)). Note that the $O(c^{1/3})$ dependence of the correction term follows directly from the assumed length scale of the cell.

The second method of modeling particle interactions assumes that the particles are positioned at the lattice points of a regular array. Because of the periodic structure of a regular array, the Stokes equations can be solved for the flow about the array, and the settling velocity of the array can be calculated as a series in increasing powers of c (Hasimoto 1959; Sangani and Acrivos 1982). For small concentrations the settling velocity is given by

$$u_o = u_s (1 - \beta_{RA} c^{1/3} + O(c)) \tag{3}$$

where the constant $\beta_{RA}$ is 1.7601 for a simple cubic array (Hasimoto 1959). As with the cell model, modeling the suspension as a regular array restricts the suspension to one in which the particles are well-separated and in which the particle spacing is of $O(ac^{-1/3})$. Again, this scaling of the lattice spacing is what causes the $c^{1/3}$ dependence of the first correction to the Stokes velocity.

Although the third type of calculation, ensemble-averaging, can in principle be applied to any suspension, it has only been applied to dilute, random suspensions in which all configurations of the particles are equally likely, provided no particles overlap. After making this assumption, using the diluteness of the suspension to justify ignoring three-particle interactions, and circumventing the well-known problem of divergent integrals, Batchelor (1972) predicted the average sedimentation velocity should be given by

$$u_o = u_s (1 - 6.55c + O(c^2)). \tag{4}$$

The final type of calculation allowing for the effect of particle interactions replaces each particle by a multipole distribution of forces located at its center. By using the diluteness of the suspension to show that only the force monopole was needed to leading order, Saffman (1973) calculated that the settling velocity for both regular arrays and random suspensions was

$$u_o = u_s (1 - \beta_{ME} c^{1/3} + O(c)) \tag{5}$$

where the constant $\beta_{ME}$ was 1.76 for simple cubic arrays but 0 for random suspensions. Mazaika (1974) later extended this approximation to include higher-order multipoles and rederived the results of both Hasimoto and

Batchelor. Furthermore, both Saffman and Mazaika recognized that the $O(c^{1/3})$ dependence of the first correction to the Stokes velocity was a consequence of assuming that the pair-probability function (i.e., the probability $P(\underset{\sim}{r})$ of a particle being at position $\underset{\sim}{x}_o + \underset{\sim}{r}$ given another particle at position $\underset{\sim}{x}_o$) for the suspension varied over a length scale of $O(ac^{-1/3})$.

Experimental measurements of the average sedimentation velocity in quiescent suspensions separate into two groups depending on the size of the particles. For large particles ($a > 2\mu m$) settling in a quiescent suspension with the particle Reynolds number much less than unity, Barnea and Mizrahi (1973) have correlated the results of many investigators and proposed a correlation of the form

$$u_o = u_s \frac{(1-c)^2}{(1+c^{1/3})(\exp \frac{5}{3} \frac{c}{1-c})} \tag{6}$$

where $u_o$ is measured in the reference frame of zero volume flux of fluid plus particles. In the dilute limit this expression becomes

$$u_o = u_s (1 - c^{1/3} + c^{2/3} + O(c)). \tag{7}$$

Note that the coefficient of the $c^{1/3}$ term is only 1.0 as opposed to 1.76 as predicted for a simple cubic array.

On the other hand, for small spherical particles ($a < 2\mu m$) four different sets of measurements of the average settling velocity have appeared in the literature. Cheng and Schachman (1955), using polystyrene latex spheres of radius $0.13\mu m$ and equating the settling velocity with the measured rate of

fall of the suspension--clear fluid interface, determined that

$$u_o = u_s (1 - 5.1c) \tag{8}$$

whereas Buscall, et al. (1982), repeating Cheng and Schachman's technique with 1.55μm particles, found that

$$u_o = u_s (1 - 5.4c). \tag{9}$$

Tackie, Bowen, and Epstein (1983) fit their data on the settling velocity of 0.6μm silica spheres to an empirical equation reducing to

$$u_o = u_s (1 - 4.44c + 7.54c^2) \tag{10}$$

for small c. Finally, the settling velocity measurements of Kops-Werkhoven and Fijnaut (1981) for spherical particles of radius 0.021μm show that

$$u_o = u_s (1-(6 \pm 1)c). \tag{11}$$

In summary, all of the methods for calculating the average sedimentation velocity of dilute, quiescent, monodisperse suspensions of spheres predict different results, and none of these predictions is in agreement with all of the experimental measurements. Furthermore, the experiments indicate a different behavior for small ($a \lesssim 2\mu m$) particles than for larger particles. For the small particles the correction to Stokes velocity is proportional to c, whereas for the larger particles it is proportional to $c^{1/3}$. Based on the

methods of Batchelor and of Saffman and Mazaika, the observed behavior of $u_o$ implies that the pair-probability function in a settling suspension varies over a length scale of O(a) for small particles and over a length scale of $O(ac^{-1/3})$ for larger particles.

## 2. Interpretation

Verifying the hypothesis that the pair-probability function of a sedimenting suspension of large (radius greater than approximately 2μm) particles varies over a length scale of $O(ac^{-1/3})$ is possible in two ways. The most direct approach, which was attempted by Smith (1968), is to determine the relative particle positions experimentally. Smith photographed a sedimenting suspension composed of 4mm spheres in silicone oil from two perpendicular planes. He then divided the domain into cubes and counted the number of particles in each cube thereby creating a distribution of the number of boxes containing a given number of particles. This distribution was then compared with that one would predict if the suspension were completely random. Unfortunately, because the pictures were not used to measure the relative particle positions and hence the pair-probability distribution directly, the method of data analysis of Smith allows one to infer from the experimental results that the pair-probability function was either random or varied on a length scale of $O(ac^{-1/3})$. Thus, definitive conclusions cannot be drawn from these experiments.

The second approach is to examine theoretically why and how this type of microscale "structure" might develop in sedimenting suspensions. Of course, because of the reversibility property of the equations of motion at zero Reynolds number, two-particle hydrodynamic interactions cannot produce relative motion between the spheres in a settling suspension and therefore can be ruled out as an explanation. However, several other possible mechanisms can be proposed.

An obvious possibility is microinertial effects which are known to cause close particles to drift apart from each other as the pair settles in an infinite fluid. These effects can be shown to be much too weak, however, by considering the time scale they require to cause a rearrangement of the particles. Since the velocity at which the particles drift apart is proportional to $u_o Re$, the time needed for a particle to migrate a distance comparable to the interparticle spacing, $ac^{-1/3}$, by microinertia is

$$T_1 \cong \frac{ac^{-1/3}}{Ku_o Re} \cong \frac{\nu c^{-1/3}}{Ku_s^2} \cong \frac{30 \text{ hours}}{K} \tag{12}$$

where the final estimate is for the values of c, $\nu$, and $u_s$ used in the experiments of Lynch and Herbolzheimer (1985a). (Here K is an O(1) constant). However, in these experiments the settling velocity was steady after no more than 30 seconds (the first time at which a measurement could be made) and did not vary from experiment to experiment.

Nonhydrodynamic interactions, such as London-Van der Waals interactions, are also a possibility, but these should be negligibly small for the relatively large particles used in the experiments cited by Barnea and Mizrahi (1973).

The only remaining possibilities are Brownian motion and multiparticle hydrodynamic interactions. The dimensionless group measuring the effect of multiparticle hydrodynamic interactions compared to the effect of Brownian motion is the Brownian-motion Peclet number $Pe = \frac{V_R a}{D}$ where D is the relative Brownian-motion diffusion coefficient and $V_R$ measures the relative velocity between some test particle in the suspension and its neighbors. The diffusion coefficient D for a monodisperse suspension of spheres should be approximately

$kT/6\pi\mu a$ where k is Boltzmann's constant and T is the absolute temperature. Making a reasonable approximation of $V_R$ is more difficult. Batchelor (1982) suggests that, because two identical spheres settling in an infinite fluid do not move relative to one another, $V_R$ and Pe should be identically zero. Particles do, however, move relative to one another in a real suspension as a result of multiparticle hydrodynamic interactions.

To estimate the magnitude of the resulting relative velocity, let us consider a pair of particles being influenced by one of its nearest neighbors. To a first approximation we can treat this pair as being immersed in a linear shear flow generated by the third particle. Then, the relative velocity between the particles should be proportional to $\left|\underset{\sim}{R} \cdot \nabla \underset{\sim}{v}\right|$ where $\underset{\sim}{R}$ is the vector joining the particle centers and where the velocity gradient generated by the third particle, $\nabla \underset{\sim}{v}$, is evaluated at the center of one of the particles in the pair. In creeping flow, $\underset{\sim}{v} \sim O(u_s \frac{a}{r})$ for large a/r so $\nabla \underset{\sim}{v} \sim O(\frac{u_s a}{r^2})$ where r is the distance from the third particle to the pair. On the average the particle spacing is $O(ac^{-1/3})$ so taking this as the estimate for both R and r, we find

$$V_R = \kappa\, u_s \frac{a}{r^2} R = \kappa u_s c^{1/3} , \tag{13}$$

where $\kappa$ is an O(1) constant accounting for the crudeness of the above approximations and the fact that many more than one additional particle influence the relative motion of the pair being considered. After substituting for D and $V_R$, the Peclet number becomes

$$Pe = \frac{4\pi a^4(\rho_S-\rho)gc^{1/3}}{3kT}\kappa \ . \qquad (14)$$

Table 1 presents results for the Peclet number calculated using this choice of $V_R$ for a variety of published sedimentation experiments. The values of the Peclet number in the three sets of experiments with particles smaller than 2μm indicate that in these experiments Brownian motion played the dominant role in determining the relative positions of the particles. Coincidentally, these were also the sets of experiments for which the first correction to the Stokes velocity was proportional to O(c), not $O(c^{1/3})$, which is consistent with the expectation that Brownian motion would insure that the pair-probability function was random. The results of these three sets of experiments do differ in the coefficient of the O(c) term; Batchelor and Wen (1982) have ascribed this difference in the O(c) coefficient between the various experiments using small particles and that predicted by Batchelor (1972) to Van der Waals attractive forces, which cause an excess of close pairs beyond that in a random suspension.

On the other hand, for the experiments listed in Table 1 with a > 2μm, the large values of Pe suggest that the influence of multiparticle hydrodynamic interactions dominated the influence of Brownian motion. Since these were also the experiments in which the sedimentation velocity was found to be proportional to $O(c^{1/3})$, a logical hypothesis might be that multiparticle hydrodynamic interactions caused the particles, as they settled, to change their relative positions in such a way as to make the pair-probability function vary over a length scale of $O(ac^{-1/3})$. Since the relative velocity between two particles as a result of interactions with a third particle is proportional to

$u_S a/r$, for the values of a, c, and $u_S$ used in the experiments of Lynch and Herbolzheimer (1985a), the time required for multiparticle hydrodynamic interactions to cause a migration comparable to the interparticle spacing is approximately

$$T_2 = \frac{ac^{-1/3}}{K_1 u_S(\frac{a}{r})} \cong \frac{ac^{-2/3}}{K_1 u_S} \cong \frac{5 \text{ seconds}}{K_1} \tag{15}$$

in which r is a distance representative of the distance between two nearby particles, $ac^{-1/3}$, and $K_1$ is another O(1) constant. Multiparticle hydrodynamic interactions are thus a reasonable possibility for the cause of the tendency of close pairs to be less likely to persist in a sedimenting suspension.

## 3. Simulation Method

To test the hypothesis that multiparticle hydrodynamic interactions result in a pair-probability function changing over a length scale of $O(ac^{-1/3})$ and in close pairs being less likely to persist, we have developed a molecular-dynamics-type simulation of a sub-ensemble (between 27 and 125 identical spheres inside a cube) of a sedimenting suspension. In the simulation the particles are allowed to settle under the influence of gravity until they reach an asymptotic "long-time" configuration from a statistical standpoint. The details for implementing this simulation are described elsewhere (Lynch and Herbolzheimer 1985b), but a brief synopsis of the simulation procedure is afforded here.

In the simulation the N spheres of radius a are initially placed in a cube with sides of length L in one of two types of initial configurations. In order to demonstrate how a suspension which initially has no close pairs would behave, we let the spheres take random perturbations about the lattice points of a simple cubic array. In other runs, in order to demonstrate the behavior of a suspension with an initial pair-probability function similar to a random suspension, we place the particles in the cube randomly with the restriction that the particles may not overlap.

The trajectories of the spheres are calculated from the initial positions by integrating the particle velocities (which are functions of the instantaneous particle positions only) forward in time using the fourth-order Adams-Moulton predictor-corrector method. To observe how the suspension evolves, the pair-probability function and the settling velocity averaged over the particles in the cube are calculated as functions of time. Since only a

relatively small number of particles can be handled in the simulation, periodic boundary conditions are applied at the sides of the cube in order to approximate the behavior of an effectively infinite suspension.

The velocity of a sphere having no near neighbors consists of three distinct parts. First, at each sphere in the cube a velocity is induced directly by the presence of all of the spheres in the cube. For a particle $\alpha$ which has no close neighbors (i.e., particles within a few particle radii of $\alpha$), we calculate this induced velocity by multiplying the translational mobility tensor for the problem of N identical spheres moving in a zero-Reynolds-number fluid (Mazur and Van Saarloos 1982) by the gravitational force acting on each sphere and by then using the first three terms of the resulting series in $\frac{a}{r_{\alpha\beta}}$. (Here $r_{\alpha\beta}$ is the distance between particle $\alpha$ and another particle in the suspension $\beta$.) The first term in this expansion is the Stokes velocity, the second term approximates the other particles in the suspension as point forces, and the third, which consists of a potential-dipole singularity situated at the center of each of the other particles, is the $(\frac{a}{r_{\alpha\beta}})^3$ term in the fluid velocity field induced by the other particles plus the Faxen's law correction of the point-force velocity field to account for the finite size of particle $\alpha$.

This contribution to the velocity of particle $\alpha$ cannot be the only contribution, however, because the particle interactions between two particles $\alpha$ and $\beta$ in zero-Reynolds-number flow decay like $\frac{1}{r_{\alpha\beta}}$ as $r_{\alpha\beta} \to \infty$; hence, increasing the size of the cube to $\infty$ (i.e., using an infinite number of particles) results in the velocities of all the particles becoming unbounded.

This divergence arises because we have ignored the effect of the backflow of fluid which is necessary to preserve continuity. With error O(c) we may calculate the effect of the backflow from particles inside the cube and thereby alleviate the problem of divergent integrals by "smearing-out" the sum of the point-force interactions over the entire cube (see Saffman (1973)).

A third contribution to the velocity of any chosen particle without close neighbors is the influence of suspension particles outside the cube. Far from the particle, we assume that the suspension becomes essentially random since we do not expect any long-range order to develop. The net result of this approximation is to make the direct effect of the particles outside the cube cancel the effect of the backflow due to the particles outside the cube.

If we now make all lengths dimensionless by using the length of the side of the cube and choose as the dimensionless time $\tau$, a time comparable to that needed for a typical suspension particle to migrate laterally a distance equal to the interparticle spacing, then in dimensionless form the velocity of any given test particle $\alpha$ is

$$N^{2/3} \frac{d}{dt}\left[\underset{\sim}{r}_\alpha - \frac{u_s \tau}{L}\, t\underset{\sim}{e}\right] = \sum_{\beta=1,\alpha\neq\beta}^{N}\left[\left(1 + \frac{2}{3r_{\alpha\beta}^2}\left(\frac{a}{L}\right)^2\right)\frac{\underset{\sim}{e}}{r_{\alpha\beta}} + \left(1 - \frac{2}{r_{\alpha\beta}^2}\left(\frac{a}{L}\right)^2\right)\frac{(\underset{\sim}{e}\cdot\underset{\sim}{r}_{\alpha\beta})\underset{\sim}{r}_{\alpha\beta}}{r_{\alpha\beta}^3}\right] - 3.17343\, N\underset{\sim}{e} \qquad (16)$$

in which $\tau$ equals $\frac{4}{3}\left(\frac{4}{3}\pi\right)^{1/3} c^{-1/3} N^{-1/3} \frac{L}{u_s}$, $\underset{\sim}{e}$ is the unit vector in the direction of gravity, $\underset{\sim}{r}_\alpha$ is the dimensionless position of particle $\alpha$, $\underset{\sim}{r}_{\alpha\beta}$ is $\underset{\sim}{r}_\alpha$

minus $\underset{\sim}{r}_\beta$, and $(\frac{a}{L})$ equals $(\frac{3}{4\pi}\ \frac{c}{N})^{1/3}$. (The first term is due to direct particle interactions, and the second represents the backflow.)

For particles having close neighbors, we need to include, in addition to these three effects, higher-order reflections due to the close spheres. For particles having one close neighbor, we include these by considering this pair of particles to be settling in a shear flow generated by the settling of the other N-2 particles. The exact solution is known for this two-particle problem, and it can be decomposed into the sum of the velocity attained by a pair settling in an infinite fluid at rest far from the pair (see Batchelor (1972)) and the relative velocity between two force-free, torque-free spheres moving in the approximately linear flow field generated by the other particles (see Batchelor and Green (1972)). This procedure is generalized for particles having more than one close neighbor by balancing the forces and torques on each of the close particles and considering the resistance and shear forces (i.e., the translational-rotational and shear resistance tensors) due to the other close particles to be pairwise-additive (for details see Lynch and Herbolzheimer (1985b)).

## 4. Results and Discussion

Results from the simulations shall be presented in terms of the pair-probability function and the settling velocity, each averaged over the particles in the cube. In the limit as $c \to 0$, the coefficient of the $O(c^{1/3})$ term in the expansion for the settling velocity may be obtained by subtracting $u_S$ from $u_O$ and dividing this result by $u_S c^{1/3}$. Since the particle velocities in the simulation do not include the Stokes velocity and are made dimensionless by the velocity $L/\tau$, we only need to multiply the averaged settling velocity by $\frac{L}{u_S \tau c^{1/3}} = \frac{3}{4} (3/4\pi)^{1/3} N^{1/3}$ to obtain the $O(c^{1/3})$ coefficient. Because the average sedimentation velocity is only proportional to $c^{1/3}$ with error $O(c)$, this procedure introduces an error of $O(c^{2/3})$ into the $O(c^{1/3})$ coefficient; however, for the small concentrations used in the simulation (e.g., $c = 0.005$), the error should be small enough so that this is still a useful way of illustrating how the value of the $O(c^{1/3})$ term changes over time. (For example, at $c = .005$ the error in the $O(c^{1/3})$ coefficient would be $-(.005)^{2/3} = .029$ for a simple cubic array and $6.55(.005)^{2/3} = .192$ for a random suspension.)

In a real suspension the rate of fall of the suspension--clear fluid interface (i.e., the generally used measure of $u_O$) corresponds to some average of the settling velocities of the spheres over some small volume of suspension and some sufficiently short time. Hence, we average the estimate of the $O(c^{1/3})$ coefficient over time once the sub-ensemble of particles has reached a long-time asymptotic state from a statistical standpoint and thereby obtain a prediction of what the first correction to the Stokes velocity (i.e., $(1-u_O^{\infty}/u_S c^{1/3})$ where $u_O^{\infty}$ is the asymptotic value of $u_O$) should be in a real suspension. This time-averaged estimate of the $O(c^{1/3})$ coefficient is presented

in Table 2, which gives a list of the completed simulation runs.

The pair-probability function is calculated in the simulation by dividing the region around each particle into concentric spherical shells, counting the number of particles whose centers lie in each shell, and dividing this count by the volume of the shell. This result is then normalized by the number of particles per unit volume of suspension, n. For simulation runs with 27, 64, and 125 particles, the shells used are, respectively, of width L/16, L/20, and L/24.* This procedure yields a pair-probability function g(r) averaged over all angles and over the width of the shell. We present in Figure 1 the pair-probability function calculated at intervals of .4 in dimensionless time for simulation run 6, a run with an initially random distribution of 64 particles at $c = .005$ and with a time step $\Delta t$ of $.001\tau$. (The vertical lines at $r = 2a$ and $r = 4a$ in Figure 1 indicate respectively the radius inside of which no particles are present because of the inpenetrability of the particles and the radius inside of which neighboring particles are treated as close neighbors.) Because the pair-probability function averaged over the particles fluctuates markedly in time (see Figure 1), we have averaged g(r) over time steps .4 dimensionless time units apart in order to remove most of these fluctuations. (More frequent averaging was found not to increase the precision of the pair-probability function noticeably.) In all subsequent discussions we present results for the time-averaged g(r). Besides the pair-probability function and average settling velocity, the simulation also produces at regular time

---

*To avoid including any effects of volume exclusion due to the finite size of the particles, we adjust the width of the first shell with its outer radius greater than 2a by changing its inner radius to 2a.

intervals statistics of the particle velocities and a picture of the particle positions; however, presentation of this material would be rather cumbersome and is not attempted here.

When in run 6 the particles are placed in the box randomly in order to simulate the behavior of an initially random suspension, the long-time results are similar to the results of sedimentation experiments on dilute, quiescent, monodisperse suspensions. In Figure 2 we see that the coefficient of the $O(c^{1/3})$ term in the expansion for the settling velocity asymptotes to a value of .778, which, although less than 1.0, is greater than that which would be expected for a random suspension (viz., 0.0). Moreover, at $c = .005$ any volume-exclusion effect of higher-order in c could not possibly produce this large a correction to the Stokes velocity. To examine how the pair-probability function progresses toward a long-time distribution, we have divided the evolution of simulation run 6 (as seen in Figure 1) into three periods: an initial period from $t = 0$ to 2.4 when very little happens, a period from $t = 2.8$ to 4.8 when the suspension evolves, and a final period from $t = 5.2$ to 8.0 when a long-time pair-probability function exists. Figures 3, 4, and 5 show the pair-probability function averaged over each of these three time periods. Obviously the initial distribution of particles changes into one with a pair-probability function varying over a length scale comparable to the interparticle spacing (about .25L in this case). The final pair-probability function shows fewer close pairs than in a random suspension but becomes essentially random as $r \to \infty$.

When the particles are initially allowed to take random perturbations about the lattice points of a simple cubic array, the long-time results are similar, but not identical, to those for the initial configuration of a random

suspension. In Figure 6 we plot the $O(c^{1/3})$ coefficient versus time for simulation run 1, which has an initial configuration of 64 particles in a randomized simple cubic array with a concentration of .005; the time step is $.001\tau$ as in run 6. For long-time the $O(c^{1/3})$ coefficient seems to level off at .785, i.e., about the same value as for run 6. However, unlike run 6 the suspension begins to evolve immediately and essentially reaches its final distribution by $t = 1.2$. Figures 7 and 8 compare the initial pair-probability function to that averaged from $t = 1.2$ to 8.0. The long-time pair-probability function is much smoother than for the initially random suspension and again shows structure on a length scale of $O(ac^{-1/3})$.

To test the effect of step size on the simulation, we repeated run 6 with time steps of .002 and .0005. In each of these three runs, a group of four close particles forms when the dimensionless time reaches about .15. Because extremely small errors in the positions of the particles in the quadruple can cause large errors in their relative velocities, the motion of the quadruple is calculated differently in each case and consequently the trajectories of the particles in these three runs quickly diverge; however, the long-time behavior of the average settling velocity is quite similar for the runs (see Figures 2, 9 and 10). As the time step is decreased, the average settling velocity becomes a smoother function of time. We observe from the pictures of the particle positions and the statistics of the particle velocities that this is the result of clusters of particles moving fast enough to come close to other particles and thereby forming larger clusters. When a cluster forms, the settling velocity of each of the particles inside the cluster increases substantially and the value of the average settling velocity "jumps" as a function of time. Hence, because clusters form far more readily at the larger

time steps, the plot of the $O(c^{1/3})$ coefficient versus time appears more jagged. The only other noticeable effect of changing the time step is that the number of particles which overlap is reduced significantly.

When N is increased to 125 in run 12, the long-time results are again similar to runs 1, 6, 7, and 8, although the asymptotic value of the $O(c^{1/3})$ coefficient is slightly lower in this case. The explanation for this anomaly is that at about t = 6.0 several particles come together to form a quadruple; the suspension becomes momentarily more random and the value of the $O(c^{1/3})$ coefficient is correspondingly reduced (see Figure 11). Because we observed that quadruples were less likely to form for smaller time steps, this problem might not occur if the time step were reduced. In Figures 12 and 13 we compare the pair-probability function for run 12 averaged from t = 0 to 1.2 to that averaged from t = 1.6 to 8.0. The initial pair-probability distribution, despite having fewer very close pairs than the final distribution, has many more moderately close pairs (i.e., pairs closer than the interparticle spacing, .2L).

Comparing the long-time pair-probability function for run 12 with 125 particles (Figure 13) to that for run 6 with 64 particles (Figure 8) and to that for run 13 with 27 particles (Figure 14), we see that for large r the pair-probability function more closely approximates a random suspension as N is increased. This is presumably due to the better statistics for larger N rather than to any effect of the periodic boundary conditions because the long-time result for the average settling velocity shows little change as N is increased. For N = 27, although fewer moderately close pairs are present than in a random suspension, an extra number of very close pairs appear; several of the other runs show similar behavior, but in none is it as pronounced as here.

Five simulation runs were completed at concentrations other than .005. Raising c to .008 and to .02 seems to have little impact on the long-time behavior of a simulation run; in run 9 with c = .008 and in run 3 with c = .02, the long-time pair-probability function is again one which varies over a length scale of $O(ac^{-1/3})$ (see Figure 15). The estimate of the $O(c^{1/3})$ coefficient at c = .008 is .764, a value in close accord with the results for the runs at c = .005. Because at c = .02 the O(c) correction term is important in the settling velocity expansion, the estimated $O(c^{1/3})$ coefficient asymptotes to a value, .965, which is slightly larger than that found at c = .005.

However, several changes worth noting do occur. First, because the particles are now larger relative to the size of the box, they overlap more frequently. Also, the variance in the velocity distribution of the particles decreases significantly as c is increased. Finally, because at this larger concentration clusters of particles are constantly forming and breaking up, the plot of the $O(c^{1/3})$ coefficient versus time becomes increasingly more jagged as c is increased (see Figure 16).

At c = .02 the simulation method shows some signs of breaking down. For computational considerations, in the simulation we can consider a maximum of 3 particles as close neighbors of a given particle $\alpha$. However, for c = .02 at times more than 3 particles come close to a given particle $\alpha$, and the simulation must consider the particles furthest from $\alpha$ to be "far away". A more difficult problem with the simulation procedure is that at t = 3.731 a quadruple of particles comes so close together that the matrix we must invert to determine the velocities of the quadruple is algorithmically singular. Because of this difficulty, we end the simulation at this point.

Surprisingly, in two of the three simulation runs with c = .001, the smallest concentration used in the simulations, the long-time behavior is profoundly different. For run 2 with an initial configuration of a randomized simple cubic array, the average settling velocity asymptotes to about $u_s(1-.855c^{1/3})$ (see Figure 17) and the long-time pair-probability function again shows the expected deficiency of close pairs. In neither of the runs for which the particles are placed in the cube randomly, however, does the distribution evolve in the expected pattern. In run 10, the simulation results show a strong tendency toward creation, and subsequent destruction, of close pairs, and the sub-ensemble does not approach any asymptotic state monotonically; nevertheless, the average settling velocity eventually does seem to level off to an asymptote from t = 9.6 to 12.0. (The asymptotic value of the $O(c^{1/3})$ coefficient for this run is listed in Table 2 as inconclusive.) Run 11 shows even more interesting results. In this run, despite the fact that the particles are initially placed in the cube randomly, the initial particle distribution has few close pairs. Hence, we see in Figure 18 that the initial settling velocity is very close to the expected asymptotic value and that the $O(c^{1/3})$ coefficient remains at this level (viz., .835) until t = 2.4. At this point close pairs begin to appear, and eventually the sub-ensemble develops into a collection of particles with even more close pairs than a random suspension (see Figure 19). Two other characteristics which make the runs for c = .001 different from the other simulation runs are the absence of any close triples and the large variance in the distribution of the particle velocities.

## 5. Conclusions

Despite the aberrant behavior of the simulation runs at c = .001, the universally similar long-time behavior of the runs with c = .005, .008, and .02 suggest that multiparticle hydrodynamic interactions can produce a microscale suspension structure changing over a length scale of $O(ac^{-1/3})$ and that this structure yields a first correction to the Stokes velocity proportional to $O(c^{1/3})$. The value of the $O(c^{1/3})$ term determined by averaging the long-time values obtained from all the runs with c = .005 (viz., ca. .752) is slightly lower than that expected from the correlation of Barnea and Mizrahi (viz., 1.0). One (probably small) contribution to this discrepancy is that force pairwise additivity, used to calculate the velocities of close triples and quadruples, consistently overestimates their absolute velocities. Another explanation is that in calculating the average settling velocity we have not calculated correctly the effects of higher-order terms in c (e.g., the term in the settling velocity expansion of $O(c^{4/3})$) which are not completely negligible for c = .005. The fact that the $O(c^{1/3})$ coefficient for simulation run 2 with c = .001 asymptotes to about .85, not .75, lends some support to this contention.

However, most likely this discrepancy is simply due to the error inherent in the correlation. As we see in Figure 20, our result for the settling velocity at each of the four concentrations used agrees significantly better with the correlation than either the result for a random suspension or a simple cubic array. (The value of $u_o$ for c = .001 is that of run 2.) Furthermore, the agreement is probably within the experimental accuracy of the correlation. Why our simulation yields the result

$$u_o = u_s (1-.752c^{1/3}) \tag{16}$$

for small c, rather than

$$u_o = u_s (1-c^{1/3} + c^{2/3} + \quad O(c)) \tag{7}$$

can be explained by observing that for small c the third term in the correlation is $1.0\ c^{2/3}$. However, because the velocity induced at some particle $\alpha$ by N other particles far away has no term proportional to $(a/r)^2$ where r is a measure of the distance between $\alpha$ and the other particles, the expansion for the settling velocity can have no term proportional to $c^{2/3}$. Since the correlation includes a spurious $c^{2/3}$ term, it overestimates the coefficient of the $c^{1/3}$ term. Indeed we see in Figure 20 that for c = .005 the predictions of equations 16 and 7 are essentially identical.

One possible explanation for why close pairs break up in a settling suspension relies on the following observation: since close pairs settle faster than particles without close neighbors, they tend to overtake single isolated particles. Suppose we consider a pair behind and slightly to the right of a single particle (see Figure 21a). The single particle induces a velocity field at the pair tending to make the particle closer to the single settle faster relative to the other member of the pair and thus tending to make the pair break apart. Eventually the pair moves even with the single (Figure 21b), creating a close triple; the middle particle in the triple settles faster than the other two, and the pair degenerates to the point where the effects of other particles become important enough to effectively destroy the pair (Figure 21c).

The rapid settling of close pairs can also have another important influence on the evolution of the suspension. Suppose a pair is about to overtake an isolated particle separated from the pair by a distance R sufficiently large so that the isolated particle has little effect on the relative velocity of the pair (which decays like $(a/R)^2$) but an important effect on the settling velocity of the pair (which decays like $(a/R)$). Then, as the close pair moves past the isolated particle, it is dragged down with the pair and the radial pair-probability function for each of these particles changes to one with more moderately close pairs. Since the isolated particle now moves faster, it also encounters other particles and the pair-probability function changes further toward one with an excess of moderately close pairs.

Because for $c = .001$ close triples are a rare occurrence, the most important effect of encounters between close pairs and isolated particles may be to change the pair-probability function, not to produce relative motion between the particles in the pair. Under this scenario the long-time pair-probability function should show three features: a spike near $r = 2a$ due to close pairs locked in lubrication layers, a dip below 1.0 due to the absence of close triples, and a substantial excess of moderately close pairs. As we see in Figure 19, the long-time pair-probability function shows this type of distribution. (In Figure 19 we have used spherical shells of width L/40, instead of L/20, in order to resolve these features.) Thus this scenario might serve as a rationale for the anomalous behavior of the runs with $c = .001$.

REFERENCES

Barnea, E. and Mizrahi, J. 1973 A generalized approach to the fluid dynamics of particulate systems. Part 1. General correlation for fluidization and sedimentation in solid multiparticle systems. Chem. Eng. J. 5, 171-189.

Batchelor, G.K. 1972 Sedimentation in a dilute dispersion of spheres. J. Fluid Mech. 52, 245-268.

Batchelor, G.K. 1982 Sedimentation in dilute polydisperse system of interacting spheres. Part 1. General theory. J. Fluid Mech. 119, 379-408.

Batchelor, G.K. and Green, J.T. 1972 The hydrodynamic interaction of two small freely-moving spheres in a linear flow field. J. Fluid Mech. 56, 375-400.

Batchelor, G.K. and Wen, C.-S. 1982 Sedimentation in a dilute polydisperse system of interacting spheres. Part 2. Numerical results. J. Fluid Mech. 124, 495-528.

Buscall, R., Goodwin, J.W., Ottewill, R.H. and Tadros, T.F. 1982 The settling of particles through Newtonian and Non-Newtonian media. J. Colloid Interface Sci. 85, 78-86.

Cheng, P.Y. and Schachman, H.K. 1955 Studies on the validity of the Einstein viscosity law and Stokes' law of sedimentation. J. Polymer Sci. 16, 19-30.

Happel, J. and Brenner, H. 1965 Low Reynolds Number Hydrodynamics. Prentice-Hall.

Hasimoto, H. 1959 On the periodic fundamental solutions of the Stokes equations and their application to viscous flow past a cubic array of spheres. J. Fluid Mech. 5, 317-328.

Kops-Werkhoven, M.M. and Fijnaut, H.M. 1981 Dynamic light scattering and sedimentation experiments on silica dispersions at finite concentrations. J. Chem. Phys. 74, 1618-1625.

Lynch, E.D. and Herbolzheimer, E. 1985a Sedimentation in sheared suspensions. (To be submitted - Chapter 3 of this thesis).

Lynch, E.D. and Herbolzheimer, E. 1985b A method for the simulation of sedimenting suspensions. (To be submitted - Chapter 2 of this thesis).

Mazaika, P.K. 1974 On the settling speed of dilute arrays of spheres. Ph.D. Thesis, Calif. Inst. Tech.

Mazur, P. and Van Saarloos, W. 1982 Many-sphere hydrodynamic interactions and mobilities in a suspension. Physica 115A, 21-57.

Oliver, D.R. 1961 The sedimentation of suspensions of closely-sized spherical particles. Chem. Eng. Sci. 15, 230-242.

Saffman, P.G. 1973 On the settling speed of free and fixed suspensions. Stud. Appl. Math 52, 115-127.

Sangani, A.S. and Acrivos, A. 1982 Slow flow through a periodic array of spheres. Int. J. Multiphase Flow 8, 343-360.

Smith, T.N. 1968 The spatial distribution of spheres falling in a viscous liquid. J. Fluid Mech. 32, 203-207.

Steinour, H.H. 1944 Rate of sedimentations. Nonflocculated suspensions of uniform spheres. Ind. Eng. Chem. 36, 618-624.

Tackie, E., Bowen, B.D. and Epstein, N. 1983 Hindered settling of uncharged and charged submicrometer spheres. Ann. NY Acad. Sci. 404, 366-67.

Table 1

Values of the Peclet Number for Several Sets of Sedimentation Experiments

| | $a_{mean}(\mu m)$ | $\rho_s(\frac{g}{cm^3})$ | $\rho(\frac{g}{cm^3})$ | c | Pe |
|---|---|---|---|---|---|
| Kops-Werkhoven and Fijnaut (1981) | .021 | 1.28 | .78 | .0078-.117 | ca. $4x10^{-7}\kappa$ |
| Cheng and Schachman (1955) | .13 | 1.052 | 1.0 | .005-.075 | ca. $5x10^{-5}\kappa$ |
| Buscall, et al. (1982) | 1.55 | 1.054 | 1.0 | .005-.085[+] | ca. $.5\kappa$-$1.4\kappa$ |
| Steinour (1944) (glass spheres) | 6.8 | 2.32 | 1.0 | .15-.5 | ca. $1.9x10^{4}\kappa$ |
| Oliver (1961) | 80 | 1.191 | 1.05 | .0033-.35 | ca. $2x10^{7}\kappa$ |
| Lynch and Herbolzheimer (1985a) | 51 | 2.8 | 1.04 | .04-.25 | ca. $5x10^{7}\kappa$ |

[+] Largest concentration for which the correction factor to the Stokes velocity was proportional to c.

Table 2.

List of Simulation Runs

| Run | Type of Initial Configuration | N | c | $\frac{a}{L}$ | $\Delta t$ | $t_{final}$ | $(1-u_o^{\infty}/u_s c^{1/3})$ |
|---|---|---|---|---|---|---|---|
| 1 | Randomized Simple Cubic Array | 64 | .005 | .0265 | .001 | 8.0 | .785 |
| 2 | Randomized Simple Cubic Array | 64 | .001 | .0155 | .0005 | 6.0 | .855 |
| 3 | Randomized Simple Cubic Array | 64 | .02 | .0421 | .001 | 3.731 | .965 |
| 4 | Randomized Simple Cubic Array | 27 | .005 | .0354 | .001 | 8.0 | .854 |
| 5 | Random Suspension | 64 | .005 | .0265 | .001 | 12.0 | .684 |
| 6 | Random Suspension | 64 | .005 | .0265 | .001 | 8.0 | .778 |
| 7 | Random Suspension | 64 | .005 | .0265 | .002 | 8.0 | .701 |
| 8 | Random Suspension | 64 | .005 | .0265 | .0005 | 8.0 | .738 |
| 9 | Random Suspension | 64 | .008 | .0310 | .001 | 8.0 | .764 |
| 10 | Random Suspension | 64 | .001 | .0155 | .0005 | 12.0 | - |
| 11 | Random Suspension | 64 | .001 | .0155 | .0005 | 8.0 | .008 |
| 12 | Random Suspension | 125 | .005 | .0212 | .001 | 8.0 | .627 |
| 13 | Random Suspension | 27 | .005 | .0354 | .001 | 8.0 | .852 |

Figure 1. Volume-averaged pair-probability function at intervals of .4 in dimensionless time for simulation run 6: initial configuration of a random suspension; N=64, c=.005, $\Delta t$=.001.

Figure 1

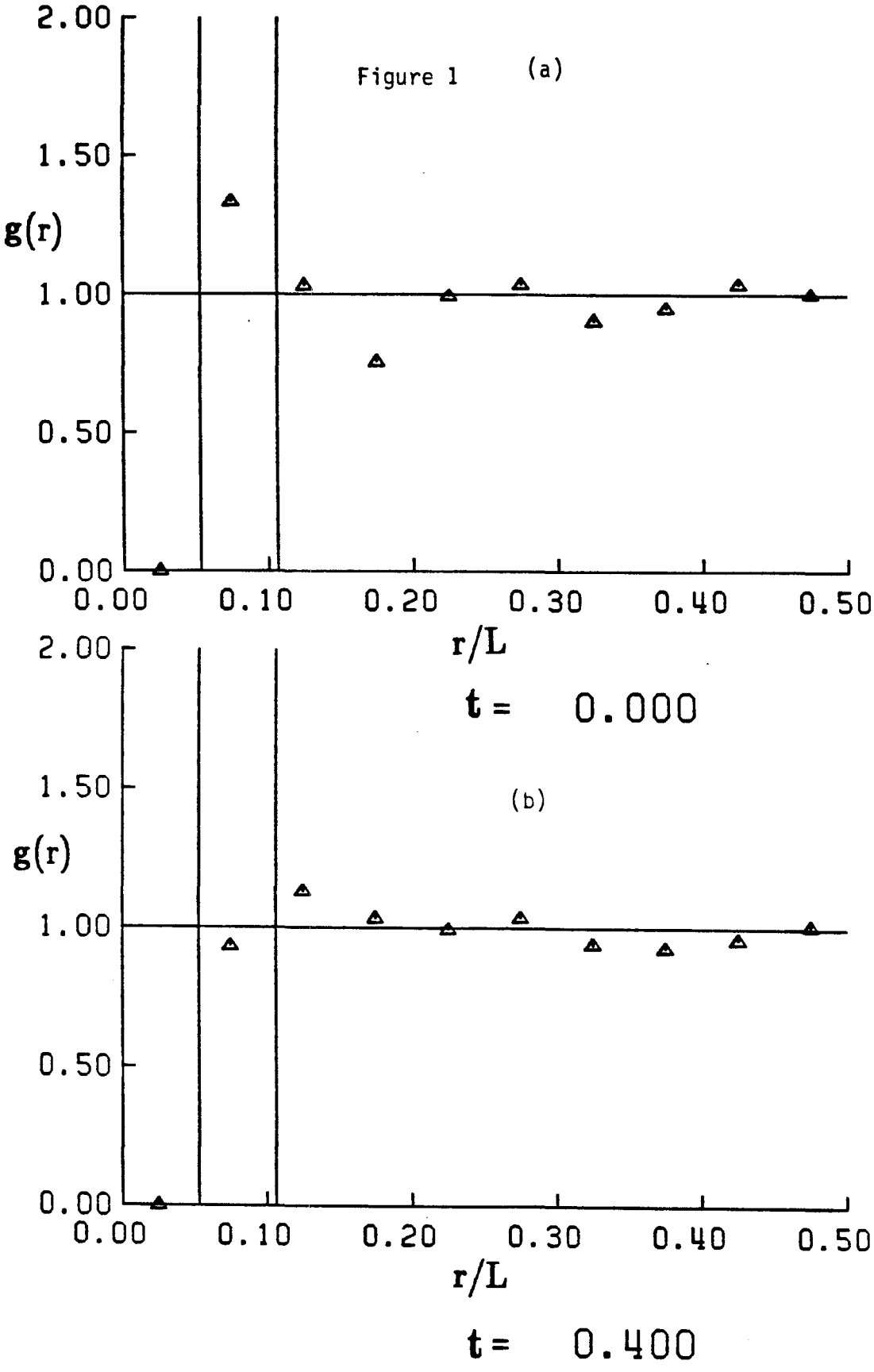
(a)
2.00
1.50
g(r)
1.00
0.50
0.00
0.00
0.10
0.20
0.30
0.40
0.50
r/L
t = 0.000
(b)
2.00
1.50
g(r)
1.00
0.50
0.00
0.00
0.10
0.20
0.30
0.40
0.50
r/L
t = 0.400

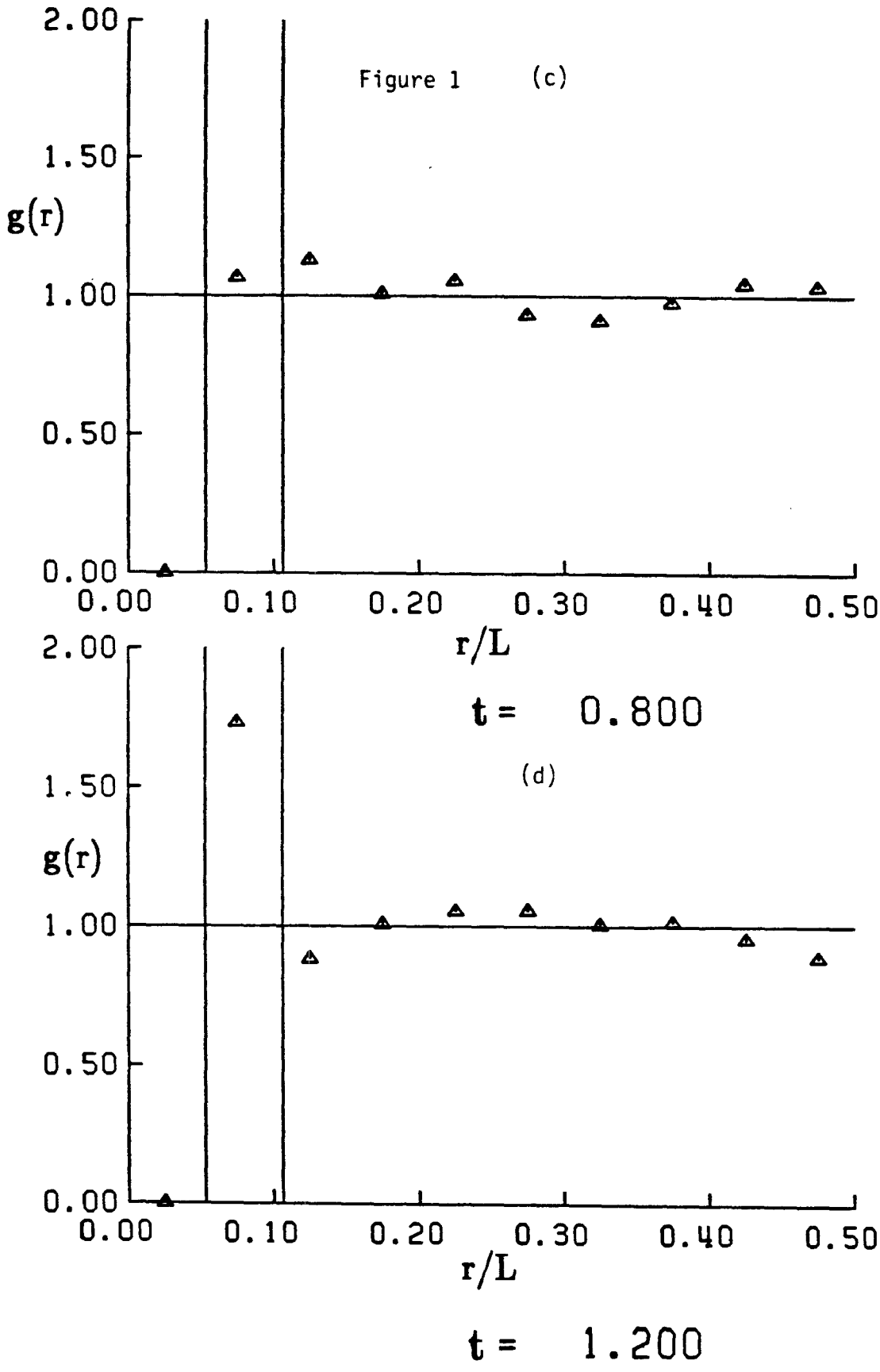
2.00
1.50
g(r)
1.00
0.50
0.00
0.00
0.10
0.20
0.30
0.40
0.50
r/L
t = 0.800
(d)
2.00
1.50
g(r)
1.00
0.50
0.00
0.00
0.10
0.20
0.30
0.40
0.50
r/L
t = 1.200

Figure 1 (c)

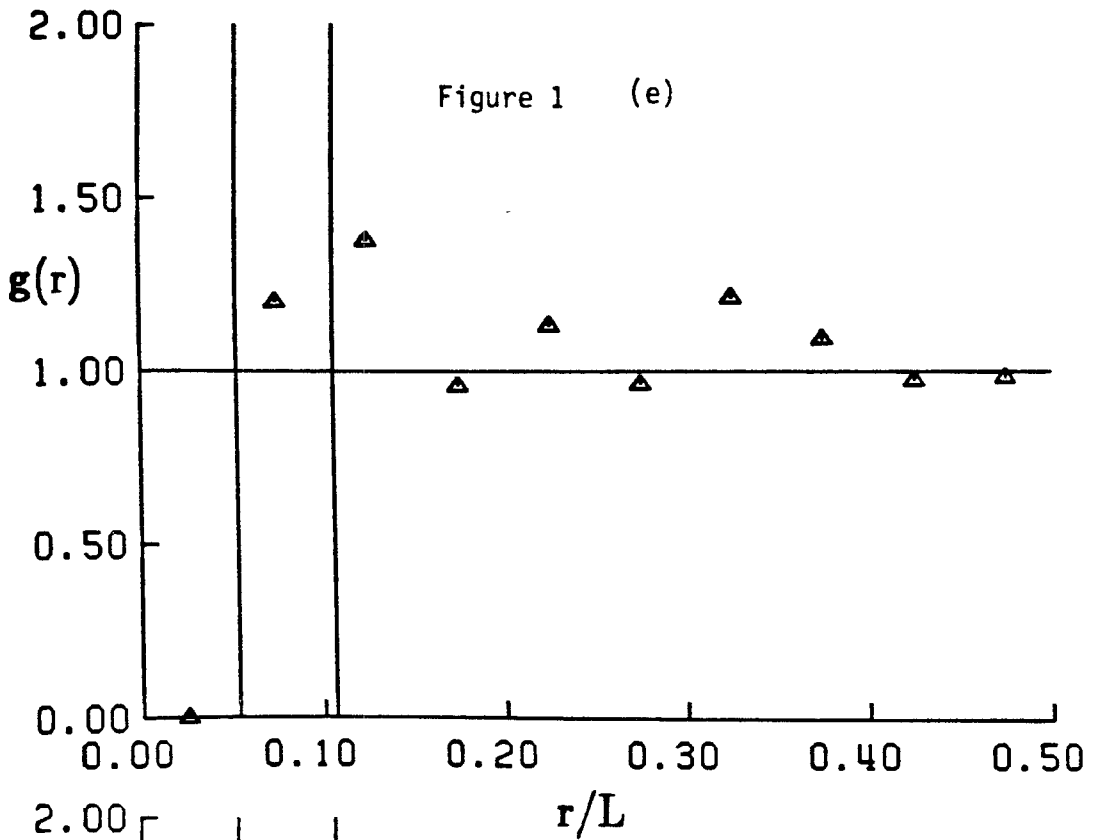


Figure 1 (e)

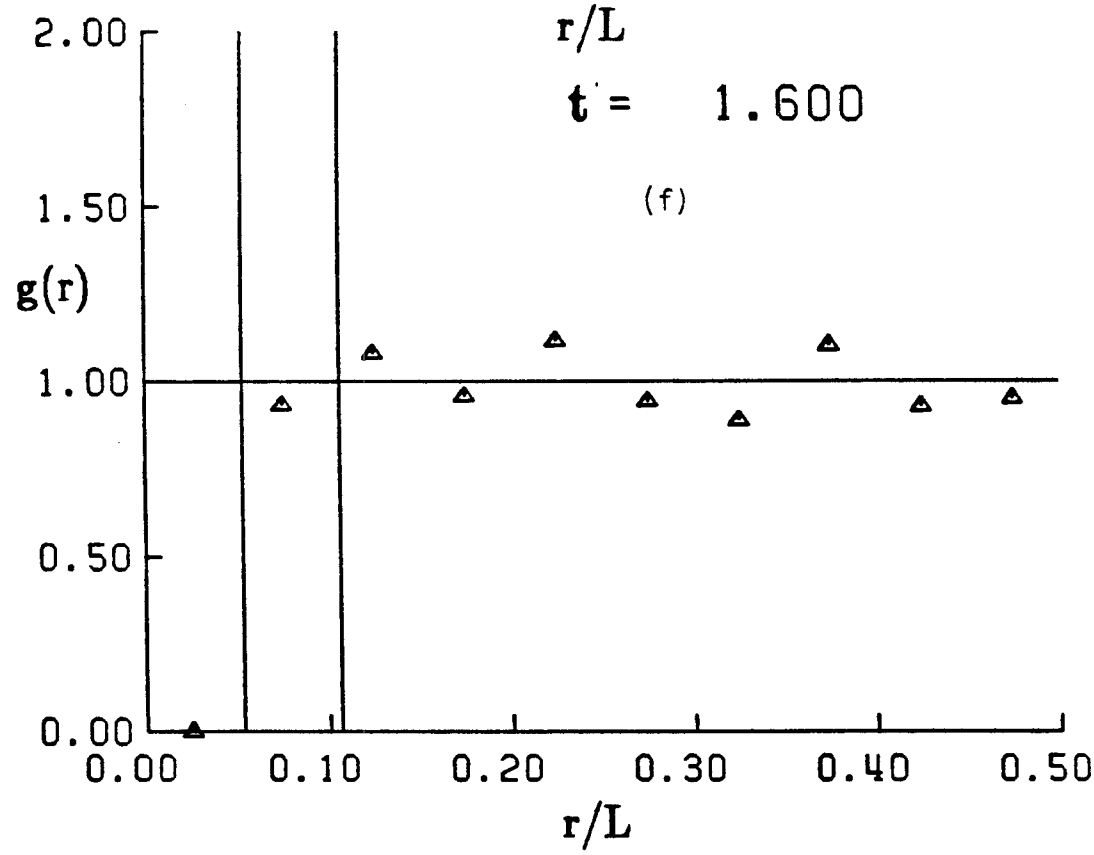


t = 1.600

(f)

t = 2.000

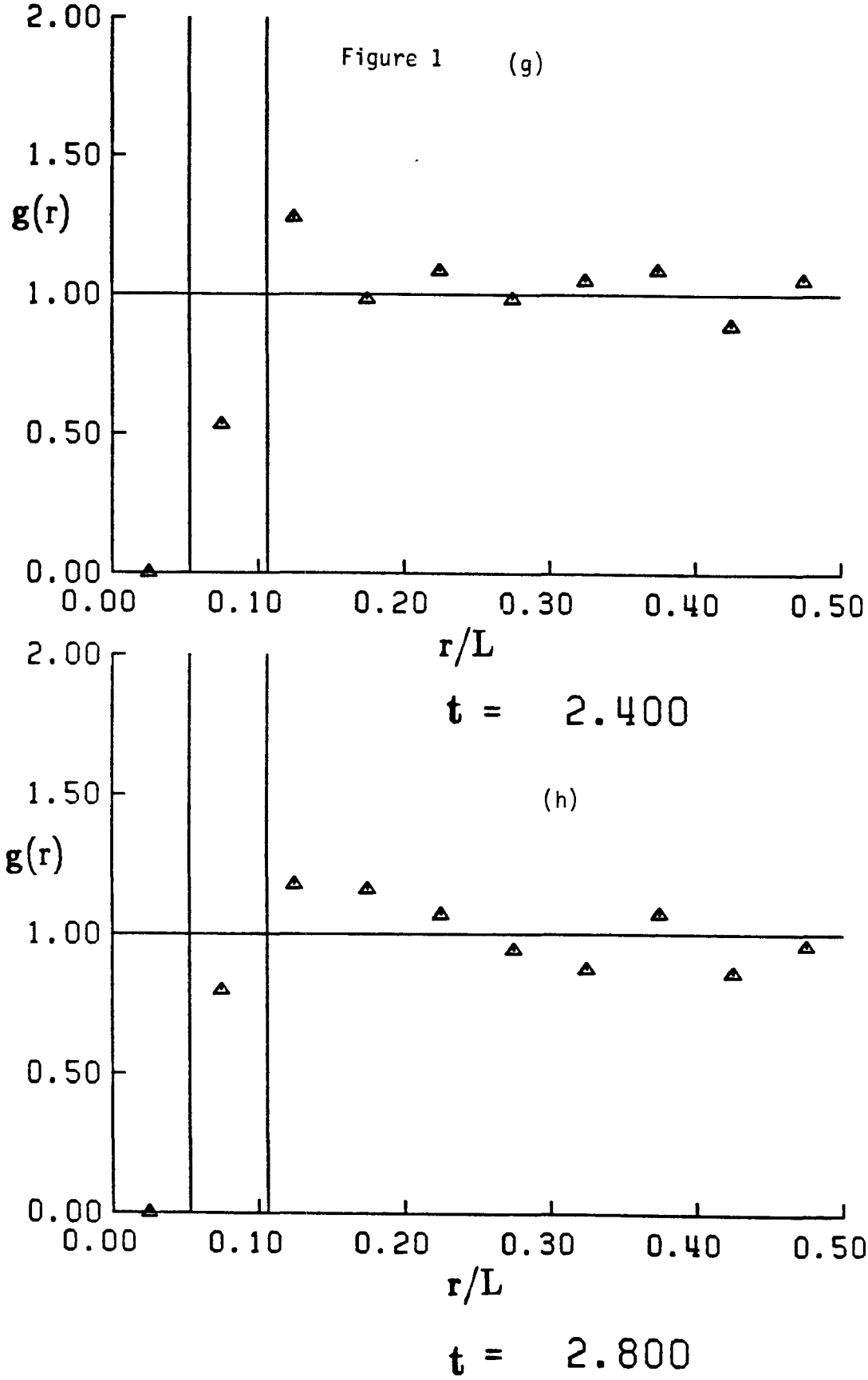
2.00
1.50
g(r)
1.00
0.50
0.00
0.00
0.10
0.20
0.30
0.40
0.50
r/L
t = 2.400
(h)
2.00
1.50
g(r)
1.00
0.50
0.00
0.00
0.10
0.20
0.30
0.40
0.50
r/L
t = 2.800

Figure 1 (g)

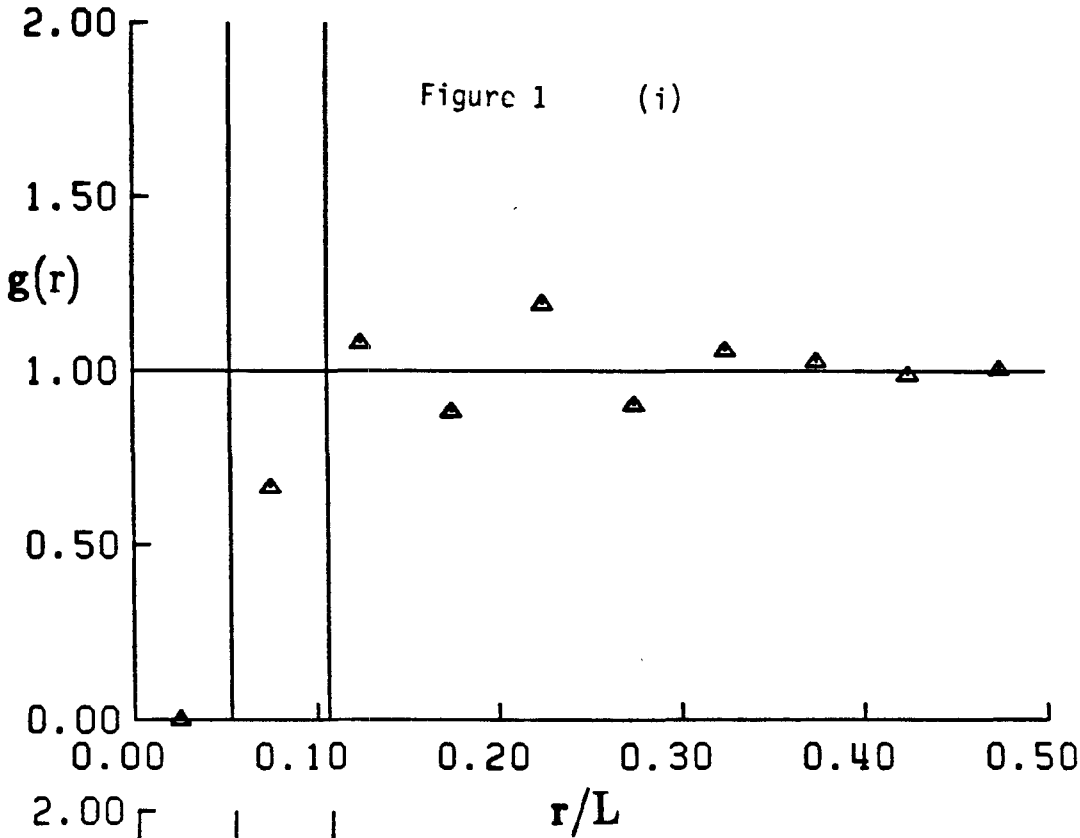


Figure 1 (i)

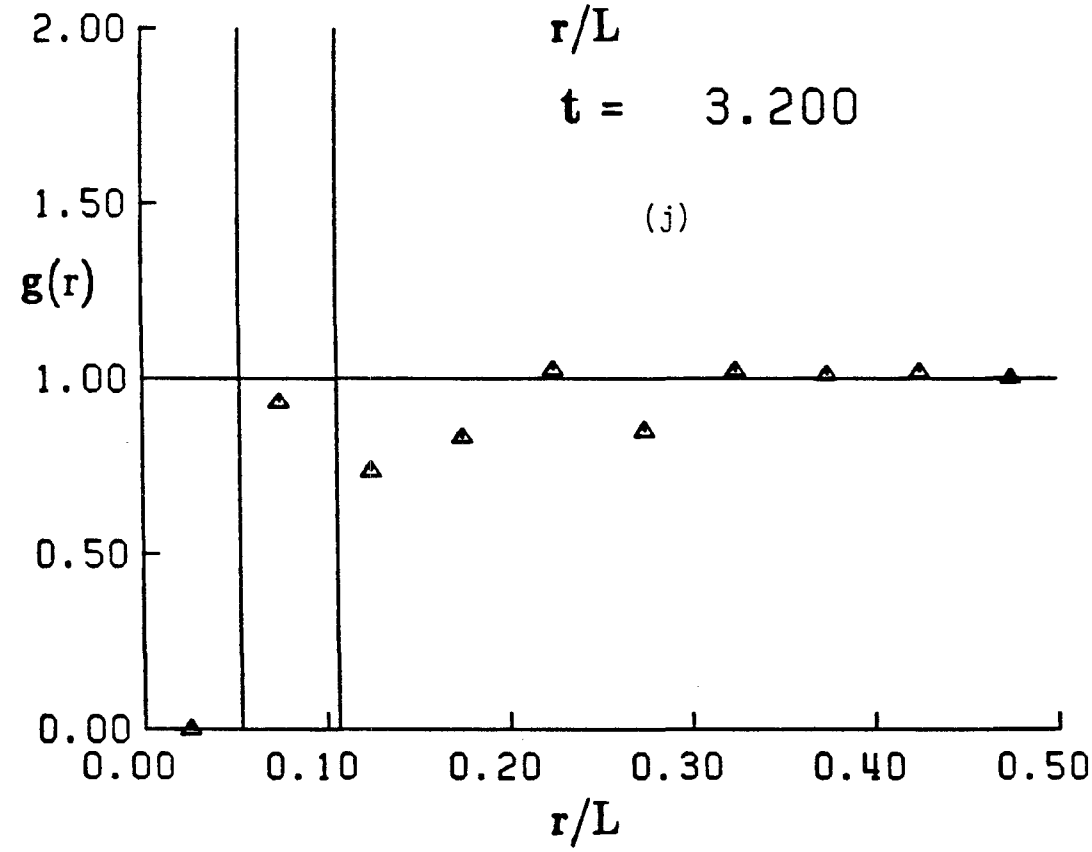


t = 3.200

(j)

t = 3.600

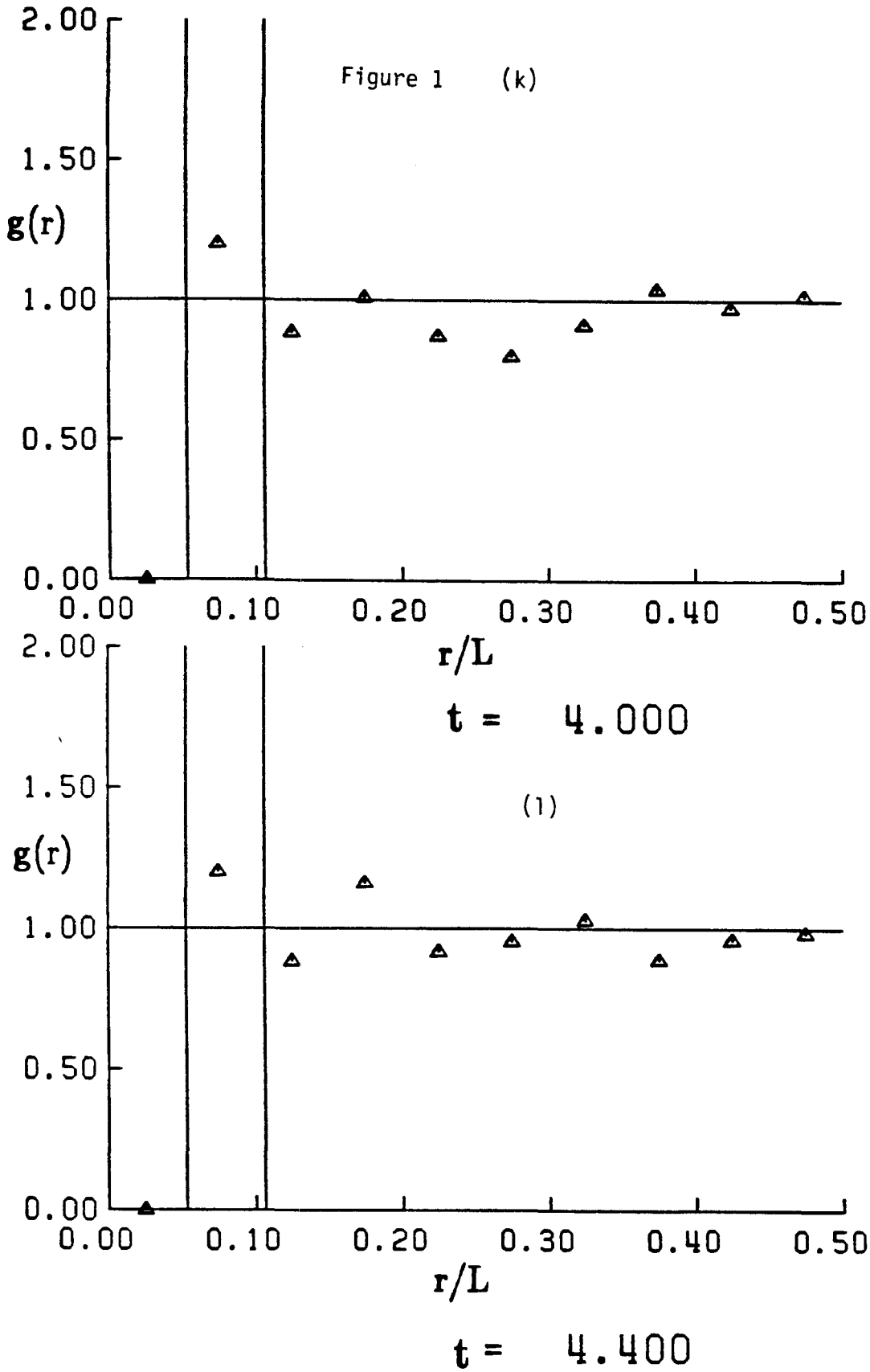
2.00
1.50
g(r)
1.00
0.50
0.00
0.00
0.10
0.20
0.30
0.40
0.50
r/L
t = 4.000
(1)
2.00
1.50
g(r)
1.00
0.50
0.00
0.00
0.10
0.20
0.30
0.40
0.50
r/L
t = 4.400

Figure 1 (k)

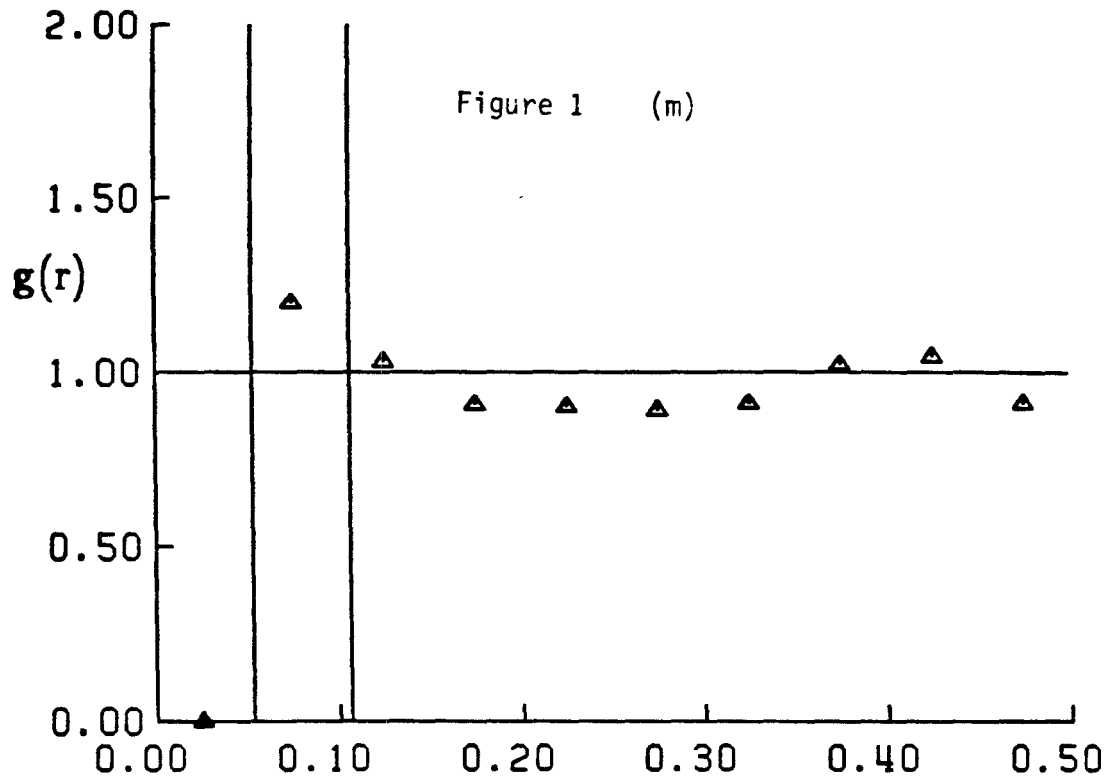


Figure 1 (m)

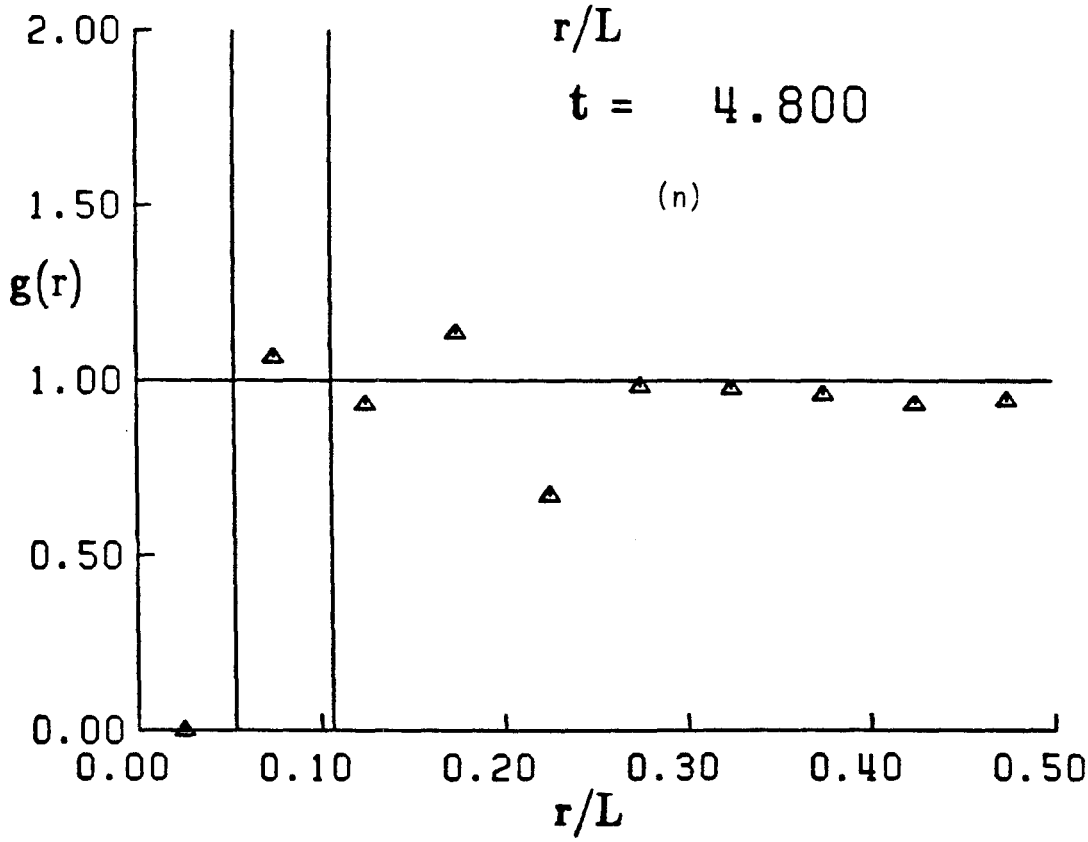


t = 4.800

(n)

t = 5.200

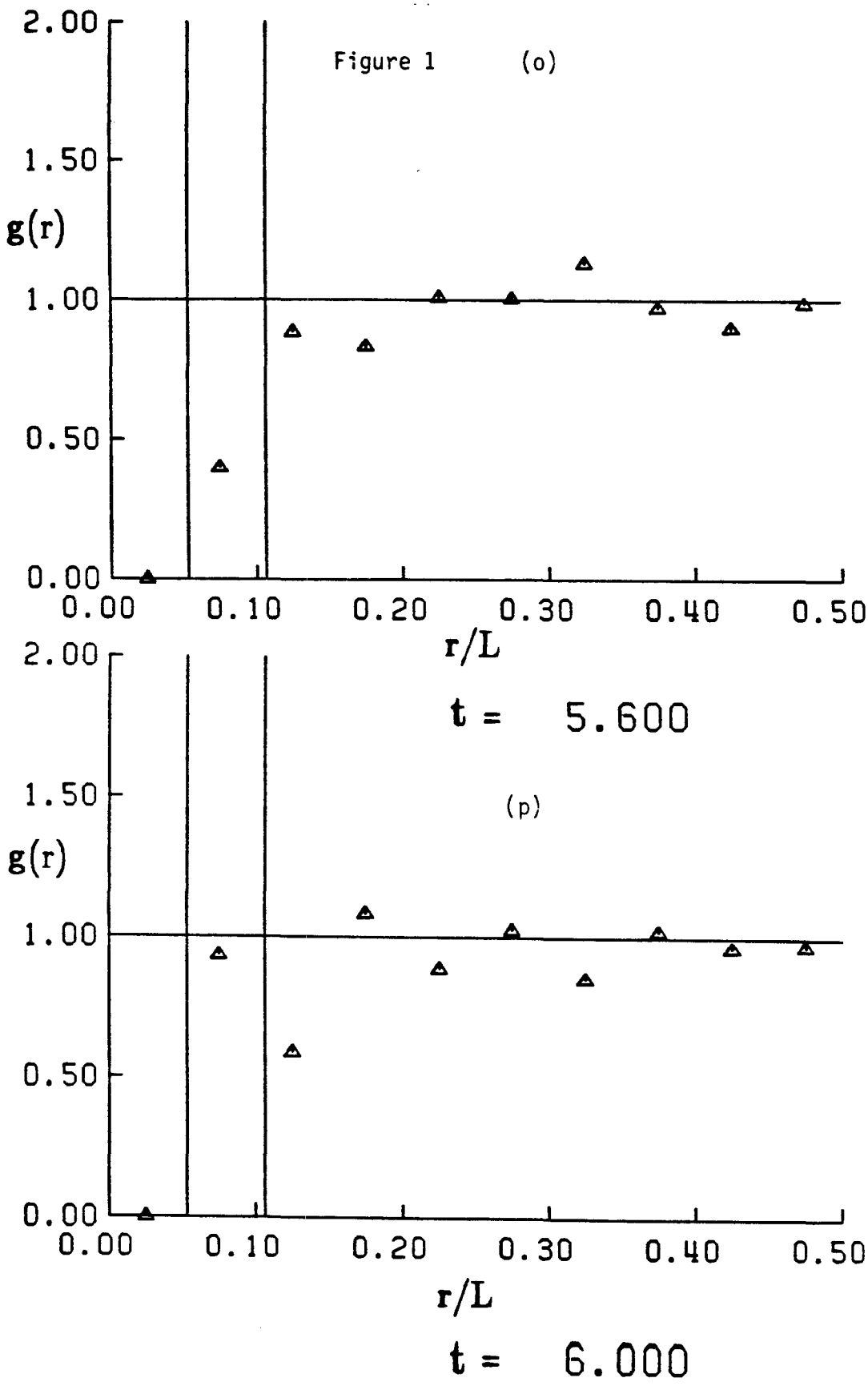
2.00
1.50
g(r)
1.00
0.50
0.00
0.00
0.10
0.20
0.30
0.40
0.50
r/L
t = 5.600
2.00
1.50
g(r)
1.00
0.50
0.00
0.00
0.10
0.20
0.30
0.40
0.50
r/L
t = 6.000

Figure 1 (o) (p)

Figure 1 (q)

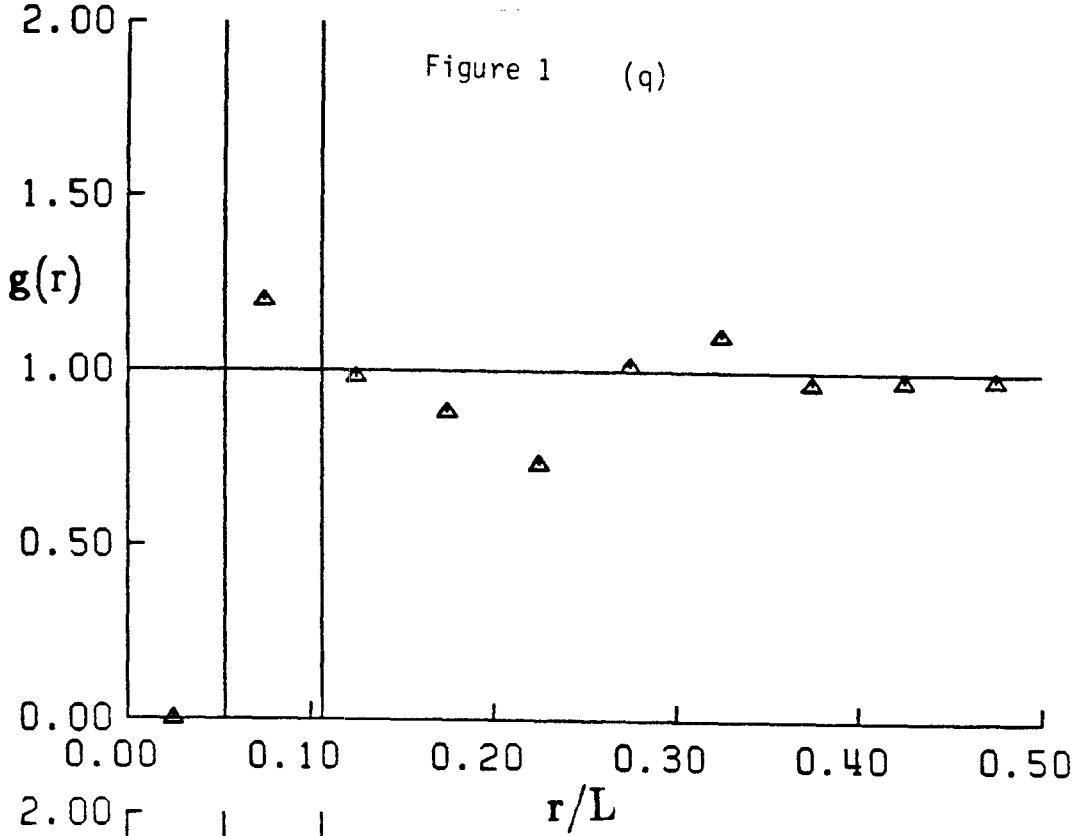
2.00
1.50
g(r)
1.00
0.50
0.00
0.00
0.10
0.20
0.30
0.40
0.50
r/L
t = 6.400

(r)

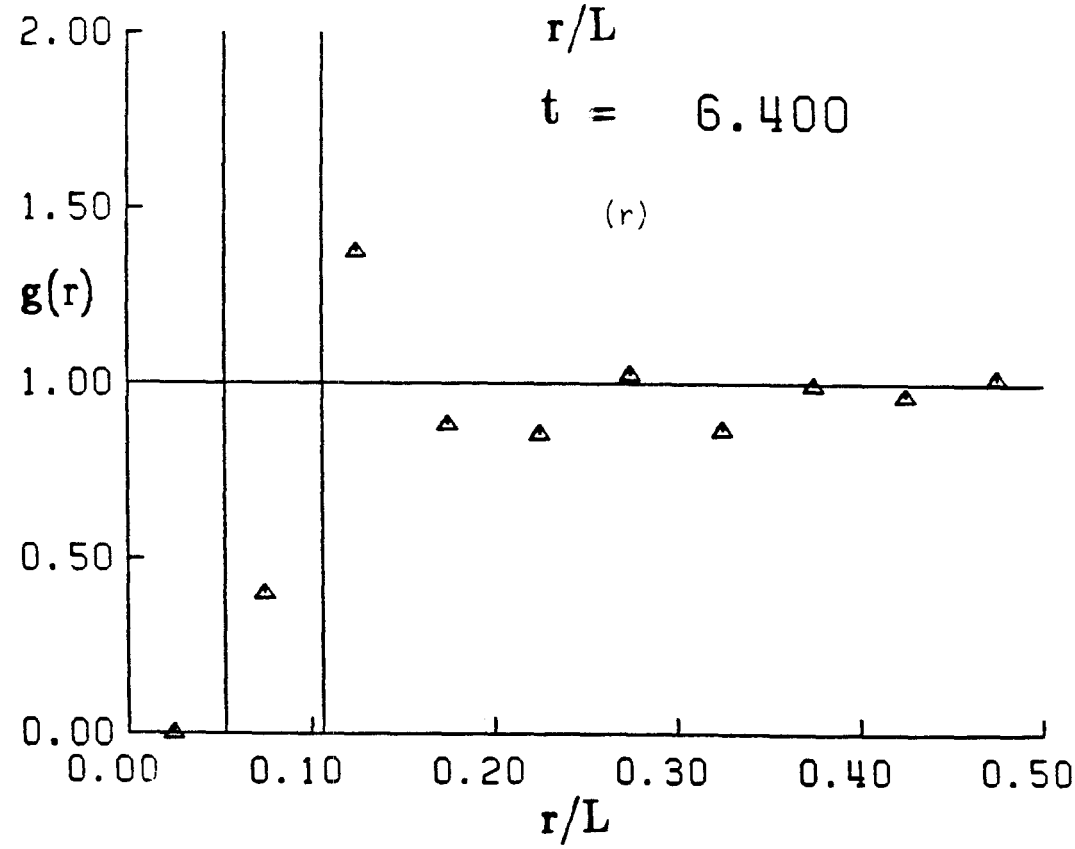
2.00
1.50
g(r)
1.00
0.50
0.00
0.00
0.10
0.20
0.30
0.40
0.50
r/L
t = 6.800

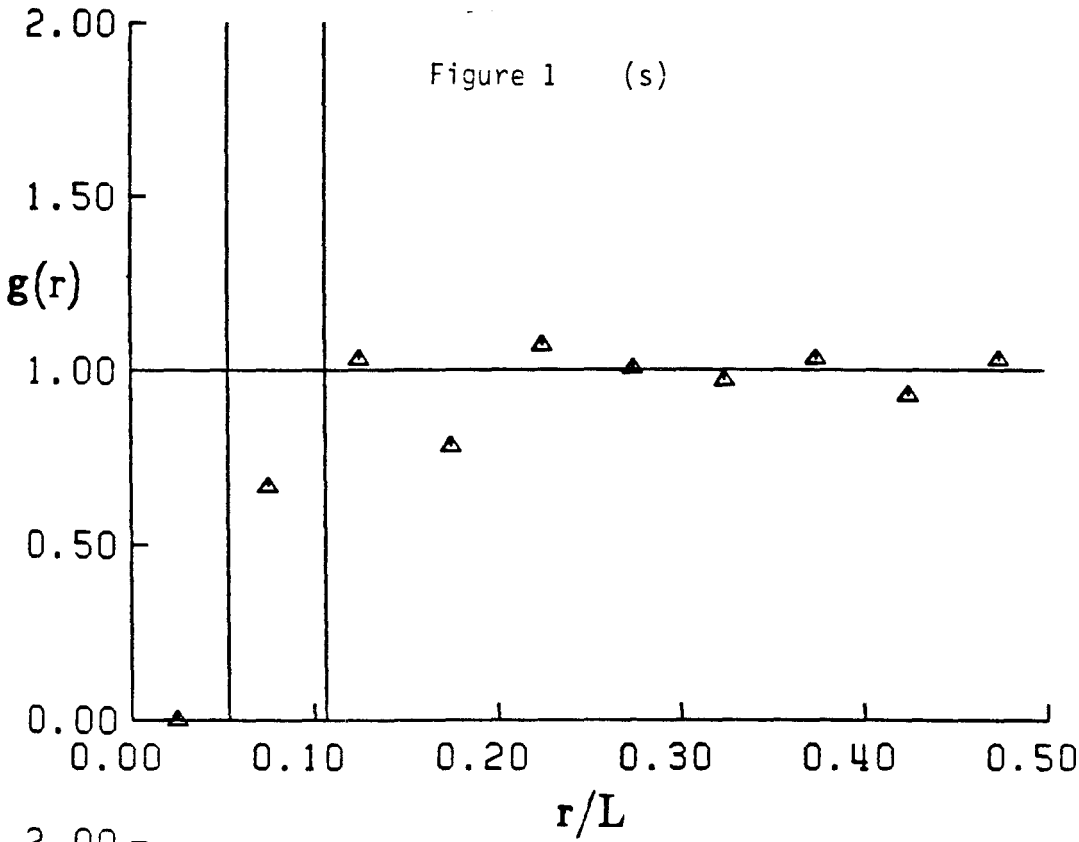


Figure 1 (s)

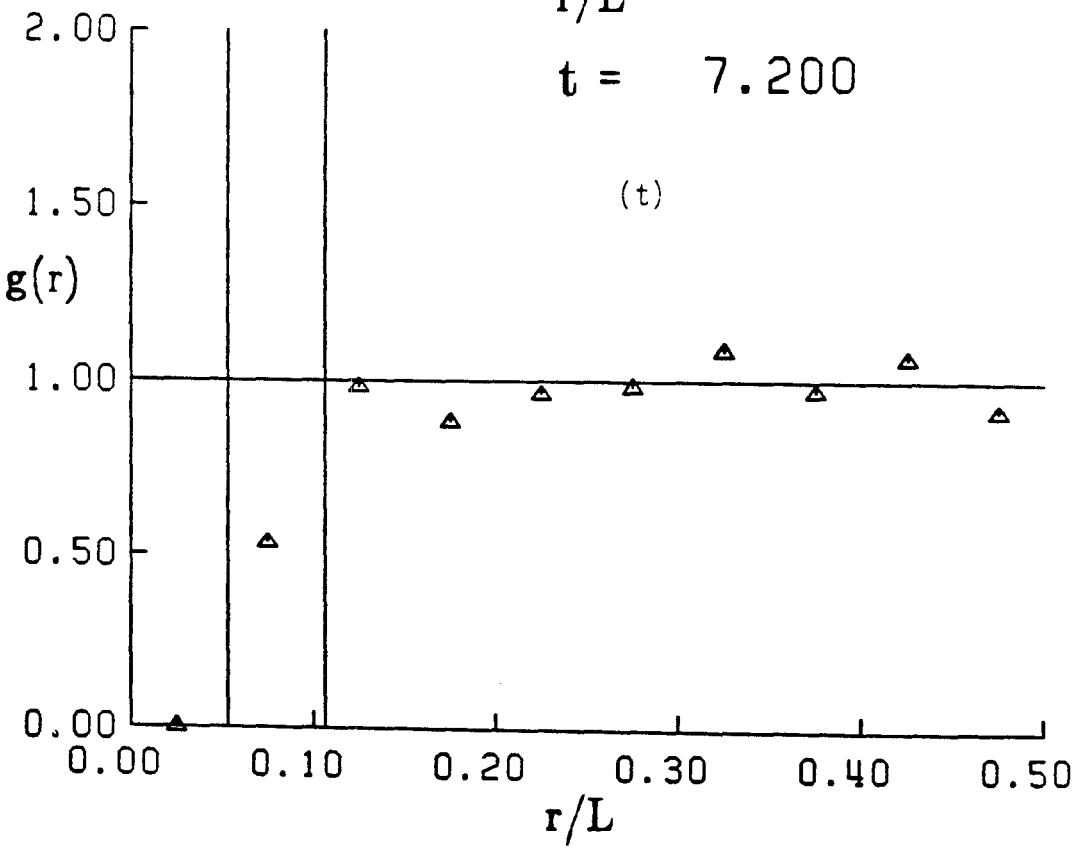


t = 7.200

(t)

t = 7.600

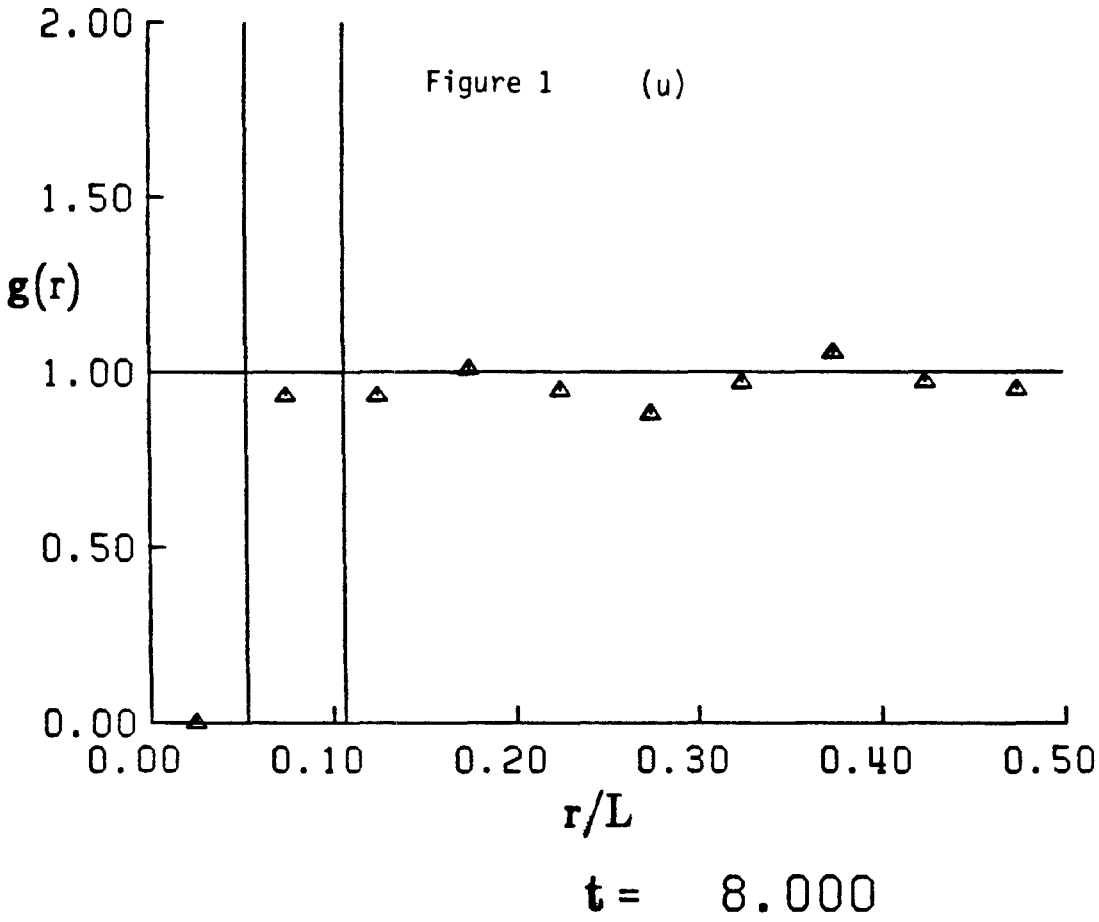


Figure 1 (u)

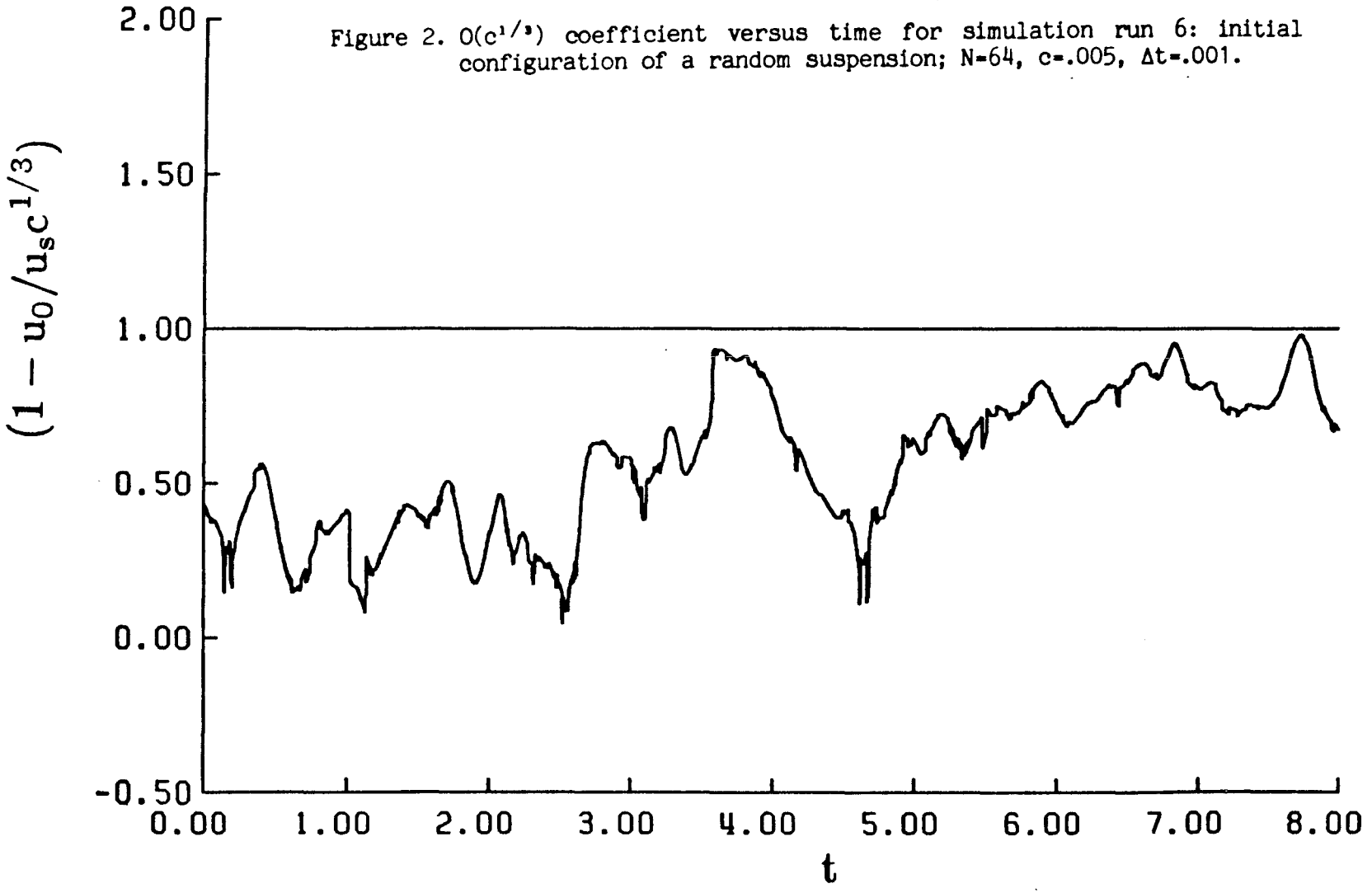


Figure 2. $O(c^{1/3})$ coefficient versus time for simulation run 6: initial configuration of a random suspension; N=64, c=.005, $\Delta t$=.001.

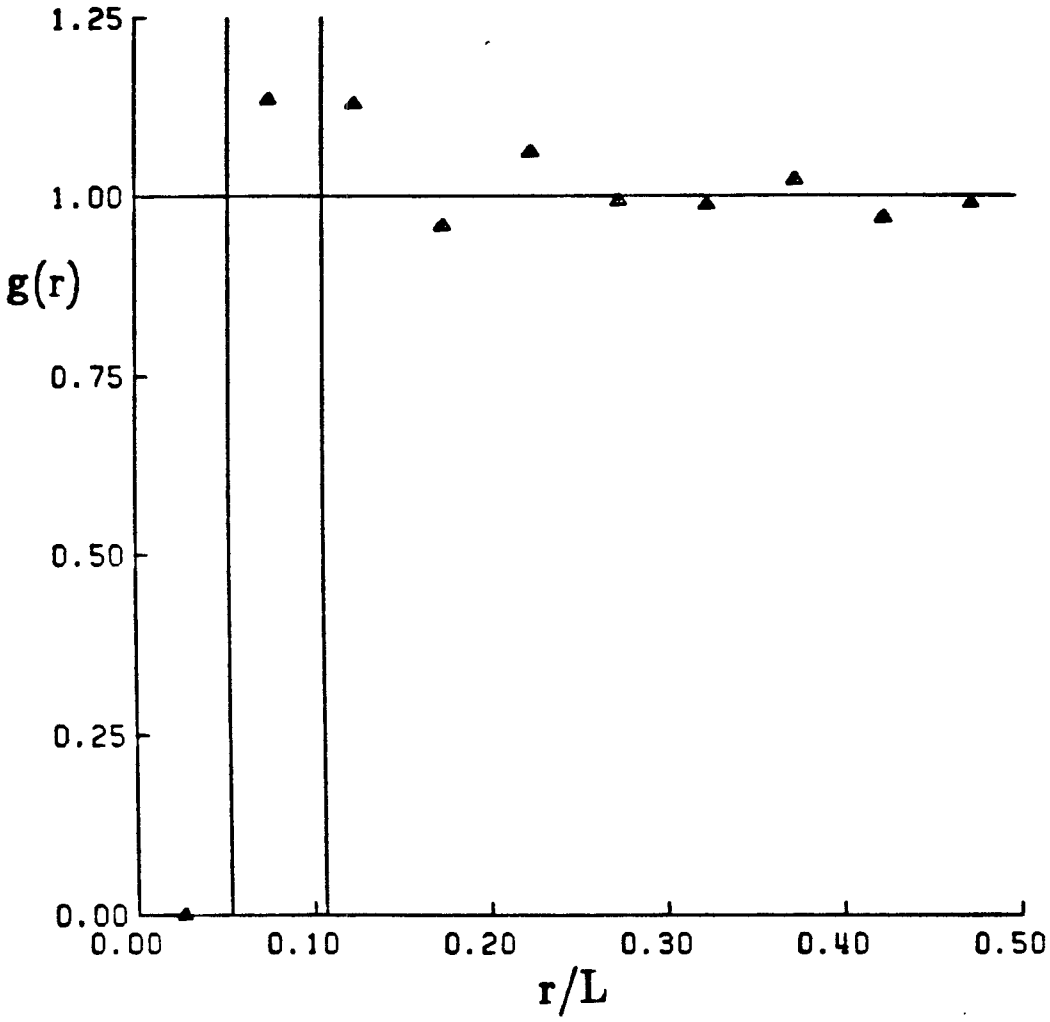


Figure 3. Pair-probability function averaged from t=0.0 to 2.4 for simulation run 6: initial configuration of a random suspension; N=64, c=.005, $\Delta t$=.001.

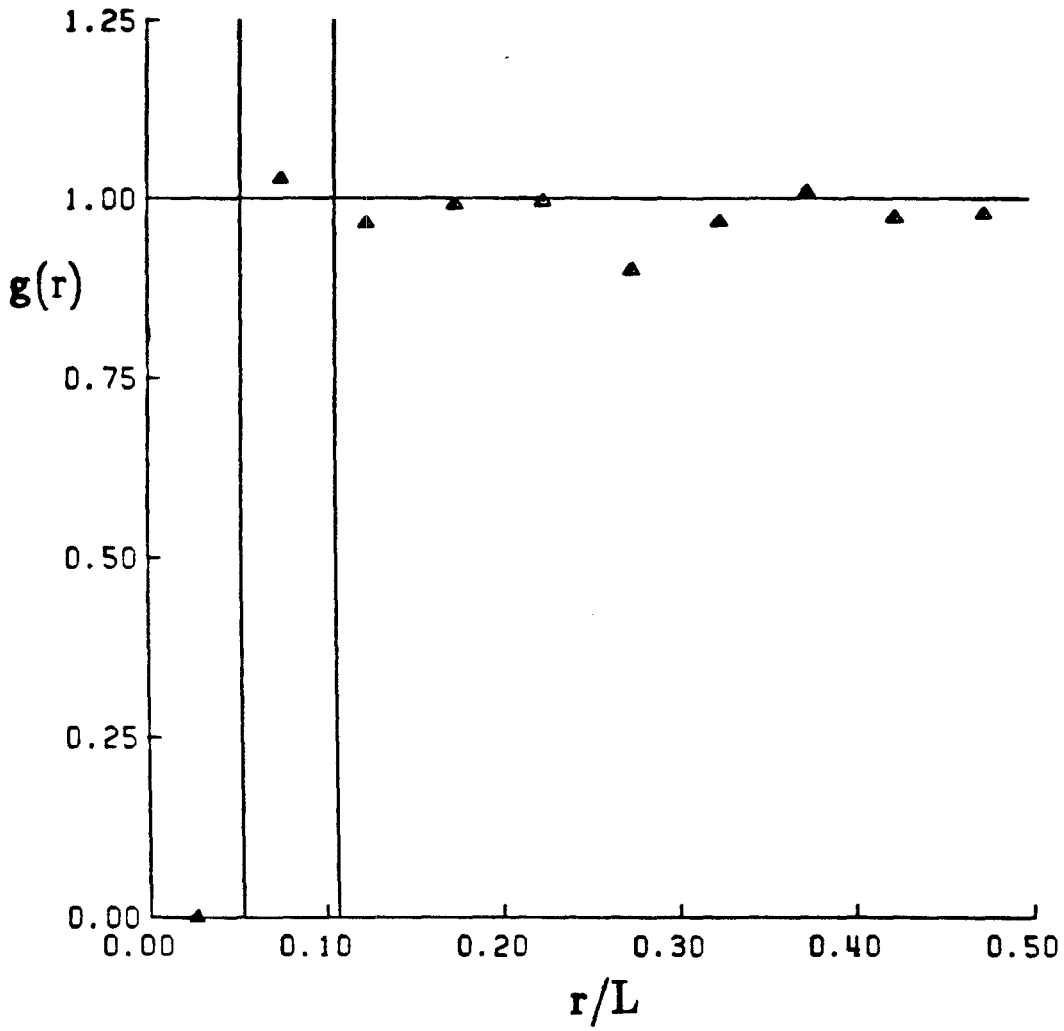


Figure 4. Pair-probability function for simulation run 6 averaged from t=2.8 to 4.8.

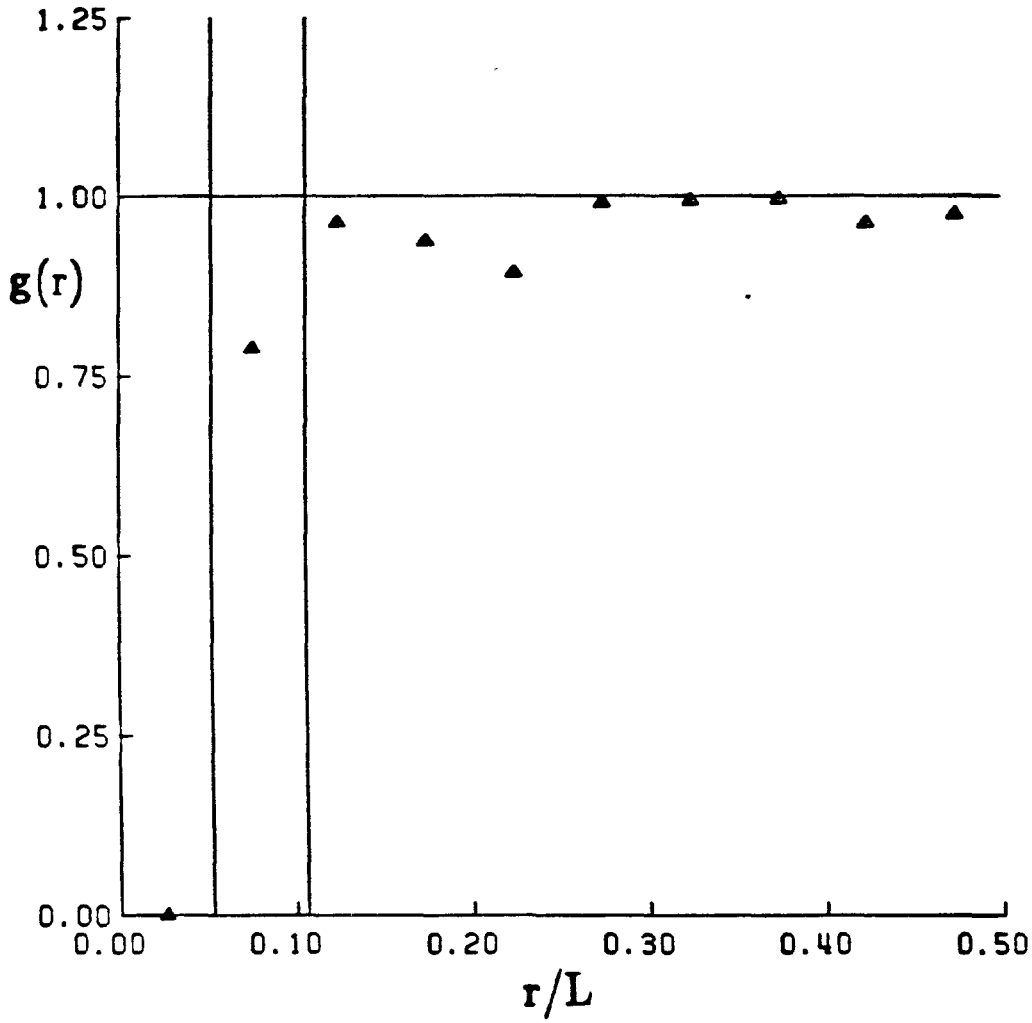


Figure 5. Pair-probability function for simulation run 6 averaged from t=5.2 to 8.0.

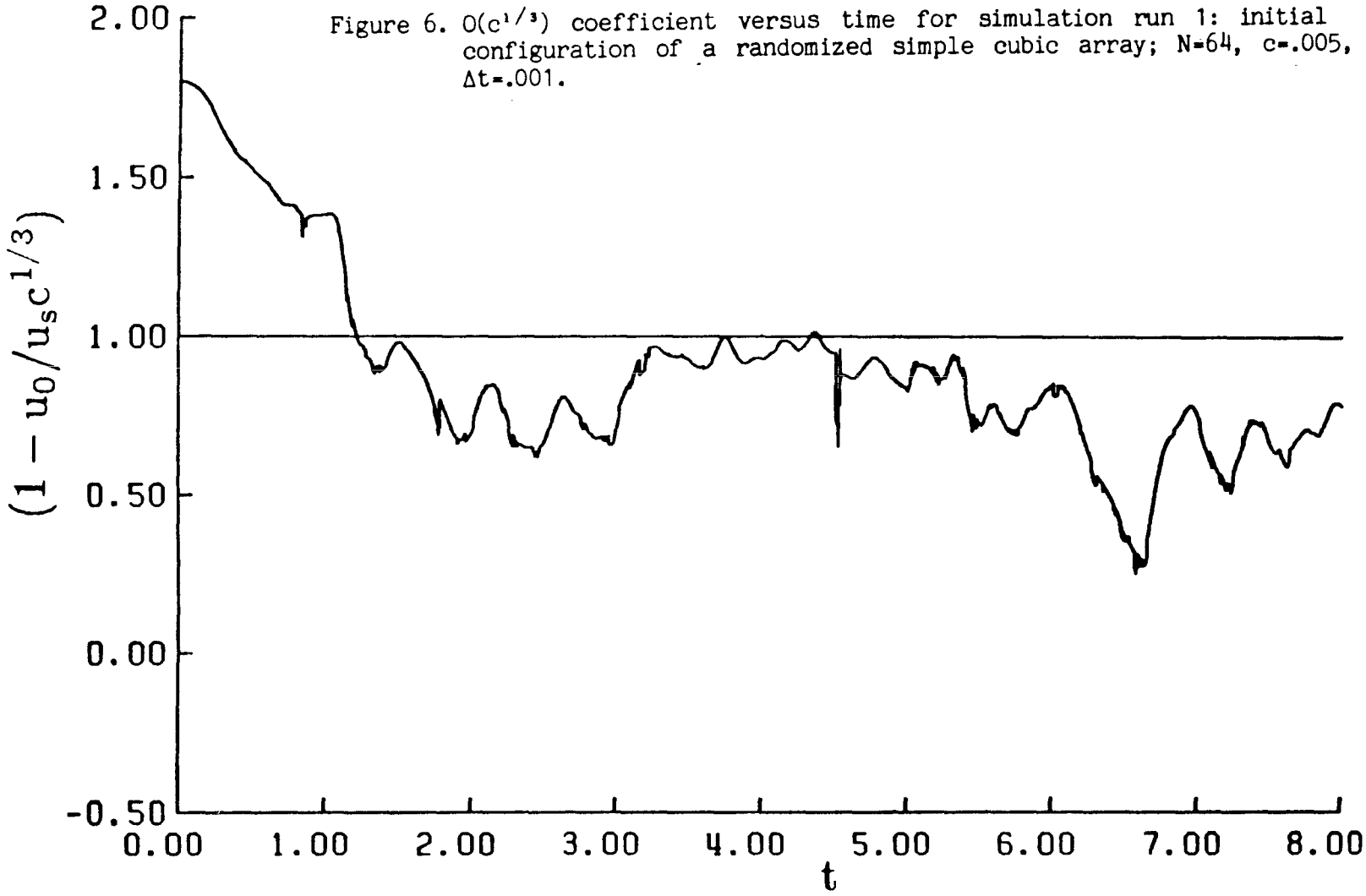


Figure 6. $O(c^{1/3})$ coefficient versus time for simulation run 1: initial configuration of a randomized simple cubic array; N=64, c=.005, $\Delta t$=.001.

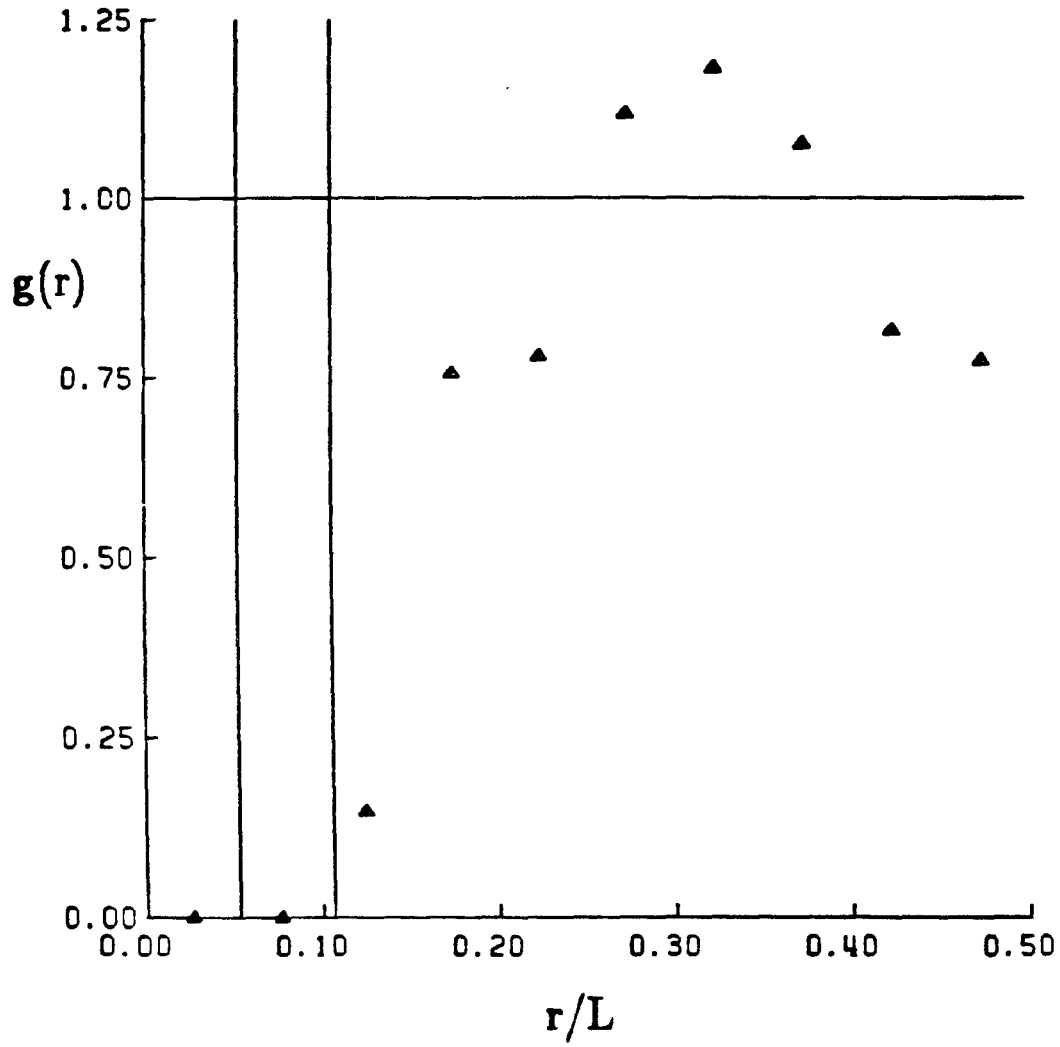


Figure 7. Initial pair-probability function for simulation run 1: initial configuration of a randomized simple cubic array; N=64, c=.005, Δt=.001.

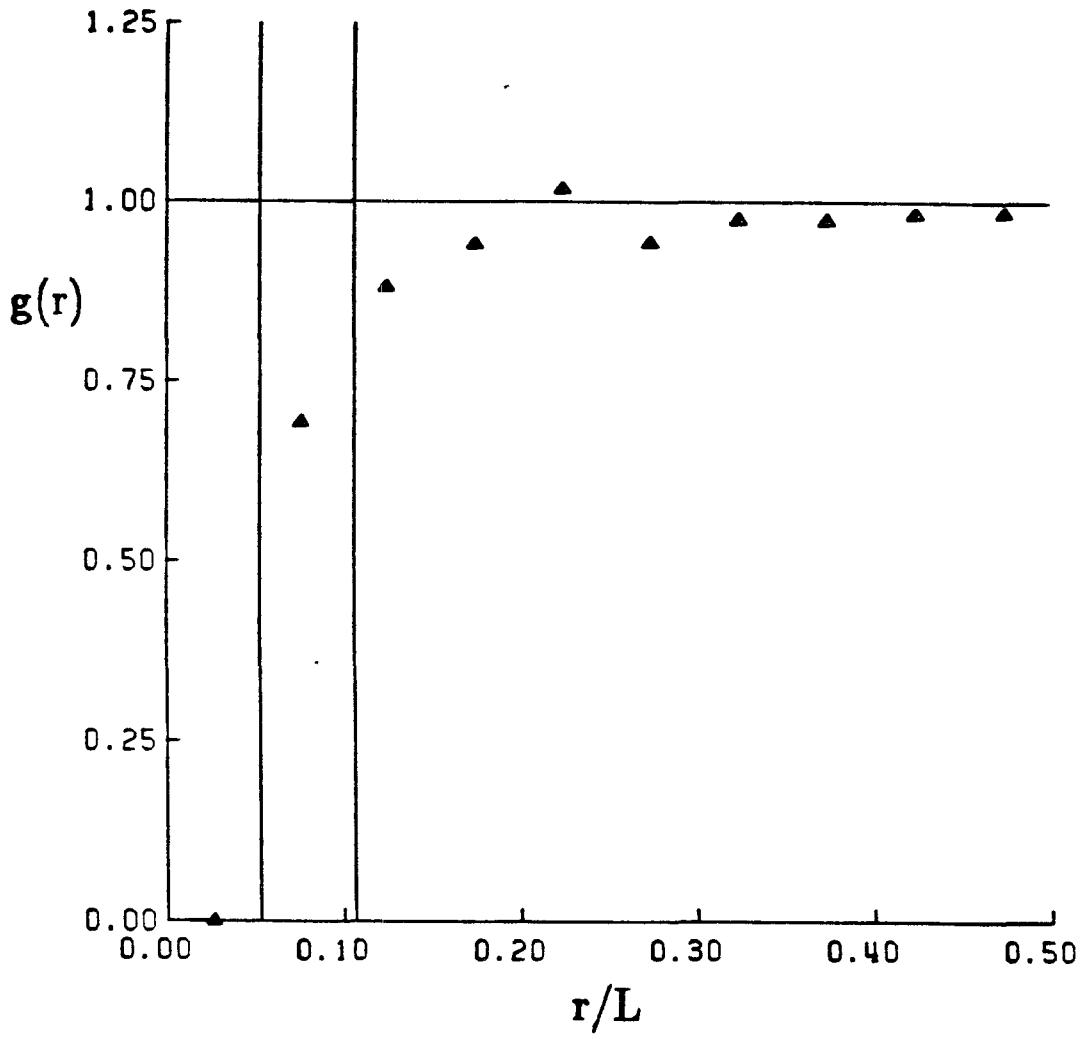


Figure 8. Pair-probability function for simulation run 1 averaged from t=1.2 to 8.0.

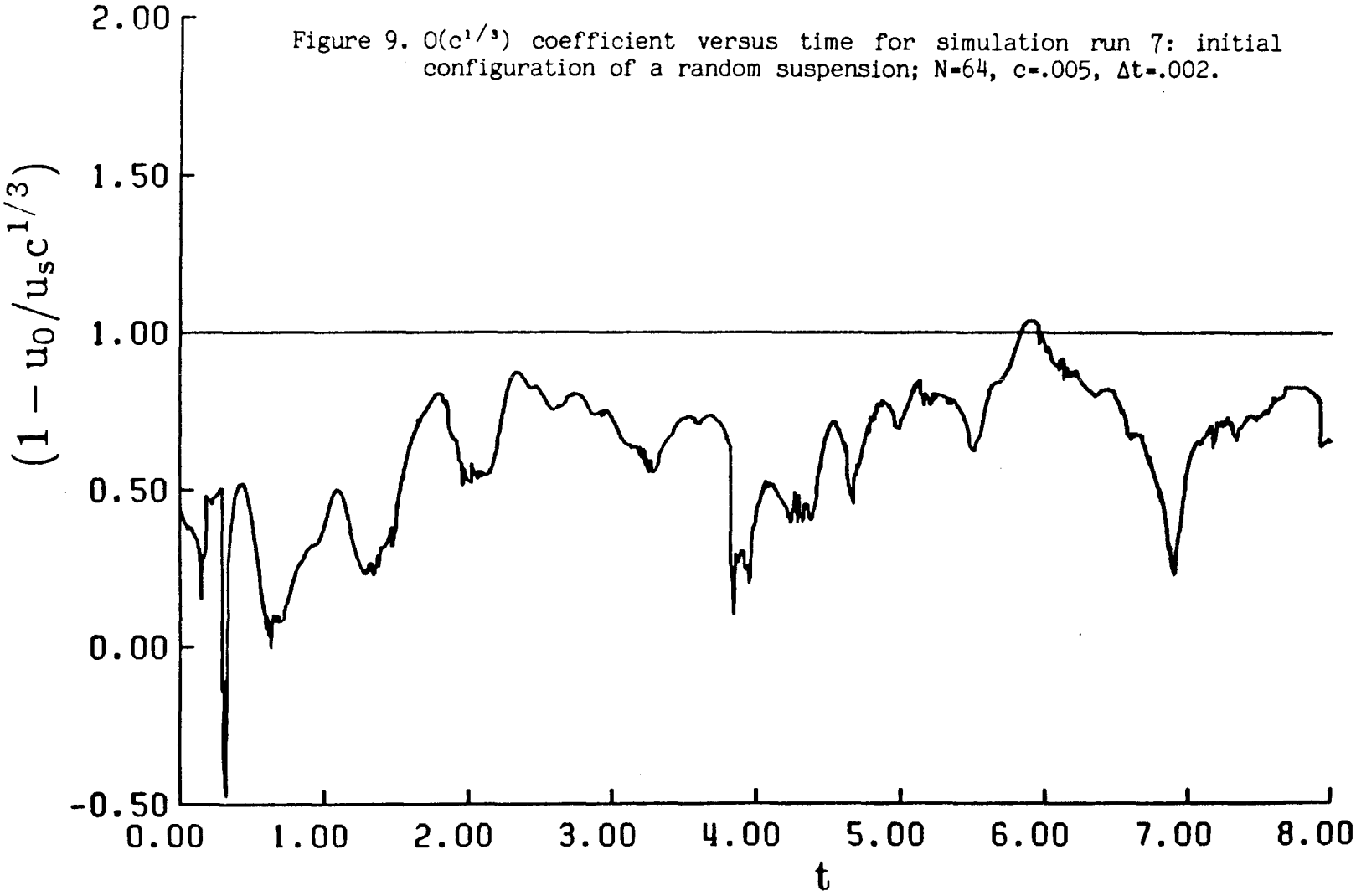


Figure 9. $O(c^{1/3})$ coefficient versus time for simulation run 7: initial configuration of a random suspension; N=64, c=.005, $\Delta t$=.002.

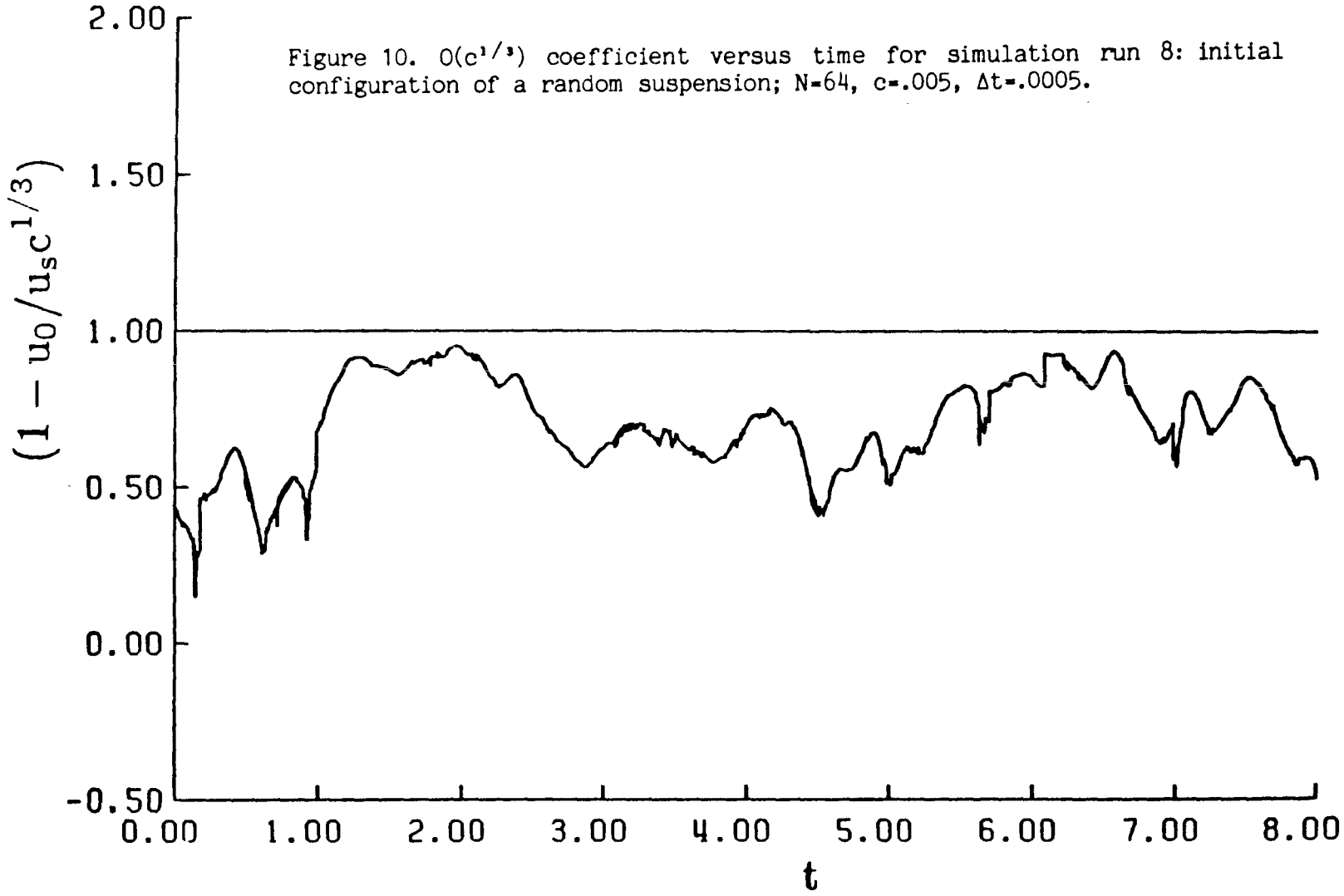


Figure 10. $O(c^{1/3})$ coefficient versus time for simulation run 8: initial configuration of a random suspension; N=64, c=.005, $\Delta t$=.0005.

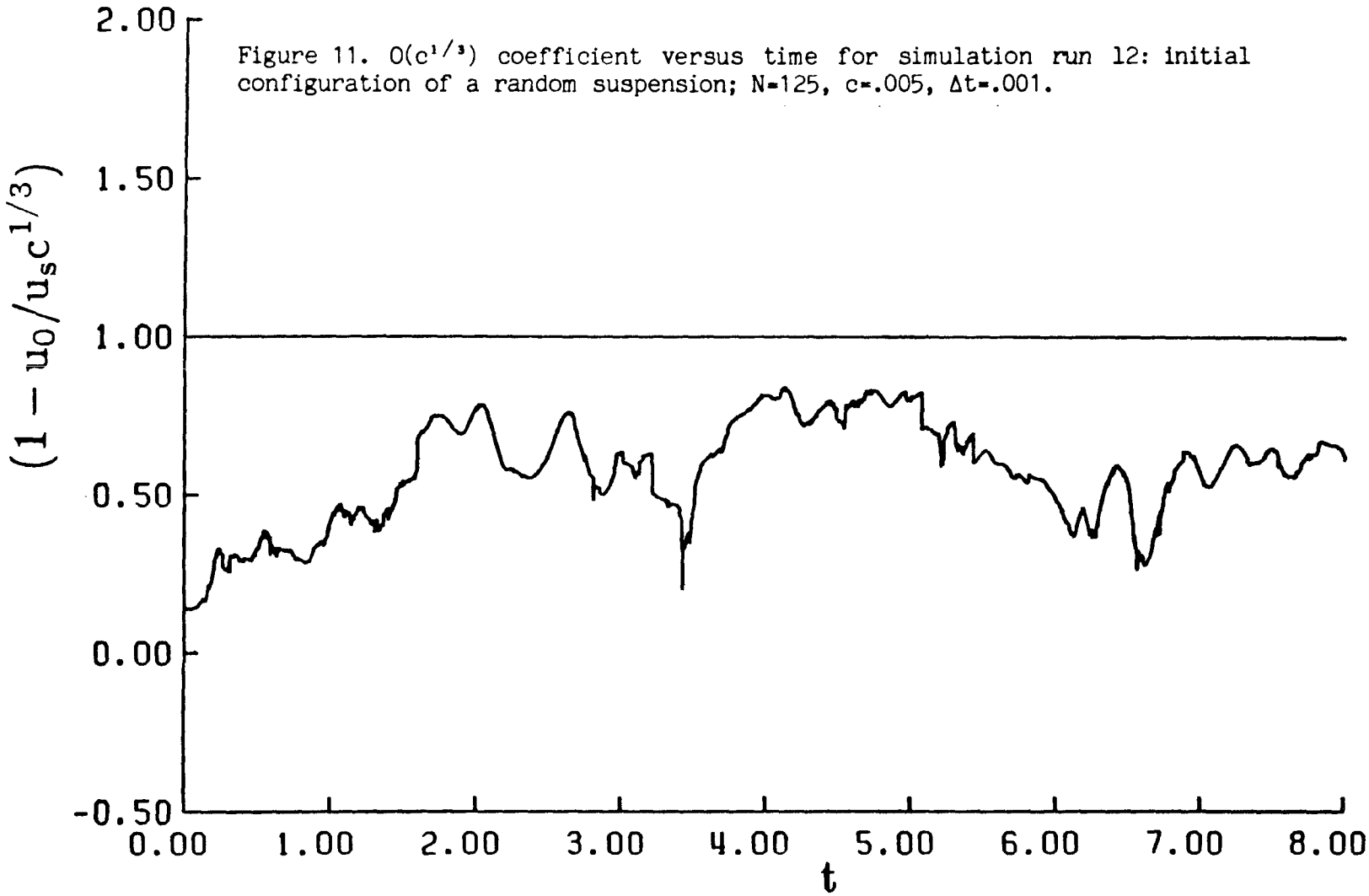


Figure 11. $O(c^{1/3})$ coefficient versus time for simulation run 12: initial configuration of a random suspension; N=125, c=.005, $\Delta t$=.001.

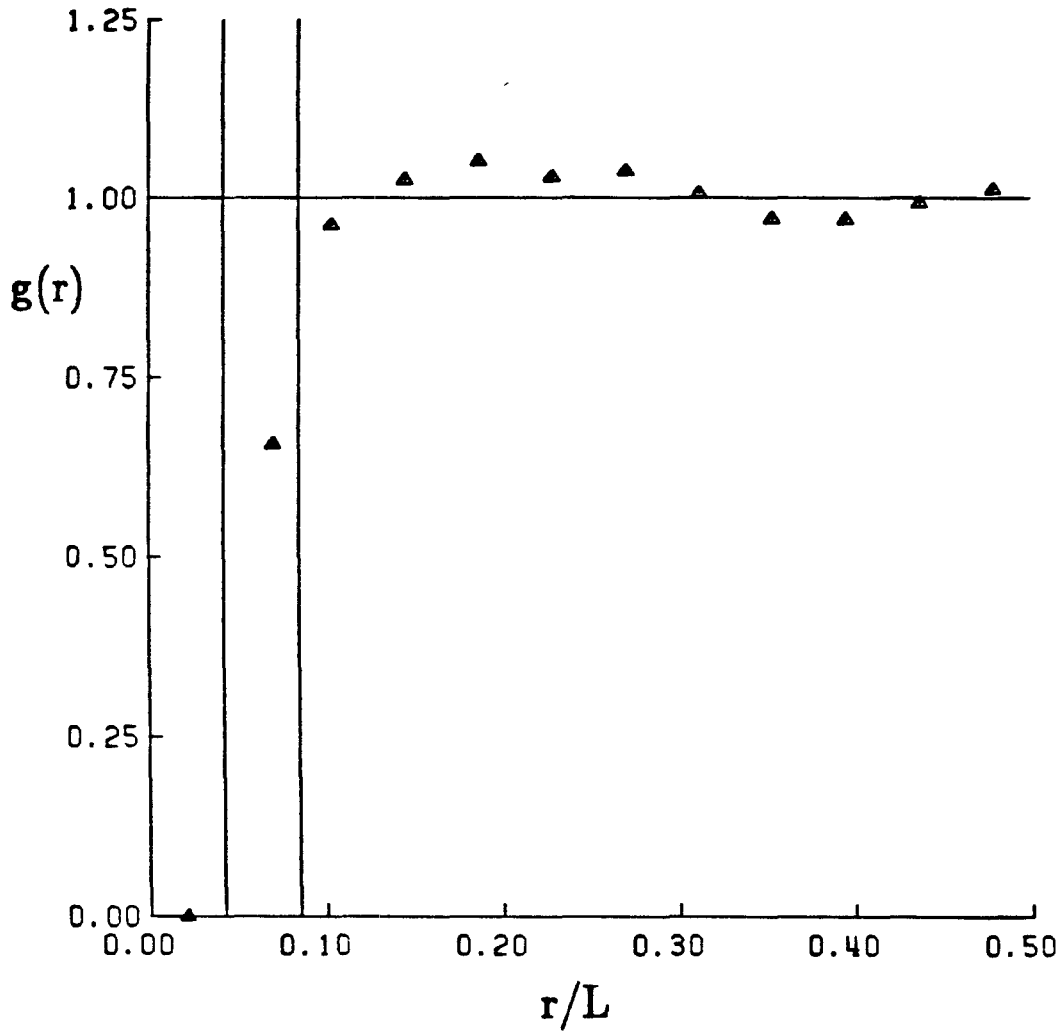


Figure 12. Pair-probability function averaged from 0 to 1.2 for simulation run 12: initial configuration of a random suspension; N=125, c=.005, $\Delta t$=.001.

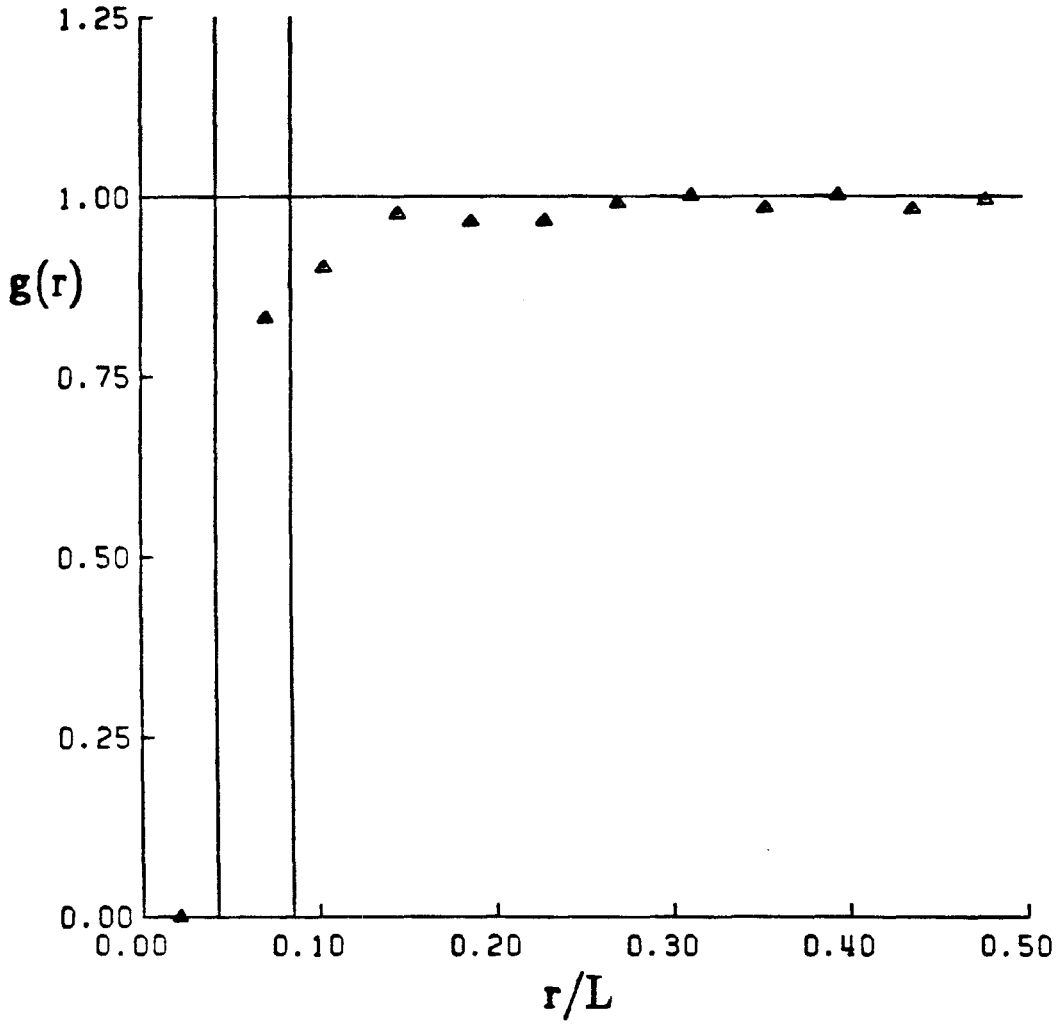


Figure 13. Pair-probability function averaged from 1.6 to 8.0 for simulation run 12.

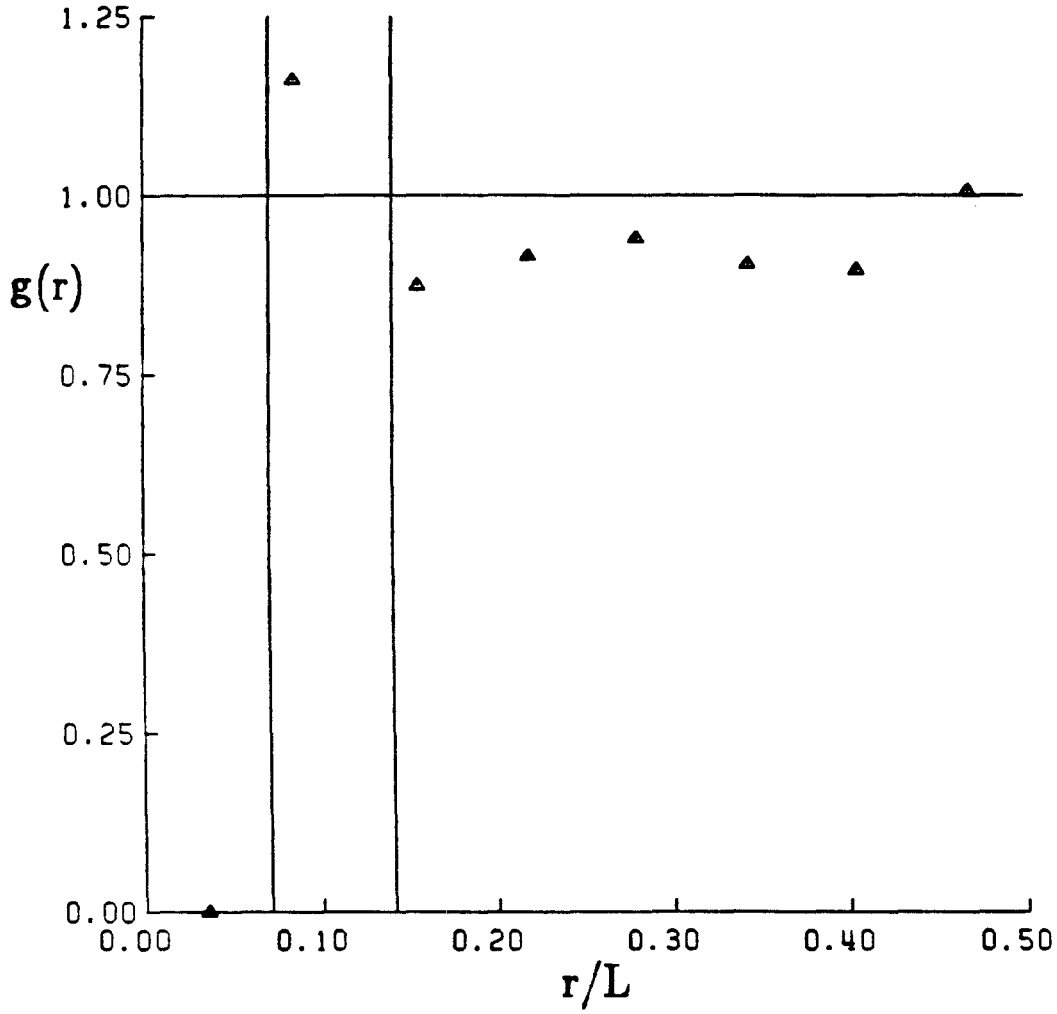


Figure 14. Pair-probability function averaged from t=0.0 to 8.0 for simulation run 13: initial configuration of a random suspension; N=27, c=.005, Δt=.001.

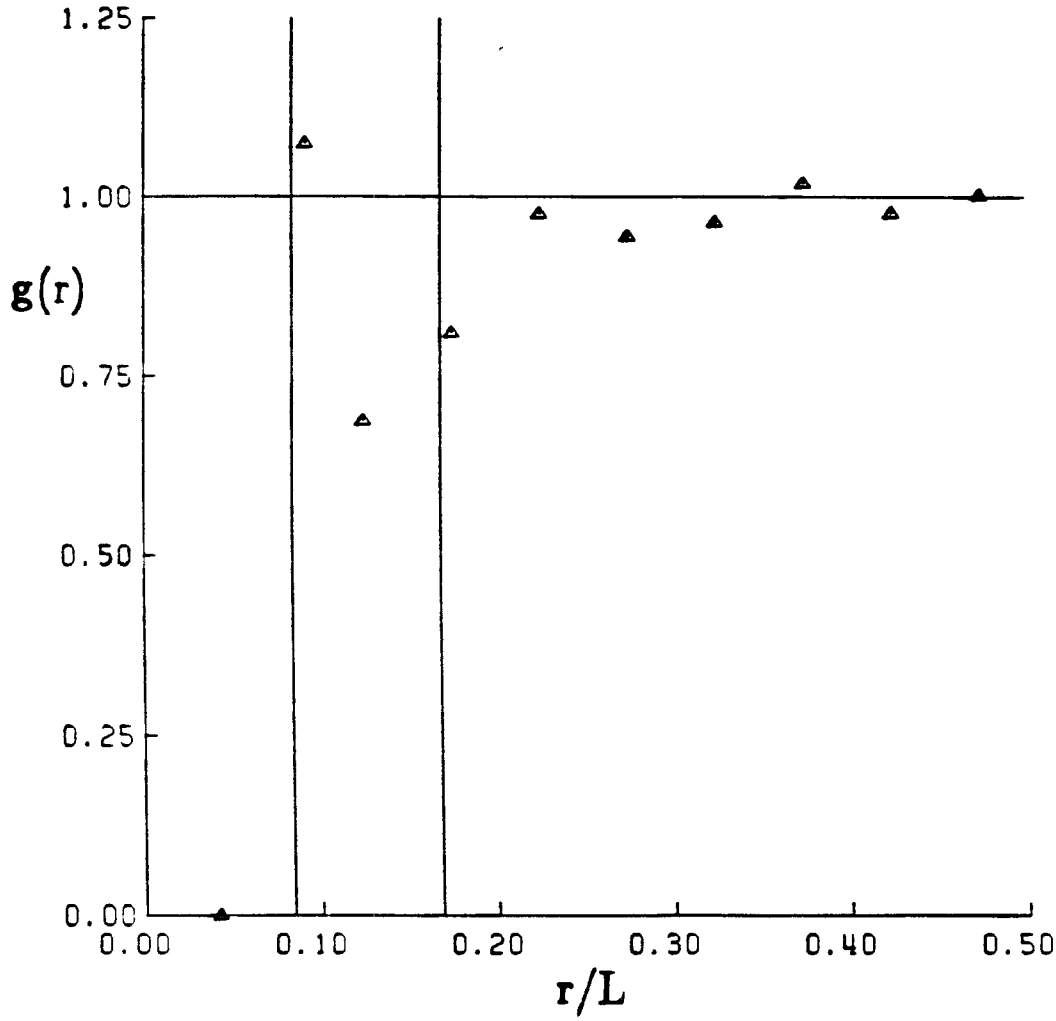


Figure 15. Pair-probability function averaged from t=1.2 to t=3.6 for simulation run 3: initial configuration of a randomized simple cubic array; N=64, c=.02, $\Delta t$=.001.

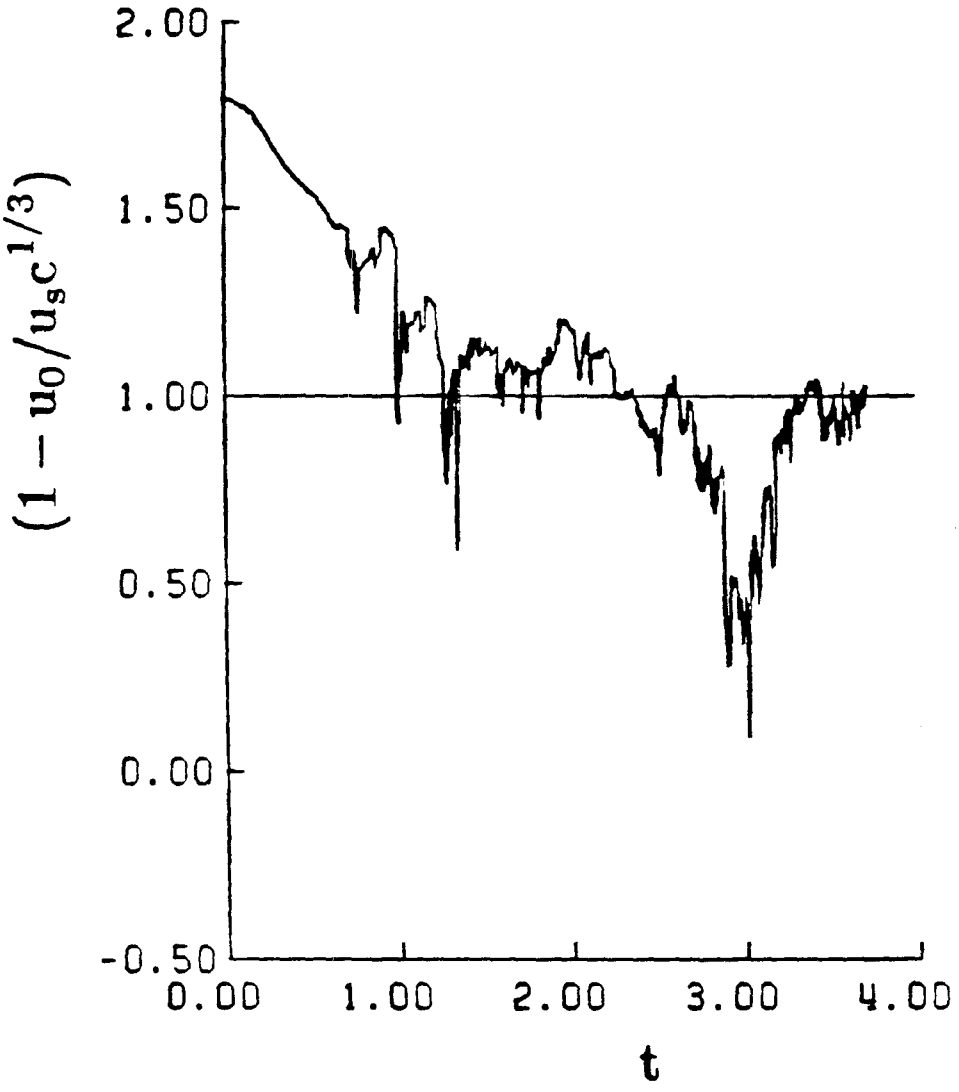


Figure 16. $O(c^{1/3})$ coefficient versus time for simulation run 3: initial configuration of a randomized simple cubic array; N=64, c=.02, $\Delta t$=.001.

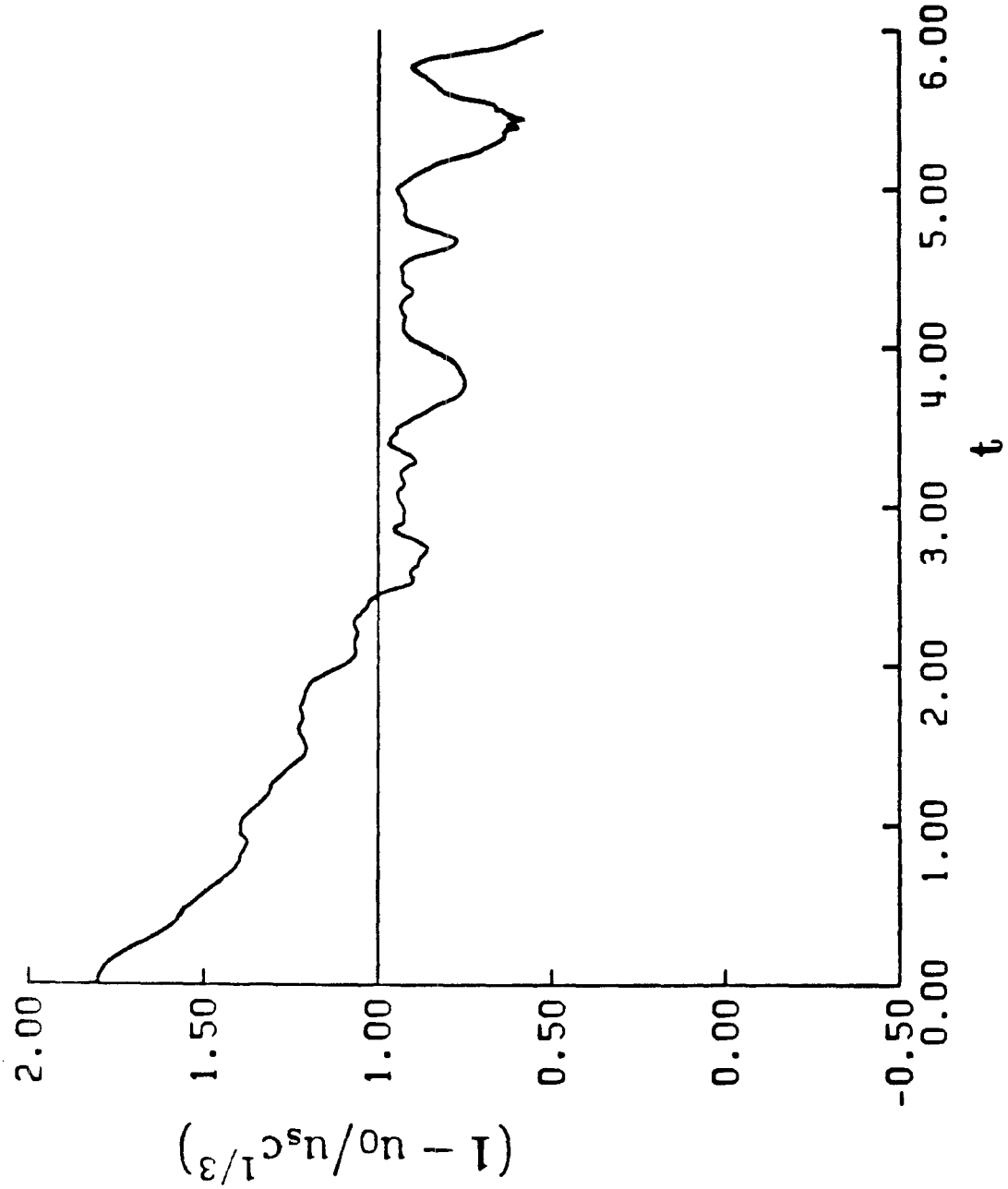


Figure 17. $O(c^{1/3})$ coefficient versus time for simulation run 2: initial configuration of a randomized simple cubic array; N=64, c=.001, $\Delta t$=.0005.

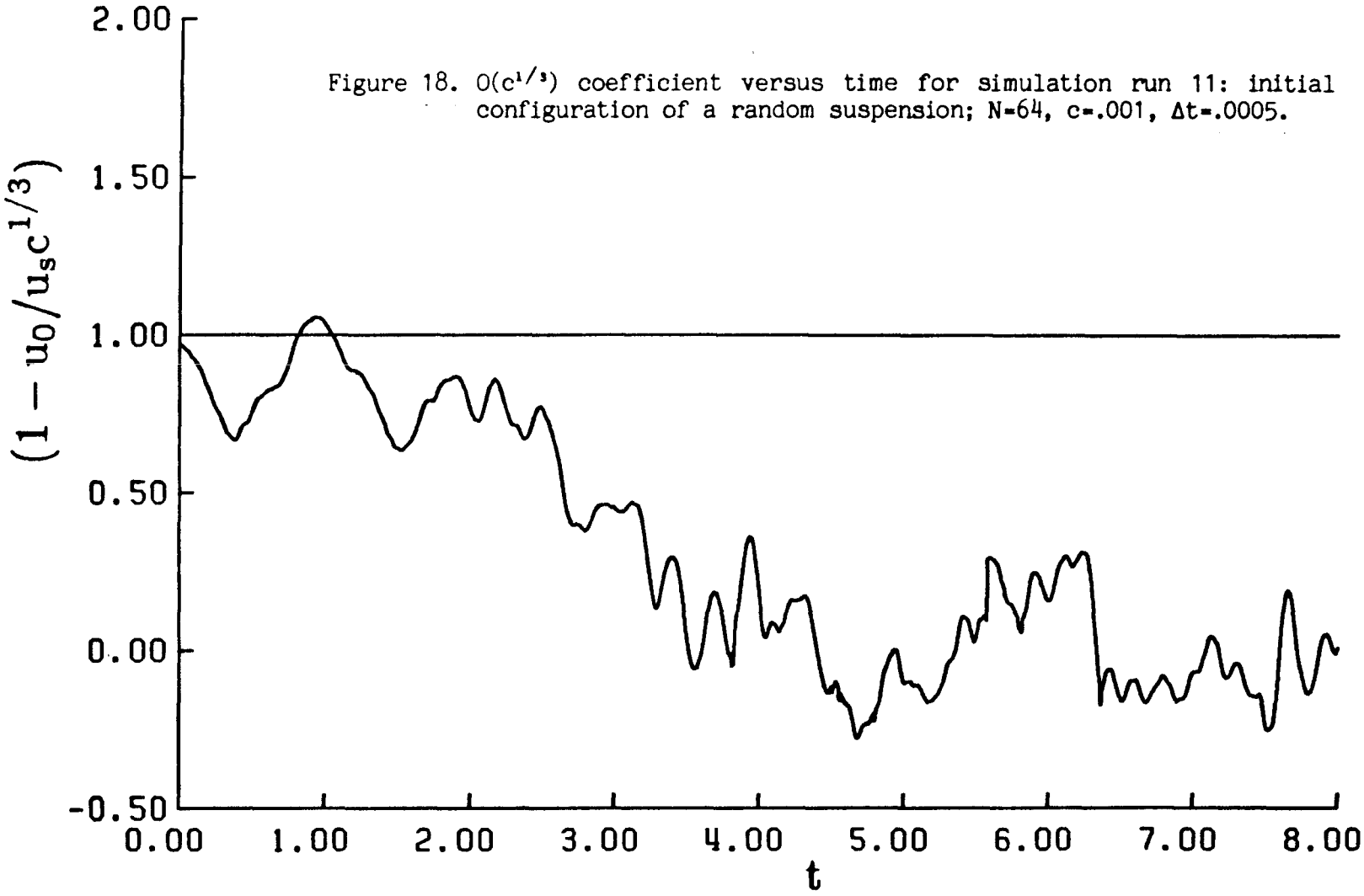


Figure 18. $O(c^{1/3})$ coefficient versus time for simulation run 11: initial configuration of a random suspension; N=64, c=.001, $\Delta t$=.0005.

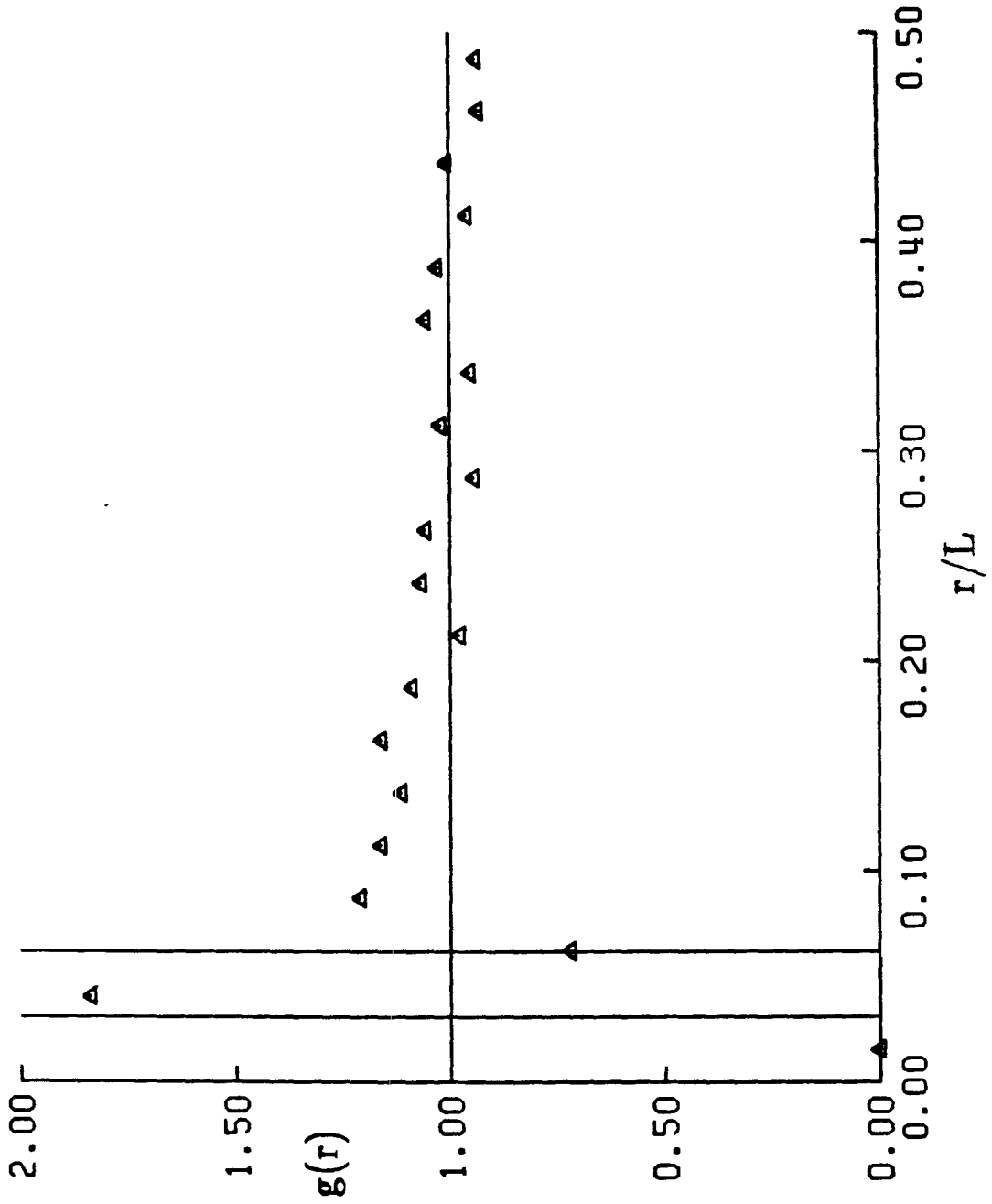


Figure 19. Pair-probability function averaged from t=3.6 to 8.0 for simulation run 11: initial configuration of a random suspension; N=64, c=.001, $\Delta t$=.0005.

Figure 20. $u_o/u_s$ versus c for various theoretical and experimental results: a - correlation of Barnea and Mizrahi (1973) (equation 6), b - first three terms of Barnea and Mizrahi's correlation (equation 7), c - first two terms of theoretical result for simple cubic array (equation 3), d - theoretical result of Batchelor (1972) for random suspensions (equation 4), e - two-term result of our simulation (equation 16). The squares indicate the settling velocity determined from our simulation at various concentrations.

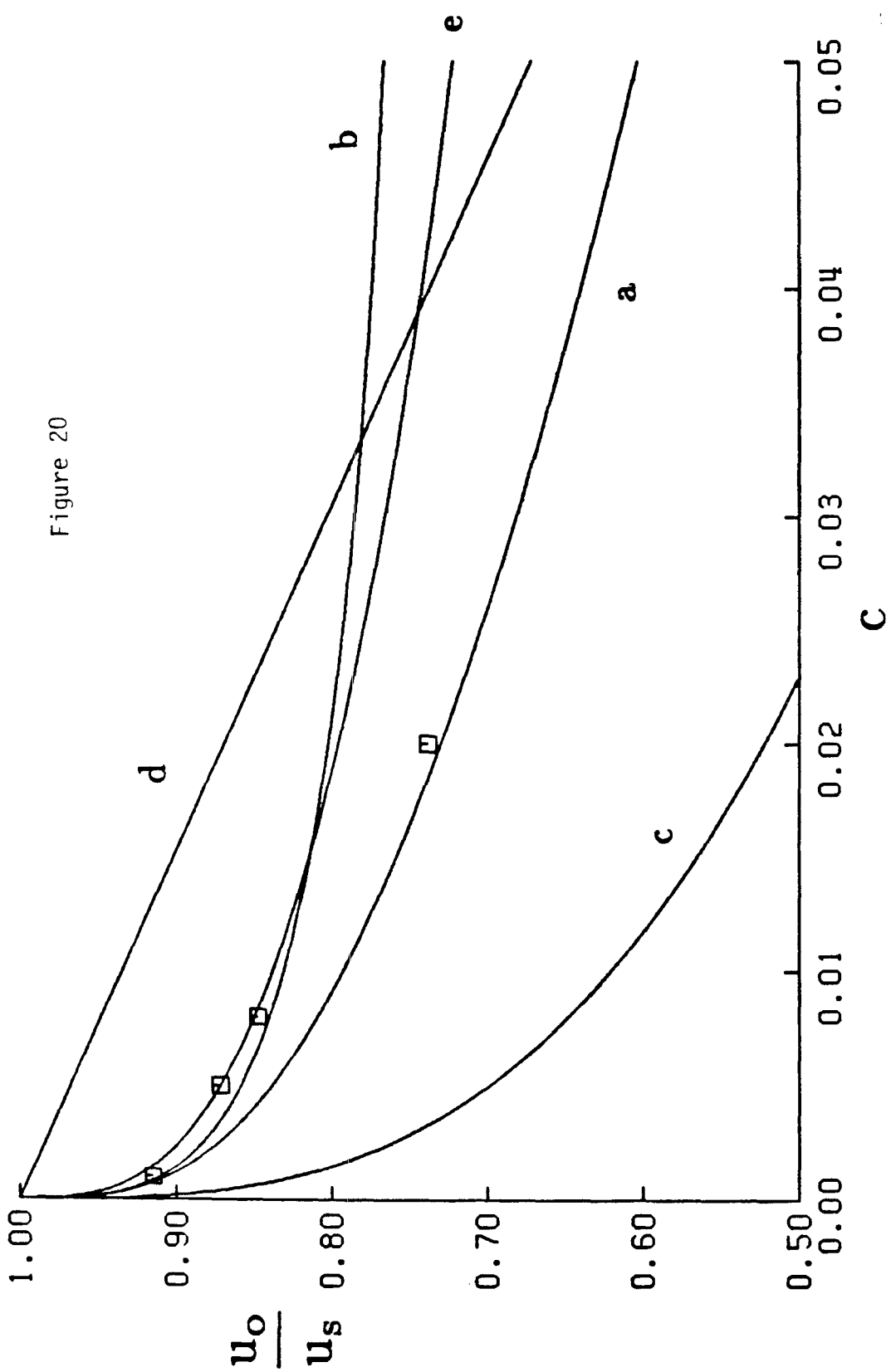
1.00
0.90
0.80
0.70
0.60
0.50
$\frac{u_o}{u_s}$
0.00
0.01
0.02
0.03
0.04
0.05
c
a
b
c
d
e

Figure 20

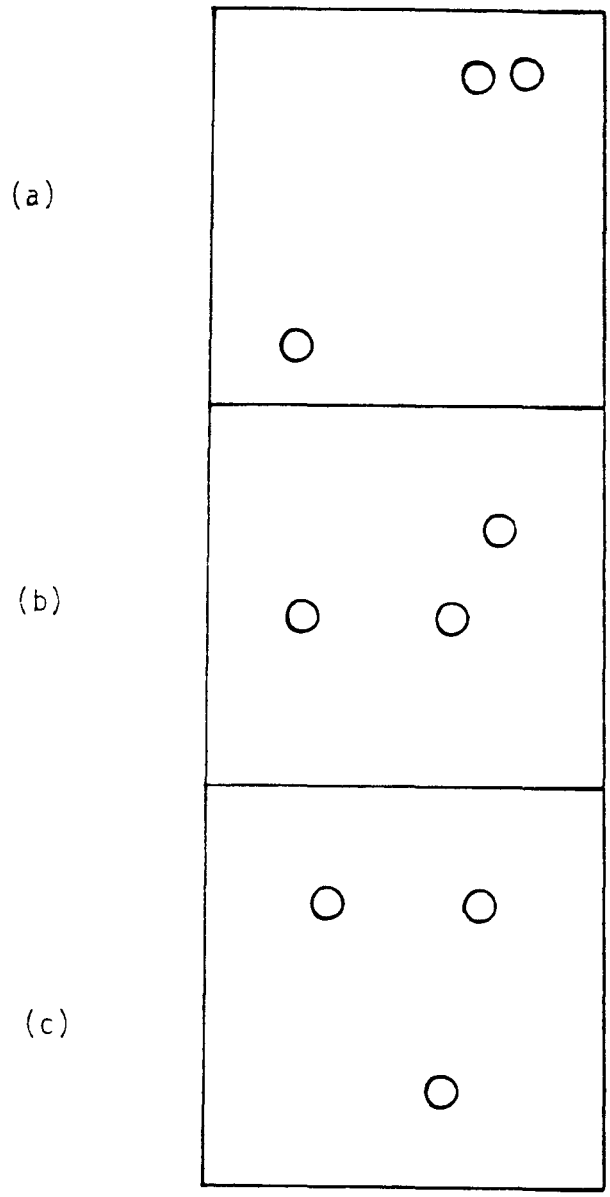


Figure 21. Illustration of the breakup of a close pair.

# CHAPTER II

A Method for the Simulation of Sedimenting Suspensions

(Chapter II consists of a paper

by Edward D. Lynch and Eric Herbolzheimer)

# A Method for the Simulation of Sedimenting Suspensions

Edward D. Lynch and Eric Herbolzheimer
California Institute of Technology
Pasadena, California 91125

## Abstract

This paper presents one method for implementing a molecular-dynamics-type simulation for a three-dimensional, sedimenting suspension. Although we are primarily interested in applying this method to the calculation of the average sedimentation velocity in dilute, quiescent suspensions (see Lynch and Herbolzheimer (1985)), the method should have application in other physical situations. The simulation follows the trajectories of a sub-ensemble (27 to 125 identical spheres inside a cube) of the suspension by imposing periodic boundary conditions at the sides of the cube. The velocity of each of the particles at each time step is decomposed into contributions due to interactions with particles far from the specified particle, to interactions with particles close to the specified particle, to interactions with particles outside the cube, and to the pure-fluid return flow. This procedure both preserves the lubrication forces which restrain particles from overlapping and calculates accurately the relative velocities between N well-separated spheres settling under low-Reynolds-number conditions. Trajectories for three interacting particles computed using this method agree remarkably well with those computed by Ganatos, Pfeffer, and Weinbaum (1978) using a collocation technique.

## 1. Introduction

Although the properties of dilute suspensions have been studied for nearly a hundred years, only recently have systematic methods been developed for treating the particle interaction effects which are important in more concentrated systems. To date, these hydrodynamic particle interactions have been incorporated into the calculation of constitutive relations for suspensions by one of four methods: cell models, regular arrays, ensemble averaging, or multipole expansions (see the discussion in Lynch and Herbolzheimer (1985)). All of these methods except ensemble averaging share one common feature: they require a priori knowledge of how the particles are arranged on the microscale. Of course, the particles in a suspension are free to move in response to the forces applied on them by the fluid, and since their relative positions can have important effects on the suspension properties, determining the microscale particle distribution is an important part of the calculation of any suspension property. In the ensemble-averaging approach, the relative particle positions are determined as part of the calculation, but with the restriction of considering the interaction of only a pair of particles in the suspension. Although this technique is adequate for calculating the stress in a dilute suspension undergoing pure straining motion, the limitation of considering only pair interactions leads to indeterminacies in the particle distributions for other shear flows and for the important problem of calculating the average sedimentation velocity of a monodisperse suspension of spheres. In this paper we describe a method which accounts for multiparticle hydrodynamic interactions in determining the motion and the positions of the particles. In particular, the pair-probability function $P(\underline{r})$

(i.e., the probability of a particle being at position $\underline{x}_o + \underline{r}$ given a particle at position $\underline{x}_o$) can be determined as part of the calculation even in the case of sedimentation.

The procedure explained in this paper involves simulating the behavior of a sub-ensemble of the sedimenting suspension in a manner similar to that used in molecular dynamics to study the macroscopic properties and pair-probability functions of dense gases and liquids. Despite their extensive use in molecular dynamics, these type of simulations have received rather limited use in studying the interaction between the hydrodynamic and nonhydrodynamic forces present in suspensions. Several authors (cf. Ermak and McCammon 1978; Bacon, et al. 1983; and Dickinson and Parker 1984) have employed Brownian-dynamics simulations which include the effects of hydrodynamic interactions to study the behavior of close pairs and triples of particles in colloidal suspensions. Although the Brownian-dynamics algorithm described by Ermak and McCammon has some similarities to the method presented here and although these references give some insight into how pairs and triples behave under the influence of Brownian motion, DLVO-type colloidal forces, and two-particle and three-particle hydrodynamic interactions, they do not treat the multiparticle hydrodynamic interactions important in suspensions. In their study of coagulation, Valioulis, List, and Pearson (Valioulis, List, and Pearson 1984; Pearson, Valioulis, and List 1984) simulated the behavior of many particles moving under the effects of Brownian motion, shear, Van der Waals forces, and hydrodynamic interactions. However, in treating the hydrodynamic interactions, they only considered at most two-particle interactions. The only previous molecular-dynamics-type simulation which treats the effects of multiparticle interactions is the work of Bossis and Brady (Bossis and Brady 1985; Brady and

Bossis 1984). They investigated the effects of multiparticle hydrodynamic forces, shearing forces, and DLVO-type colloidal forces on a suspension in a sheared monolayer by approximating the multiparticle hydrodynamic interactions using the assumption of pairwise additivity of either the velocities of the particles or the hydrodynamic forces on the particles.

In this paper we propose a simulation procedure which calculates the hydrodynamic interactions using a method similar to pairwise additivity of the velocities for particles which are well-spaced from each other and using pairwise additivity of the forces for particles which are close together. This hybrid method both preserves the important lubrication forces between close pairs of particles and calculates the velocities of the particles which are far from each other in a manner which agrees with exact asymptotic results for the problem of N particles settling in a quiescent fluid. The other important difference between this and previous work is that we are mainly interested in the interplay between these interactions and gravity, not DLVO-type forces or shearing forces (although the method is explained in a way which makes obvious how other types of forces could be included).

## 2. General Method

In the next three sections, we explain a general procedure for calculating the macroscopic properties of a suspension via a molecular-dynamics-type simulation; parenthetically the special features of the calculation particular to our application are noted. In order to reduce the number of variable parameters, we have assumed the particles in the simulation are identical spheres of radius a and density $\rho_s$, but the extension of the method to other cases should be obvious.

Although a real suspension has an extremely large number (typically millions) of particles, for reasons of computing speed, memory, and cost a molecular-dynamics-type simulation is capable of handling at most hundreds of particles. Hence, we assume the suspension can be replaced by a N-particle sub-ensemble, contained within a cube with side of length L, with periodic boundary conditions. Periodic boundary conditions mean first that the cube containing the N particles is repeated periodically throughout space. In this implementation we assume each of the N particles is affected by only the closest image of each of the other particles. Periodic boundary conditions also mean in our application that wall effects are assumed unimportant, that the actual side walls of the container are moved to infinity, and that particles leaving through one side of the cube reenter from the point directly opposite on the other side of the cube. The assumption of periodic boundary conditions is justifiable because we expect no long-range structure or long-range forces to be present in a sedimenting suspension. (We consider this point in more detail later.)

Hence, to begin the simulation, N particles are placed in a cube in any desired configuration. We are interested in two types of initial conditions. First, to simulate the behavior of suspensions in which the particles are initially well-spaced, the particles are allowed to take random perturbations within a specified distance about the lattice points of a cubic array. In other situations where determining the behavior of suspensions with initial close pairs is important, the initial configuration of particles is prescribed by placing the particles randomly within the cube with the restriction that they may not overlap.

From the specified initial configuration, we determine the trajectories of the particles by numerically integrating the velocities of the particles forward in time. The evolution of the suspension is observed by calculating the pair-probability function and the average settling velocity as functions of time. The pair-probability function is computed by counting the number of particles in spherical shells centered on each particle, dividing by the volume of the shell, and then averaging this result over the N particles. This volume-averaged pair-probability function is then time averaged over time steps 400 time steps apart once the suspension reaches a long-time asymptotic state from a statistical standpoint. The average settling velocity is similarly determined by first averaging the settling velocities of the N particles and then time averaging this result once the suspension reaches a long-time asymptotic configuration.

To explain the method used for determining the velocities of the N particles, let us focus on our application, the sedimentation of a semi-dilute suspension of identical spheres under conditions of small particle Reynolds number. First, since the suspension is dilute, most of the particles are

separated from each other by a distance large compared with the particle radius, a. Specifically, by definition of the volume fraction we have

$$c = \frac{N}{L^3} \frac{4}{3} \pi a^3. \tag{1}$$

Hence, the average particle spacing (which is proportional to $L/N^{1/3}$) divided by a is proportional to $c^{-1/3}$. For the moment, let us assume that the particle we are calculating the velocity of (particle $\alpha$, say) does not have any close neighbors (i.e., all of its neighbors are a distance of $O(ac^{-1/3})$ away).

Now, the velocity field induced at $\alpha$ can be decomposed into three distinct parts. First, a portion of the velocity of particle $\alpha$ is the velocity with which $\alpha$ would move in the presence of the other N-1 particles in the cube (or their closest image). Since the Reynolds number is assumed to be small, we may approximate this velocity to O(c) as the sum of three contributions. The first term is the Stokes settling velocity of particle $\alpha$

$$\underline{u}_S = \frac{2}{9} a^2(\rho_S - \rho) g \, \underline{e}/\mu, \tag{2}$$

and is the velocity with which $\alpha$ would settle in an infinite fluid at rest far from $\alpha$. (Here g is the gravitational acceleration, $\underline{e}$ is the unit vector in the direction of gravity, and $\rho$, $\mu$, and $\nu$ are the fluid density, viscosity and kinematic viscosity, respectively.) The second contribution is the fluid velocity induced at sphere $\alpha$ by the other N-1 spheres and consists, to O(c), of a Stokeslet and a potential-dipole singularity at the centers of each of the N-1 other particles. The final term is the Faxen's law modification of the

Stokeslet velocity field at particle $\alpha$ to account for the presence of $\alpha$. The next higher-order term comes from the first reflection of the Stokeslet velocity field of each of the N particles off of the N-1 particles other than $\alpha$ and is $O(c^{4/3})$. Since this term is a three-body interaction and evaluating it requires $O(N^2)$ operations, whereas the first three terms are one-body and two-body interactions and require only $O(N)$ operations to evaluate them, for computational efficiency we restrict our expression for the velocity $\underset{\sim}{V}'_\alpha$ particle $\alpha$ attains due to direct particle interactions to the first three terms. After combining these three terms together, we find

$$\underset{\sim}{V}'_\alpha = u_s\left[\underset{\sim}{e} + \frac{3}{4}\sum_{\beta=1,\alpha\neq\beta}^{N}\left(\frac{a}{r_{\alpha\beta}}\right)\left(\underset{\sim}{e} + \frac{(\underset{\sim}{e}\cdot\underset{\sim}{r}_{\alpha\beta})}{r_{\alpha\beta}^2}\,\underset{\sim}{r}_{\alpha\beta}\right) - \frac{3}{2}\sum_{\beta=1,\alpha\neq\beta}^{N}\left(\frac{a}{r_{\alpha\beta}}\right)^3\left[\frac{(\underset{\sim}{e}\cdot\underset{\sim}{r}_{\alpha\beta})}{r_{\alpha\beta}^2}\,\underset{\sim}{r}_{\alpha\beta} - \frac{1}{3}\,\underset{\sim}{e}\right] + O(c^{4/3})\right] \tag{3}$$

in which $\underset{\sim}{r}_{\alpha\beta}$ is the vector from the position of particle $\beta$ to the position of particle $\alpha$, and $r_{\alpha\beta}$ is the magnitude of $\underset{\sim}{r}_{\alpha\beta}$.

This induced velocity cannot be the only contribution to the velocity of particle $\alpha$, however, since the particle interactions in zero-Reynolds-number flow decay so slowly (like $\frac{1}{r_{\alpha\beta}}$ for two particles $\alpha$ and $\beta$) as the particles get far apart that increasing the number of particles in the simulation would increase without bound the result for the velocity of particle $\alpha$. The problem is that this analysis has not included some of the essential physics. When particles settle downward, they carry their own volume and some volume of fluid with them. Hence to preserve overall continuity, a backflow of fluid

arises and must be accounted for in the simulation. This backflow can be computed with error O(c) by "smearing-out" the sum of the point-force interactions over the entire cube (i.e., multiplying the Stokeslet velocity field by the number of particles per unit volume n and integrating this result over the cube) (Saffman 1973). This procedure introduces the same error of O(c) into the velocity of each of the particles; however, for dilute suspensions this term is small compared with the leading term of $O(c^{1/3})$ in the particle interactions. The effect of the backflow due to the particles in the cube is thus

$$-\int_{\text{cube}} \underline{e} \cdot \left[\frac{3}{4} u_S \left(\frac{a}{r}\right)\left(\underline{\underline{I}} + \frac{\underline{r}\underline{r}}{r^2}\right)n\right] dV = -1.4765\, u_S c^{1/3} N^{2/3} \underline{e}. \qquad (4)$$

The final influence on the velocity of a particle $\alpha$ without close neighbors is the effect of particles outside the cube. If no long-range order exists in the suspension, far from particle $\alpha$ the particle positions become random so the pair-probability function equals n independent of radius and angle. Hence, because the distribution of particles outside the cube is unknown in our simulation, it is replaced by a random distribution. To determine the effect of this approximation on the velocity of particle $\alpha$, we observe that with error O(c), the velocity of particle $\alpha$ is given by the sum of the point-force interactions due to the other particles in the suspension minus the backflow:

$$\underline{V}_\alpha = \frac{3}{4} a u_s \underline{\underline{e}} \cdot \int \left( \sum_{\beta, \alpha \neq \beta} \delta(\underline{r}_\alpha - \underline{r}_\beta) - n \right) \left[ \frac{1}{r_{\alpha\beta}} \left( \underline{\underline{I}} + \frac{\underline{r}_{\alpha\beta} \underline{r}_{\alpha\beta}}{r_{\alpha\beta}^2} \right) \right] dV \qquad (5)$$

in which the integral is taken over the entire suspension volume. Assuming that the distribution of particles is random far from particle $\alpha$ is equivalent to replacing the actual distribution of particles outside the cube (represented in equation 5 by the sum of delta functions at the centers of all the other particles) by its ensemble-averaged value, n. Thus, with an error of O(c), this replacement eliminates the effects of the particles outside the cube, for their contribution to the backflow exactly cancels their direct influence as point forces (Saffman 1973).

Because the particle interactions in zero-Reynolds-number flow decay so slowly, any deviation in the actual distribution of particles outside the cube from a random distribution can cause substantial changes in the velocities of the particles in the cube; therefore, for our assumption to be valid, very little structure should be present in the pair-probability function at a distance of L/2 from a given test particle. Certainly this premise is true if the edge of the cube is very far from the test particle (i.e., if N is very large). However, if N is small, then the assumption of a random distribution may only be approximately correct, and the effect of the particles outside the cube on the macroscopic properties cannot be proved to be negligible. Nevertheless, for simulation runs with numbers of particles ranging from 27 to 125, the pair-probability function far from a test particle seemed to converge to the constant n as the number of particles was increased. Moreover, the long-time asymptotic value for the average settling velocity for the particles

in the cube remained relatively constant over this range of N (Lynch and Herbolzheimer 1985); thus, the assumption of a random suspension outside the cube appears to be a reasonable one.

To determine the dimensionless velocity of a settling sphere $\alpha$ without close neighbors, we combine the velocity fields induced by the direct particle interactions and the backflow, and then nondimensionalize lengths with respect to the length of the cube and time with respect to $\tau$, a time comparable to that needed for a particle to migrate an average particle spacing:

$$\tau = \frac{4}{3}\left(\frac{4}{3}\pi\right)^{1/3} c^{-1/3} N^{-1/3} \frac{L}{u_s}. \tag{6}$$

Finally, we find that the dimensionless velocity of particle $\alpha$ is given by

$$N^{2/3}\frac{d}{dt}\left[\tilde{\underline{r}}_\alpha - \frac{u_s\tau}{L}\, t\underline{e}\right] = \sum_{\beta=1,\alpha\neq\beta}^{N}\left[\left(1 + \frac{2}{3\tilde{r}_{\alpha\beta}^2}\left(\frac{a}{L}\right)^2\right)\frac{\underline{e}}{\tilde{r}_{\alpha\beta}} + \left(1 - \frac{2}{\tilde{r}_{\alpha\beta}^2}\left(\frac{a}{L}\right)^2\right)\frac{(\underline{e}\cdot\tilde{\underline{r}}_{\alpha\beta})\tilde{\underline{r}}_{\alpha\beta}}{\tilde{r}_{\alpha\beta}^3}\right] - 3.17343\, N\underline{e} + O(c) \tag{7}$$

in which $\tilde{\underline{r}}_\alpha$ is the dimensionless position of particle $\alpha$, $\tilde{\underline{r}}_{\alpha\beta}$ is $\tilde{\underline{r}}_\alpha - \tilde{\underline{r}}_\beta$, and $\left(\frac{a}{L}\right) = \left(\frac{3c}{4\pi N}\right)^{1/3}$.

## 3. Refinement of Velocity Calculation

Equation 7 is accurate only to $O(c^{2/3})$ because of the method of calculating the backflow; however, in order to increase the accuracy of the particle trajectories, we may wish to refine the calculation of the relative velocities between the particles, which are, of course, independent of the backflow since this contribution is the same for all the particles. The principal problem with the method presented in section 2 is that the approximations made in calculating the particle interaction terms breakdown when particle $\alpha$ has one or more close neighbors. For example, if the distance between particles $\alpha$ and $\gamma$ becomes $O(a)$, $r_{\alpha\gamma}/a$ becomes $O(1)$ instead of $O(c^{-1/3})$ as was assumed above. Hence, the higher-order reflection terms between $\alpha$ and $\gamma$ no longer become negligible as the concentration becomes small. This difficulty does not arise with the remaining particles, which are well-separated from $\alpha$, so we seek to develop a technique for incorporating the influence of close particles within the context of the scheme outlined in section 2. This modification is crucial to the success of the simulation since these higher-order interactions and the corresponding lubrication forces for very closely spaced particles are responsible for preventing the particles from overlapping each other. Hence, an accurate representation of the dynamics of close pairs of particles is needed to obtain a reasonable representation of the pair-probability distribution.

To start, let us reconsider in a more systematic and more general way the problem of determining the effect of the direct particle interactions on particle $\alpha$. The essence of this problem is to calculate the motion of N particles moving in an incompressible, Newtonian fluid given some known external forces on the particles.

This N-particle problem may be described in terms of the multiparticle resistance tensor formalism explained by Brenner and O'Neill (1972). To use this formalism, we need to make some assumptions. We assume that the fluid is being sheared at a uniform, steady rate and that the motion of the particles is pseudosteady. Assuming the appropriate particle Reynolds number (viz., $\frac{au_s}{\nu}$ in our application) is much less than unity and that the ratio of the densities of the particles and the fluid is O(1) allows us to neglect particle inertial effects. Finally, since in suspensions of interest to us the relative velocity due to multiparticle hydrodynamic interactions, $V_R$, is much greater than the Brownian-motion diffusion coefficient divided by the particle radius, $\frac{D}{a}$, (i.e., the Brownian-motion Peclet number $Pe = \frac{V_R a}{D}$ is much greater than unity (Lynch and Herbolzheimer 1985)), we assume Brownian-motion effects are negligible.

Under these assumptions the forces and torques on the particles are linearly related to the translational and rotational velocities of the particles. Hence we can write 6N equations balancing the forces and torques on each of the particles (see Brenner and O'Neill (1972)):

$$-\underline{F} = \underline{\underline{R}} \cdot \underline{U} + \underline{\underline{\phi}} : \underline{\underline{E}} \tag{8}$$

in which $\underline{F}$ is the force-torque vector, a 6N-component vector containing the sum of the external forces and the sum of the external torques on each of the N particles; $\underline{\underline{R}}$ is the N-particle grand resistance tensor, a 6Nx6N-component tensor describing the translational and rotational hydrodynamic resistance forces on the particles; $\underline{U}$ is the velocity-spin vector, a 6N-component vector containing the difference between the particle velocities and the undisturbed fluid velocity at each of the particles and the difference between the particle rotational velocities and one-half the undisturbed fluid vorticity at each of the particles; $\underline{\underline{\underline{\phi}}}$ is the shear resistance triadic, a 6Nx3x3 third-order tensor describing the shear resistance forces on the particles; and $\underline{\underline{E}}$ is the local fluid rate-of-strain tensor, $\frac{1}{2}(\nabla\underline{u} + \nabla\underline{u}^T)$, where $\underline{u}$ is the undisturbed fluid velocity in the system of N particles (i.e., the fluid velocity in the absence of the N particles). Alternatively, these 6N equations can be solved for the velocity-spin vector to yield

$$-\underline{\underline{R}}^{-1} \cdot \underline{F} = \underline{U} + \underline{\underline{R}}^{-1} \cdot \underline{\underline{\underline{\phi}}} : \underline{\underline{E}} \tag{9}$$

where $\underline{\underline{R}}^{-1}$ is the N-particle grand mobility tensor and is the inverse of the N-particle grand resistance tensor.

Calculating the velocities of the particles (i.e., the velocity-spin vector) given the external forces on the particles (i.e., the force-torque vector) requires knowing either the grand resistance tensor $\underline{\underline{R}}$ or the grand mobility tensor $\underline{\underline{R}}^{-1}$ and also the shear resistance forces $\underline{\underline{\underline{\phi}}} : \underline{\underline{E}}$. One possibility for determining these tensors is to assume that the shear resistance triadic and either the grand resistance or the grand mobility tensor

are pairwise-additive. Bossis and Brady (1985) explored both of these possibilities for fairly concentrated suspensions and found that assuming the hydrodynamic forces and torques to be pairwise-additive was the best approach because it preserved the lubrication forces between the particles and restrained the particles from overlapping. However, for fairly dilute suspensions where the particles are widely separated, this method has two serious disadvantages. It does not accurately predict the particle velocities because for a collection of particles all separated by distances of $O(ac^{-1/3})$, whereas the velocities of the particles are pairwise-additive with error $O(c^{4/3})$, the farfield expansion for the hydrodynamic forces upon the particles contains terms at $O(c^{2/3})$ which are three-body interactions and are not pairwise-additive (Mazur 1982). Furthermore, using the force equations is computationally inefficient because it unnecessarily requires inverting very large matrices in order to determine the velocities of the particles.

Therefore, we take a hybrid approach, in which the velocity of particle $\alpha$ is calculated differently depending upon whether zero, one, or more than one particle is within a few particle radii of $\alpha$. If $\alpha$ has no close neighbors, then we may find its velocity from the farfield solution for the N-particle mobility tensors and the force-torque vector for the N-particle system. For the case of N spheres, Mazur and Van Saarloos have calculated the grand mobility tensor when no bounding walls are present (Mazur and Van Saarloos 1982) and when a bounding wall is present (Beenakker, Van Saarloos, and Mazur 1984) and have shown how to calculate the shear resistance triadic when no bounding walls are present (Mazur and Van Saarloos 1982). These equations simplify considerably in our application since no bounding walls or external flow field are present, the only force acting on the particles is gravity, no

body torques act on the particles, and the particles are all identical spheres; therefore, the first 3N terms of the force-torque vector consist of N repetitions of $(0, 0, \frac{4}{3}\pi a^3(\rho_s-\rho)g)$ and the remaining terms equal 0, and the N-sphere shear resistance triadic is not needed. By multiplying the appropriate row of the N-sphere grand mobility tensor for an unbounded fluid by the force-torque vector, we find that the velocity of particle $\alpha$ is given, with an error $O(c^{4/3})$, by equation 3, which was previously developed based on physical arguments.

If the test particle $\alpha$ is within a few particle radii of another particle (let us call it $\gamma$), then the farfield solution of Mazur and Van Saarloos does not give an accurate representation of the velocities of particles $\alpha$ and $\gamma$ because of the neglect of higher-order reflections between these two particles. Therefore, when two particles $\alpha$ and $\gamma$ are sufficiently close together (viz., their centers are within 4a in our implementation), we treat them as a pair moving under the prescribed external forces in the velocity field created by the remaining N-2 particles in the cube (or by the nearest image of a particle). (To simplify the discussion at this point, we restrict our attention to the case of identical spheres which are far away from any bounding walls and not situated in any external flow field.)

The hydrodynamic interactions between the particles $\alpha$ and $\gamma$ in the close pair and the remaining particles in the suspension separate physically into several different types. First, we can analyze the effect of $\alpha$ and $\gamma$ upon each other as the problem of two particles moving under prescribed external forces and torques in the flow field (i.e., the undisturbed fluid velocity field minus the undisturbed fluid velocity at the midpoint between $\alpha$ and $\gamma$)

generated by the other N-2 particles. Because the equations of motion at zero Reynolds number are linear, we may decompose this problem into that of two particles moving under imposed external forces and torques in an infinite fluid at rest far from the particles and that of two force-free, torque-free particles moving in the flow field generated by the other N-2 particles. Note that in making this decomposition we have neglected the reflections of the velocity field generated by particles $\alpha$ and $\gamma$ off of the remaining N-2 particles. Since $\alpha$ and $\gamma$ are well-separated from the other particles, this approximation introduces an error of $O(c^{4/3})$ into the velocities of $\alpha$ and $\gamma$.

To calculate the velocities of the two particles moving in an infinite, quiescent fluid, we multiply the two-particle grand mobility tensor by the vector containing the external forces and torques imposed on the particles. Since no body torques act on the particles and gravity is the only external force acting on them, the velocity of both $\alpha$ and $\gamma$ is that attained by two spheres settling in an infinite, quiescent fluid and can be computed by knowing how the velocity of two particles settling parallel to the line joining their centers and the velocity of two particles settling perpendicular to the line joining their centers depend upon the separation distance $r_{\alpha\gamma}$ between the particles. Both of these problems have been solved for almost touching spheres, for spheres very far apart, and for separations in between these two extremes (Wakiya 1967; Goldman, Cox and Brenner 1966; Happel and Brenner 1965; Batchelor 1972; and O'Neill 1969).

The remaining problem of determining the motion of two force-free, torque-free particles immersed in the flow field generated by the remaining N-2 particles simplifies considerably by noting that within an error of $O(c)$ this flow field is a linear shear centered at the midpoint between $\alpha$ and $\gamma$, that

within an additional error of $O(c)$ the rate-of-strain tensor $\tilde{\underline{\underline{E}}}$ and vorticity $\tilde{\underline{\Omega}}$ of this shear at the midpoint may be approximated by their values at particle $\alpha$, and that within an error of $O(c^{4/3})$ $\tilde{\underline{\underline{E}}}$ and $\tilde{\underline{\Omega}}$ can be calculated by treating the N-2 remaining particles as point forces. Recalling that both $\tilde{\underline{\underline{E}}}$ and $\tilde{\underline{\Omega}}$ must be made dimensionless by $\frac{1}{t}$, we find after making these approximations that

$$N^{2/3}\,\tilde{\underline{\underline{E}}} = \sum_{\beta=1,\beta\neq\alpha,\gamma}^{N} \frac{(\underline{e}\cdot\tilde{\underline{r}}_{\alpha\beta})}{\tilde{r}^3_{\alpha\beta}} \left[\underline{\underline{I}} - 3\,\frac{\tilde{\underline{r}}_{\alpha\beta}\tilde{\underline{r}}_{\alpha\beta}}{(\tilde{r}^2_{\alpha\beta})}\right] + O(c^{2/3}) \tag{10}$$

and

$$N^{2/3}\,\tilde{\underline{\Omega}} = \sum_{\beta=1,\beta\neq\alpha,\gamma}^{N} \frac{2}{\tilde{r}^3_{\alpha\beta}}\,(\underline{e}\times\underline{r}_{\alpha\beta}) + O(c^{2/3}). \tag{11}$$

Fortunately, the motion of two force-free, torque-free particles immersed in a linear shear field has been determined by Batchelor and Green (1972). Their result for the relative motion between $\alpha$ and $\gamma$ is comprised of two terms: a term resulting from particle interactions between $\alpha$ and $\gamma$ and a term representing the difference between the undisturbed fluid velocity field created by the N-2 other particles at $\alpha$ and that created at $\gamma$. The term due to particle interactions may be included without modification in calculating the velocities of $\alpha$ and $\gamma$; however, the difference in the fluid velocity field is not included here.

It instead is incorporated into the final influence on the velocities of $\alpha$ and $\gamma$: the effect of the N-2 other particles. With error $O(c^{4/3})$ we may approximate this effect at either of the particles $\alpha$ or $\gamma$ (choose particle $\alpha$, say) as the sum of the undisturbed fluid velocity field at $\alpha$ produced by the

particles other than α and γ and of the Faxen's law correction of this velocity to reflect the finite size of α. In other words, the effect of the remaining N-2 particles is identical to their effect in the case where α had no close neighbors (cf. equation 3), and therefore the velocity induced at particle α by these particles in dimensional form is:

$$\underline{V}_\alpha^n = \left[\frac{3}{4}\sum_{\beta=1,\beta\neq\alpha,\gamma}^{N}\frac{a}{r_{\alpha\beta}}\left(\underline{e}+\frac{(\underline{e}\cdot\underline{r}_{\alpha\beta})}{r_{\alpha\beta}^2}\,r_{\alpha\beta}\right)-\frac{3}{2}\sum_{\beta=1,\beta\neq\alpha,\gamma}^{N}\left(\frac{a}{r_{\alpha\beta}}\right)^3\left[\frac{(\underline{e}\cdot\underline{r}_{\alpha\beta})}{r_{\alpha\beta}^2}\,r_{\alpha\beta}-\frac{1}{3}\,\underline{e}\right]+O(c^{4/3})\right] \tag{12}$$

Because we treat the effect of the particles far away in the same way in both cases, particles α and γ do not suffer a change in velocity when their centers come within 4a.

After combining the results for the settling motion of α and γ with that for the relative motion between α and γ in the created linear flow field and after incorporating the backflow and equation 12, the velocities of particles α and γ are given in dimensionless form by

$$N^{2/3}\frac{d}{dt}\left[\tilde{\underline{r}}_\alpha-\frac{u_S\tau}{L}\,\underline{e}t\right]=\sum_{\beta=1,\beta\neq\alpha,\gamma}^{N}\left[\left(1+\frac{2}{3\tilde{r}_{\alpha\beta}^2}\left(\frac{a}{L}\right)^2\right)\frac{\underline{e}}{\tilde{r}_{\alpha\beta}}+\left(1-\frac{2}{\tilde{r}_{\alpha\beta}^2}\left(\frac{a}{L}\right)^2\right)\frac{(\underline{e}\cdot\tilde{\underline{r}}_{\alpha\beta})\tilde{\underline{r}}_{\alpha\beta}}{\tilde{r}_{\alpha\beta}^3}\right]-3.17343\,N\underline{e}+$$

$$u_S\frac{\tau}{L}N^{2/3}\left[(\lambda_1(r_{\alpha\gamma})-\lambda_2(r_{\alpha\gamma}))\frac{\tilde{\underline{r}}_{\alpha\gamma}(\tilde{\underline{r}}_{\alpha\gamma}\cdot\underline{e})}{\tilde{r}_{\alpha\gamma}^2}+(\lambda_2(r_{\alpha\gamma})-1)\underline{e}\right]+$$

$$\frac{1}{2} N^{2/3} \left[ (B(r_{\alpha\gamma}) - A(r_{\alpha\gamma})) \tilde{\underset{\sim}{r}}_{\alpha\gamma} \cdot \tilde{\underset{\approx}{E}} \cdot \frac{\tilde{\underset{\sim}{r}}_{\alpha\gamma}}{\tilde{r}^2_{\alpha\gamma}} \tilde{\underset{\sim}{r}}_{\alpha\gamma} - B(r_{\alpha\gamma}) (\tilde{\underset{\approx}{E}} \cdot \tilde{\underset{\sim}{r}}_{\alpha\gamma}) \right] \qquad (13)$$

and

$$N^{2/3} \frac{d}{dt} \left[ \tilde{\underset{\sim}{r}}_{\gamma} - \frac{u_s \tau}{L} \underset{\sim}{e} t \right] = \sum_{\beta=1, \beta \neq \alpha, \gamma}^{N} \left[ \left(1 + \frac{2}{3\tilde{r}^2_{\gamma\beta}} \left(\frac{a}{L}\right)^2\right) \frac{\underset{\sim}{e}}{r_{\gamma\beta}} + \left(1 - \frac{2}{\tilde{r}^2_{\gamma\beta}} \left(\frac{a}{L}\right)^2\right) \frac{(\underset{\sim}{e} \cdot \tilde{\underset{\sim}{r}}_{\gamma\beta}) \tilde{\underset{\sim}{r}}_{\gamma\beta}}{(\tilde{r}^3_{\gamma\beta})} \right] - 3.17343 N \underset{\sim}{e} + u_s \frac{\tau}{L} N^{2/3}$$

$$\left[ (\lambda_1(r_{\alpha\gamma}) - \lambda_2(r_{\alpha\gamma})) \frac{\tilde{\underset{\sim}{r}}_{\alpha\gamma} (\tilde{\underset{\sim}{r}}_{\alpha\gamma} \cdot \underset{\sim}{e})}{\tilde{r}^2_{\alpha\gamma}} + (\lambda_2(r_{\alpha\gamma}) - 1) \underset{\sim}{e} \right] -$$

$$\frac{1}{2} N^{2/3} \left[ (B(r_{\alpha\gamma}) - A(r_{\alpha\gamma})) \frac{(\tilde{\underset{\sim}{r}}_{\alpha\gamma} \cdot \tilde{\underset{\approx}{E}} \cdot \tilde{\underset{\sim}{r}}_{\alpha\gamma})}{\tilde{r}^2_{\alpha\gamma}} \tilde{\underset{\sim}{r}}_{\alpha\gamma} - B(r_{\alpha\gamma}) (\tilde{\underset{\approx}{E}} \cdot \tilde{\underset{\sim}{r}}_{\alpha\gamma}) \right] \qquad (14)$$

in which $\tilde{\underset{\approx}{E}}$ is given by equation 10. The functions $\lambda_1(r_{\alpha\gamma})$ and $\lambda_2(r_{\alpha\gamma})$ and the functions $A(r_{\alpha\gamma})$ and $B(r_{\alpha\gamma})$ are coefficients determining respectively the settling motion of two spheres parallel and perpendicular to the line joining their centers and the motion of two spheres in a linear flow field. They are functions only of $r_{\alpha\gamma}$, the distance between $\alpha$ and $\gamma$, and in the simulation are calculated by using the lubrication and farfield results when the spheres are close together or far apart, respectively, and by using Akima's method (Akima 1970) to fit an interpolant through the known numerical values of the coefficients when the spheres are neither close together nor far apart. Because the accuracy of the available farfield and nearfield forms differs for the various coefficients, the ranges of $r_{\alpha\gamma}$ over which the nearfield and farfield forms are used also differs. In equations 13 and 14 the first term is the effect of the other N-2 particles, the second term is the backflow, the

third term arises because of the settling of the pair in an infinite, quiescent fluid, and the fourth represents the relative motion of $\alpha$ and $\gamma$ in the linear flow field created by the other N-2 particles.

In addition to being justifiable on physical grounds, equations 13 and 14 can be derived from the farfield result for the N-sphere mobility tensor (Mazur and Van Saarloos 1982). If the pair $\alpha$ and $\gamma$ have a separation distance of O(a) whereas the other particles in the suspension are separated from $\alpha$ and $\gamma$ by a length of $O(ac^{-1/3})$, then the result of multiplying the farfield form of the mobility tensor by the gravitational force on each particle is the velocities of $\alpha$ and $\gamma$ in the form of a sum of terms in increasing powers of $(\frac{a}{r_{\alpha\gamma}})$ and c. With error of at most $O((\frac{a}{r_{\alpha\gamma}})c)$, this sum is the combination of terms in equations 13 and 14 due to direct particle interactions if the functions $\lambda_1(r_{\alpha\gamma})$, $\lambda_2(r_{\alpha\gamma})$, $A(r_{\alpha\gamma})$, and $B(r_{\alpha\gamma})$ are replaced by farfield forms accurate to $O(\frac{a}{r_{\alpha\gamma}})^7$ (which is the same order as the smallest terms in the exact N-sphere solution).

When more than one particle comes with 4a of particle $\alpha$, we generalize the procedure used for a close pair by considering the M close particles (where we are interested in the cases of M=3 or 4, i.e., close triples and quadruples) to be settling in the linear flow field generated by the other N-M particles. The motion of these M particles may thus be described by 6M equations balancing the forces and torques on each of the close spheres (Brenner and O'Neill 1972):

$$-\tilde{\underline{F}} = \tilde{\underline{\underline{R}}} \cdot (\tilde{\underline{U}} + \frac{u_{ST}}{L}\underline{e}^*) + \tilde{\underline{\underline{\phi}}} : \tilde{\underline{\underline{E}}} \qquad (15)$$

where $\underline{e}^*$ is the 6M-component vector with M repetitions of (0, 0, 1) as its first 3M components and with 0 for all its other components and where $\underline{\tilde{F}}$, $\underline{\underline{\tilde{R}}}$, $\underline{\tilde{U}}$, $\underline{\underline{\tilde{\phi}}}$, and $\underline{\underline{\tilde{E}}}$ have the same interpretation as their counterparts in equation 8 except that now all the tensors are 6Mx6M-component tensors, all the vectors are 6M-component vectors, and $\underline{\tilde{F}}$, $\underline{\underline{\tilde{R}}}$, $\underline{\tilde{U}}$, $\underline{\underline{\tilde{\phi}}}$, and $\underline{\underline{\tilde{E}}}$ are now in dimensionless form.

To calculate the velocities of the particles, we observe that the first 3M components of $\underline{\tilde{U}}$ contain the dimensionless velocities of the particles minus the dimensionless undisturbed fluid velocity at each of the particles and that the undisturbed fluid velocity may be approximated with error O(c) by the velocity induced by the N-M particles far away at each of the close particles (i.e., by treating the other particles in the same fashion as when only two particles are close together). Therefore, calculating the velocities of the particles requires only determining $\underline{\tilde{F}}$, $\underline{\underline{\tilde{R}}}$, $\underline{\underline{\tilde{\phi}}}$, and $\underline{\underline{\tilde{E}}}$ and inverting the matrix $\underline{\underline{\tilde{R}}}$. In the situation where no body torques act on the particles and the only external force acting on the particles is gravity, $\underline{\tilde{F}}$ is the vector $\frac{u_S \tau}{L} \underline{e}^*$ defined above. Equation 10 gives the rate-of-strain tensor $\underline{\underline{\tilde{E}}}$ at particle $\alpha$ as in the two-particle case except that the sum is now over only N-M particles.

Thus, the main difficulty in determining the velocities of a close triple or quadruple is in calculating $\underline{\underline{\tilde{R}}}$ and $\underline{\underline{\tilde{\phi}}}$, the grand and shear resistance tensors made dimensionless by $6\pi\mu a$. Because the multiparticle problem for determining $\underline{\underline{\tilde{\phi}}}$ and $\underline{\underline{\tilde{R}}}$ has not been solved for particles close together, we choose to approximate $\underline{\underline{\tilde{\phi}}}$ and $\underline{\underline{\tilde{R}}}$ by assuming the forces and torques on the particles are pairwise-additive; this procedure preserves the lubrication forces which

restrain the particles from overlapping. (For a triple of particles $\alpha$, $\gamma_1$, and $\gamma_2$, pairwise additivity means that the force on particle $\alpha$ with particles $\gamma_1$ and $\gamma_2$ nearby is the force on $\alpha$ with only $\gamma_1$ nearby plus the force on $\alpha$ with only $\gamma_2$ nearby minus the force on $\alpha$ with neither $\gamma_1$ nor $\gamma_2$ nearby.)

This procedure necessitates knowing the complete set of two-sphere resistance tensors as a function of the separation distance between the spheres. Although Jeffrey and Onishi (1984) have recently tabulated this information in one reference, this tabulation was not available at the time the simulation was prepared; therefore, the resistance tensors are computed from the solutions (tabulated in terms of 13 scalar parameters) to the variety of two-sphere motion problems (cf. Batchelor 1976; Cooley and O'Neill 1969; Happel and Brenner 1965; Hansford 1970; Arp and Mason 1977; Majumdar 1967; Takagi 1974; Reuland, Felderhof, and Jones 1978; Jeffery 1915; Davis 1969; O'Neill and Majumdar 1970; Brenner and O'Neill 1972; Brenner 1964; and Wacholder and Sather 1974). For large and small values of the separation distance between the particles, the farfield and lubrication results, respectively, are used to calculate the resistance coefficients in the simulation; at intermediate separation distances Akima's method (Akima 1970) is used to interpolate between the known numerical values of the resistance coefficients. As before, because the accuracy of the nearfield and farfield forms varies for the 13 coefficients, the range of separation distances over which these forms are used also varies.

## 4. Numerical Implementation

The net result of sections 2 and 3 is a set of equations for the velocity of each of the N particles in the cube given the instantaneous particle positions. The trajectories of the particles are determined by integrating these equations forward in time using a fixed-time-step predictor-corrector method. The fourth-order Adams-Bashforth method is the predictor, and the fourth-order Admas-Moulton method is the corrector. The fourth-order Runge-Kutta method starts the calculation for the first few time steps. The method has several advantages: it requires only two function evaluations per time step, it has good stability properties, and it is reasonably low-order. The order of the method should be reasonably low since, as we explain below, the time step must be set fairly small.

In order to capture most of the details of the motion of the particles, we must select a time step less than the smallest of the four time scales of the problem. When the particles are well-separated, their motion changes over the time scale of the interparticle spacing divided by the relative velocity between two well-separated particles

$$T_1 \simeq \frac{ac^{-1/3}}{u_s c^{1/3}} = \frac{a}{u_s} c^{-2/3} = \frac{3}{4} \left(\frac{3}{4\pi}\right)^{2/3} \tau \qquad (16)$$

This time scale is roughly 1/3 of the dimensionless time for the simulation, which is the time scale over which the suspension rearranges due to settling and the time scale which determines the final time of the simulation. If this were the only important time scale, then a time step of approximately $.01\tau$ to $.005\tau$ would probably suffice. However, when two particles come close together, they move with a velocity of approximately $u_s$ relative to the other particles in the suspension (which are separated from the pair by a distance of $O(ac^{-1/3})$). Thus, another important time scale is

$$T_2 \simeq \frac{ac^{-1/3}}{u_s} = \frac{a}{u_s} c^{-1/3} = T_1 c^{1/3}. \tag{17}$$

Since the concentration is small, $T_1 > T_2$. In particular, for the typical value of $c=.5\%$, $T_2=.17T_1$. The relative motion between a pair of particles proceeds over the time scale of the particle radius divided by the relative velocity of the pair. Hence, because the relative velocity is proportional to the radius of the particles and to the rate-of-strain tensor of the linear shear flow created by the other N-2 particles and because the rate-of-strain tensor is proportional to $u_s \frac{a}{(ac^{-1/3})^2}$,

$$T_3 \simeq \frac{a}{u_s c^{2/3}} = \frac{a}{u_s} c^{-2/3} = T_1. \tag{18}$$

The final important time scale occurs when two particles come close enough so that the important length scale is the gap distance $\delta$ between the particles. Then, the relative velocity along the lines of centers of the

particles is approximately $(A(r)-1)a\left|\underline{\underline{E}}\right|$ where A(r) is given in Batchelor and Green (1972). For $\frac{\delta}{a}<<1$, $A(r) \simeq (1-4.0\ \frac{\delta}{a})$ and thus

$$T_4 \simeq \left|\frac{\delta}{(1-4.0\ \frac{\delta}{a}-1)\ u_s c^{2/3}}\right| = \frac{1}{4}\ \frac{a}{u_s}\ c^{-2/3} = \frac{1}{4}\ T_1$$

Of these four time scales, the smallest is $T_2$, which is approximately $\frac{\tau}{20}$. The results of simulation runs with a time step of $.02T_2$ or $.001\tau$ (Lynch and Herbolzheimer 1985) suggest this time step is sufficiently small for most physical situations.

Because of the approximations made in calculating the velocities of the particles and because the time scale of the relative motion between two very close particles is small, the lubrication forces between the particles are not always strong enough to prevent the particles from overlapping. Although reducing the time step reduces significantly the number of overlapping particles, setting a time step small enough to eliminate overlapping particles would be prohibitively costly. Therefore, this problem is corrected in the simulation by moving the particles apart a small distance (viz., .008a) whenever they overlap.

Another numerical aspect of the simulation is that when more than one particle is close to a given particle $\alpha$, determining the velocities of the close particles requires inverting $\tilde{\underline{\underline{R}}}$, the grand resistance tensor describing the translational and rotational forces between the close particles. Because many of the resistance coefficients become infinite as the gap between the close particles shrinks to zero, a large difference may exist in the magnitude

of the matrix elements of $\tilde{\underline{R}}$. To prevent this from affecting the accuracy of the matrix inversion and of the relative velocities between the close particles, the simulation uses equilibration and partial pivoting in inverting $\tilde{\underline{R}}$ and if the initial result is not sufficiently accurate corrects it through iterative improvement. Because of the symmetry of the resistance tensor (as required by the reciprocal theorem for Stokes flow), we may enhance computation speed by inverting $\tilde{\underline{R}}$ using the method of Bunch for indefinite symmetric matrices (Bunch and Parlett 1971; Bunch 1971).

A possible difficulty in the simulation might arise because we calculate the velocity of a given particle differently depending upon how close its nearest neighbor is. We have assumed that the change in the computed velocity of a particle when it comes within 4a of another particle has little effect on the overall behavior of the particle trajectories. When a set of two isolated particles becomes a pair, the velocities of the pair remain essentially unchanged; however, when three particles form a triple their velocities change because of the difference between the predictions of force pairwise additivity and of the farfield result for the velocities, which is similar to the result of velocity pairwise additivity. In test runs with small numbers of particles (see section 5), the particle trajectories showed no unphysical behavior obviously attributable to this velocity jump.

## 5. Results and Discussion

To study how the approximations made in determining the velocities of the spheres might affect the behavior of the simulation, we have examined how well our simulation predicts the trajectories of three settling spheres which are initially placed in a horizontal line. The trajectories of the spheres in this problem, first examined theoretically by Hocking (1964) who approximated the spheres as point forces, have been calculated numerically by Ganatos, Pfeffer, and Weinbaum (1978) using a four-point collocation scheme.

Ganatos, et al. present their results in the form of scale drawings of the sphere trajectories for an initial sphere configuration where the centers of the outer spheres are separated by 12a and where $\chi$ (called C by Ganatos, et al.), the ratio of the distance between the central and rightmost sphere to the distance between the central and leftmost sphere, varies from 1.0 to 2.0. We present in Figures 1a through 8a the sphere trajectories under these initial conditions calculated by our method for determining the velocities and in Figures 1b through 8b those calculated by the alternative method of assuming the forces on the particles are pairwise-additive. (Calculating the velocities using force pairwise additivity is possible in our program by changing the distance at which the particles start to interact as near neighbors from 4a to infinity.) The vertical distance in sphere radii travelled by the uppermost sphere, $\tilde{d}$, and $\tilde{t}$, the time made dimensionless by the characteristic time $\frac{a}{u_s}$ appear at the left of each diagram of the particle positions. In these three-particle calculations the time step is approximately .74 $\frac{a}{u_s}$ or approximately 6 times larger than in the simulation with many particles. With the exception of

this change, the procedure for determining the trajectories is essentially identical to that in the simulation. When the velocities were computed by our method, all of these three-particle calculations required less than 15 seconds of time for calculations in single precision on the VAX 11/780 computer. (By contrast, a simulation run with 64 particles and 8000 time steps required approximately 5 hours of CPU time.)

Comparing the diagrams of the trajectories to those of Ganatos, et al. reveals that, although both methods predict the qualitative features of the trajectories relatively well, the results of Ganatos, et al. are noticeably closer to the trajectories calculated from our method than those calculated from force pairwise additivity. For example, for $\chi$=1.1 and $\chi$=1.5 the long-time behavior of the trajectories of Ganatos, et al. is similar to our results, but not to those of force pairwise additivity, and for $\chi$=1.4 our method reproduces many more of the details in the trajectories of the numerical solution than force pairwise additivity does.

However, even when both methods produce results qualitatively similar to the exact solution, our method yields better quantitative results because it is, as explained earlier, accurate to $O(\frac{a}{r_{\alpha\beta}})^3$ for two well-separated spheres $\alpha$ and $\beta$ whereas the forces on the particles are pairwise-additive only to $O(\frac{a}{r_{\alpha\beta}})$. For example for $\chi$=1.6, although the trajectories for both methods agree qualitatively well with the numerical solution, the distance settled by the uppermost sphere at $\tilde{t}$=400, the final time of the calculation, is 489.7 for the numerical solution, 489.9 for our method, and 505.0 for force pairwise additivity. Similarly, for $\chi$=1.0, the time at which all three spheres settle with equal velocities in the numerical solution, $\tilde{t}$=107.8, is far better

predicted by our method (for which $\tilde{t}$=105.8) than by force pairwise additivity (for which $\tilde{t}$=132.7).

The main qualitative differences in the trajectories of Ganatos, et al. and our trajectories generally result from instances when two particles pass close to each other (e.g., see the diagram of $\tilde{t}$=350 for $\chi$=1.4). Because in the lubrication layers around the particles, the relative velocity between the particles changes quite rapidly as a function of separation distance, initially small differences in the computed positions of the particles can grow into large differences between the two sets of trajectories.

The trajectories produced by our method for the case of equally spaced spheres show two unphysical features which deserve further elaboration. For reasons of efficiency, in the simulation the rate-of-strain tensor $\tilde{\tilde{E}}$ due to the particles far away is evaluated on one of the particles; for this three-particle calculation, however, this procedure adds a perturbation which is unsymmetric about the centerline to an otherwise symmetric problem and eventually causes the result to be unsymmetric (see the diagrams for $\tilde{t}$=158.3 and $\tilde{t}$=175 in Figure 1a$_1$). For this reason the result of evaluating $\tilde{\tilde{E}}$ as the average of the values of $\tilde{\tilde{E}}$ at the centers of the close particles (i.e., an estimate of $\tilde{\tilde{E}}$ at the midpoint between the particles) is shown in the diagrams for $\tilde{t}$=158.3 and $\tilde{t}$=175 in Figure 1a$_2$ and is observed to be symmetric about the centerline. (Until $\tilde{t}$=158.3 the results of the two procedures are identical.) The case $\chi$=1.0 is the only case where the position at which $\tilde{\tilde{E}}$ was evaluated had a significant impact on the trajectories. For the case in which the average value of $\tilde{\tilde{E}}$ is used, the particles overlap at $\tilde{t}$=162.9; the particles overlap, as they do in the numerical solution of Ganatos, et al., because the time step is too large and because of the approximations made in calculating

the particle velocities, not because of neglect of the lubrication forces between the particles. After $\tilde{t}$=158.3 Ganatos, et al. separate particles 1 and 3 and restrain them from rotating or moving laterally, so their results for $\tilde{t}$=175 must be regarded as somewhat questionable.

Obviously for these three-sphere problems the trajectories generated by our simulation agree extremely well with those calculated by Ganatos, et al. Because of this result, we can likewise be confident that our hybrid method for calculating the velocities of the particles will yield reasonable results in simulation runs with many particles.

## REFERENCES

Akima, H. 1970 A new method of interpolation and smooth curve fitting based on local procedures. J. Assoc. Computing Machinery 17, 589-602.

Arp, P.A. and Mason, S.G. 1977 The kinetics of flowing dispersions. VIII. Doublets of rigid spheres (theoretical). J. Colloid Interface Sci. 61, 21-43.

Bacon, J., Dickinson, E., Parker, R., Anastasiou, N. and Lal, M. 1983 Motion of flocs of two or three interacting colloidal particles in a hydrodynamic medium. J. Chem. Soc., Faraday Trans. 2, 91-109.

Batchelor, G.K. 1972 Sedimentation in a dilute dispersion of spheres. J. Fluid Mech. 52, 245-268.

Batchelor, G.K. 1976 Brownian diffusion of particles with hydrodynamic interaction. J. Fluid Mech. 74, 1-29.

Batchelor, G.K. and Green, J.T. 1972 The hydrodynamic interaction of two small freely-moving spheres in a linear flow field. J. Fluid Mech. 56, 375-400.

Beenakker, C.W.J., Van Saarloos, W. and Mazur, P. 1984 Many-sphere hydrodynamic interactions. III. The influence of a plane wall. Physica 127A, 451-472.

Brenner, H. 1964 The Stokes resistance of an arbitrary particle-II. An extension. Chem. Engng. Sci. 19, 599-629.

Brenner, H. and O'Neill, M.E. 1972 On the Stokes resistance of multiparticle systems in a linear shear field. Chem. Engng Sci. 27, 1421-1439.

Bossis, G. and Brady, J.F. 1984 Dynamic simulation of sheared suspensions. I. General method. J. Chem. Phys. 80, 5141-5154.

Brady, J.F. and Bossis, G. 1984 Dynamic simulation of sheared suspensions: rheology. Proc. IX Int. Cong. Rheol. 2, 456-480.

Bunch, J.R. 1971 Analysis of the diagonal pivoting method. SIAM J. Numer. Anal. 8, 656-680.

Bunch, J.R. and Parlett, B.N. 1971 Direct methods for solving symmetric indefinite systems of linear equations. SIAM J. Numer. Anal. 8, 639-655.

Cooley, M.D.A. and O'Neill, M.E. 1969 On the slow motion of two spheres in contact along their line of centres through a viscous fluid. Proc. Camb. Phil. Soc. 66, 407-415.

Davis, M.H. 1969 The slow translation and rotation of two unequal spheres in a viscous fluid. Chem. Engng. Sci. 24, 1769-1776.

Dickinson, E. and Parker, R. 1984 Brownian encounters in a polydisperse sedimenting system of interacting colloidal particles. J. Colloid Interface Sci. 97, 220-231.

Ermak, D.L., and McCammon, J.A. 1978 Brownian dynamics with hydrodynamic interactions. J. Chem. Phys. 69, 1352-1360.

Ganatos, P., Pfeffer, R. and Weinbaum, S. 1978 A numerical-solution technique for three-dimensional Stokes flows, with application to the motion of strongly interacting spheres in a plane. J. Fluid Mech. 84, 79-111.

Goldman, A.J., Cox, R.G. and Brenner, H. 1966 The slow motion of two identical arbitrarily oriented spheres through a viscous fluid. Chem. Engng. Sci. 21, 1151-1170.

Hansford, R.E. 1970 On converging solid spheres in a highly viscous fluid. Mathematika 17, 250-254.

Happel, J. and Brenner, H. 1965 Low Reynolds Number Hydrodynamics. Prentice-Hall.

Hocking, L.M. 1964 The behavior of clusters of spheres falling in a viscous fluid. Part 2. Slow motion theory. J. Fluid Mech. 20, 129-139.

Jeffery, G.B. 1915 On the steady rotation of a solid of revolution in a viscous fluid. Proc. Lond. Math. Soc. 14, 327-338.

Jeffrey, D.J. and Onishi, Y. 1984 Calculation of the resistance and mobility functions for two unequal rigid spheres in low-Reynolds-number flow. J. Fluid Mech. 139, 261-290.

Lynch, E.D. and Herbolzheimer, E. 1985 Sedimentation in quiescent suspensions. (To be submitted - Chapter 1 of this thesis).

Majumdar, S.R. 1967 Slow motion of an incompressible viscous liquid generated by the rotation of two spheres in contact. Mathematika 14, 43-46.

Mazur, P. 1982 On the motion and Brownian motion of N spheres in a viscous fluid. Adv. Colloid Interface Sci. 17, 1-19.

Mazur, P. and Van Saarloos, W. 1982 Many-sphere hydrodynamic interactions and mobilities in a suspension. Physica 115A, 21-57.

O'Neill, M.E. 1969 On asymmetrical slow viscous flows caused by the motion of two equal spheres almost in contact. Proc. Camb. Phil. Soc. 65, 543-556.

O'Neill, M.E. and Majumdar, S.R. 1970 Asymmetrical slow viscous fluid motions caused by the translation or rotation of two spheres. Part I: The

determination of exact solutions for any values of the ratio of radii and separation parameters. Z. angew. Math. Phys. 21, 164-179.

Pearson, H.J., Valioulis, I.A. and List, E.J. 1984 Monte Carlo simulation of coagulation in discrete particle-size distributions. Part I. Brownian motion and fluid shearing. J. Fluid Mech. 143, 367-385 (1984).

Reuland, P., Felderhof, B.U. and Jones, R.B. 1978 Hydrodynamic interaction of two spherically symmetric polymers. Physica 93A, 465-475.

Saffman, P. 1973 On the settling speed of free and fixed suspensions. Stud. Appl. Math. 52, 115-127.

Takagi, H. 1974 Slow rotation of two touching spheres in viscous fluid. J. Phys. Soc. Japan 36, 875-877.

Valioulis, I.A., List, E.J. and Pearson, H.J. 1984 Monte Carlo simulation of coagulation in discrete particle-size distributions. Part 2. Interparticle forces and the quasi-stationary equilibrium hypothesis. J. Fluid Mech. 143, 387-411.

Wacholder, E. and Sather, N.F. 1974 The hydrodynamic interaction of two unequal spheres moving under gravity through quiescent viscous fluid. J. Fluid Mech. 65, 417-437.

Wakiya, S. 1967 Slow motions of a viscous fluid around two spheres. J. Phys. Soc. Japan 22, 1101-1109.

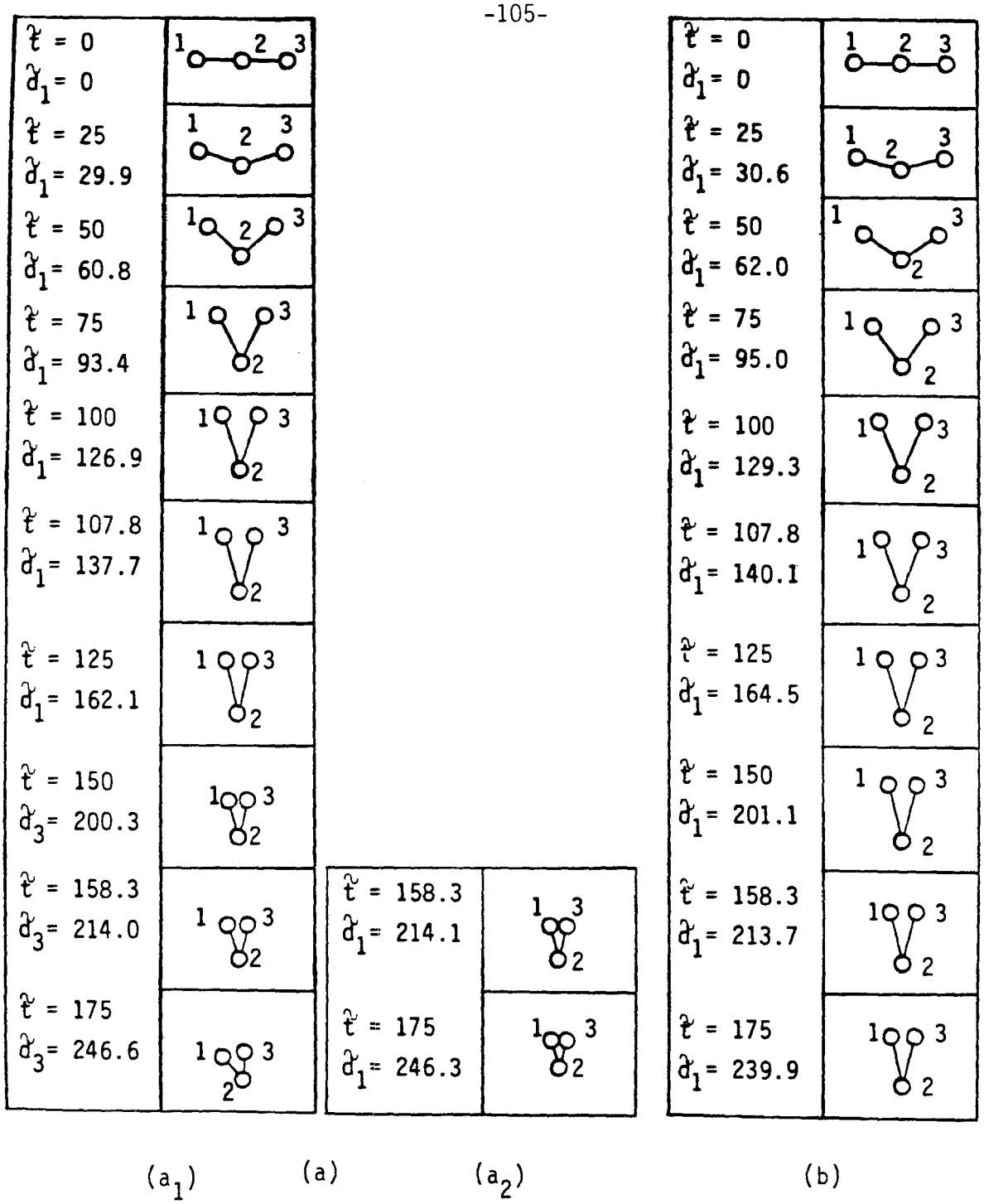


Figure 1. Trajectories for three equally spaced settling spheres initially in a horizontal line, $\chi$=1.0; predictions of: our method - (a), force pairwise additivity - (b).

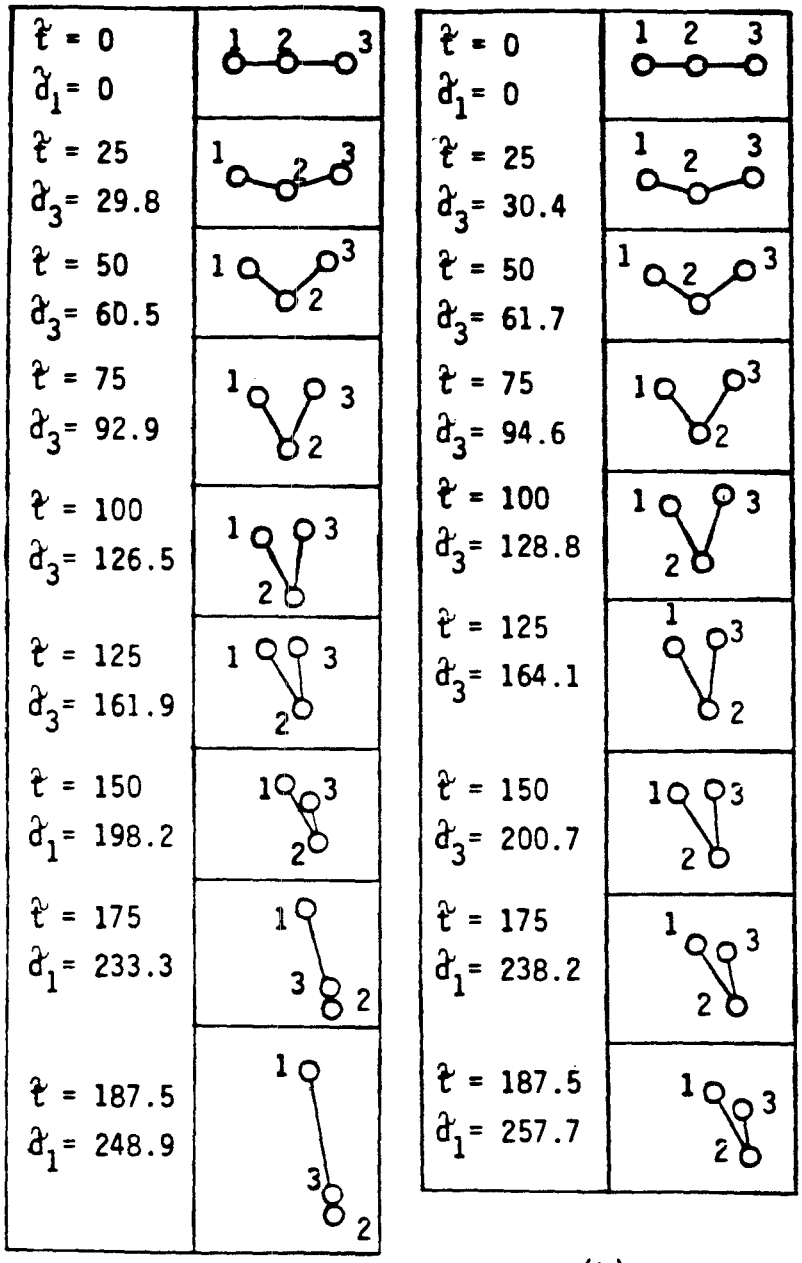


Figure 2. Trajectories for three settling spheres initially in a horizontal line, $\chi$=1.1; predictions of: our method - (a), force pairwise additivity - (b).

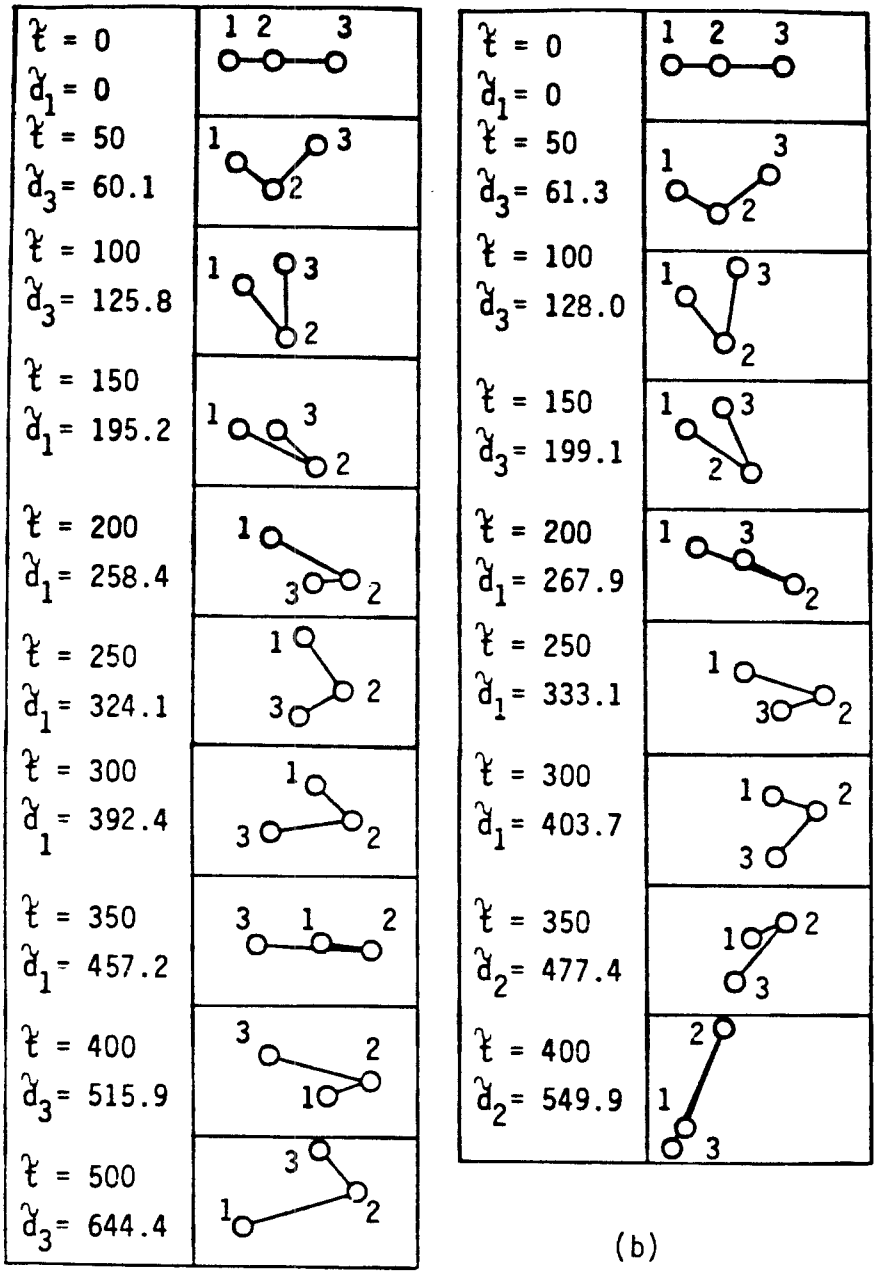


Figure 3. Trajectories for three settling spheres initially in a horizontal line, $\chi$=1.3; predictions of: our method - (a), force pairwise additivity - (b).

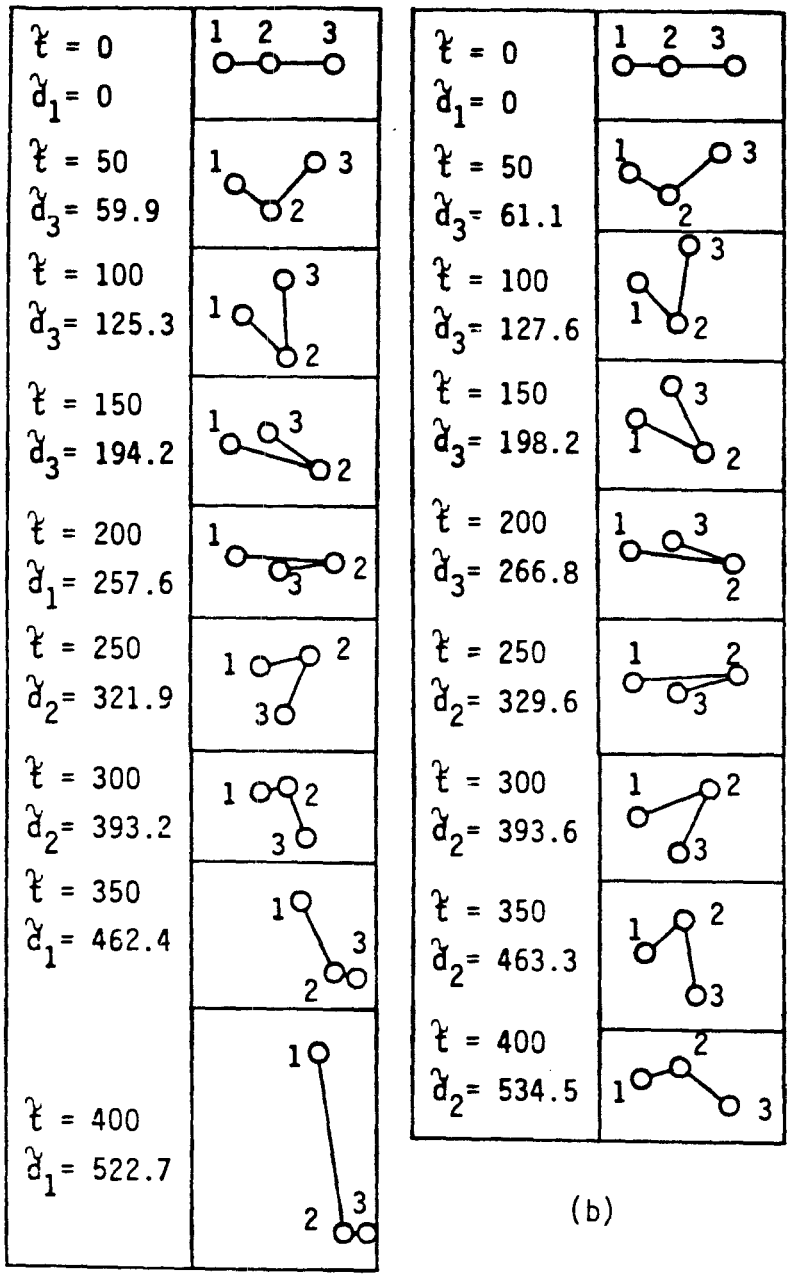


Figure 4. Trajectories for three settling spheres initially in a horizontal line, $\chi$=1.4; predictions of: our method - (a), force pairwise additivity - (b).

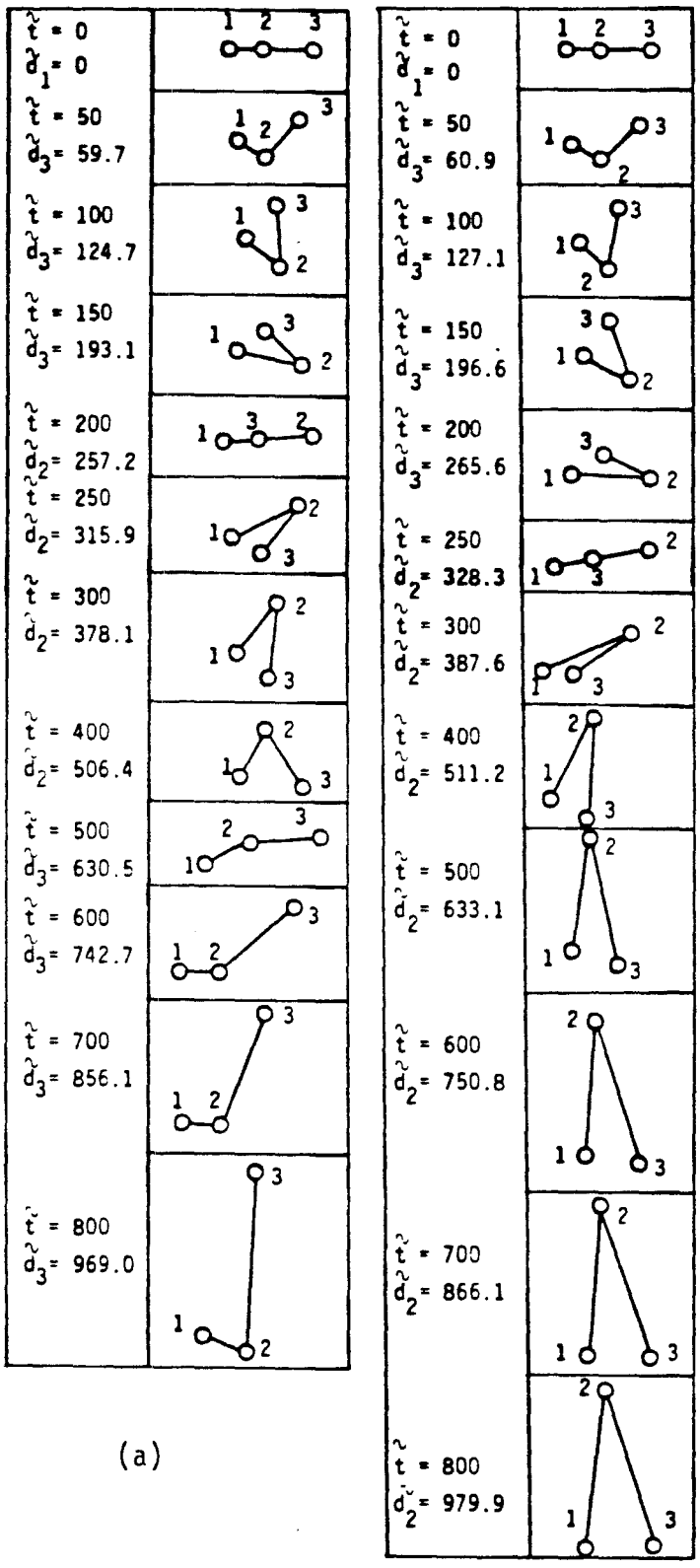


Figure 5. Trajectories for three settling spheres initially in a horizontal line, $\chi$=1.5; predictions of: our method - (a), force pairwise additivity - (b).

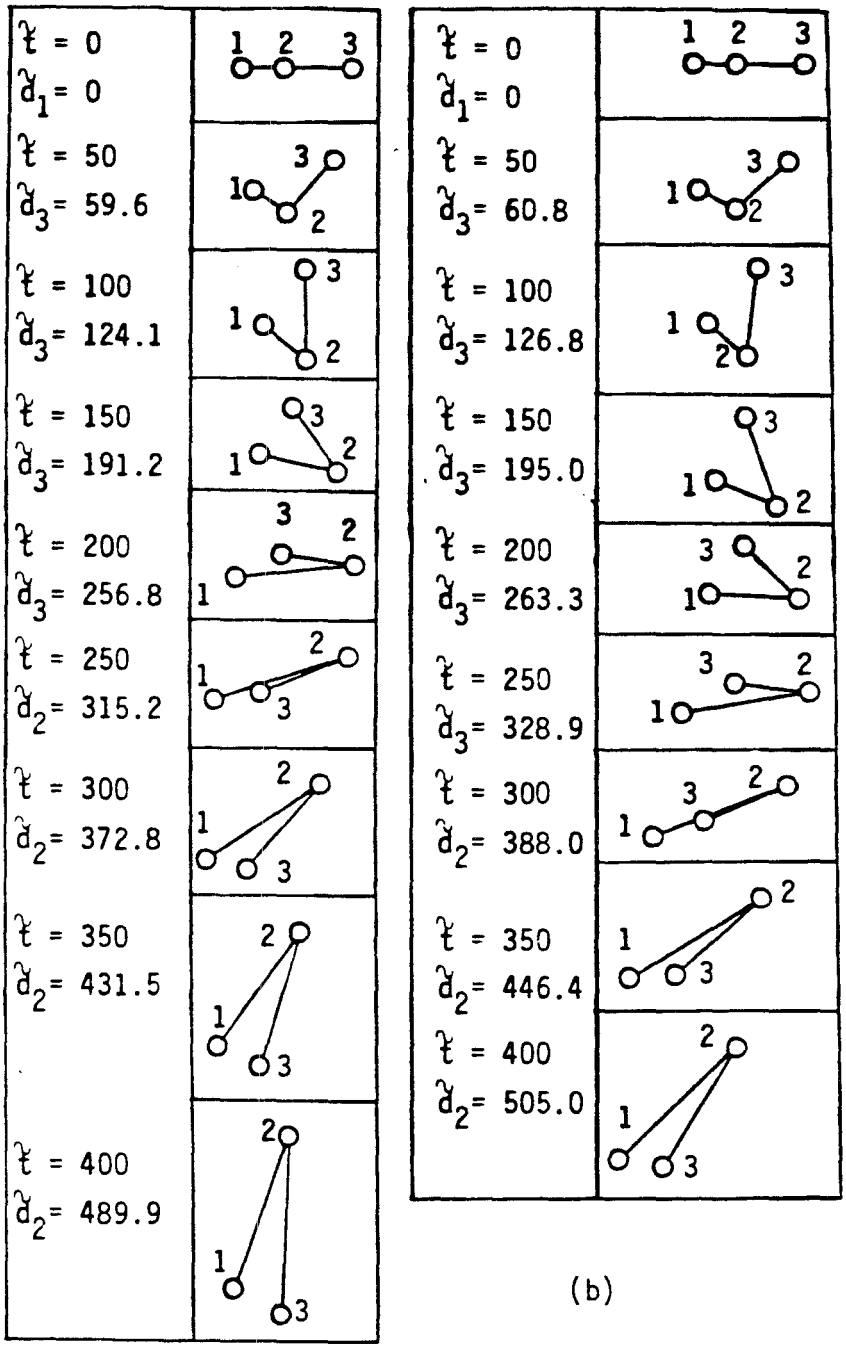


Figure 6. Trajectories for three settling spheres initially in a horizontal line, $\chi$=1.6; predictions of: our method - (a), force pairwise additivity - (b).

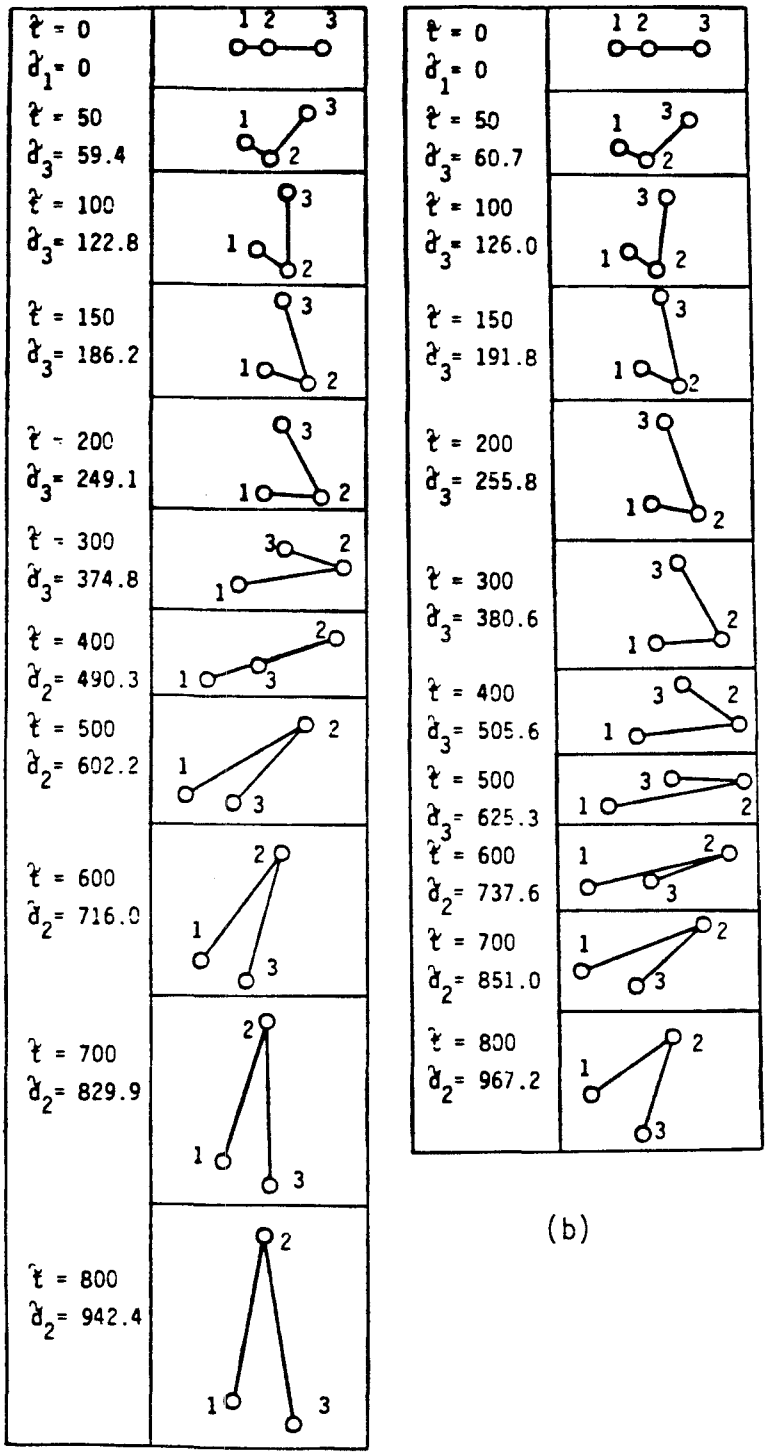


Figure 7. Trajectories for three settling spheres initially in a horizontal line, $\chi$=1.8; predictions of: our method - (a), force pairwise additivity - (b).

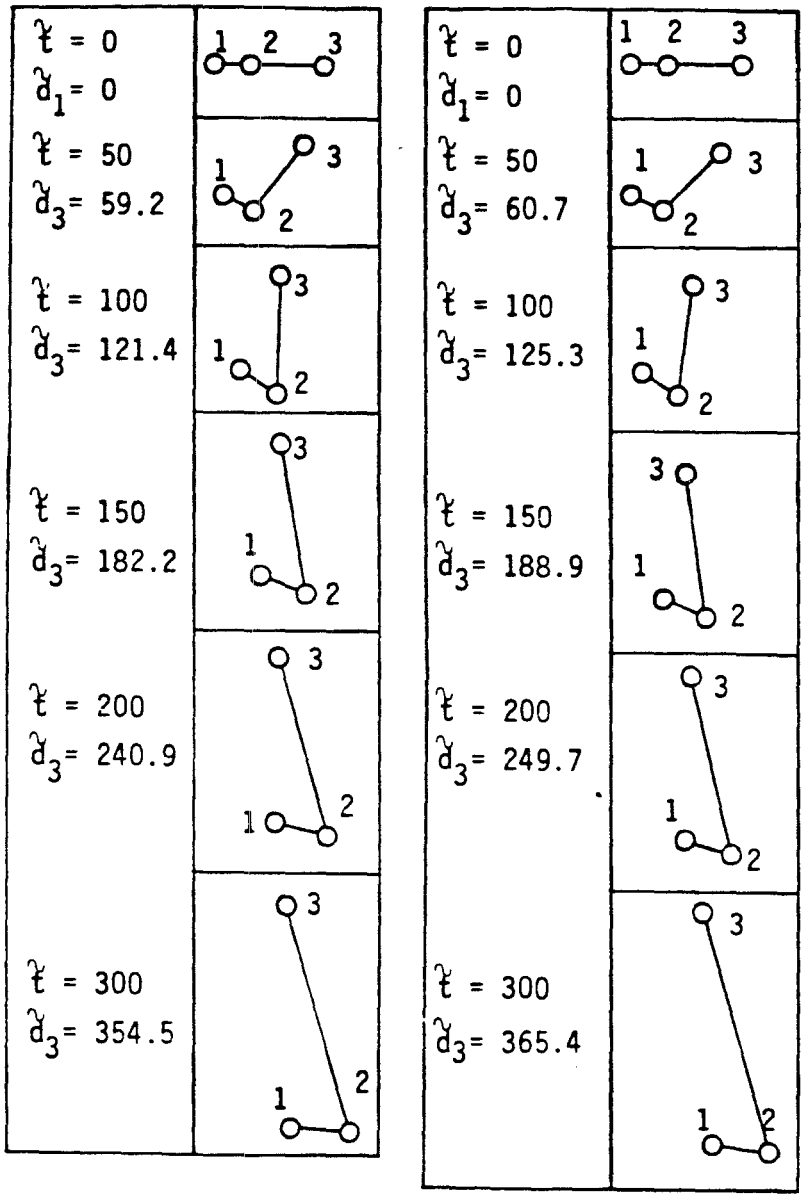


Figure 8. Trajectories for three settling spheres initially in a horizontal line, $\chi$=2.0; predictions of: our method - (a), force pairwise additivity - (b).

# CHAPTER III

## Sedimentation in Sheared Suspensions

(Chapter III consists of a paper
by Edward D. Lynch and Eric Herbolzheimer)

# Sedimentation in Sheared Suspensions

Edward D. Lynch and Eric Herbolzheimer
California Institute of Technology
Pasadena, California 91125

## Abstract

When a suspension of identical sedimenting rigid spheres in an incompressible, Newtonian fluid is sheared, the sedimentation velocity should depend not only on the volume fraction of solids in the suspension, but also on the shear rate and flow type. Although the sedimentation velocity has been studied both experimentally and theoretically for quiescent suspensions (cf. Lynch and Herbolzheimer 1985), sheared suspensions of non-flocculating particles have not received such attention; consequently, the effect of bulk flow on the settling velocity remains unknown.

In this paper we first calculate that for a suspension undergoing "rapid" shearing in a uniaxial extensional flow the settling velocity is given by $u_s(1-4.52c + O(c^2))$ where $u_s$ is the Stokes velocity and c is the volume fraction of particles. This result agrees very well with our experimental measurements made for a suspension undergoing "rapid" simple shear in a cylindrical Couette device. We also examine experimentally the effects of shear rates which are not asymptotically large as well as what the proper dimensionless shear rate should be for use in constitutive relations for the sedimentation velocity.

## 1. Introduction

Calculating macroscopic flows of suspensions requires constitutive relations for the sedimentation velocity and the stress of the suspension as a function of c, the volume fraction of particles in the suspension, and of the local bulk flow conditions of the suspension. Until now studies of the sedimentation velocity in suspensions have only considered quiescent suspensions (i.e., suspensions for which no overall bulk motion occurs). However, because the bulk flow affects the microscale distribution of particles in the suspension, it can play a significant role in determining the suspension sedimentation velocity, even in non-flocculating suspensions. In this paper we shall use both theoretical and experimental techniques to investigate the effect shear has on the sedimentation velocity.

The results for the quiescent sedimentation problem, reviewed in Lynch and Herbolzheimer (1985), may be summarized briefly as follows. If the particles in the suspension are randomly arranged (i.e., all positions of the particles are equally likely given the particles do not overlap), then the sedimentation velocity of a monodisperse suspension (with respect to axes situated so that the mean flux of fluid plus particles is zero) is

$$u_o = u_s \, (1 - 6.55c + O(c^2)) \tag{1}$$

(cf. Batchelor 1972). Here $u_s$ is the Stokes velocity, $\frac{2}{9} a^2(\rho_s - \rho) \frac{g}{u}$, a is the sphere radius, $\rho_s$ is the particle density, $\rho$ is the fluid density, g is the gravitational acceleration, and $\mu$ is the fluid viscosity. On the other hand, if

the particles are positioned at the lattice points of a cubic array, then the settling velocity is

$$u_o = u_s(1 - 1.7601c^{1/3} + O(c)) \tag{2}$$

(cf. Hasimoto 1959; Sangani and Acrivos 1982). Both of these results are inconsistent with the correlation developed by Barnea and Mizrahi (1973) from previous experimental work for quiescent, monodisperse suspensions of spheres with radius greater than 2μm; they found that

$$u_o = u_s \frac{(1-c)^2}{(1+c^{1/3})(\exp(\frac{5}{3}\frac{c}{1-c}))} , \tag{3a}$$

which for dilute suspensions asymptotes to

$$u_o = u_s (1-c^{1/3} + c^{2/3} + O(c)) . \tag{3b}$$

We have explained in a previous paper (Lynch and Herbolzheimer 1985) that previous experimental work can be shown to be consistent with a suspension having a pair-probability function (i.e., the probability $P(\underline{r})$ of a particle being at position $\underline{x}_o + \underline{r}$ given another particle at position $\underline{x}_o$) changing over a length scale of $O(ac^{-1/3})$ and have shown that a molecular-dynamics-type simulation of a sedimenting suspension can be used to predict such a pair-probability function. Apparently, in a quiescent settling suspension as a result of multiparticle hydrodynamic interactions close pairs of particles are less likely to persist, and instead most particles are separated from their

nearest neighbors by a distance comparable to the average particle spacing; i.e., by a distance of $O(ac^{-1/3})$. Consequently, the first correction to the Stokes velocity is proportional to $c^{1/3}$. Specifically, we find from the simulations in Lynch and Herbolzheimer (1985) that

$$u_o = u_s (1 - .75c^{1/3} + O(c)) \tag{4}$$

and that the $c^{2/3}$ term in (3b) is an artifact of Barnea and Mizrahi's assumed form for the correlation. We might point out that this concentration dependence is very strong with the settling velocity being only 79% of the Stokes velocity when the volume fraction is only .01 rather than 94% of $u_s$ as predicted by Batchelor's (1972) theory.

Let us now suppose the sedimenting suspension is sheared by some external means. We now have on the one hand the multiparticle hydrodynamic interactions which in a quiescent settling suspension tend to make the particles become "well-spaced" competing against the imposed shear flow which carries at least some of the particles into close proximity to their neighbors. Hence, shearing the suspension should produce more close pairs thereby changing the pair-probability function. In fact, if the shear is fast enough for the effects of shearing to dominate those of sedimentation, the pair-probability function should become identical to that calculated by Batchelor and Green (1972b) and should change over a length scale of O(a), not of $O(ac^{-1/3})$. Consequently, in this case the sedimentation velocity should be of the form

$$u_o = u_s (1 - \beta_s c + O(c^2)). \tag{5}$$

where $\beta_S$ is an O(1) constant. In the next three sections, we examine this hypothesis in greater detail both theoretically and experimentally.

## 2. Theory

Let us begin by extending Batchelor's (1972) calculation for the sedimentation velocity in a dilute, quiescent suspension to include the effects of an imposed linear shear flow. First, we note that the shear does not alter Batchelor's technique for overcoming the well-known divergence problems which arise in calculating the sedimentation velocity when the full multiparticle hydrodynamics problem is reduced (via the assumed diluteness of the suspension) to a two-particle problem. Specifically, his equations (3.3), (3.4), (3.9), and (3.13) still apply, but the pair-probability function, the flow field around a single particle, and the velocity of a particle in the presence of one neighbor are all altered by the shear.

The pair-probability distribution in a sheared suspension of neutrally buoyant particles has already been found by Batchelor and Green (1972b). Since the particles cannot overlap and since for large separations the pair-probability function should asymptote to n, the average number of particles per unit volume in the suspension, let us define

$$P(\underset{\sim}{x}_o+\underset{\sim}{r}|\underset{\sim}{x}_o) = \begin{cases} 0 & \text{for } r < 2a \\ np(\underset{\sim}{r}) & \text{for } r > 2a \end{cases} \tag{6}$$

The function $p(\underset{\sim}{r})$ can be found from the conservation equation for particle pairs,

$$\frac{\partial p}{\partial t} + \underset{\sim}{V}_R \cdot \nabla p = -p\nabla \cdot \underset{\sim}{V}_R \tag{7}$$

where $\underset{\sim}{V}_R$ is the relative velocity between the centers of the particles in the pair. If the suspension is sufficiently dilute, then the relative motion of any pair is not significantly affected by the other particles in the suspension. Under this assumption $\underset{\sim}{V}_R$ can be determined from the relative motion of a pair of particles immersed in an infinite fluid undergoing the prescribed shear motion. Batchelor and Green (1972a,b) have compiled the known results for $\underset{\sim}{V}_R$ for neutrally buoyant particles in a linear shear flow and have solved for $p(\underset{\sim}{r})$. Of course, in the limit of pair interactions, the sedimentation of identical particles has no effect on the relative motion of the particles so Batchelor and Green's results apply to sheared sedimenting suspensions as well. As pointed out by Batchelor and Green (1972b), in some cases the particles can execute closed trajectories about one another resulting in an indeterminacy in $p(\underset{\sim}{r})$. This problem does not arise in pure extensional flow, however, since all particle trajectories start from and pass to infinity. In this case Batchelor and Green (1972b) have shown that $p(\underset{\sim}{r})$ is independent of direction so

$$p(\underset{\sim}{r}) = q(r) \tag{8}$$

where $q(r)$ is shown in their Figure 1 and Table 1.

All that remains now is to evaluate the integrals in Batchelor's (1972) equations (3.4), (3.9), and (3.13). Since the unconditioned probability of finding a particle at $\underset{\sim}{x}_o + \underset{\sim}{r}$ equals n, these integrals become

$$\overline{\underset{\sim}{u}}_o = \underset{\sim}{u}_S + \overline{\underset{\sim}{V}}' + \overline{\underset{\sim}{V}}'' + \overline{\underset{\sim}{W}} \tag{9}$$

with

$$\overline{\underset{\sim}{V}}' = n \int_{r\geq 2a} \underset{\sim}{u}(\underset{\sim}{x}_o, \underset{\sim}{x}_o+\underset{\sim}{r})(q(r)-1)d\underset{\sim}{r} - n \int_{r<2a} \underset{\sim}{u}(\underset{\sim}{x}_o,\underset{\sim}{x}_o+\underset{\sim}{r})d\underset{\sim}{r} \tag{10}$$

$$\overline{\underset{\sim}{V}}'' = n \int_{r\geq 2a} \frac{1}{6} a^2\{\nabla^2 \underset{\sim}{u}(\underset{\sim}{x}, \underset{\sim}{x}_o+\underset{\sim}{r})\}_{\underset{\sim}{x}=\underset{\sim}{x}_o} (q(r)-1)d\underset{\sim}{r} \tag{11}$$

$$-n \int_{a<r<2a} \frac{1}{6} a^2\{\nabla^2 \underset{\sim}{u}(\underset{\sim}{x},\underset{\sim}{x}_o+\underset{\sim}{r})\}_{\underset{\sim}{x}=\underset{\sim}{x}_o} d\underset{\sim}{r} + \frac{1}{2} c\underset{\sim}{u}_s$$

and

$$\overline{\underset{\sim}{W}} = n \int_{r\geq 2a} \underset{\sim}{W}(\underset{\sim}{x}_o,\underset{\sim}{x}_o+\underset{\sim}{r})q(r)d\underset{\sim}{r} \tag{12}$$

where

$$\underset{\sim}{W}(\underset{\sim}{x}_o,\underset{\sim}{x}_o+\underset{\sim}{r}) = \underset{\sim}{U}(\underset{\sim}{x}_o,\underset{\sim}{x}_o+\underset{\sim}{r}) - \underset{\sim}{u}_s - \underset{\sim}{u}(\underset{\sim}{x}_o,\underset{\sim}{x}_o+\underset{\sim}{r}) - \frac{1}{6} a^2\{\nabla^2 \underset{\sim}{u}(\underset{\sim}{x},\underset{\sim}{x}_o+\underset{\sim}{r})\}_{\underset{\sim}{x}=\underset{\sim}{x}_o} \tag{13}$$

(The definitions of the various symbols are as in Batchelor (1972) with the exceptions that the symbol for the average settling velocity is now $\overline{\underset{\sim}{u}}_o$ and Batchelor's symbol for the settling velocity of an isolated particle, $\underset{\sim}{U}_o$, is replaced by $\underset{\sim}{u}_s$, the Stokes velocity times $\underset{\sim}{e}$, the vector in the direction of gravity.) For a particle immersed in a pure straining flow, we have

$$\underset{\sim}{u}(\underset{\sim}{x}_o,\underset{\sim}{x}_o+\underset{\sim}{r}) = \underset{\sim}{u}_s(\frac{3a}{4r} + \frac{a^3}{4r^3}) + \underset{\sim}{u}_s\cdot\frac{\underset{\sim}{rr}}{r^2}(\frac{3a}{4r} - \frac{3a^3}{4r^3})$$
$$- (1 - \frac{a^5}{r^5})\underset{\approx}{E}\cdot\underset{\sim}{r} - (\frac{5a^5}{2r^7} - \frac{5a^3}{2r^5})\underset{\sim}{r}\cdot\underset{\approx}{E}\cdot\underset{\sim}{rr} \tag{14}$$

and

$$\{\nabla^2 \underset{\sim}{u}(\underset{\sim}{x},\underset{\sim}{x}_o+\underset{\sim}{r})\}_{\underset{\sim}{x}=\underset{\sim}{x}_o} = \underset{\sim}{u}_s \frac{3a}{2r^3} - \underset{\sim}{u}_s \cdot \frac{\underset{\sim}{\underset{\sim}{rr}}}{r^2} \frac{9a}{2r^3} + 10 \frac{a^3}{r^5} \underset{\approx}{E} \cdot \underset{\sim}{r}$$
$$- 25 \frac{a^3}{2r^7} \underset{\sim}{r} \cdot \underset{\approx}{E} \cdot \underset{\sim}{r}\underset{\sim}{r} \qquad (15)$$

where $\underset{\approx}{E}$ is the rate of strain tensor which is symmetric for a pure straining flow. When these expressions, which are identical to those in sedimentation except for the terms proportional to $\underset{\approx}{E}$, are substituted into the expressions for $\overline{\underset{\sim}{V}}'$and $\overline{\underset{\sim}{V}}''$ above, the terms arising from the shear are proportional to either $\int \underset{\sim}{r} dS$ or $\underset{\approx}{E}:\int \underset{\sim}{r}\underset{\sim}{r}\underset{\sim}{r} dS$ evaluated over the surface of a sphere with radius r. Since both of these integrals vanish, the terms proportional to $\underset{\approx}{E}$ do not contribute to the sedimentation velocity. Although the details will not be given, the same argument applies to the integral for $\overline{\underset{\sim}{W}}$.

Hence, the only effect of the shear is to alter the pair-probability distribution. Since Batchelor (1972) assumed that q(r) = 1 in a quiescent suspension, the difference between his result and that for a suspension undergoing pure straining motion is given by

$$\overline{\underset{\sim}{V}}'_{sh} + \overline{\underset{\sim}{V}}''_{sh} + \overline{\underset{\sim}{W}}_{sh} \qquad (16)$$

where

$$\overline{\underset{\sim}{V}}'_{sh} = n \int_{r \geq 2a} \underset{\sim}{u}(\underset{\sim}{x}_o,\underset{\sim}{x}_o+\underset{\sim}{r})(q(r)-1)d\underset{\sim}{r} \qquad (17)$$

$$\underline{\overline{V}}'_{sh} = n \int_{r\geq 2a} \frac{1}{6} a^2 \{\nabla^2 \underline{u}(\underline{x},\underline{x}_o+\underline{r})\}_{\underline{x}=\underline{x}_o} (q(r)-1)d\underline{r} \tag{18}$$

$$\underline{\overline{W}}_{sh} = n \int_{r\geq 2a} \underline{W}(\underline{x}_o, \underline{x}_o+\underline{r}) \, (q(r)-1)d\underline{r} \tag{19}$$

and where $\underline{W}(\underline{x}_o,\underline{x}_o+\underline{r})$ and $\underline{u}(\underline{x}_o,\underline{x}_o+r)$ are as given in Batchelor (1972). Noting that $\int_s \frac{\underline{r}\underline{r}}{r^2} dS = \frac{4}{3} \pi r^2 \underline{\underline{I}}$ and using Batchelor's (1972) equation (5.6) for $\underline{U}(\underline{x}_o,\underline{x}_o+\underline{r})$, these expressions become

$$\underline{\overline{V}}'_{sh} = \underline{u}_s c \int_{\overline{r}=2}^{\infty} 3\overline{r}(q(\overline{r})-1)d\overline{r} \tag{20}$$

$$\underline{\overline{V}}''_{sh} = 0 \tag{21}$$

$$\underline{\overline{W}}_{sh} = \underline{u}_s c \int_{\overline{r}=2}^{\infty} \{\lambda_1+2\lambda_2-3(1+\frac{1}{\overline{r}})\}(q(\overline{r})-1)\overline{r}^2 d\overline{r} \tag{22}$$

where $\overline{r} = r/a$. The functions $q(\overline{r})$, $\lambda_1(\overline{r})$, and $\lambda_2(\overline{r})$ are known analytically for small separations (lubrication theory) and large $\overline{r}$ (method of reflections) and are tabulated in Batchelor and Green (1972b) and Batchelor (1972) for intermediate values of $\overline{r}$. Evaluating the integrals analytically for $2 \leq \overline{r} \leq 2.0025$ and for $\overline{r} \geq 8$ and numerically using Simpson's rule for the intermediate

values of $\overline{r}$, we find that $\overline{\underset{\sim}{V}}'_{sh} = 2.27\ c\underset{\sim}{u}_s$ and $\overline{\underset{\sim}{W}}_{sh} = -0.24\ c\underset{\sim}{u}_s$. Combining this with the result for quiescent sedimentation, we have

$$\underset{\sim}{u}_o = \underset{\sim}{u}_s(1-c(6.55-2.03) + O(c^2)). \tag{23}$$

or

$$\underset{\sim}{u}_o = \underset{\sim}{u}_s(1-4.52c + O(c^2)). \tag{24}$$

Hence, the pure extensional flow increases the sedimentation velocity. This effect occurs because as the shear forces the particles to flow past each other, their relative velocity decreases when they are close together. Thus, on the average the shear causes the particles to spend a greater fraction of their time close to a neighbor, and since the settling velocity of the pair is greater when the particle spacing is small, the average sedimentation velocity increases.

Two major problems are apparent with this approach. First, in determining $\underset{\sim}{V}_R$, the relative velocity between the centers of two particles, we have neglected the effects of all the other particles in the suspension. As mentioned earlier, however, in the limit of no shear multiparticle hydrodynamic interactions result in the particles becoming "well-spaced" with q(r) varying over a length scale of $O(ac^{-1/3})$ rather than of O(a) as we find above for a sheared suspension. Since the present method cannot easily be extended to include multiparticle interactions, the particle arrangement is controlled solely by the shear, i.e., the shear is on or it is off, and the settling velocity is independent of the shear rate. In reality one would expect a competition between these effects with their relative importance being given by the dimensionless shear rate $\gamma^* = \gamma a/u_s$. When this parameter is small, we

should have $\underset{\sim}{u}_o=\underset{\sim}{u}_s(1-0.75c^{1/3} + o(c))$ (cf. Lynch and Herbolzheimer 1985a), and when it is asymptotically large, $\underset{\sim}{u}_o=\underset{\sim}{u}_s(1-4.5c + o(c))$. Unfortunately, the intermediate range of $\gamma^*$ cannot be treated using the present technique. We note that the importance of multiparticle interactions greatly amplifies the significance of the increase in the sedimentation velocity at small concentration caused by the shear.

Another problem with this approach is that it is difficult to apply when some particle streamlines are closed as they are in the physically important case of a simple shear flow. In this case, if only pair interactions are considered in determining $\underset{\sim}{V}_R$, $p(\underset{\sim}{r})$ always depends on the initial conditions in the suspension and never reaches a steady state. Modifying the method to eliminate these unphysical results would require including some other effect (e.g., Brownian motion or multiparticle hydrodynamic interactions), which although possibly small compared to the effect of the shear, could cause migration across particle streamlines. In suspensions of relatively large particles (greater than 5μm), the multiparticle hydrodynamic interactions would most likely be the important effect. Since this effect is again hard to include in the calculations, let us turn to experiments.

## 3. Experimental

Because of the difficulties involved in extending the theory to determine the dependence of the sedimentation velocity on dimensionless shear rate and shear type, we have investigated the importance of these effects by measuring the sedimentation velocity of a suspension of spheres in the simple shear flow created by a Couette device. These experiments had four goals: to confirm that the sedimentation velocity did increase with shear; to determine the dependence of the sedimentation velocity on the volume fraction of particles and the dimensionless shear rate; to check whether the result which holds for asymptotically large shear rates in a pure straining flow also holds for asymptotically large shear rates in a simple shear flow; and to determine whether the dimensionless group $\frac{\gamma a}{u_s}$ representing the time scale for settling to the time scale for shearing is the correct dimensionless shear rate for use in constitutive relations for $u_o$.

The experiments were conducted in a cylindrical Couette device (see Figure 1) in which the outer cylinder (a precision-bore glass tube with an inner diameter of 4.5 in) was rotated while the inner cylinder (a solid anodized aluminum rod with a diameter of 3.98 in) was held fixed. With these inner and outer radii, the shear rate varied across the gap by about $\pm 12\%$ from the average shear rate. The inner cylinder was held stationary to prevent the formation of clear fluid there due to radial settling of the particles resulting from the centrifugal force. If pure fluid were formed at the inner cylinder, it would rapidly rise creating a convection current which would enhance the sedimentation rate much as in a vessel with inclined walls (see,

for example, Acrivos and Herbolzheimer (1979)). A teflon ring attached to the bottom of the inner cylinder precluded the formation of clear fluid under the rotor. Eliminating the formation of clear fluid at the inner cylinder and underneath the rotor was important because the sedimentation velocity was measured by observing the rate of fall of the suspension--clear fluid interface with a cathetometer; therefore, clear fluid formed at the inner cylinder would have erroneously enhanced the observed settling velocity of the suspension. Also to prevent the introduction of inclined-settling effects, the walls of the device were very carefully aligned parallel to the direction of gravity; the alignment was then tested in quiescent settling experiments.

The suspension consisted of glass spheres in UCON oils LB-385 ($\mu$=1.78P, $\rho$=.99 $\frac{g}{cm^3}$ at T=22°C) and 50-HB-400 ($\mu$=1.85P, $\rho$=1.04 $\frac{g}{cm^3}$ at 22°C) and in a mixture of UCON oils 50-HB-400 and 50-HB-2000 ($\mu$=3.82P, $\rho$=1.04 $\frac{g}{cm^3}$ at 22°C). Two different types of glass spheres were used for different experiments. The first set of particles had a density of 2.69 $\frac{g}{cm^3}$ and an effective particle radius of 52.5$\mu$m*. The second set of particles, filtered in an air-fluidized bed to narrow the range of size differences between the particles, had a density of 2.80 $\frac{g}{cm^3}$ and an effective particle radius of 51$\mu$m. The ratio of the particle radius to the gap width in the experiments was approximately 120; in test experiments with different gap-to-radius ratios, this ratio resulted in

---

*The effective particle radius, obtained by extrapolating the results for the settling velocity in a large beaker back to infinite dilution, matched within a few microns the mean radius obtained from a photograph of the particles.

no observable difference in the rate of fall of the interface from experiments with much larger ratios.

Two secondary effects could have influenced the results of the experiments if we had not been careful to minimize their importance. First, since the no-slip boundary condition at the bottom of the device is not equivalent to the free-surface condition at the top of the device, a small secondary flow appears. Because the effect of this secondary flow is assumed small at fluid points whose height above the bottom of the device is sufficiently large when compared to the gap size, we filled the device with suspension to an initial height of 10 in and only allowed the suspension to settle approximately halfway down the device.

Another potential problem is that under sufficiently rapid shearing the centrifugal force on the particles can be strong enough to change the particle volume fraction in the suspension; consequently, we must fix a maximum shear rate for the experiments below which the concentration changes only a few percent from the initial concentration. Otherwise, the measured sedimentation velocity would not reflect the actual sedimentation velocity at the initial volume fraction and shear rate. By using the particle continuity equation to calculate the concentration profiles in the device as a function of time (see Appendix 1), we may estimate the magnitude of the concentration change for a given shear rate and decide upon a maximum shear rate for the experiments. From Appendix 1 an estimate of the maximum dimensionless shear rate is

$$\gamma^* = \frac{\gamma a}{u_s} < 16.2. \tag{25}$$

The procedure of the experiments was as follows. The suspension was mixed thoroughly in a large beaker, and the settling velocity was measured in the beaker. After the suspension had settled 2-2.5cm, the suspension was remixed and poured into the device. The sedimentation velocity of the suspension was then measured with the shear off until the suspension had settled a distance of about 2cm. The shear was then turned on, and the settling velocity was observed for an additional 2-2.5cm. Finally the shear was turned off, and the quiescent settling velocity in the device was remeasured. The temperature of the suspension was measured at the beginning and end of each of these four steps in the procedure. Although for a truly monodisperse suspension the three measurements of the settling velocity without shear would all be identical, in the slightly polydisperse suspensions of these experiments this result was not necessarily true. A detailed explanation for why this occurs is furnished in Appendix 2.

## 4. Results and Discussion

Let us first consider the results for the effect of the volume fraction of particles upon the sedimentation velocity at asymptotically large shear rates. Since the filtered particles were less polydisperse than the unfiltered particles, the experiments with filtered particles showed less spreading of the interface at lower volume fraction (for an explanation see Appendix 2) and thus could be performed over a wider range of c. Hence, when examining the effect of c on the settling velocity at asymptotically large shear rates, we present only the results of the experiments with the filtered particles; however, the behavior of the settling velocity in the experiments with unfiltered particles was very similar.

In Figure 2 we plot the sedimentation velocity as a function of particle volume fraction for shear rates which are asymptotically large. Obviously the measurements of the settling velocity in a sheared suspension seem to follow the theoretical result for a pure straining flow for $c < .14$ and the correlation of Barnea and Mizrahi (1973) for quiescent suspensions for $c > .14$. The measurements of the settling velocity in a quiescent suspension follow the quiescent correlation except for small c where the effects of polydispersity are important. The result that the first correction to the Stokes settling velocity is proportional to O(c) for dilute, sheared suspensions is quite significant because it implies both a dramatic increase in the sedimentation velocity from the quiescent result and a pair-probability function dependent on a length scale of O(a), not a length scale of $O(ac^{-1/3})$.

Next we consider the behavior of the settling velocity at constant c and shear rates less than the asymptotic limit. In Figure 3 we present results for the sheared sedimentation velocity divided by the sedimentation velocity in the device before shearing as a function of dimensionless shear rate at three

different volume fractions: $c = .08$, $.10$, and $.14$. The value of the shear rate used is that of the bulk average shear rate in the device. The 10% suspension consisted of unfiltered particles whereas the 8% and 14% suspensions consisted of filtered particles. (Normalizing the sheared sedimentation velocity by the quiescent sedimentation velocity in the device partially eliminates from the results the effect of variation in the particle size distribution between experiments and in the initial volume fraction between experiments and between different parts of the suspension.) Because of the polydispersity of the particles, the interface became very diffuse as the experiments proceeded, and the measurements of $u_o$ show a large degree of scatter. However, the measurements of $u_o$ at $c = .08$ and $.10$ are of sufficient accuracy to show a definite decline in the settling velocity as the shear rate is decreased to zero. At $c = .14$ apparently $u_o$ is independent of the shear rate. Thus for dilute suspensions some competition does seem to exist between the effects of shear and sedimentation; however, we could not establish a constitutive relation for $u_o = u_s f(c, \gamma^*)$ because of the scatter in the data and because of the difficulty in producing a steady shear rate with the present Couette device with $\gamma^* < .5$ .

To examine whether $\gamma^* = \frac{\gamma a}{u_s}$ is the appropriate dimensionless shear rate for use in constitutive relations for $u_o$, we have plotted in Figure 4 $u_o$ versus $\gamma^*$ for two different suspensions with $c = .08$, one with a value of $\frac{u_s}{a}$ of 1.14 $sec^{-1}$ and one with a value of $\frac{u_s}{a}$ of .55 $sec^{-1}$. Although the settling velocity at the same value of $\gamma^*$ for the two suspensions is roughly equal, the large amount of scatter in the data makes any substantive conclusions impossible.

Furthermore, the data seem to indicate that the degree of experimental accuracy required to establish what the appropriate dimensionless shear rate is may well be above the degree of accuracy which can be attained through the present experimental method.

## 5. Conclusions

Shear indeed does increase the sedimentation velocity of dilute, monodisperse suspensions of spheres; in fact, under conditions of sufficiently rapid shearing, the sedimentation velocity measured in a simple shear flow is that calculated for a pure straining flow. For a suspension with $c \cong .1$ in a simple shear flow, reaching the condition of asymptotically large shear rate within 5% requires a dimensionless shear rate $\gamma^* = \frac{\gamma a}{u_s}$ of about 9. Translated into dimensional terms for particles of radius 50μm and of Stokes velocity .34 $^{cm}/_{min}$, $\gamma$ is about 10 $^{radians}/_{sec}$. The experiments described here are rather tedious and difficult, and a large degree of scatter exists in the measured sedimentation velocities; however, because they demonstrate that shear has an effect on the microscale structure of sedimenting suspensions, they can serve as a basis for more exact light-scattering experiments.

Acknowledgement The authors wish to recognize the help of Thomas Remmers, who helped carry out many of the experiments described here.

## Appendix 1. Calculation of the concentration change during a typical experiment

To estimate the concentration change in the Couette device due to the centrifugal force on the particles in the suspension, we use the particle continuity equation

$$\frac{\partial c}{\partial t} + \underset{\sim}{V}_p \cdot \nabla c = -c\nabla \cdot \underset{\sim}{V}_s \tag{26}$$

in which $\underset{\sim}{V}_p$ is the velocity of an average particle in the suspension, and $\underset{\sim}{V}_s$ is the slip velocity, the difference between the average particle velocity and average bulk velocity of the suspension. We assume that the slip velocity is in the local direction of the body force and is a function of the local volume concentration and shear rate (i.e.,

$$\underset{\sim}{V}_s = u_s f(c(R), \gamma^*(R))\underset{\sim}{e} \tag{27}$$

where $\underset{\sim}{e}$ is the vector $\left[-1, \frac{\omega^2(R)R}{g}, 0\right]$ in a cylindrical coordinate system ($\hat{z}$, $\hat{R}$, $\hat{\theta}$) aligned with the cylinder axis, R is the radial distance from the center of the device, $\omega(R)$ is the angular velocity of the suspension at some radius R, and $\gamma^*(R)$ is the dimensionless shear rate, $\gamma(R)a/u_s$, at some radius R.) Furthermore, we assume that no secondary flows occur in the device and that no bulk suspension flow occurs in either the radial or the vertical directions; therefore, the slip velocity and particle velocity are identical in these directions.

After substitution for the well-known profiles for $\omega(R)$ and $\gamma^*(R)$ in an infinite-length Couette device, the particle continuity equation becomes

$$\frac{\partial c}{\partial \tilde{t}} + Af\left(\frac{(\tilde{R}^2-1)^2}{\tilde{R}^3}\right)\frac{\partial c}{\partial \tilde{R}} = -Ac\left(\frac{(\tilde{R}^2-1)^2}{\tilde{R}^3}\right)\left(\frac{\partial f}{\partial c}\right)_{\gamma^*}\frac{\partial c}{\partial \tilde{R}} + 2A\gamma_i^* c\left(\frac{(\tilde{R}^2-1)^2}{\tilde{R}^6}\right)\left(\frac{\partial f}{\partial \gamma^*}\right)_c - 2Afc\left(\frac{\tilde{R}^4-1}{\tilde{R}^4}\right) \tag{28}$$

in which $\tilde{t}$ is the dimensionless time, $\frac{tu_s}{\ell}$, $\ell$ is 2cm, the vertical distance travelled by particles during an experiment; A is $\frac{\chi^4}{(\chi^2-1)^2}\frac{\Omega^2\ell}{g}$, the ratio of the lateral acceleration of the particles to the vertical acceleration; $\Omega$ is the rotation speed of the outer cylinder in radians per second; $\tilde{R}$ is R divided by $R_i$, the radius of the inner cylinder; $\chi$ is 1.13, the ratio of the outer-cylinder radius to the inner-cylinder radius; and $\tilde{\gamma}_i^*$ is $\frac{2\chi^2}{\chi^2-1}\frac{\Omega a}{u_s}$, the dimensionless shear rate at the inner cylinder. The left-hand side of equation 28 represents the change in c along a particle streamline whereas the right-hand side consists of forcing terms, which arise because in a rotating fluid the slip velocity is not independent of position. The sum of the first two terms on the right-hand side represents how the slip velocity changes due to concentration and shear rate changes in the radial direction. The third term is the result of the change in the direction of the body force as a function of $\tilde{R}$.

We have solved equation 28 for $c(\tilde{R},\eta(\tilde{t},\tilde{R}))$ by the method of characteristics. The characteristics are given in terms of the characteristic variable $\xi$ by

$$\left(\frac{d\tilde{R}}{d\xi}\right)_\eta = A\,\frac{(\tilde{R}^2-1)^2}{\tilde{R}^3}\,\frac{\partial}{\partial c}\,(fc)_{\gamma^*} \tag{29}$$

$$\left(\frac{d\tilde{t}}{d\xi}\right)_\eta = 1\ . \tag{30}$$

The differential equation in characteristic variables is therefore

$$\left(\frac{dc}{d\xi}\right)_\eta = A\left[-2fc\,\frac{\tilde{R}^4-1}{\tilde{R}^4} + 2\tilde{\gamma}_1^*\,\frac{(\tilde{R}^2-1)^2}{\tilde{R}^6}\,c\,\frac{\partial f}{\partial \gamma^*}_{c}\right] \tag{31}$$

If the initial concentration is uniform for $1 \le \tilde{R} \le 1.13$ and equal to $c_o$, then an appropriate initial condition is specifying $c = c_o$ along the parametric curve $t = 0$, $\tilde{R} = \eta$, $1 < \eta \le 1.13$. Since the inner cylinder does not rotate, the wall of the inner cylinder is a characteristic, and no boundary condition is needed at $\tilde{R} = 1$. The general solution to this problem is

$$\tilde{t} = \frac{1}{A}\int_\eta^{\tilde{R}} \frac{\tilde{R}^3 d\tilde{R}}{(\tilde{R}^2-1)^2}\left[\frac{1}{\frac{\partial}{\partial c}\,(fc)_{\gamma^*}}\right],\quad c = c(\tilde{R},\eta) \tag{32}$$

$$\frac{f(c,\gamma^*(\tilde{R}))c}{f(c_o,\gamma^*(\tilde{R}))c_o} = \left[\left(\frac{\eta^2-1}{\tilde{R}^2-1}\right)\frac{\tilde{R}}{\eta}\right]^2 \tag{33}$$

Determining $c\,(\tilde{R},\tilde{t})$ in more detail requires specifying f, the constitutive relation for the slip velocity. If the suspension is dilute and is being

sheared extremely rapidly, then f is approximately 1 - 4.52c. (Rapid shearing of the suspension causes the largest possible body force changes, and thus the largest concentration changes possible in the device.) If $c_o$ is small, then equations 16 and 17 simplify in the case of rapid shearing to

$$\frac{c}{c_o} = \left[\frac{\eta^2-1}{\tilde{R}^2-1}\,\frac{\tilde{R}}{\eta}\right]^2 (1-4.52c_o) + 4.52c_o\left[\frac{\eta^2-1}{\tilde{R}^2-1}\,\frac{\tilde{R}}{\eta}\right]^4 + O(c_o^2) \tag{34}$$

$$\tilde{At} = \frac{1}{2}\left[\frac{\tilde{R}^2-\eta^2}{(\tilde{R}^2-1)(\eta^2-1)} + \ln\left[\frac{\tilde{R}^2-1}{\eta^2-1}\right]\right] + 1.51c_o\left[\left(\frac{\eta^2-1}{\eta}\right)^2\left[\frac{\eta^6}{(\eta^2-1)^3} - \frac{\tilde{R}^6}{(\tilde{R}^2-1)^3}\right]\right] + O(c_o^2)\,. \tag{35}$$

For the typical experimental value of .08 for $c_o$, Figure 5 shows the isoconcentration curves as a function of $\tilde{At}$ and $\tilde{R}$. If we require that the average volume concentration at the conclusion of the experiment differ by at most 10% from the initial concentration (so that the average settling velocity at the conclusion of the experiment differs by at most 6% from the initial settling velocity), then from Figure 5

$$\tilde{At} = \frac{u_s t_f}{\ell}\,\frac{\chi^4}{(\chi^2-1)^2}\,\frac{\Omega^2\ell}{g} < .3 \tag{36}$$

where $t_f$, the time required for an experiment is $\frac{\ell}{u_o}$. Since we measure the shear rate in the experiments by the bulk average shear rate in a very long Couette device (i.e.,

$$\bar{\gamma} = \frac{4\chi^2 \ln\chi}{(\chi^2-1)^2}\,\Omega = 8.14\Omega\,, \tag{37}$$

we find, after rearranging terms, that equation 36 becomes

$$\gamma^* < \frac{4a\ln\chi}{u_s(\chi^2-1)}\sqrt{\frac{.3gu_o}{\ell u_s}}\,. \tag{38}$$

Choosing $a = 51\mu m$, $\rho_s - \rho = 1.76\ \frac{g}{cm^3}$, $\mu = 1.85$ P, and $c_o = .08$ as typical values of these parameters, we have

$$\gamma^* = \frac{\gamma a}{u_s} < 16.2\,. \tag{39}$$

## Appendix 2. Effect of polydispersity upon measurement of the settling velocity

For a monodisperse sedimenting suspension, a sharp interface forms between the suspension and the clear fluid above it because particles which "fall behind" the interface find themselves in a region without other particles and therefore settle faster. On the other hand, in a polydisperse suspension smaller particles with smaller Stokes velocities can settle slower than a typical particle in the suspension, altering the sharp interface of a monodisperse suspension into a broad band in which the concentration changes from the bulk suspension concentration to zero. This effect is more apparent for smaller concentrations, where the difference between the observed settling velocity of the suspension and the Stokes settling velocity of a typical particle is very small.

In the experiments the settling velocity was measured by making the particles appear light against a dark background and observing as a function of time the point in this band at which the suspension became visually opaque. Two different people carried out the experiments described here, and their judgments about where the suspension became visually opaque did not always agree; however, because the effective radius of the particles was determined from the experiments and because measuring different points on the interface corresponds roughly to measuring the settling velocity of different size particles, this should not be a major difficulty. Because the radius of the beaker was much greater than the gap size, viewing the suspension in the beaker meant peering through many more particles than in the device; consequently, in the device the point of visual opacity was different, slightly larger particles seemed to define the interface, and the measured settling

velocity was slightly greater than in the beaker. This problem was alleviated by assuming the particles in the device had a slightly larger effective radius and correspondingly larger Stokes velocity than the particles in the beaker. This explanation for why the settling velocity in the beaker was different was confirmed by measuring the settling velocity in the beaker with and without a black plate inserted vertically into the suspension in order to simulate the effect of the small gap of the device.

The fact that the settling velocity in the device was not always the same after shearing as it was before shearing can be explained as follows. Because shearing the suspension made the difference between the suspension settling velocity and the Stokes velocity of a typical suspension particle smaller, the interface generally became more diffuse upon shearing. After the shear was turned off, this difference increased, and the interface became less diffuse as it readjusted to the new conditions; because the interface position was difficult to measure during this transient readjustment period, a corresponding error was made in determining the settling velocity after shearing.

References

Acrivos, A. and Herbolzheimer, E. 1979 Enhanced sedimentation in settling tanks with inclined walls. J. Fluid Mech., 92, 435-57.

Barnea, E. and Mizrahi, J. 1973 A generalized approach to the fluid dynamics of particulate systems. Part 1. General correlation for fluidization and sedimentation in solid multiphase systems. Chem. Eng. J. 5, 171-189.

Batchelor, G.K. 1972 Sedimentation in a dilute dispersion of spheres. J. Fluid Mech. 52, 245-268.

Batchelor, G.K. and Green, J.T. 1972a The hydrodynamic interaction of two small freely-moving spheres in a linear flow field. J. Fluid Mech. 56, 375-400.

Batchelor, G.K. and Green, J.T. 1972b The determination of the bulk stress in a suspension of spherical particles to order $c^2$. J. Fluid Mech. 56, 401-427.

Hasimoto, H. 1959 On the periodic fundamental solutions of the Stokes equations and their application to viscous flow past a cubic array of spheres. J. Fluid Mech. 5, 317-328.

Lynch, E.D. and Herbolzheimer, E. 1985 Sedimentation in quiescent suspensions. (To be submitted - Chapter 1 of this thesis).

Sangani, A.S. and Acrivos, A. 1982 Slow flow through a periodic array of spheres. Int. J. Multiphase Flow 8, 343-360.

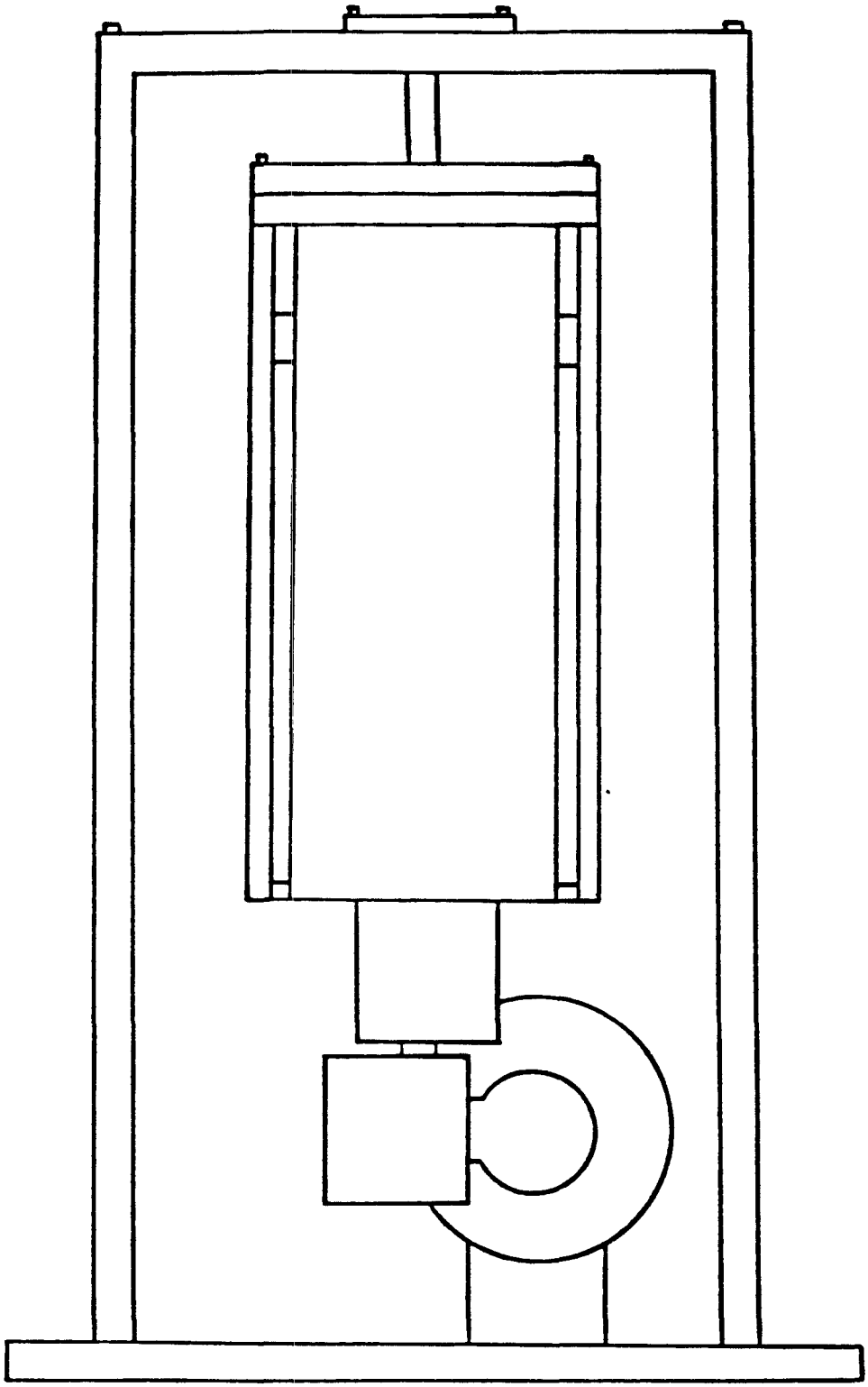

Figure 1. Couette device for sedimentation experiments.

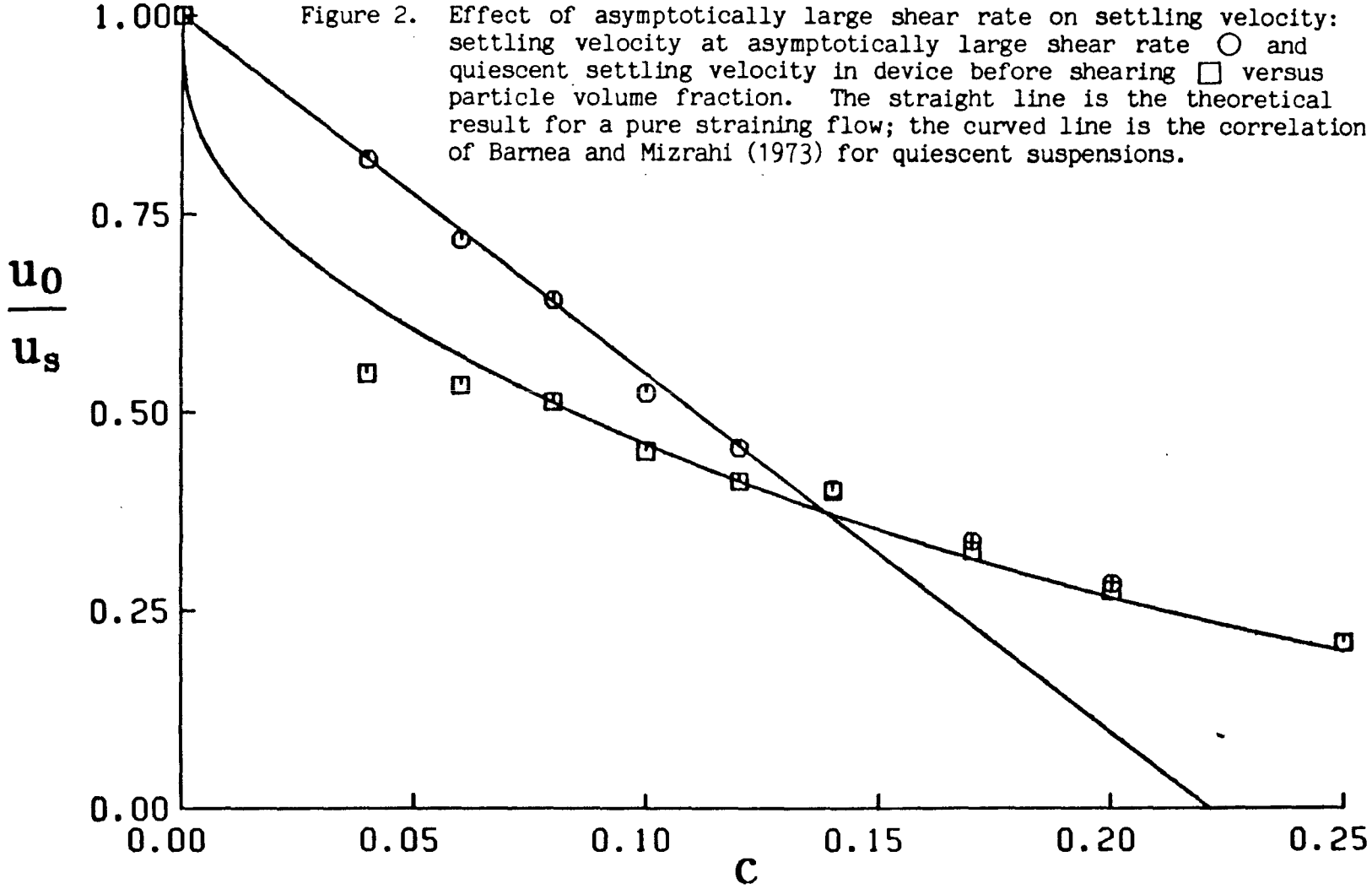


Figure 2. Effect of asymptotically large shear rate on settling velocity: settling velocity at asymptotically large shear rate ○ and quiescent settling velocity in device before shearing □ versus particle volume fraction. The straight line is the theoretical result for a pure straining flow; the curved line is the correlation of Barnea and Mizrahi (1973) for quiescent suspensions.

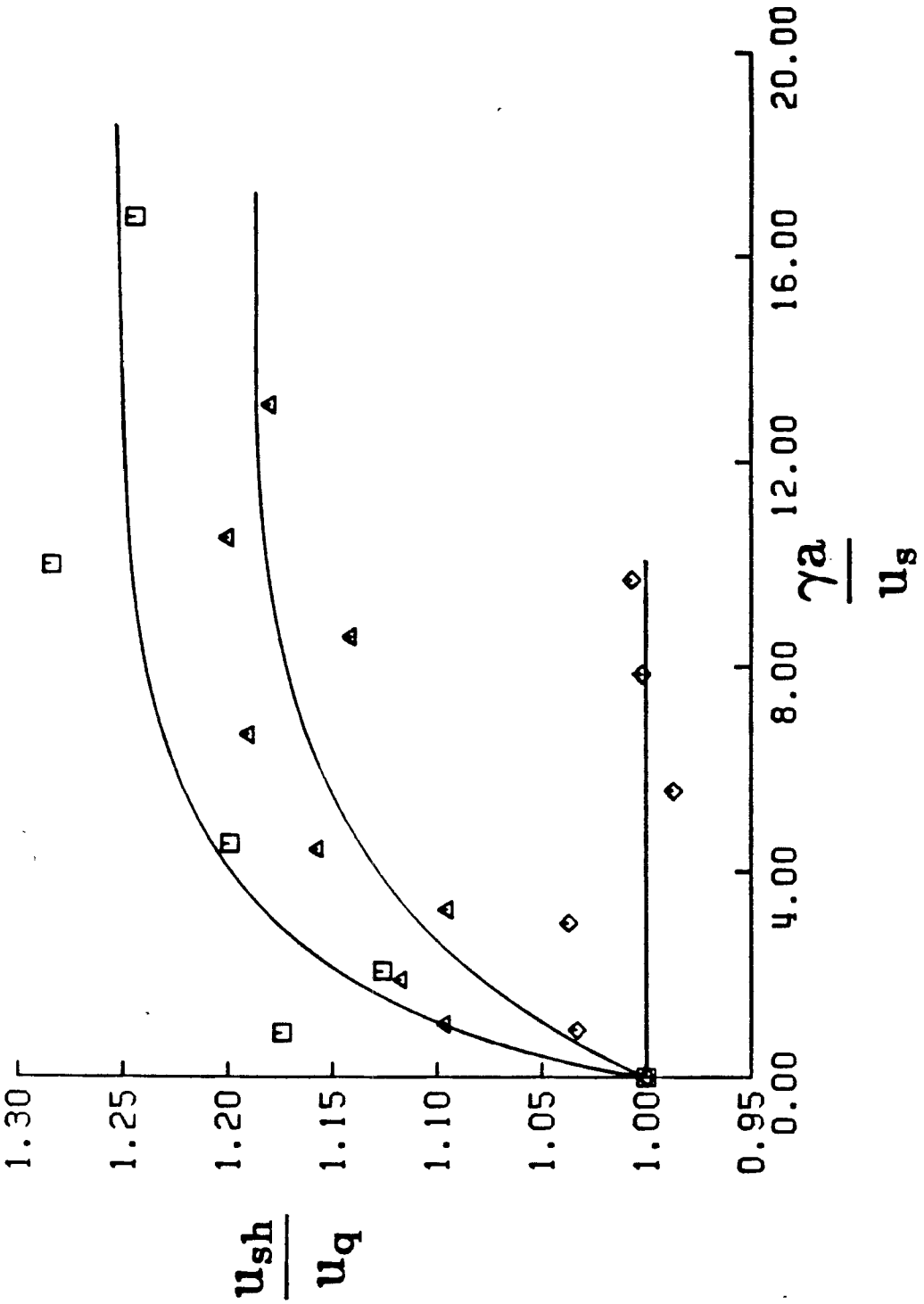


Figure 3. Sheared settling velocity divided by quiescent settling velocity in device versus dimensionless shear rate for three different particle volume fractions: □ - .08, △ - .10, ◇ - .14.

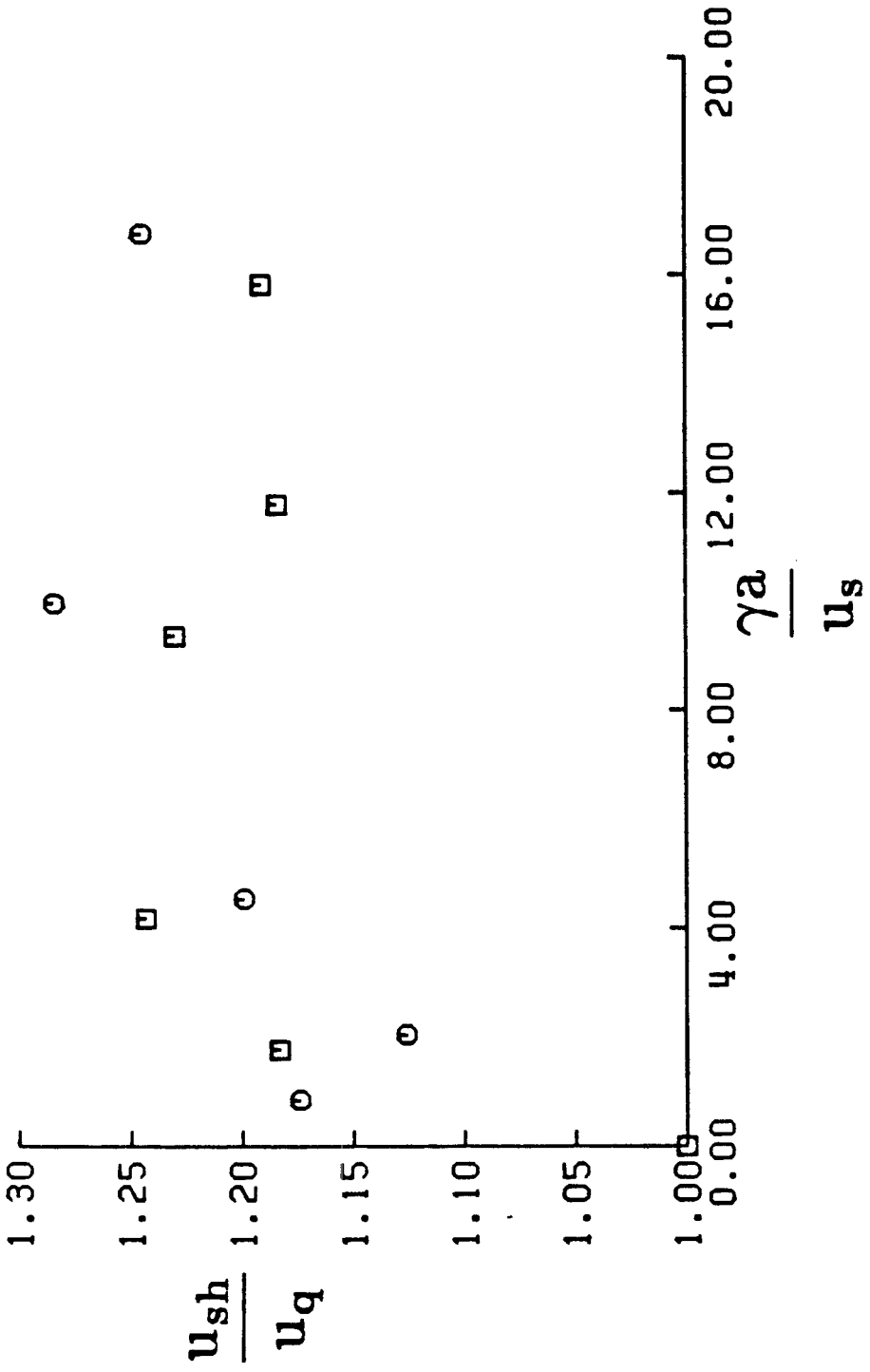


Figure 4. Sheared settling velocity divided by quiescent settling velocity in device versus dimensionless shear rate for two different suspensions: ○ - $u_s/a = 1.14 sec^{-1}$, □ - $u_s/a = .55 sec^{-1}$.

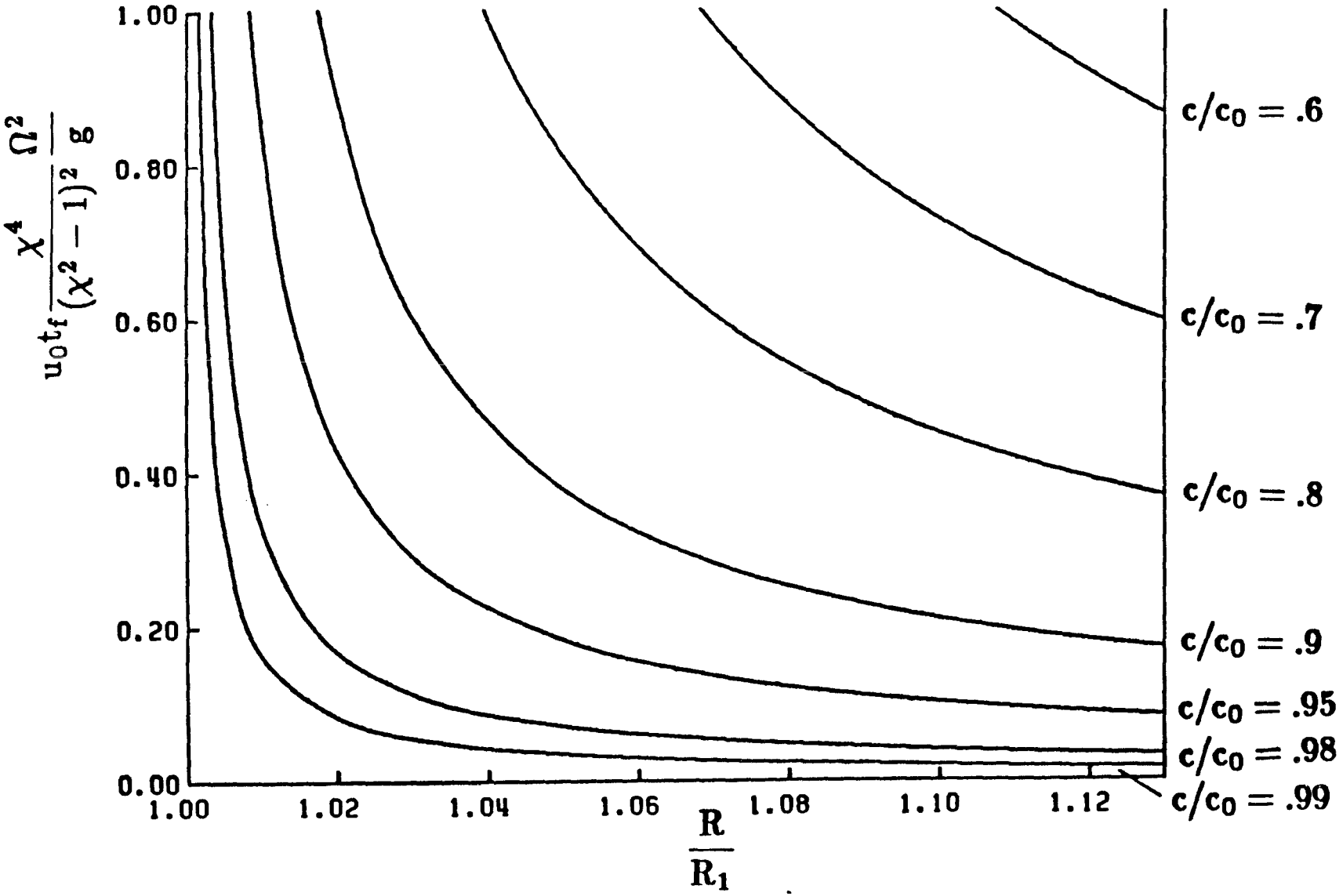


Figure 5. Isoconcentration curves in Couette device for various values of $c/c_0$.

# APPENDIX

**APPENDIX 1:** Additional plots of the $O(c^{1/3})$ coefficient in the expansion for the average sedimentation velocity versus time.

Appendix 1 shows how the $O(c^{1/3})$ coefficient varies with time for the five simulation runs for which results were not presented in Chapter 1. The method of calculating the $O(c^{1/3})$ coefficient is identical to that in Chapter 1.

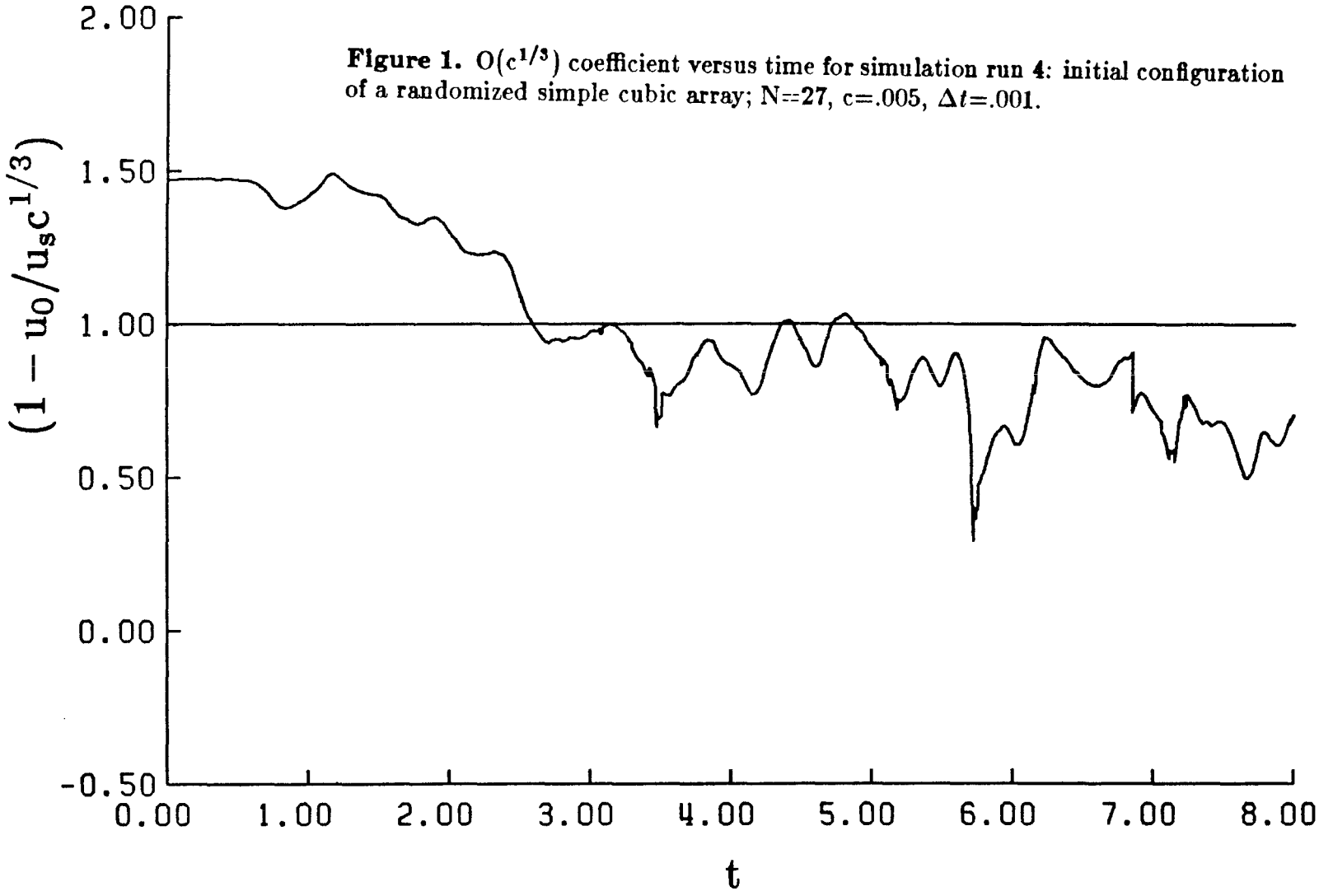


**Figure 1.** $O(c^{1/3})$ coefficient versus time for simulation run 4: initial configuration of a randomized simple cubic array; N=27, c=.005, $\Delta t$=.001.

**Figure 2.** $O(c^{1/3})$ coefficient versus time for simulation run 5: initial configuration of a random suspension; N=64, c=.005, $\Delta t$=.001.

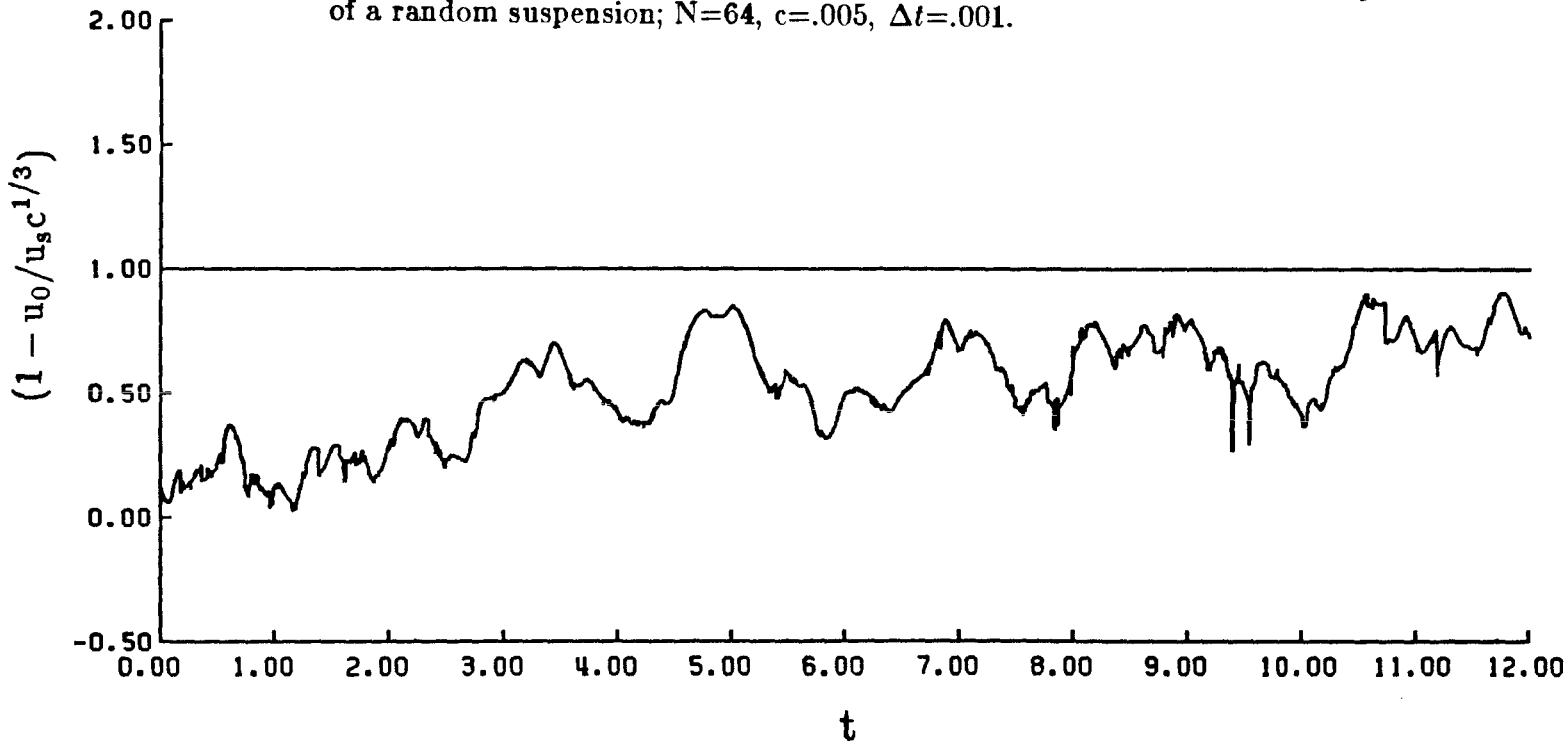

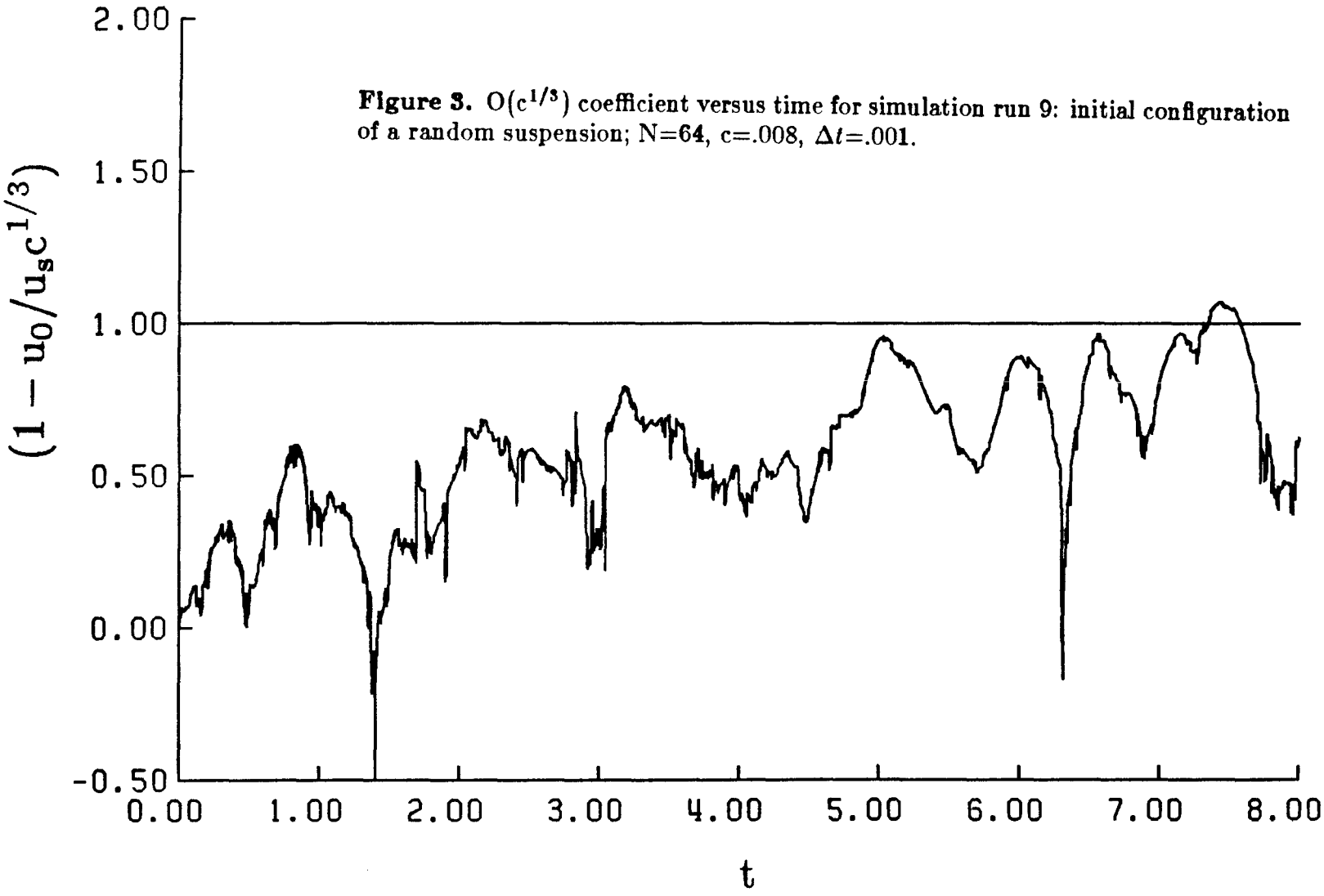


**Figure 3.** $O(c^{1/3})$ coefficient versus time for simulation run 9: initial configuration of a random suspension; N=64, c=.008, $\Delta t$=.001.

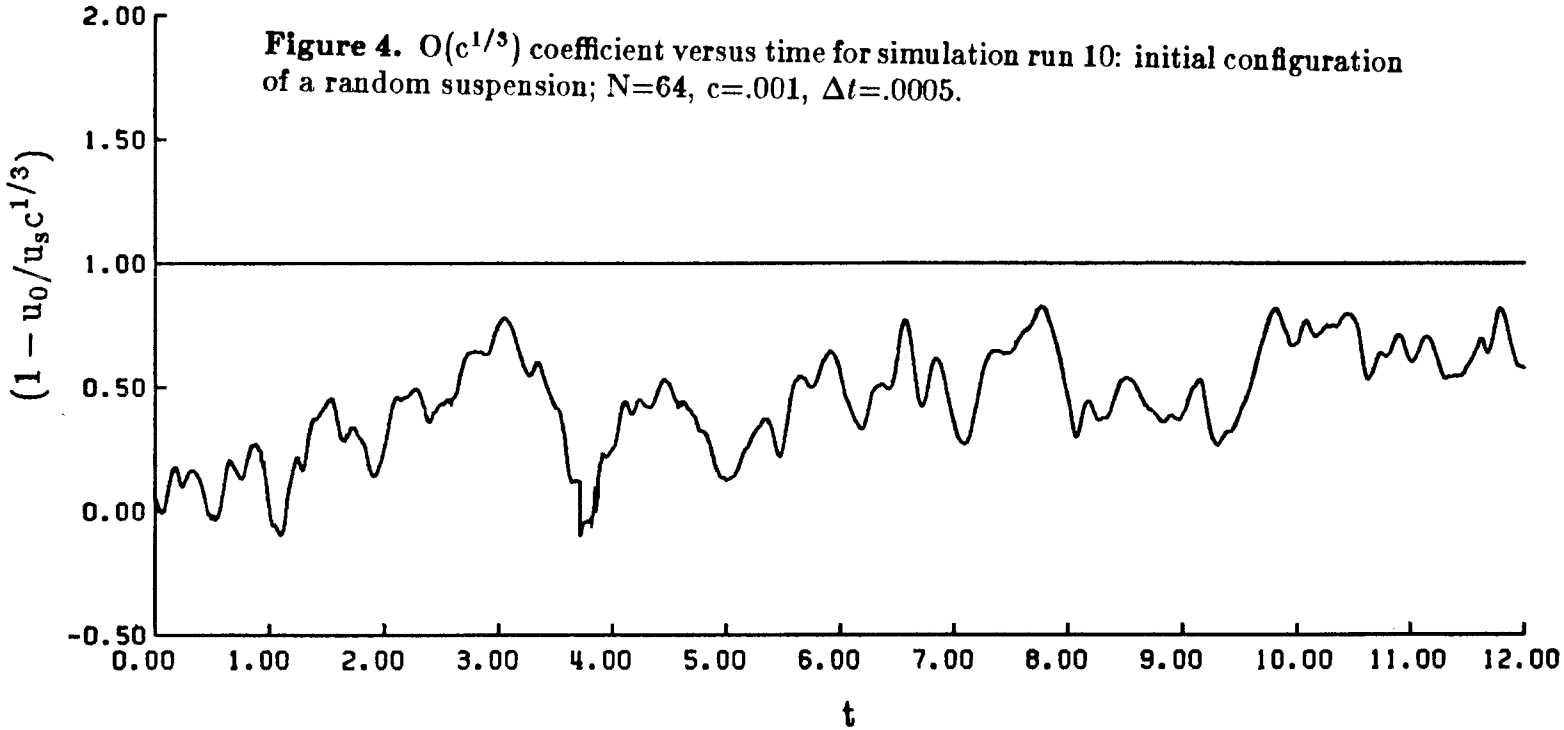


**Figure 4.** $O(c^{1/3})$ coefficient versus time for simulation run 10: initial configuration of a random suspension; N=64, c=.001, $\Delta t$=.0005.

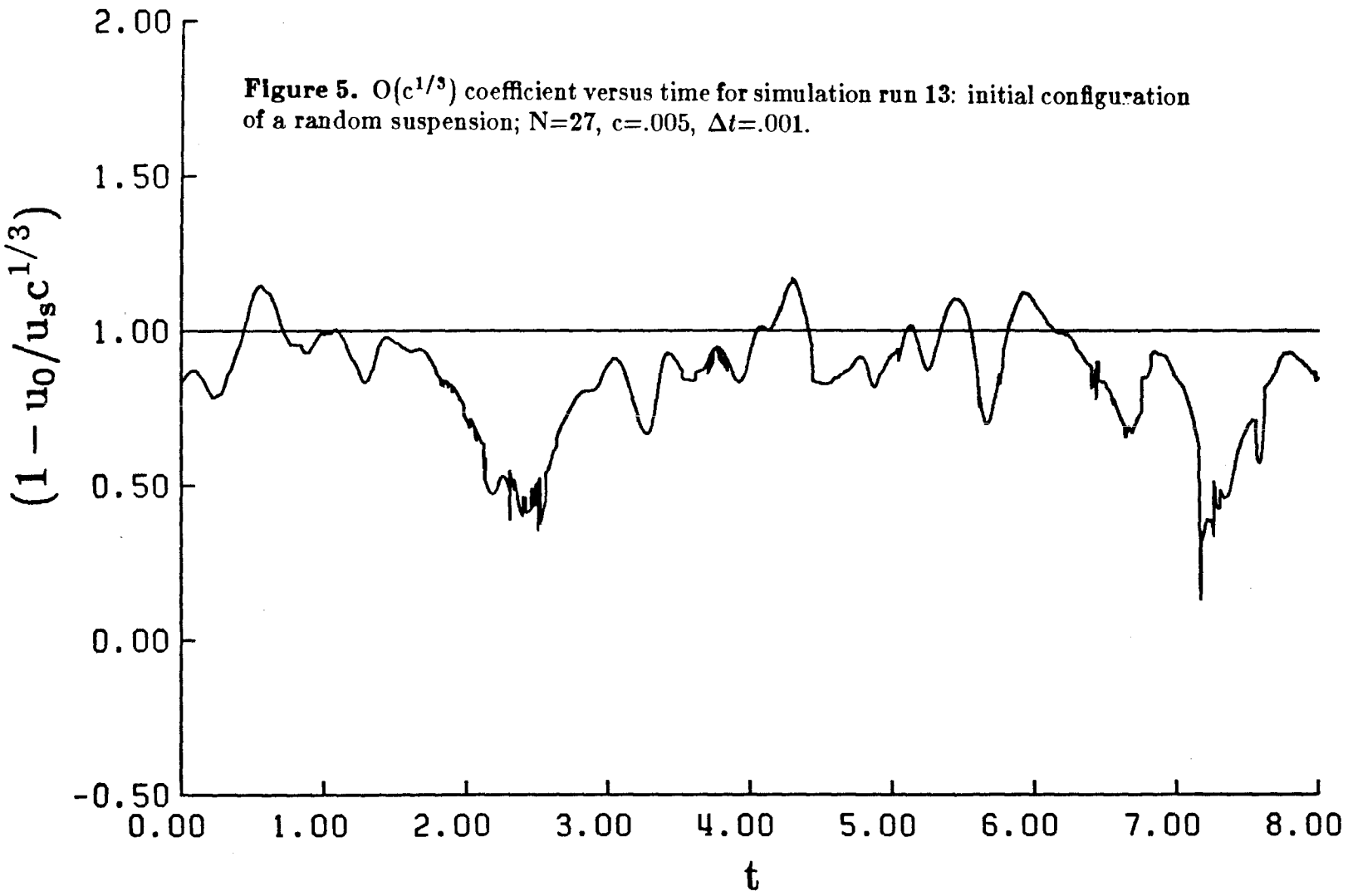


**Figure 5.** $O(c^{1/3})$ coefficient versus time for simulation run 13: initial configuration of a random suspension; N=27, c=.005, $\Delta t$=.001.

**APPENDIX 2:** Additional plots of the time-averaged pair-probability function

Appendix 2 presents additional results for the time-averaged pair-probability function. The meaning of the plots and the method of calculating g(r) are both identical to those in Chapter 1 except that now two sets of spherical shells are used to calculate g(r). The second set of shells, represented in the plots by squares, has a gap distance exactly half that of the original set of shells.

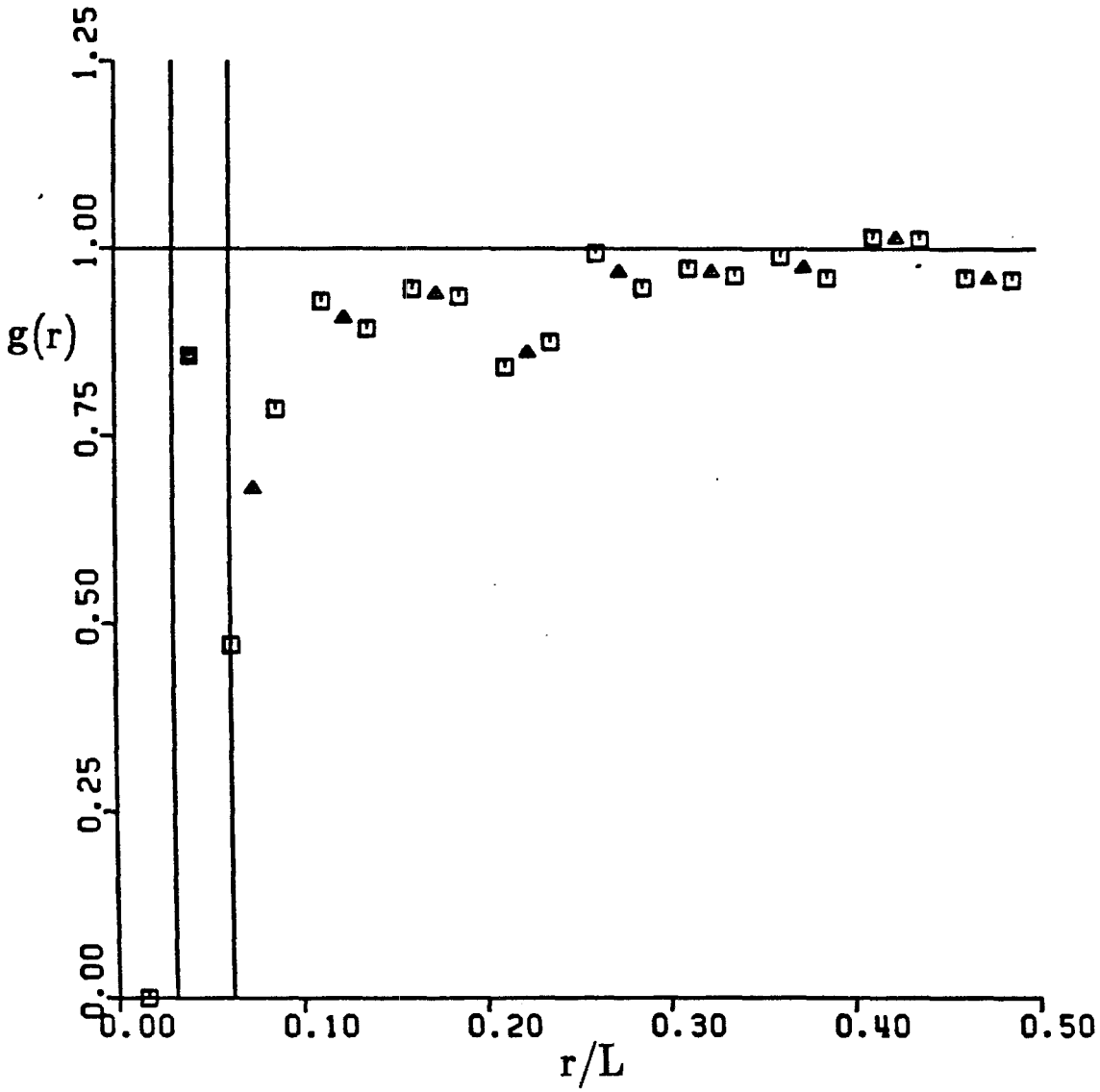


**Figure 6.** Pair-probability function for simulation run 2 averaged from t=2.4 to 6.0.

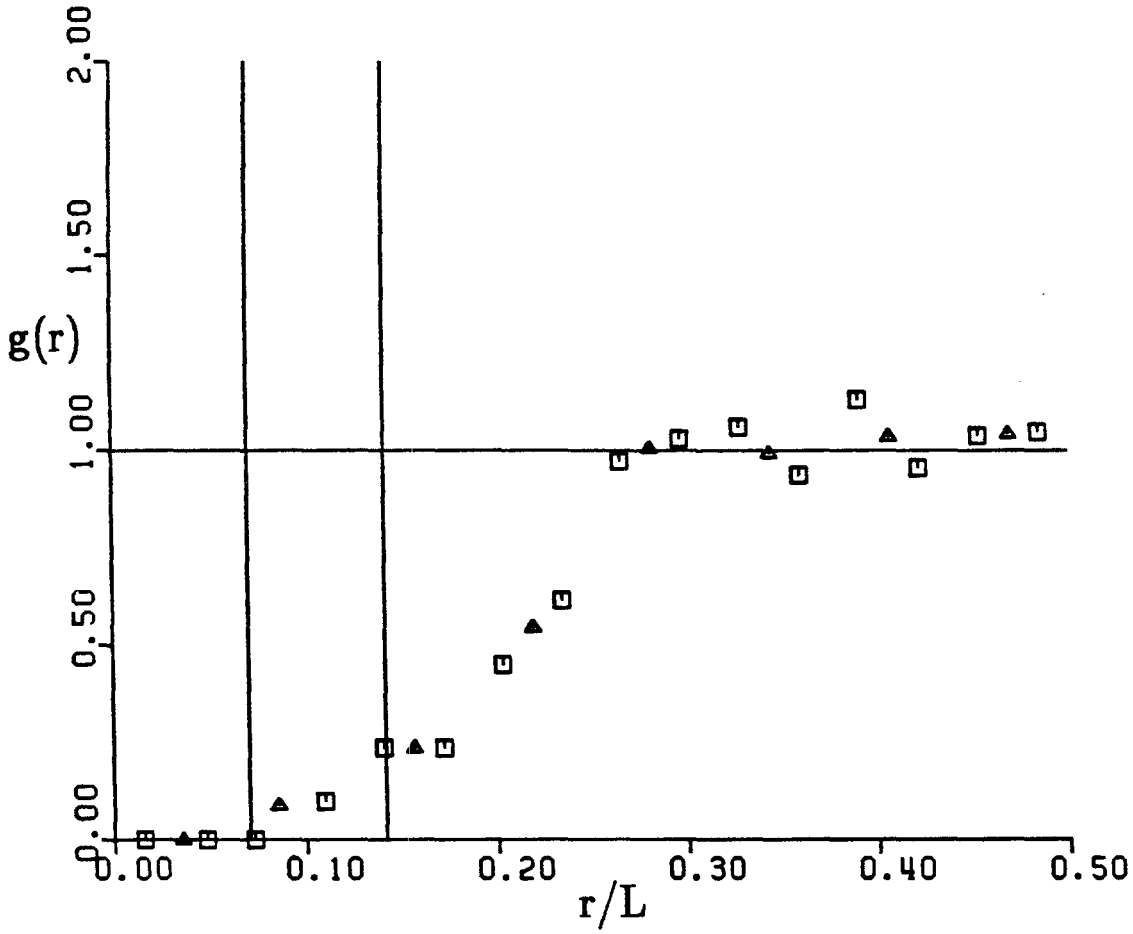


**Figure 7.** Pair-probability function for simulation run 4 averaged from t=0 to 2.0.

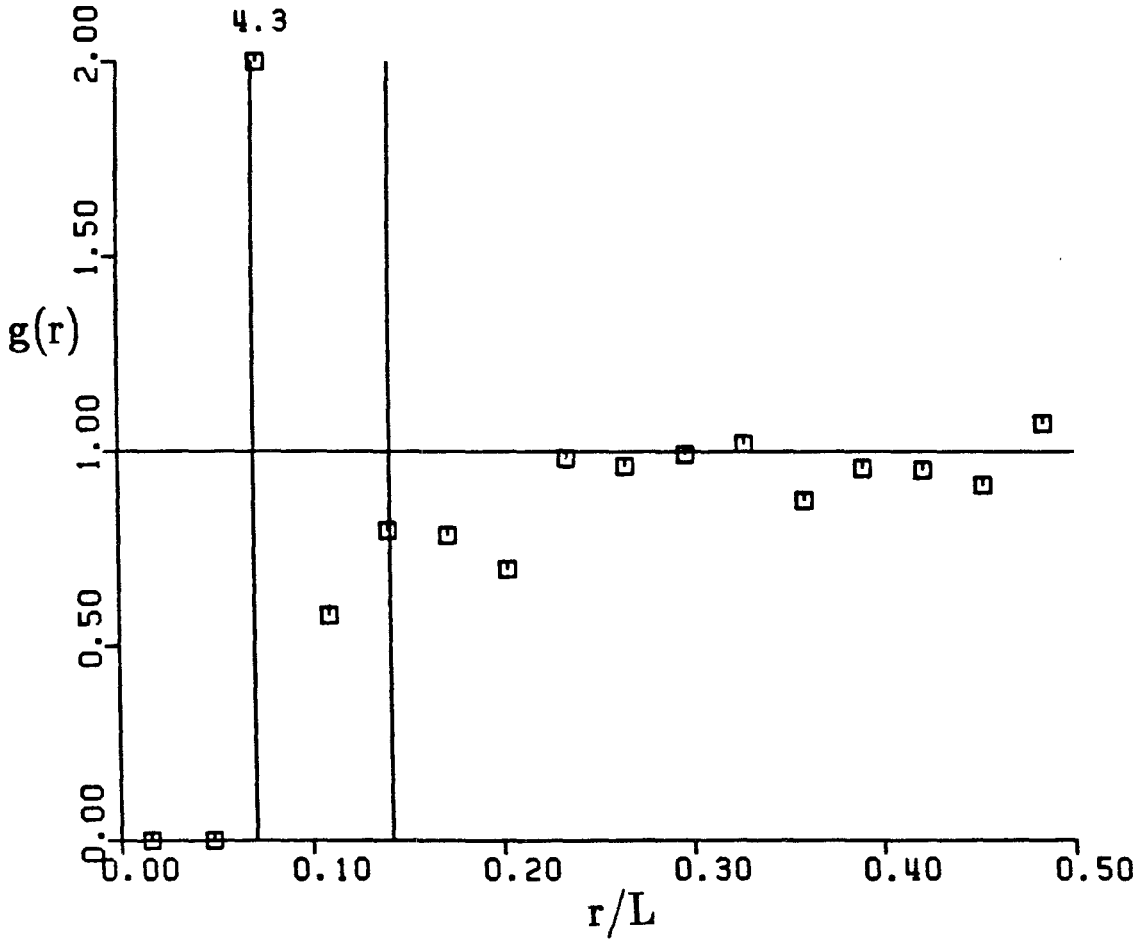


**Figure 8.** Pair-probability function for simulation run 4 averaged from t=2.4 to 8.0.

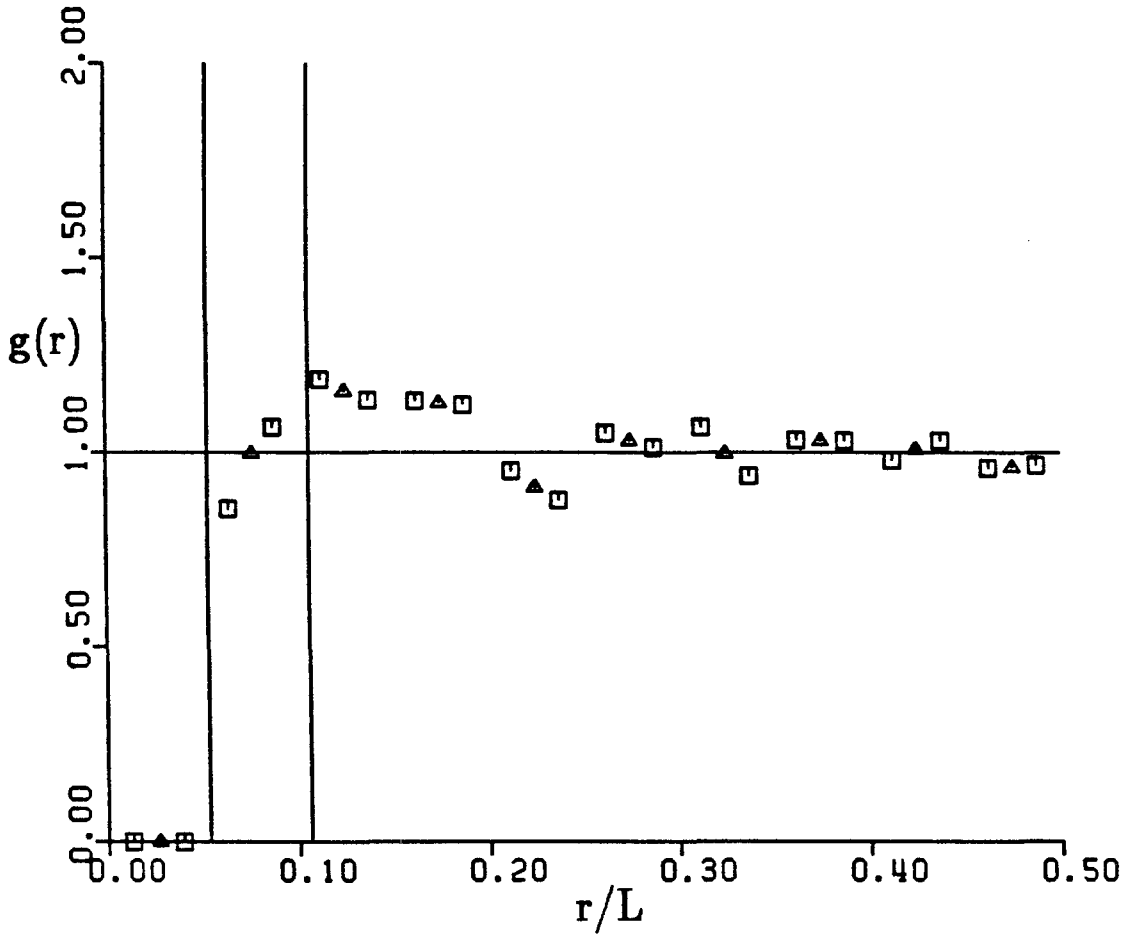


**Figure 9.** Pair-probability function for simulation run 5 averaged from t=0 to 2.4.

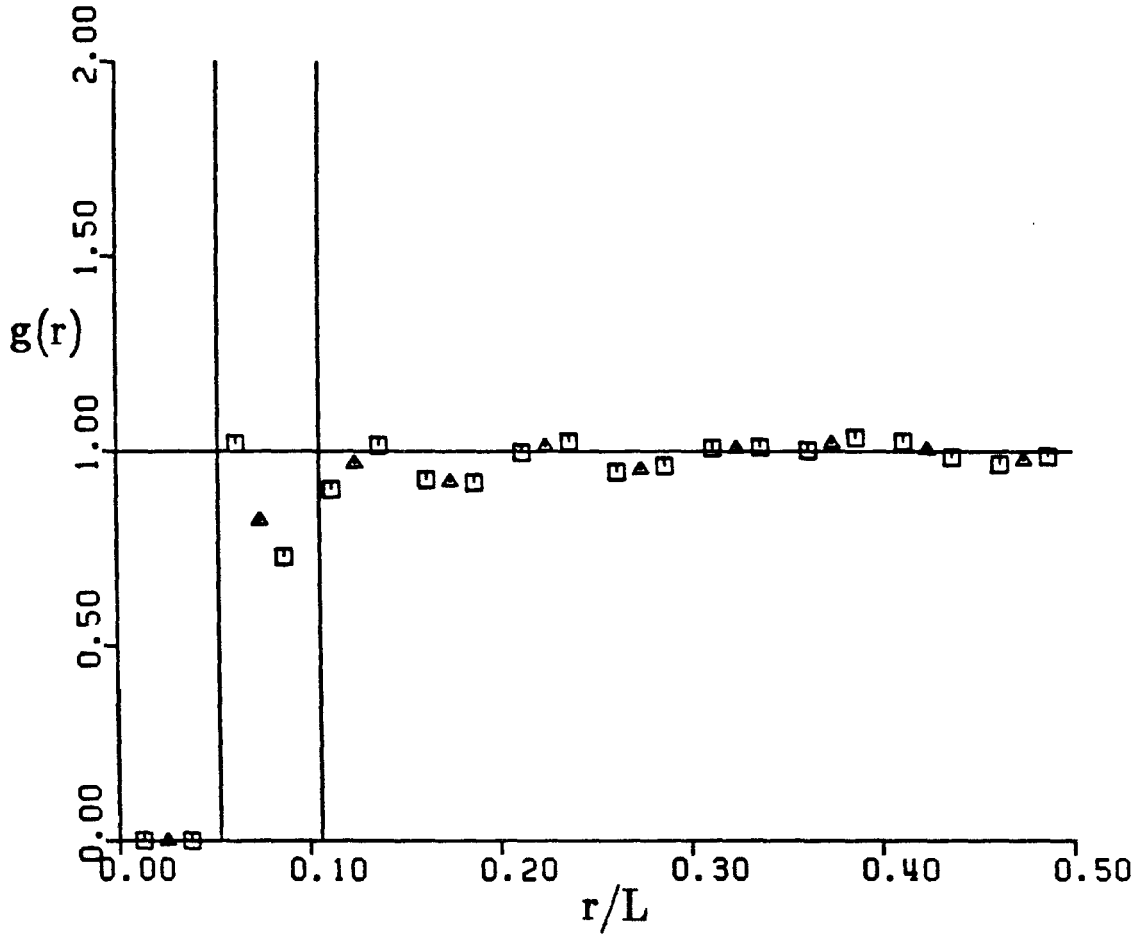


**Figure 10.** Pair-probability function for simulation run 5 averaged from t=2.8 to 7.6.

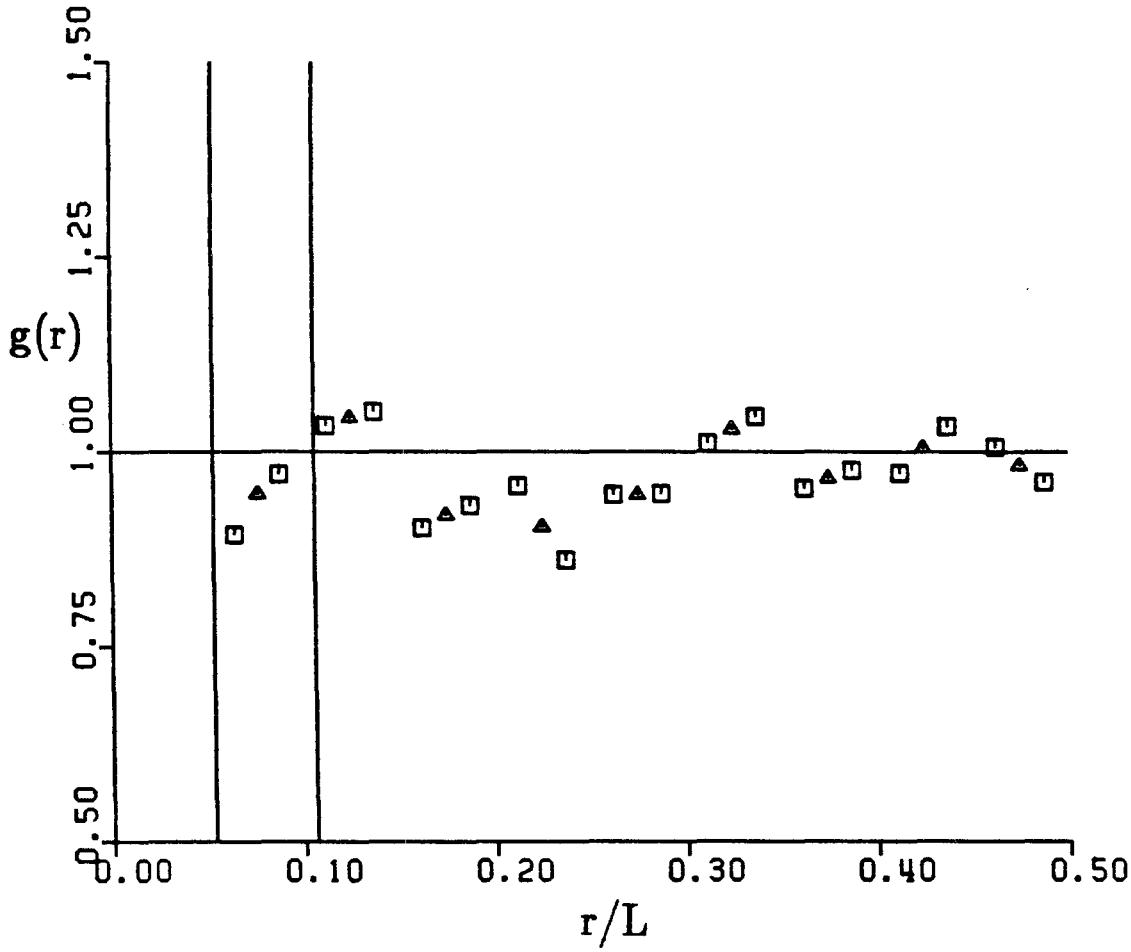


**Figure 11.** Pair-probability function for simulation run 5 averaged from t=8.0 to 12.0.

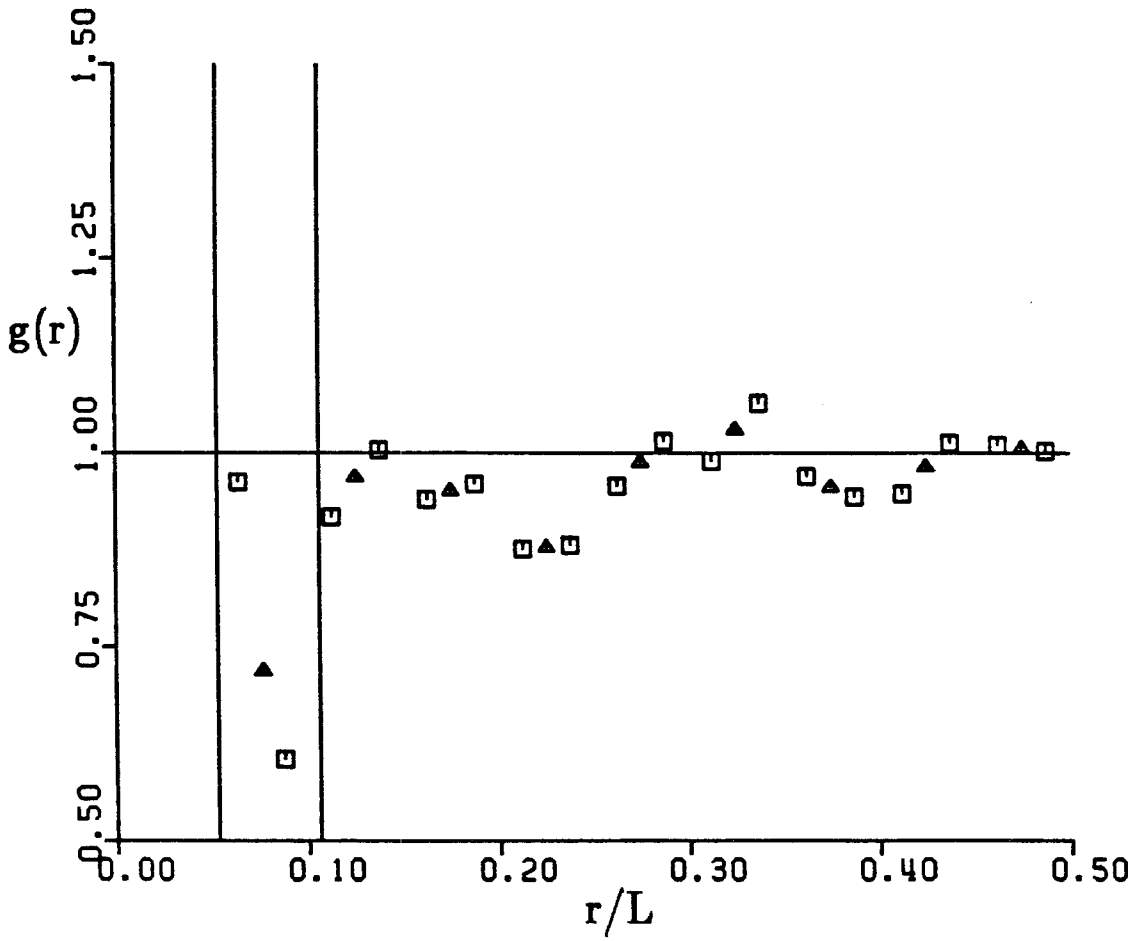


**Figure 12.** Pair-probability function for simulation run 5 averaged from t=10.8 to 12.0.

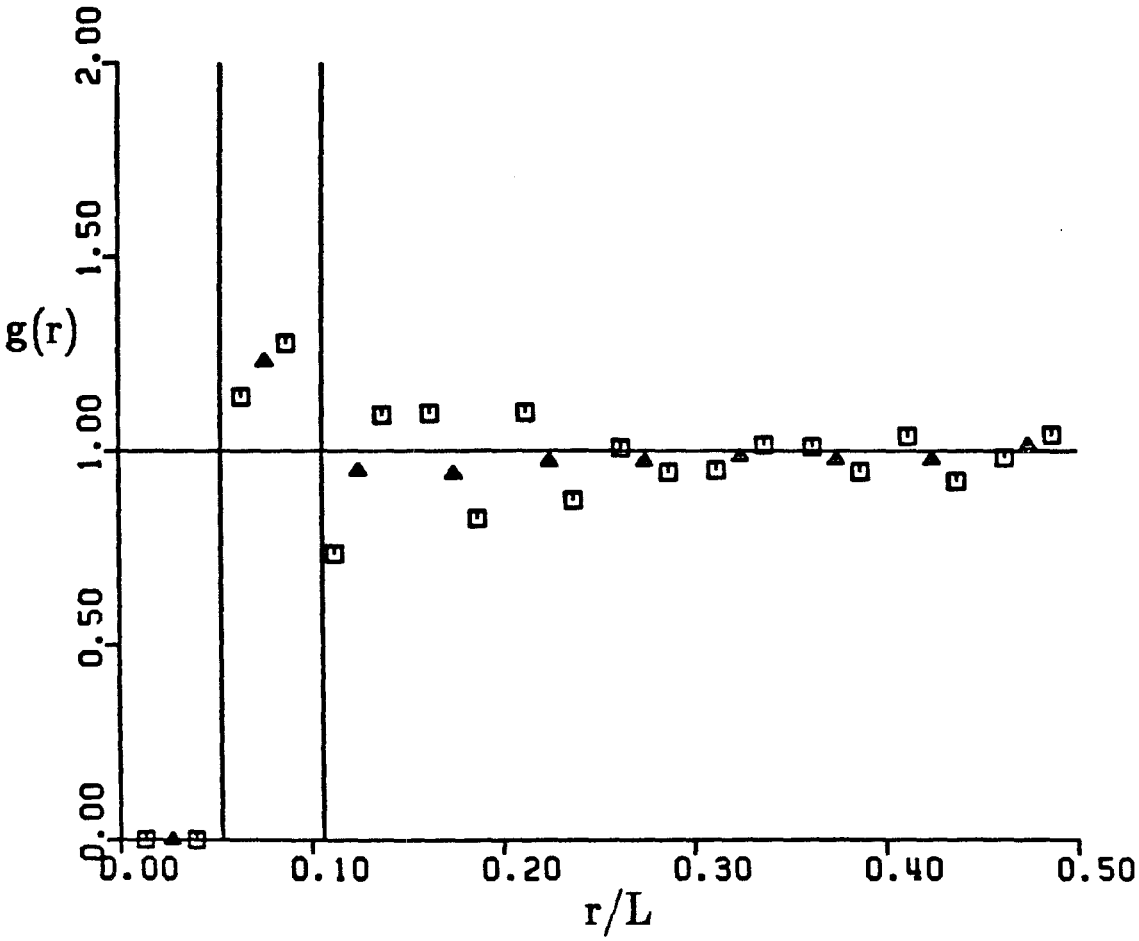


**Figure 13.** Pair-probability function for simulation run 7 averaged from t=0 to 1.6.

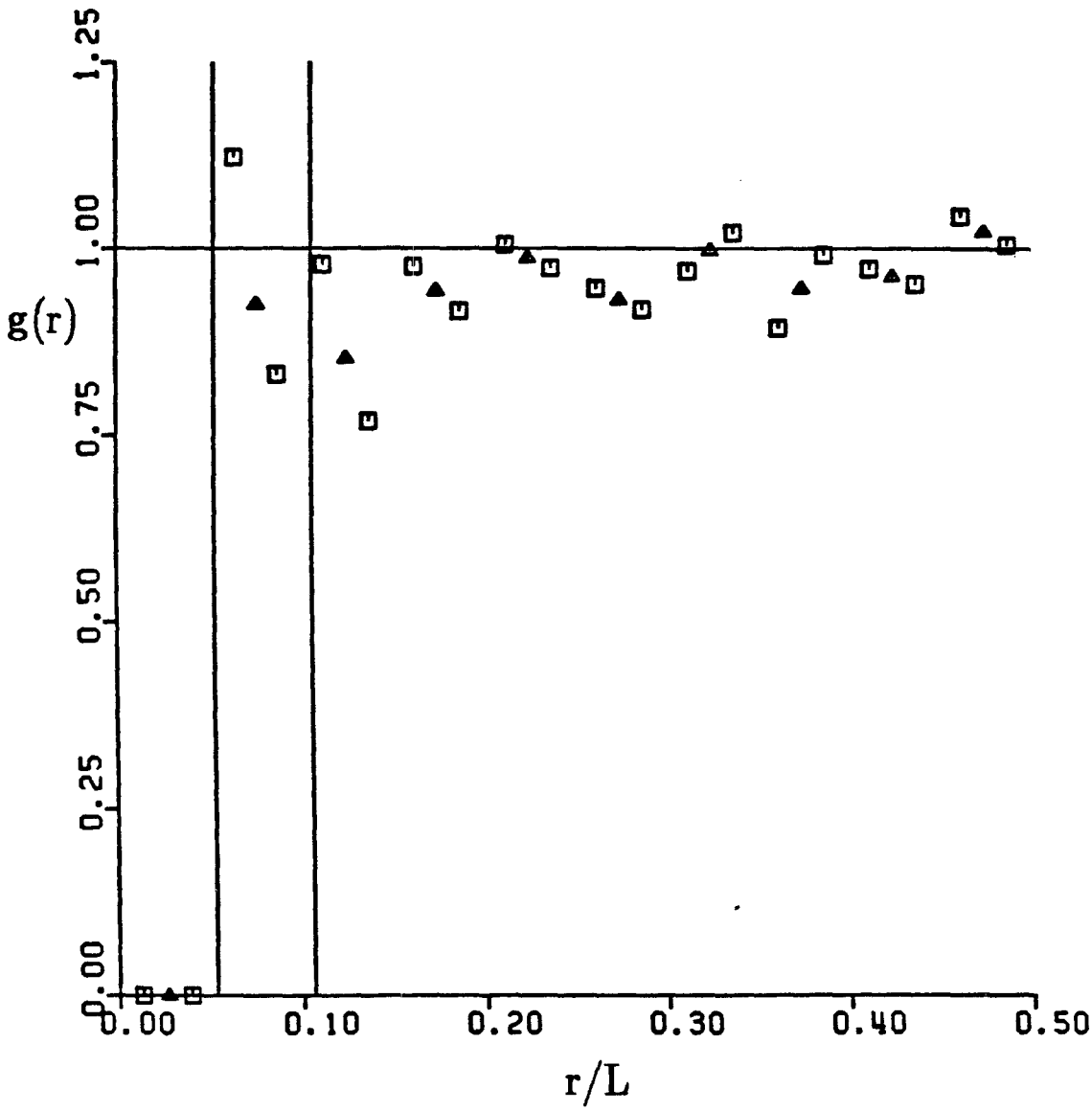


**Figure 14.** Pair-probability function for simulation run 7 averaged from t=2.4 to 8.0.

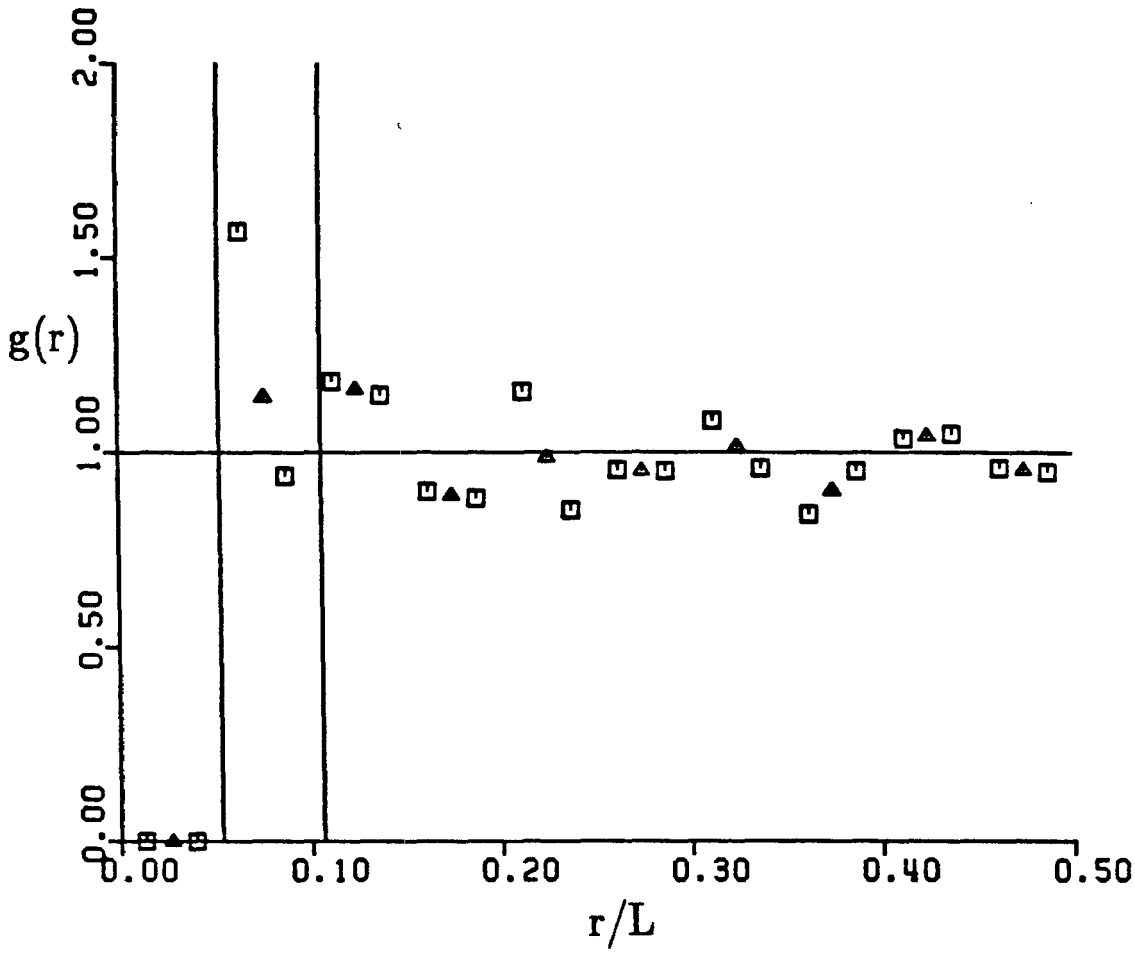


**Figure 15.** Pair-probability function for simulation run 8 averaged from t=0 to .8.

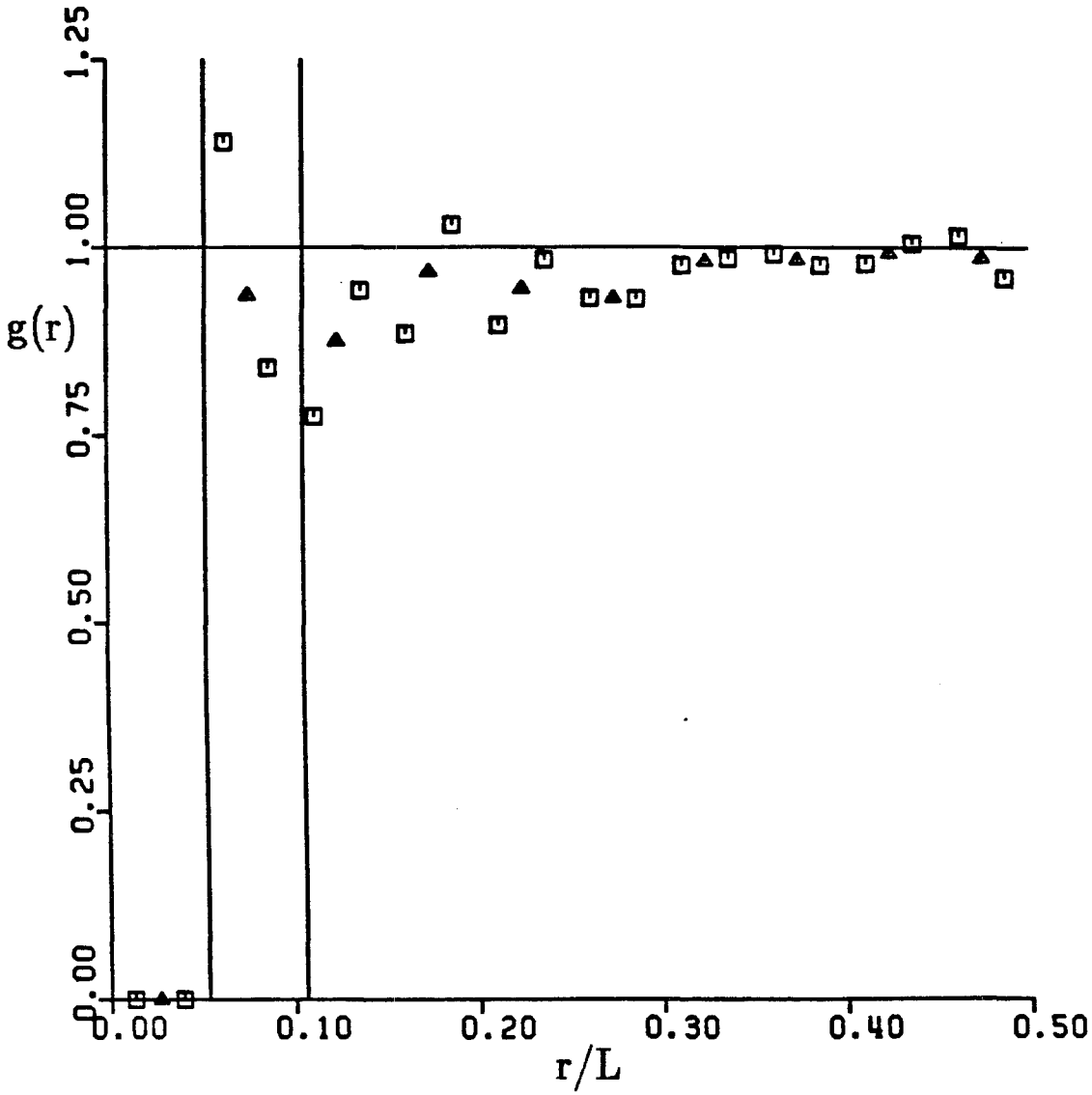


**Figure 16.** Pair-probability function for simulation run 8 averaged from t=1.2 to 8.0.

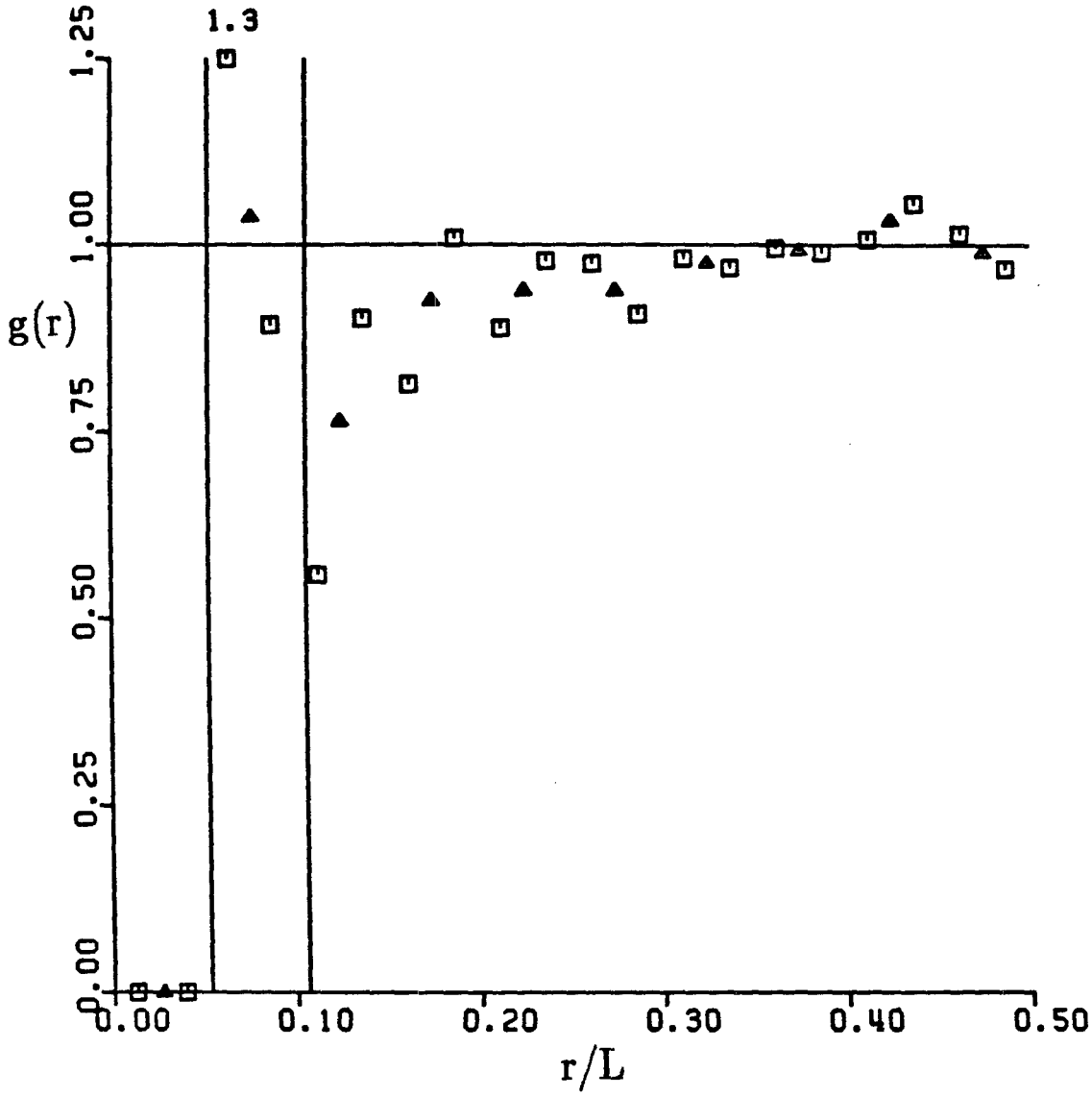


**Figure 17.** Pair-probability function for simulation run 8 averaged from t=5.6 to 8.0.

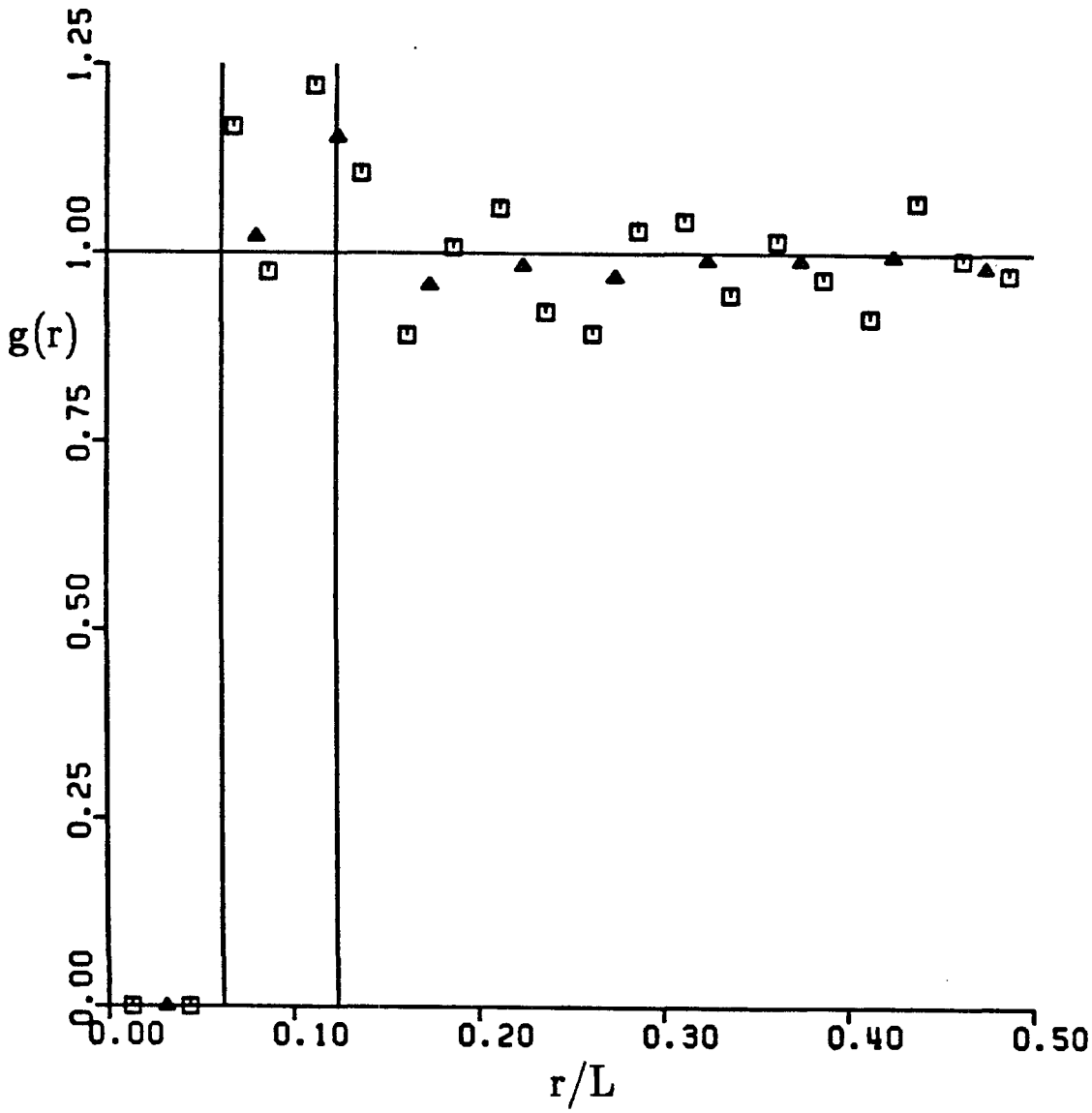


**Figure 18.** Pair-probability function for simulation run 9 averaged from 0 to 2.0.

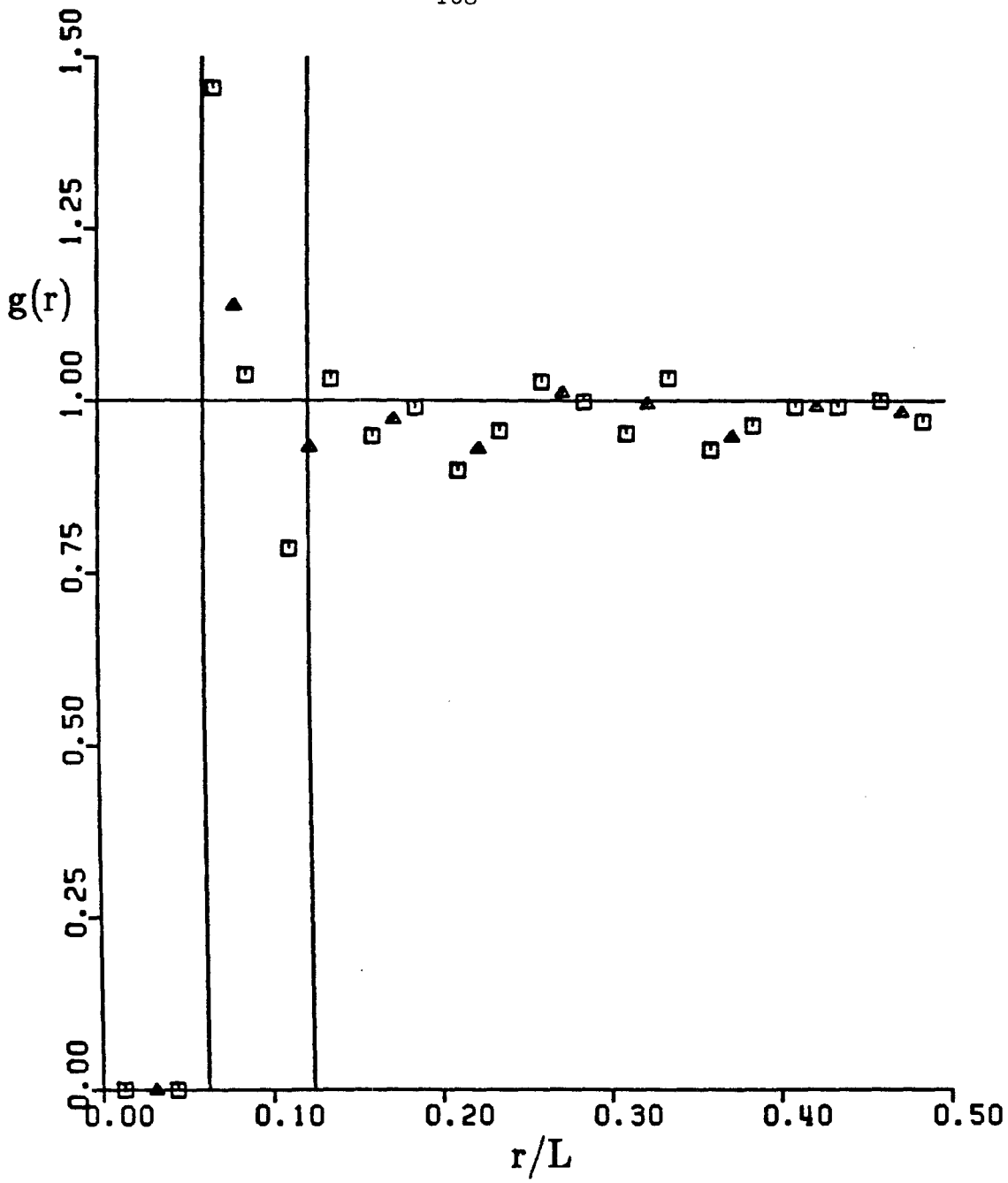


**Figure 19.** Pair-probability function for simulation run 9 averaged from t=2.4 to 4.8.

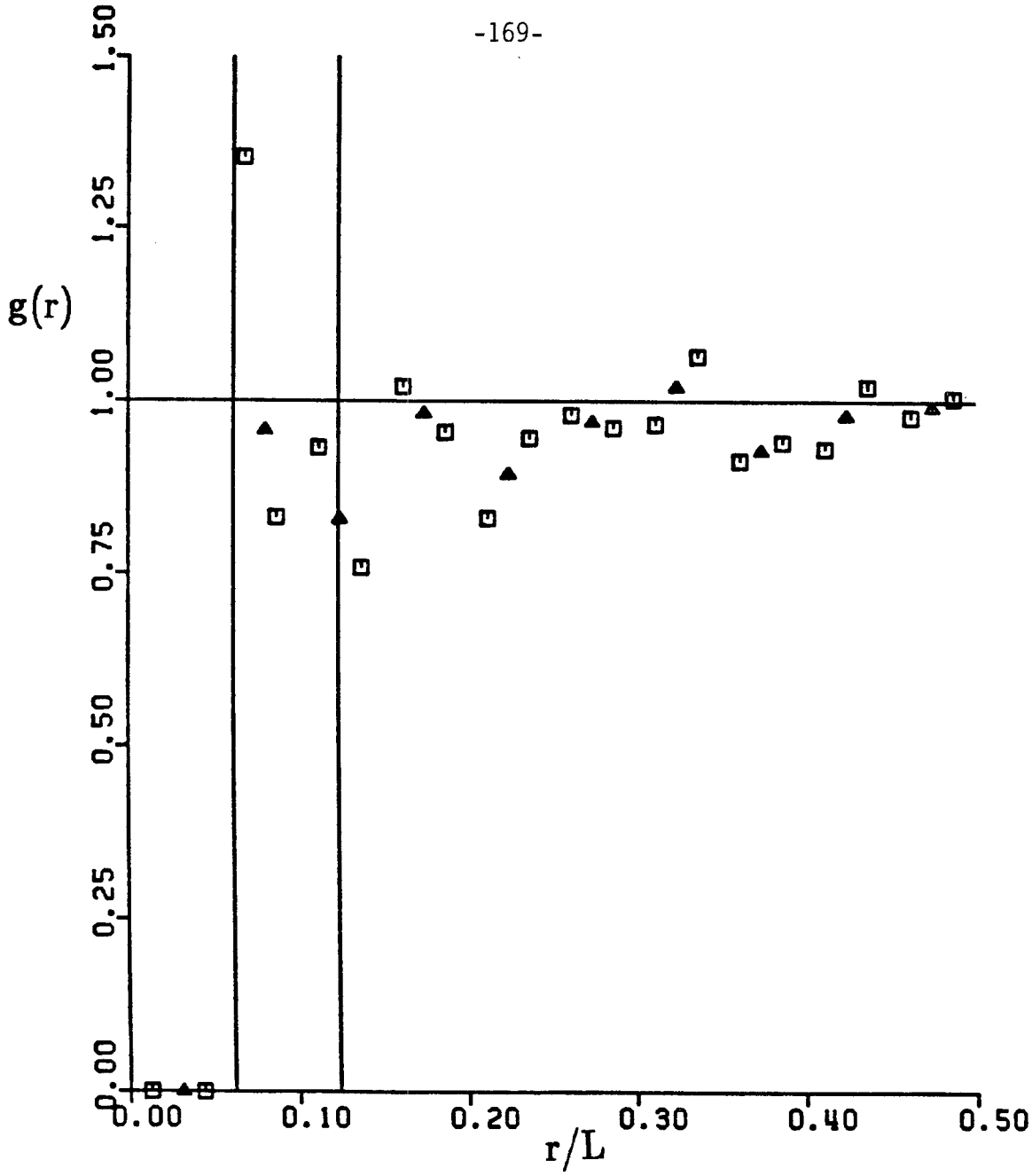


**Figure 20.** Pair-probability function for simulation run 9 averaged from t=5.2 to 8.0.

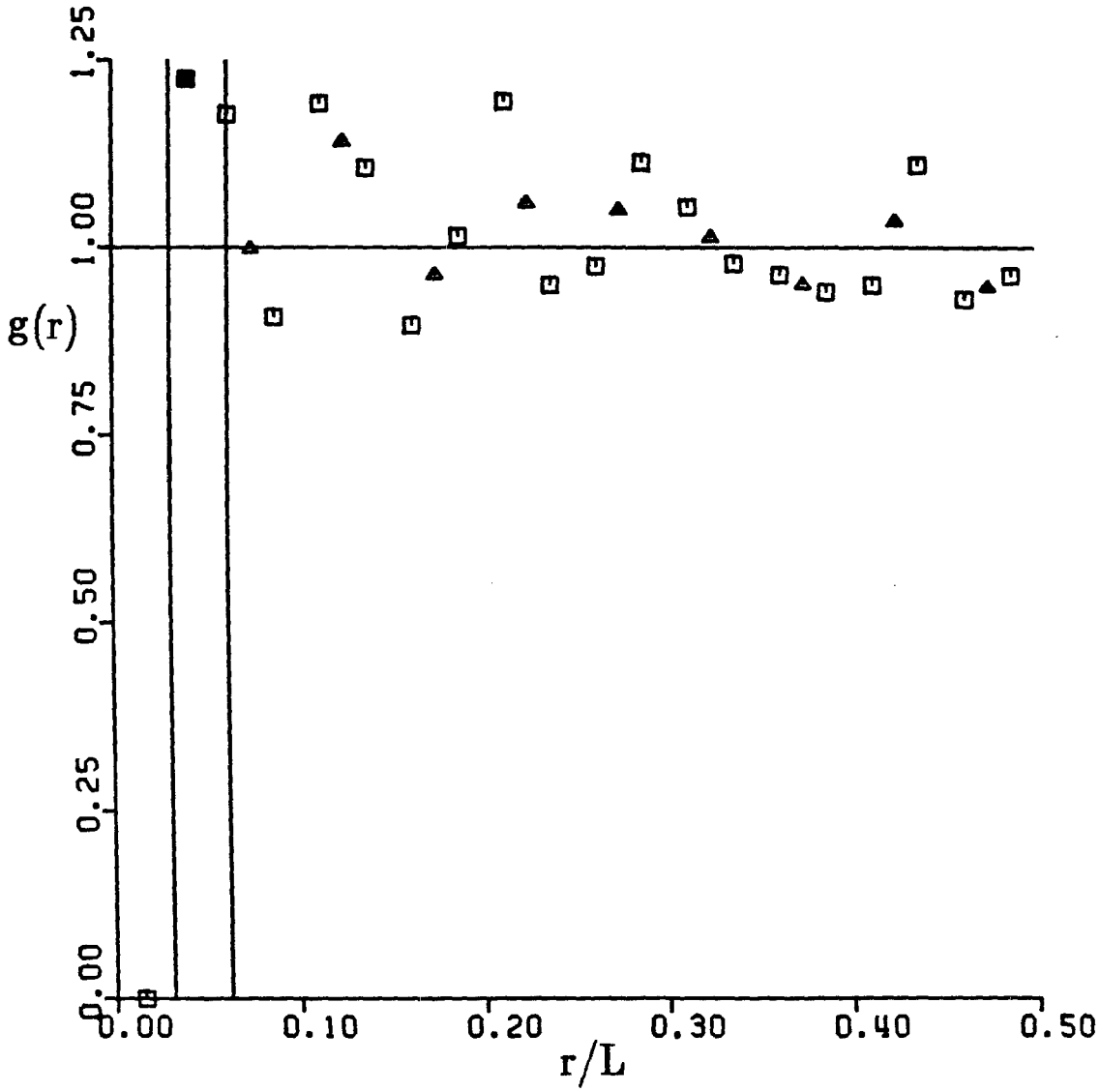


**Figure 21.** Pair-probability function for simulation run 10 averaged from t=0 to 1.2.

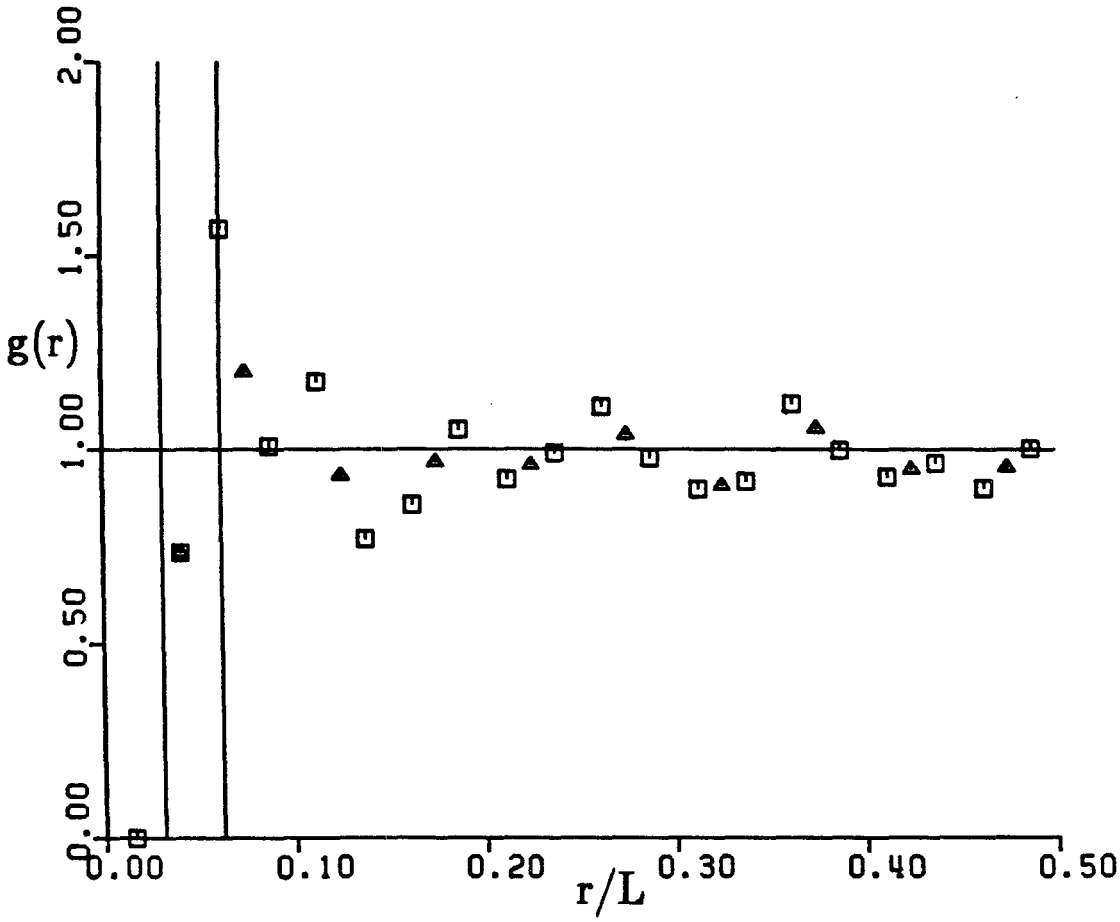


**Figure 22.** Pair-probability function for simulation run 10 averaged from t=1.6 to 3.2.

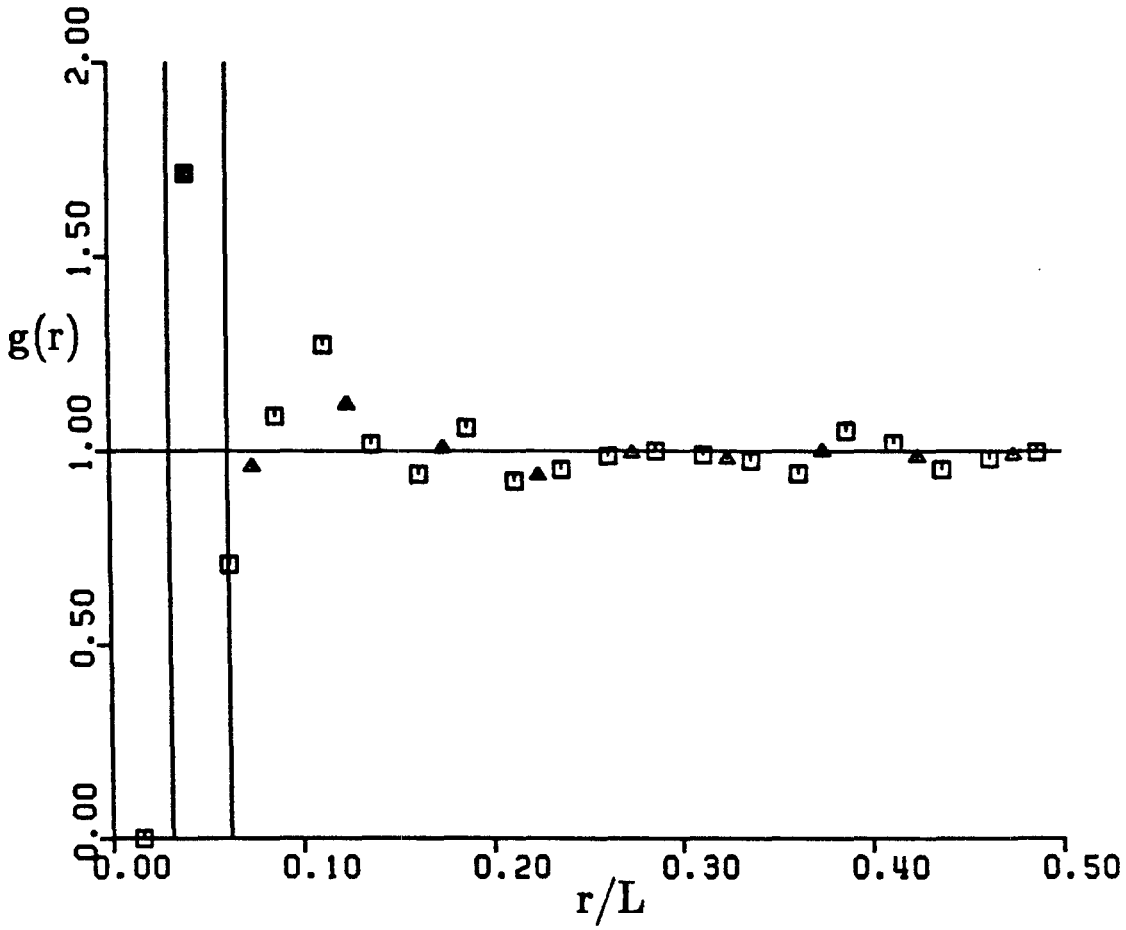


**Figure 23.** Pair-probability function for simulation run 10 averaged from t=3.6 to 5.2.

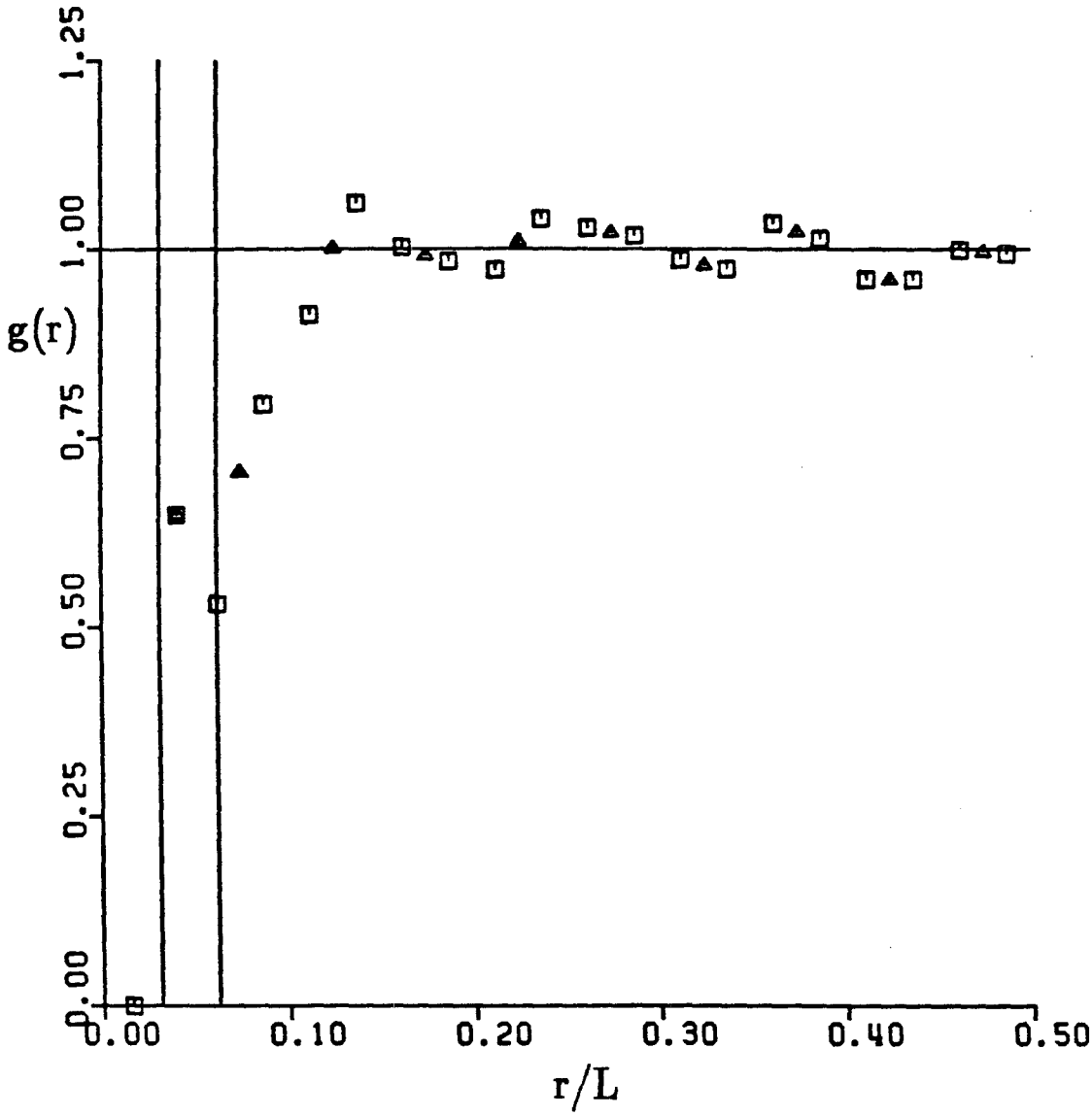


**Figure 24.** Pair-probability function for simulation run 10 averaged from t=5.6 to 12.0.

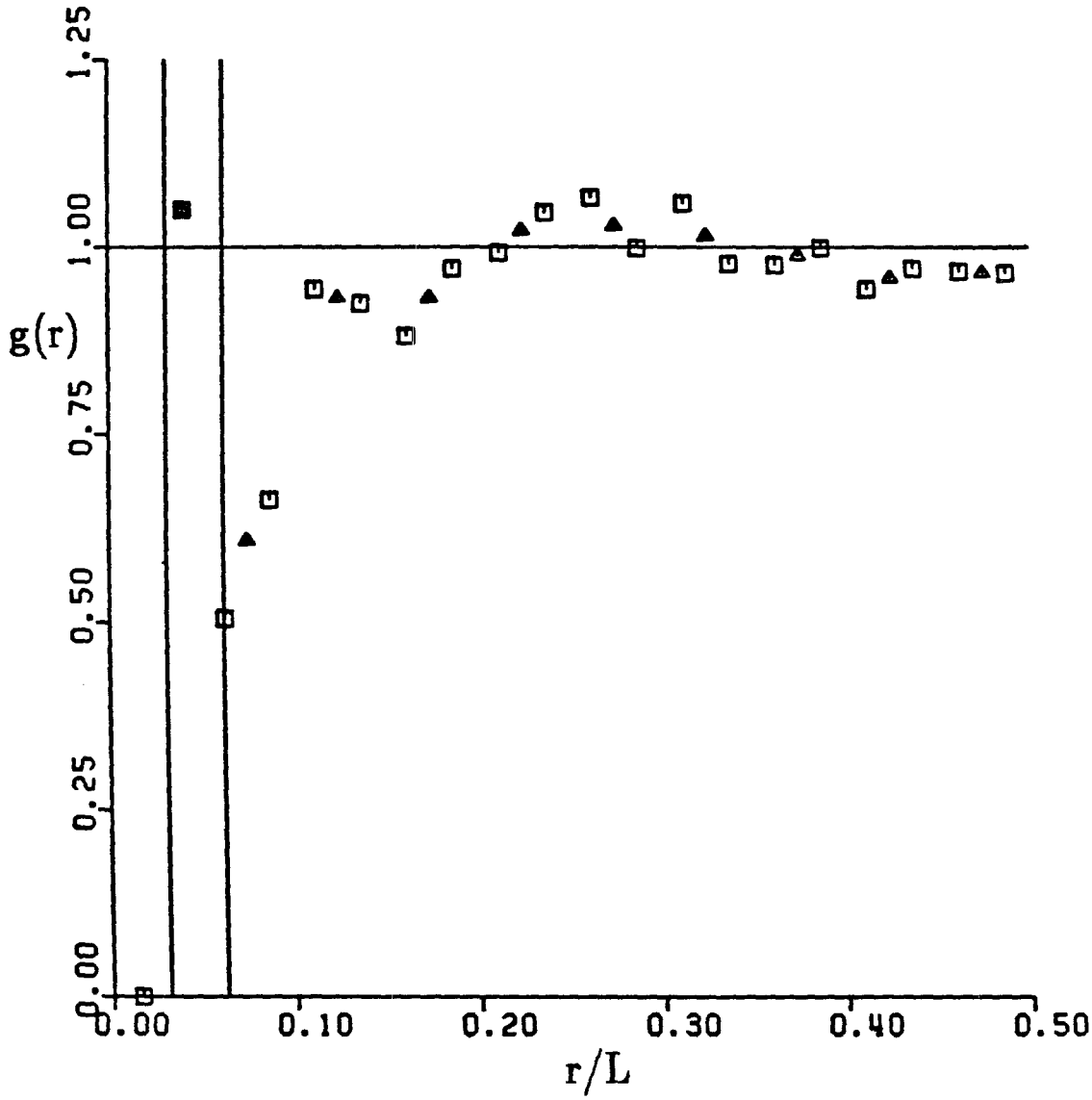


**Figure 25.** Pair-probability function for simulation run 10 averaged from t=9.6 to 12.0.

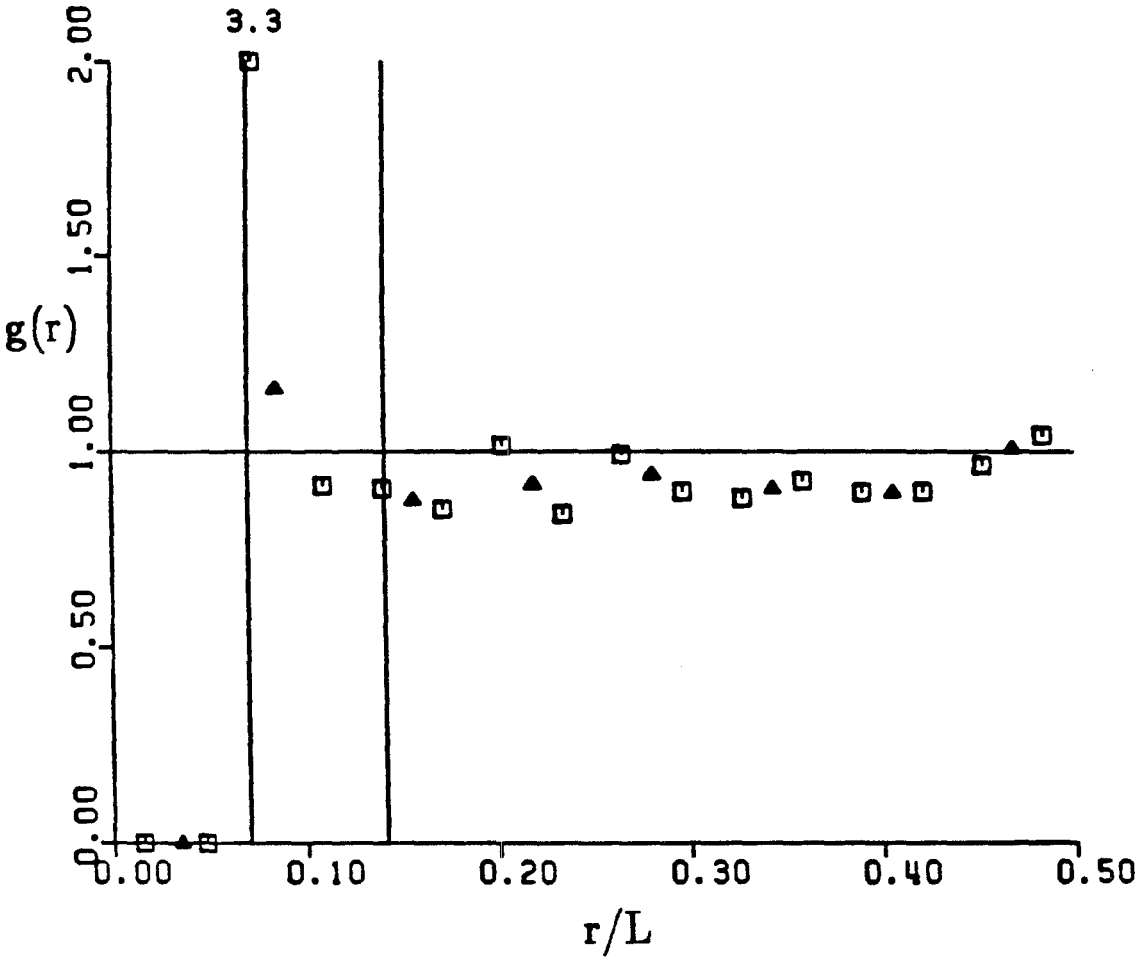


**Figure 26.** Pair-probability function for simulation run 13 averaged from t=0 to 8.0.

**APPENDIX 3:** Example distributions of the particle velocities

Appendix 3 shows an example (viz., that of run 3) of how the distribution of particle velocities develops over time. The number of particles with a velocity within a given range is plotted against the $O(c^{1/3})$ coefficient in the expansion for the settling velocity (which is a measure of the velocity of a particle). Although the distribution of particle velocities is initially very narrow, it eventually develops into a very wide distribution which is skewed toward one end.

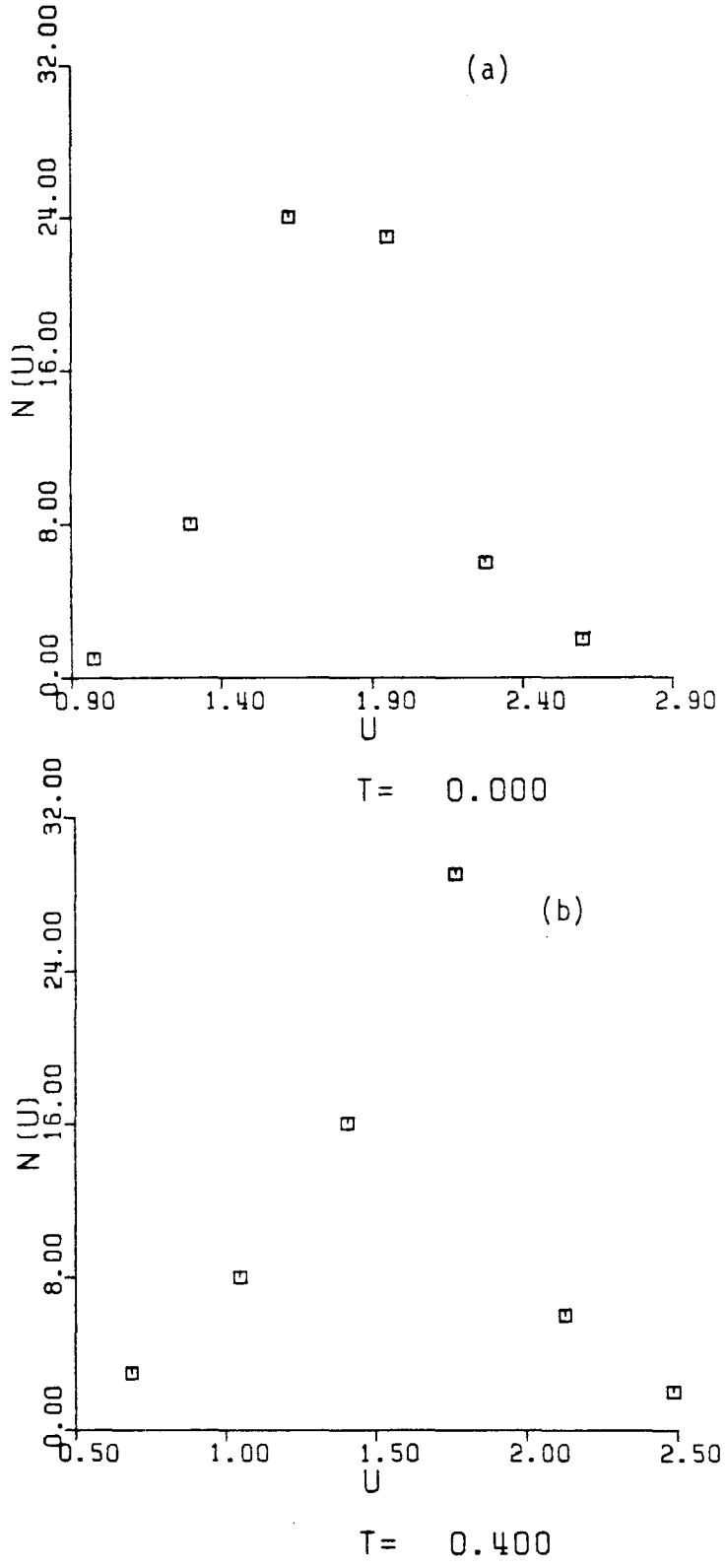


**Figure 27.** Histograms of the particle velocities for simulation run 3.

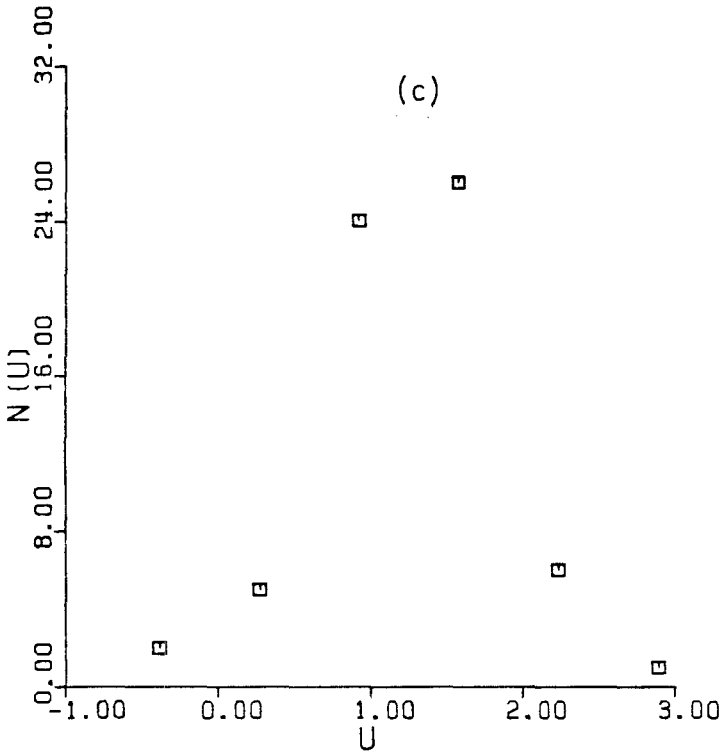
(c)
32.00
24.00
16.00
8.00
0.00
N (U)
-1.00
0.00
1.00
2.00
3.00
U

T= 1.200

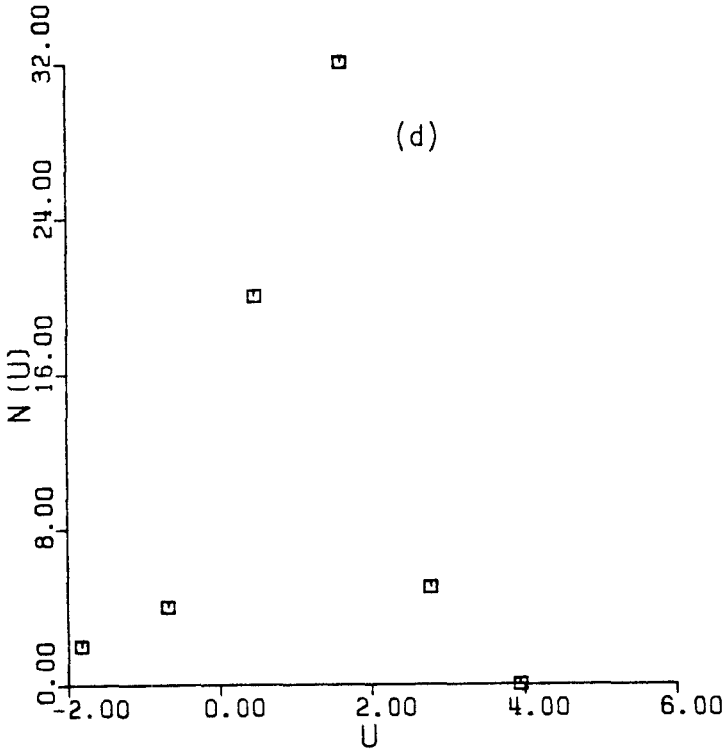
(d)
32.00
24.00
16.00
8.00
0.00
N (U)
-2.00
0.00
2.00
4.00
6.00
U

T= 1.600

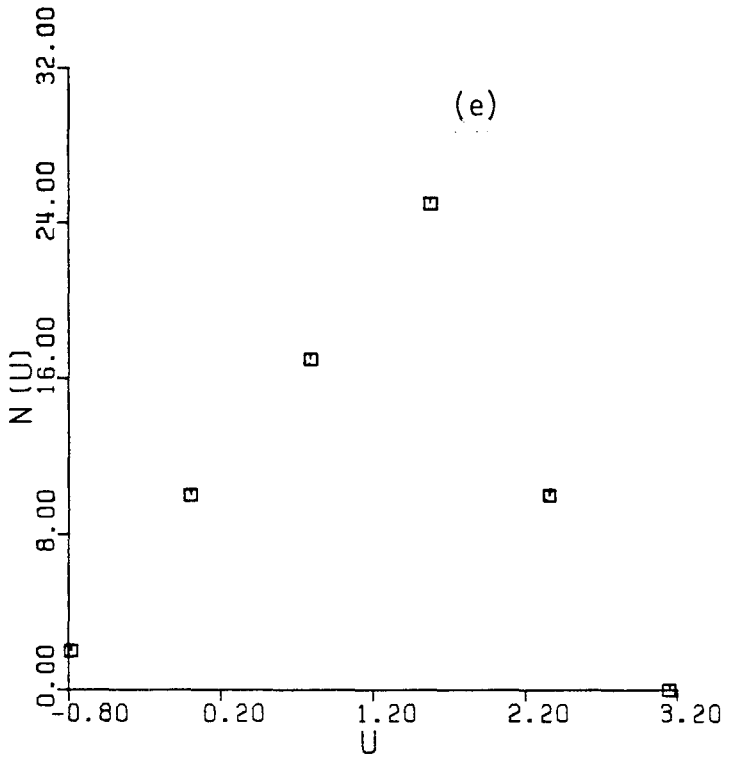
(e)
32.00
24.00
16.00
8.00
0.00
N (U)
-0.80
0.20
1.20
2.20
3.20
U

T= 2.000

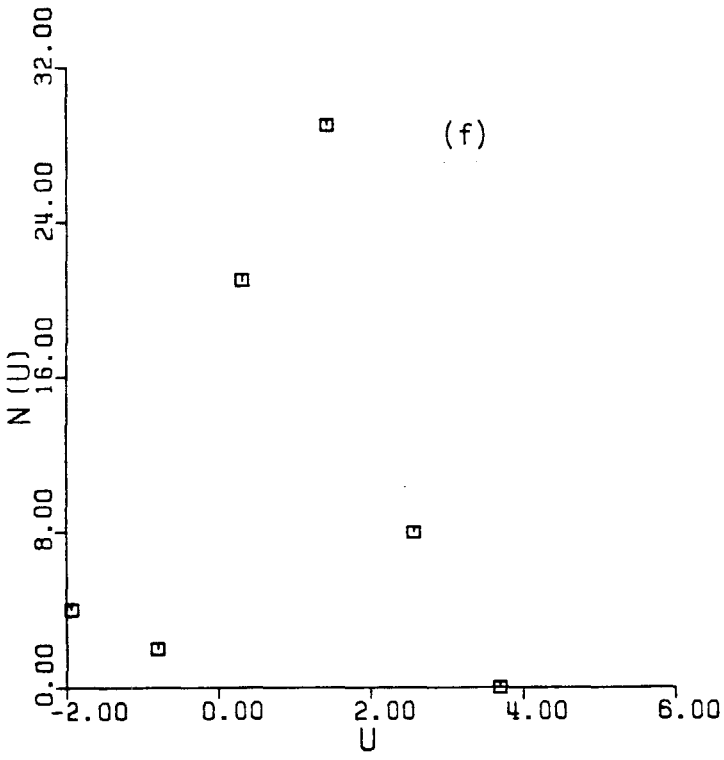
(f)
32.00
24.00
16.00
8.00
0.00
N (U)
-2.00
0.00
2.00
4.00
6.00
U

T= 3.200

**APPENDIX 4:** Plots of the volume-averaged pair-probability function at different instants in time

Appendix 4 presents results for the pair-probability function, averaged over the particles in the cube, as a function of time. The method of calculation of the pair-probability function is identical to that in Chapter 1 except that the first interval no longer has its inside radius adjusted to eliminate any effects of volume exclusion. In the plots the axes have the same meaning as in Figure 1 of Chapter 1. For simulation run 12 two sets of intervals are used; the second set of intervals, represented in the plots by squares, has a gap distance exactly half that of the original set of intervals.

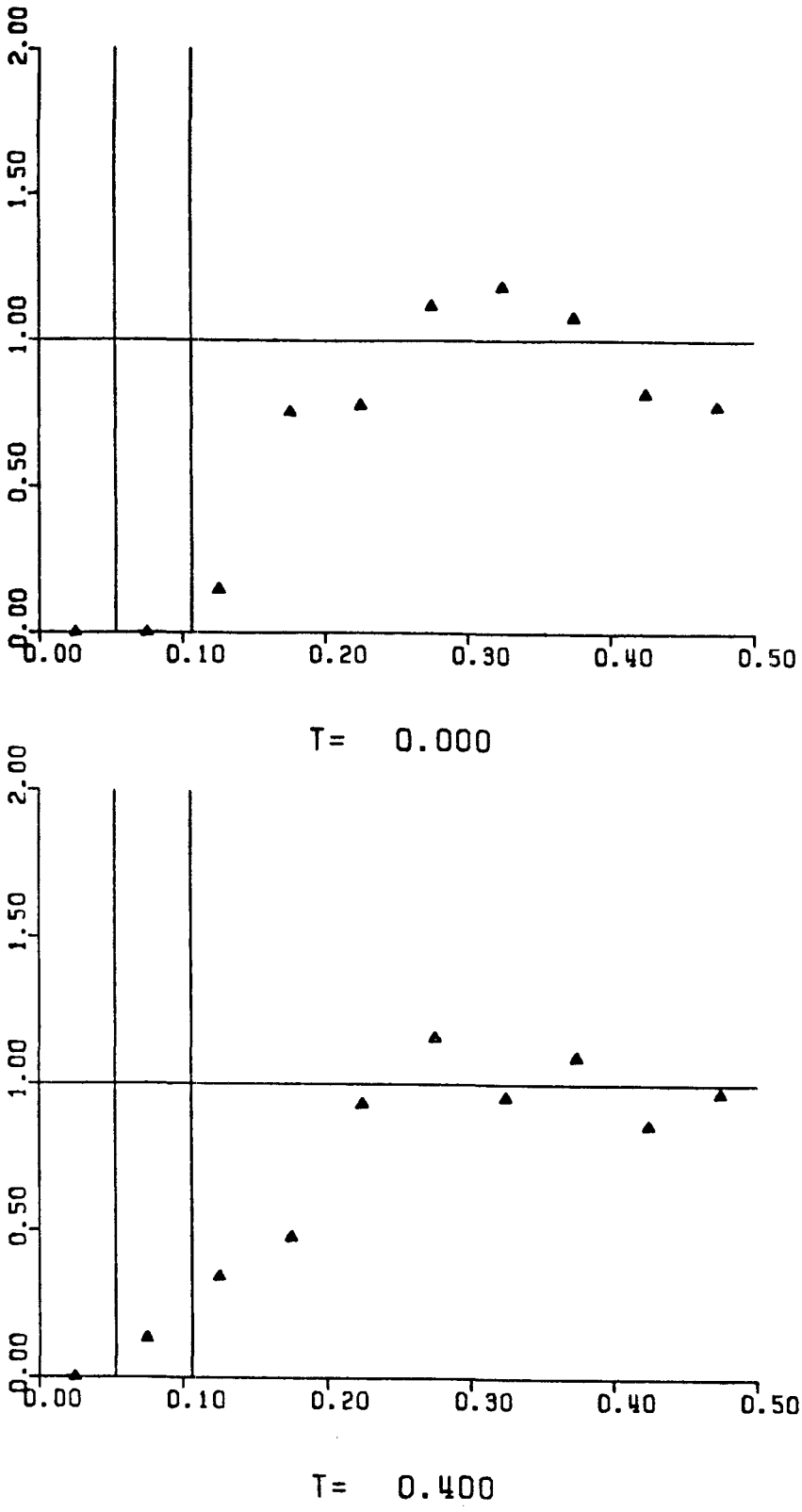


**Figure 28.** Pair-probability function for simulation run 1 at different instants in time.

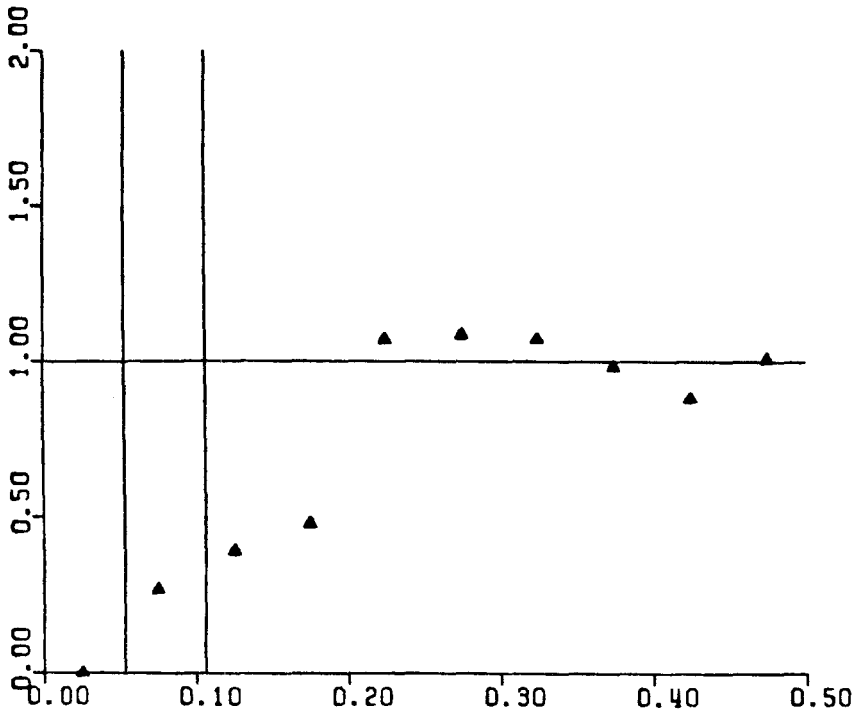
2.00
1.50
1.00
0.50
0.00
0.00
0.10
0.20
0.30
0.40
0.50

T= 0.800

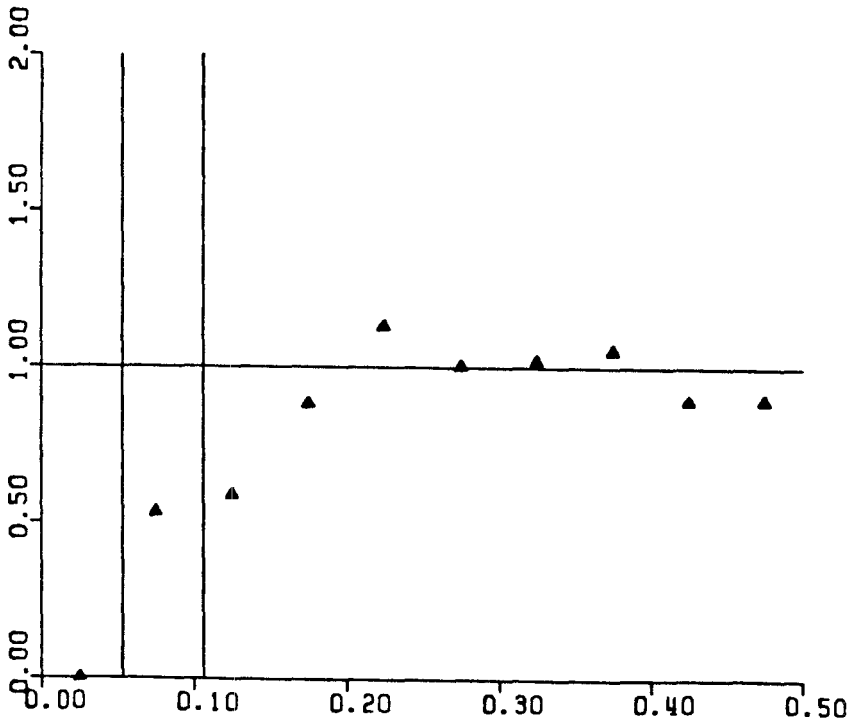
2.00
1.50
1.00
0.50
0.00
0.00
0.10
0.20
0.30
0.40
0.50

T= 1.200

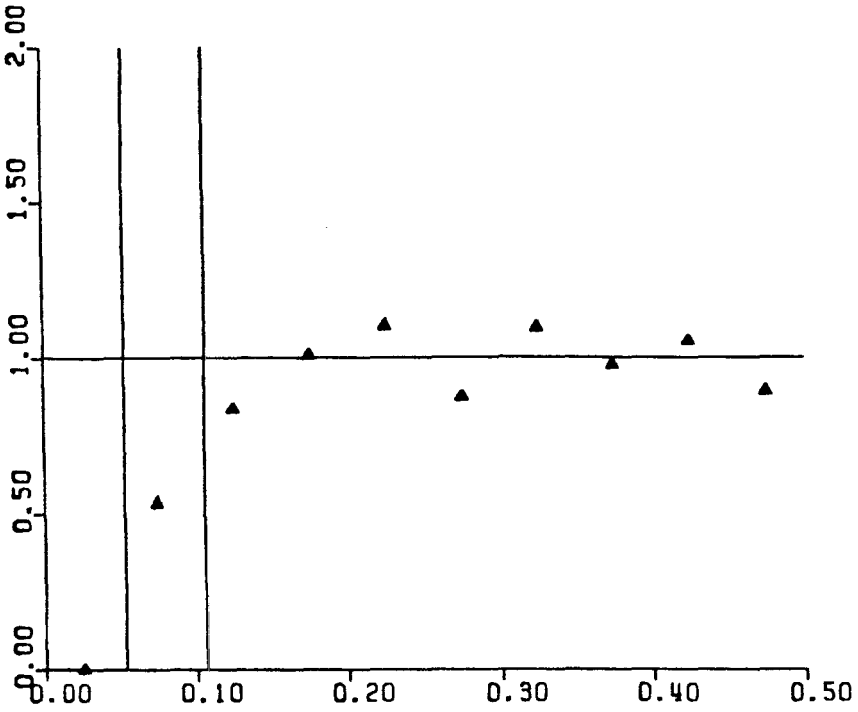
2.00
1.50
1.00
0.50
0.00
0.00
0.10
0.20
0.30
0.40
0.50

T= 1.600

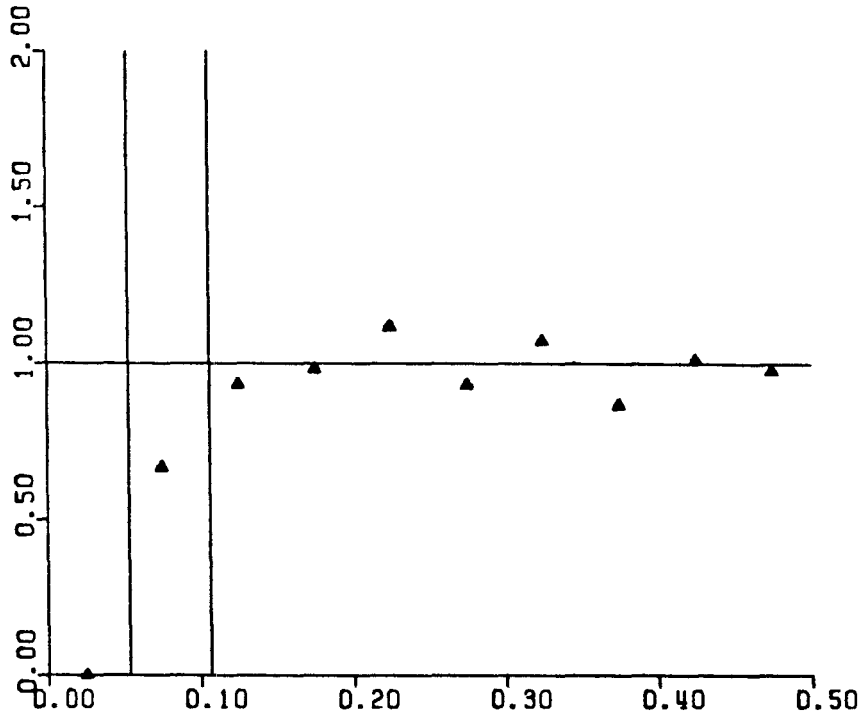
2.00
1.50
1.00
0.50
0.00
0.00
0.10
0.20
0.30
0.40
0.50

T= 2.000

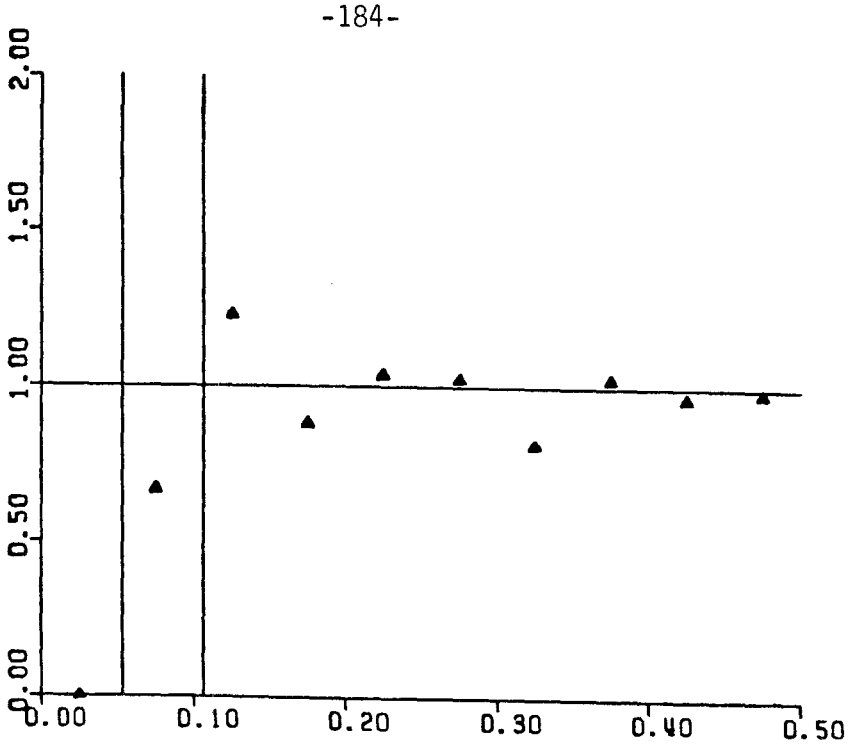
2.00
1.50
1.00
0.50
0.00
0.00
0.10
0.20
0.30
0.40
0.50

T= 2.400

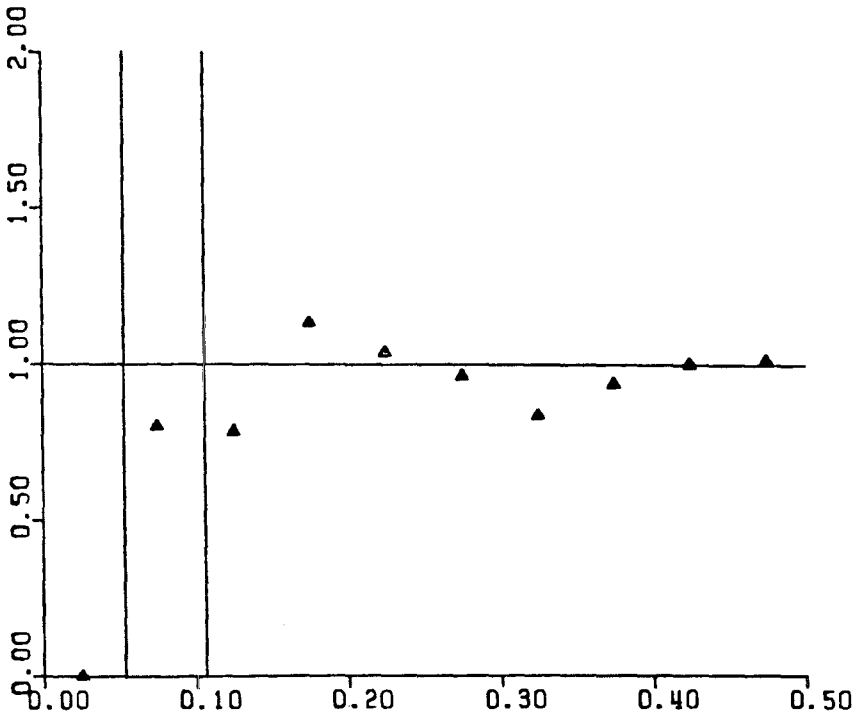
2.00
1.50
1.00
0.50
0.00
0.00
0.10
0.20
0.30
0.40
0.50

T= 2.800

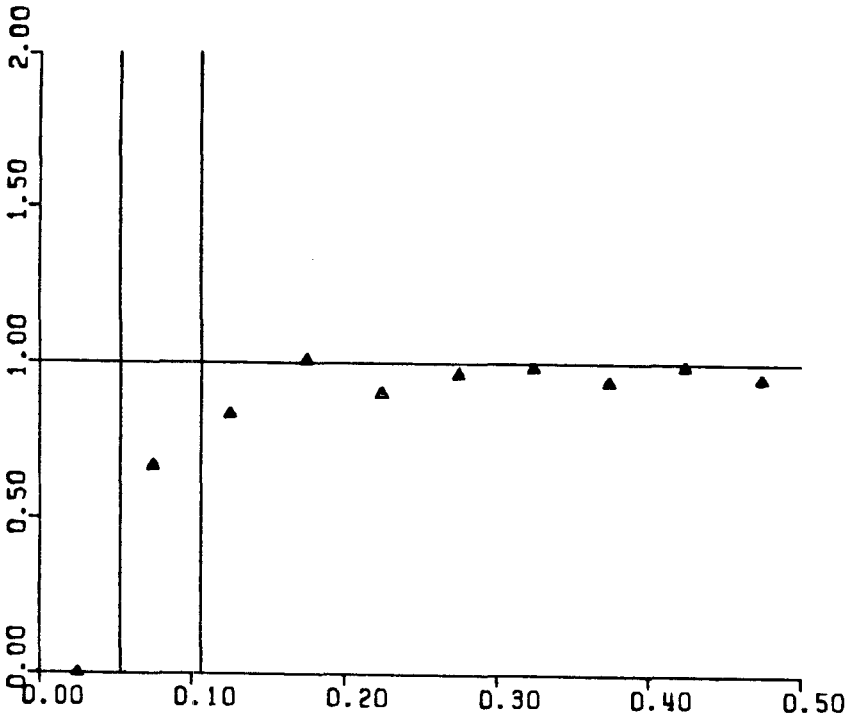
2.00
1.50
1.00
0.50
0.00
0.00
0.10
0.20
0.30
0.40
0.50

T= 3.200

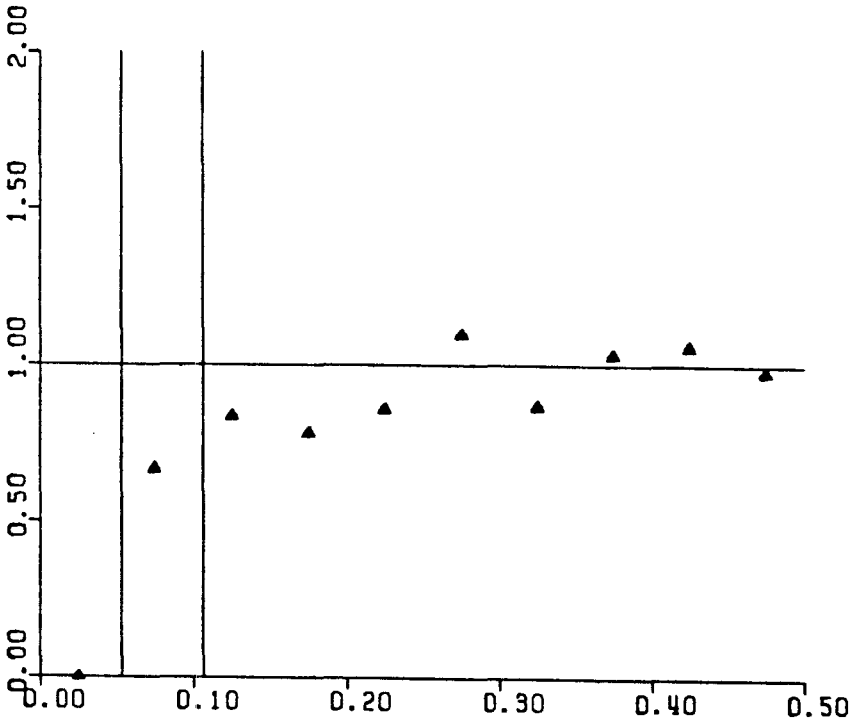
2.00
1.50
1.00
0.50
0.00
0.00
0.10
0.20
0.30
0.40
0.50

T= 3.600

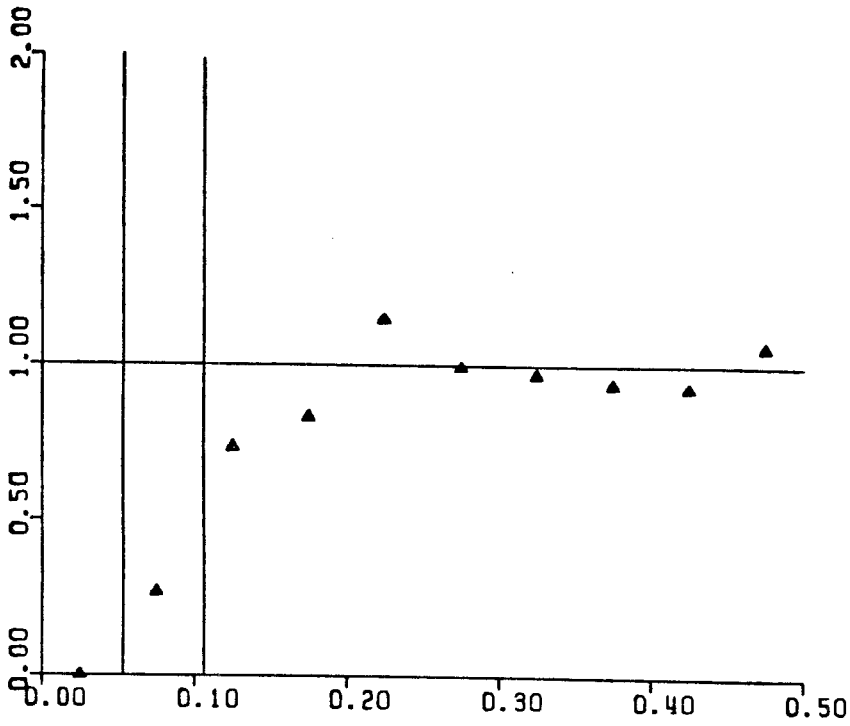
2.00
1.50
1.00
0.50
0.00
0.00
0.10
0.20
0.30
0.40
0.50

T= 4.000

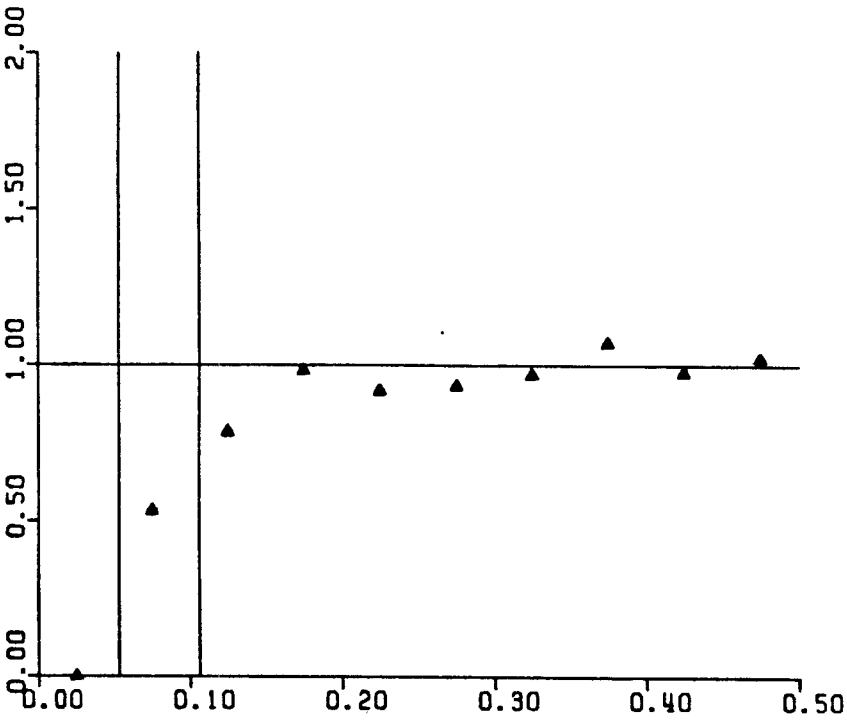
2.00
1.50
1.00
0.50
0.00
0.00
0.10
0.20
0.30
0.40
0.50

T= 4.400

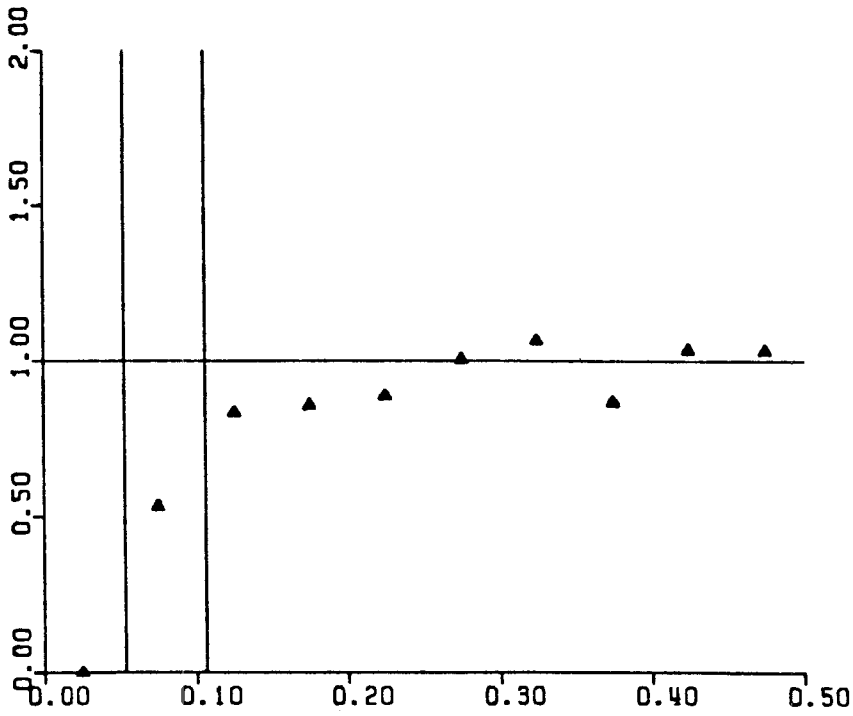
2.00
1.50
1.00
0.50
0.00
0.00
0.10
0.20
0.30
0.40
0.50

T= 4.800

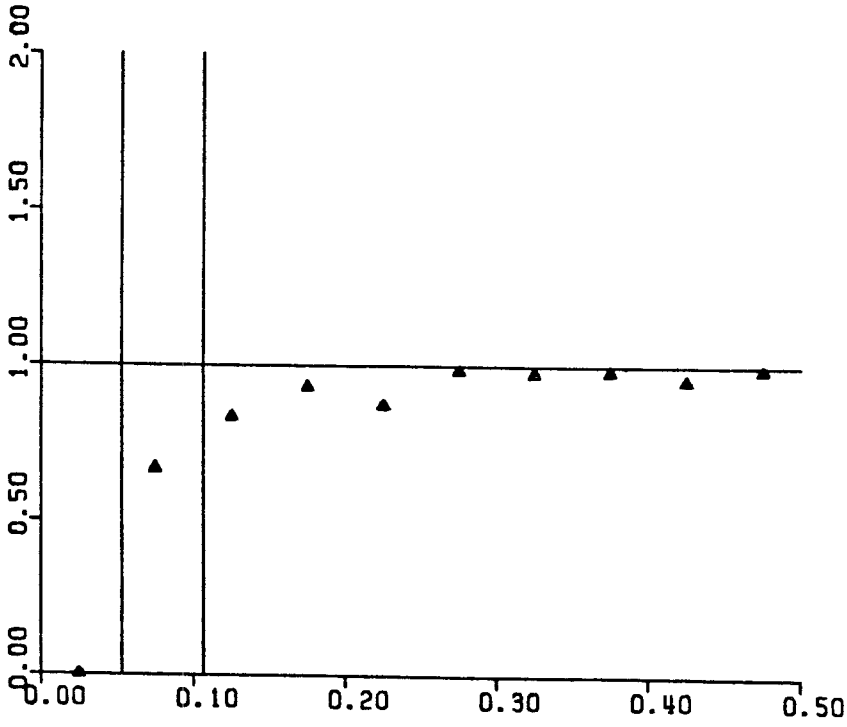
2.00
1.50
1.00
0.50
0.00
0.00
0.10
0.20
0.30
0.40
0.50

T= 5.200

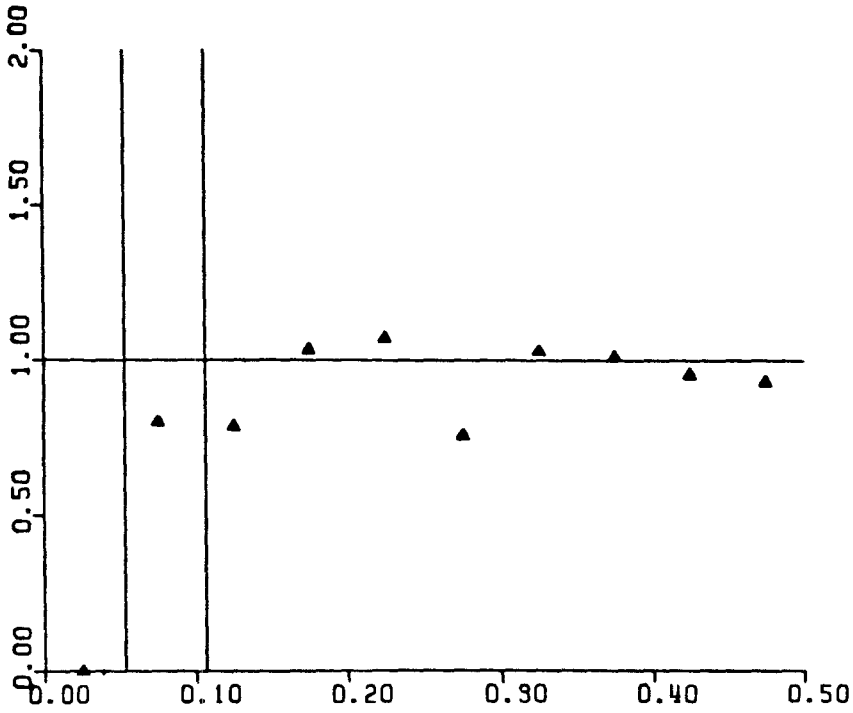
2.00
1.50
1.00
0.50
0.00
0.00
0.10
0.20
0.30
0.40
0.50

T= 5.600

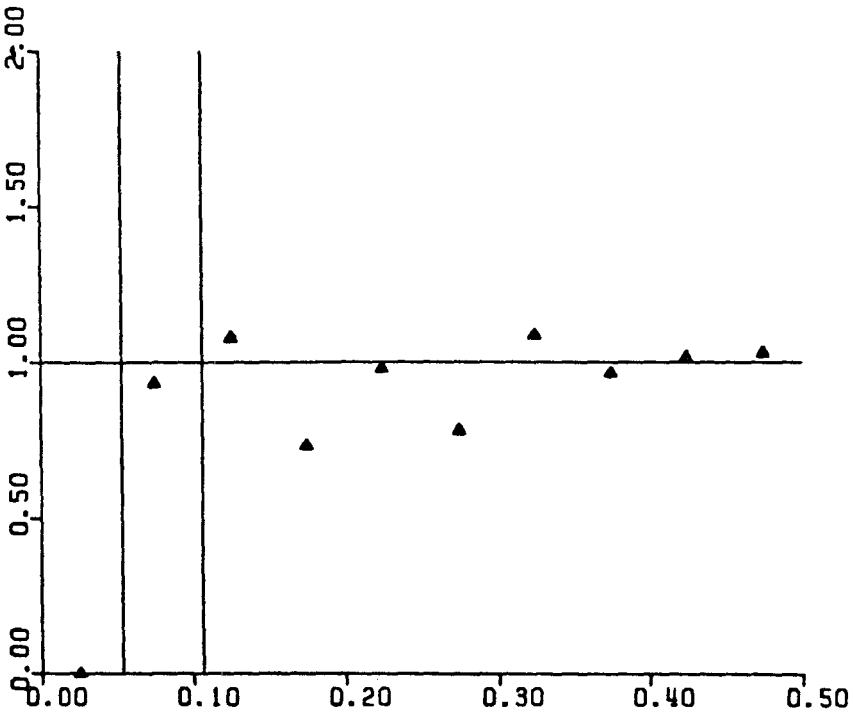
2.00
1.50
1.00
0.50
0.00
0.00
0.10
0.20
0.30
0.40
0.50

T= 6.000

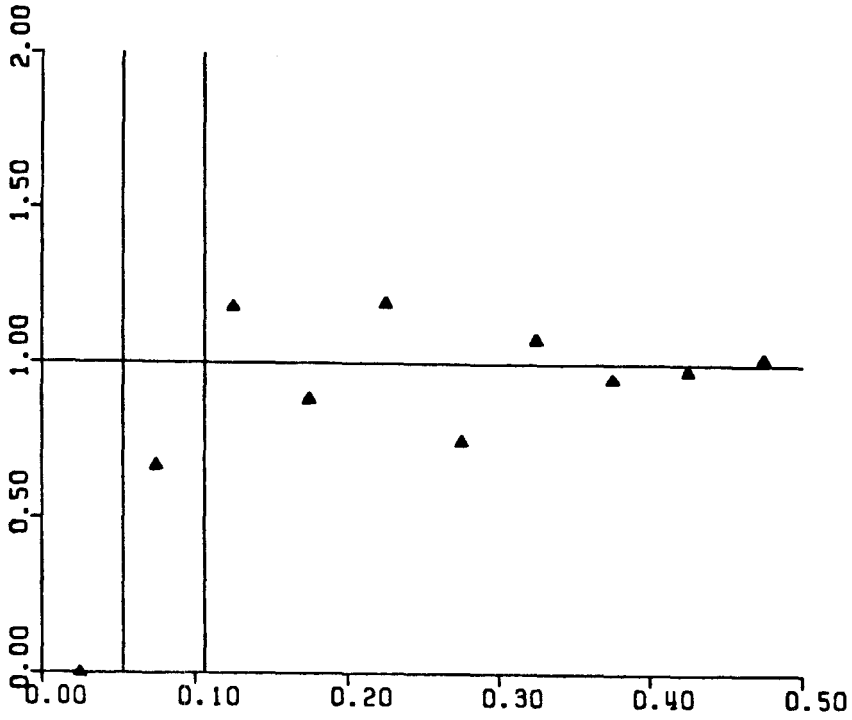
2.00
1.50
1.00
0.50
0.00
0.00
0.10
0.20
0.30
0.40
0.50

T= 6.400

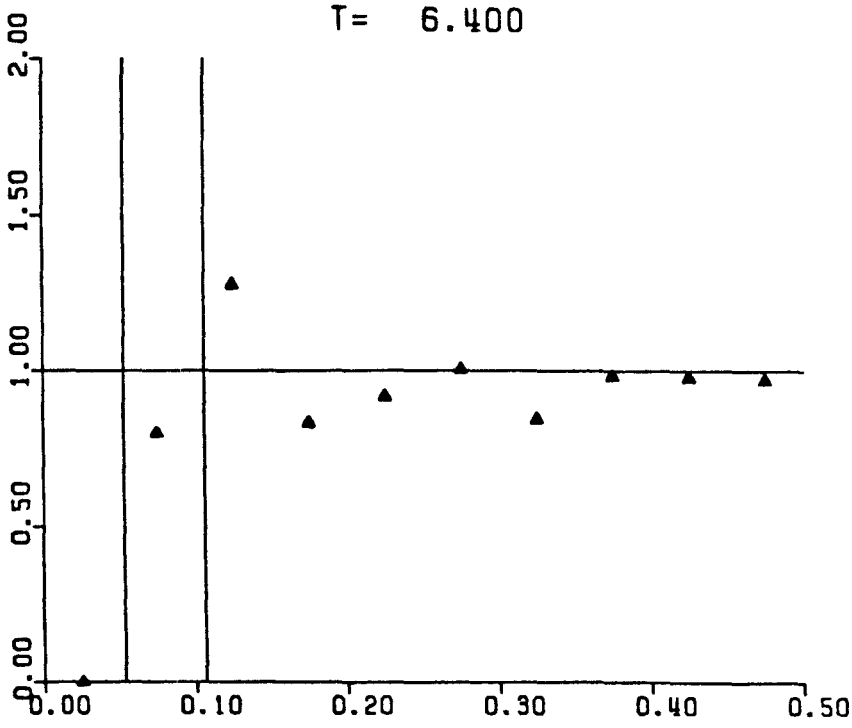
2.00
1.50
1.00
0.50
0.00
0.00
0.10
0.20
0.30
0.40
0.50

T= 6.800

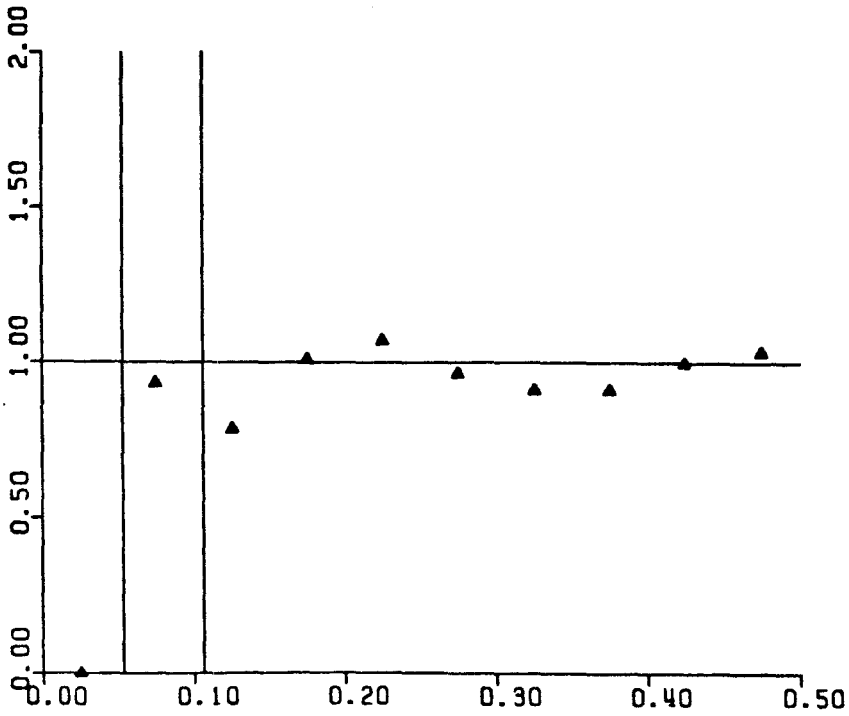
2.00
1.50
1.00
0.50
0.00
0.00
0.10
0.20
0.30
0.40
0.50

T= 7.200

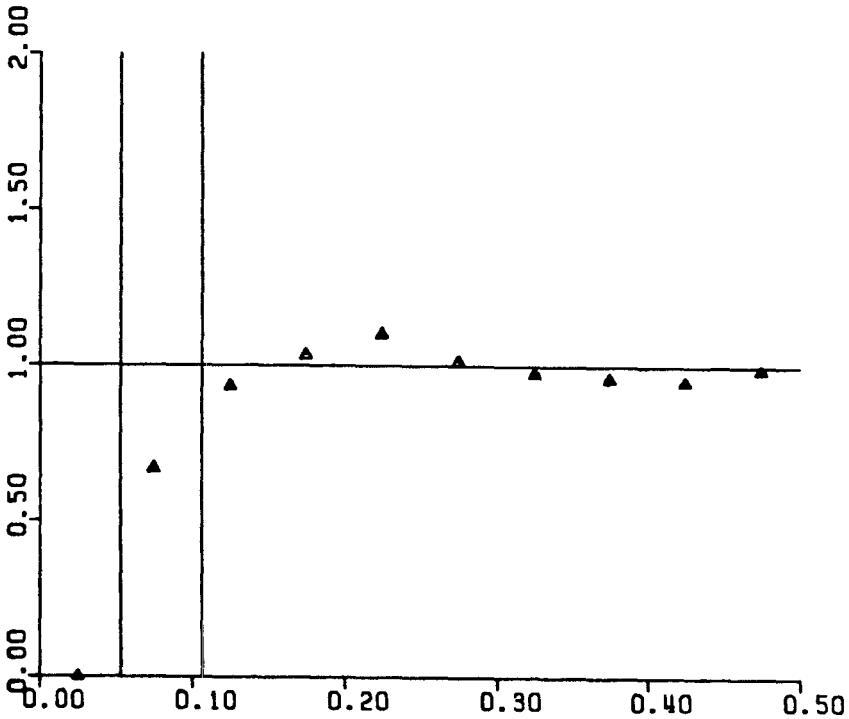
2.00
1.50
1.00
0.50
0.00
0.00
0.10
0.20
0.30
0.40
0.50

T= 7.600

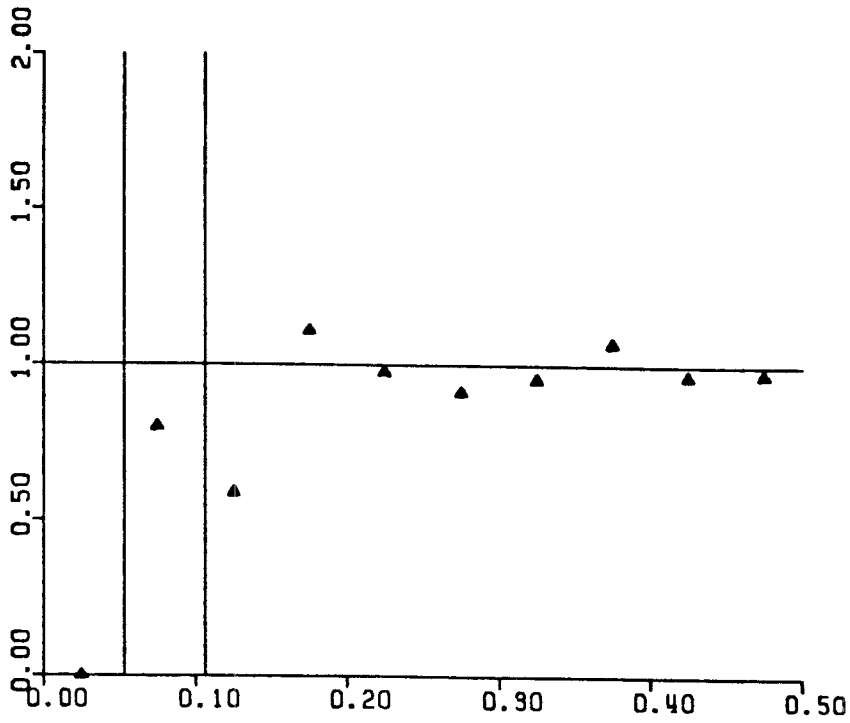


T= 8.000

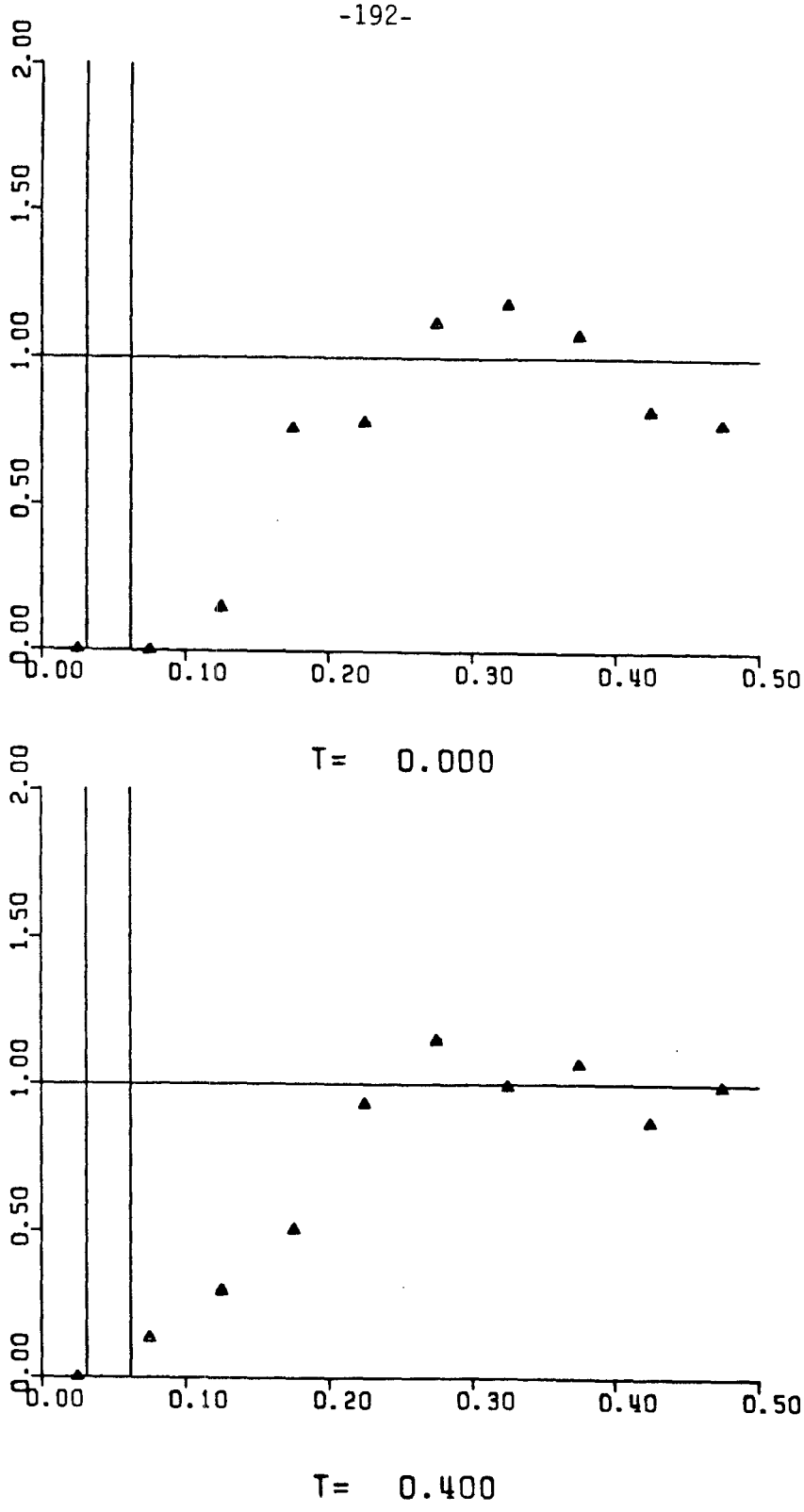


**Figure 29.** Pair-probability function for simulation run 2.

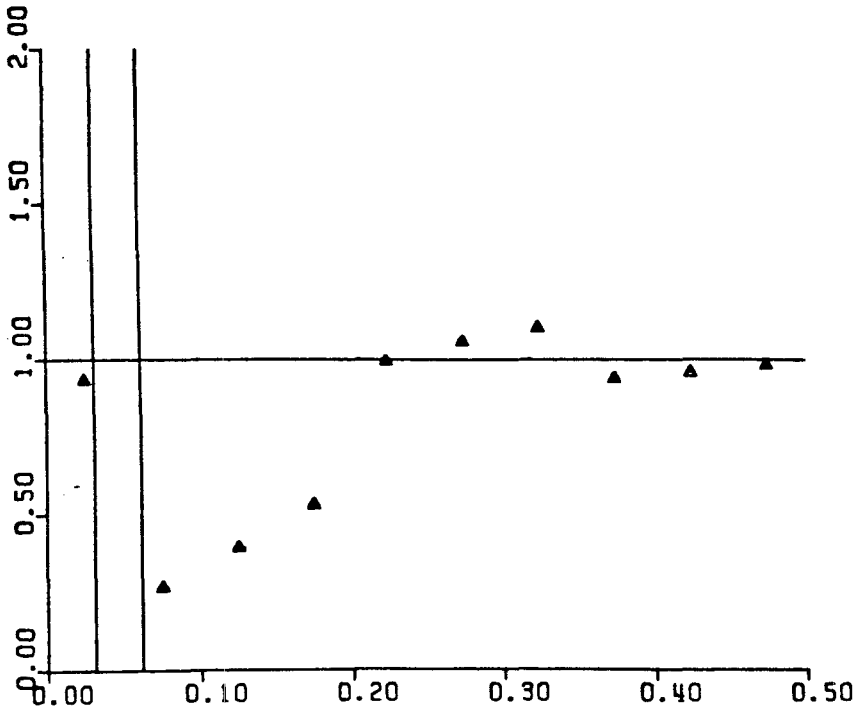
2.00
1.50
1.00
0.50
0.00
0.00
0.10
0.20
0.30
0.40
0.50

T= 0.800

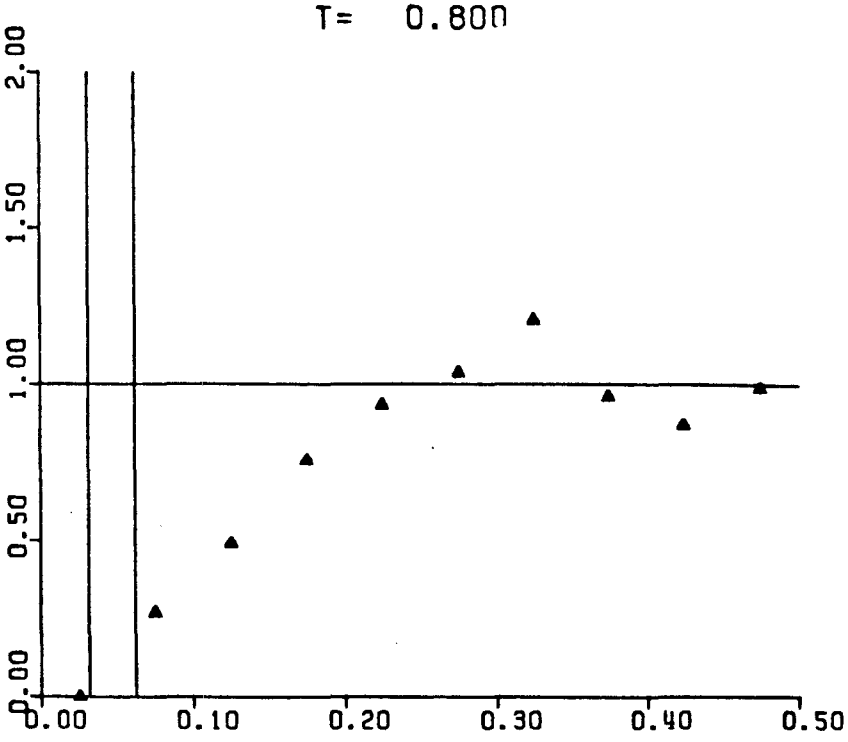
2.00
1.50
1.00
0.50
0.00
0.00
0.10
0.20
0.30
0.40
0.50

T= 1.200

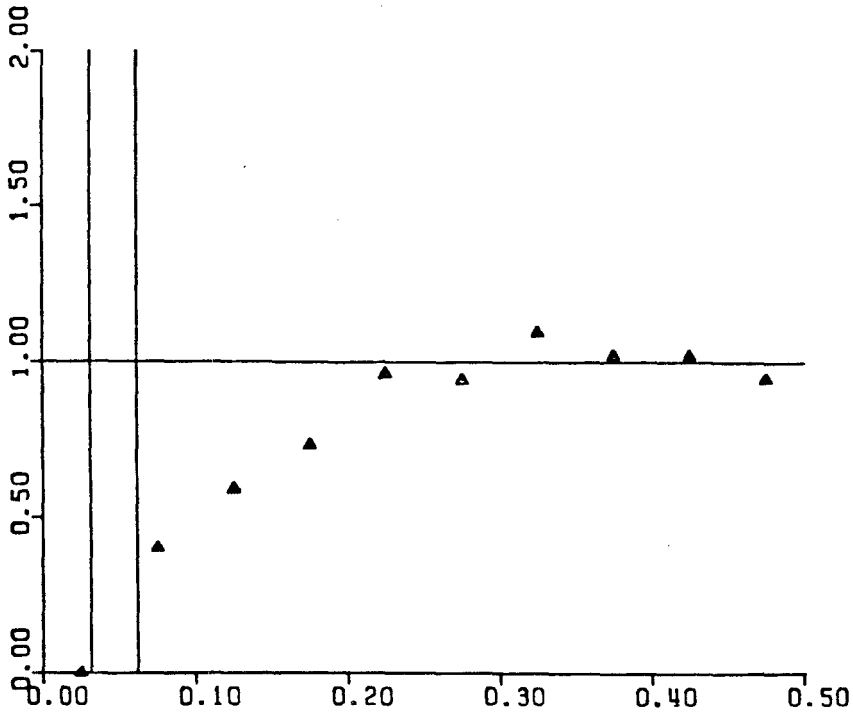
2.00
1.50
1.00
0.50
0.00
0.00
0.10
0.20
0.30
0.40
0.50

T= 1.600

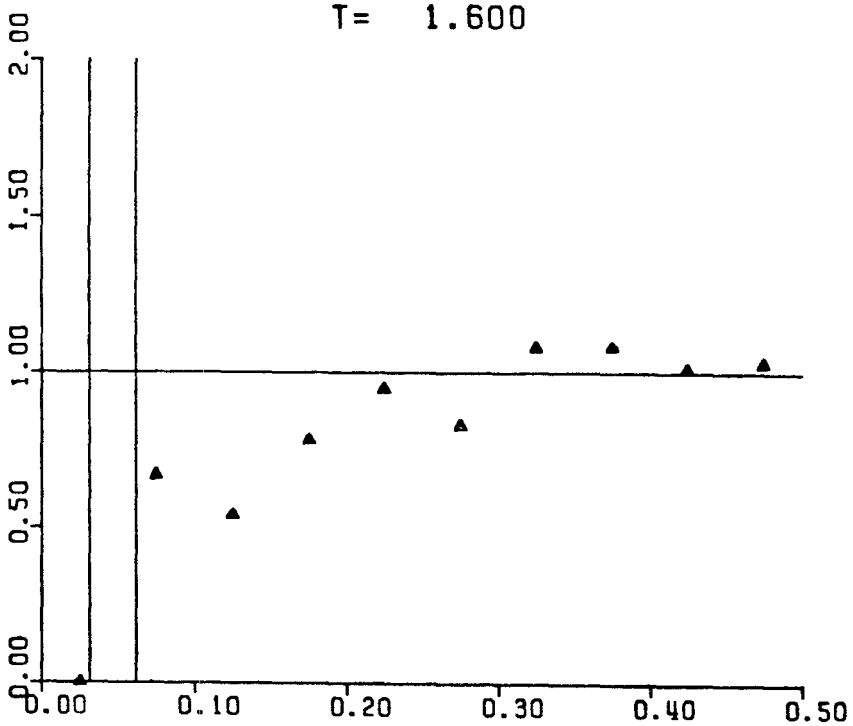
2.00
1.50
1.00
0.50
0.00
0.00
0.10
0.20
0.30
0.40
0.50

T= 2.000

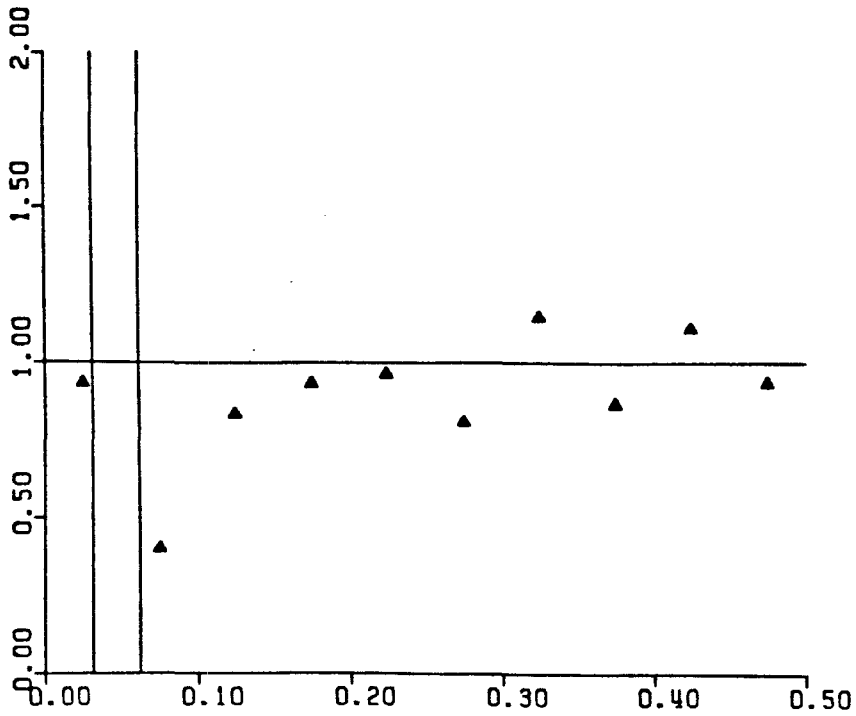
2.00
1.50
1.00
0.50
0.00
0.00
0.10
0.20
0.30
0.40
0.50

T= 2.400

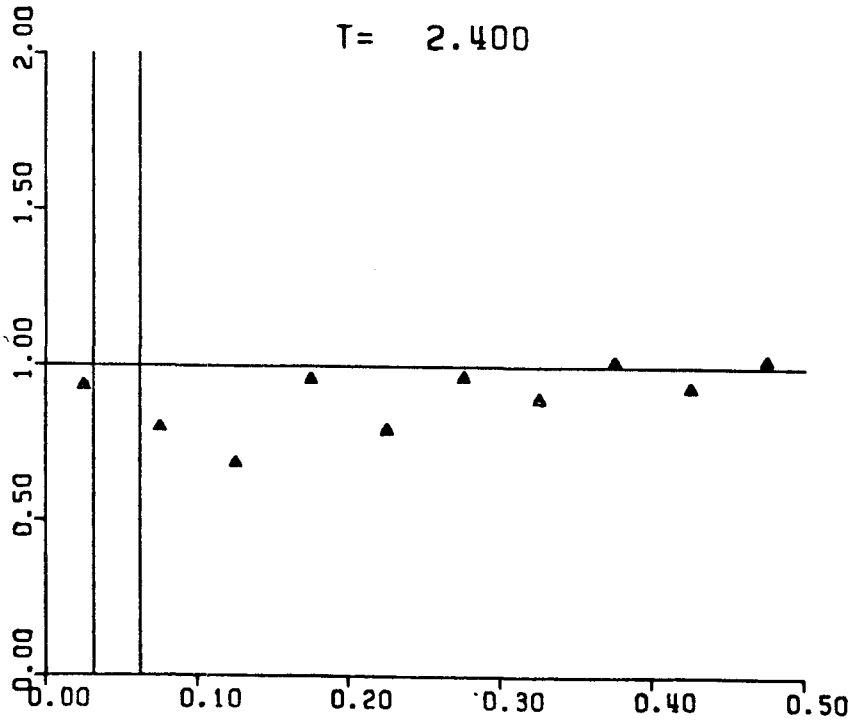
2.00
1.50
1.00
0.50
0.00
0.00
0.10
0.20
0.30
0.40
0.50

T= 2.800

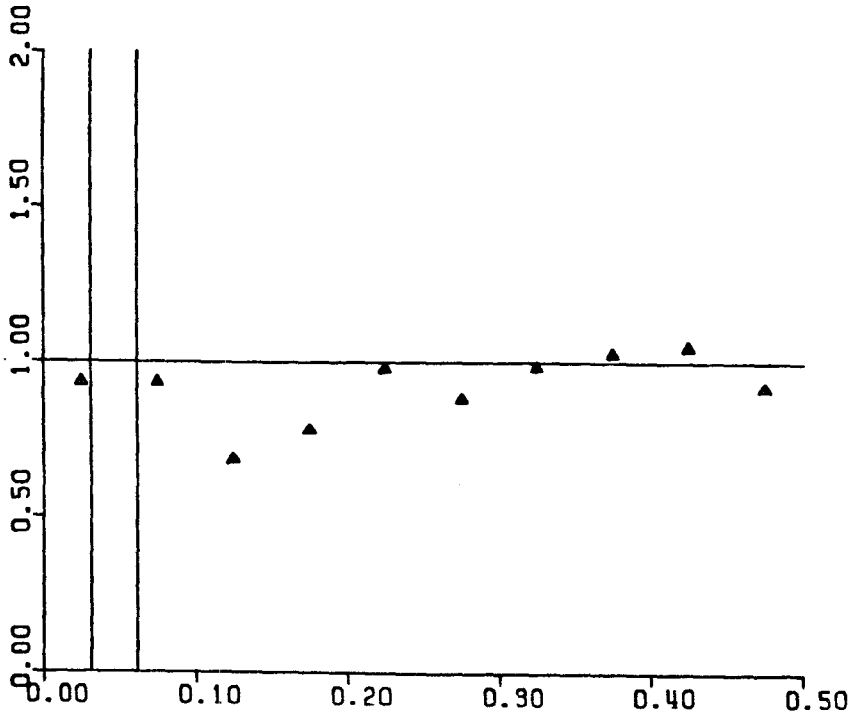
2.00
1.50
1.00
0.50
0.00
0.00
0.10
0.20
0.30
0.40
0.50

T= 3.200

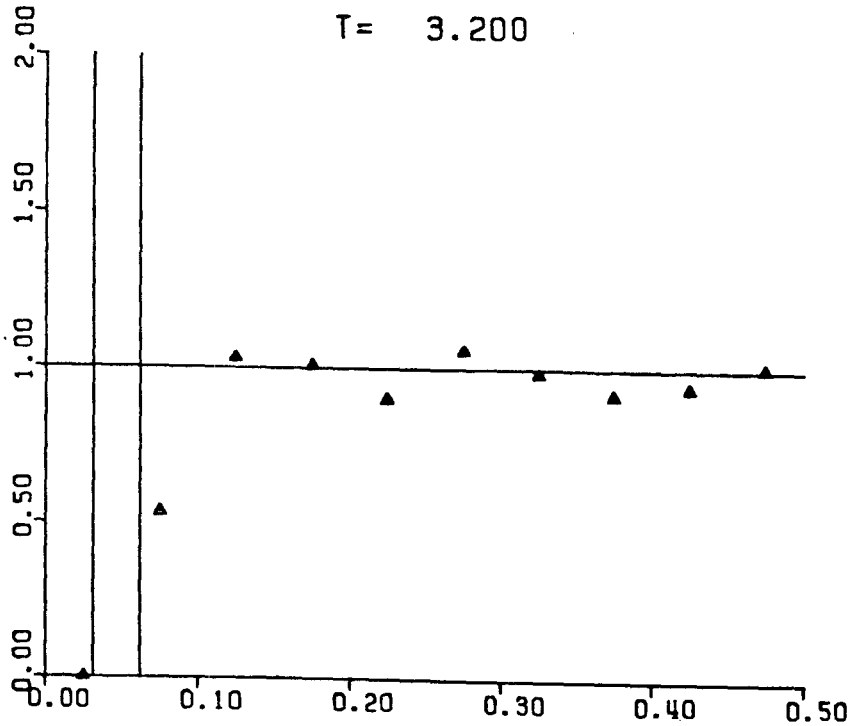
2.00
1.50
1.00
0.50
0.00
0.00
0.10
0.20
0.30
0.40
0.50

T= 3.600

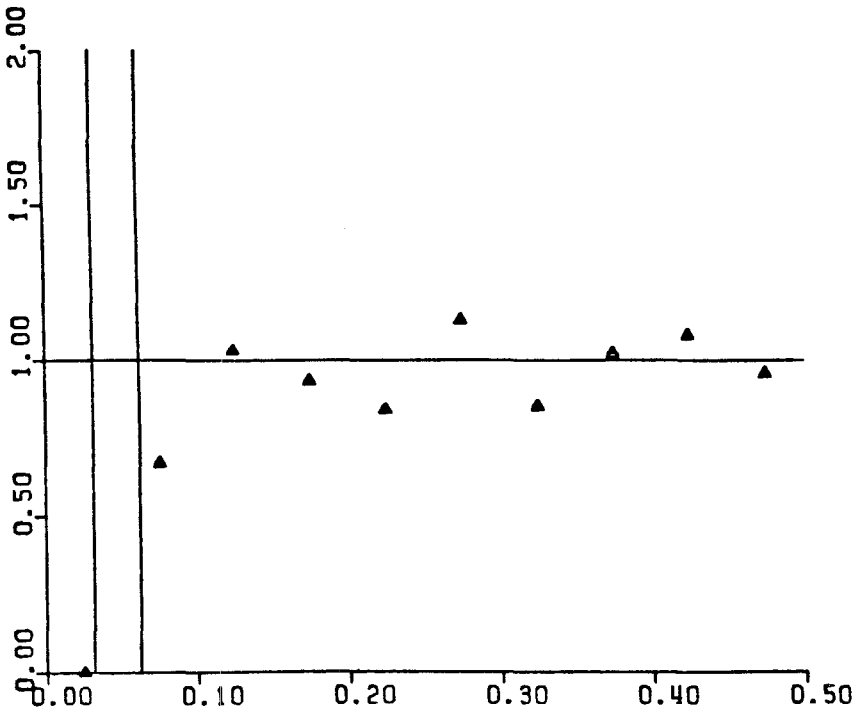
2.00
1.50
1.00
0.50
0.00
0.00
0.10
0.20
0.30
0.40
0.50

T= 4.000

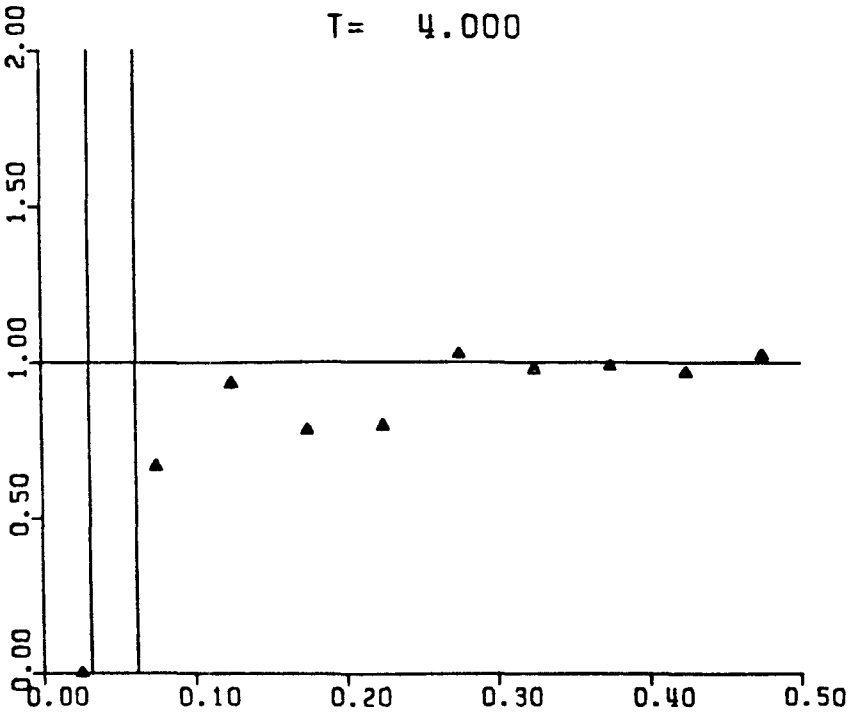
2.00
1.50
1.00
0.50
0.00
0.00
0.10
0.20
0.30
0.40
0.50

T= 4.400

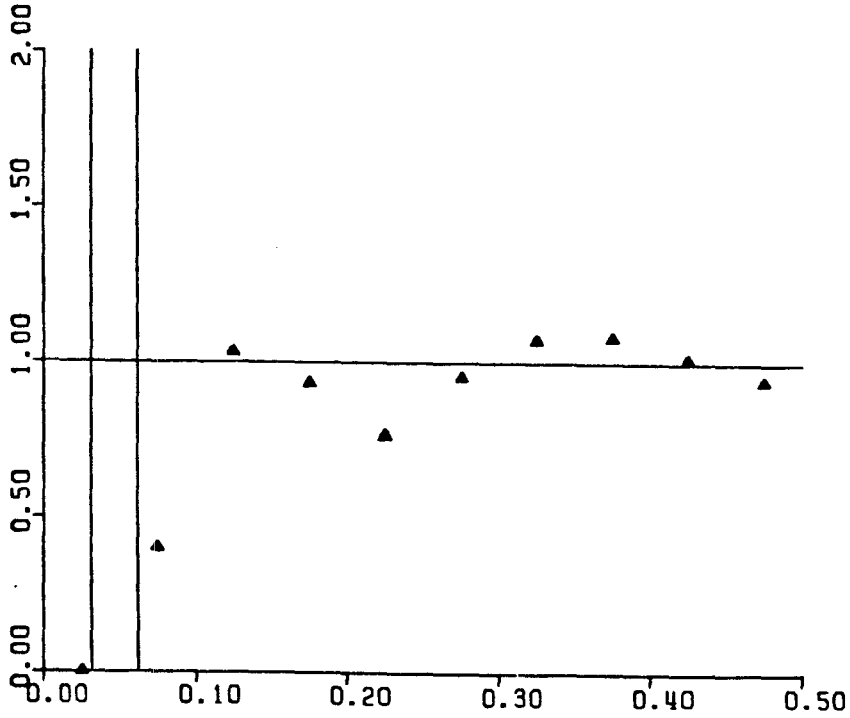
2.00
1.50
1.00
0.50
0.00
0.00
0.10
0.20
0.30
0.40
0.50

T= 4.800

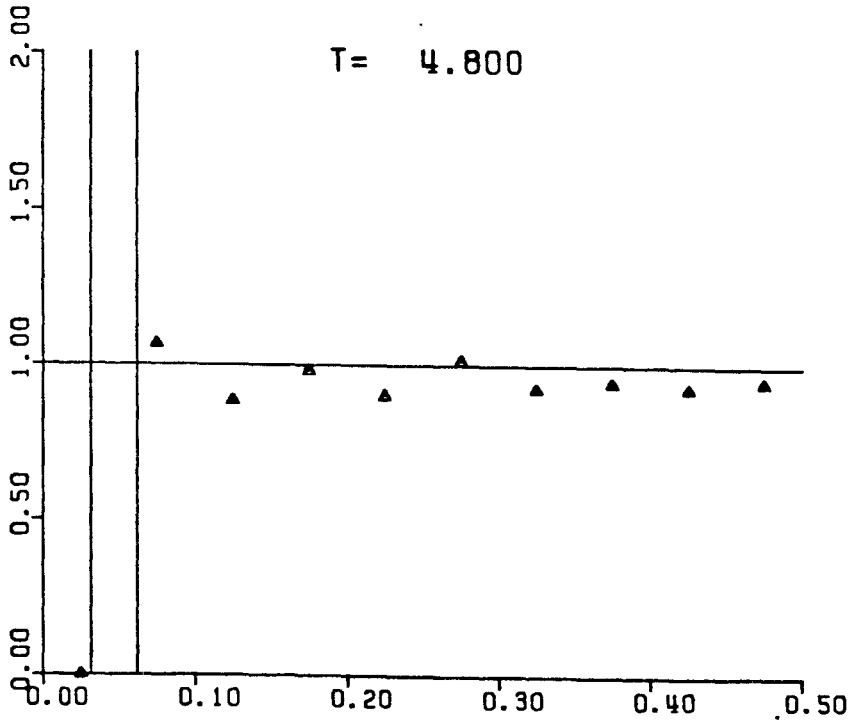
2.00
1.50
1.00
0.50
0.00
0.00
0.10
0.20
0.30
0.40
0.50

T= 5.200

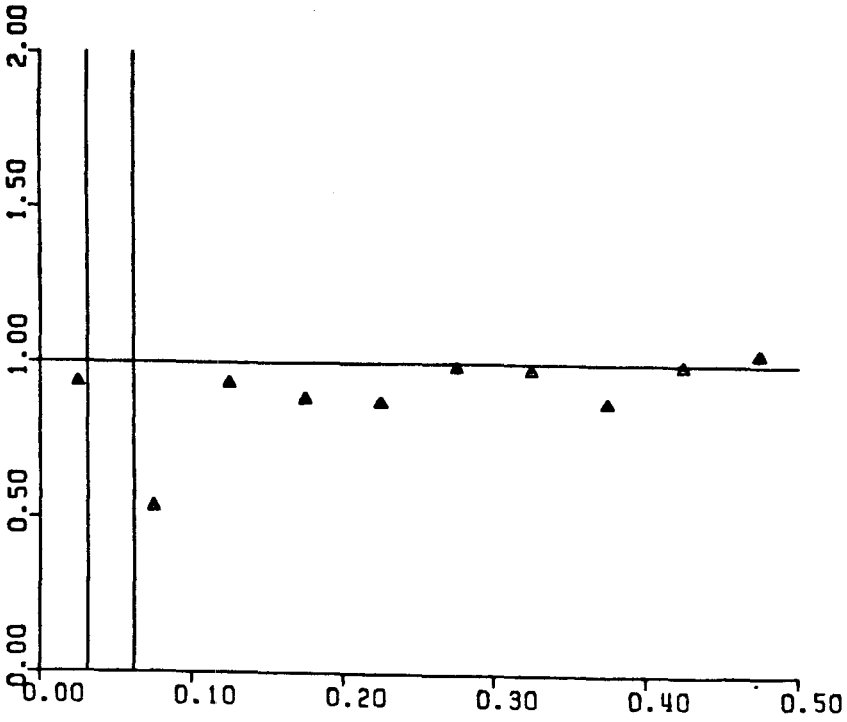
2.00
1.50
1.00
0.50
0.00
0.00
0.10
0.20
0.30
0.40
0.50

T= 5.600

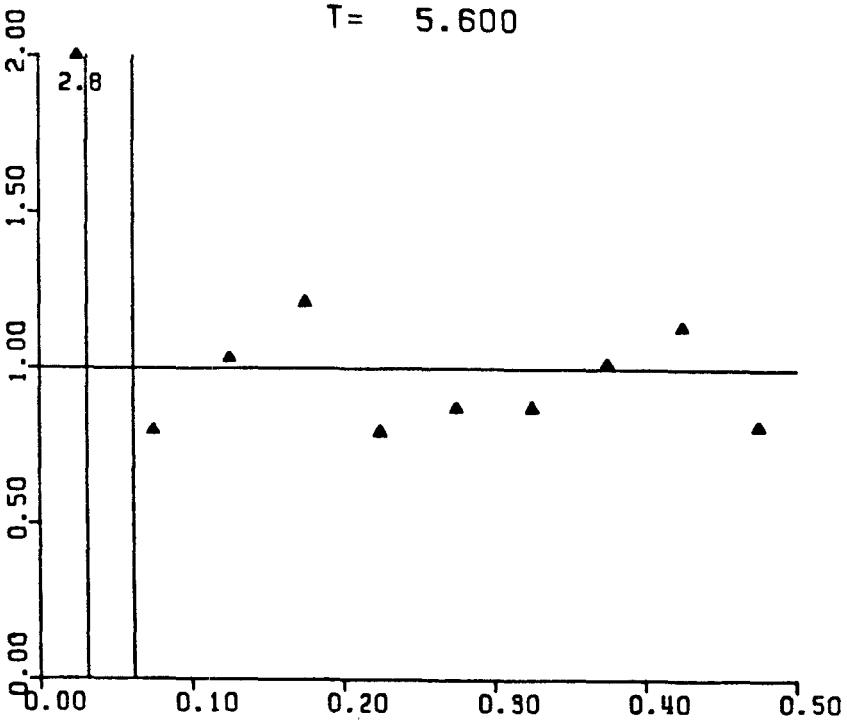
2.00
1.50
1.00
0.50
0.00
2.8
0.00
0.10
0.20
0.30
0.40
0.50

T= 6.001

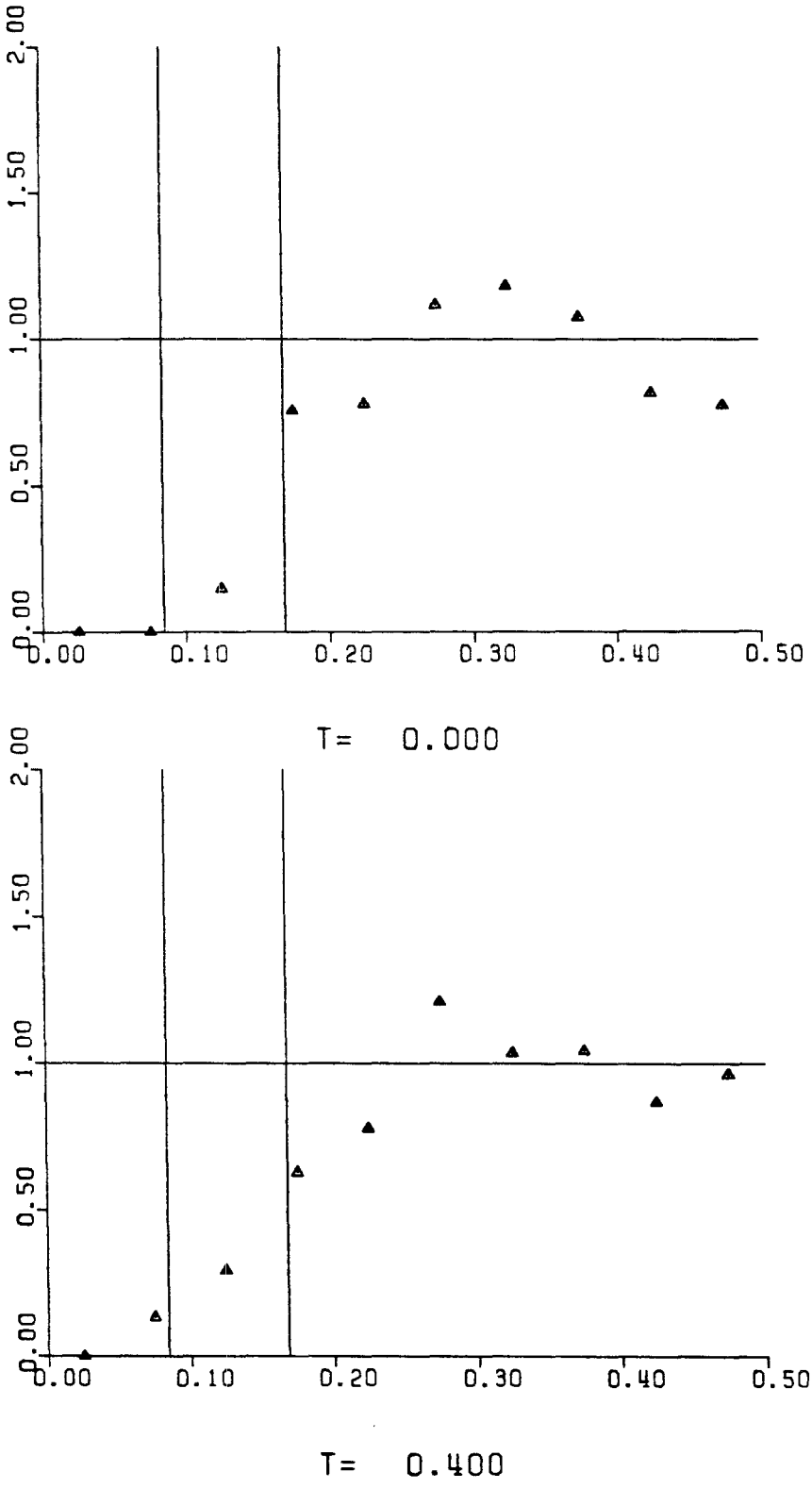


**Figure 30.** Pair-probability function for simulation run 3.

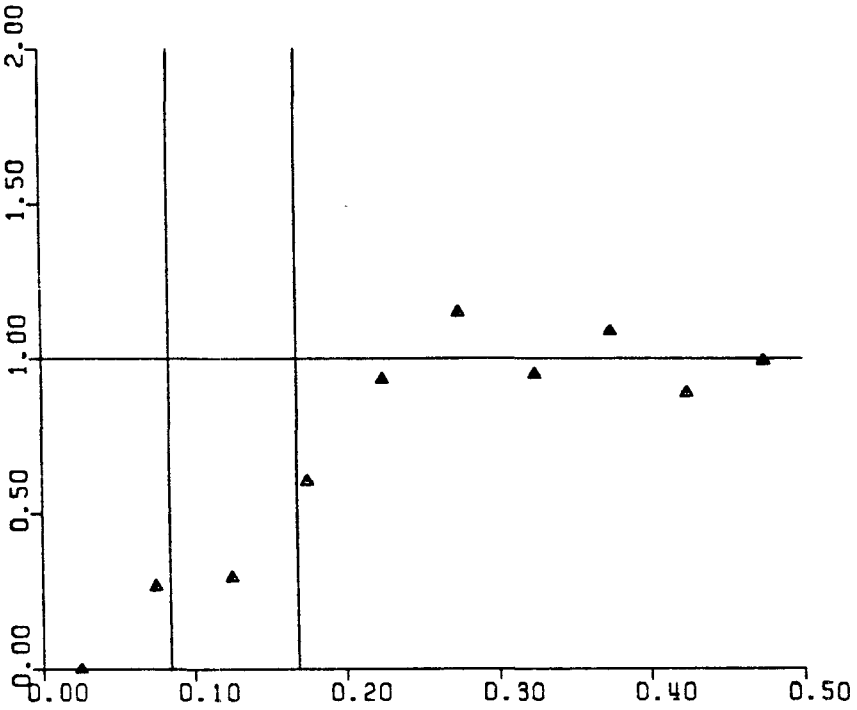
2.00
1.50
1.00
0.50
0.00
0.00
0.10
0.20
0.30
0.40
0.50

0.800

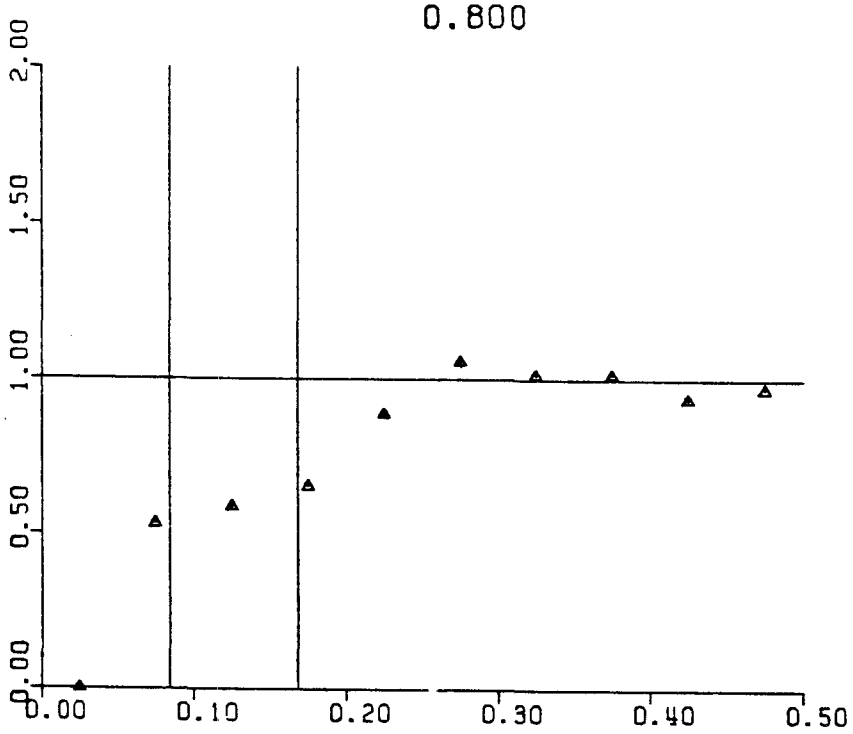
2.00
1.50
1.00
0.50
0.00
0.00
0.10
0.20
0.30
0.40
0.50

T= 1.200

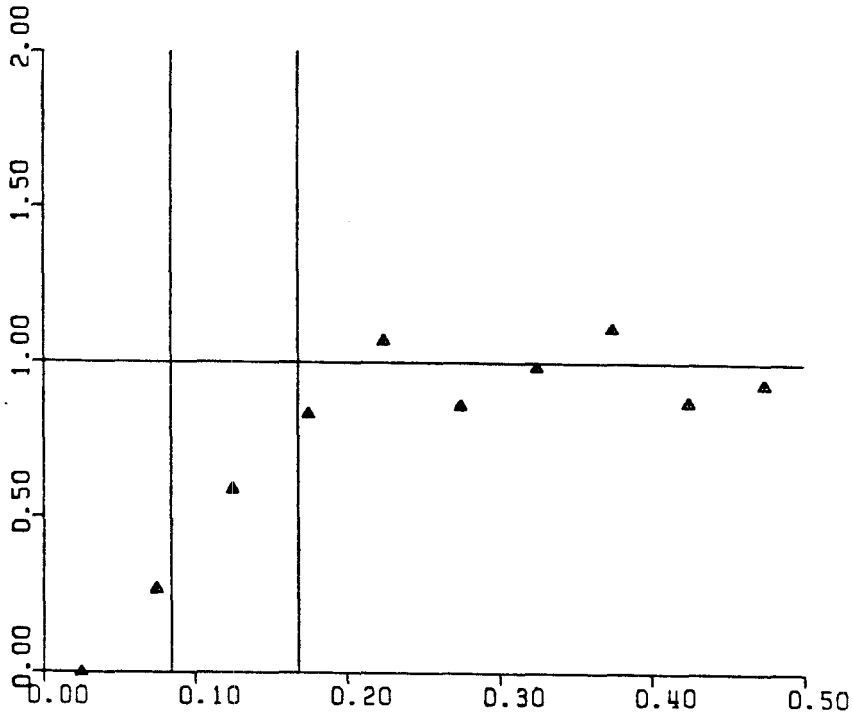
2.00
1.50
1.00
0.50
0.00
0.00
0.10
0.20
0.30
0.40
0.50

T= 1.600

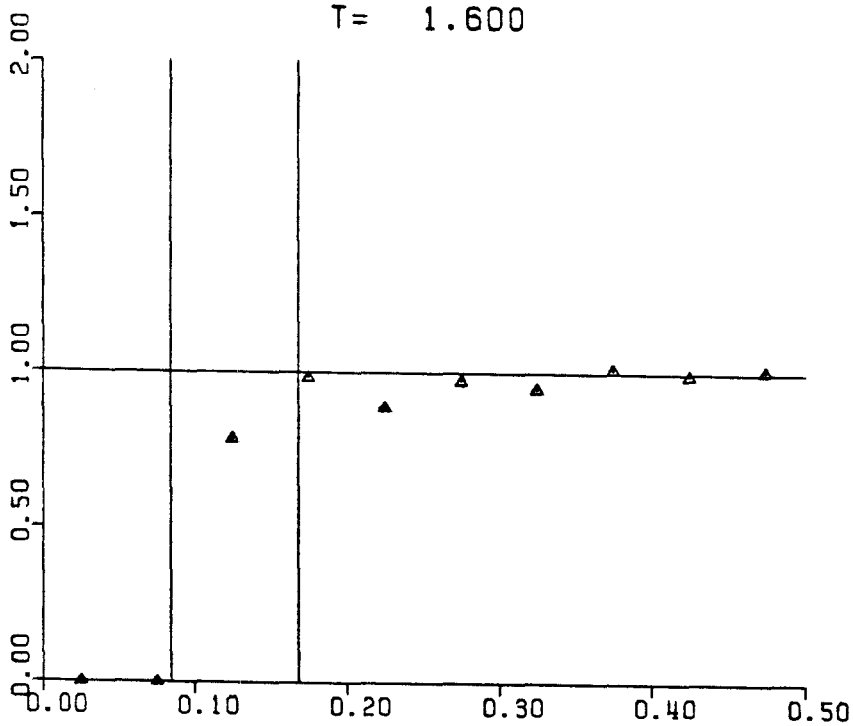
2.00
1.50
1.00
0.50
0.00
0.00
0.10
0.20
0.30
0.40
0.50

T= 2.000

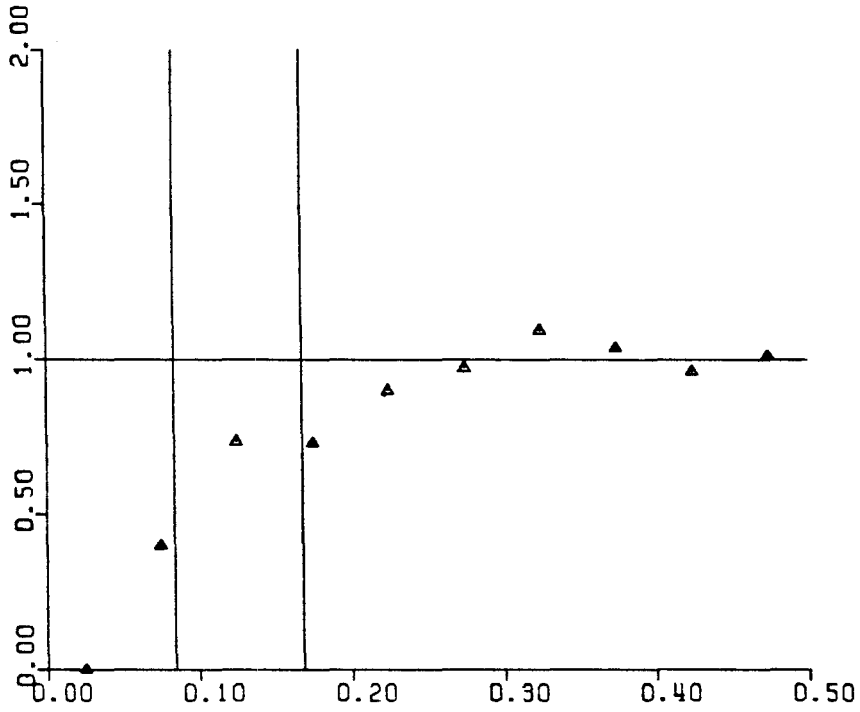
2.00
1.50
1.00
0.50
0.00
0.00
0.10
0.20
0.30
0.40
0.50

T= 2.400

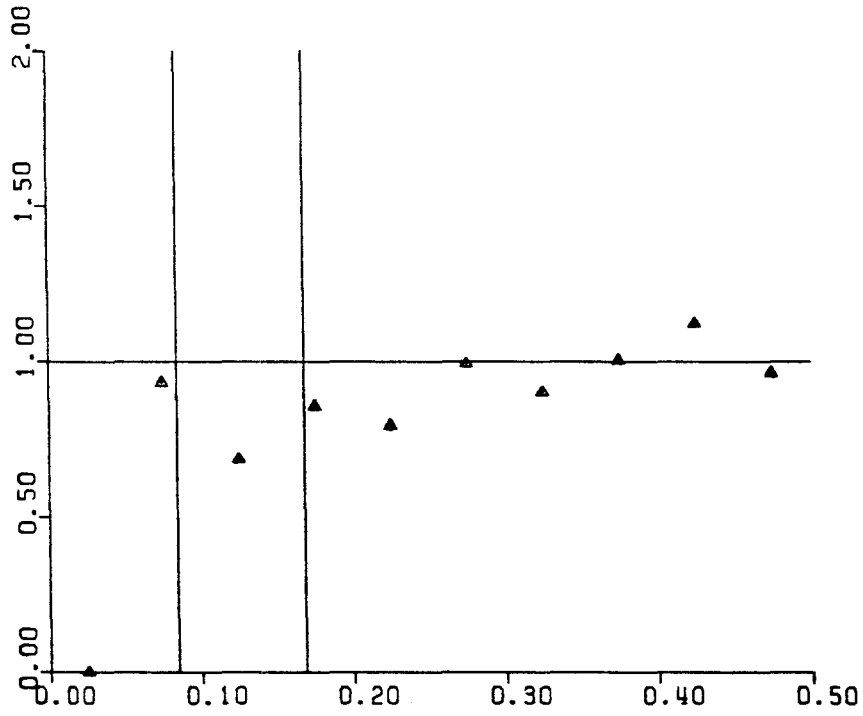
2.00
1.50
1.00
0.50
0.00
0.00
0.10
0.20
0.30
0.40
0.50

T= 2.800

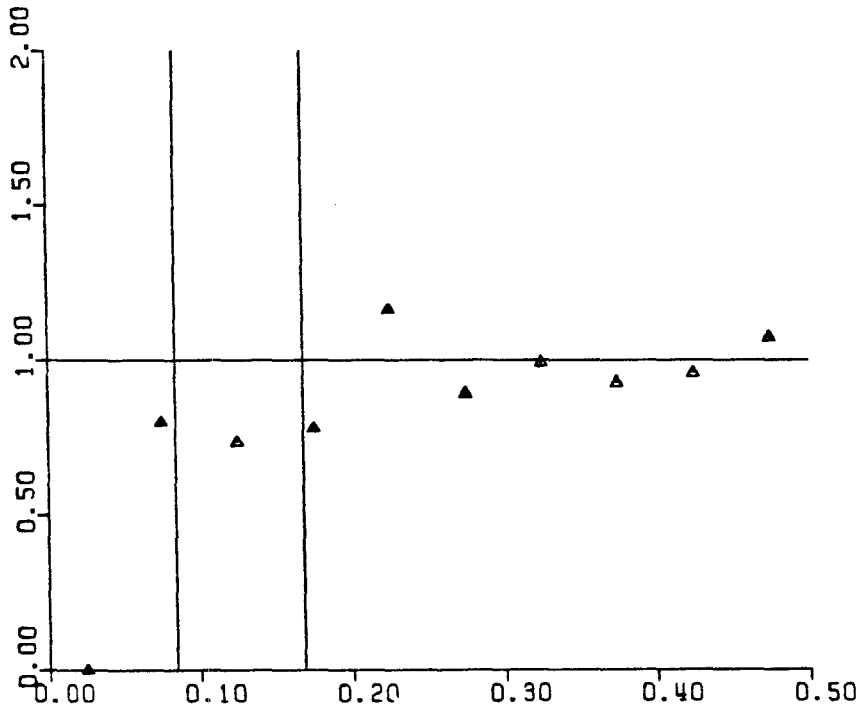
2.00
1.50
1.00
0.50
0.00
0.00
0.10
0.20
0.30
0.40
0.50

T= 3.200

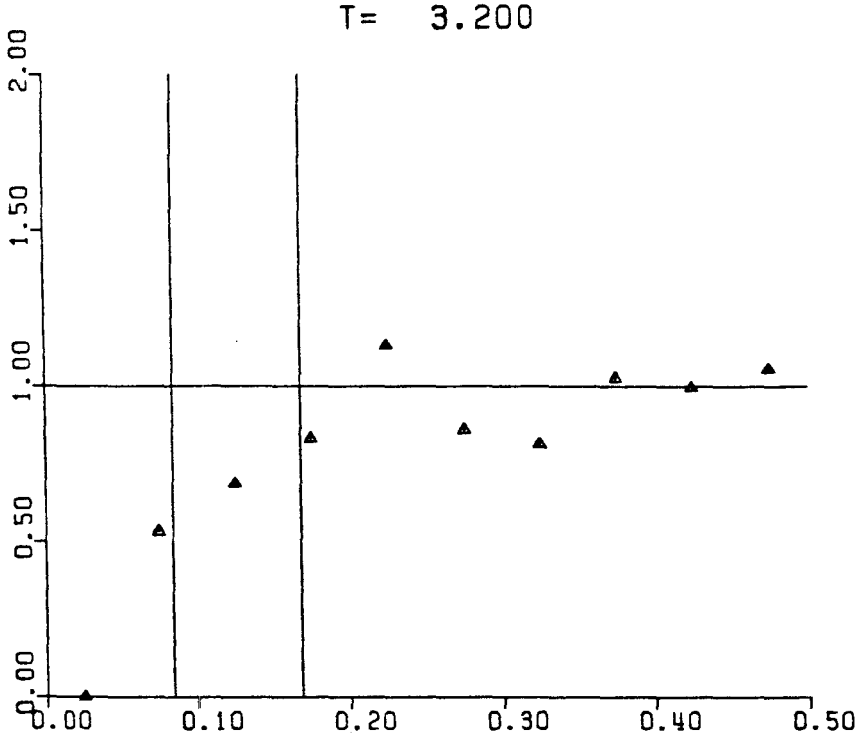
2.00
1.50
1.00
0.50
0.00
0.00
0.10
0.20
0.30
0.40
0.50

T= 3.600

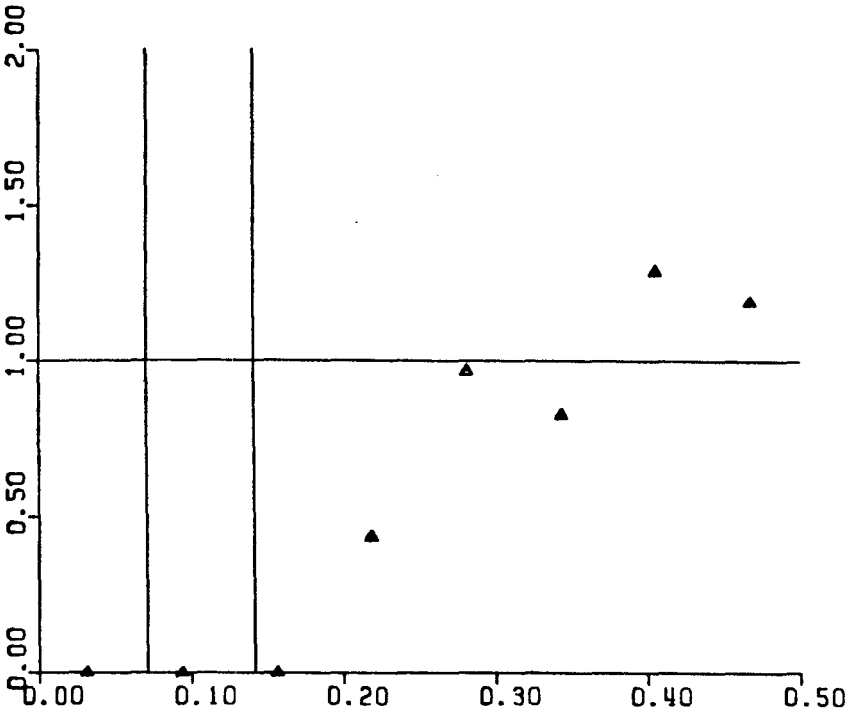


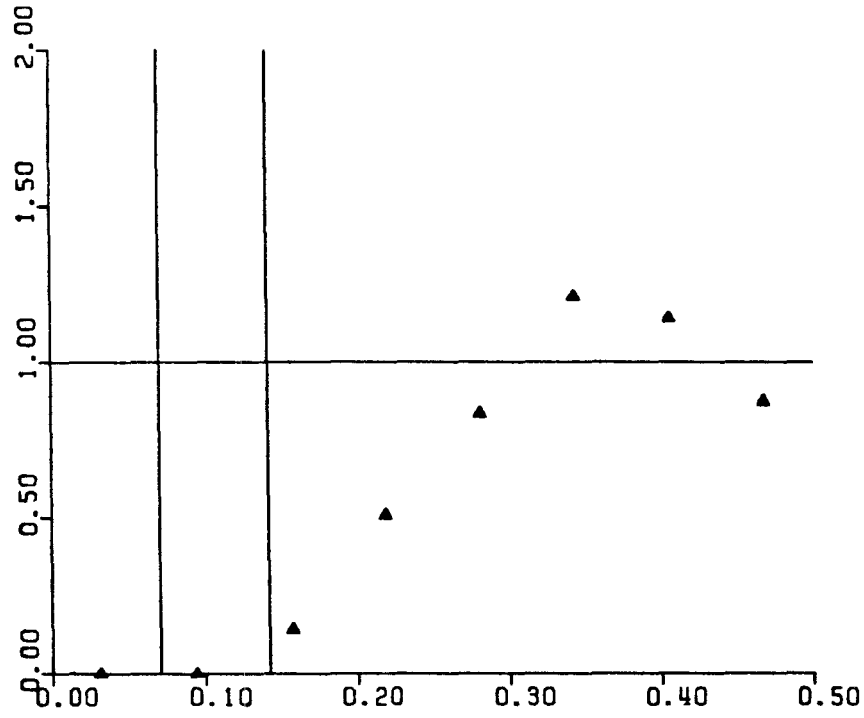


**Figure 31.** Pair-probability function for simulation run 4.

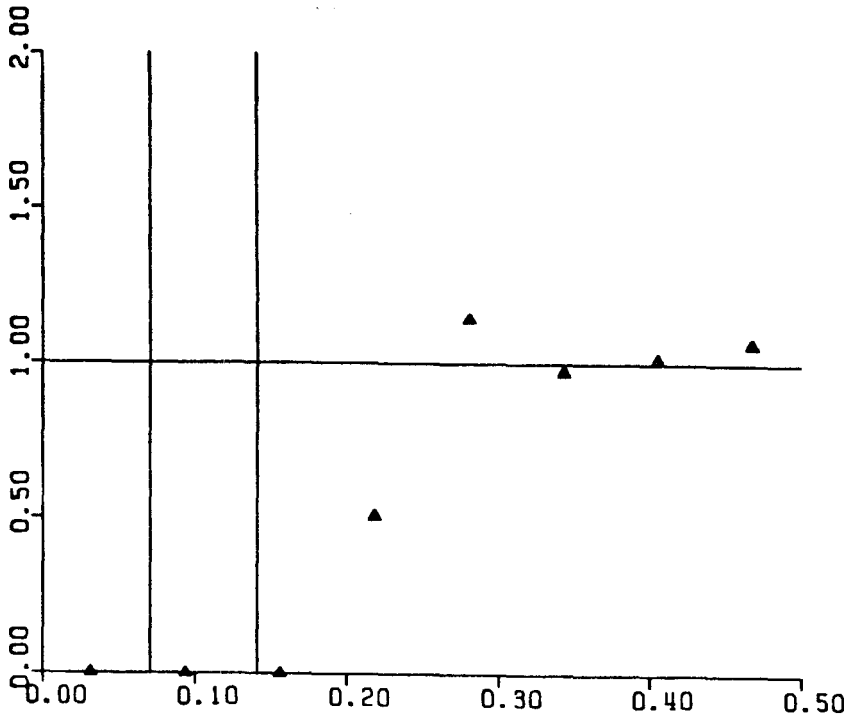
2.00
1.50
1.00
0.50
0.00
0.00
0.10
0.20
0.30
0.40
0.50

T= 0.800

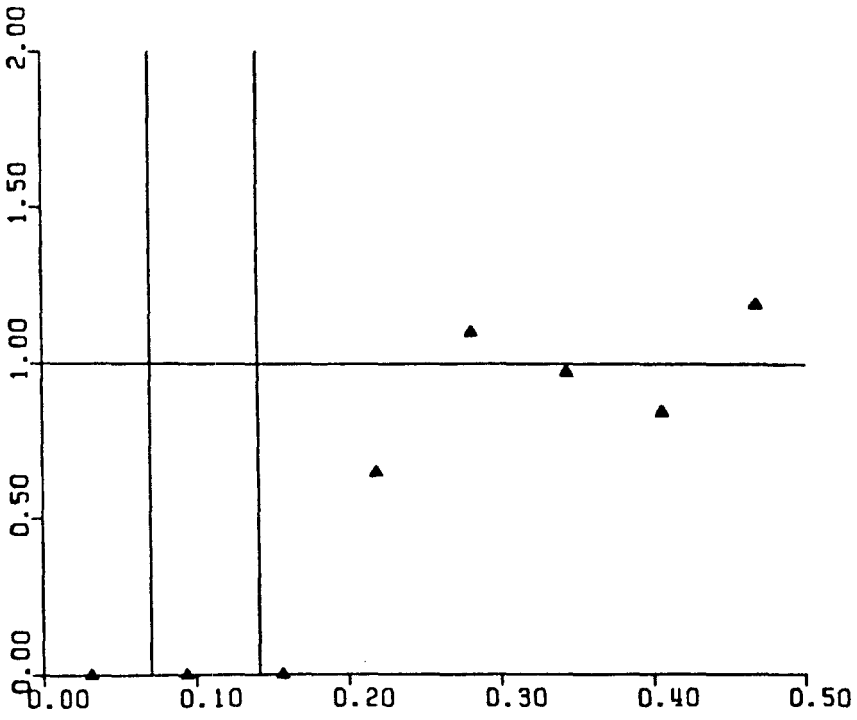
2.00
1.50
1.00
0.50
0.00
0.00
0.10
0.20
0.30
0.40
0.50

T= 1.200

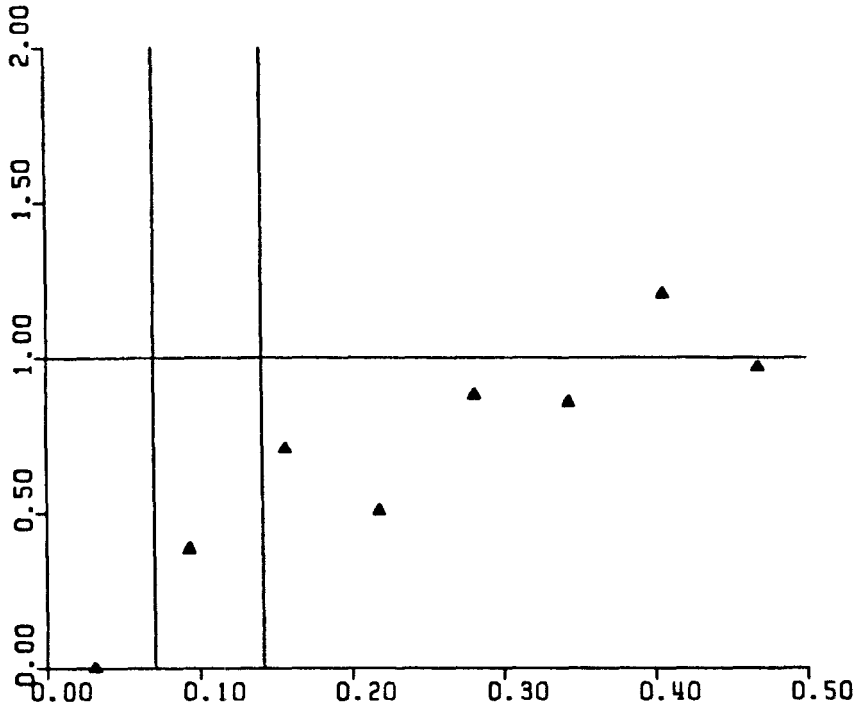
2.00
1.50
1.00
0.50
0.00
0.00
0.10
0.20
0.30
0.40
0.50

T= 1.600

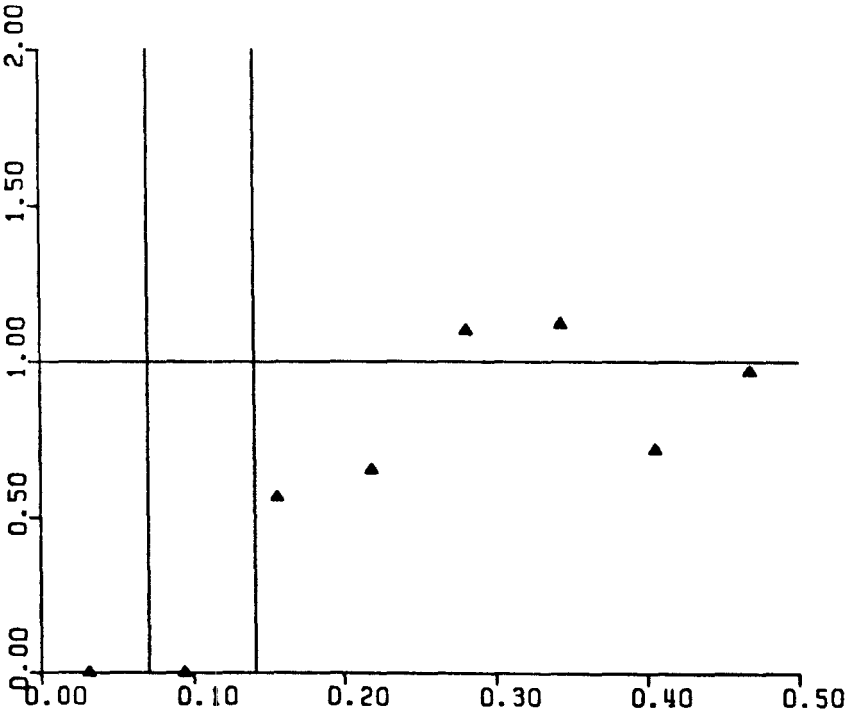
2.00
1.50
1.00
0.50
0.00
0.00
0.10
0.20
0.30
0.40
0.50

T= 2.000

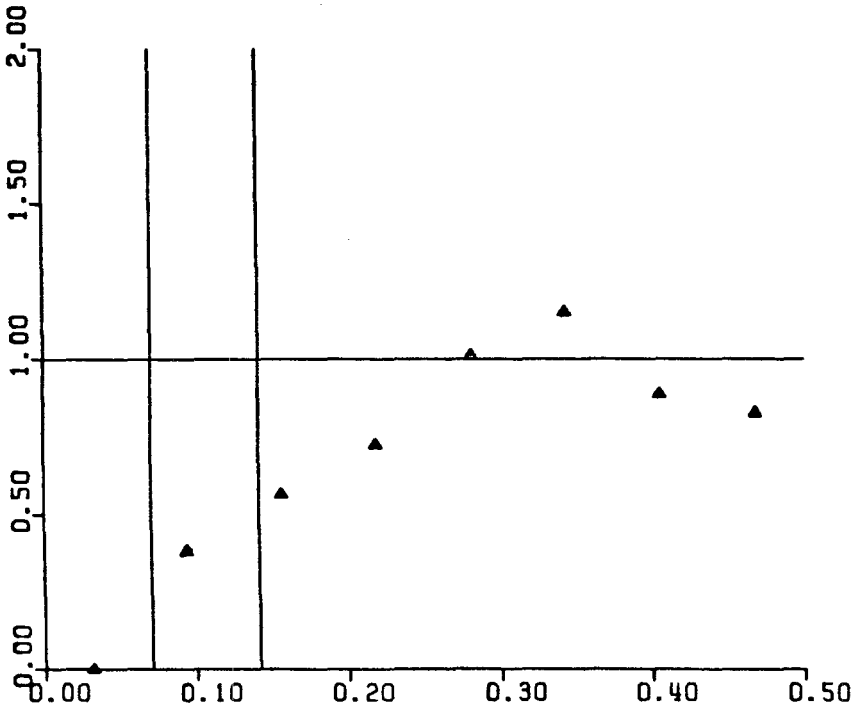
2.00
1.50
1.00
0.50
0.00
0.00
0.10
0.20
0.30
0.40
0.50

T= 2.400

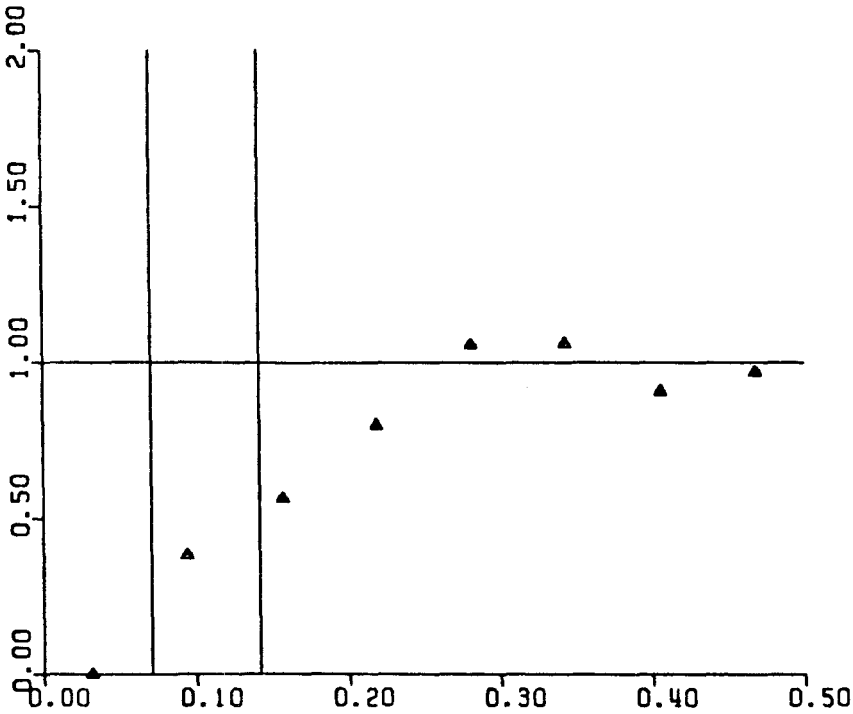
2.00
1.50
1.00
0.50
0.00
0.00
0.10
0.20
0.30
0.40
0.50

T= 2.800

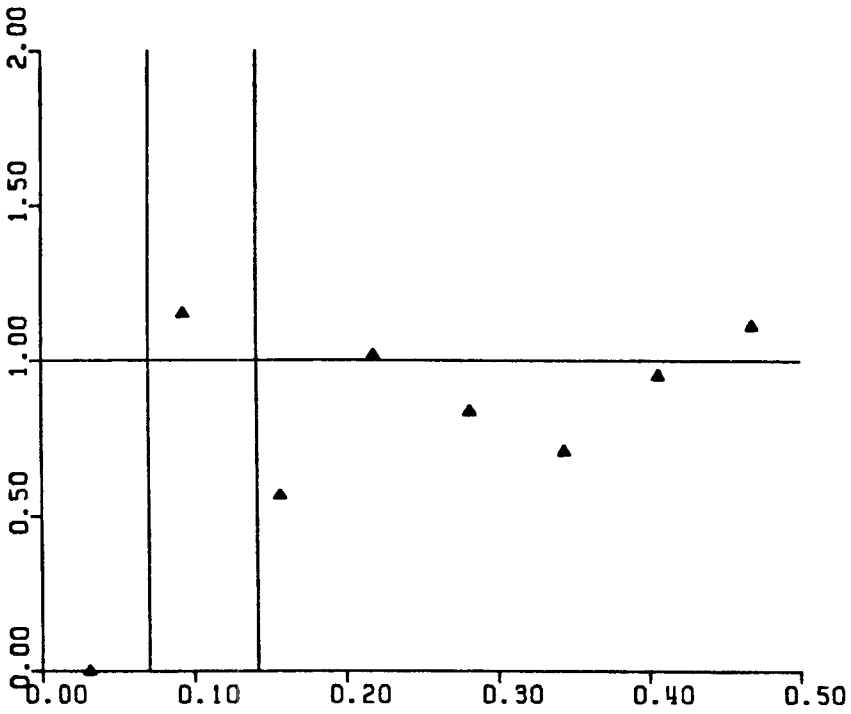
2.00
1.50
1.00
0.50
0.00
0.00
0.10
0.20
0.30
0.40
0.50

T= 3.200

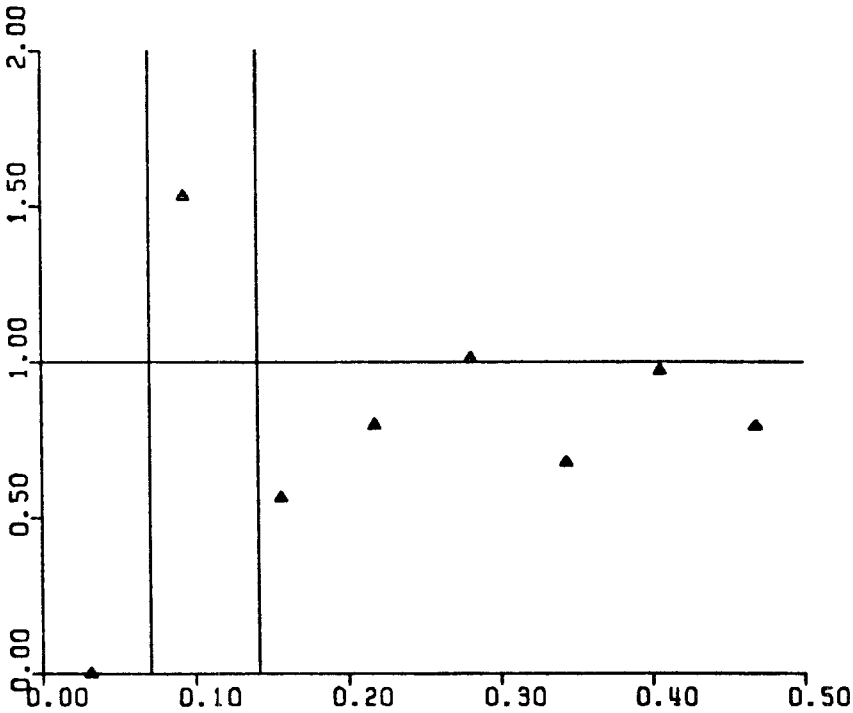
2.00
1.50
1.00
0.50
0.00
0.00
0.10
0.20
0.30
0.40
0.50

T= 3.600

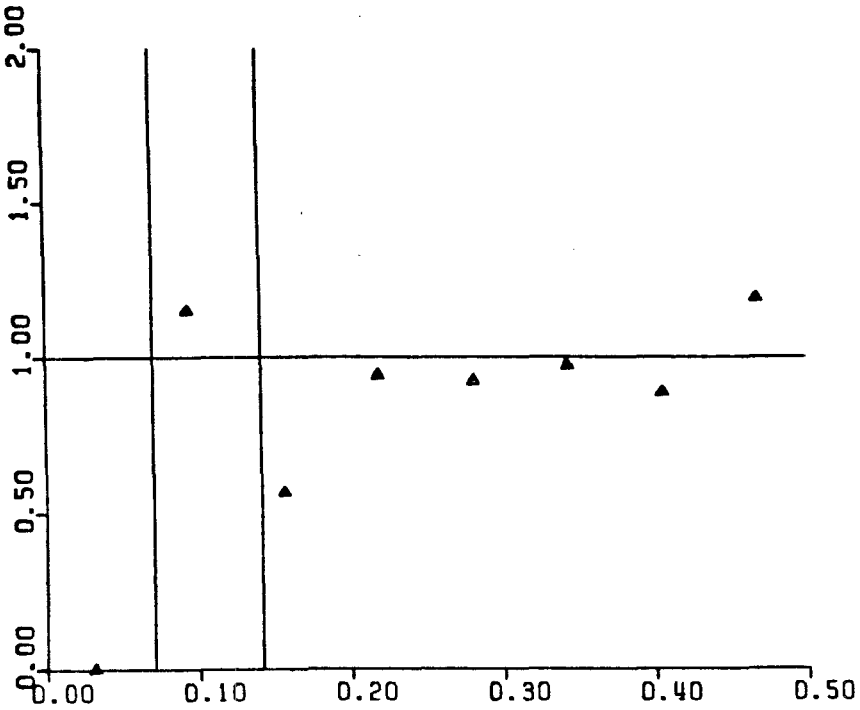
2.00
1.50
1.00
0.50
0.00
0.00
0.10
0.20
0.30
0.40
0.50

T= 4.000

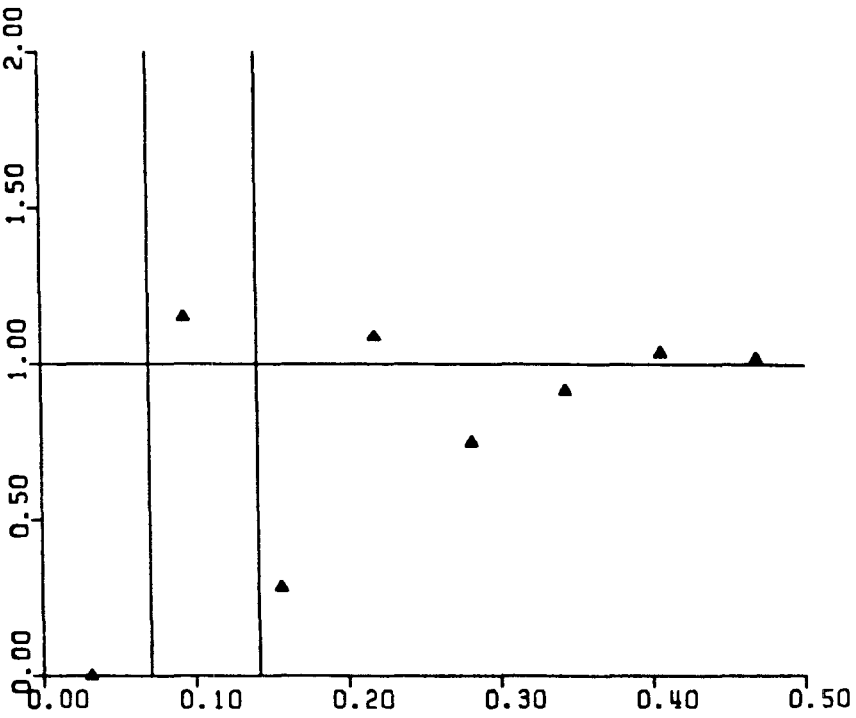
2.00
1.50
1.00
0.50
0.00
0.00
0.10
0.20
0.30
0.40
0.50

T= 4.400

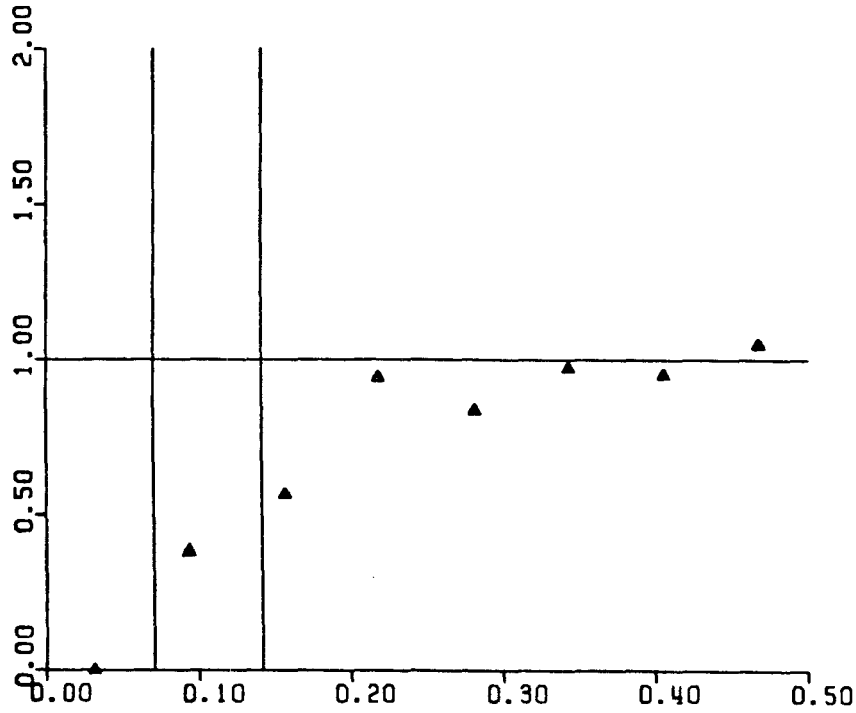
2.00
1.50
1.00
0.50
0.00
0.00
0.10
0.20
0.30
0.40
0.50

T= 4.800

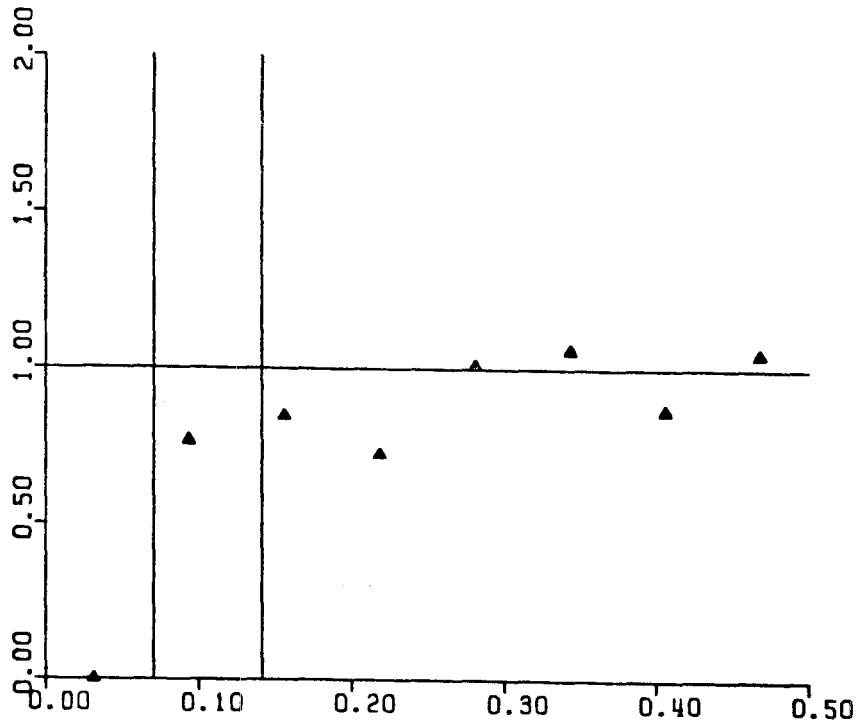
2.00
1.50
1.00
0.50
0.00
0.00
0.10
0.20
0.30
0.40
0.50

T= 5.200

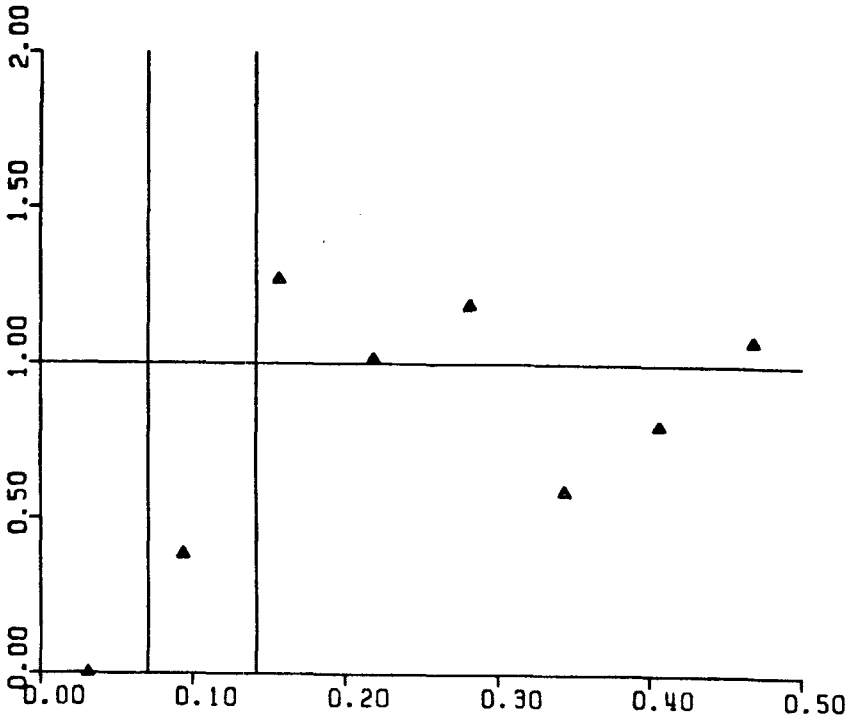
2.00
1.50
1.00
0.50
0.00
0.00
0.10
0.20
0.30
0.40
0.50

T= 5.600

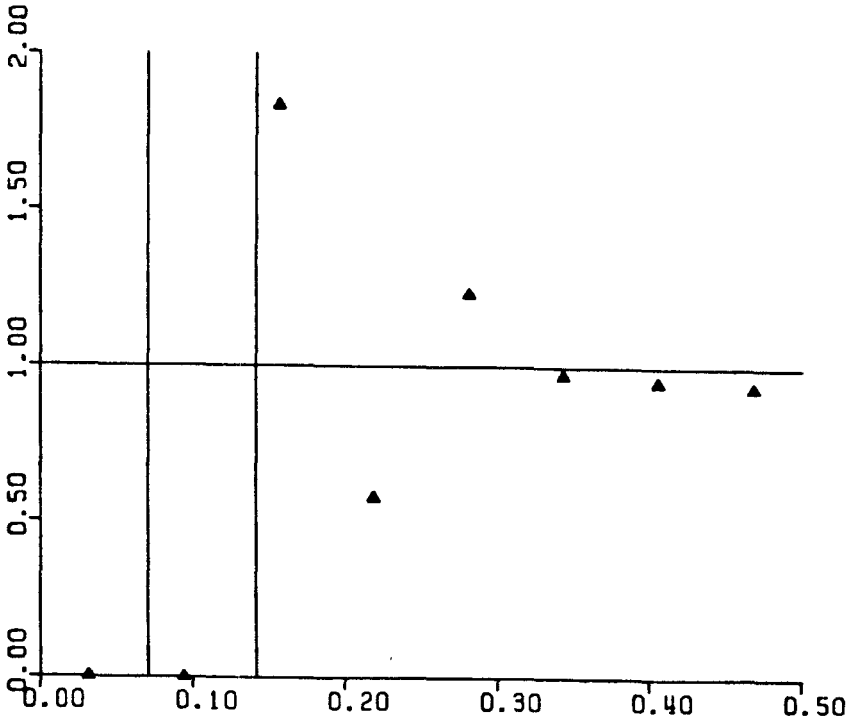
2.00
1.50
1.00
0.50
0.00
0.00
0.10
0.20
0.30
0.40
0.50

T= 6.000

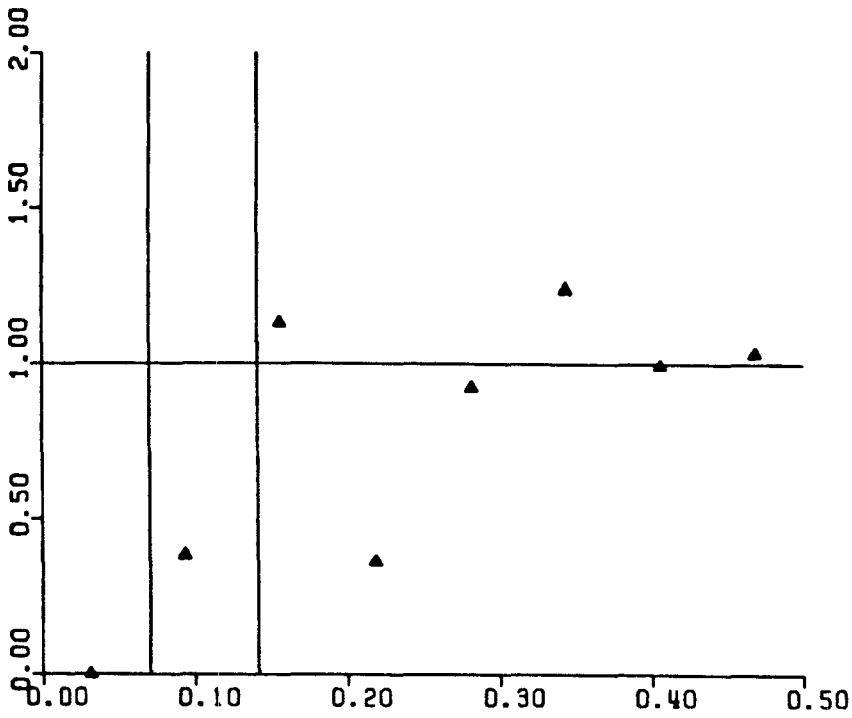
2.00
1.50
1.00
0.50
0.00
0.00
0.10
0.20
0.30
0.40
0.50

T= 6.400

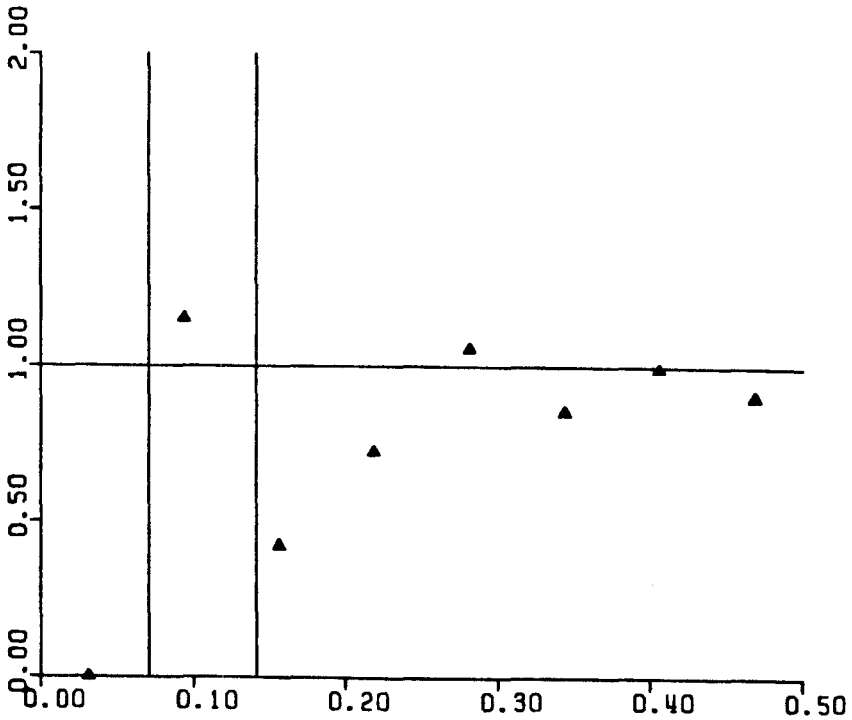
2.00
1.50
1.00
0.50
0.00
0.00
0.10
0.20
0.30
0.40
0.50

T= 6.800

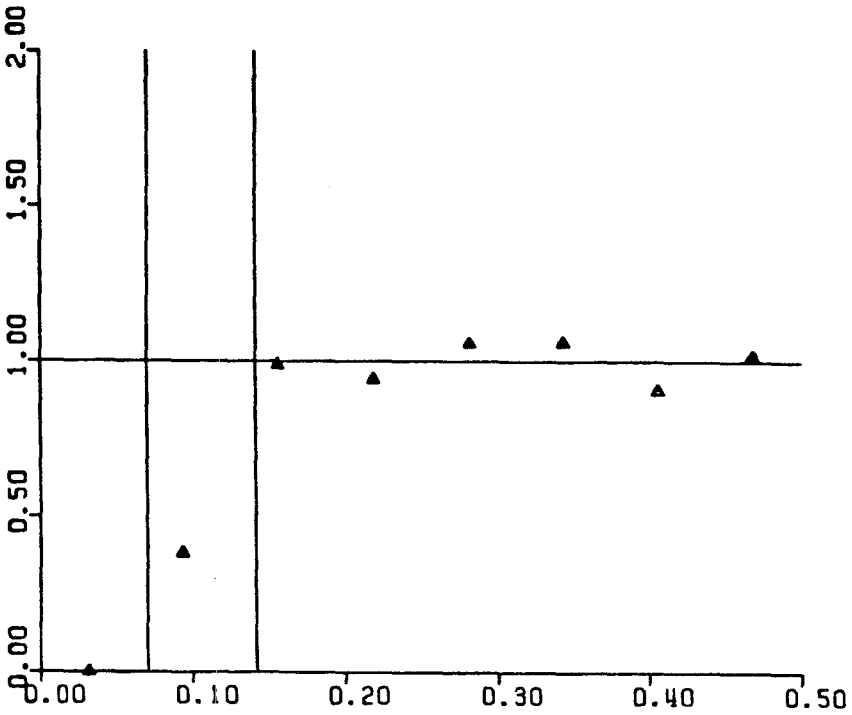
2.00
1.50
1.00
0.50
0.00
0.00
0.10
0.20
0.30
0.40
0.50

T= 7.200

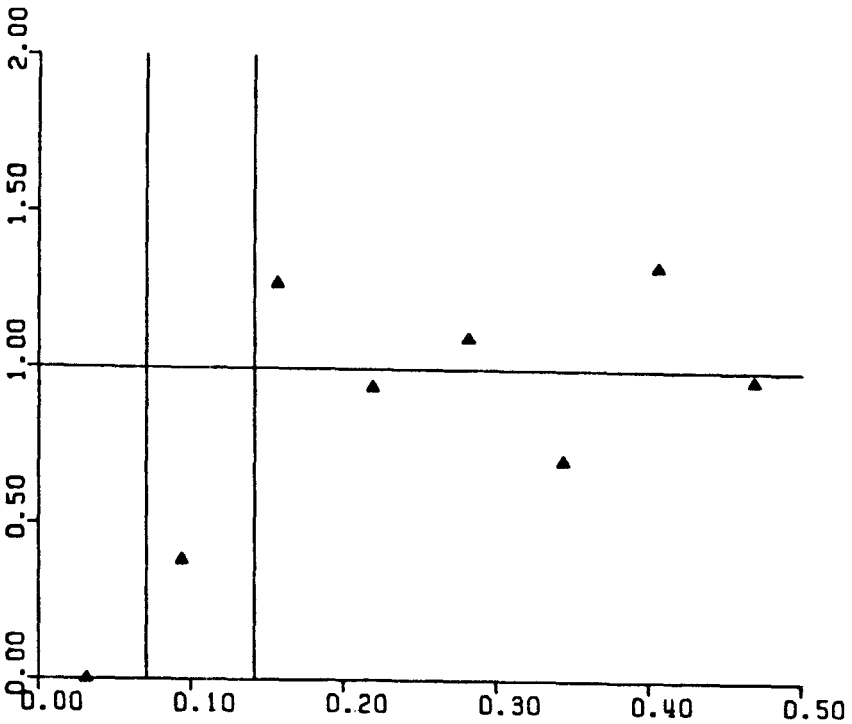
2.00
1.50
1.00
0.50
0.00
0.00
0.10
0.20
0.30
0.40
0.50

T= 7.600

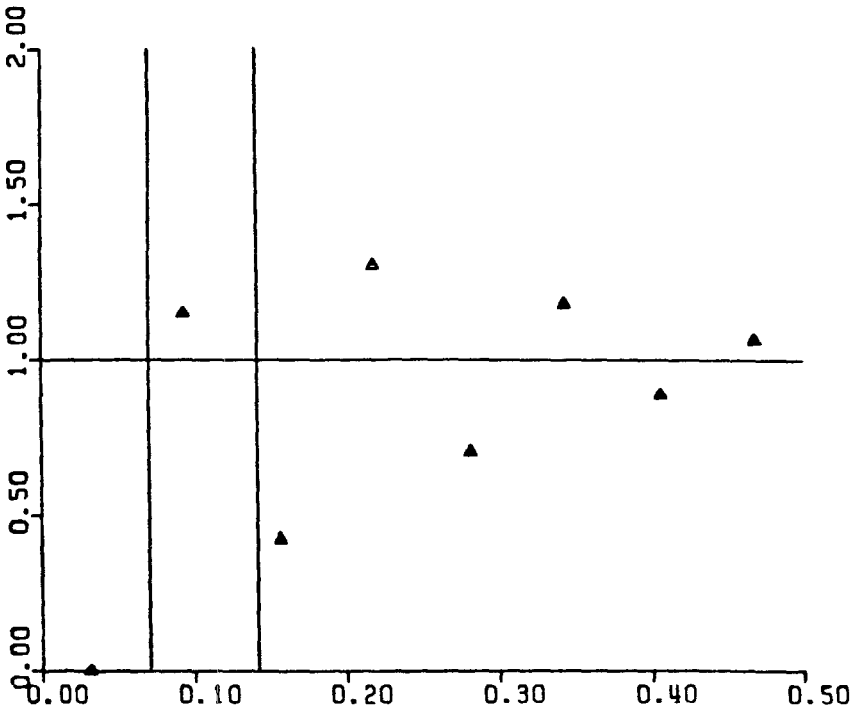


T= 8.000

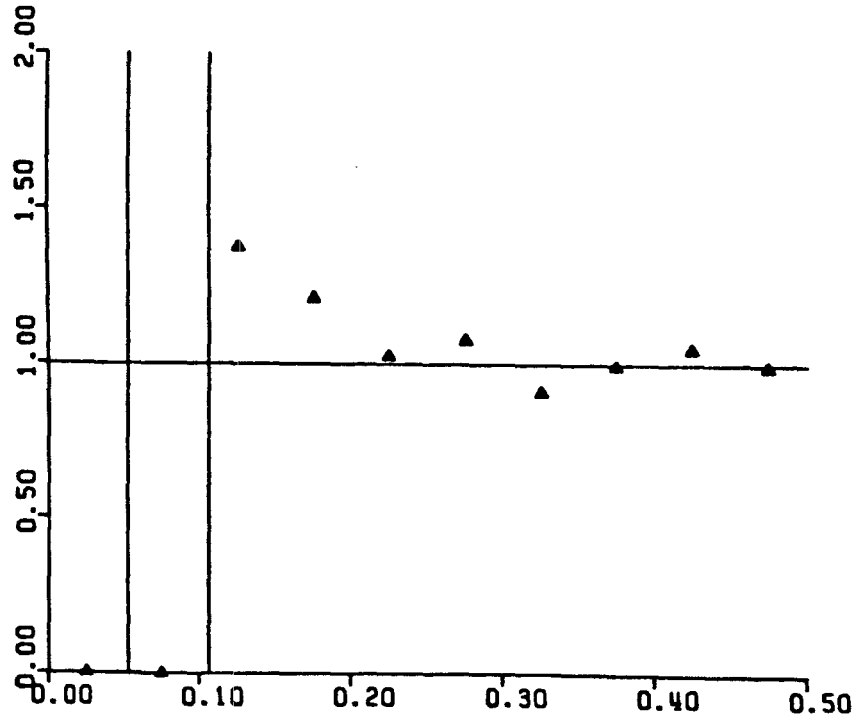


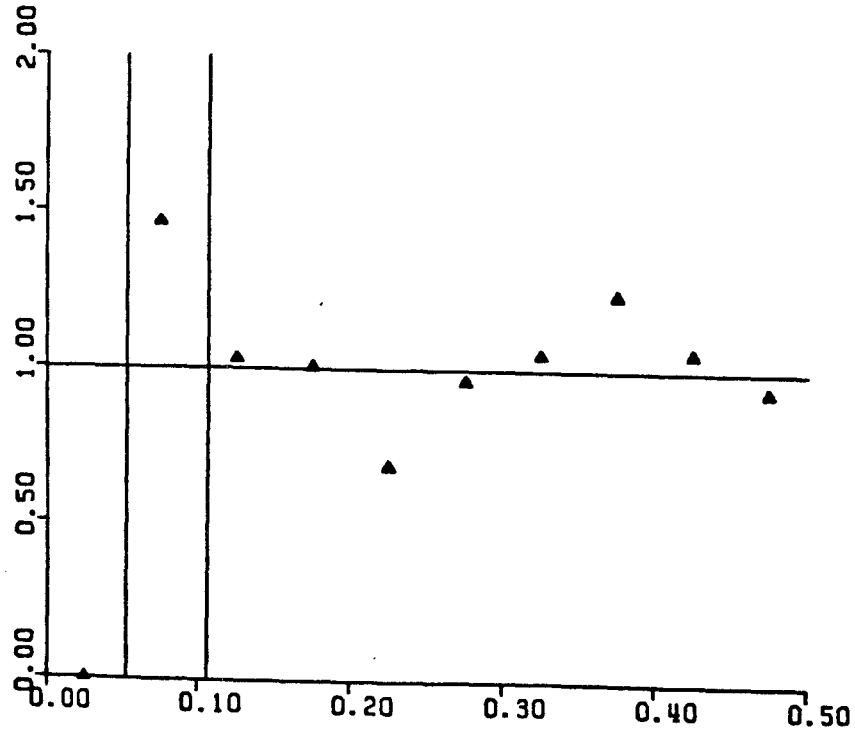


**Figure 32.** Pair-probability function for simulation run 5.

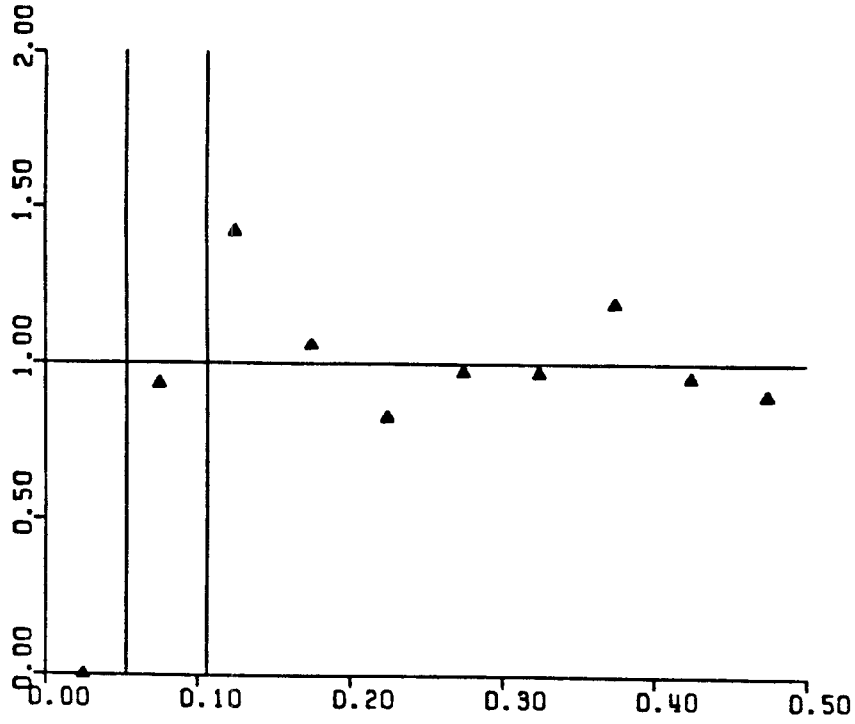
2.00
1.50
1.00
0.50
0.00
0.00
0.10
0.20
0.30
0.40
0.50

T= 0.800

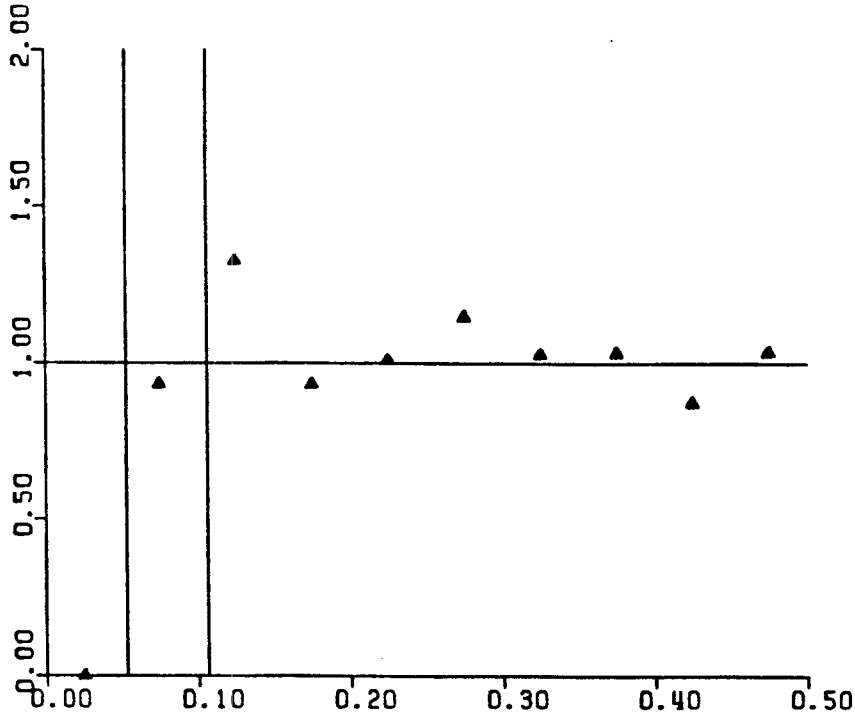
2.00
1.50
1.00
0.50
0.00
0.00
0.10
0.20
0.30
0.40
0.50

T= 1.200

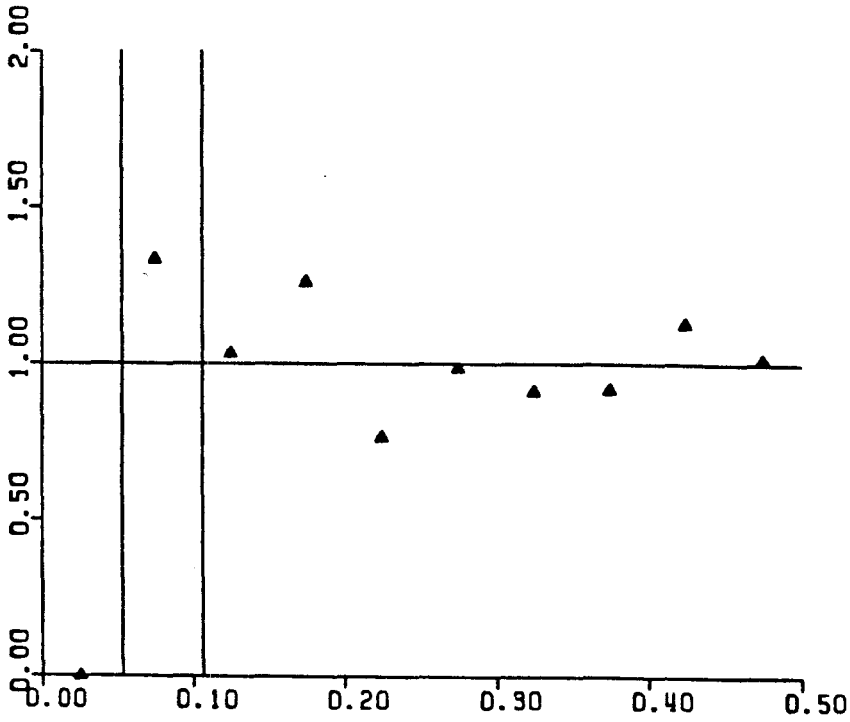
2.00
1.50
1.00
0.50
0.00
0.00
0.10
0.20
0.30
0.40
0.50

T= 1.600

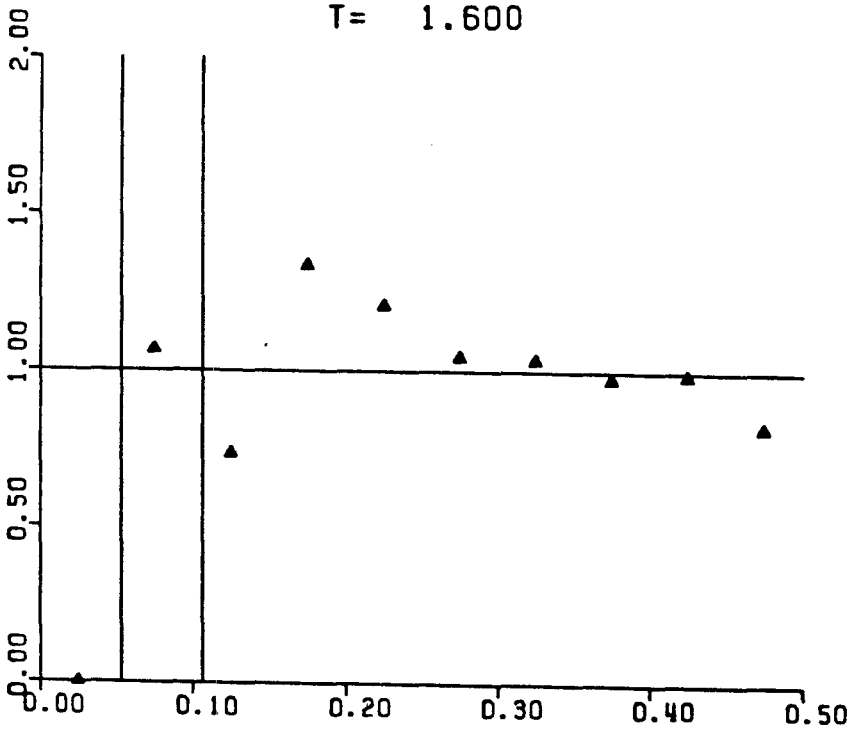
2.00
1.50
1.00
0.50
0.00
0.00
0.10
0.20
0.30
0.40
0.50

T= 2.000

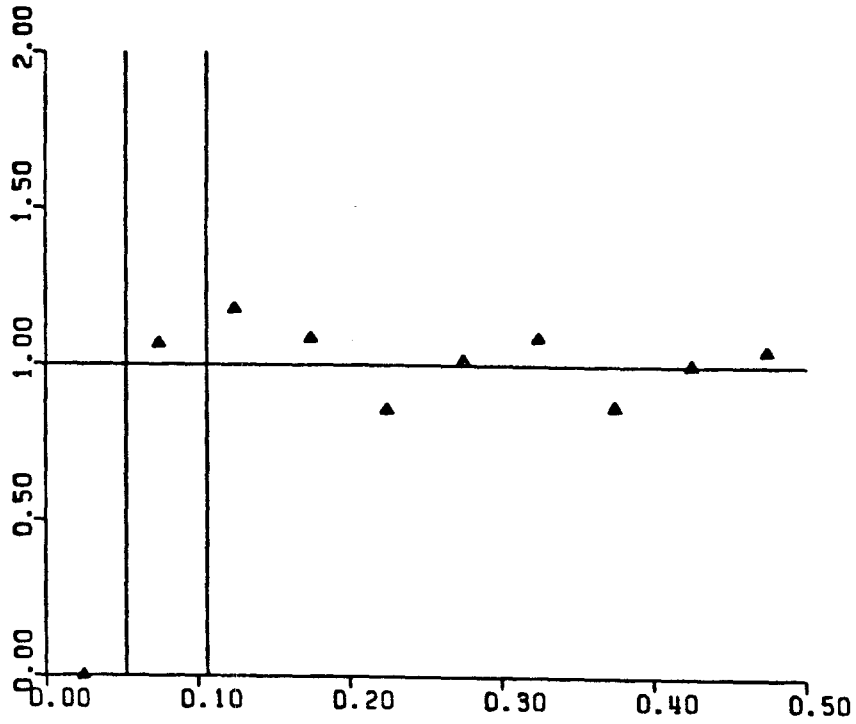
2.00
1.50
1.00
0.50
0.00
0.00
0.10
0.20
0.30
0.40
0.50

T= 2.400

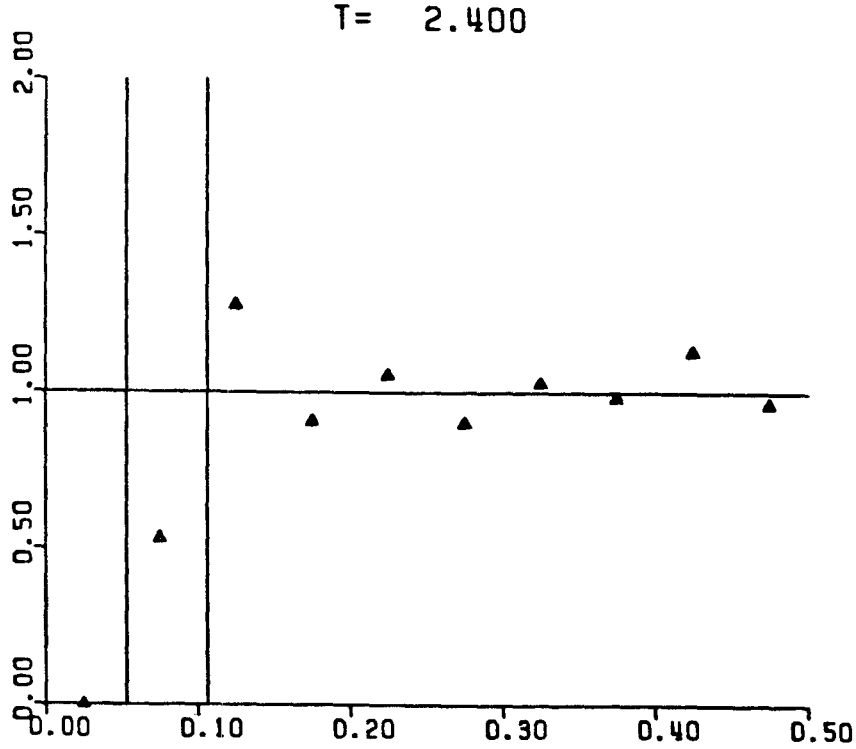
2.00
1.50
1.00
0.50
0.00
0.00
0.10
0.20
0.30
0.40
0.50

T= 2.800

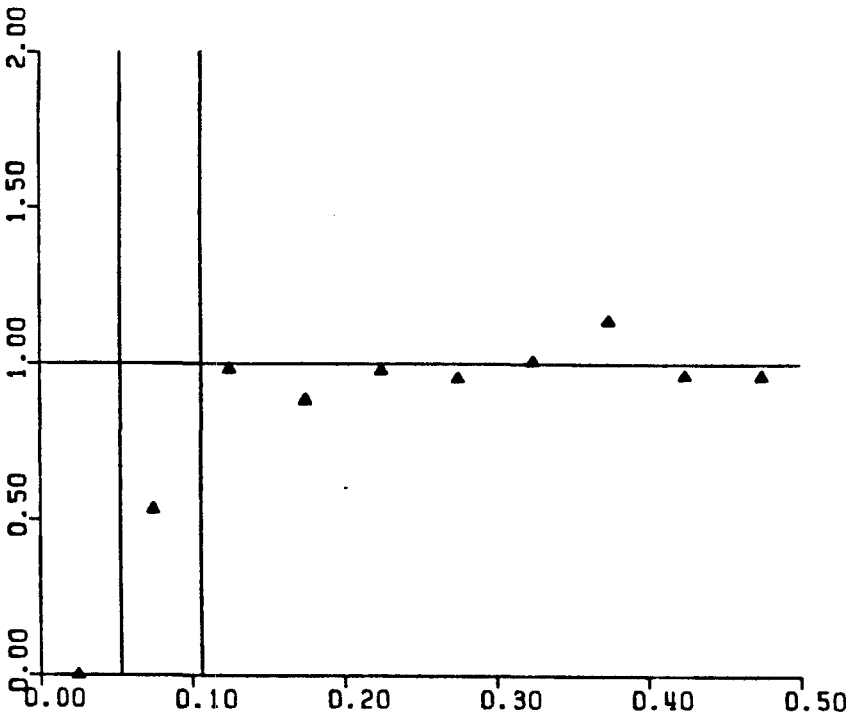
2.00
1.50
1.00
0.50
0.00
0.00
0.10
0.20
0.30
0.40
0.50

T= 3.200

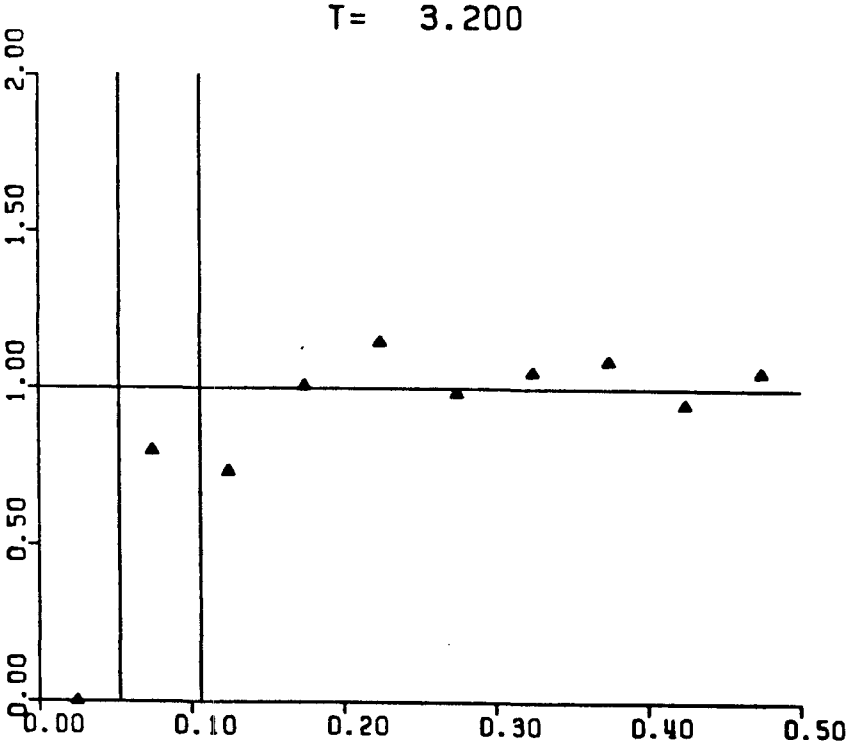
2.00
1.50
1.00
0.50
0.00
0.00
0.10
0.20
0.30
0.40
0.50

T= 3.600

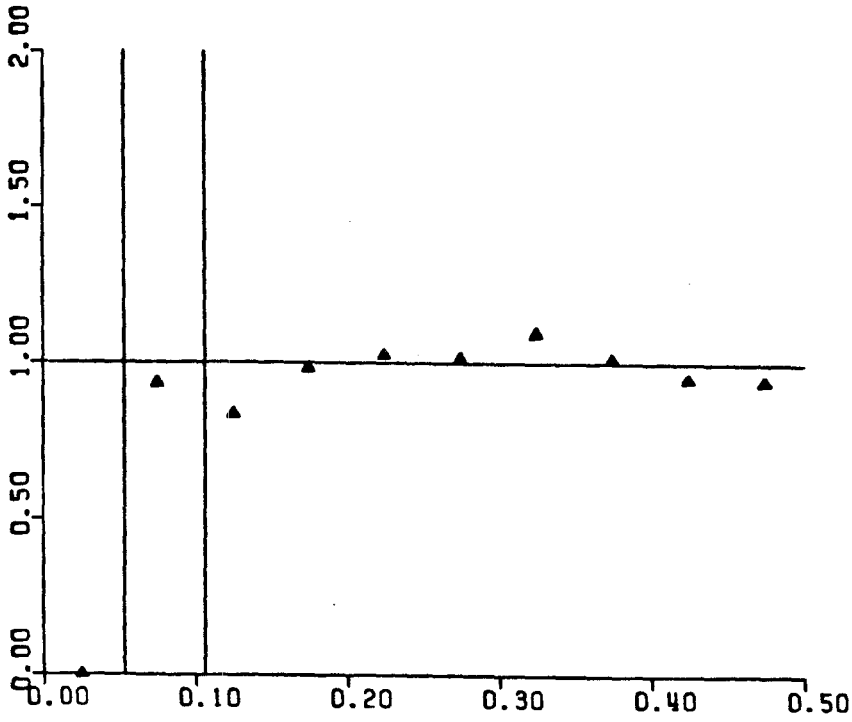
2.00
1.50
1.00
0.50
0.00
0.00
0.10
0.20
0.30
0.40
0.50

T= 4.000

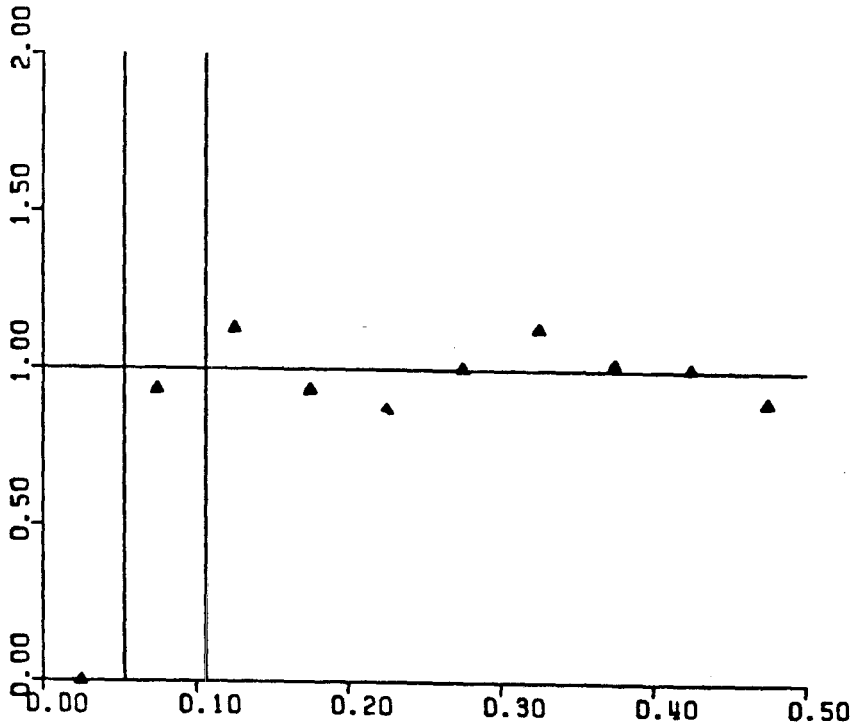
2.00
1.50
1.00
0.50
0.00
0.00
0.10
0.20
0.30
0.40
0.50

T= 4.400

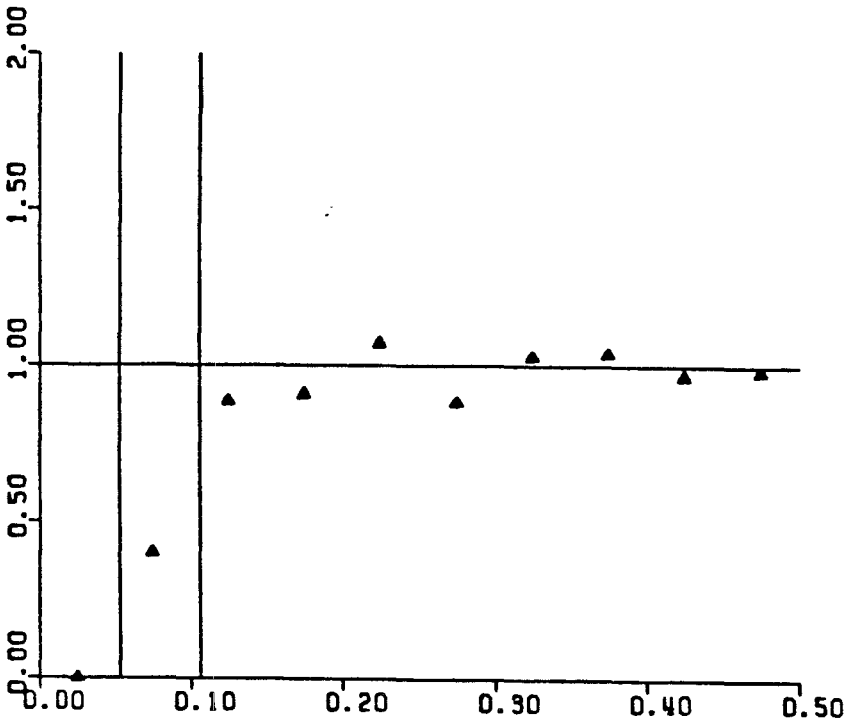
2.00
1.50
1.00
0.50
0.00
0.00
0.10
0.20
0.30
0.40
0.50

T= 4.800

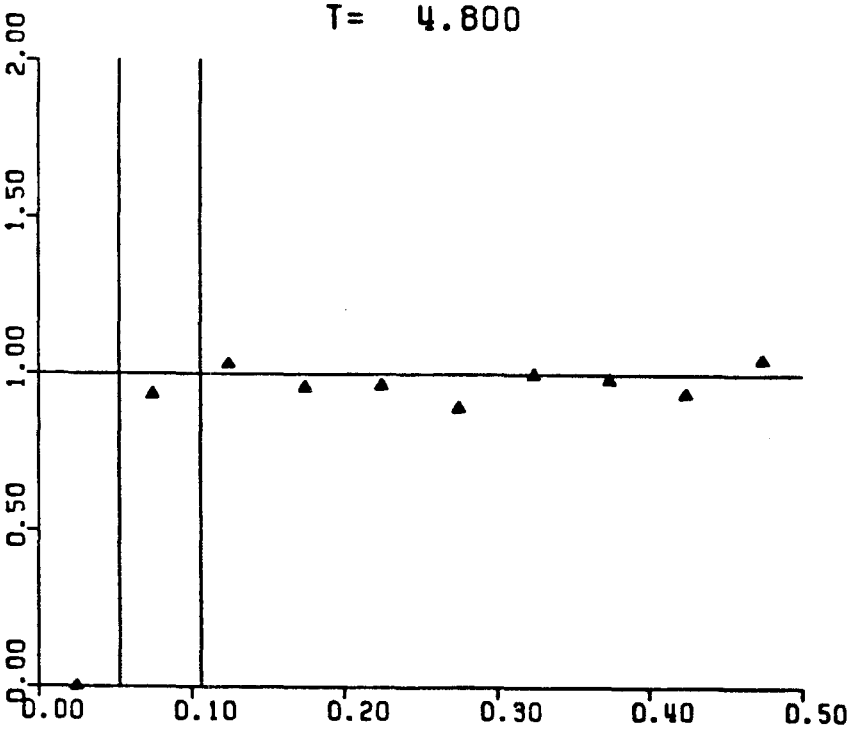
2.00
1.50
1.00
0.50
0.00
0.00
0.10
0.20
0.30
0.40
0.50

T= 5.200

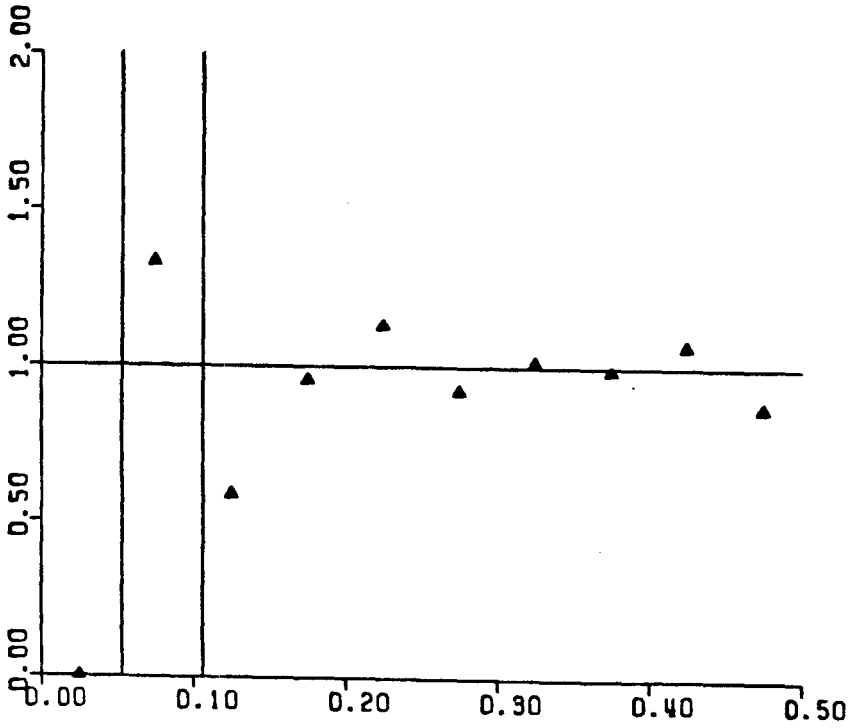
2.00
1.50
1.00
0.50
0.00
0.00
0.10
0.20
0.30
0.40
0.50

T= 5.600

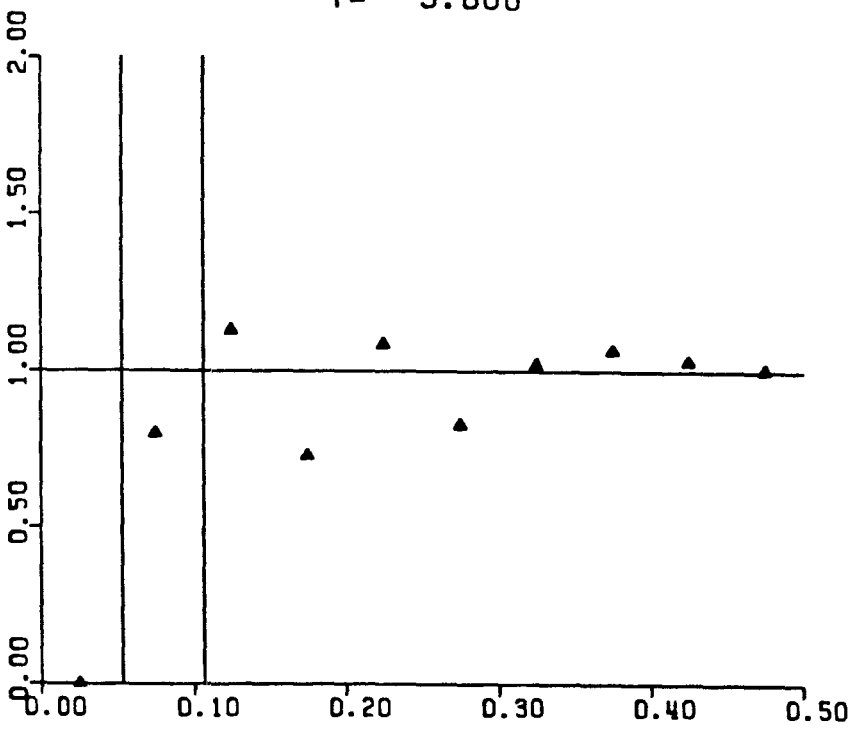
2.00
1.50
1.00
0.50
0.00
0.00
0.10
0.20
0.30
0.40
0.50

T= 6.000

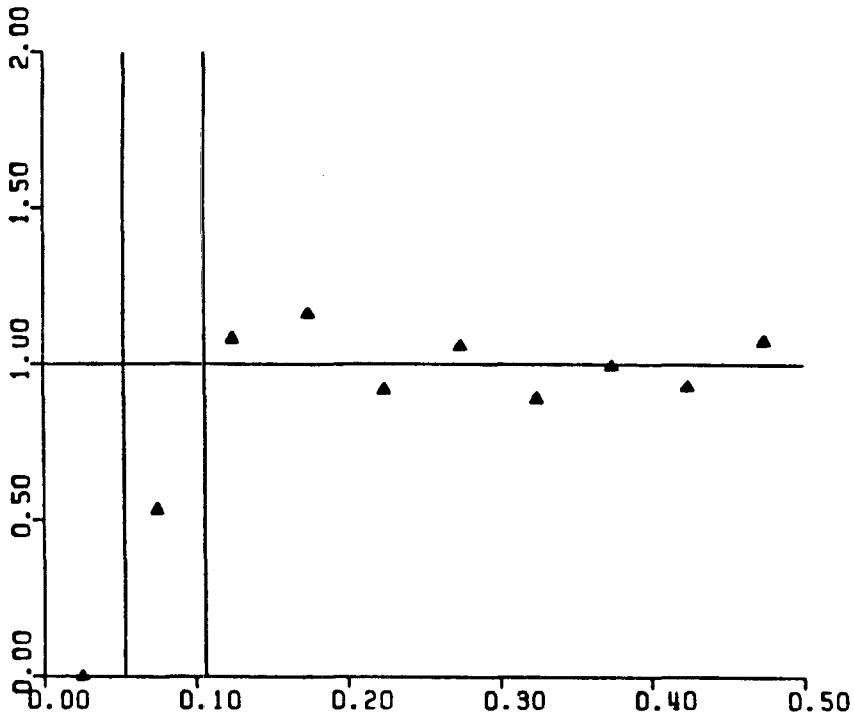
2.00
1.50
1.00
0.50
0.00
0.00
0.10
0.20
0.30
0.40
0.50

T= 6.400

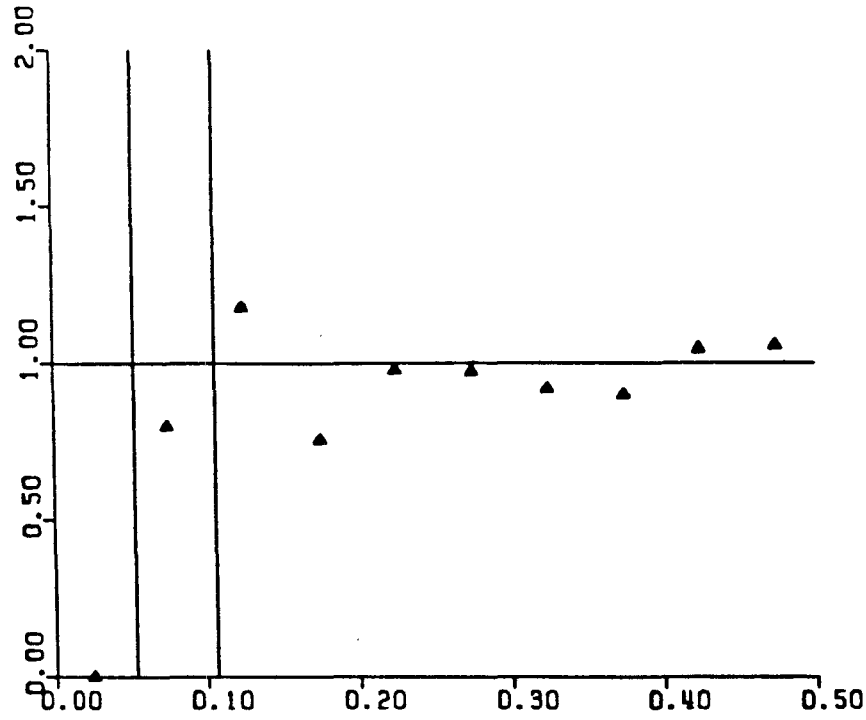
2.00
1.50
1.00
0.50
0.00
0.00
0.10
0.20
0.30
0.40
0.50

T= 6.800

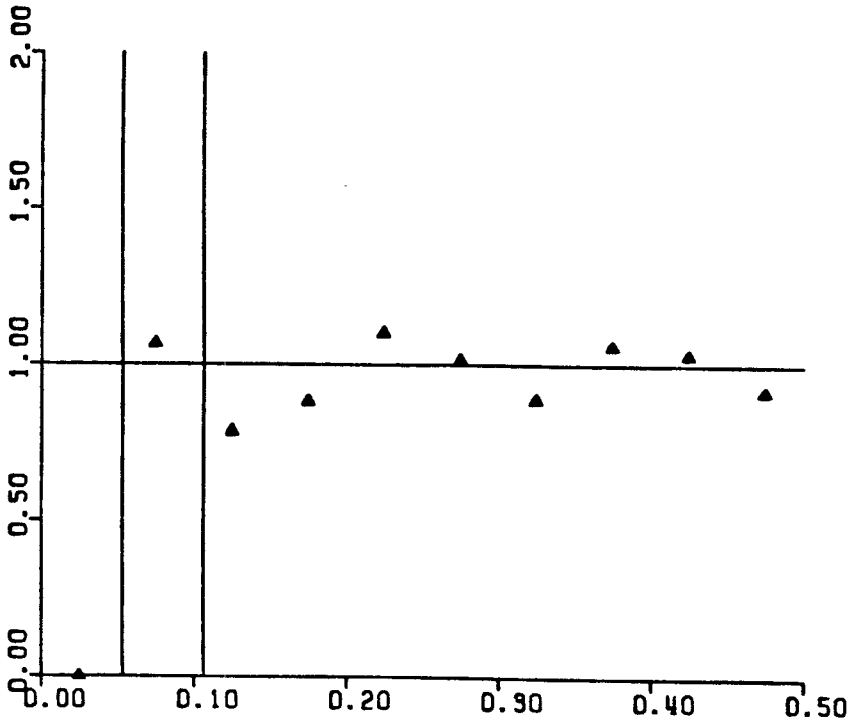
2.00
1.50
1.00
0.50
0.00
0.00
0.10
0.20
0.30
0.40
0.50

T= 7.200

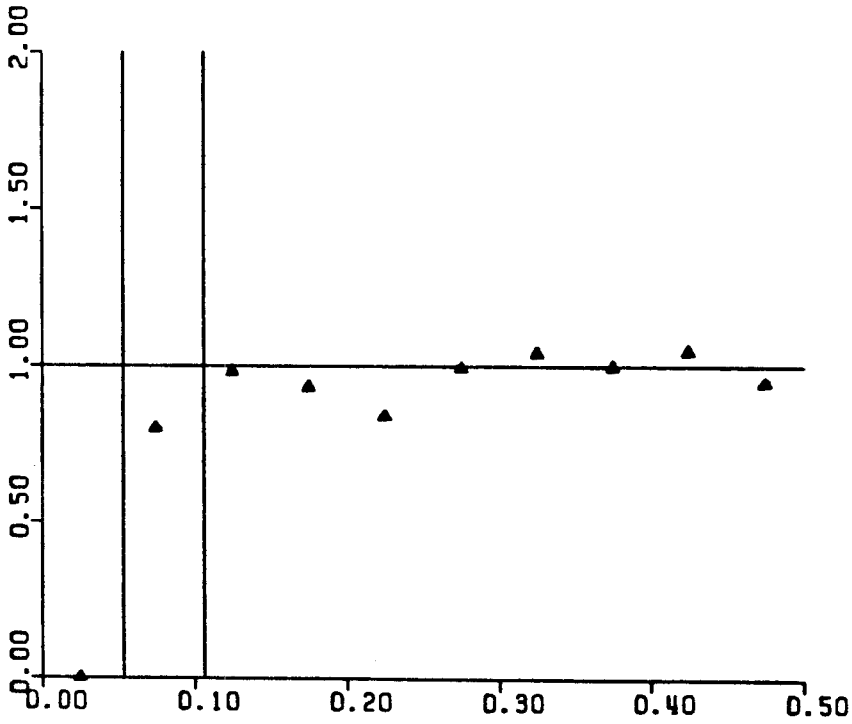
2.00
1.50
1.00
0.50
0.00
0.00
0.10
0.20
0.30
0.40
0.50

T= 7.600

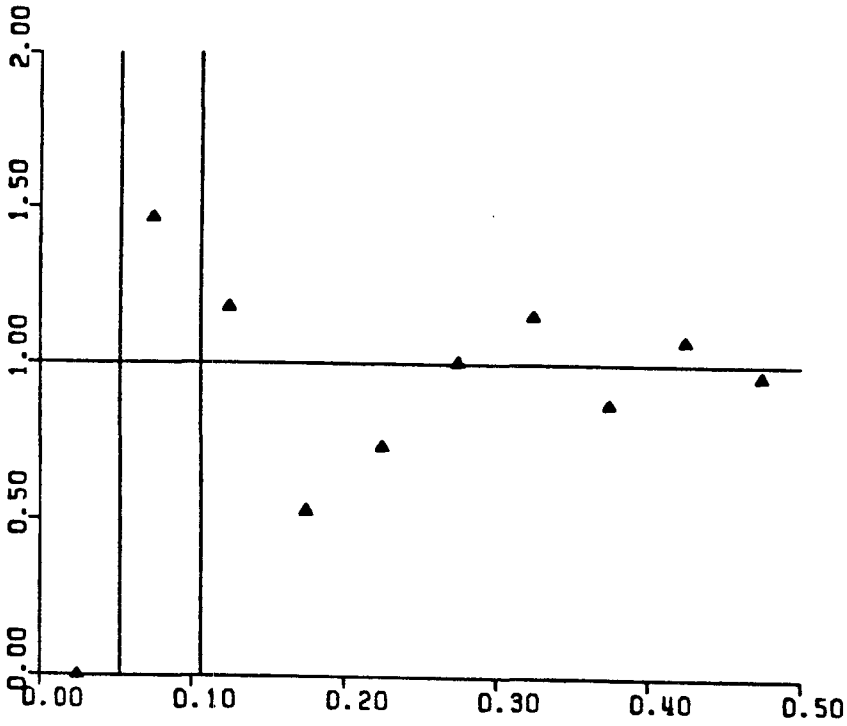
2.00
1.50
1.00
0.50
0.00
0.00
0.10
0.20
0.30
0.40
0.50

T= 8.000

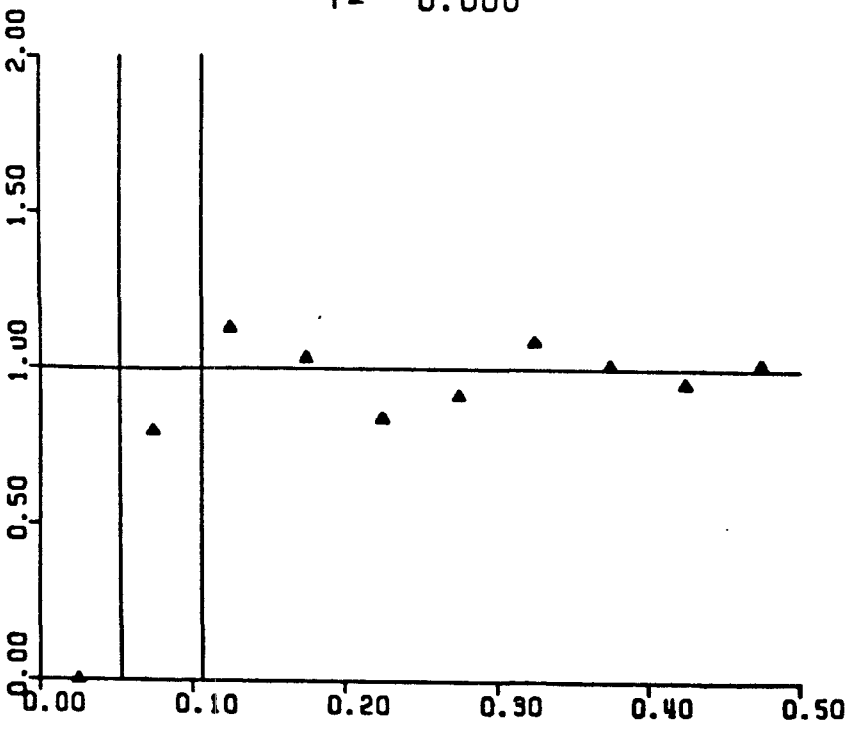
2.00
1.50
1.00
0.50
0.00
0.00
0.10
0.20
0.30
0.40
0.50

T= 8.400

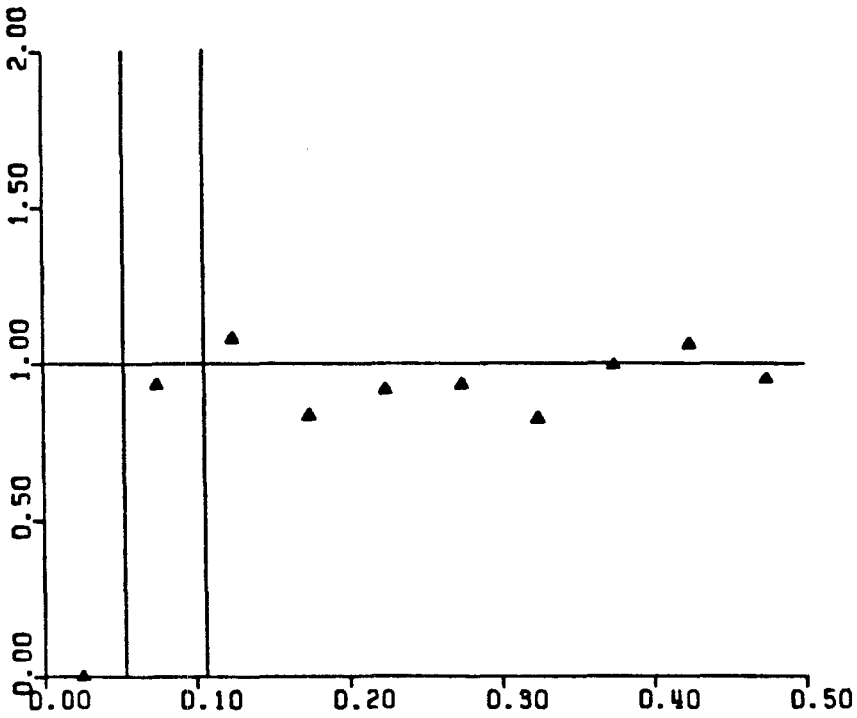
2.00
1.50
1.00
0.50
0.00
0.00
0.10
0.20
0.30
0.40
0.50

T= 8.800

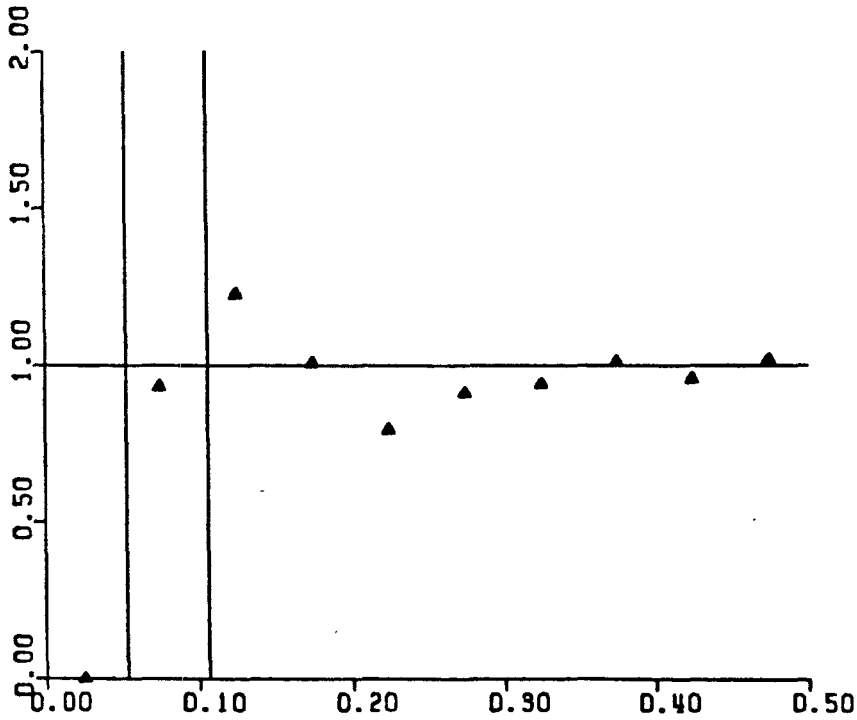
2.00
1.50
1.00
0.50
0.00
0.00
0.10
0.20
0.30
0.40
0.50

T= 9.200

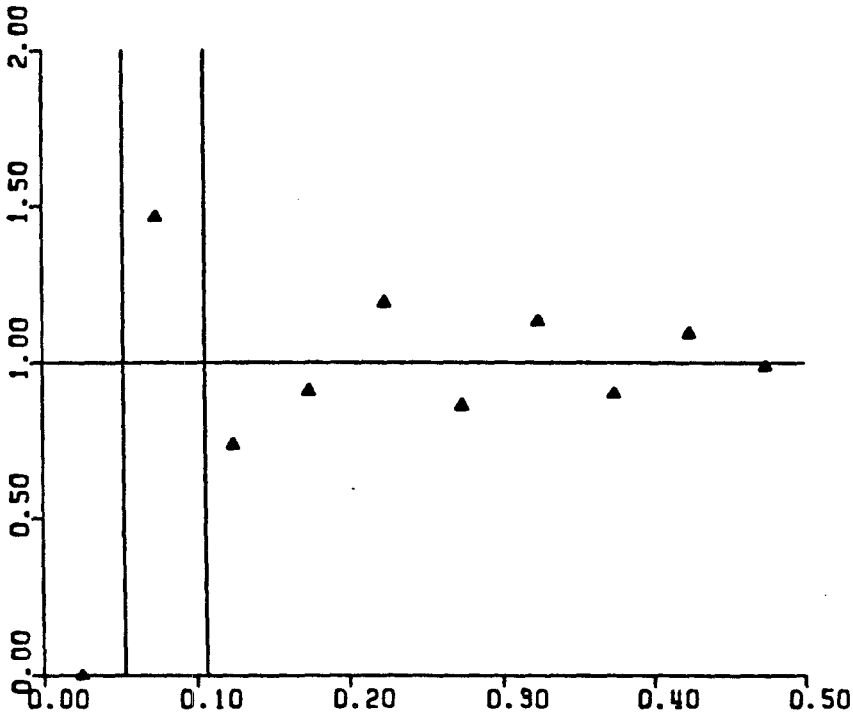


T= 9.600

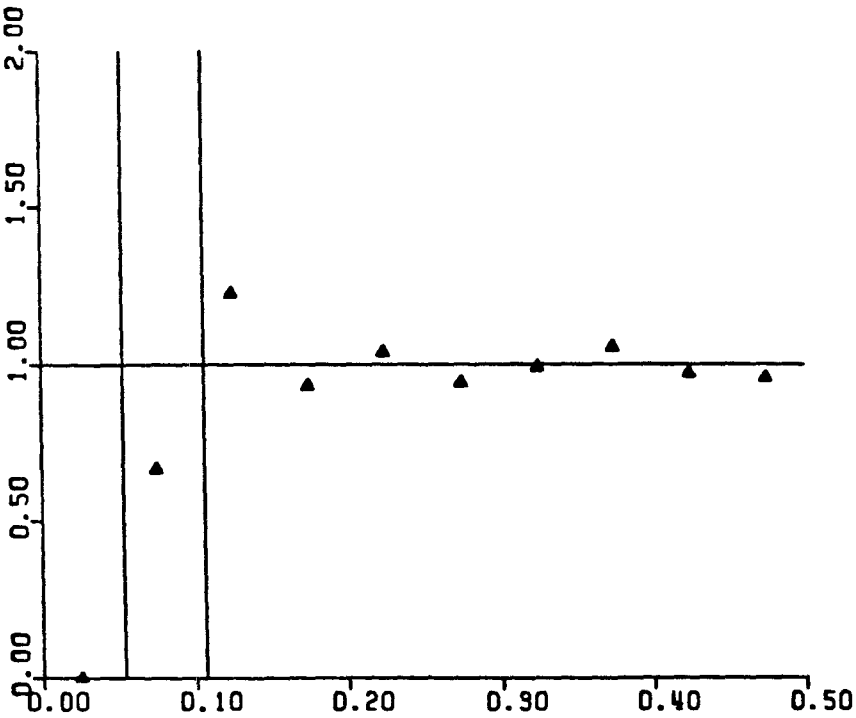


T= 10.000

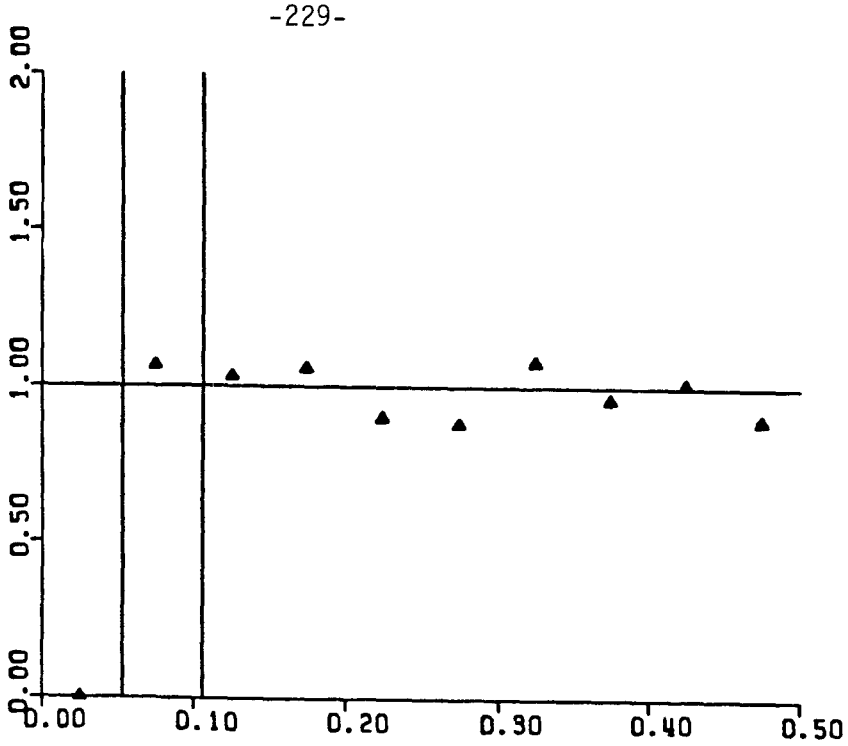


T= 10.401

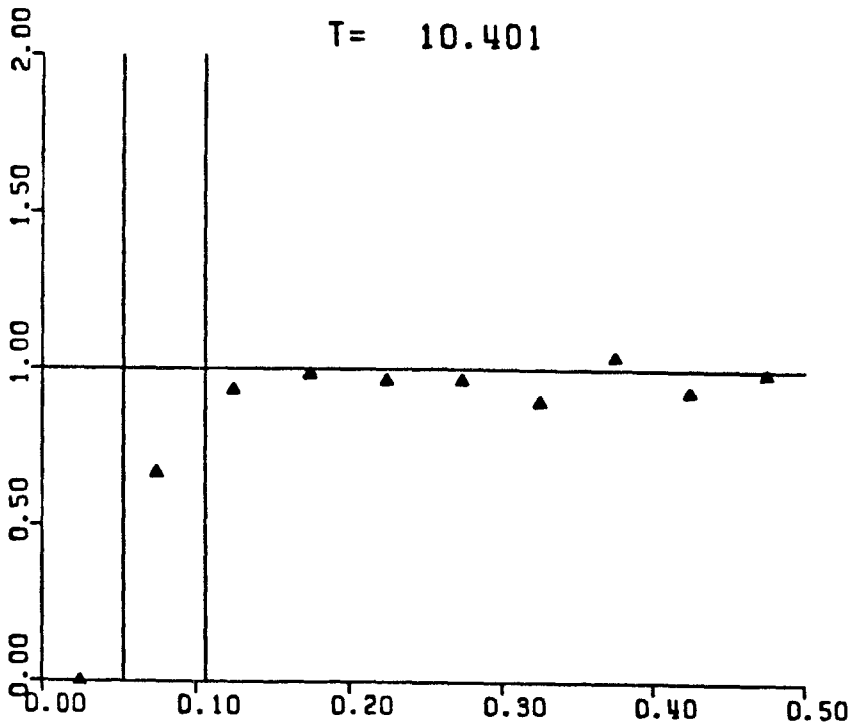


T= 10.801

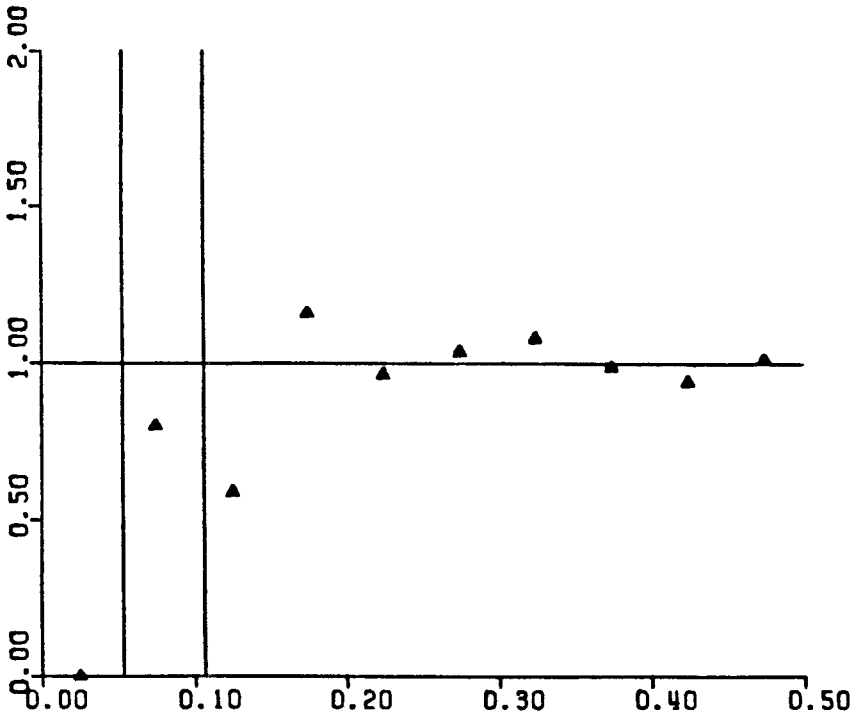


T= 11.201

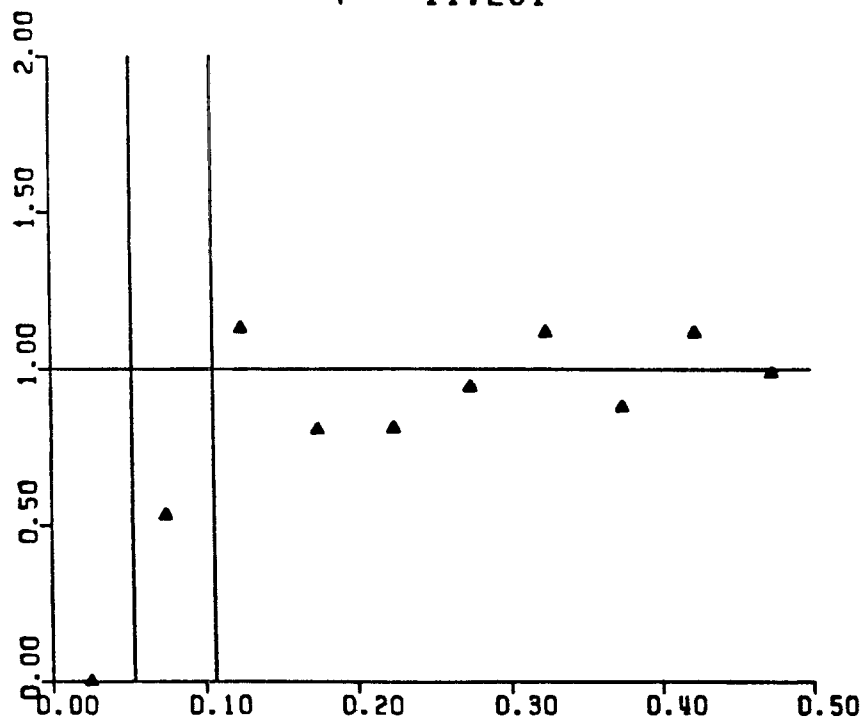


T= 11.601

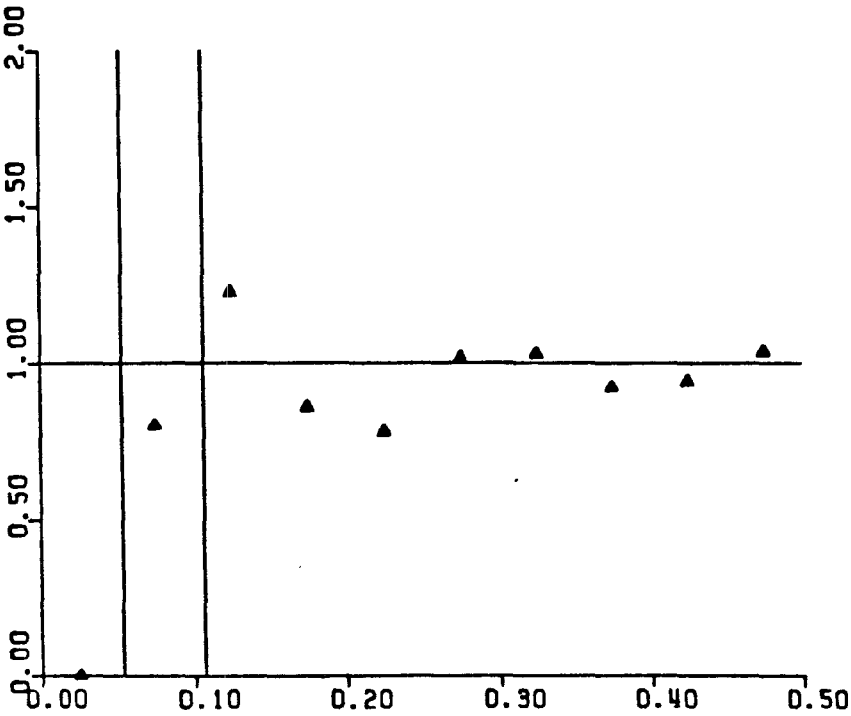


T= 12.001

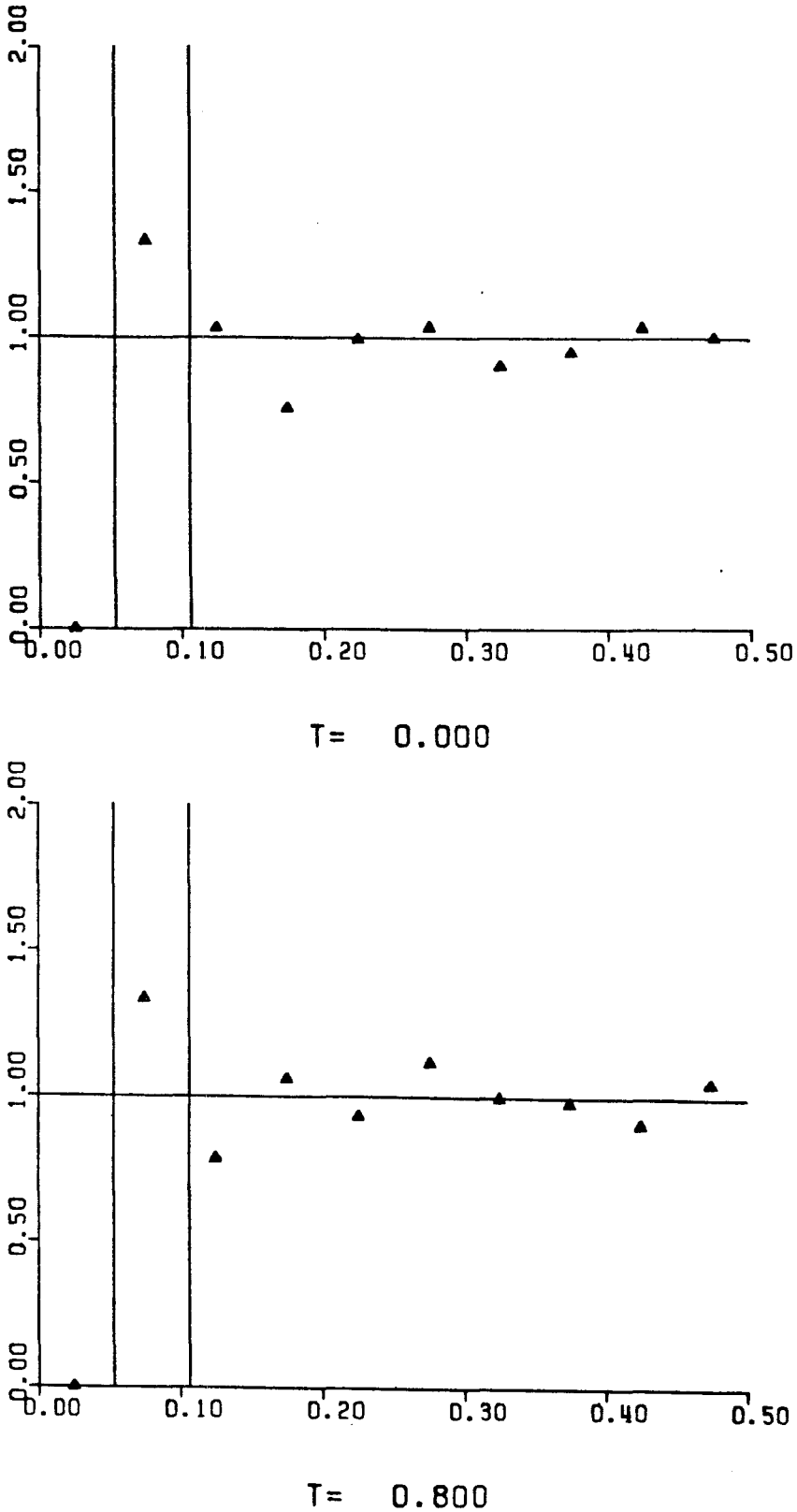


**Figure 33.** Pair-probability function for simulation run 7.

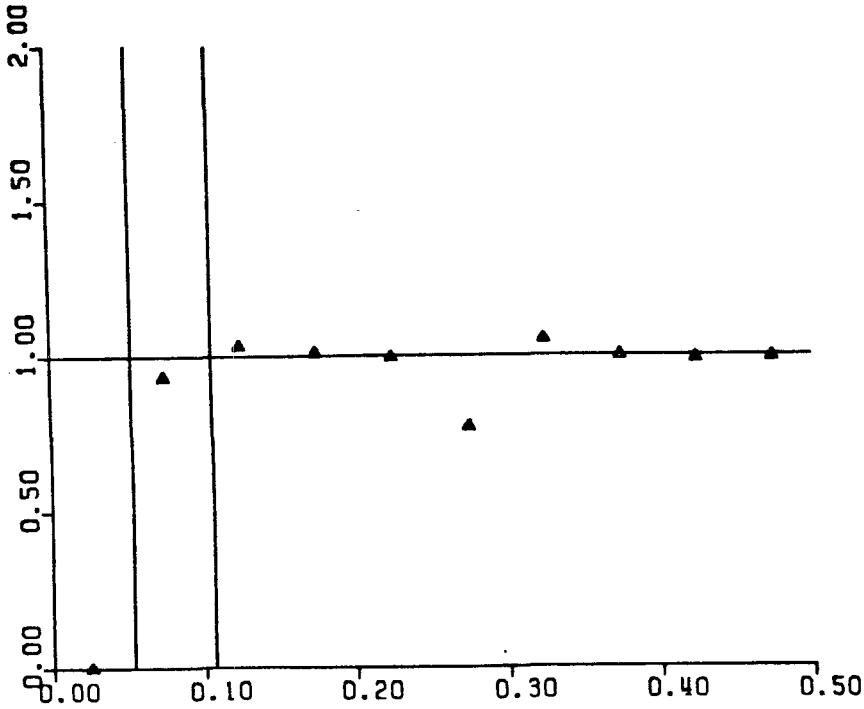
2.00
1.50
1.00
0.50
0.00
0.00
0.10
0.20
0.30
0.40
0.50

T= 1.600

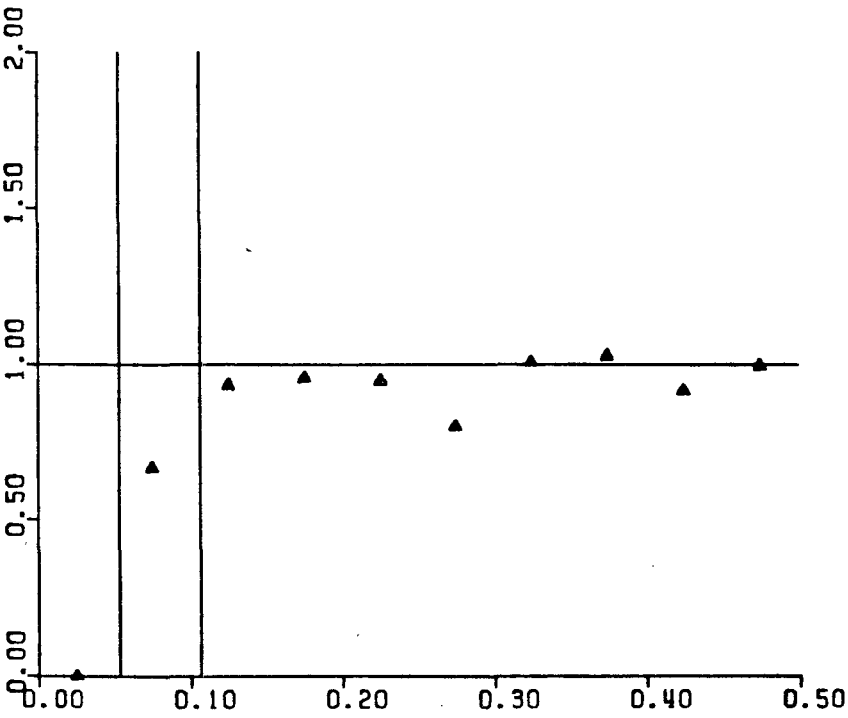
2.00
1.50
1.00
0.50
0.00
0.00
0.10
0.20
0.30
0.40
0.50

T= 2.400

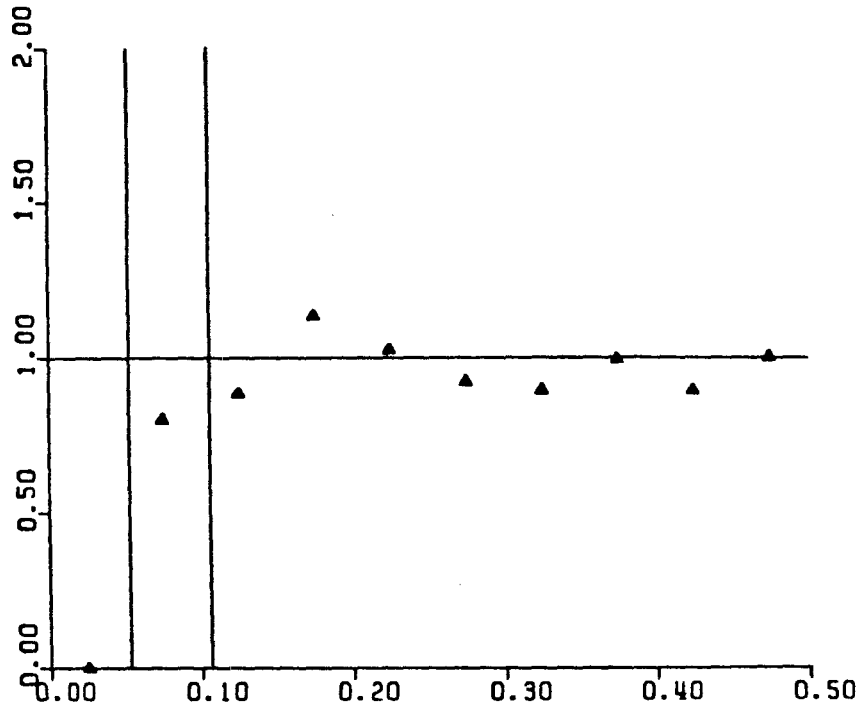
2.00
1.50
1.00
0.50
0.00
0.00
0.10
0.20
0.30
0.40
0.50

T= 3.200

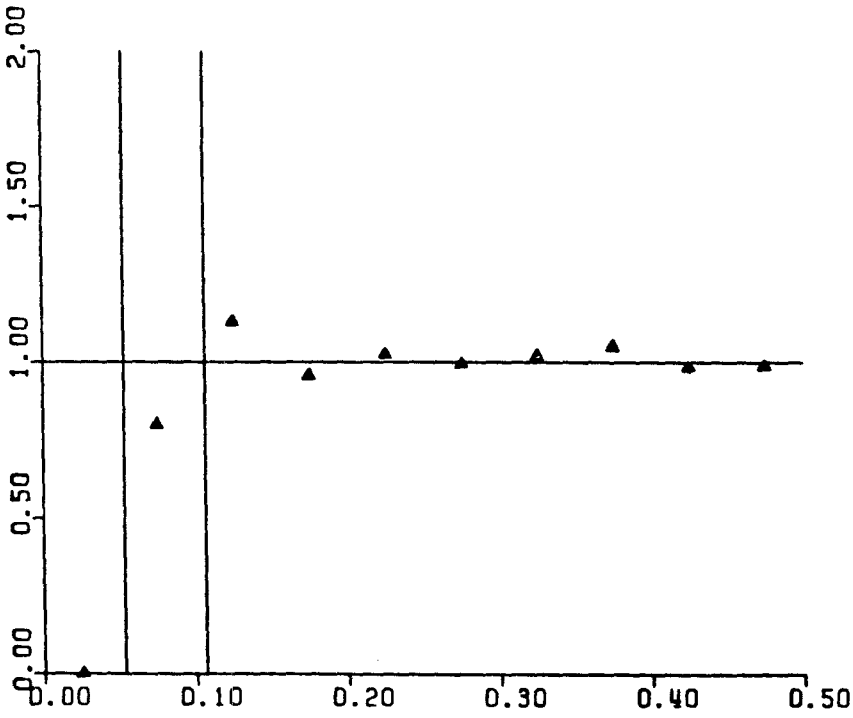
2.00
1.50
1.00
0.50
0.00
0.00
0.10
0.20
0.30
0.40
0.50

T= 4.000

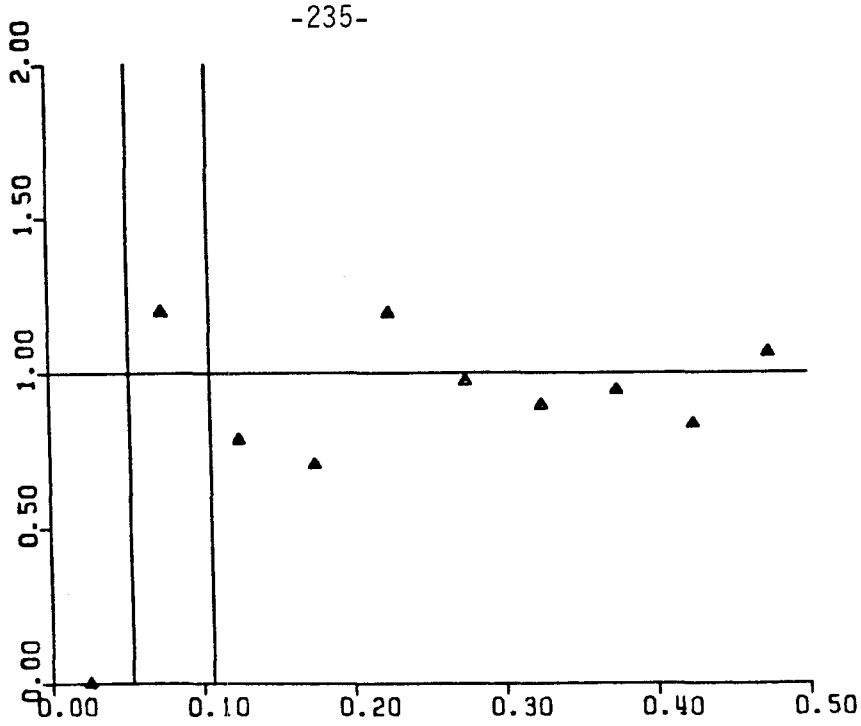
2.00
1.50
1.00
0.50
0.00
0.00
0.10
0.20
0.30
0.40
0.50

T= 4.800

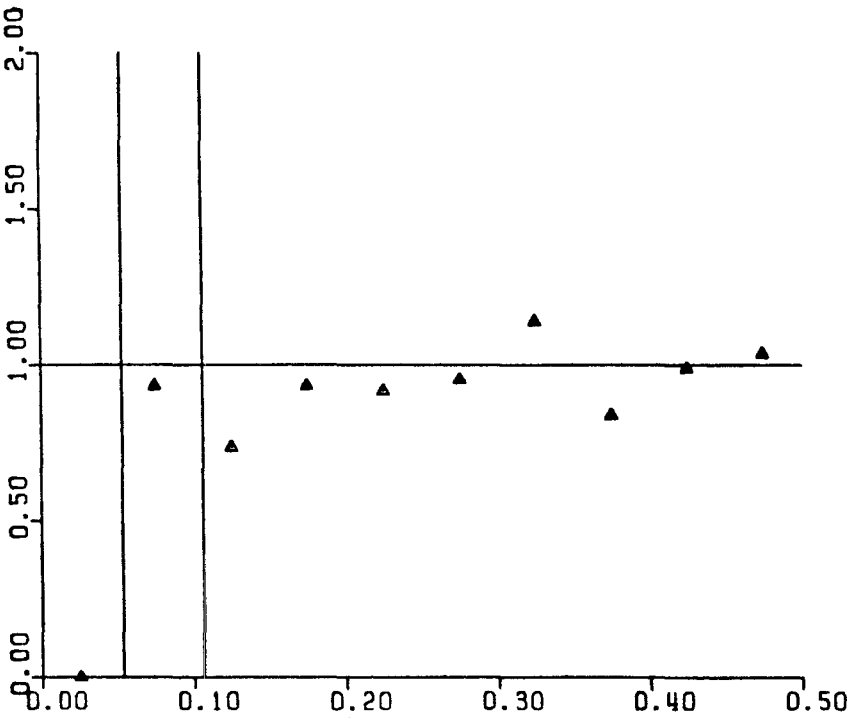
2.00
1.50
1.00
0.50
0.00
0.00
0.10
0.20
0.30
0.40
0.50

T= 5.600

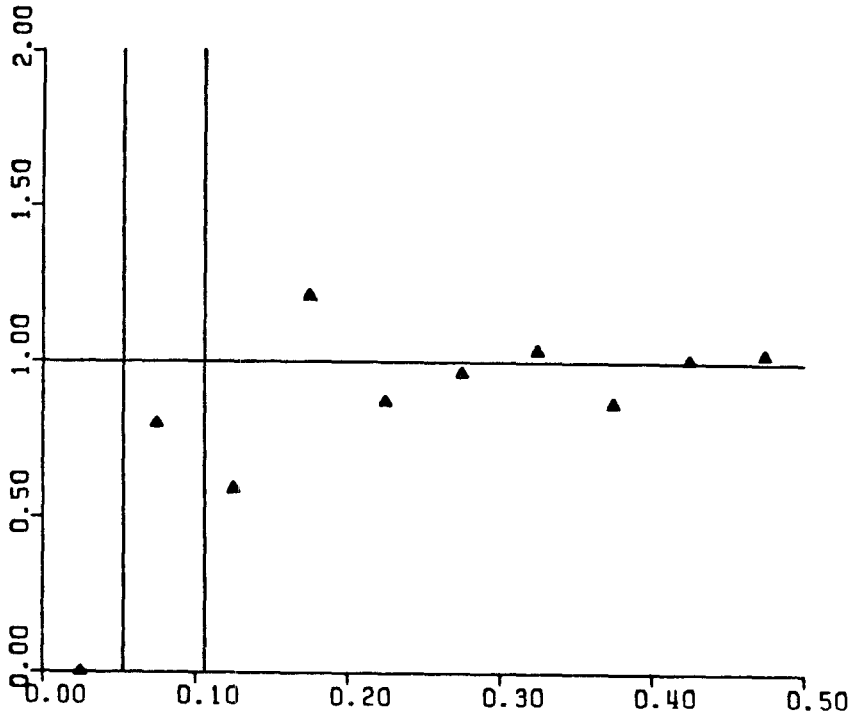
2.00
1.50
1.00
0.50
0.00
0.00
0.10
0.20
0.30
0.40
0.50

T= 6.400

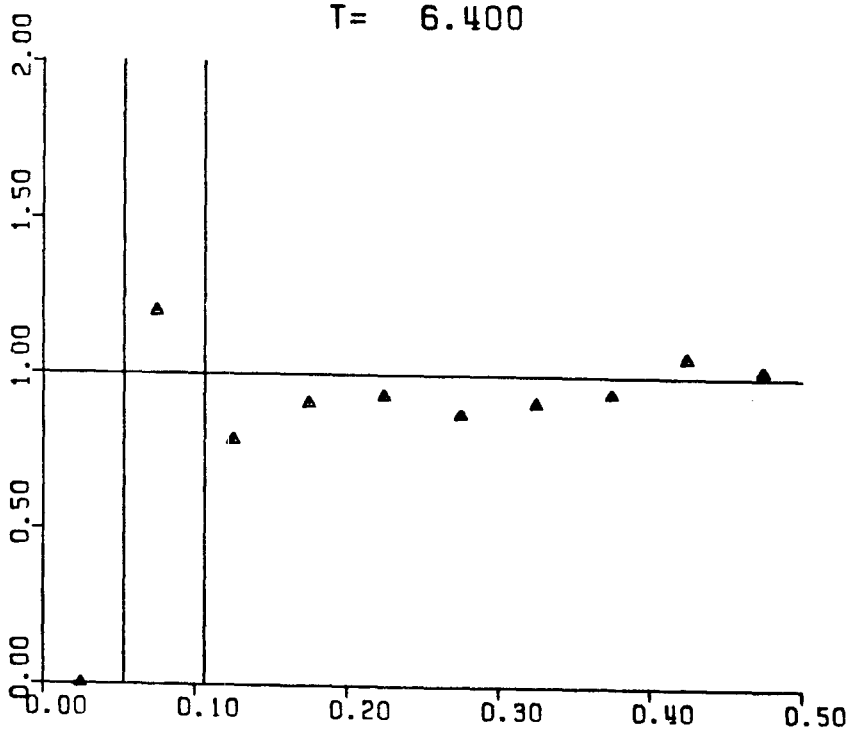
2.00
1.50
1.00
0.50
0.00
0.00
0.10
0.20
0.30
0.40
0.50

T= 7.200

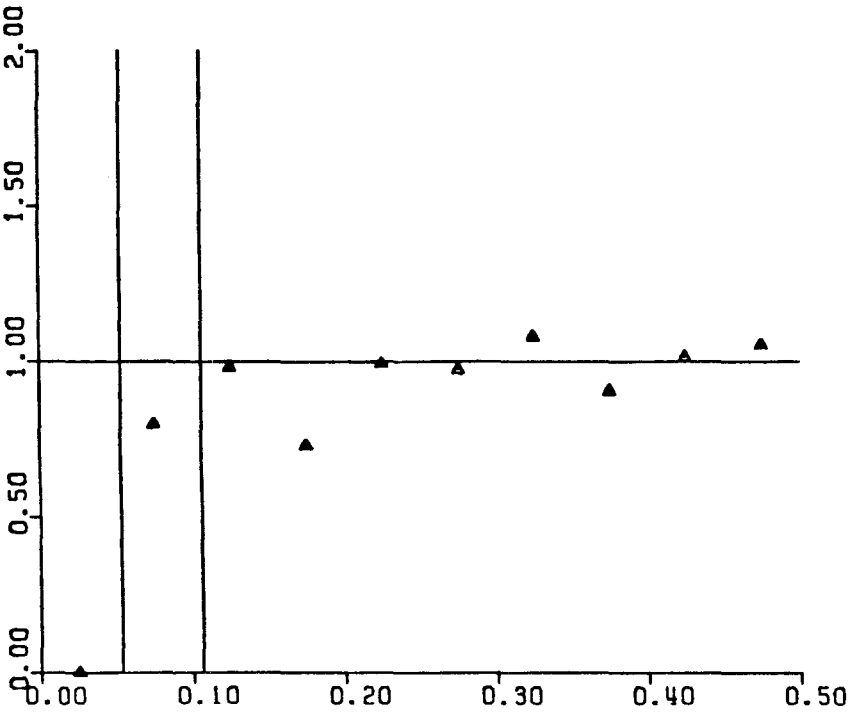


T= 8.000

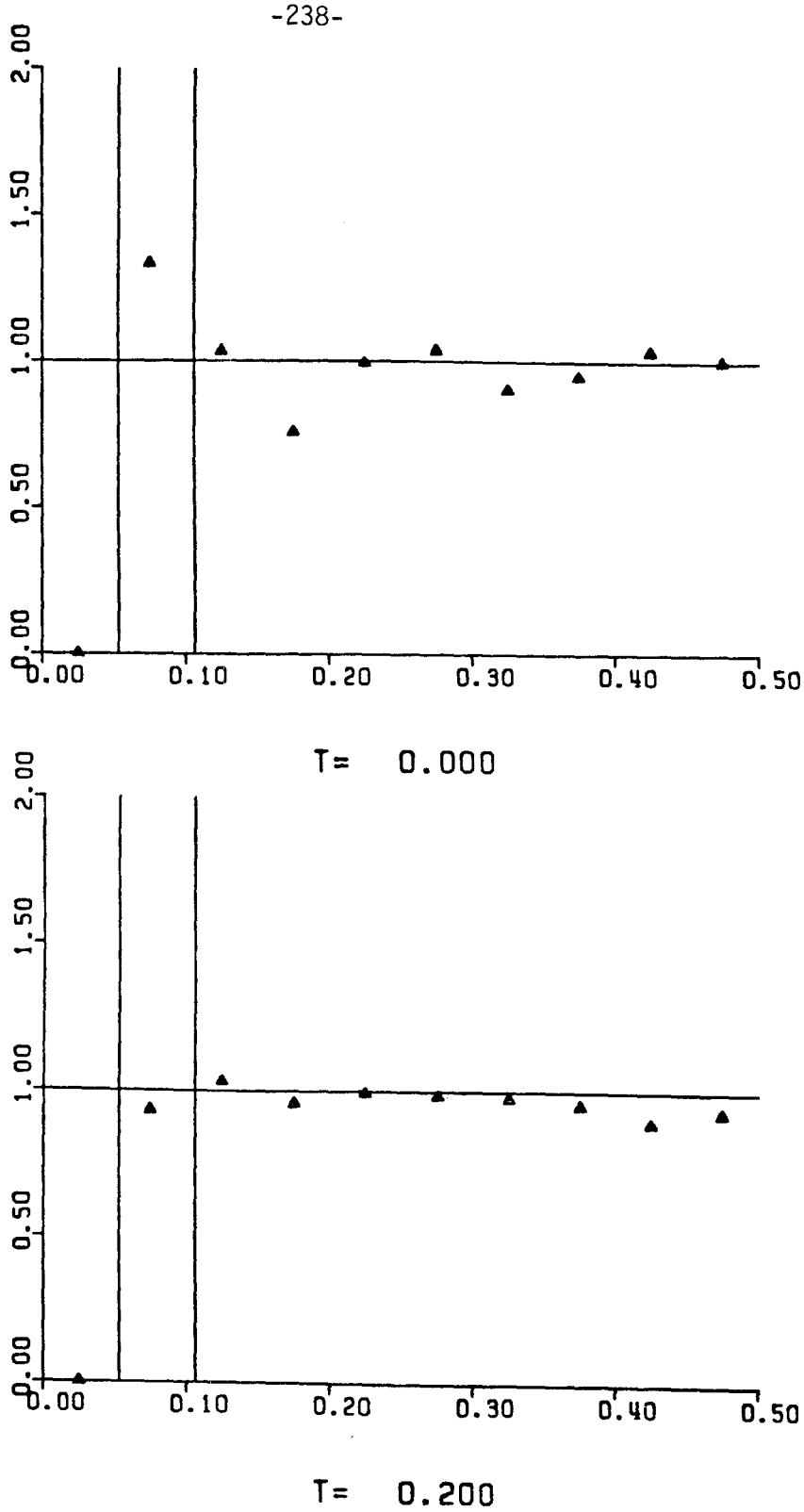


**Figure 34.** Pair-probability function for simulation run 8.

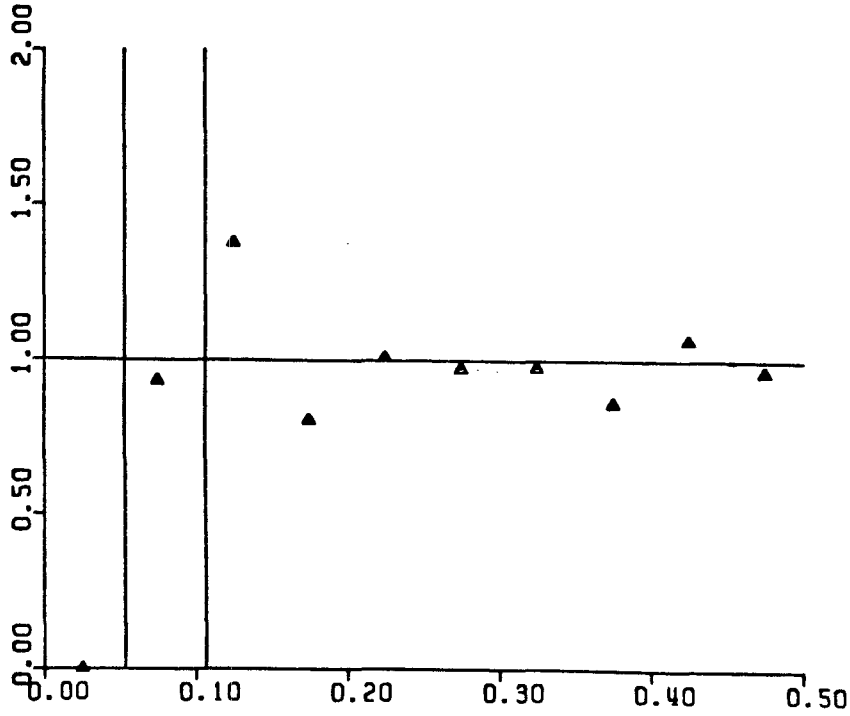
2.00
1.50
1.00
0.50
0.00
0.00
0.10
0.20
0.30
0.40
0.50

T= 0.400

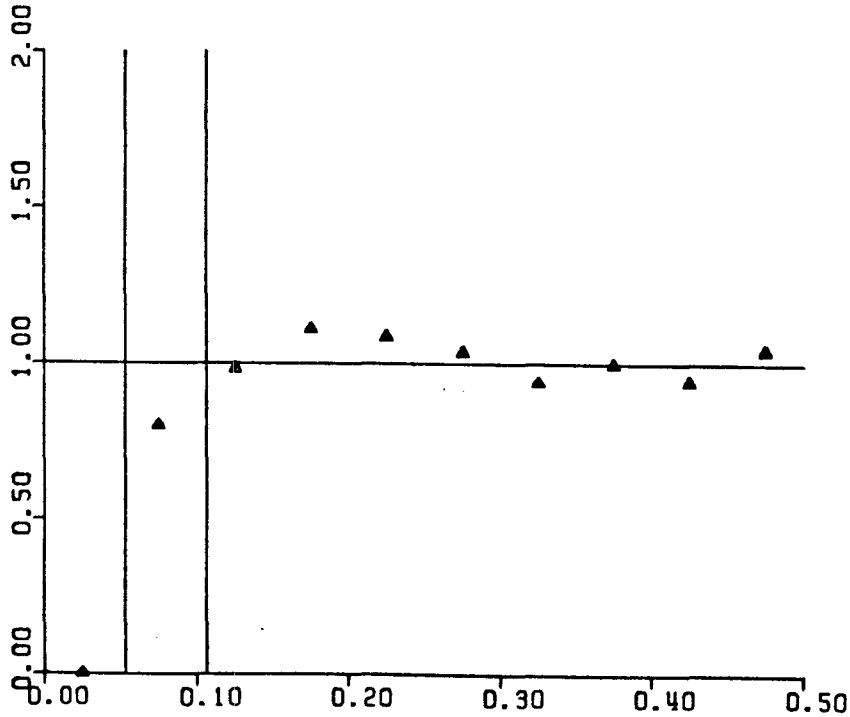
2.00
1.50
1.00
0.50
0.00
0.00
0.10
0.20
0.30
0.40
0.50

T= 0.600

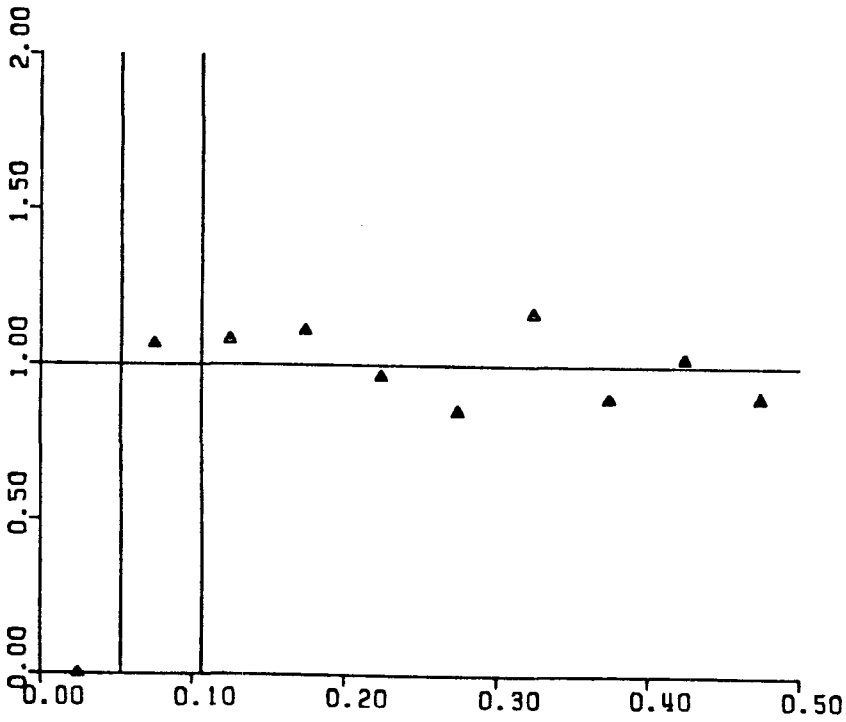
2.00
1.50
1.00
0.50
0.00
0.00
0.10
0.20
0.30
0.40
0.50

T= 0.800

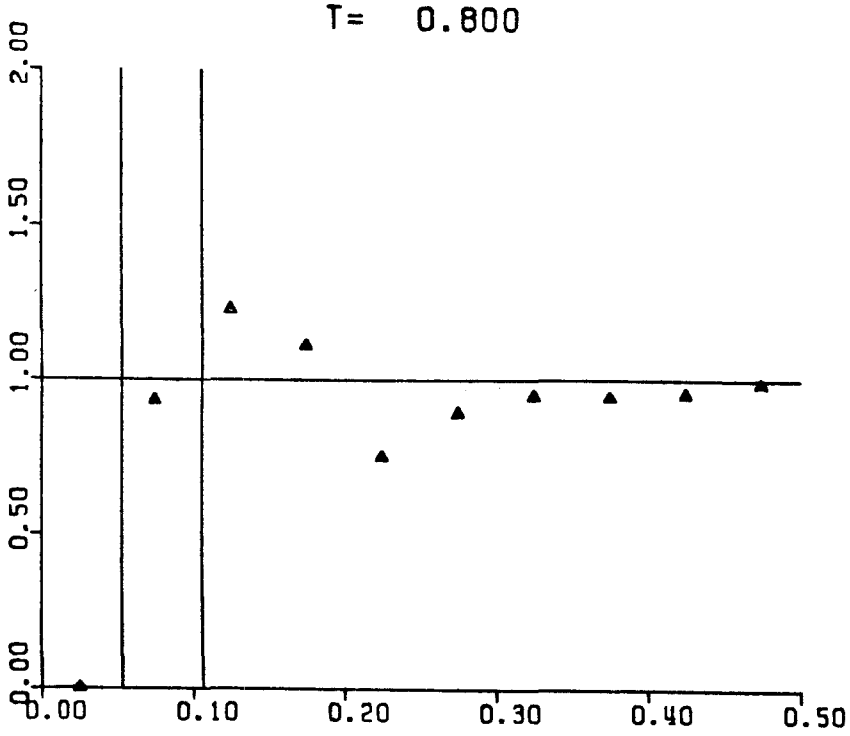
2.00
1.50
1.00
0.50
0.00
0.00
0.10
0.20
0.30
0.40
0.50

T= 1.000

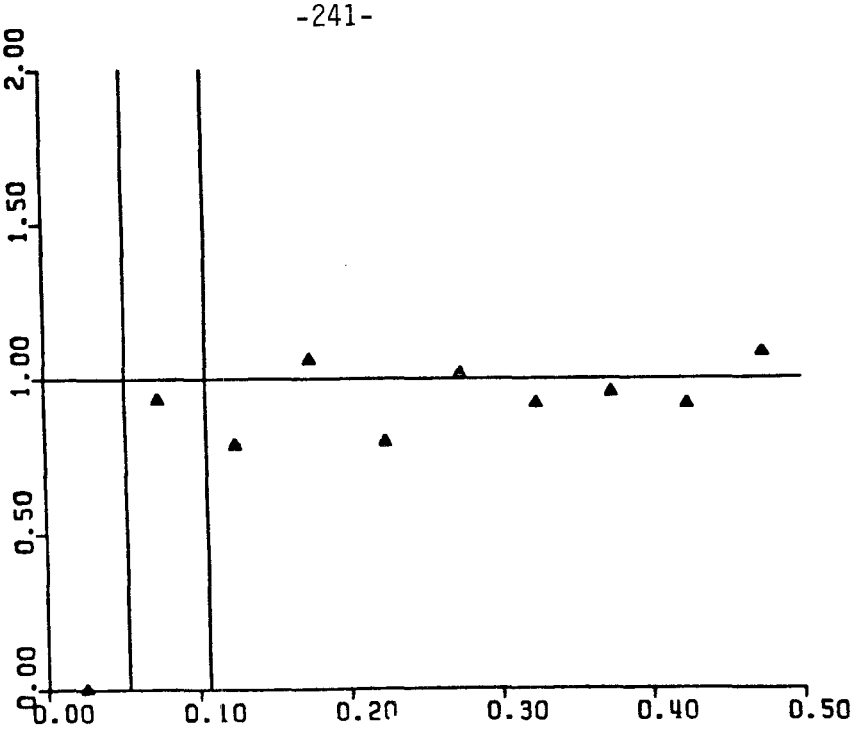
2.00
1.50
1.00
0.50
0.00
0.00
0.10
0.20
0.30
0.40
0.50

T= 1.200

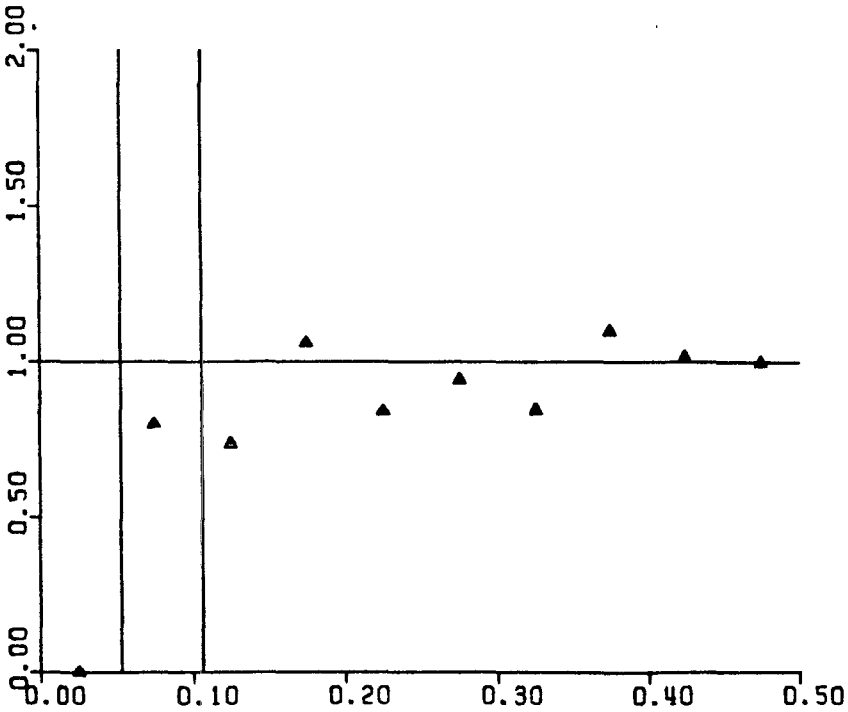
2.00
1.50
1.00
0.50
0.00
0.00
0.10
0.20
0.30
0.40
0.50

T= 1.400

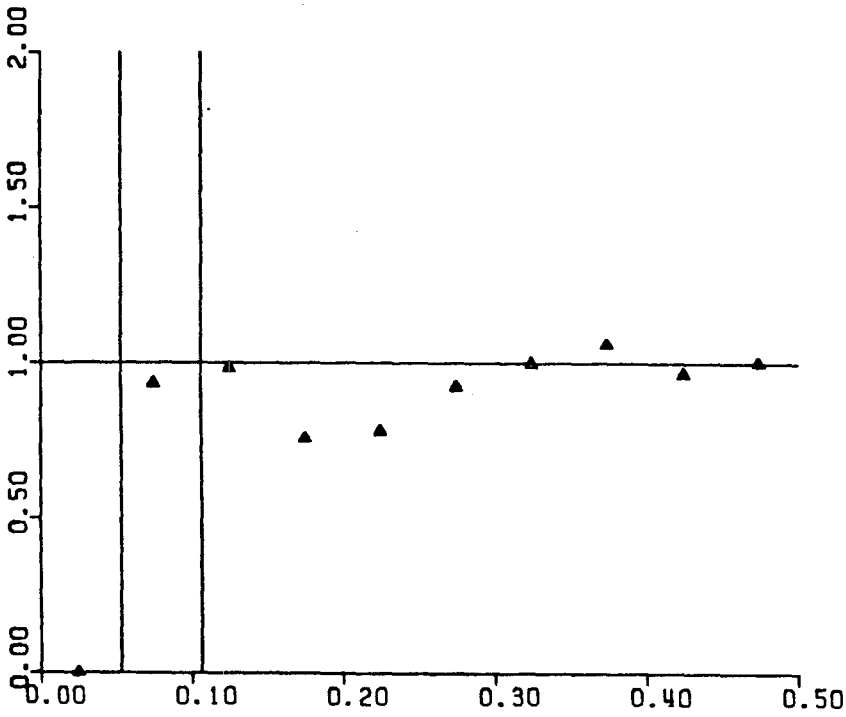
2.00
1.50
1.00
0.50
0.00
0.00
0.10
0.20
0.30
0.40
0.50

T= 1.600

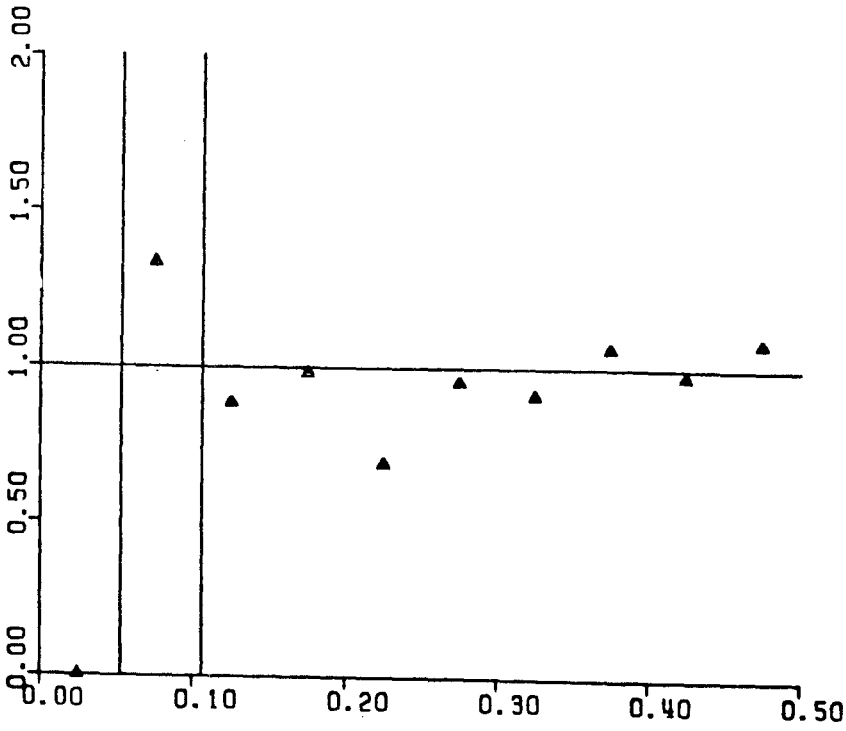
2.00
1.50
1.00
0.50
0.00
0.00
0.10
0.20
0.30
0.40
0.50

T= 1.800

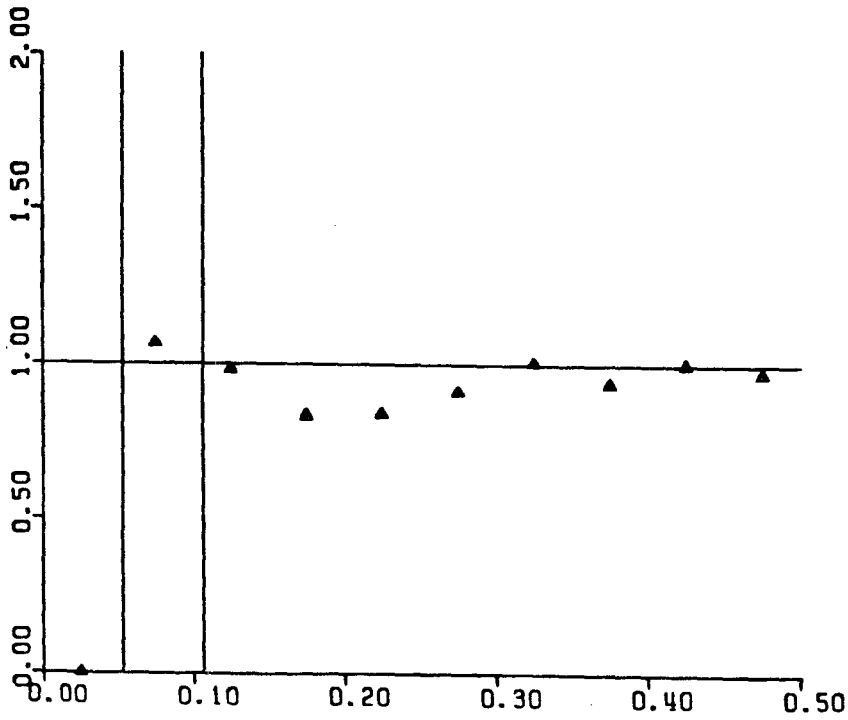
2.00
1.50
1.00
0.50
0.00
0.00
0.10
0.20
0.30
0.40
0.50

T= 2.000

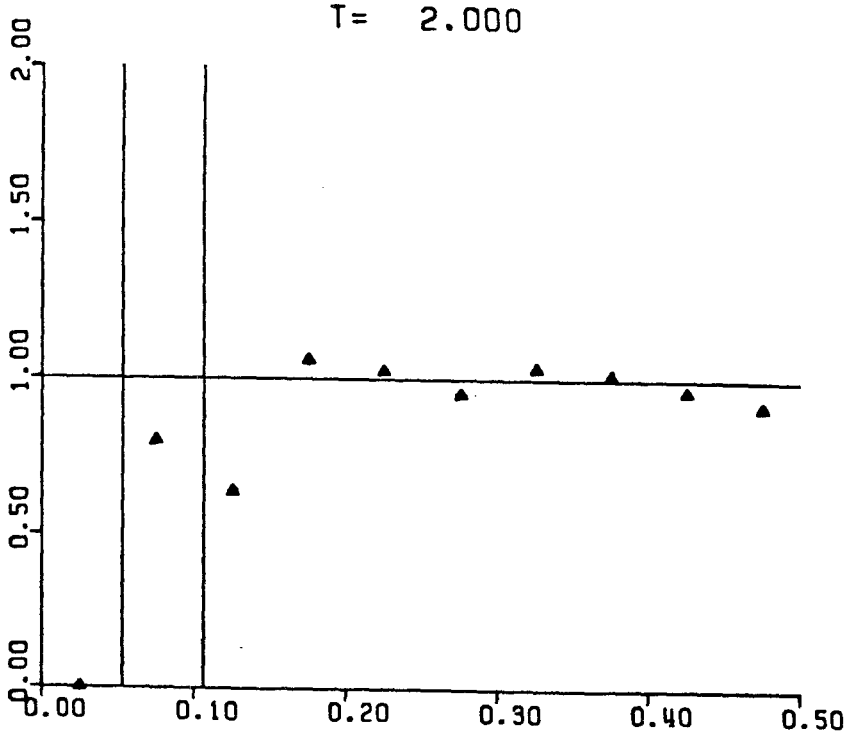
2.00
1.50
1.00
0.50
0.00
0.00
0.10
0.20
0.30
0.40
0.50

T= 2.400

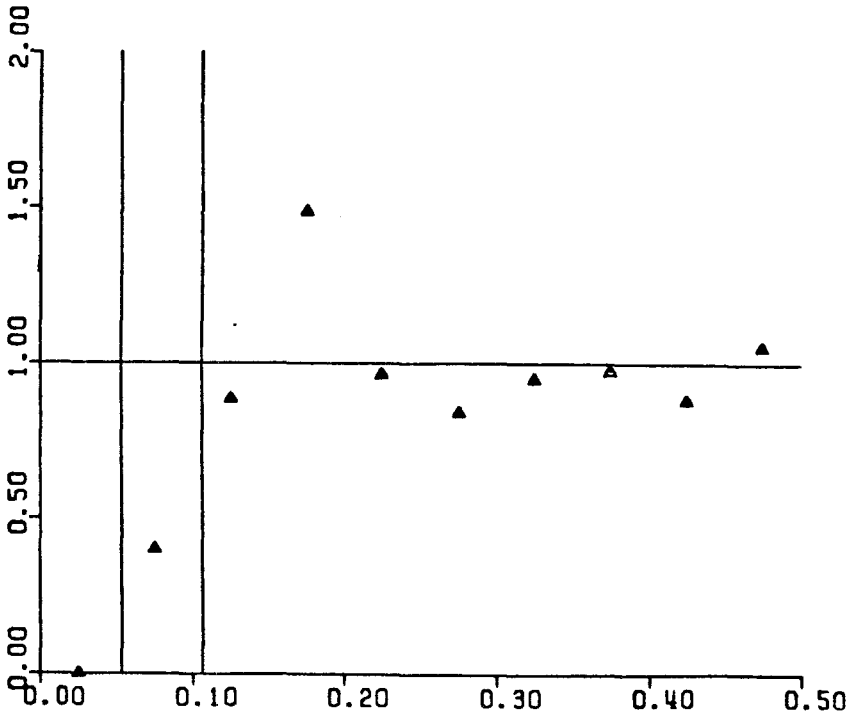
2.00
1.50
1.00
0.50
0.00
0.00
0.10
0.20
0.30
0.40
0.50

T= 2.800

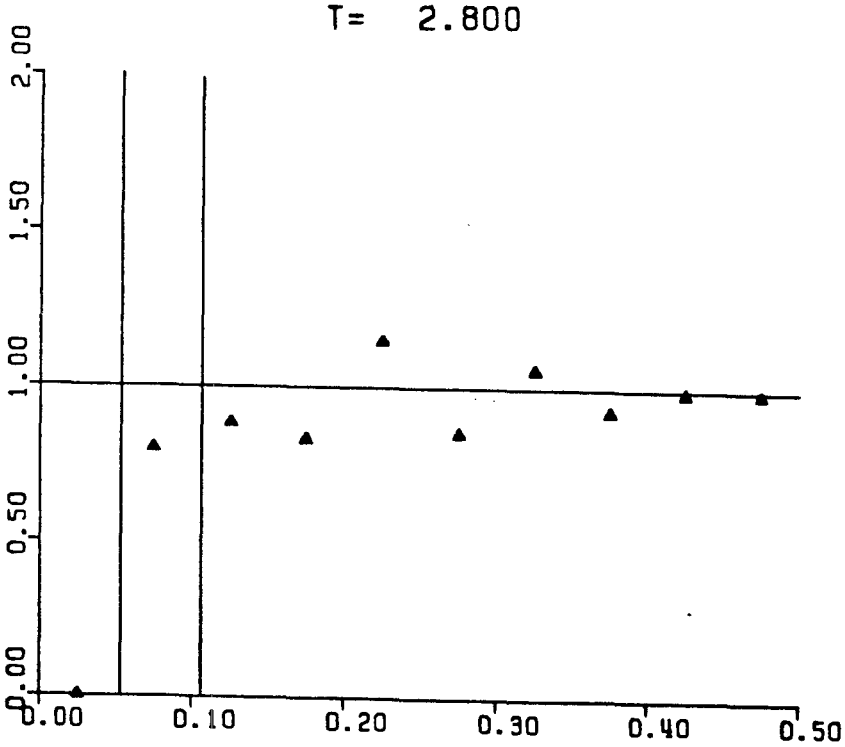
2.00
1.50
1.00
0.50
0.00
0.00
0.10
0.20
0.30
0.40
0.50

T= 3.200

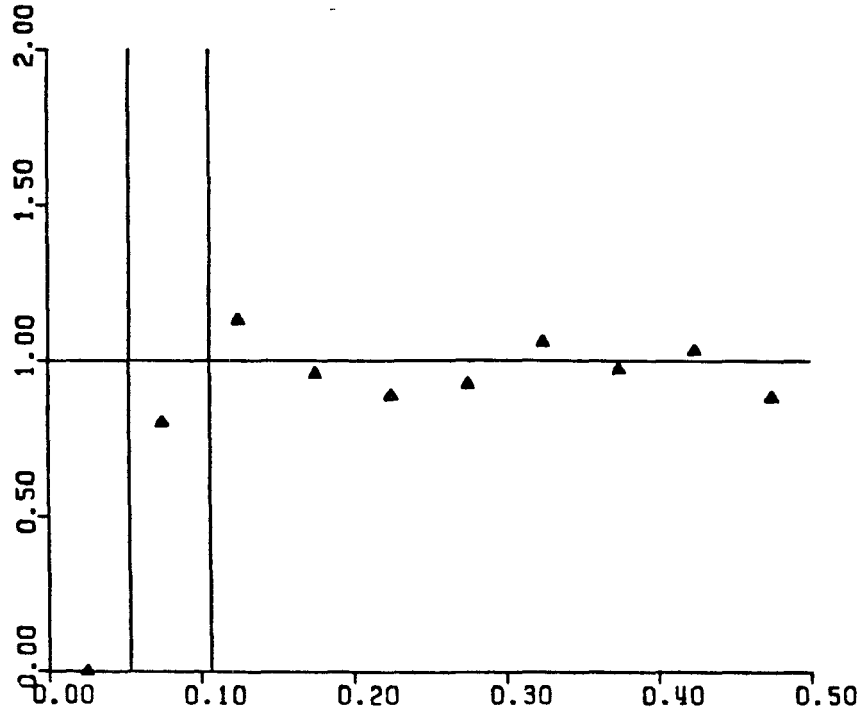
2.00
1.50
1.00
0.50
0.00
0.00
0.10
0.20
0.30
0.40
0.50

T= 3.600

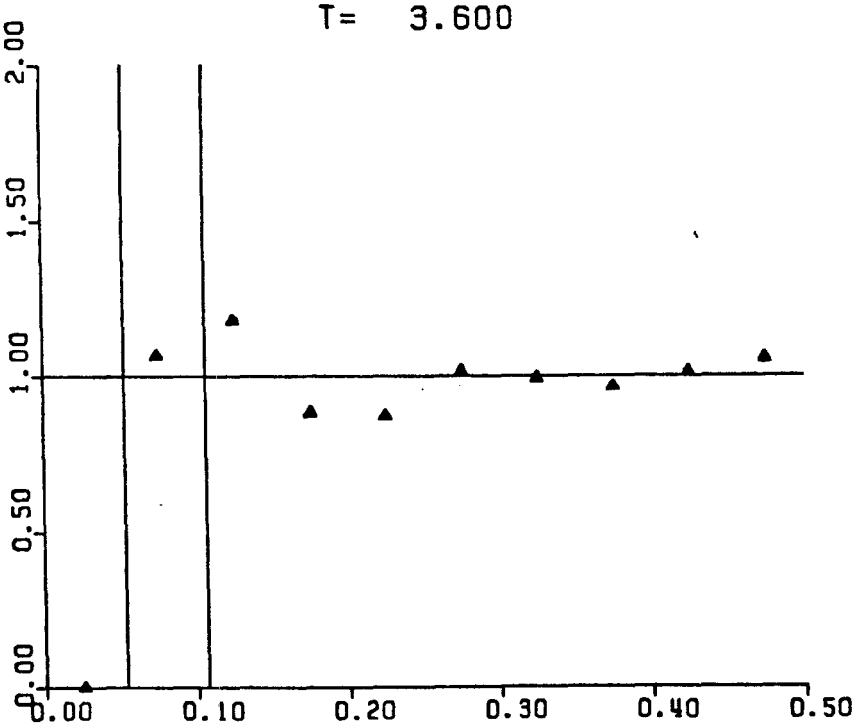
2.00
1.50
1.00
0.50
0.00
0.00
0.10
0.20
0.30
0.40
0.50

T= 4.000

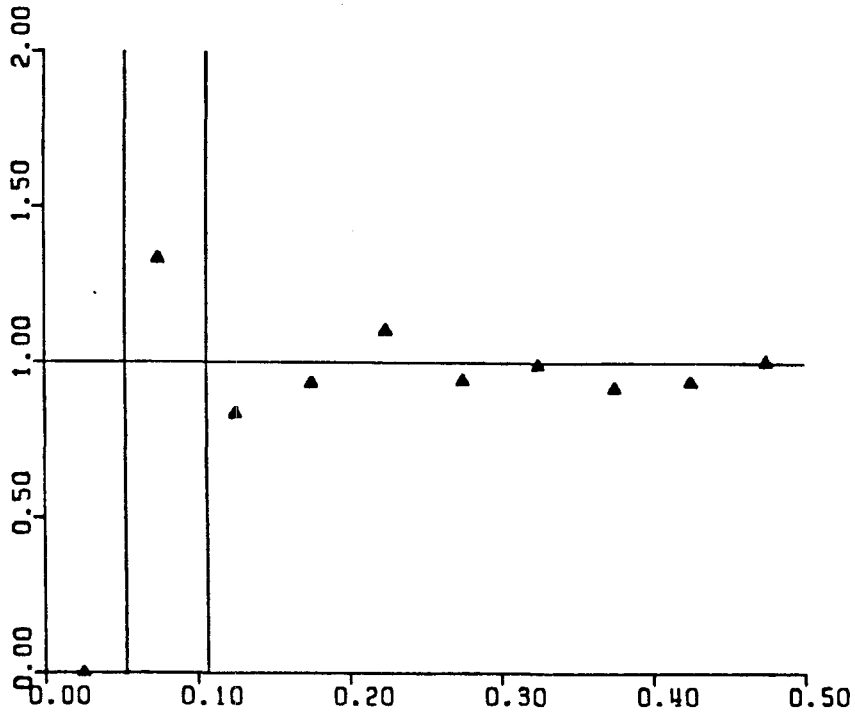
2.00
1.50
1.00
0.50
0.00
0.00
0.10
0.20
0.30
0.40
0.50

T= 4.400

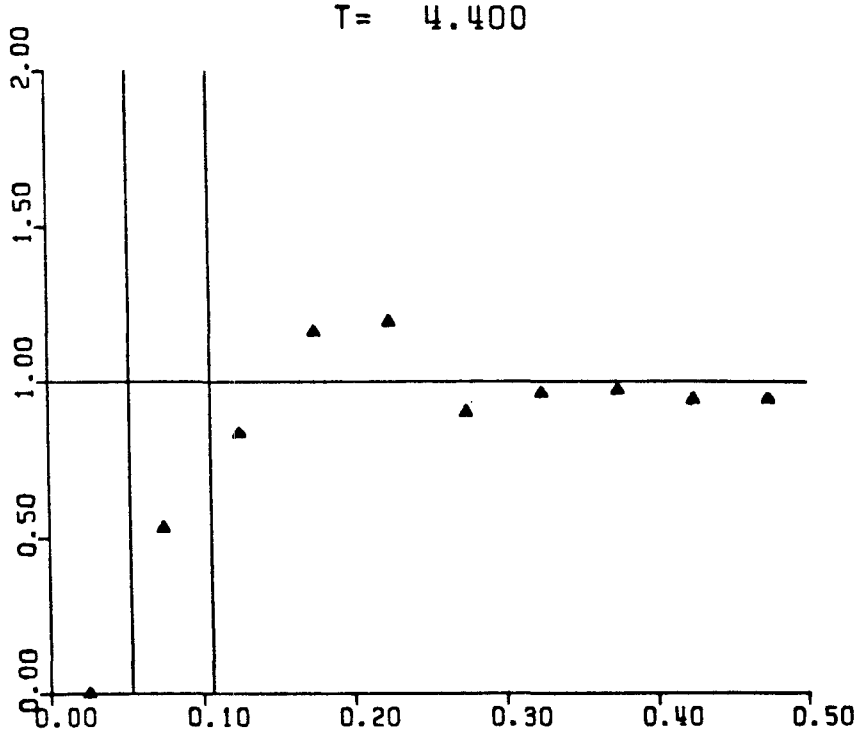
2.00
1.50
1.00
0.50
0.00
0.00
0.10
0.20
0.30
0.40
0.50

T= 4.800

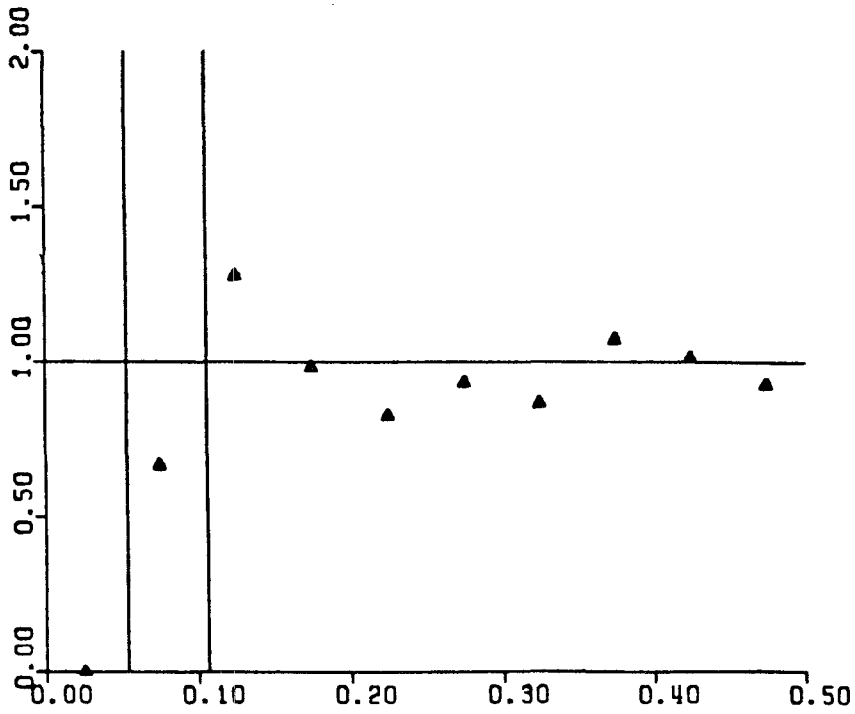
2.00
1.50
1.00
0.50
0.00
0.00
0.10
0.20
0.30
0.40
0.50

T= 5.200

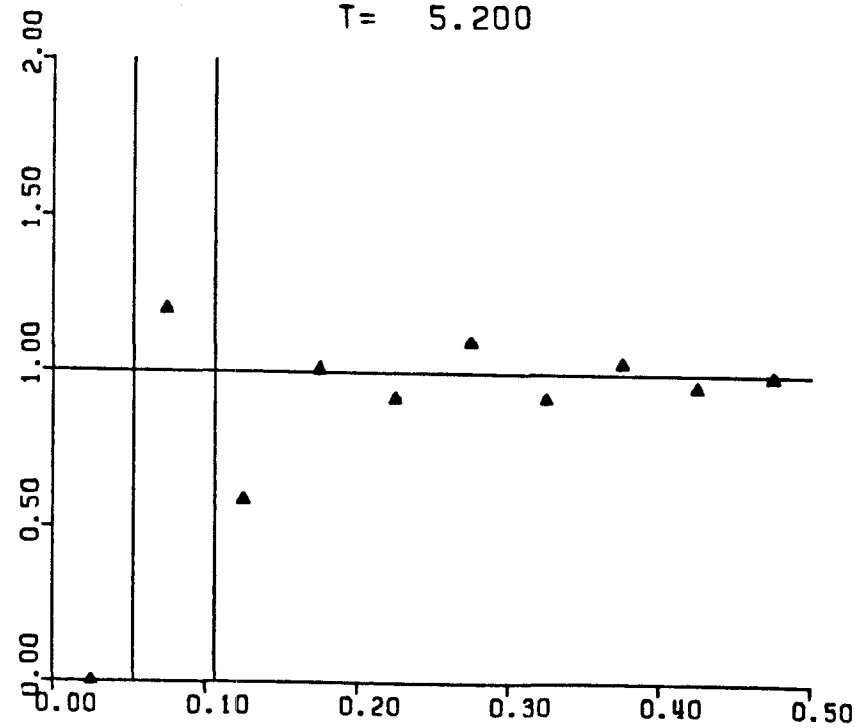
2.00
1.50
1.00
0.50
0.00
0.00
0.10
0.20
0.30
0.40
0.50

T= 5.600

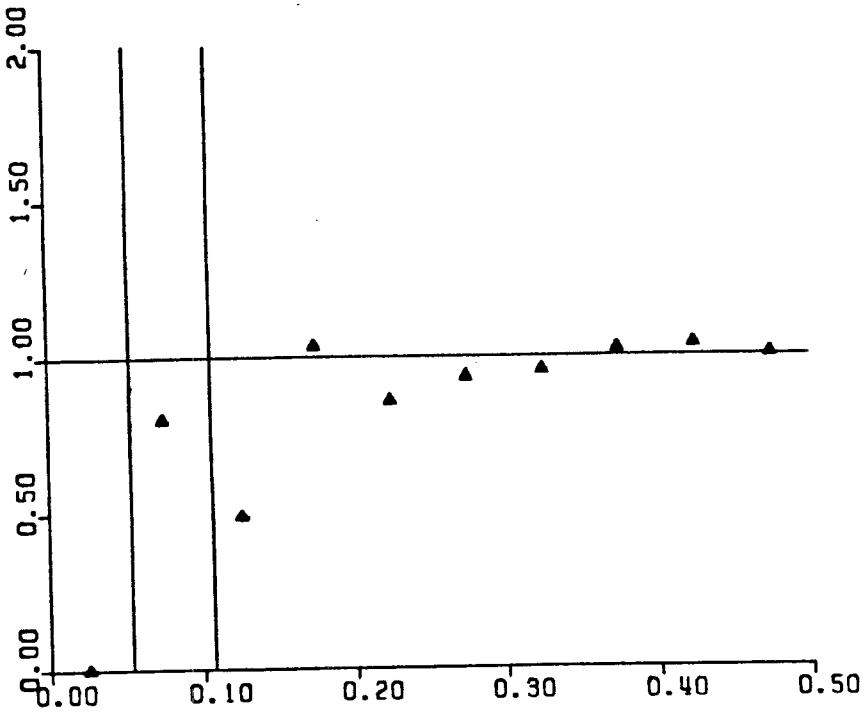
2.00
1.50
1.00
0.50
0.00
0.00
0.10
0.20
0.30
0.40
0.50

T= 6.001

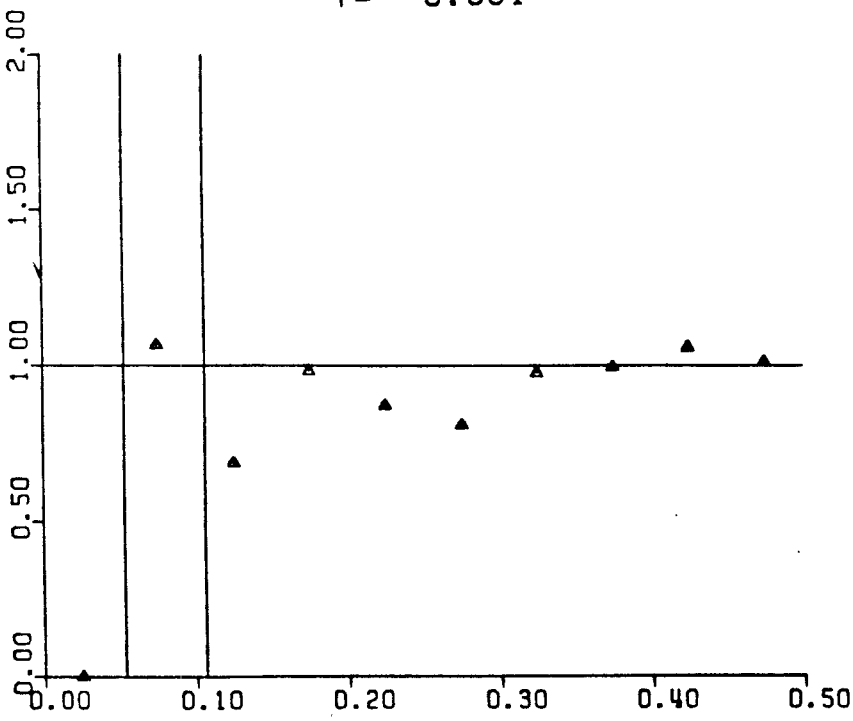
2.00
1.50
1.00
0.50
0.00
0.00
0.10
0.20
0.30
0.40
0.50

T= 6.201

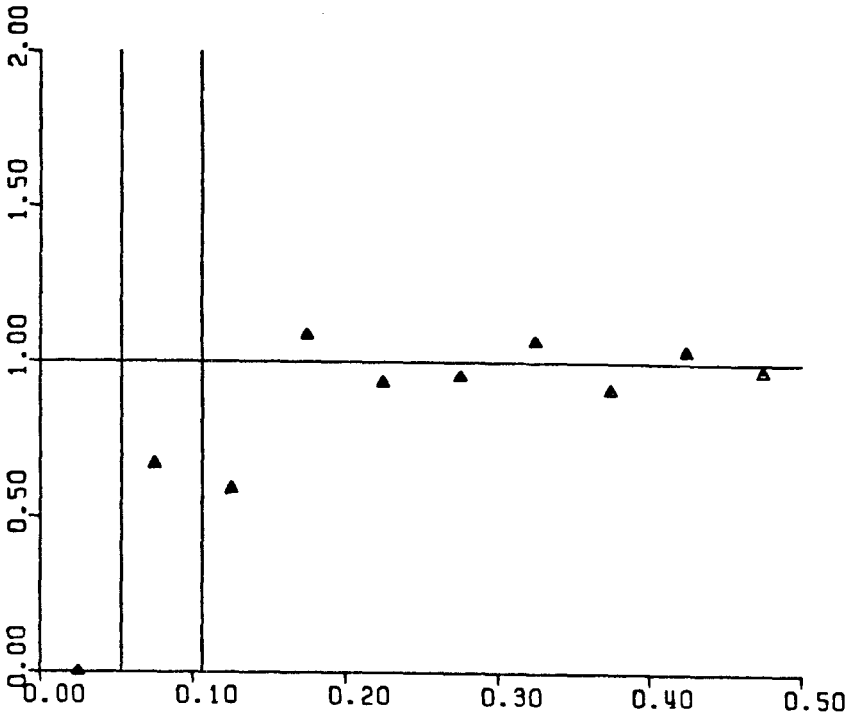
2.00
1.50
1.00
0.50
0.00
0.00
0.10
0.20
0.30
0.40
0.50

T= 6.401

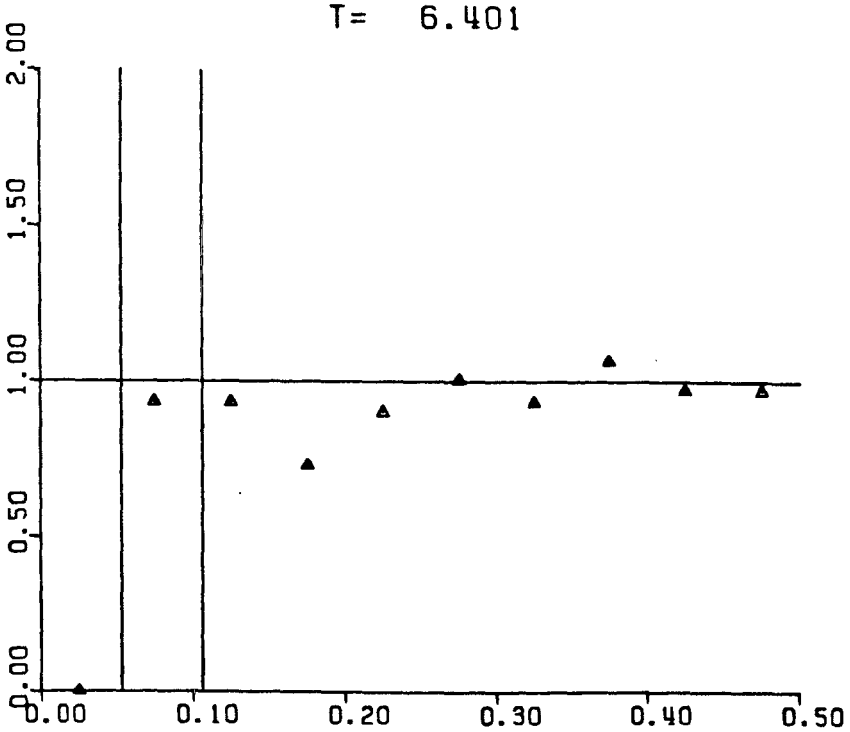
2.00
1.50
1.00
0.50
0.00
0.00
0.10
0.20
0.30
0.40
0.50

T= 6.601

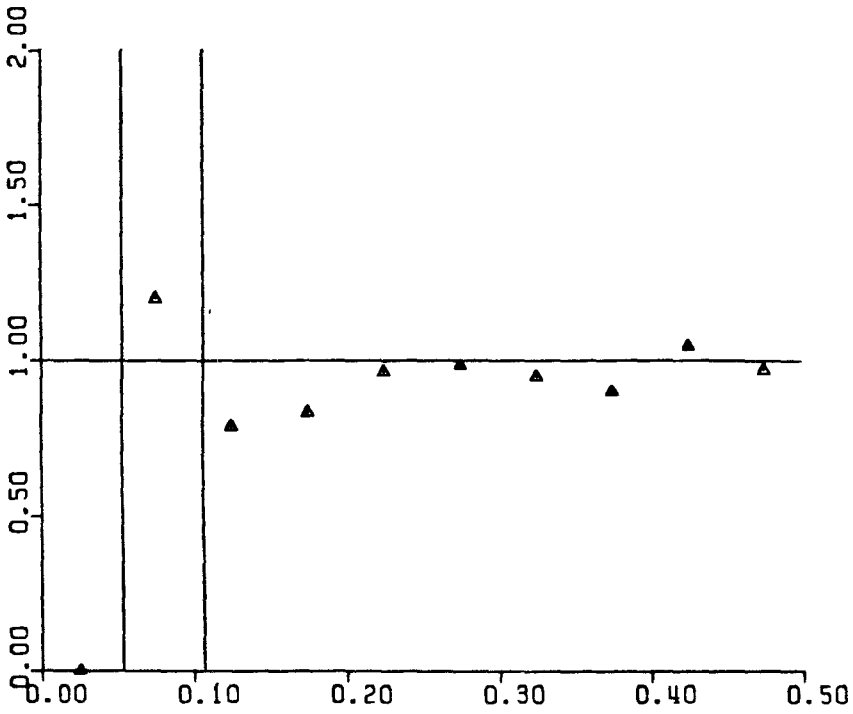
2.00
1.50
1.00
0.50
0.00
0.00
0.10
0.20
0.30
0.40
0.50

T= 6.801

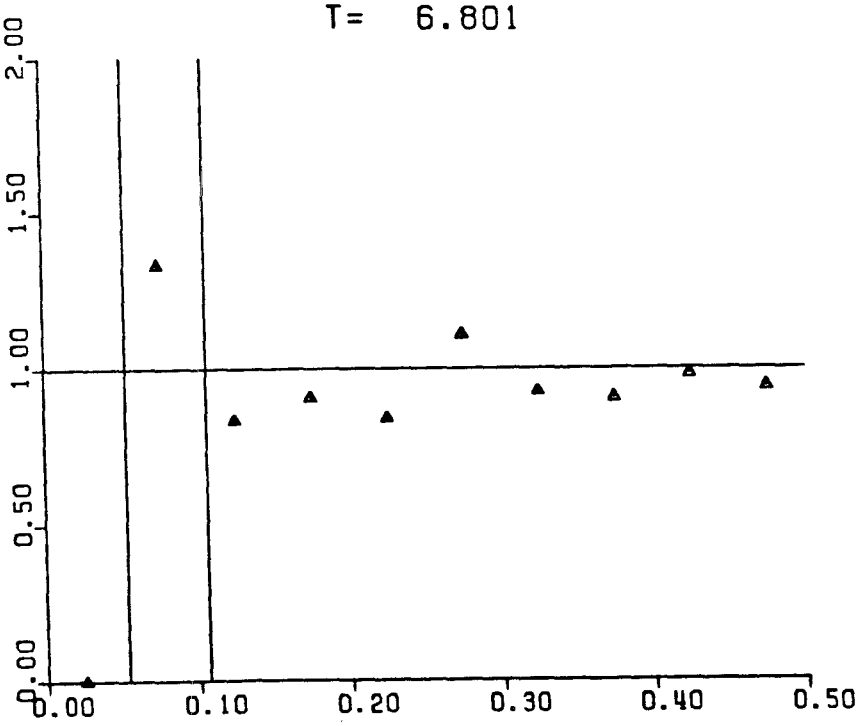
2.00
1.50
1.00
0.50
0.00
0.00
0.10
0.20
0.30
0.40
0.50

T= 7.001

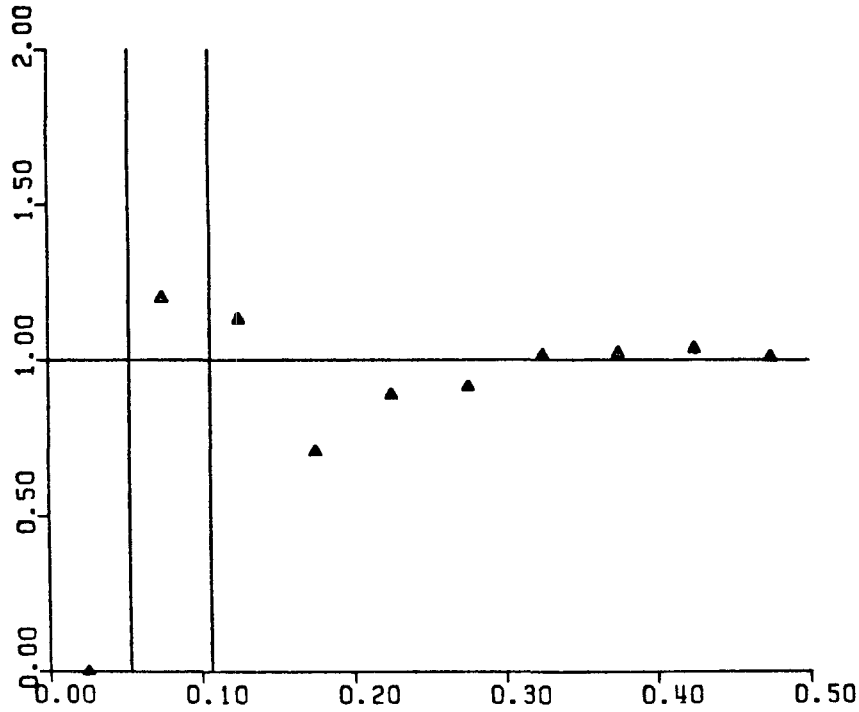
2.00
1.50
1.00
0.50
0.00
0.00
0.10
0.20
0.30
0.40
0.50

T= 7.201

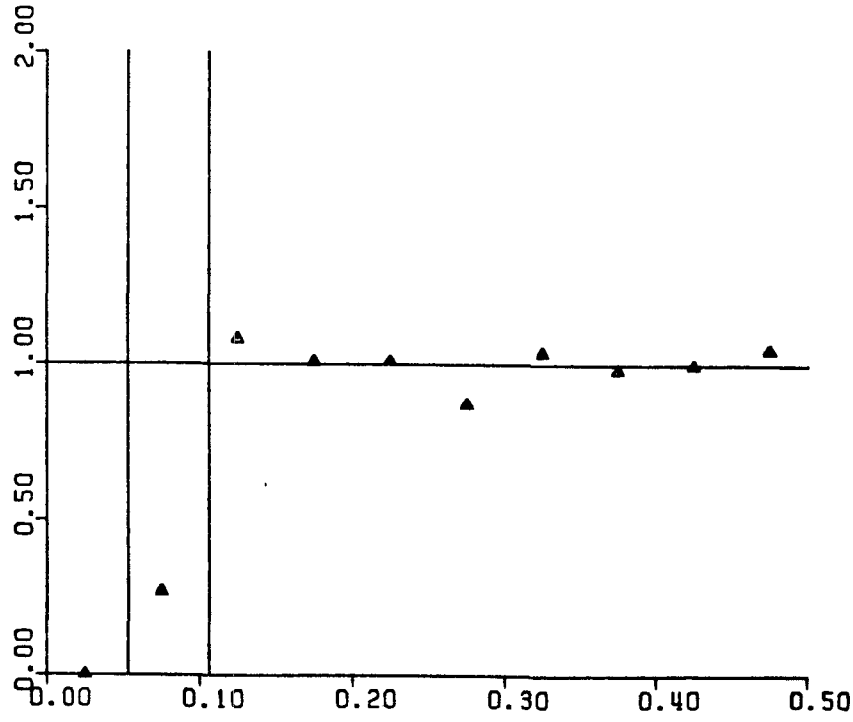
2.00
1.50
1.00
0.50
0.00
0.00
0.10
0.20
0.30
0.40
0.50

T= 7.401

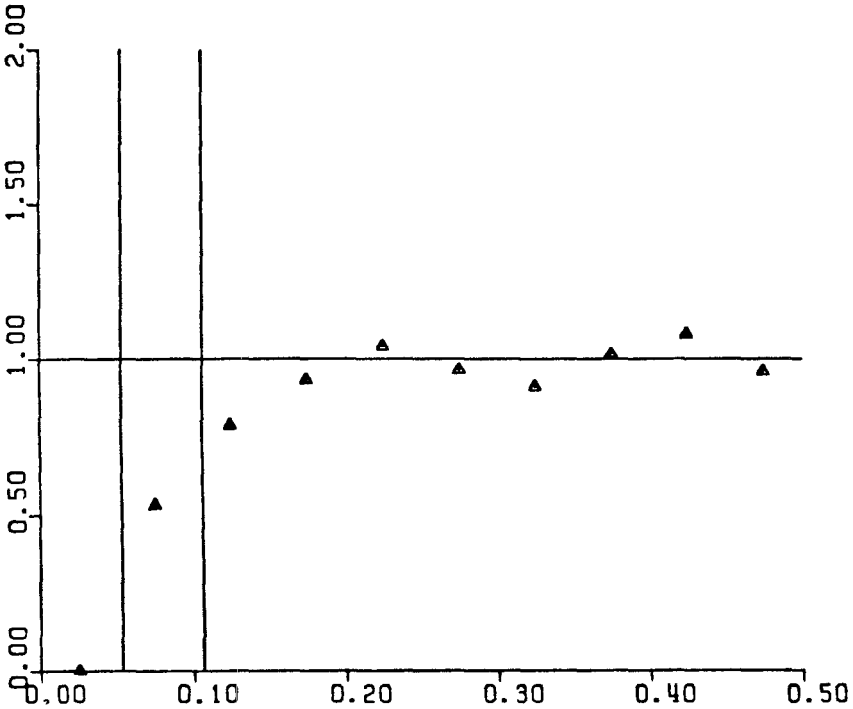
2.00
1.50
1.00
0.50
0.00
0.00
0.10
0.20
0.30
0.40
0.50

T= 7.601

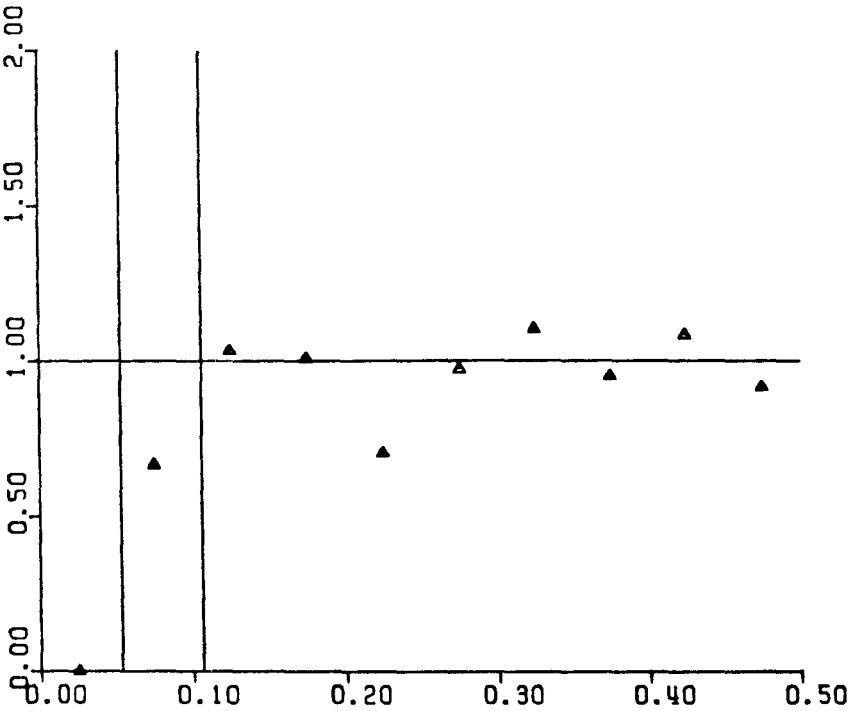
2.00
1.50
1.00
0.50
0.00
0.00
0.10
0.20
0.30
0.40
0.50

T= 7.801

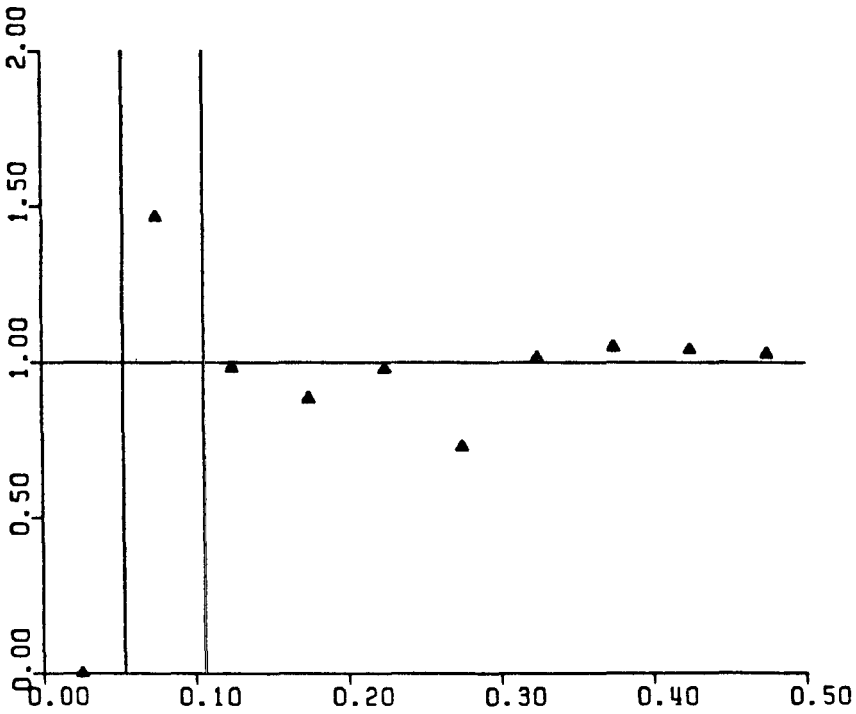


T= 8.001

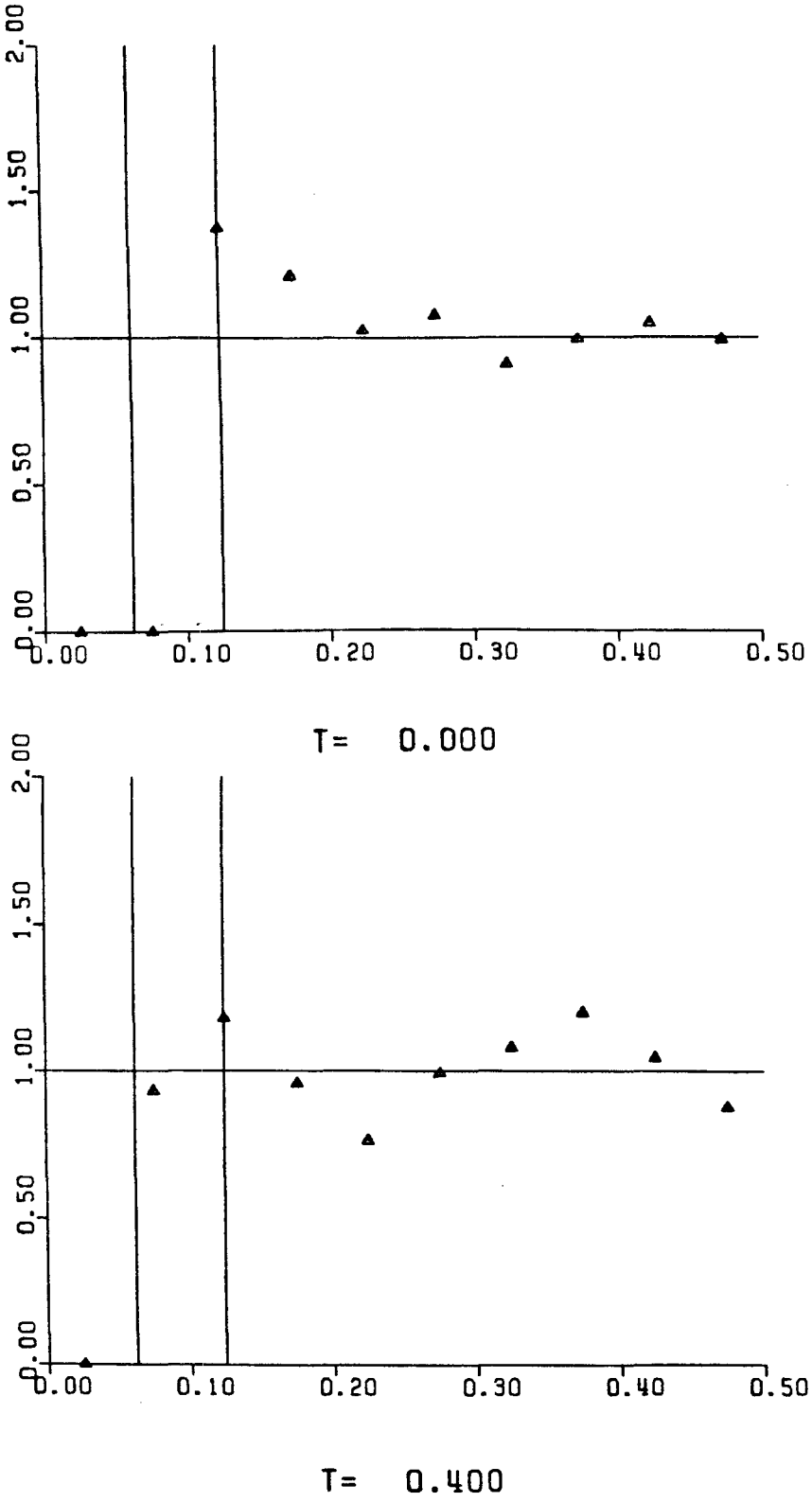


**Figure 35.** Pair-probability function for simulation run 9.

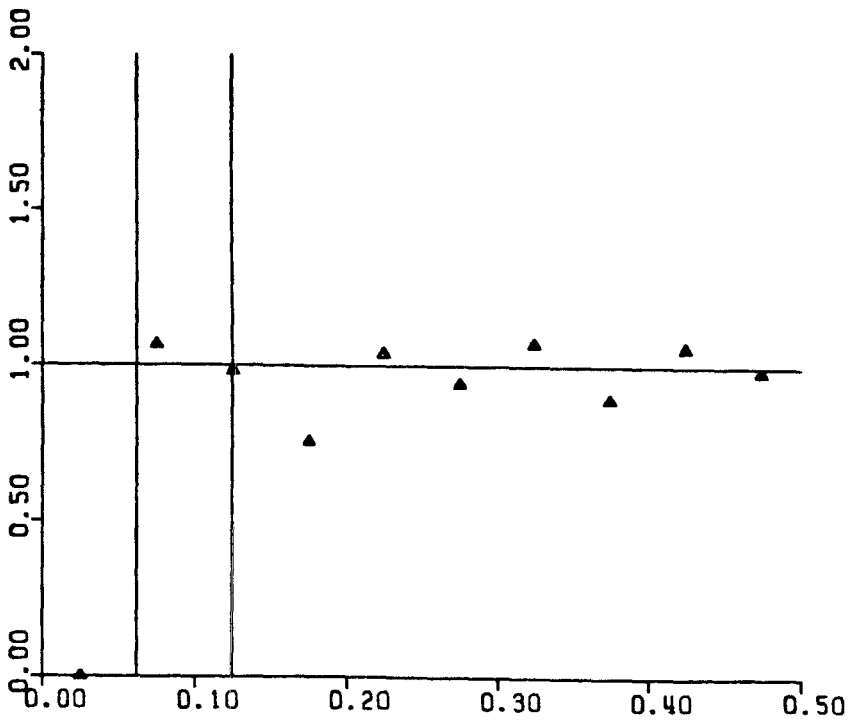
2.00
1.50
1.00
0.50
0.00
0.00
0.10
0.20
0.30
0.40
0.50

T= 0.800

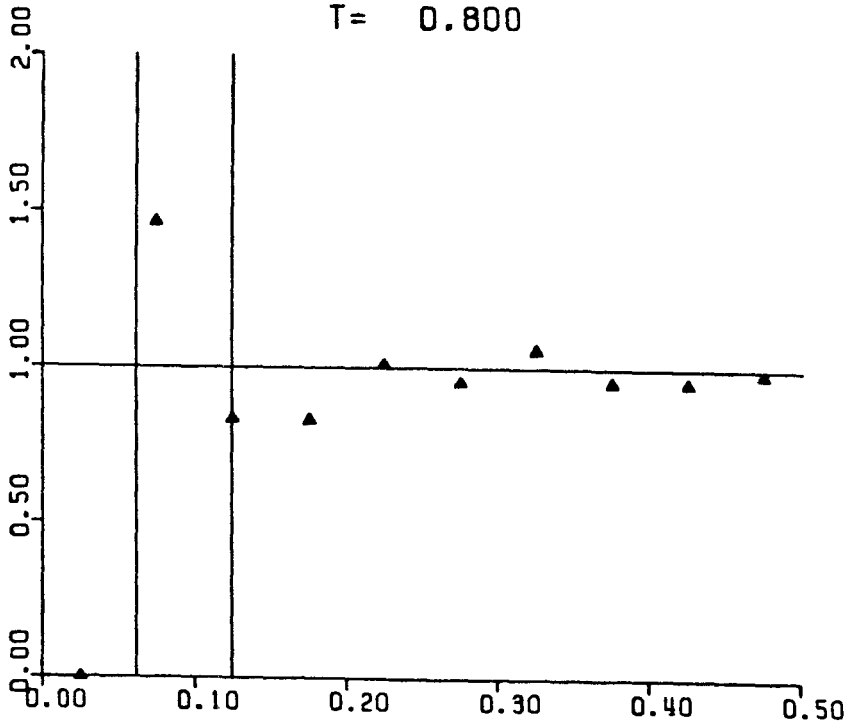
2.00
1.50
1.00
0.50
0.00
0.00
0.10
0.20
0.30
0.40
0.50

T= 1.200

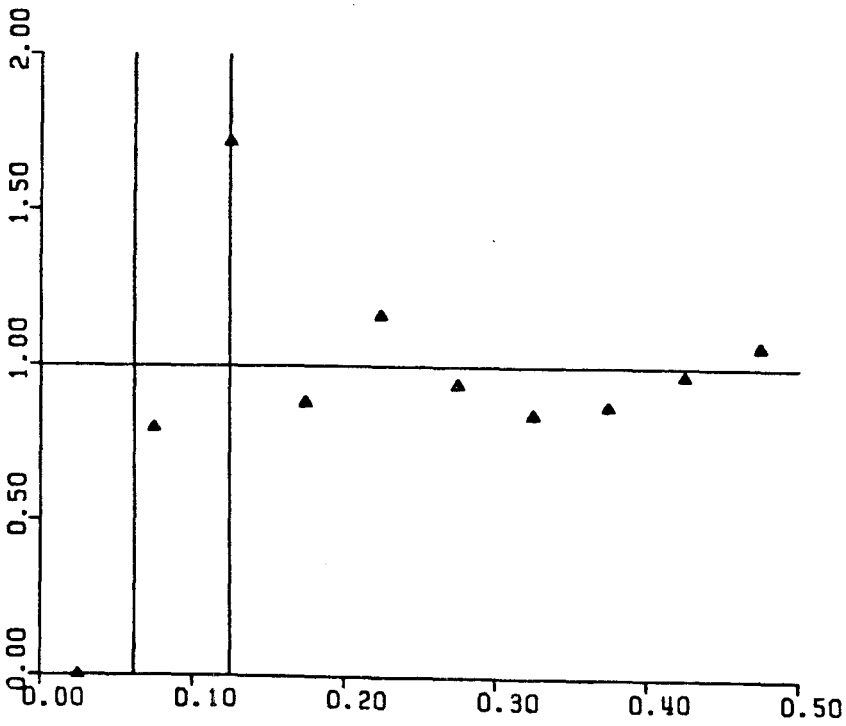
2.00
1.50
1.00
0.50
0.00
0.00
0.10
0.20
0.30
0.40
0.50

T= 1.600

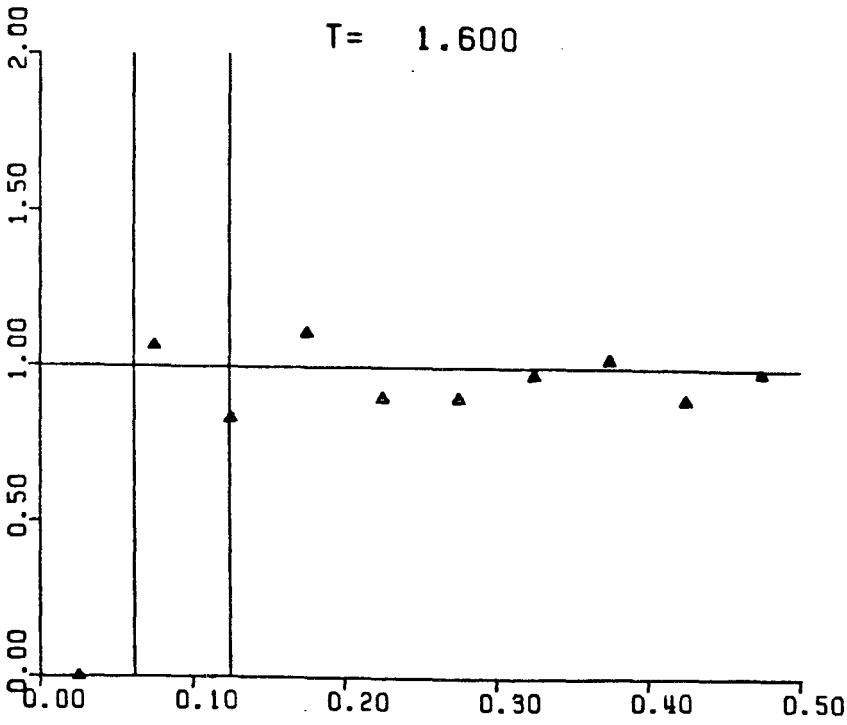
2.00
1.50
1.00
0.50
0.00
0.00
0.10
0.20
0.30
0.40
0.50

T= 2.000

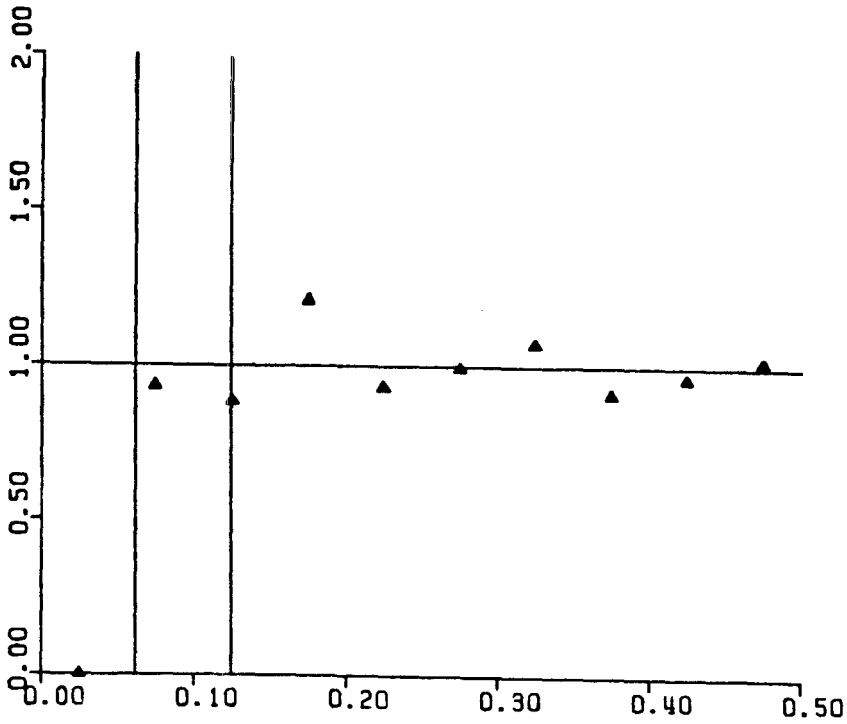
2.00
1.50
1.00
0.50
0.00
0.00
0.10
0.20
0.30
0.40
0.50

T= 2.400

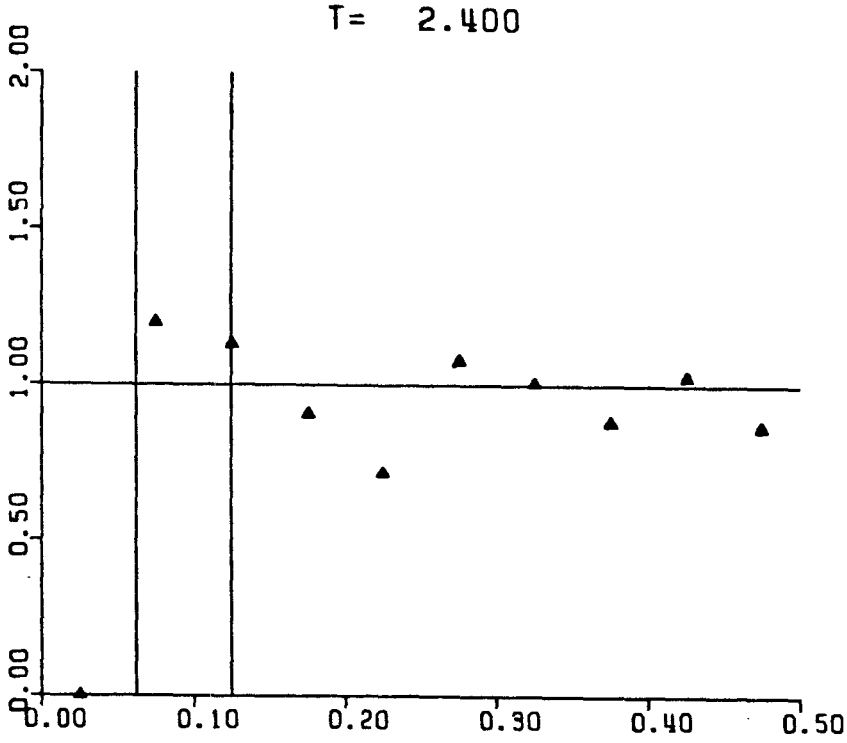
2.00
1.50
1.00
0.50
0.00
0.00
0.10
0.20
0.30
0.40
0.50

T= 2.800

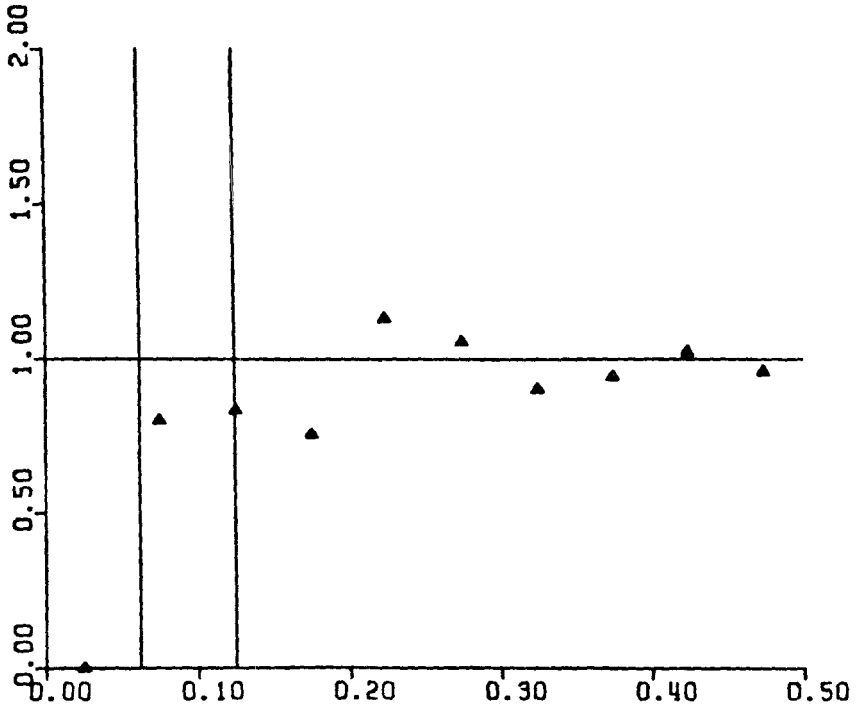
2.00
1.50
1.00
0.50
0.00
0.00
0.10
0.20
0.30
0.40
0.50

T= 3.200

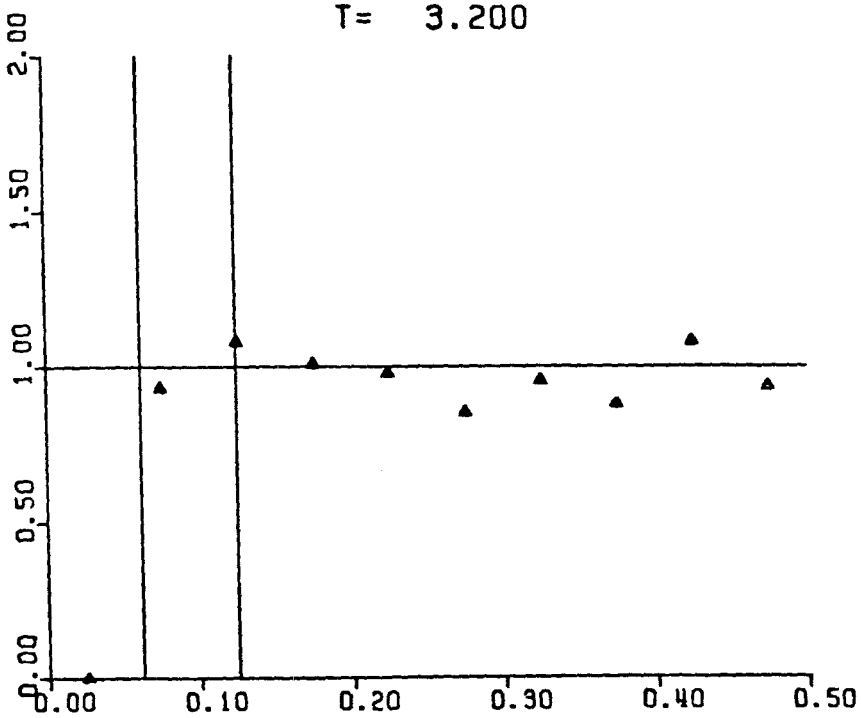
2.00
1.50
1.00
0.50
0.00
0.00
0.10
0.20
0.30
0.40
0.50

T= 3.600

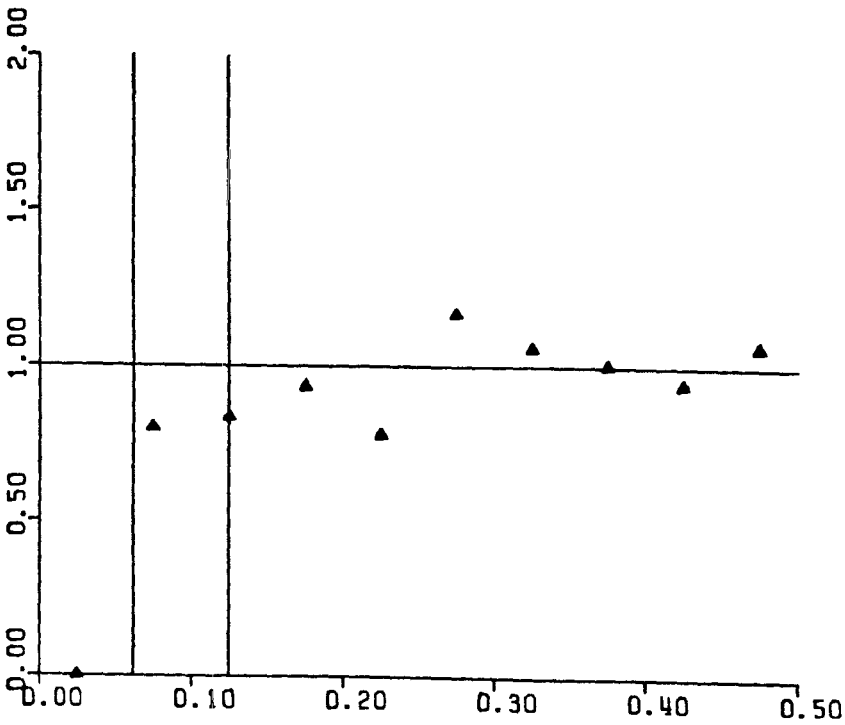
2.00
1.50
1.00
0.50
0.00
0.00
0.10
0.20
0.30
0.40
0.50

T= 4.000

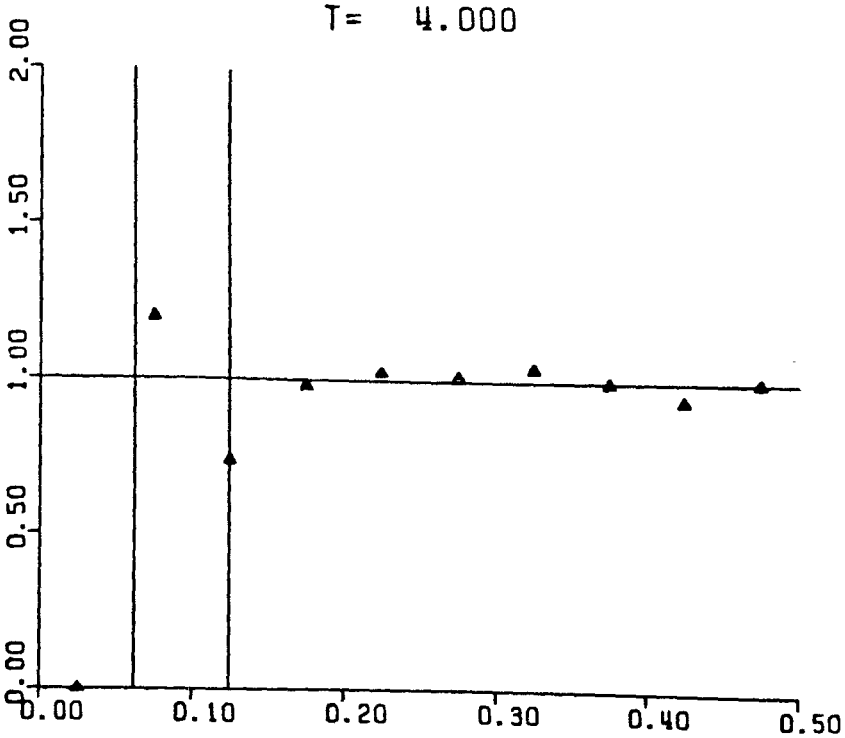
2.00
1.50
1.00
0.50
0.00
0.00
0.10
0.20
0.30
0.40
0.50

T= 4.400

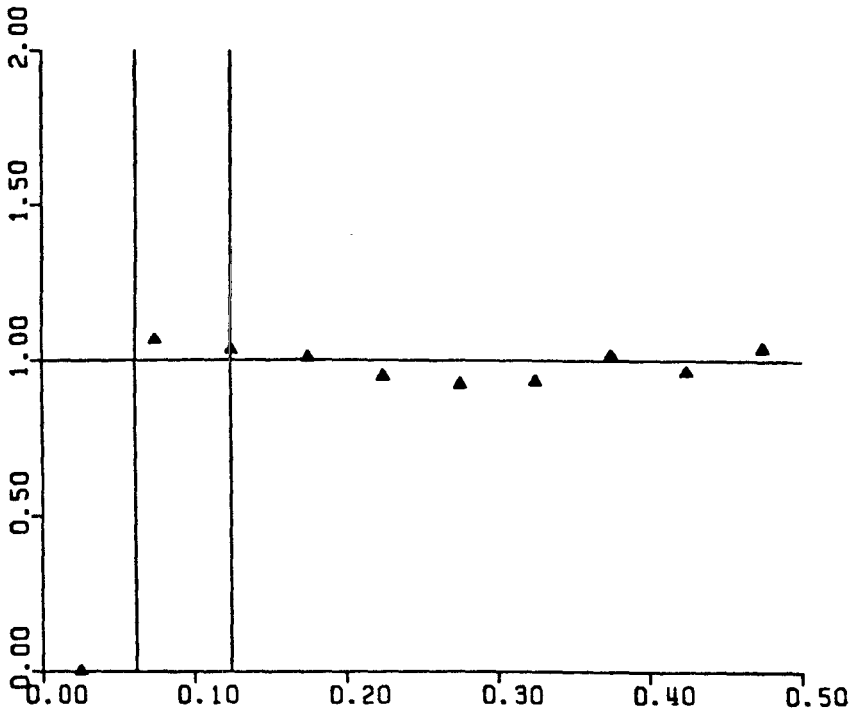
2.00
1.50
1.00
0.50
0.00
0.00
0.10
0.20
0.30
0.40
0.50

T= 4.800

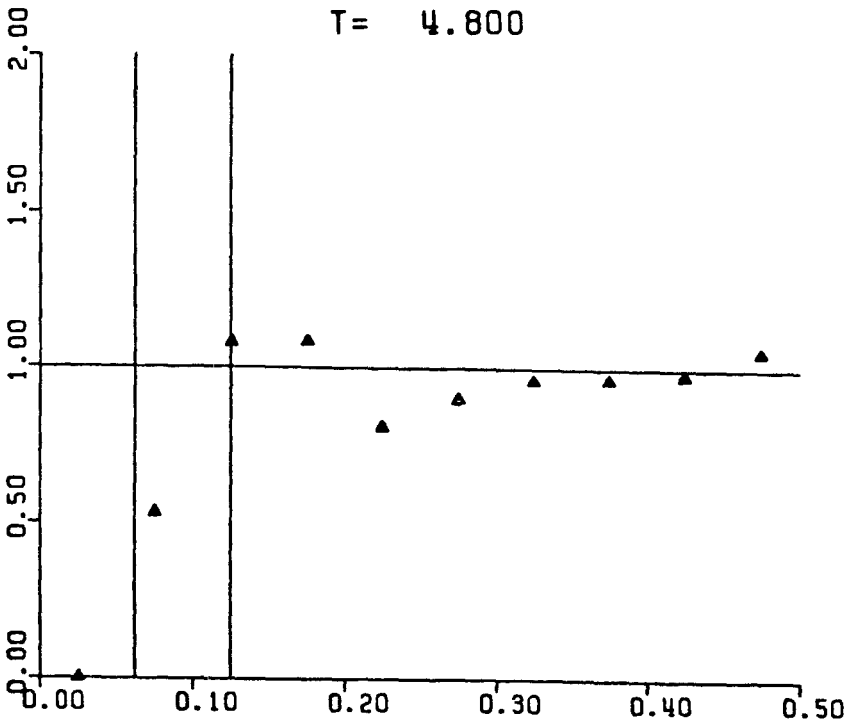
2.00
1.50
1.00
0.50
0.00
0.00
0.10
0.20
0.30
0.40
0.50

T= 5.200

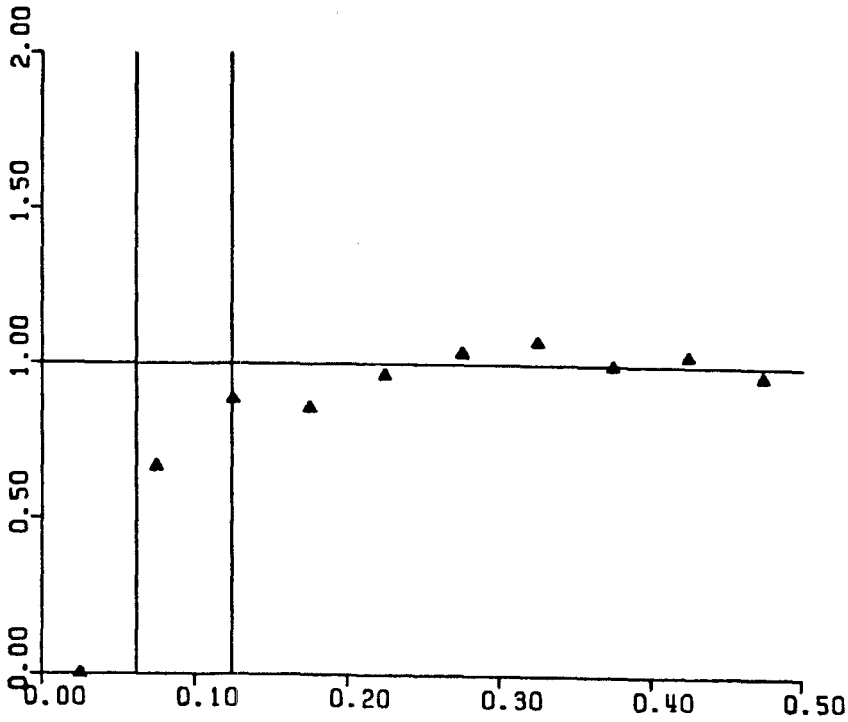
2.00
1.50
1.00
0.50
0.00
0.00
0.10
0.20
0.30
0.40
0.50

T= 5.600

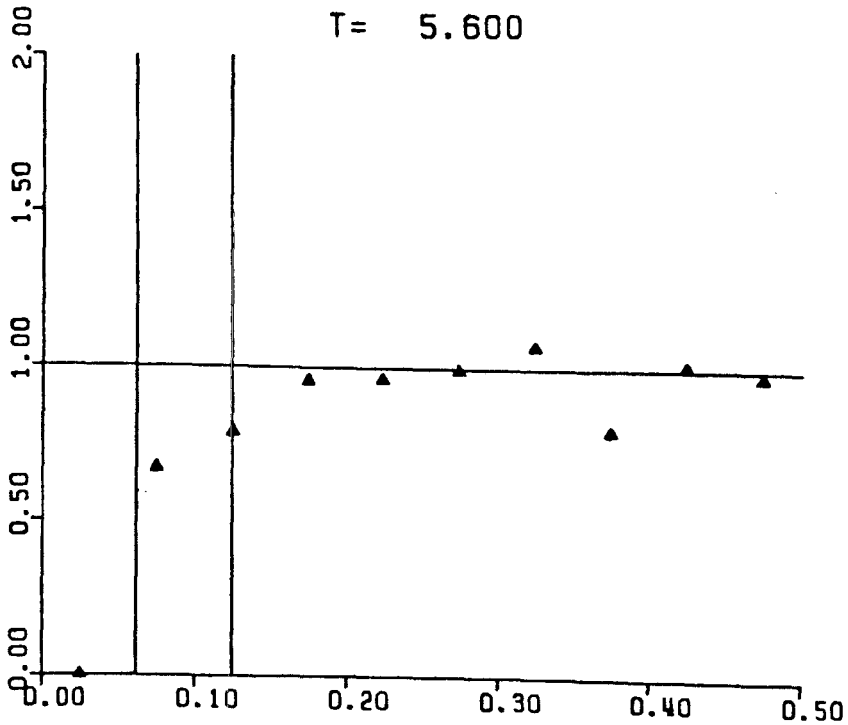
2.00
1.50
1.00
0.50
0.00
0.00
0.10
0.20
0.30
0.40
0.50

T= 6.000

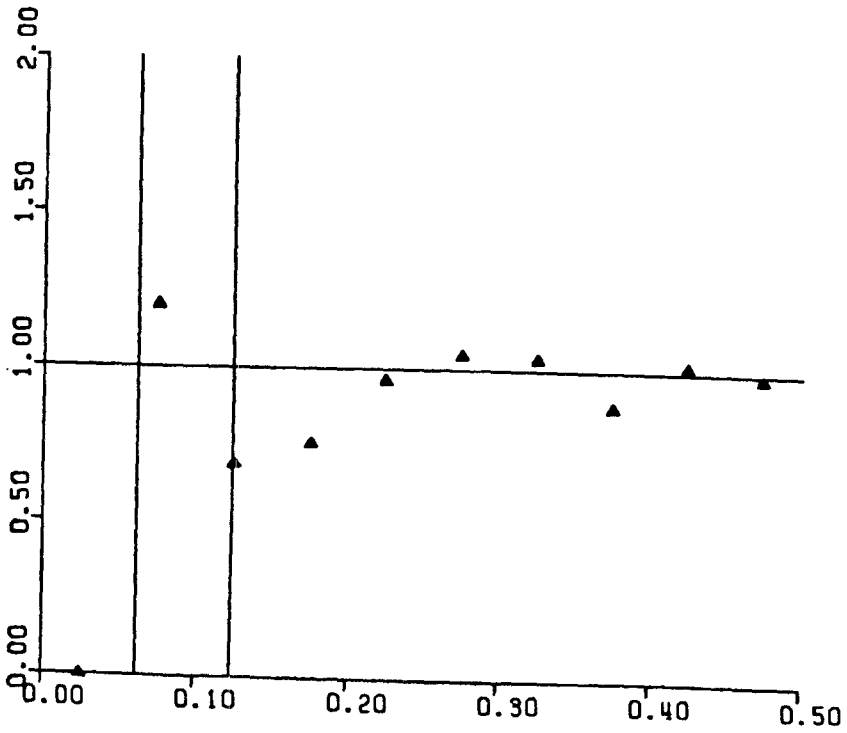
2.00
1.50
1.00
0.50
0.00
0.00
0.10
0.20
0.30
0.40
0.50

T= 6.400

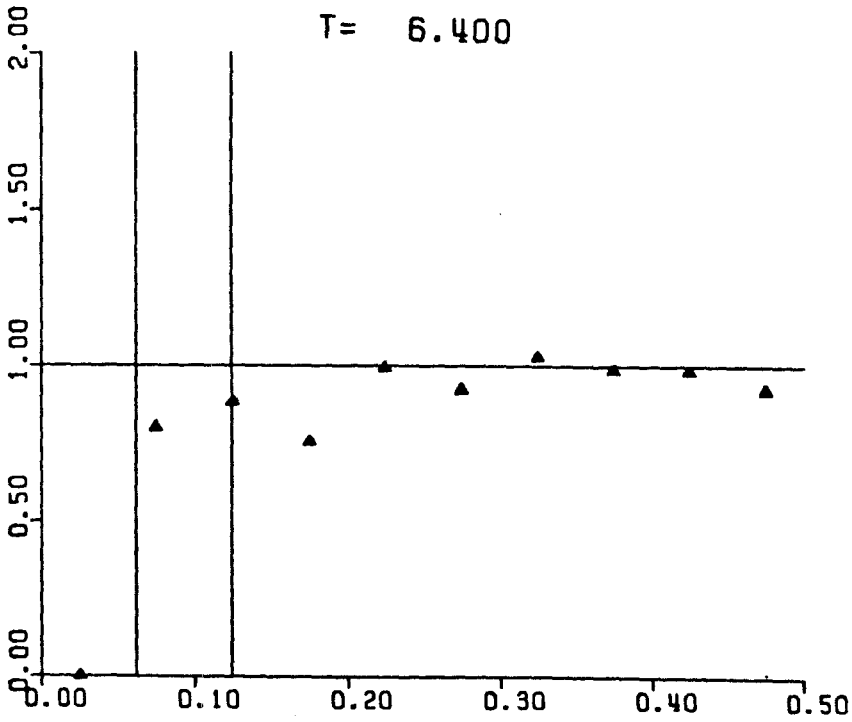
2.00
1.50
1.00
0.50
0.00
0.00
0.10
0.20
0.30
0.40
0.50

T= 6.800

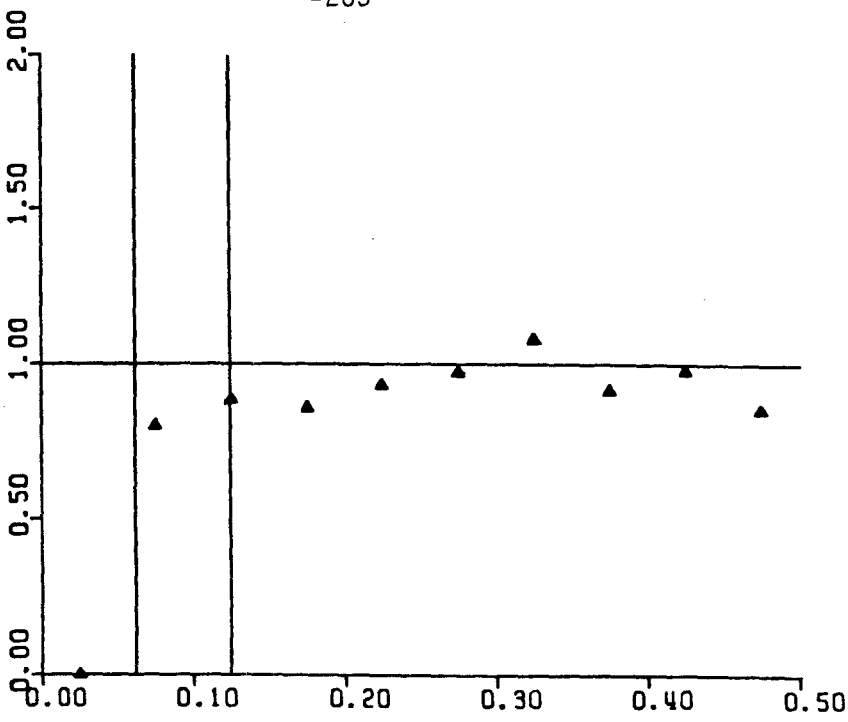
2.00
1.50
1.00
0.50
0.00
0.00
0.10
0.20
0.30
0.40
0.50

T= 7.200

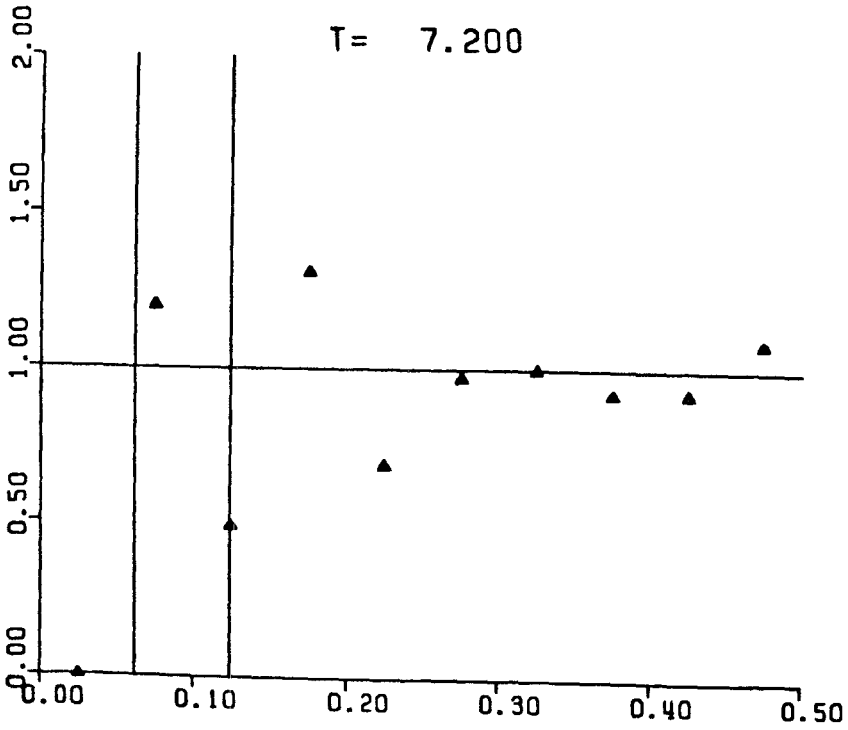
2.00
1.50
1.00
0.50
0.00
0.00
0.10
0.20
0.30
0.40
0.50

T= 7.600

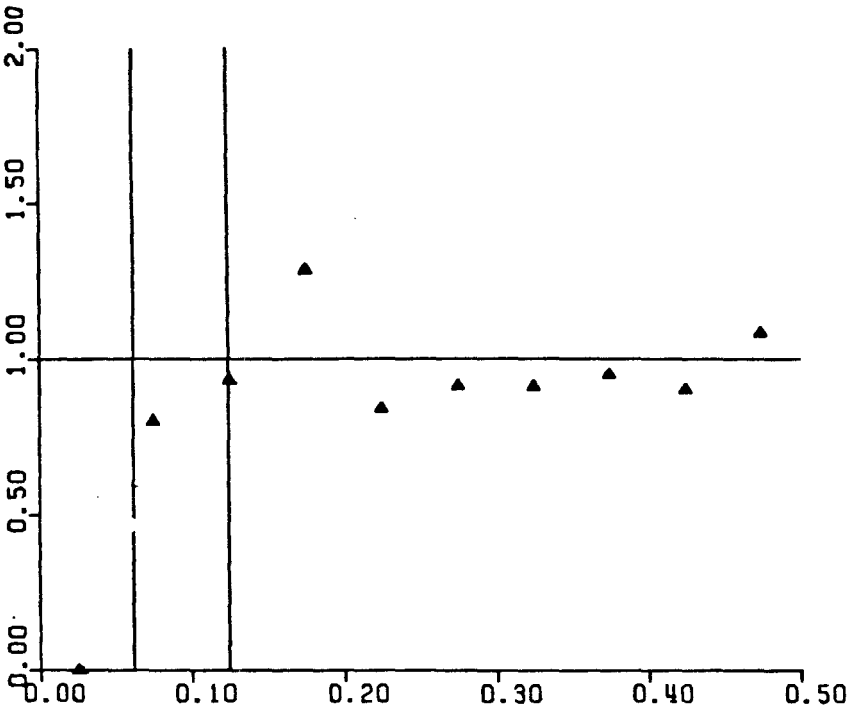


T= 8.000

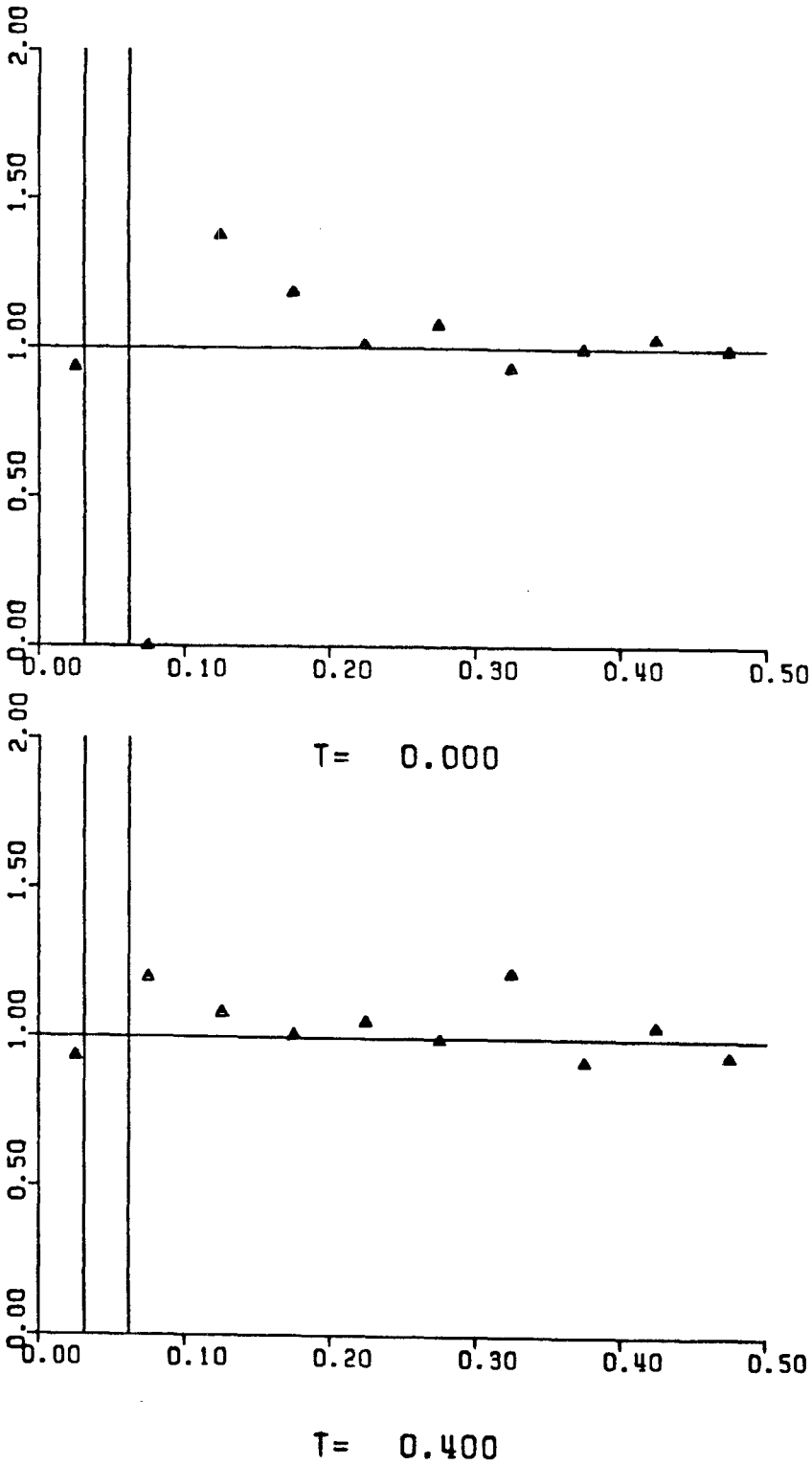


**Figure 36.** Pair-probability function for simulation run 10.

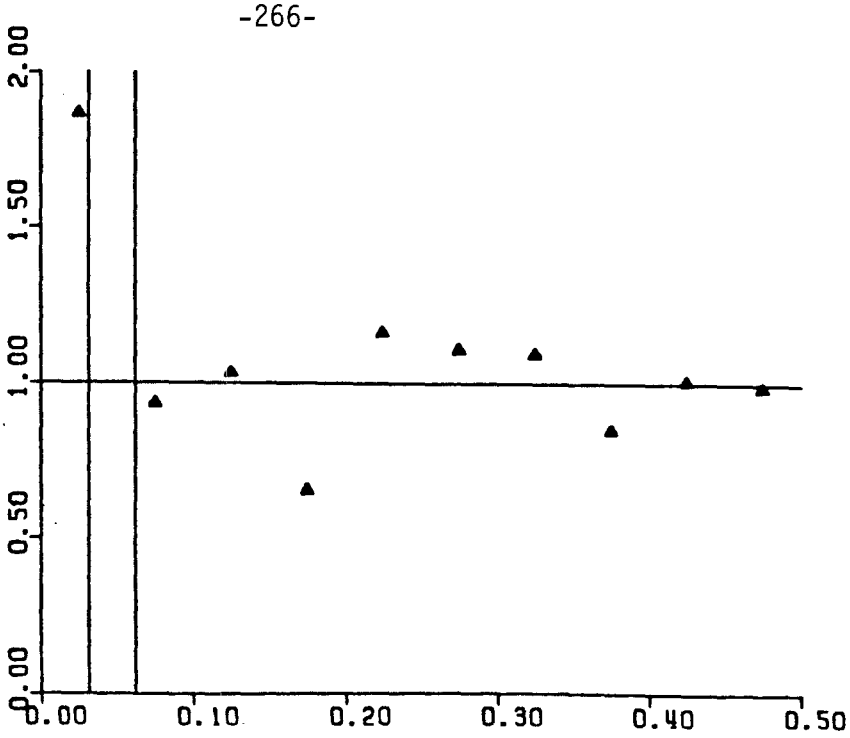
2.00
1.50
1.00
0.50
0.00
0.00
0.10
0.20
0.30
0.40
0.50

T= 0.800

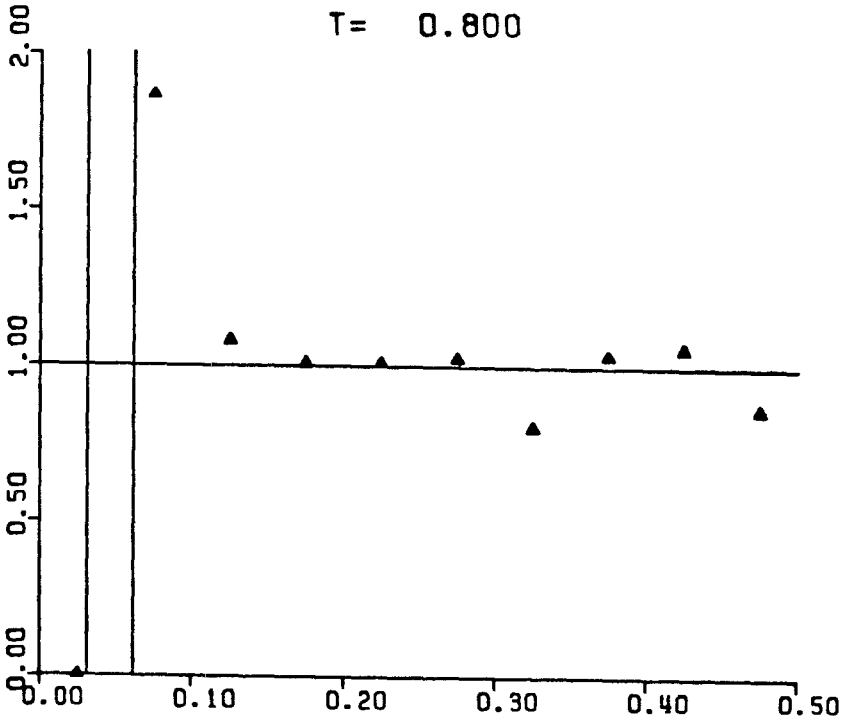
2.00
1.50
1.00
0.50
0.00
0.00
0.10
0.20
0.30
0.40
0.50

T= 1.200

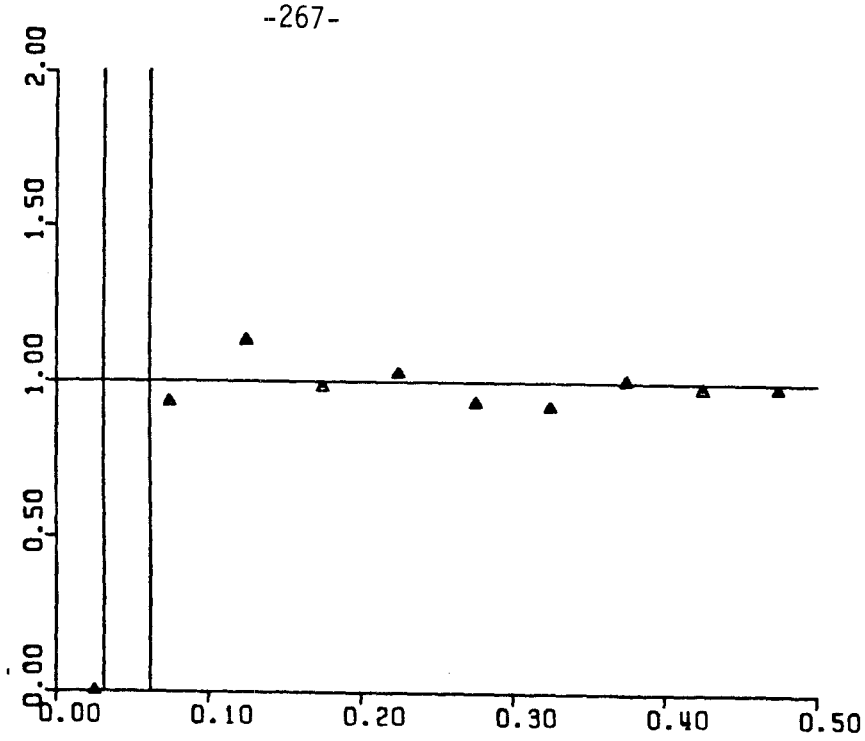
2.00
1.50
1.00
0.50
0.00
0.00
0.10
0.20
0.30
0.40
0.50

T= 1.600

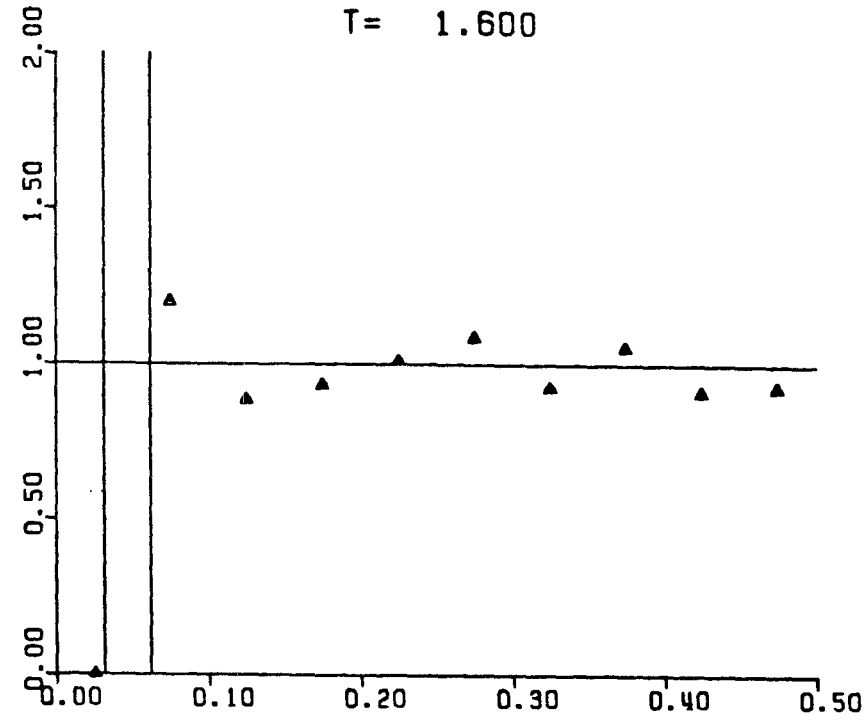
2.00
1.50
1.00
0.50
0.00
0.00
0.10
0.20
0.30
0.40
0.50

T= 2.000

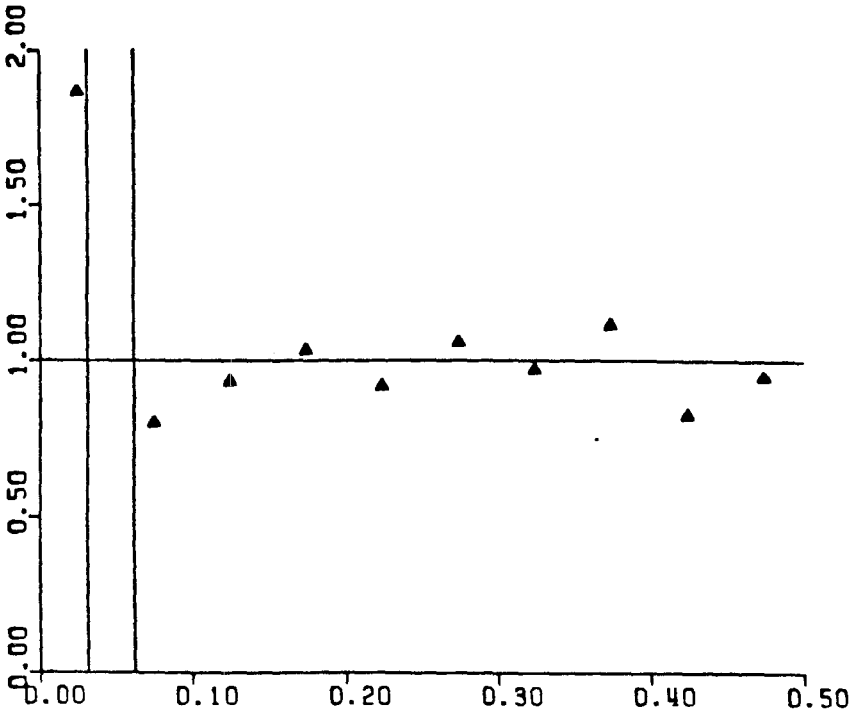
2.00
1.50
1.00
0.50
0.00
0.00
0.10
0.20
0.30
0.40
0.50

T= 2.400

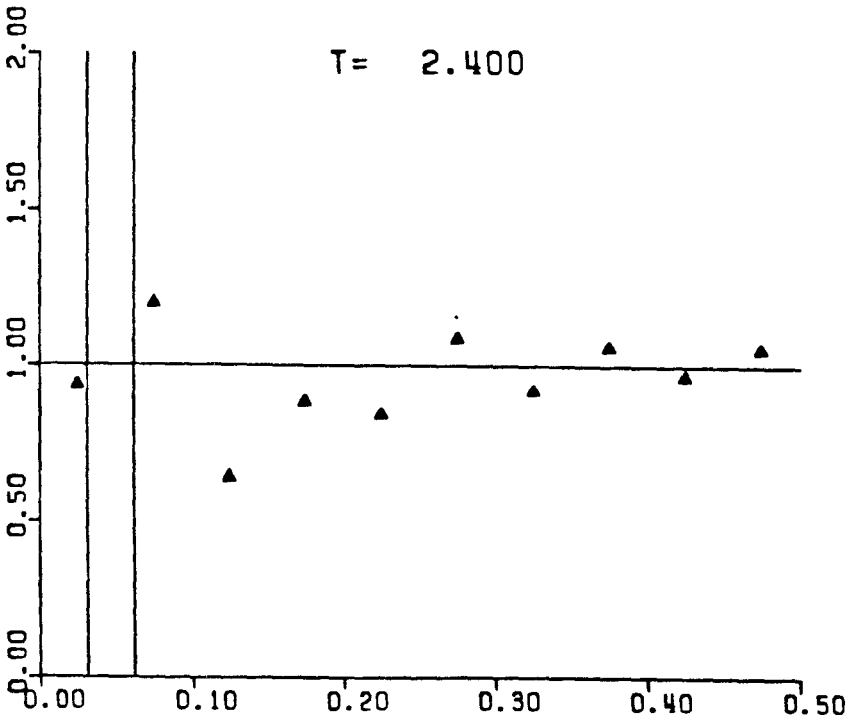
2.00
1.50
1.00
0.50
0.00
0.00
0.10
0.20
0.30
0.40
0.50

T= 2.800

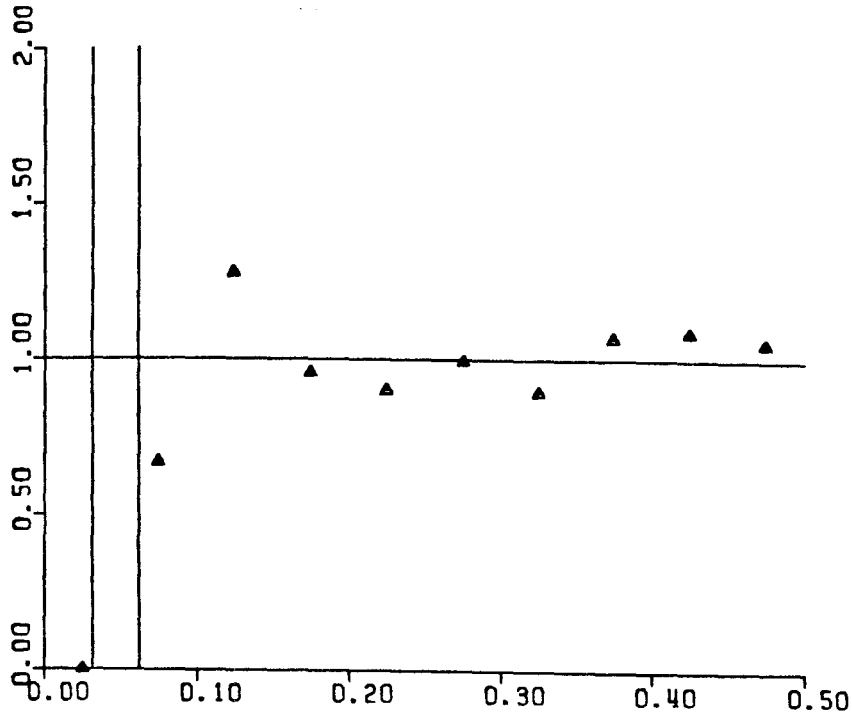
2.00
1.50
1.00
0.50
0.00
0.00
0.10
0.20
0.30
0.40
0.50

T= 3.200

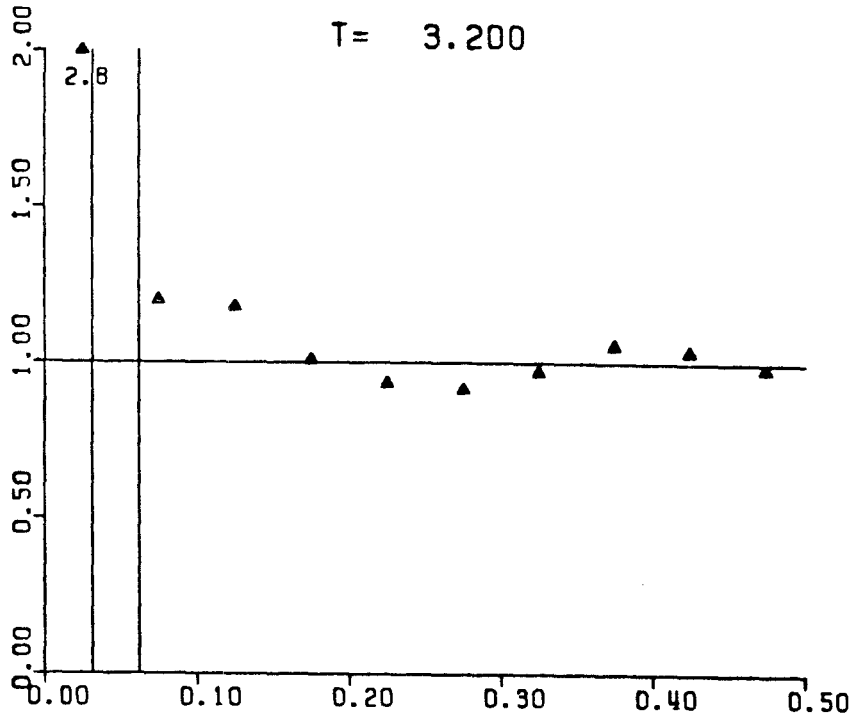
2.8
2.00
1.50
1.00
0.50
0.00
0.00
0.10
0.20
0.30
0.40
0.50

T= 3.600

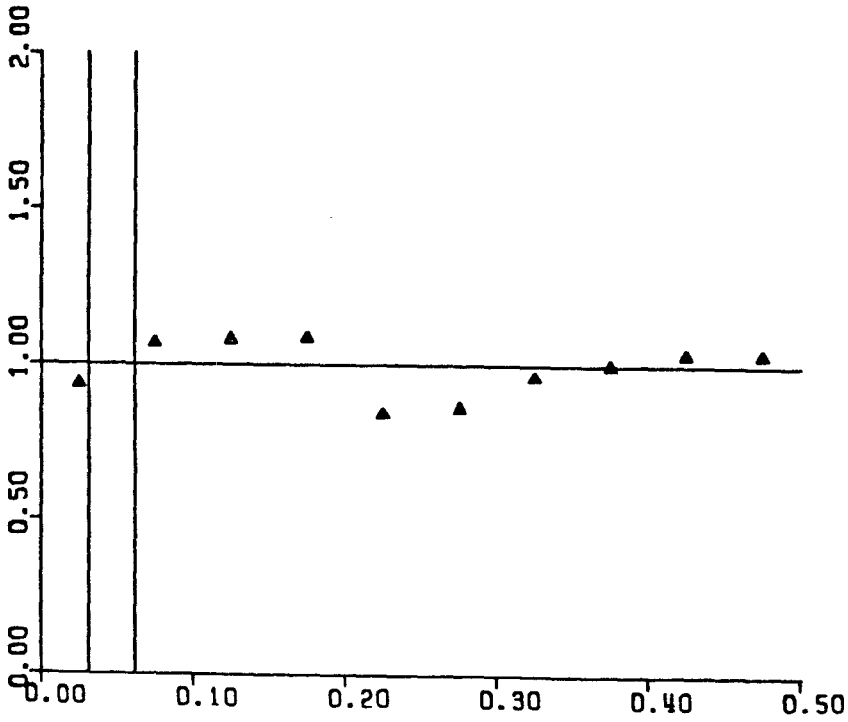
2.00
1.50
1.00
0.50
0.00
0.00
0.10
0.20
0.30
0.40
0.50

T= 4.000

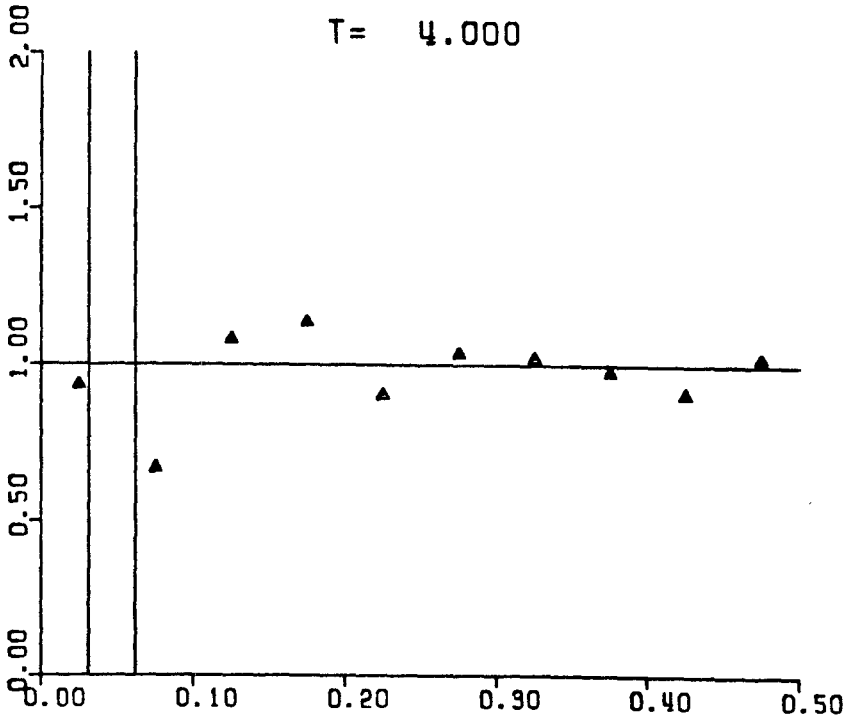
2.00
1.50
1.00
0.50
0.00
0.00
0.10
0.20
0.30
0.40
0.50

T= 4.400

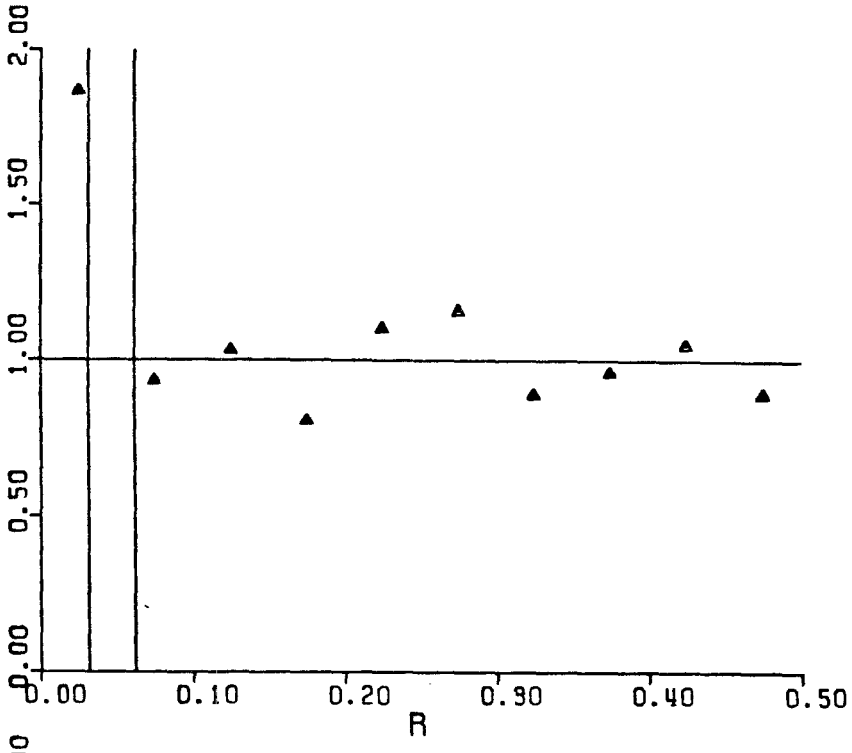
2.00
1.50
1.00
0.50
0.00
0.00
0.10
0.20
0.30
0.40
0.50
R

T= 4.800

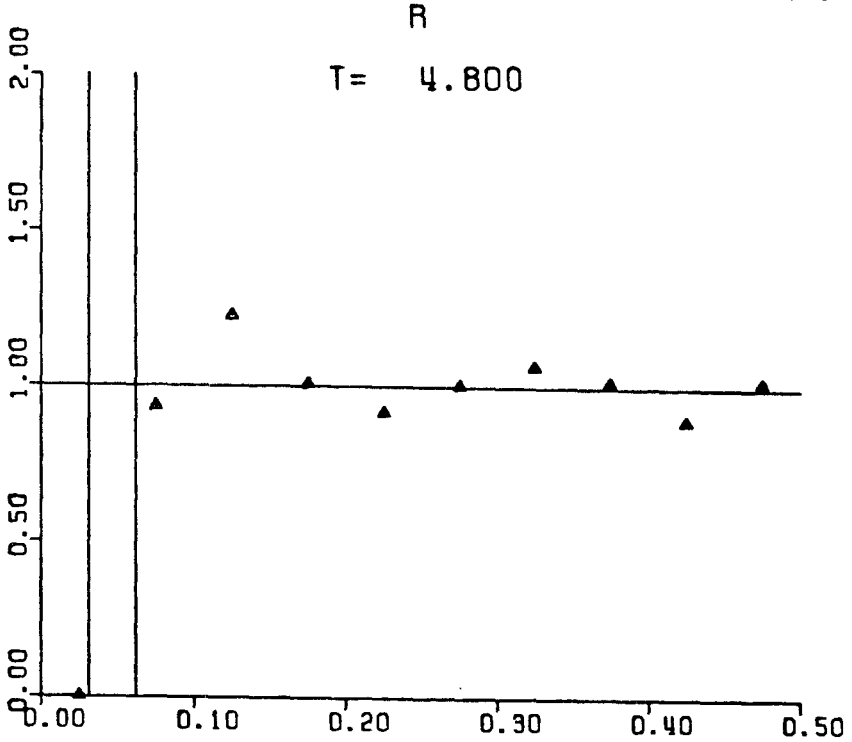
2.00
1.50
1.00
0.50
0.00
0.00
0.10
0.20
0.30
0.40
0.50

T= 5.200

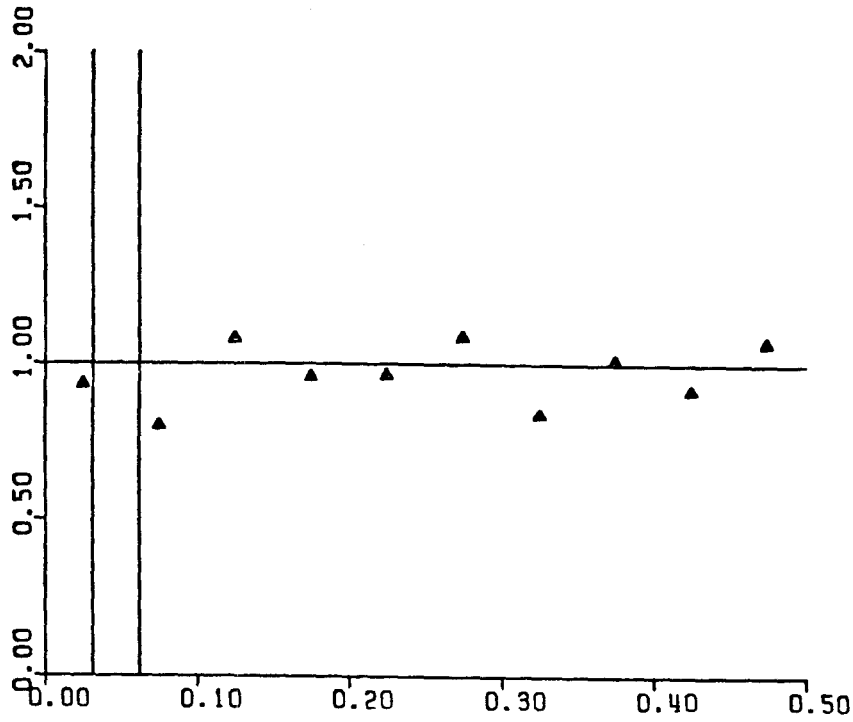
2.00
1.50
1.00
0.50
0.00
0.00
0.10
0.20
0.30
0.40
0.50

T= 5.600

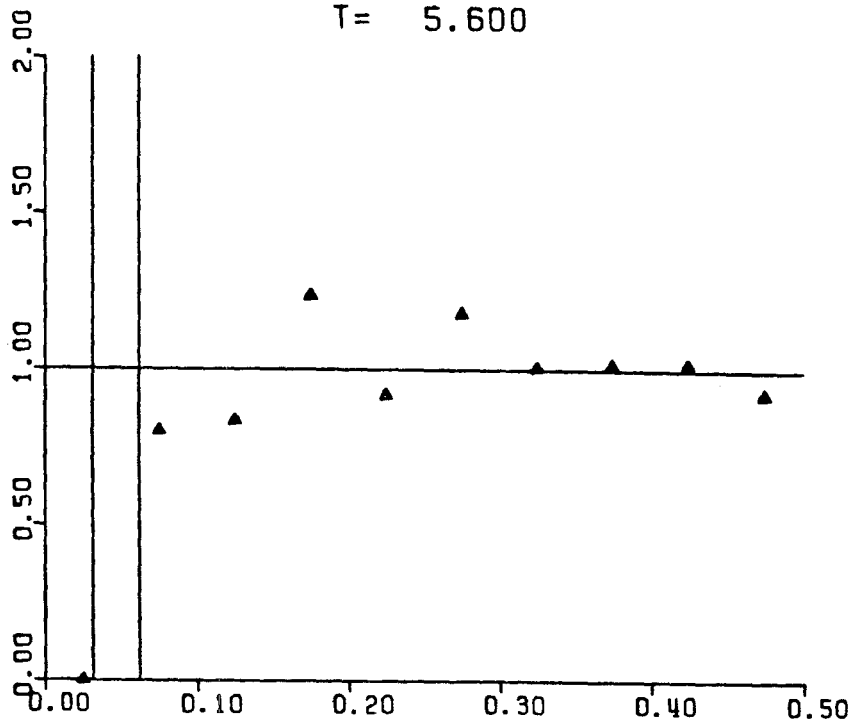
2.00
1.50
1.00
0.50
0.00
0.00
0.10
0.20
0.30
0.40
0.50

T= 6.001

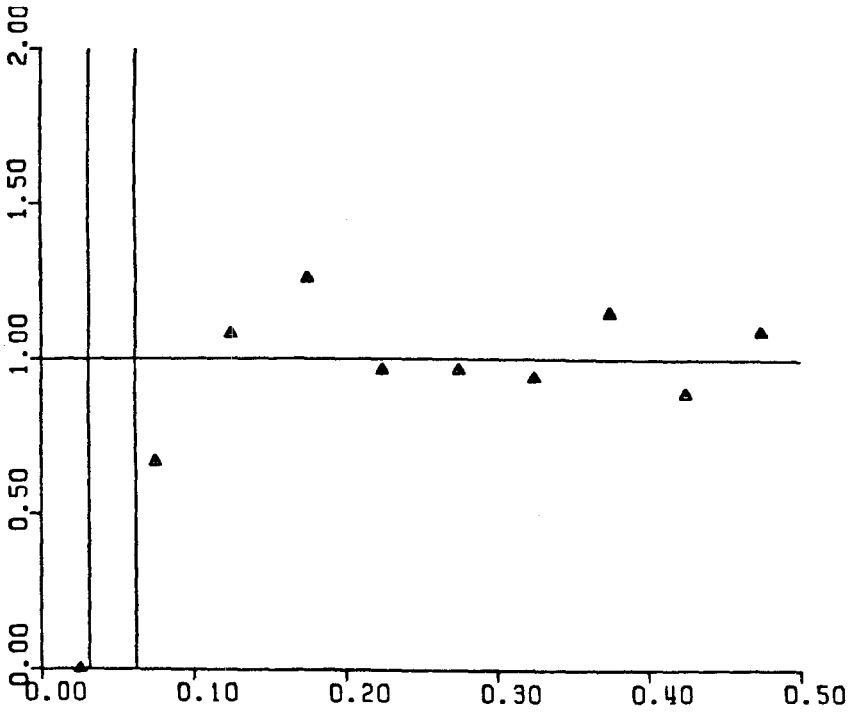
2.00
1.50
1.00
0.50
0.00
0.00
0.10
0.20
0.30
0.40
0.50

T= 6.401

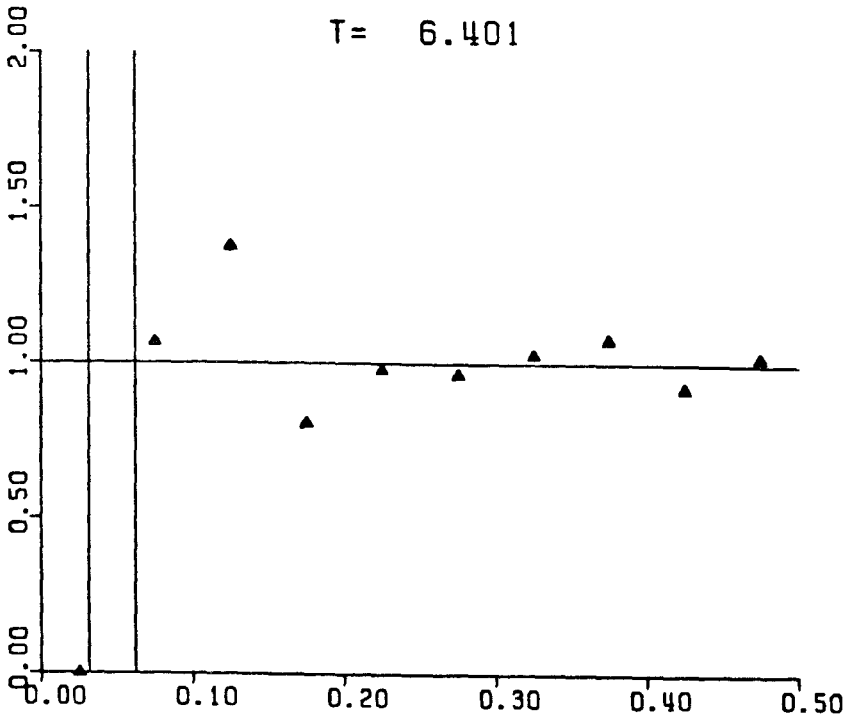
2.00
1.50
1.00
0.50
0.00
0.00
0.10
0.20
0.30
0.40
0.50

T= 6.801

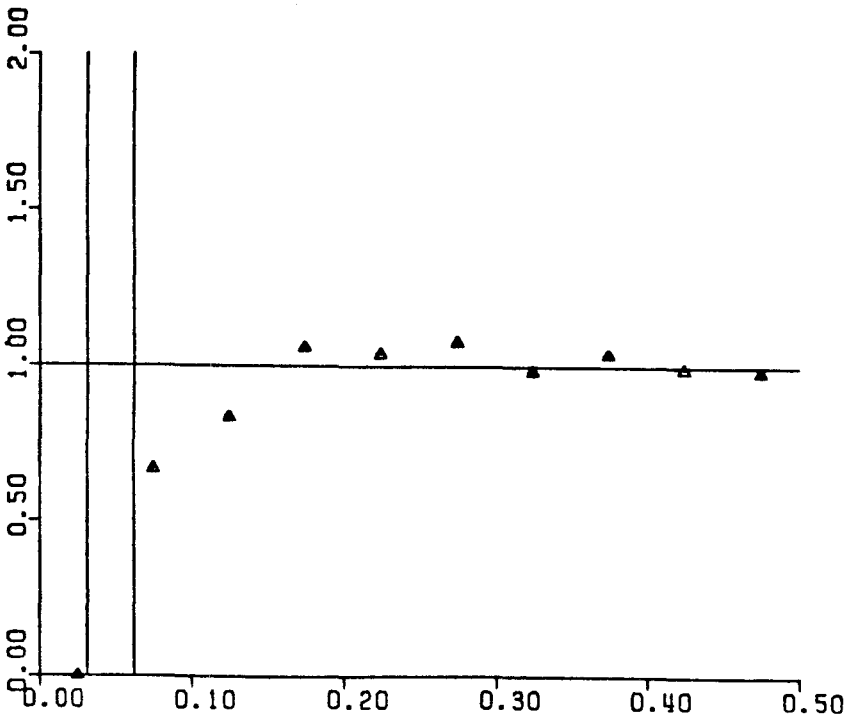
2.00
1.50
1.00
0.50
0.00
0.00
0.10
0.20
0.30
0.40
0.50

T= 7.201

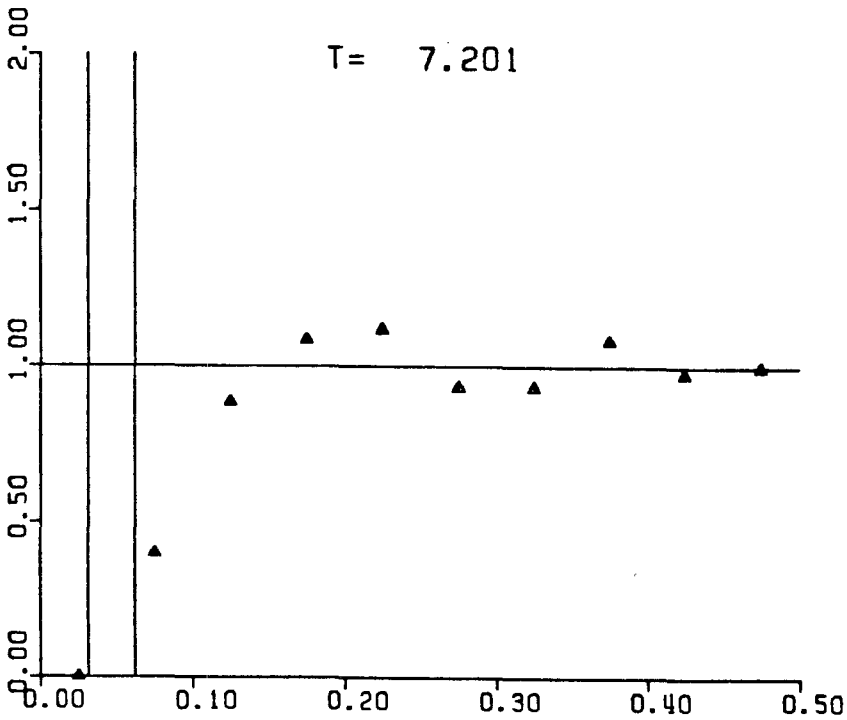
2.00
1.50
1.00
0.50
0.00
0.00
0.10
0.20
0.30
0.40
0.50

T= 7.601

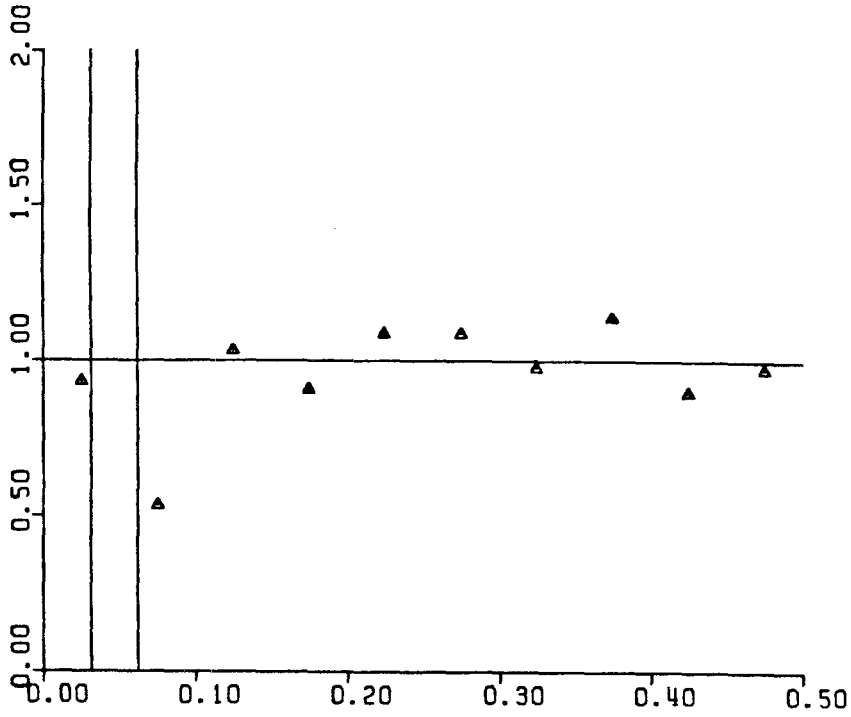
2.00
1.50
1.00
0.50
0.00
0.00
0.10
0.20
0.30
0.40
0.50

T= 8.001

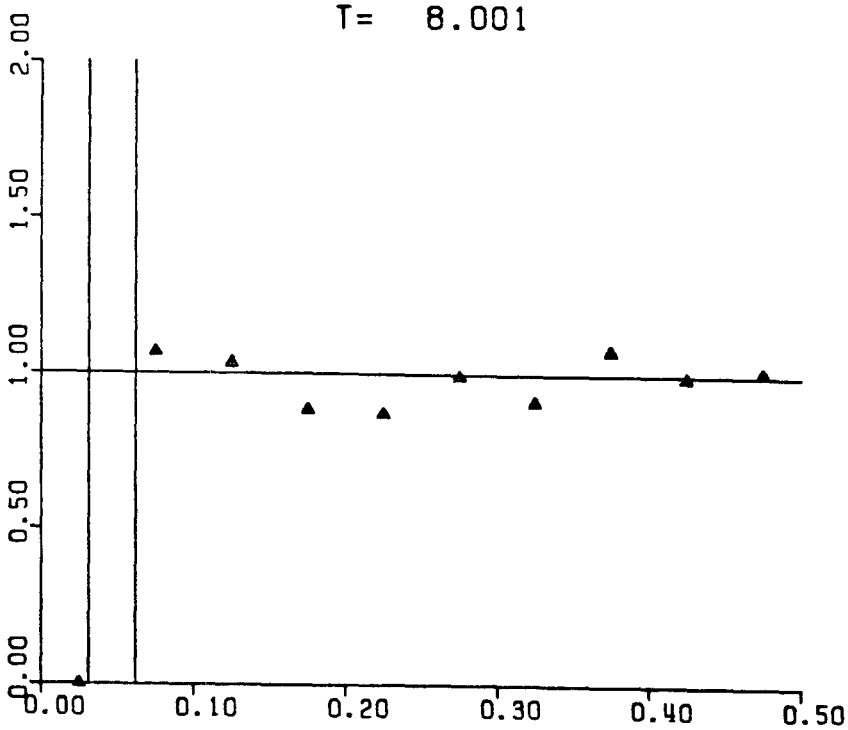
2.00
1.50
1.00
0.50
0.00
0.00
0.10
0.20
0.30
0.40
0.50

T= 8.401

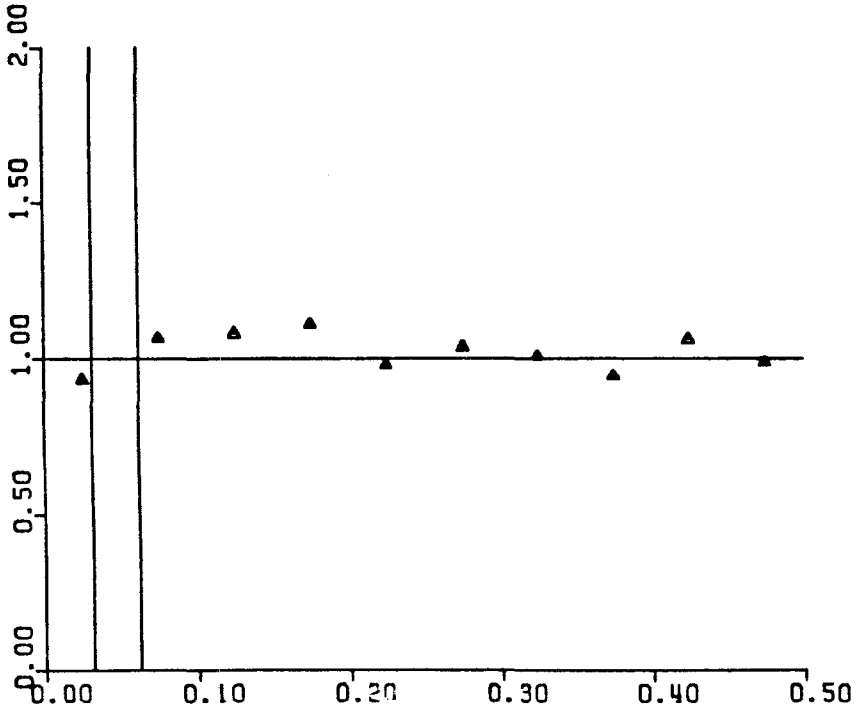
2.00
1.50
1.00
0.50
0.00
0.00
0.10
0.20
0.30
0.40
0.50

T= 8.801

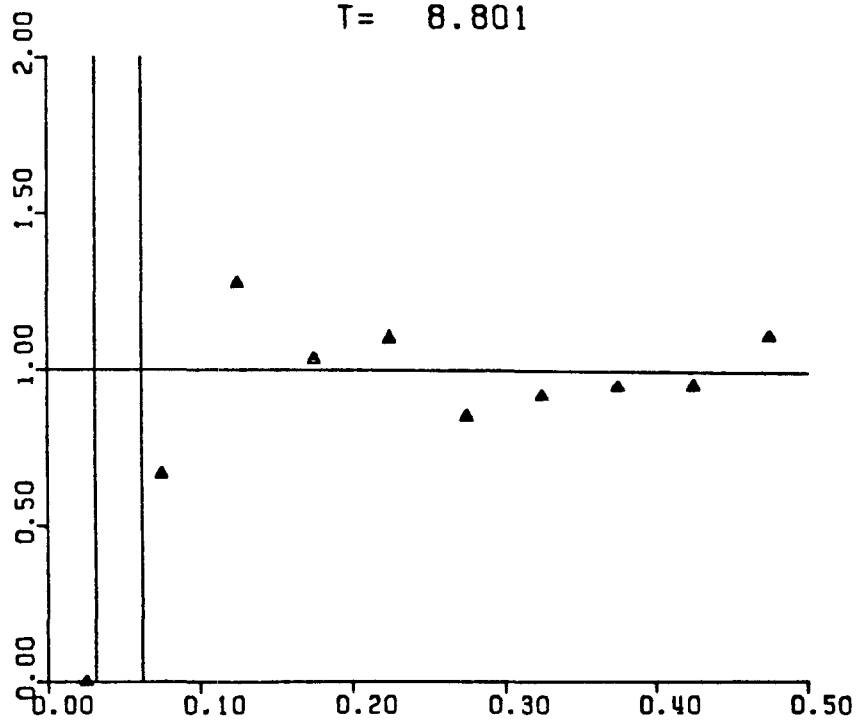
2.00
1.50
1.00
0.50
0.00
0.00
0.10
0.20
0.30
0.40
0.50

T= 9.201

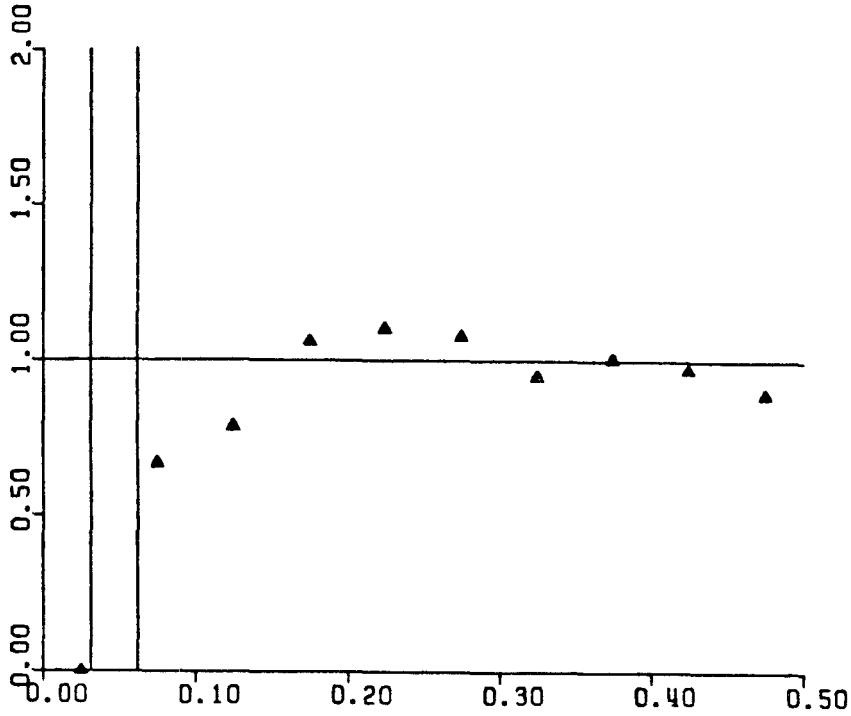


T= 9.601

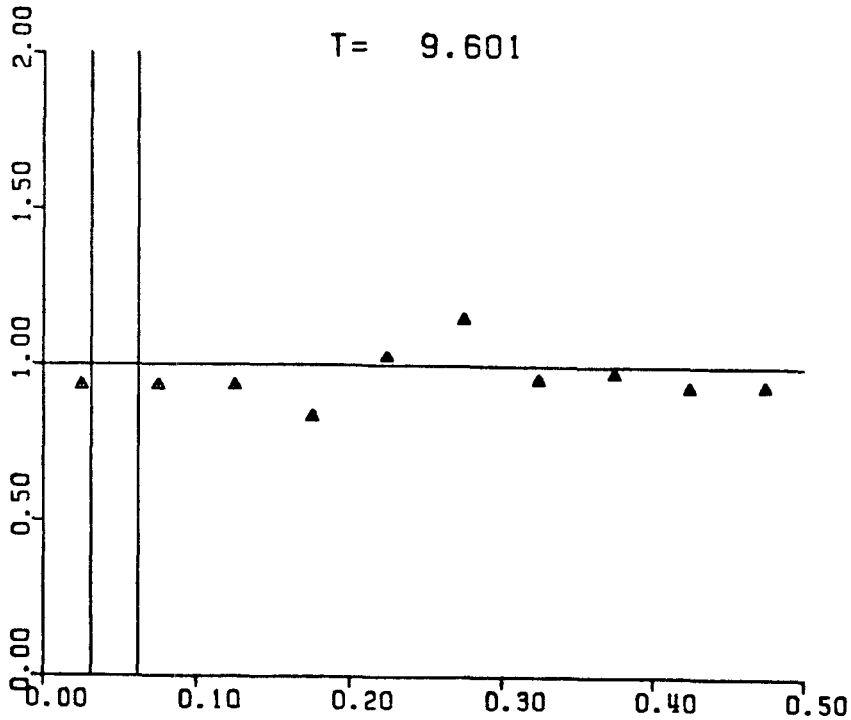


T= 10.000

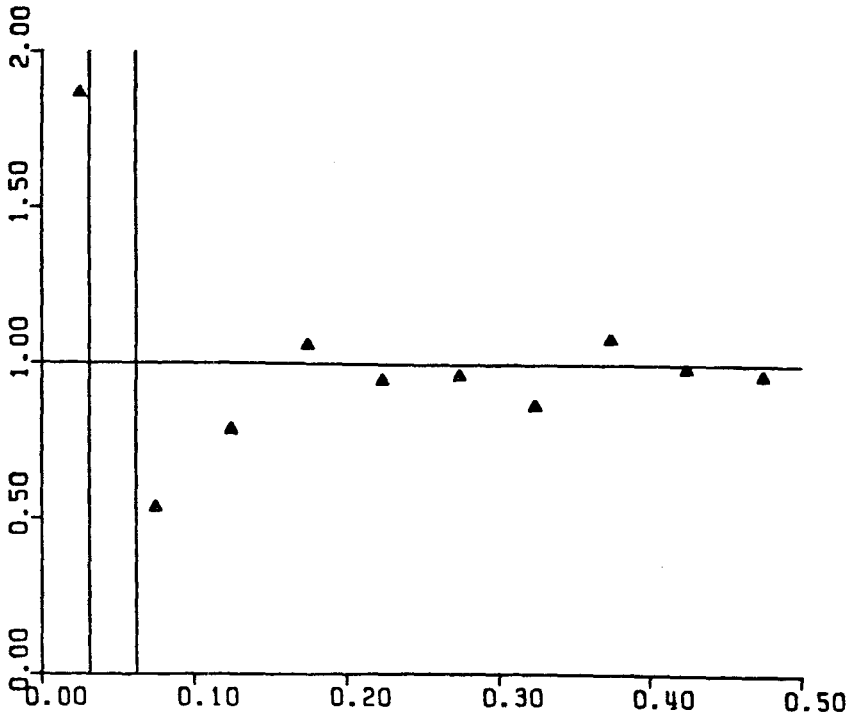


T= 10.400

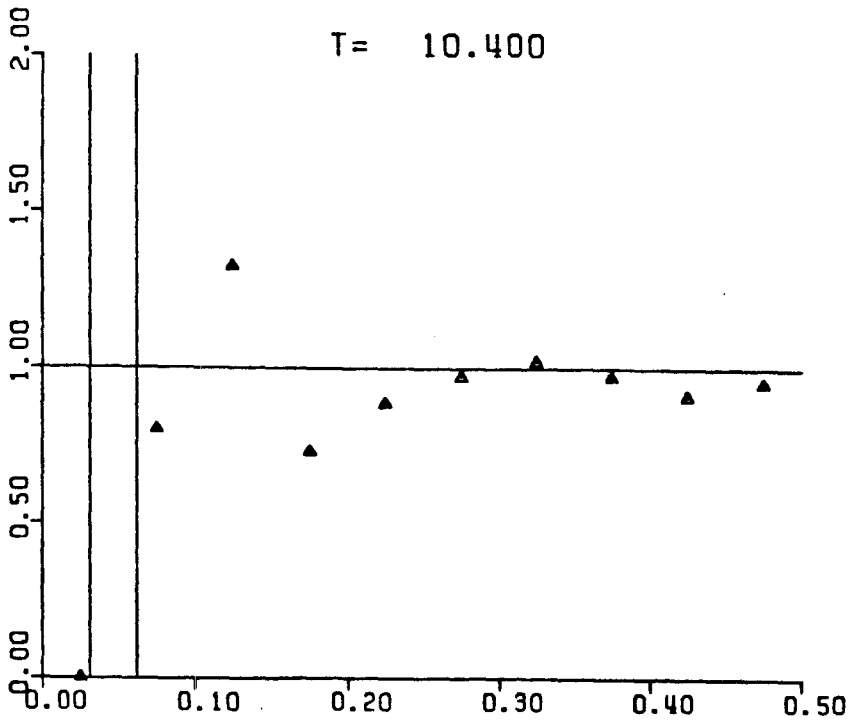


T= 10.800

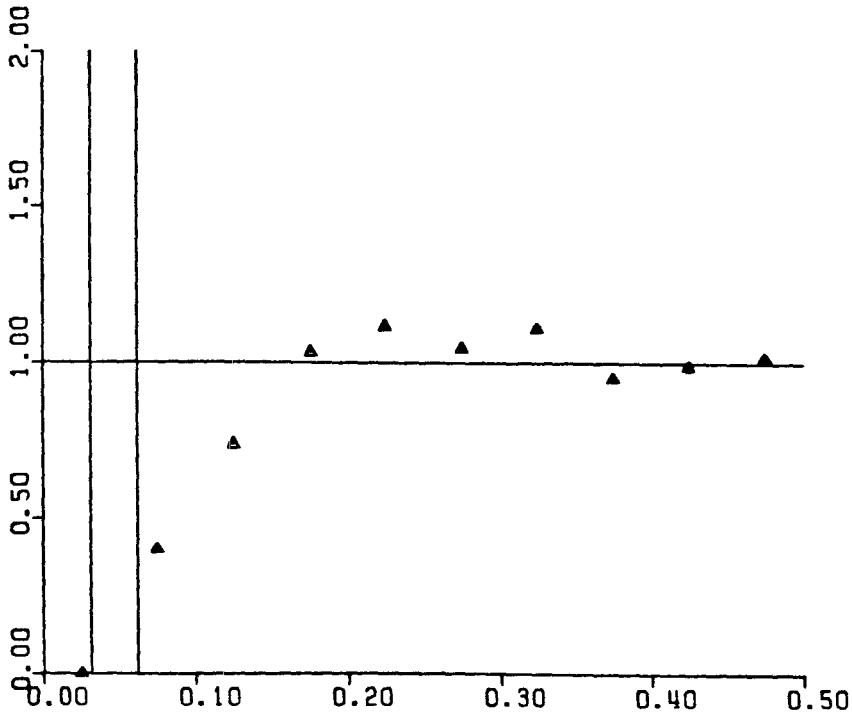


T= 11.200

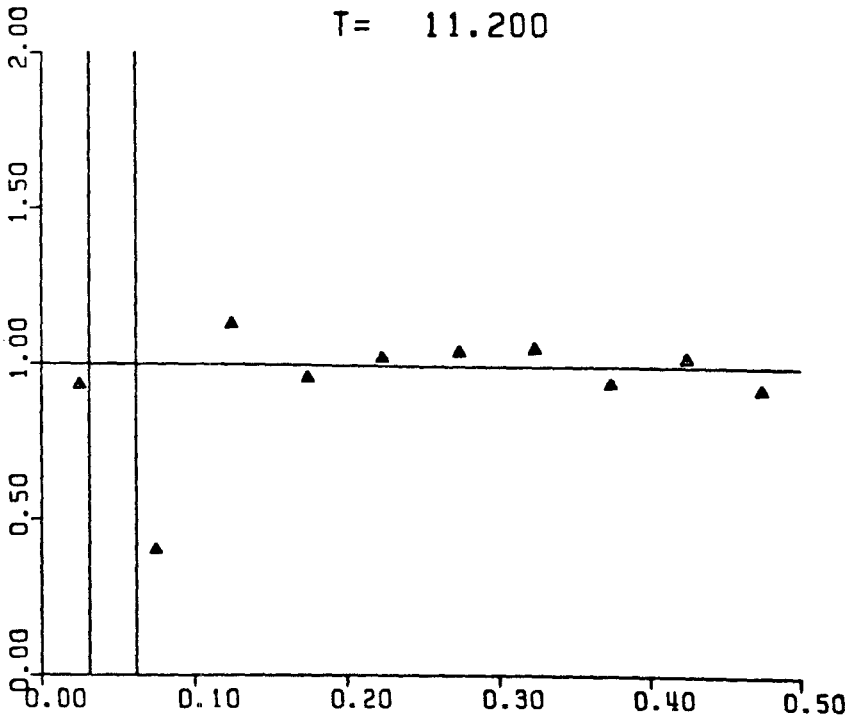


T= 11.599

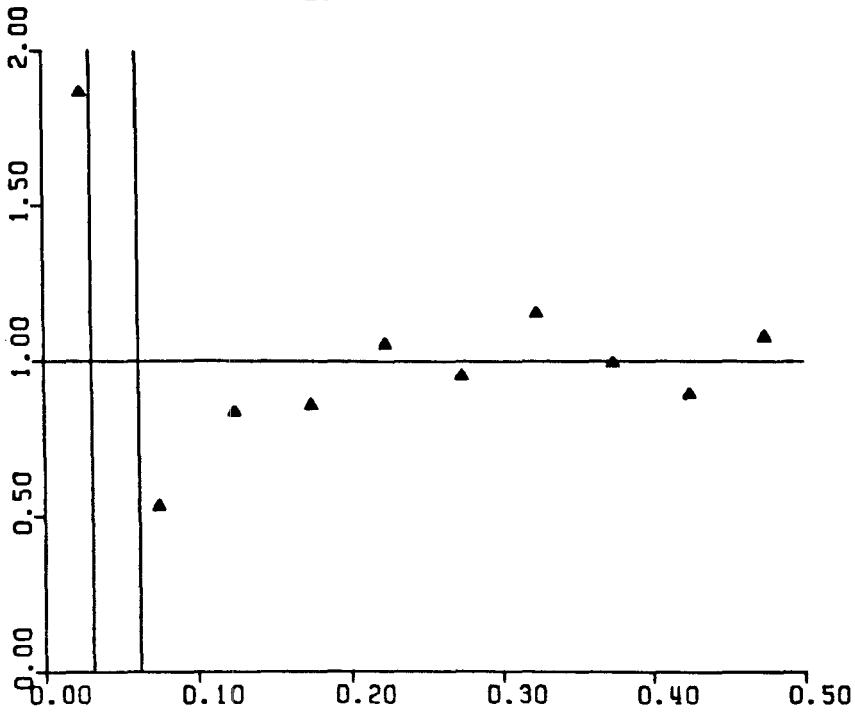


T= 11.999

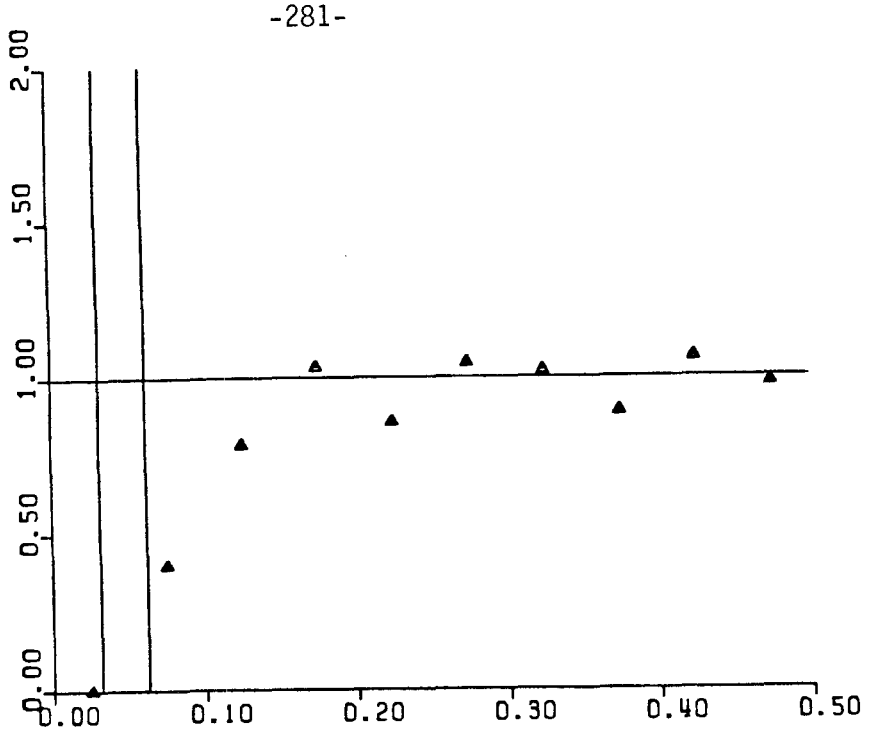


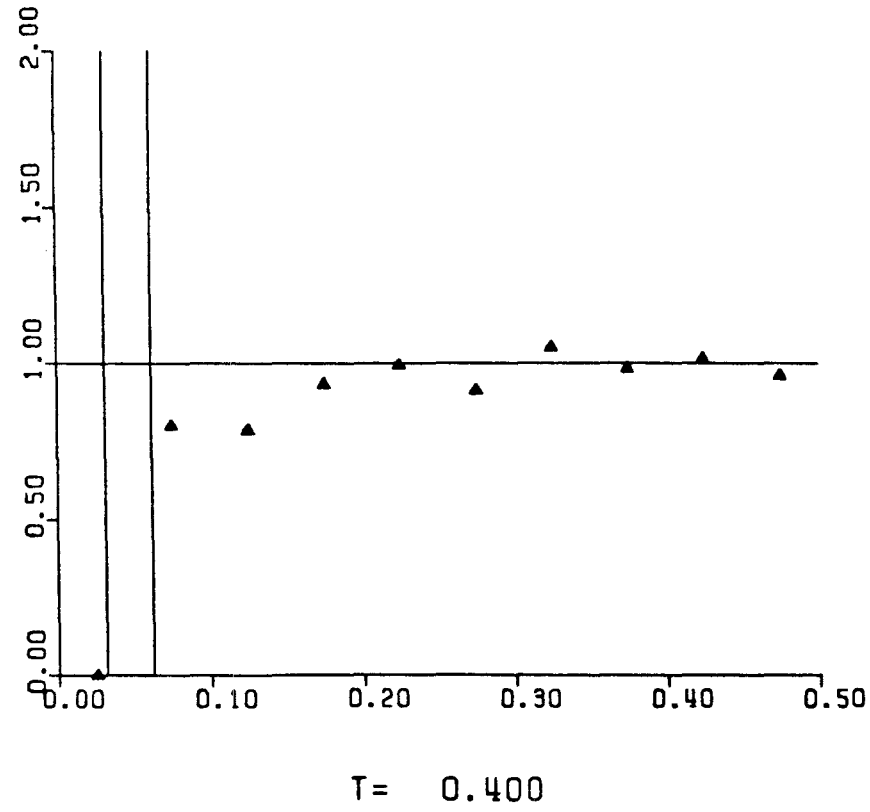


**Figure 37.** Pair-probability function for simulation run 11.

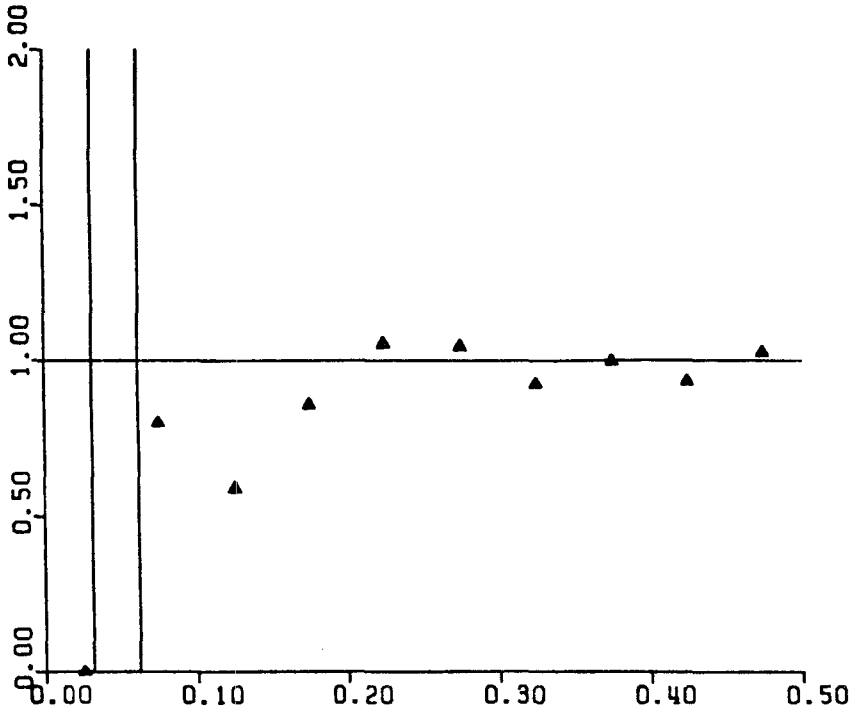
2.00
1.50
1.00
0.50
0.00
0.00
0.10
0.20
0.30
0.40
0.50

T= 0.800

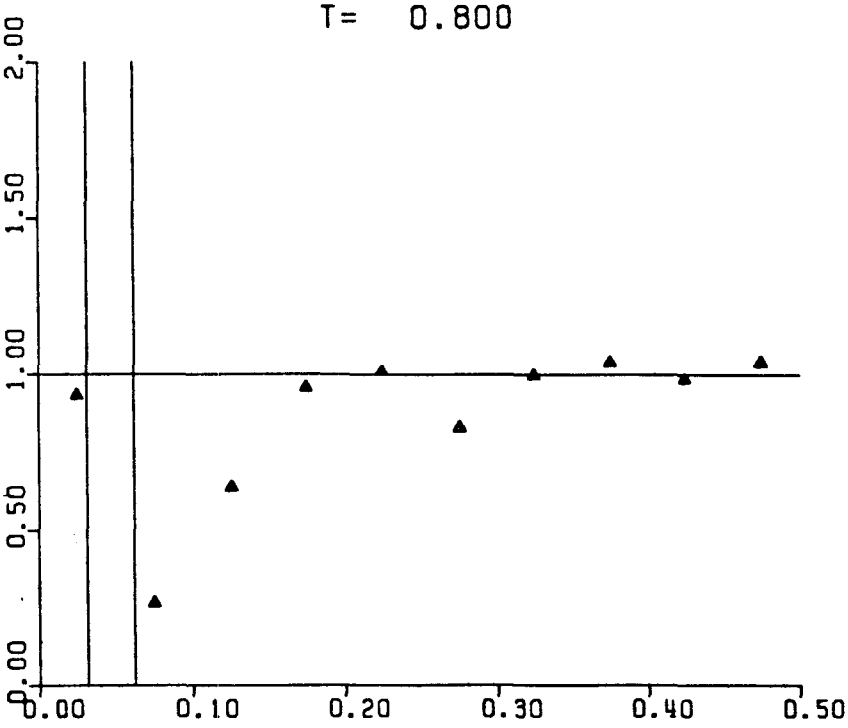
2.00
1.50
1.00
0.50
0.00
0.00
0.10
0.20
0.30
0.40
0.50

T= 1.200

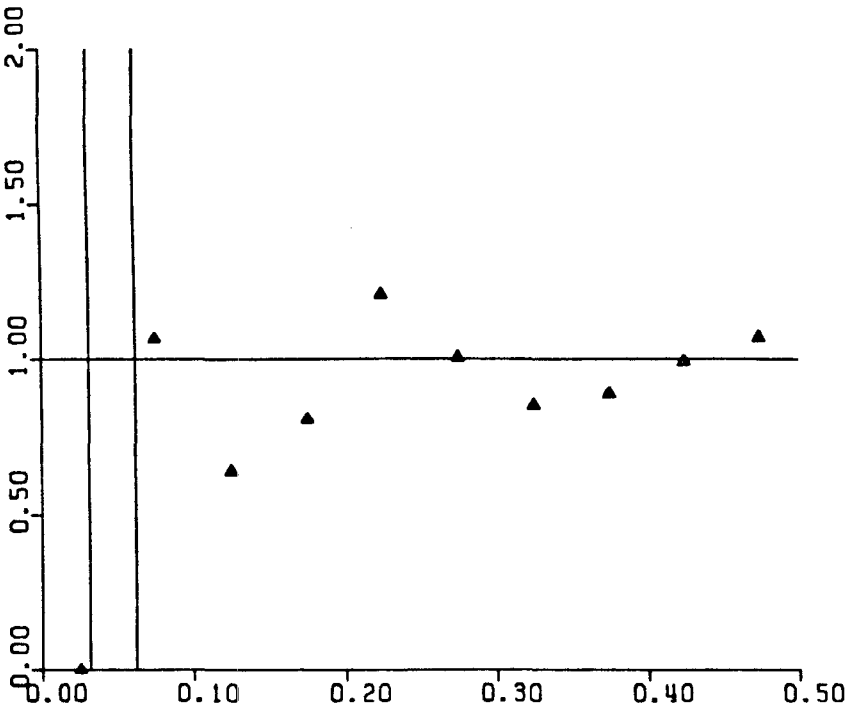
2.00
1.50
1.00
0.50
0.00
0.00
0.10
0.20
0.30
0.40
0.50

T= 1.600

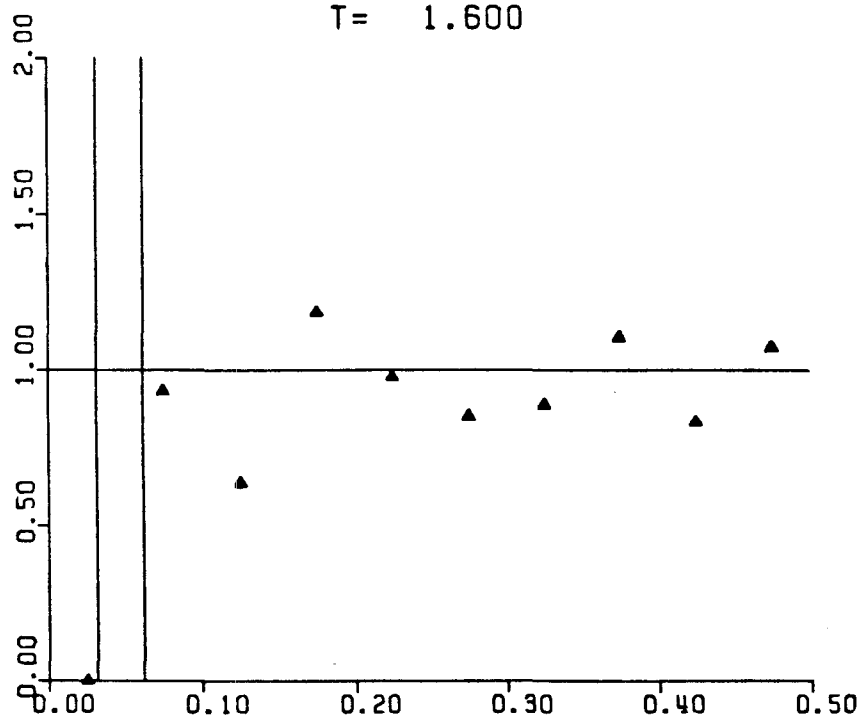
2.00
1.50
1.00
0.50
0.00
0.00
0.10
0.20
0.30
0.40
0.50

T= 2.000

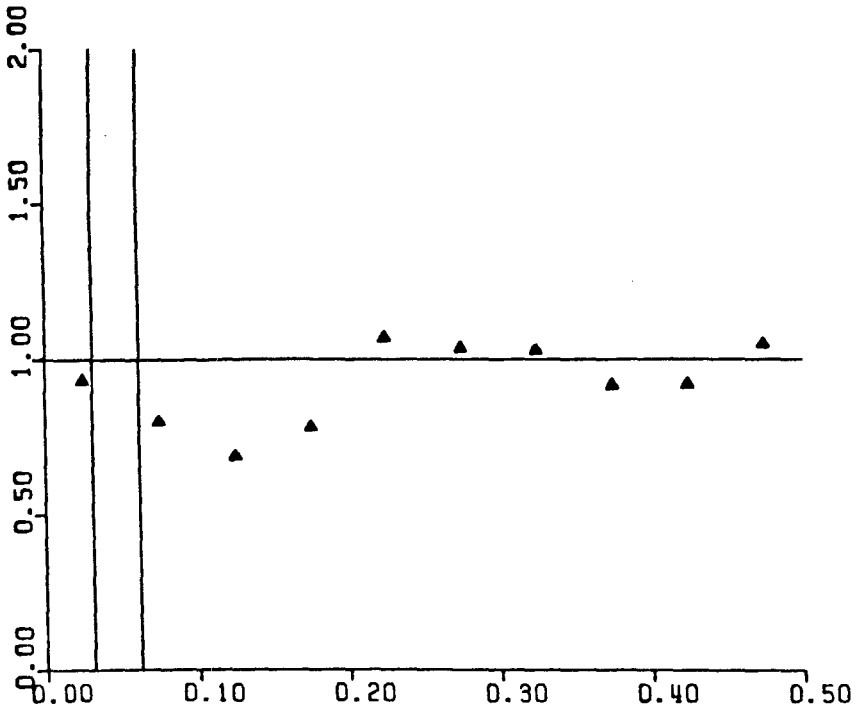
2.00
1.50
1.00
0.50
0.00
0.00
0.10
0.20
0.30
0.40
0.50

T= 2.400

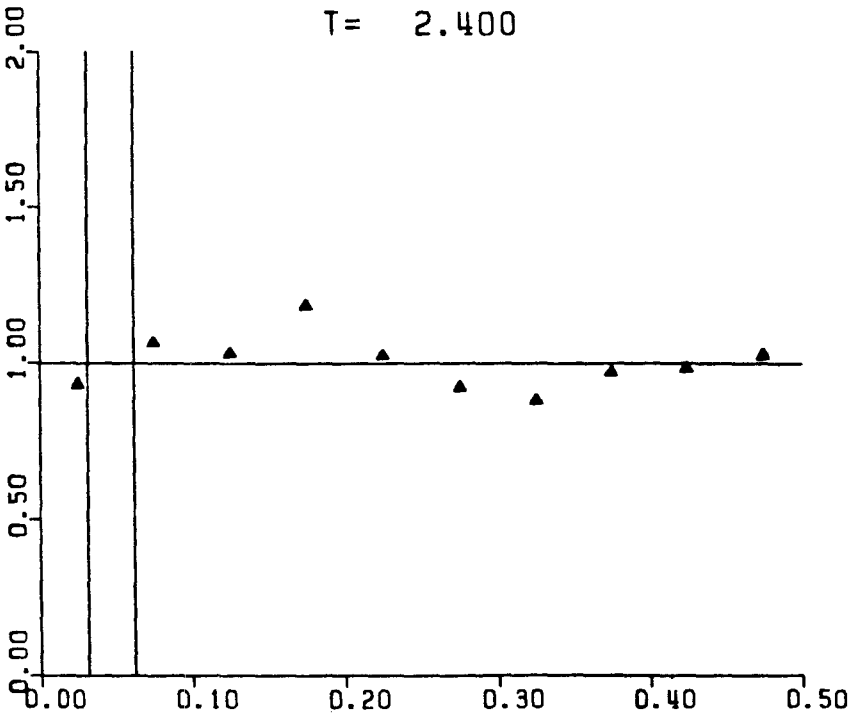
2.00
1.50
1.00
0.50
0.00
0.00
0.10
0.20
0.30
0.40
0.50

T= 2.800

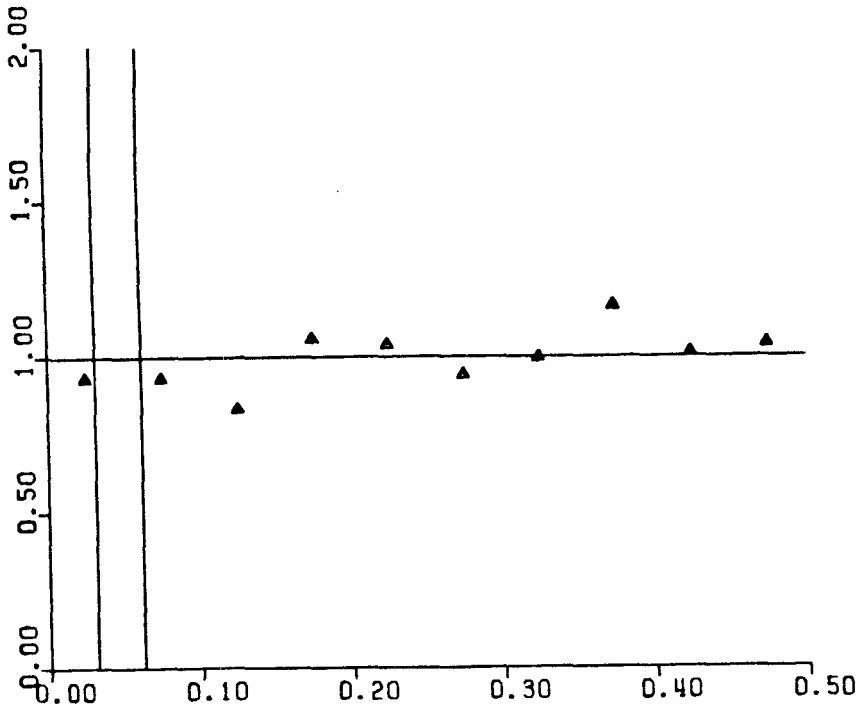
2.00
1.50
1.00
0.50
0.00
0.00
0.10
0.20
0.30
0.40
0.50

T= 3.200

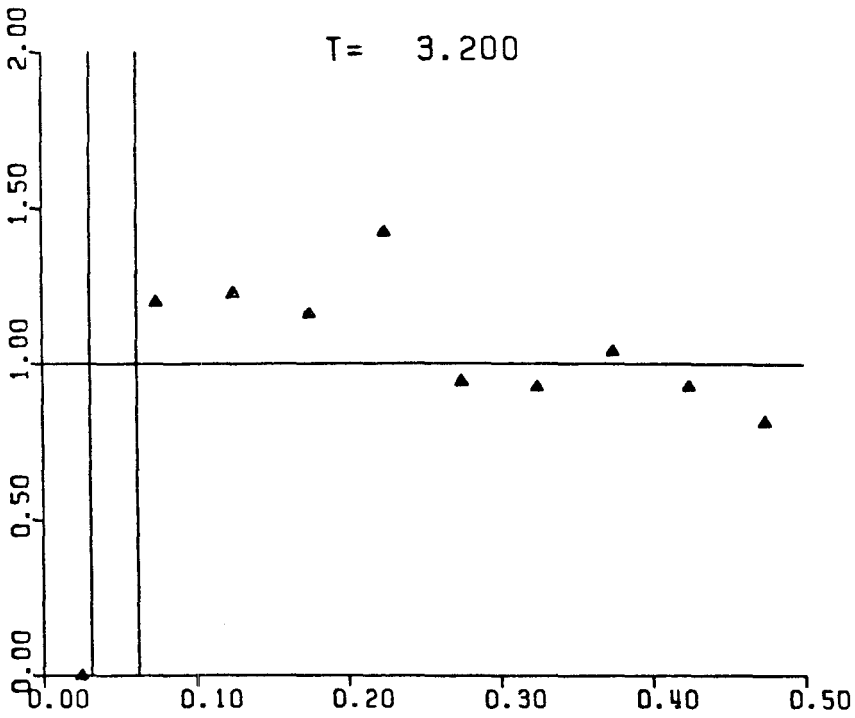
2.00
1.50
1.00
0.50
0.00
0.00
0.10
0.20
0.30
0.40
0.50

T= 3.600

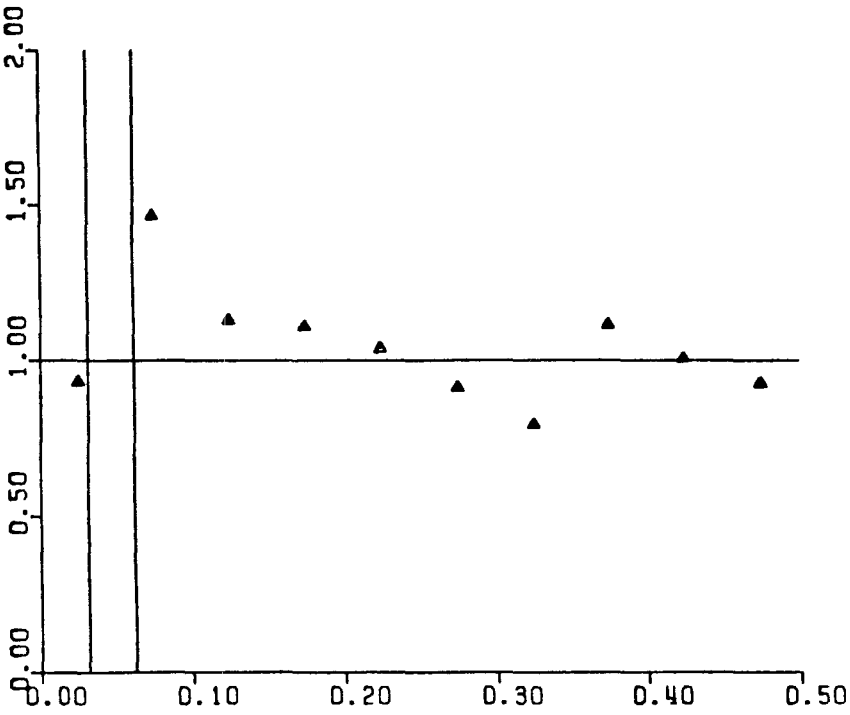
2.00
1.50
1.00
0.50
0.00
0.00
0.10
0.20
0.30
0.40
0.50

T= 4.000

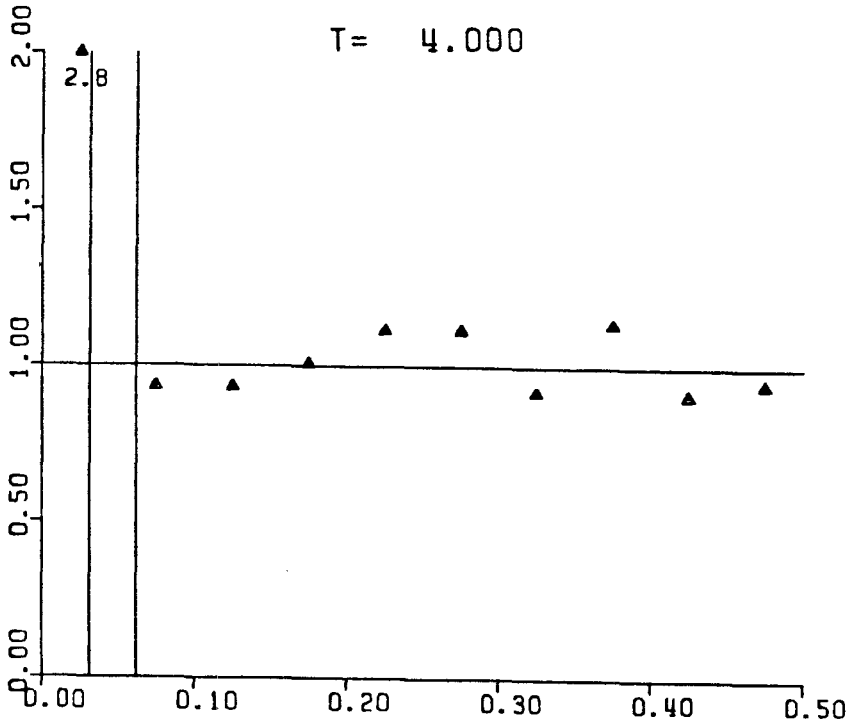
2.00
1.50
1.00
0.50
0.00
2.8
0.00
0.10
0.20
0.30
0.40
0.50

T= 4.400

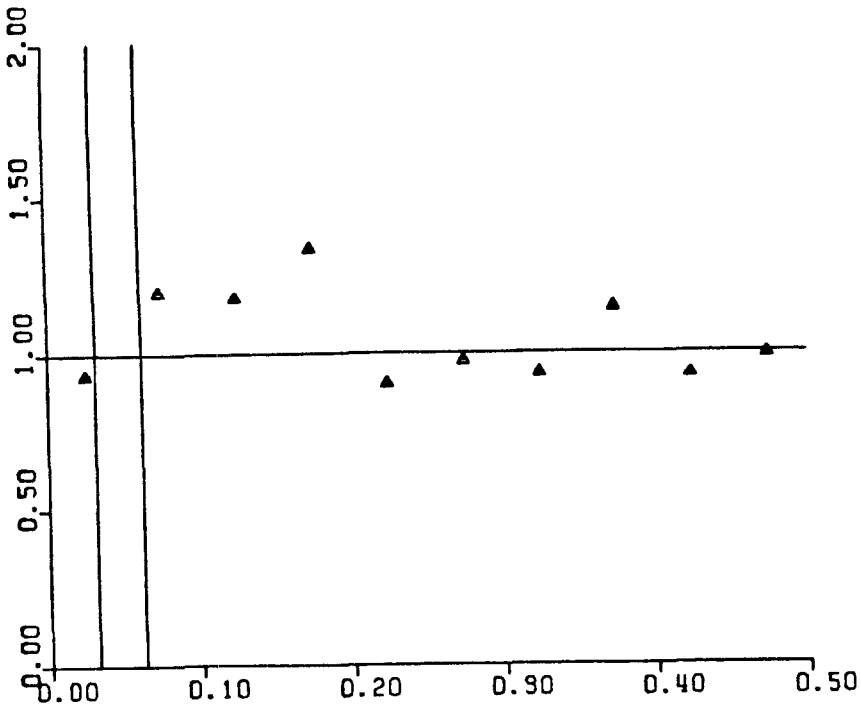
2.00
1.50
1.00
0.50
0.00
0.00
0.10
0.20
0.30
0.40
0.50

T= 4.800

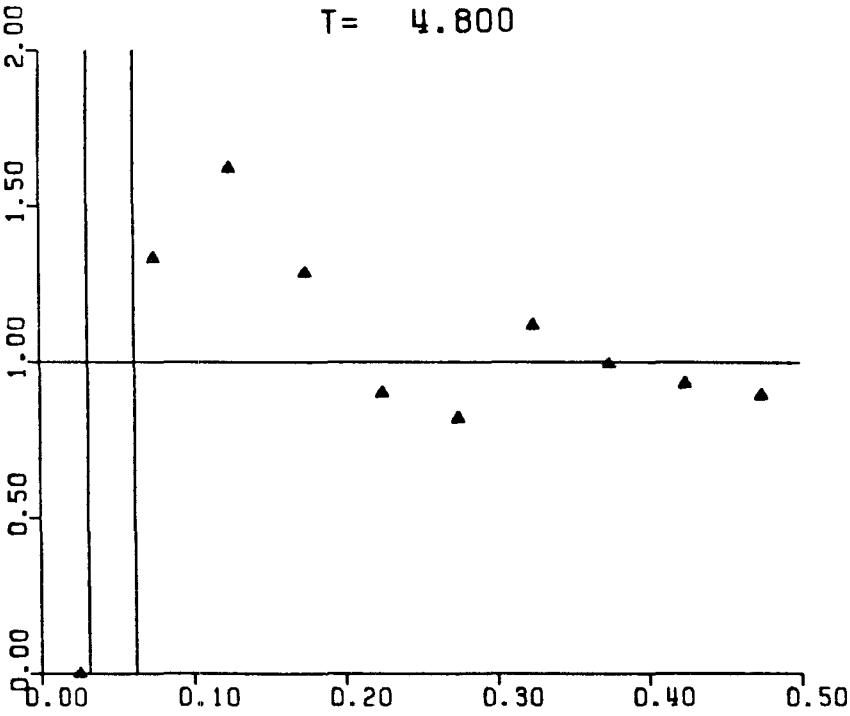
2.00
1.50
1.00
0.50
0.00
0.00
0.10
0.20
0.30
0.40
0.50

T= 5.200

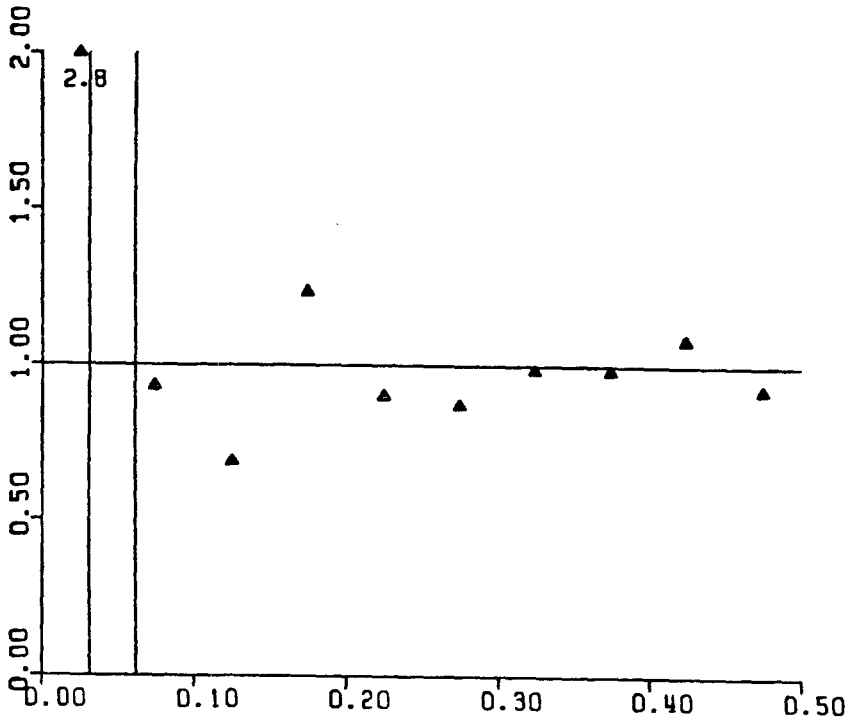
2.00
1.50
1.00
0.50
0.00
2.8
0.00
0.10
0.20
0.30
0.40
0.50

T= 5.600

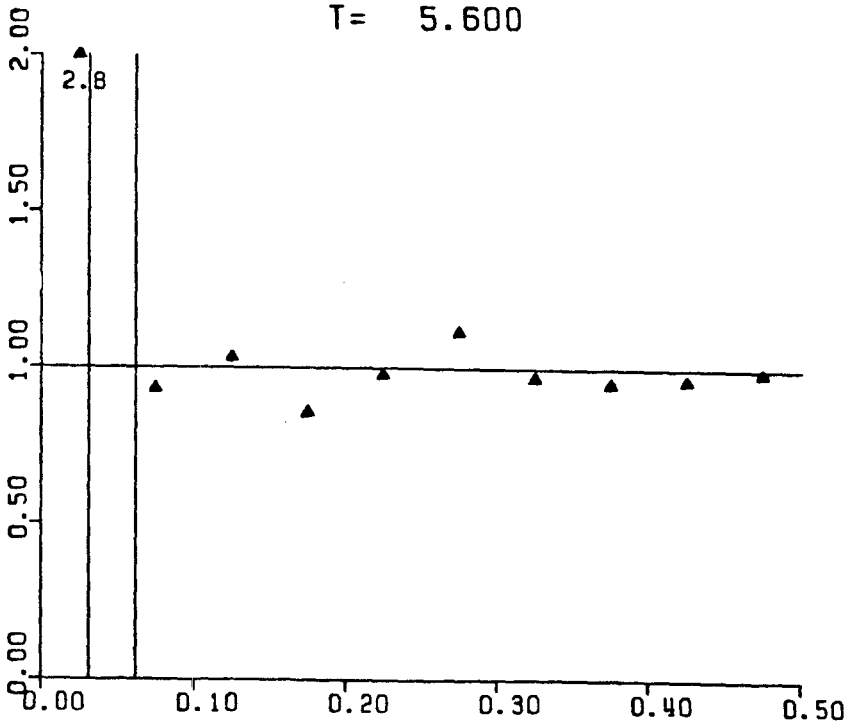
2.00
1.50
1.00
0.50
0.00
2.8
0.00
0.10
0.20
0.30
0.40
0.50

T= 6.001

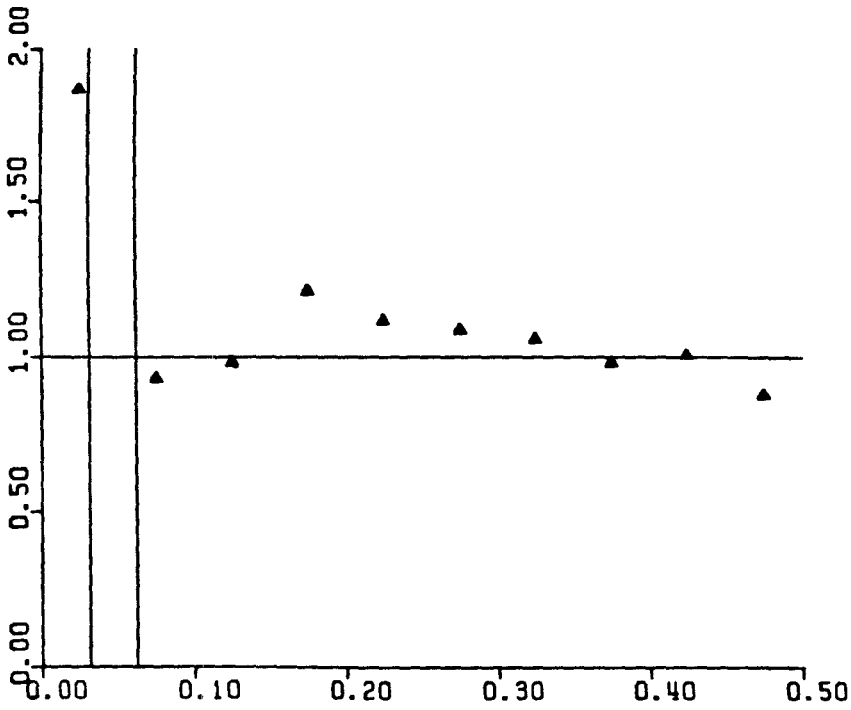
2.00
1.50
1.00
0.50
0.00
0.00
0.10
0.20
0.30
0.40
0.50

T= 6.401

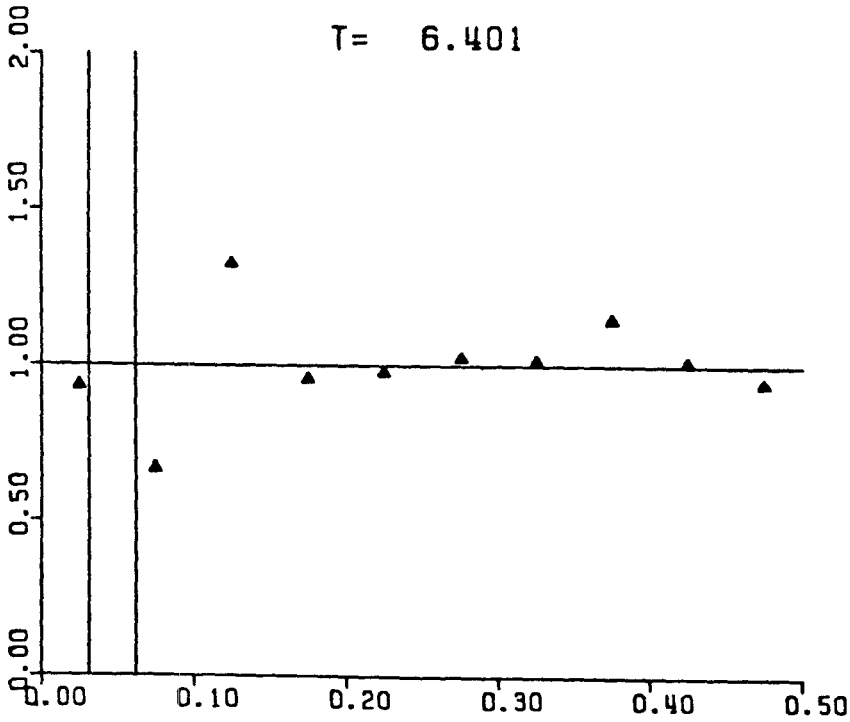
2.00
1.50
1.00
0.50
0.00
0.00
0.10
0.20
0.30
0.40
0.50

T= 6.801

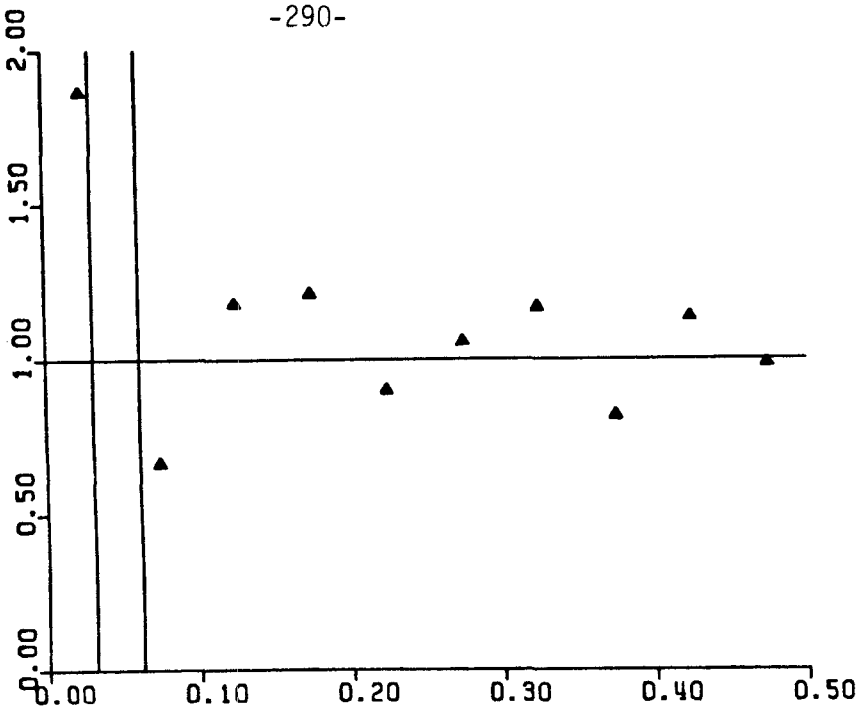
2.00
1.50
1.00
0.50
0.00
0.00
0.10
0.20
0.30
0.40
0.50

T= 7.201

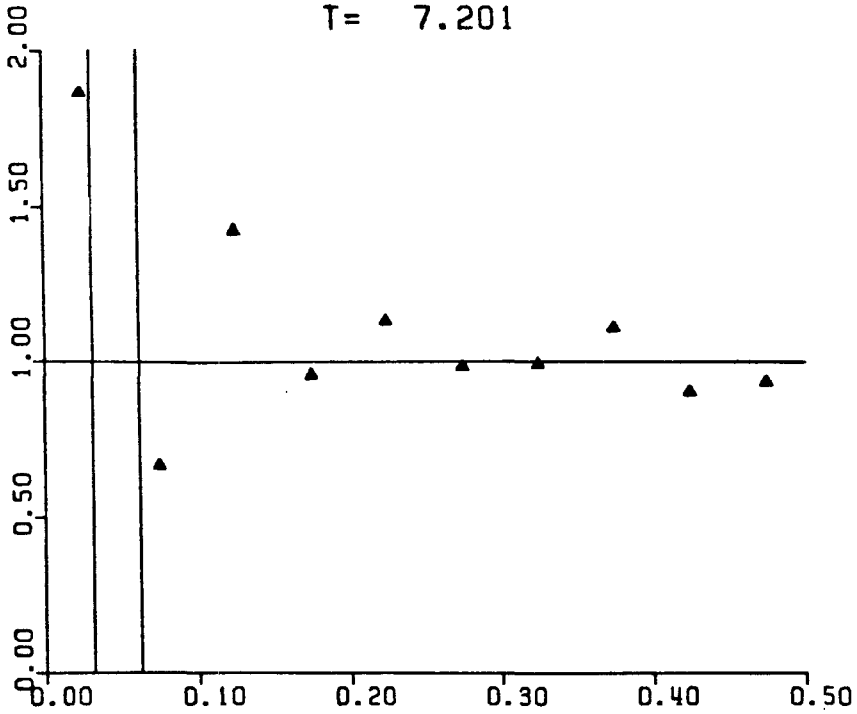
2.00
1.50
1.00
0.50
0.00
0.00
0.10
0.20
0.30
0.40
0.50

T= 7.601

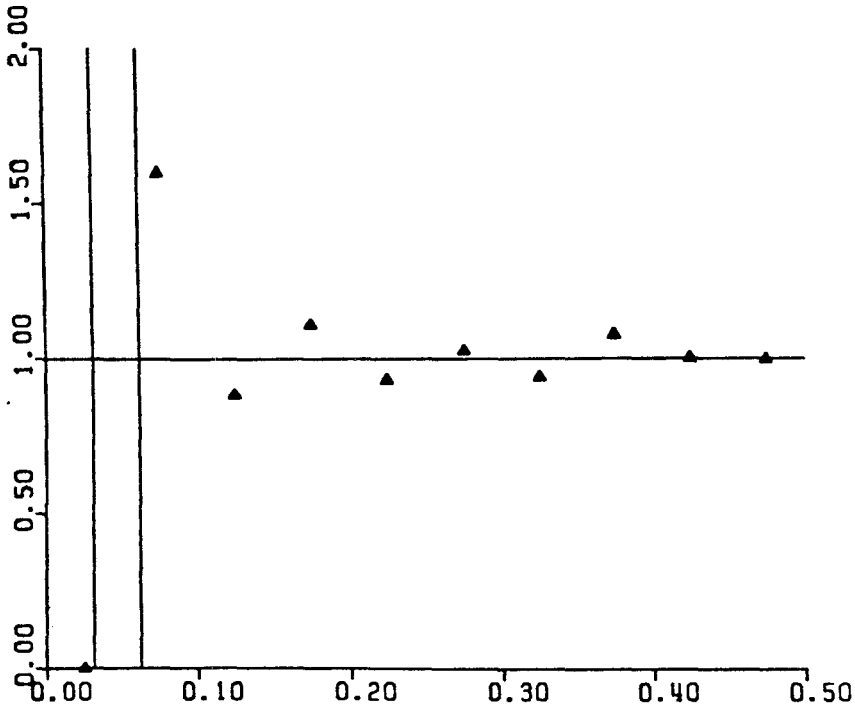


T= 8.001

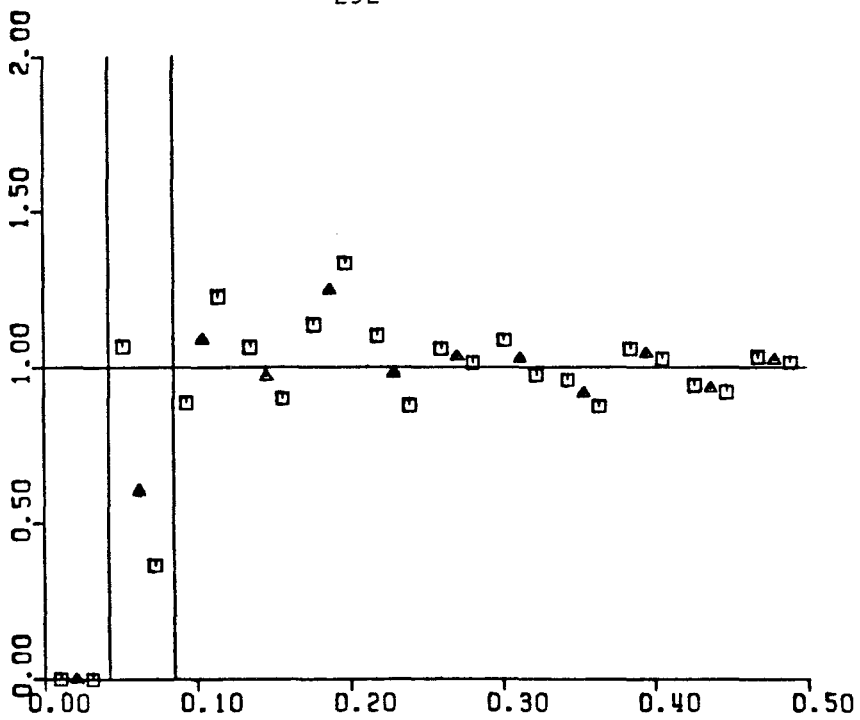


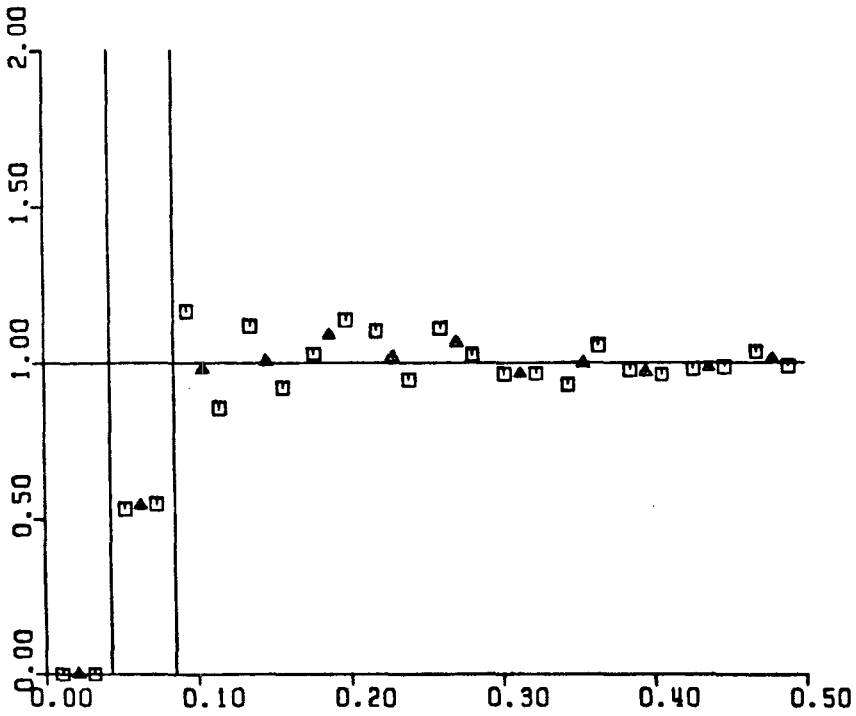


**Figure 38.** Pair-probability function for simulation run 12.

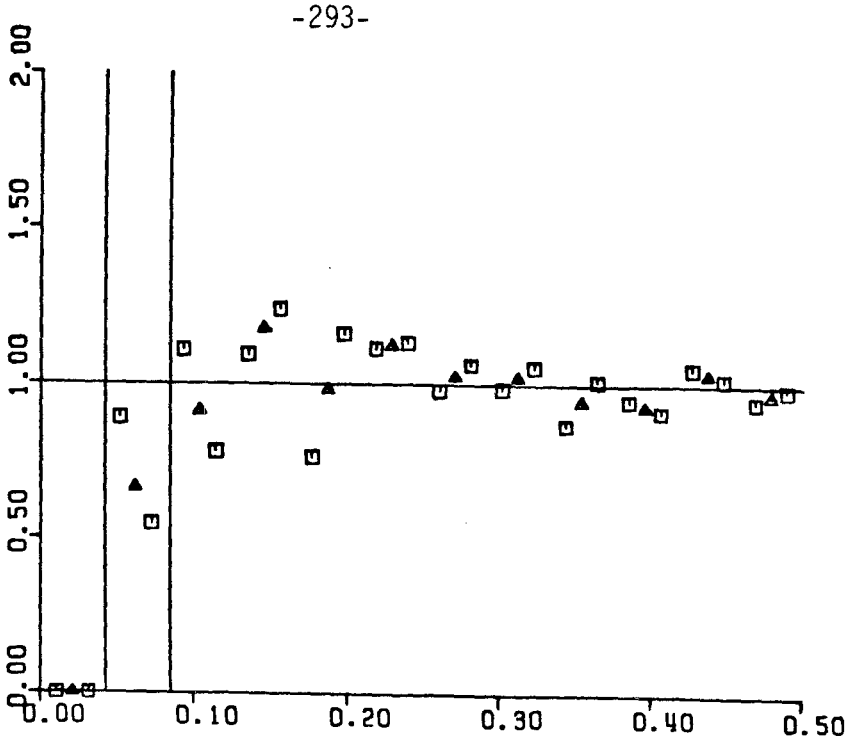
2.00
1.50
1.00
0.50
0.00
0.00
0.10
0.20
0.30
0.40
0.50

T= 0.800

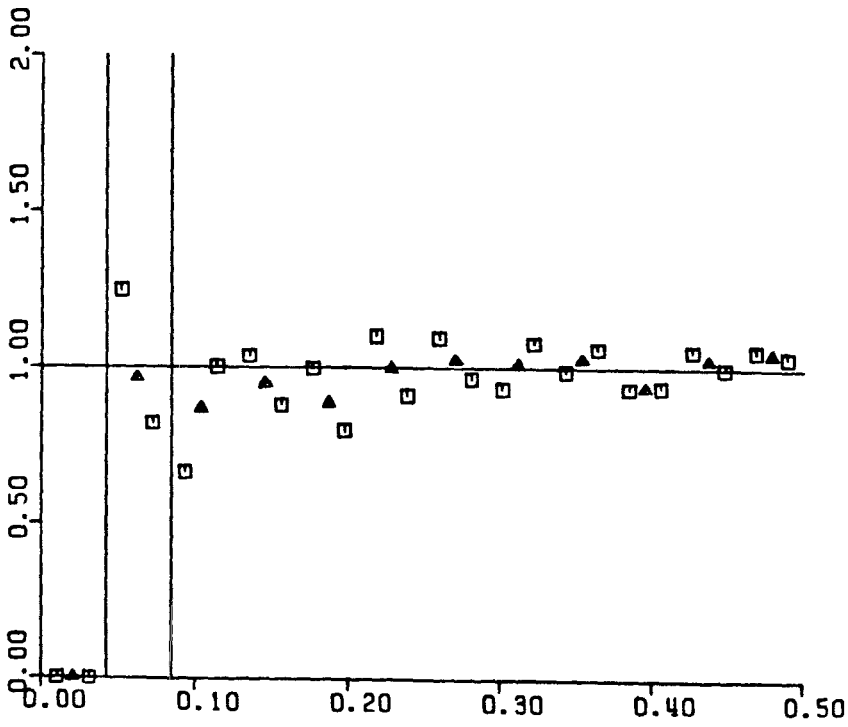
2.00
1.50
1.00
0.50
0.00
0.00
0.10
0.20
0.30
0.40
0.50

T= 1.200

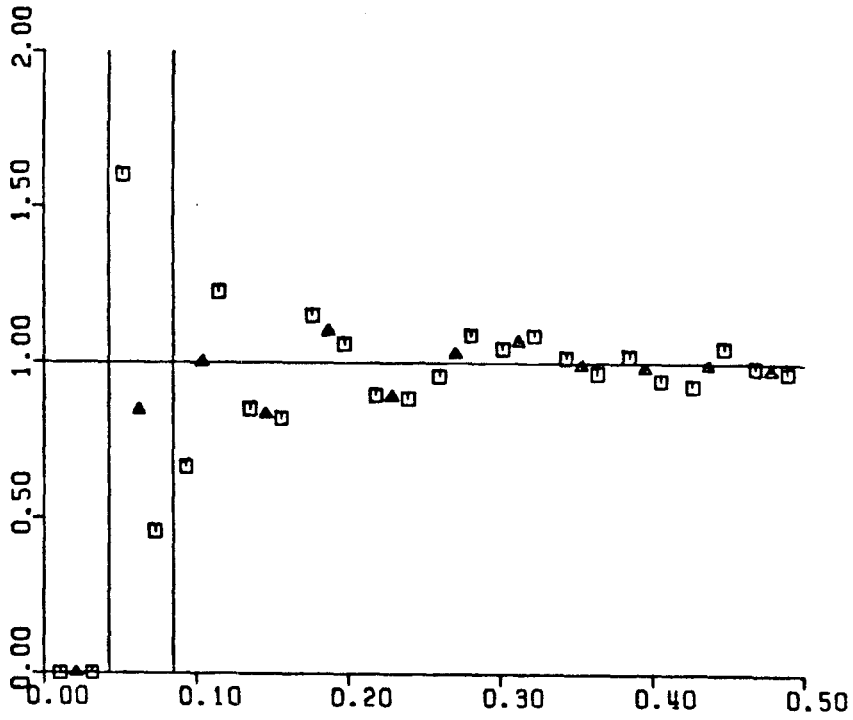
2.00
1.50
1.00
0.50
0.00
0.00
0.10
0.20
0.30
0.40
0.50

T= 1.600

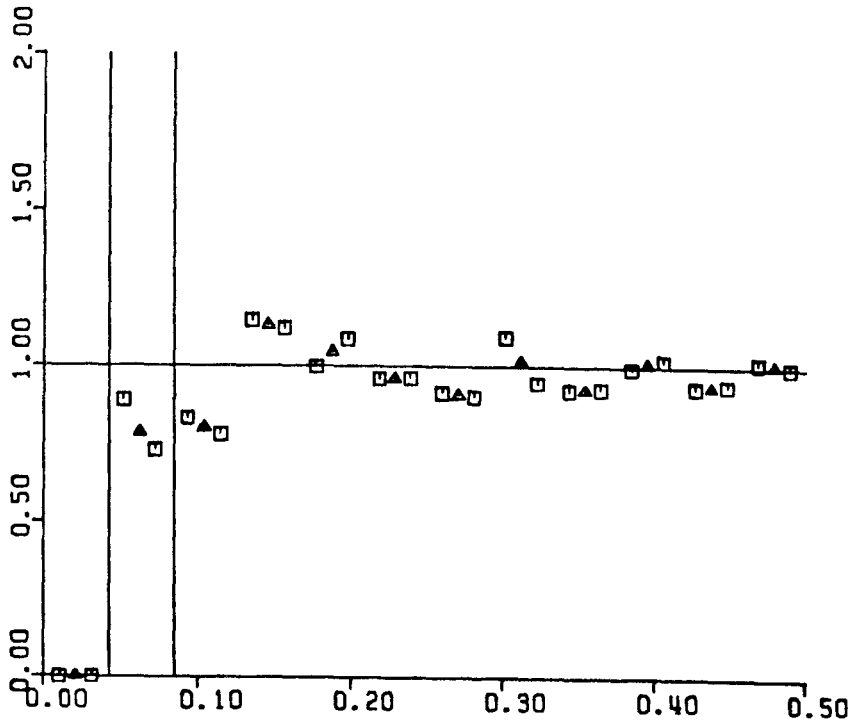
2.00
1.50
1.00
0.50
0.00
0.00
0.10
0.20
0.30
0.40
0.50

T= 2.000

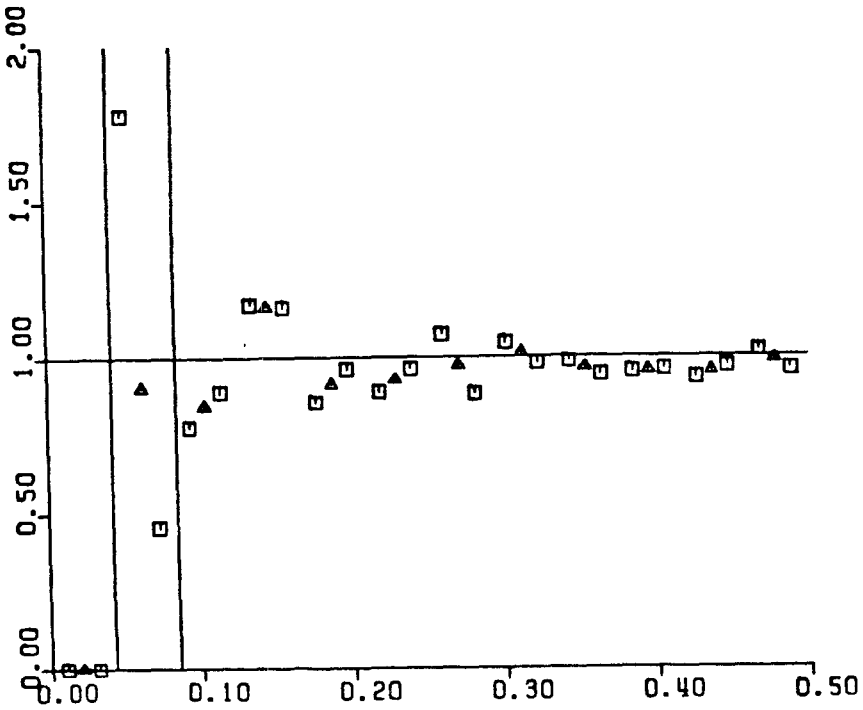
2.00
1.50
1.00
0.50
0.00
0.00
0.10
0.20
0.30
0.40
0.50

T= 2.400

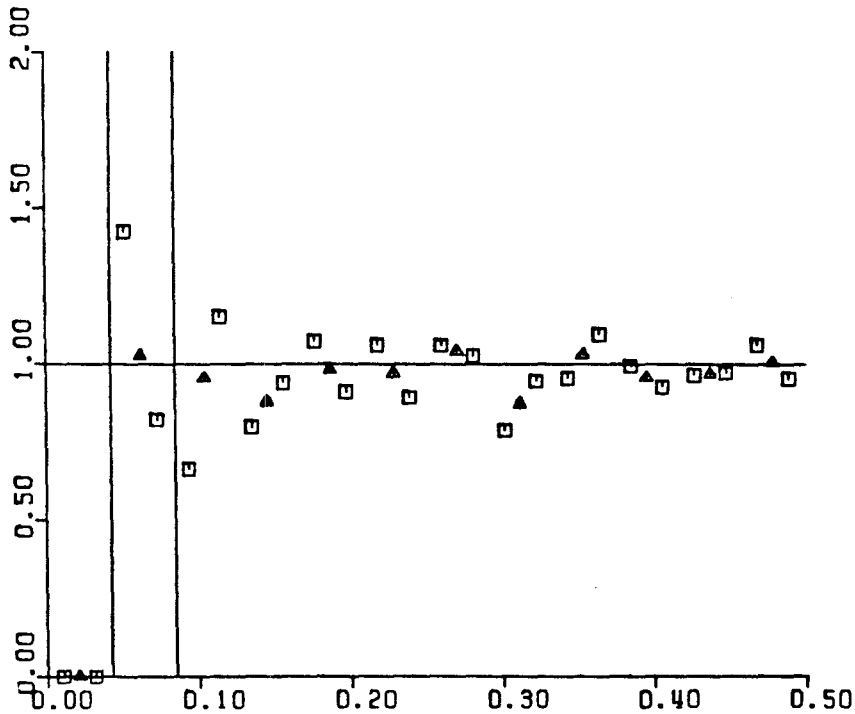
2.00
1.50
1.00
0.50
0.00
0.00
0.10
0.20
0.30
0.40
0.50

T= 2.800

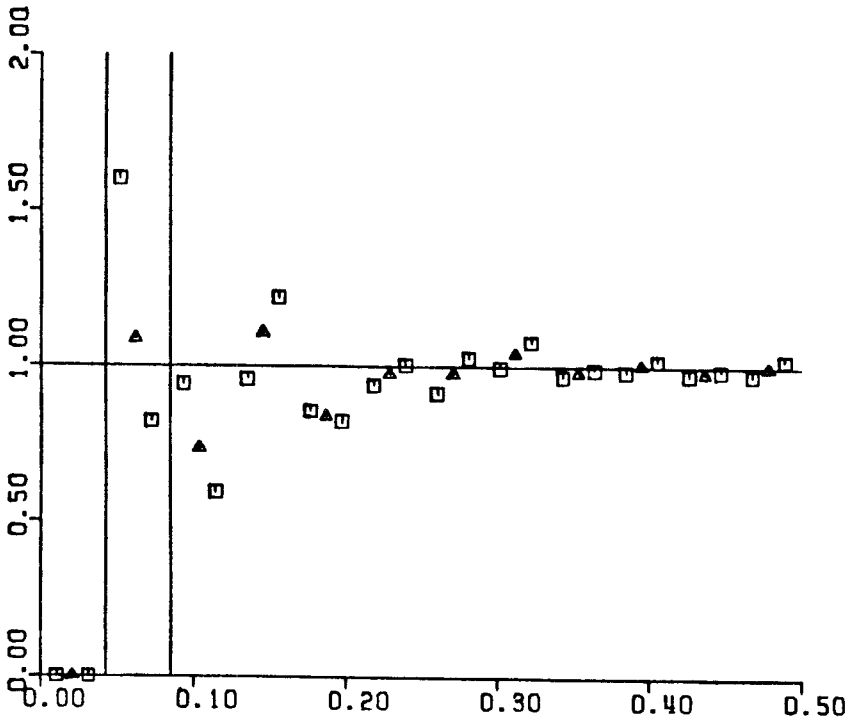
2.00
1.50
1.00
0.50
0.00
0.00
0.10
0.20
0.30
0.40
0.50

T= 3.200

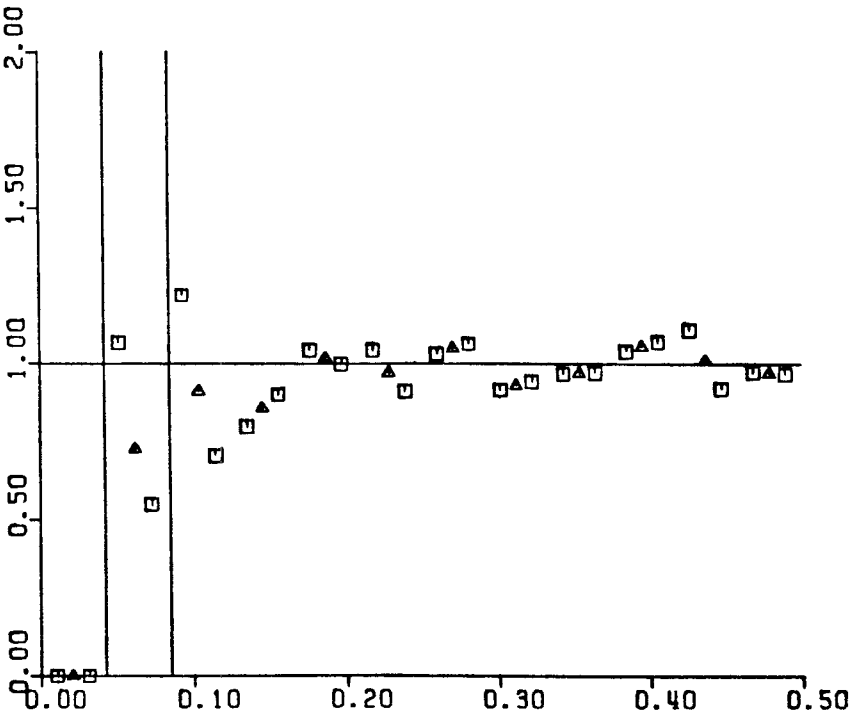
2.00
1.50
1.00
0.50
0.00
0.00
0.10
0.20
0.30
0.40
0.50

T= 3.600

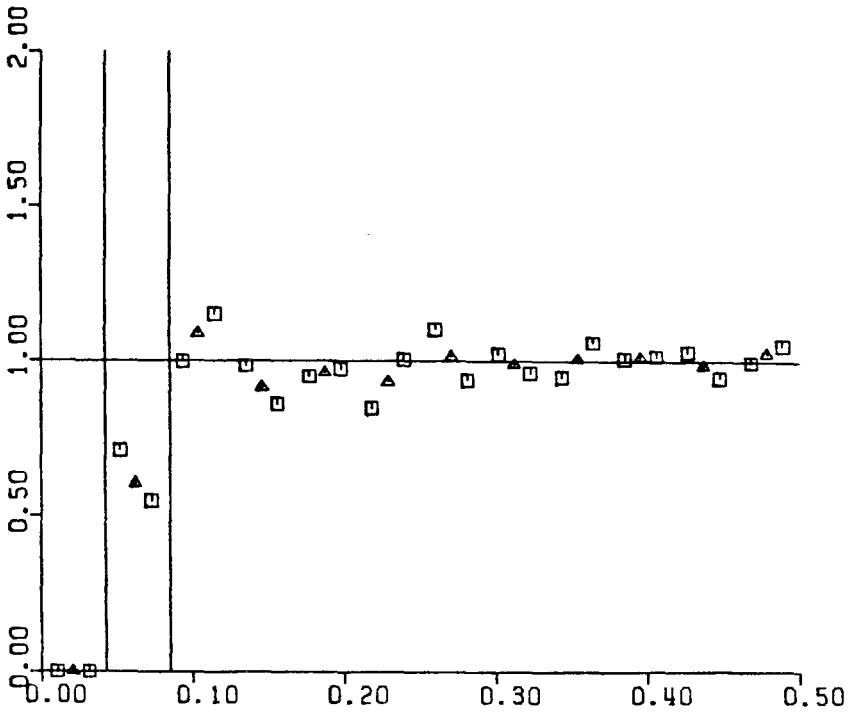
2.00
1.50
1.00
0.50
0.00
0.00
0.10
0.20
0.30
0.40
0.50

T= 4.000

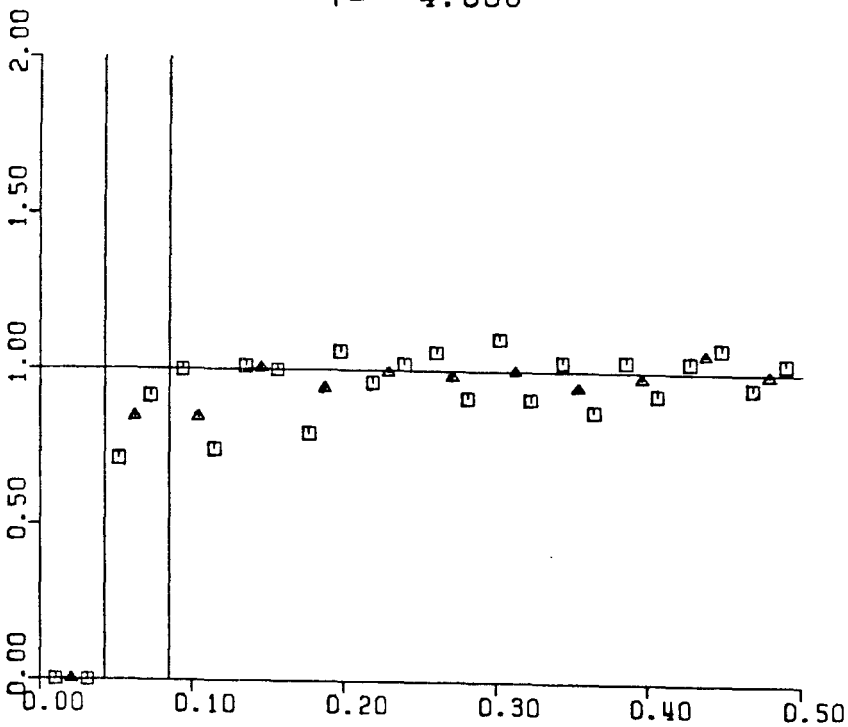
2.00
1.50
1.00
0.50
0.00
0.00
0.10
0.20
0.30
0.40
0.50

T= 4.400

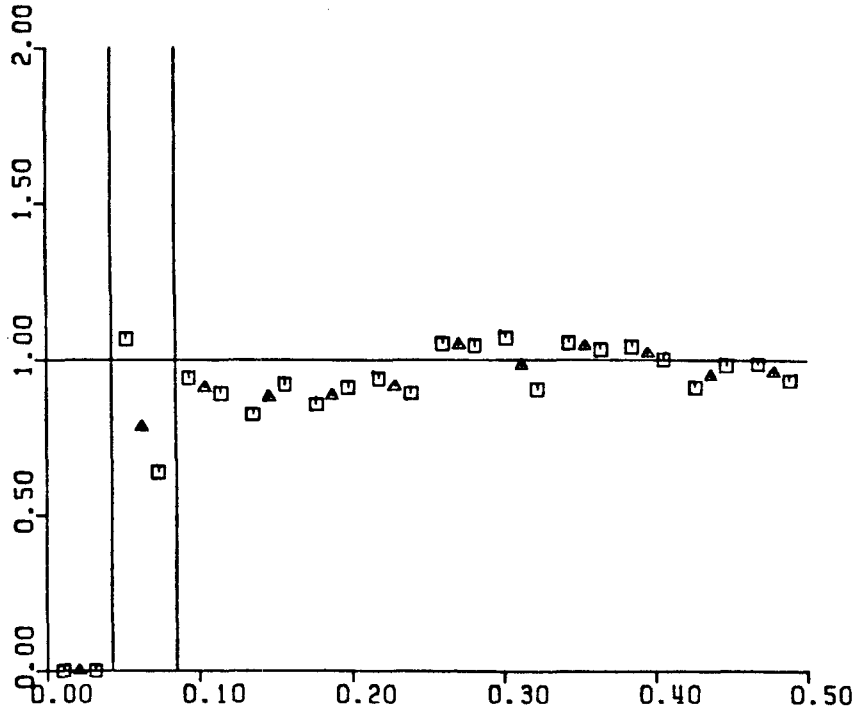
2.00
1.50
1.00
0.50
0.00
0.00
0.10
0.20
0.30
0.40
0.50

T= 4.800

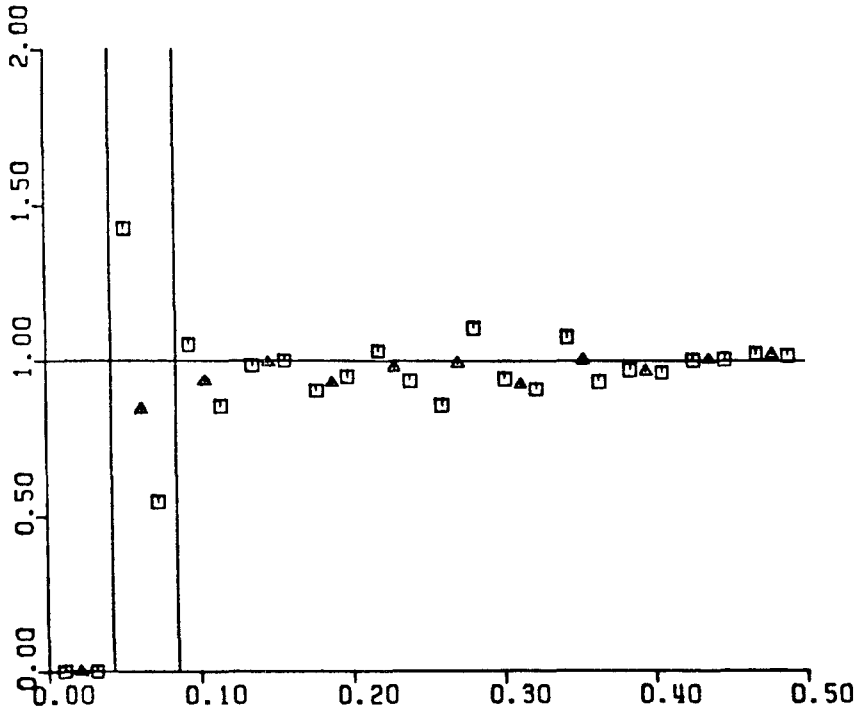
2.00
1.50
1.00
0.50
0.00
0.00
0.10
0.20
0.30
0.40
0.50

T= 5.200

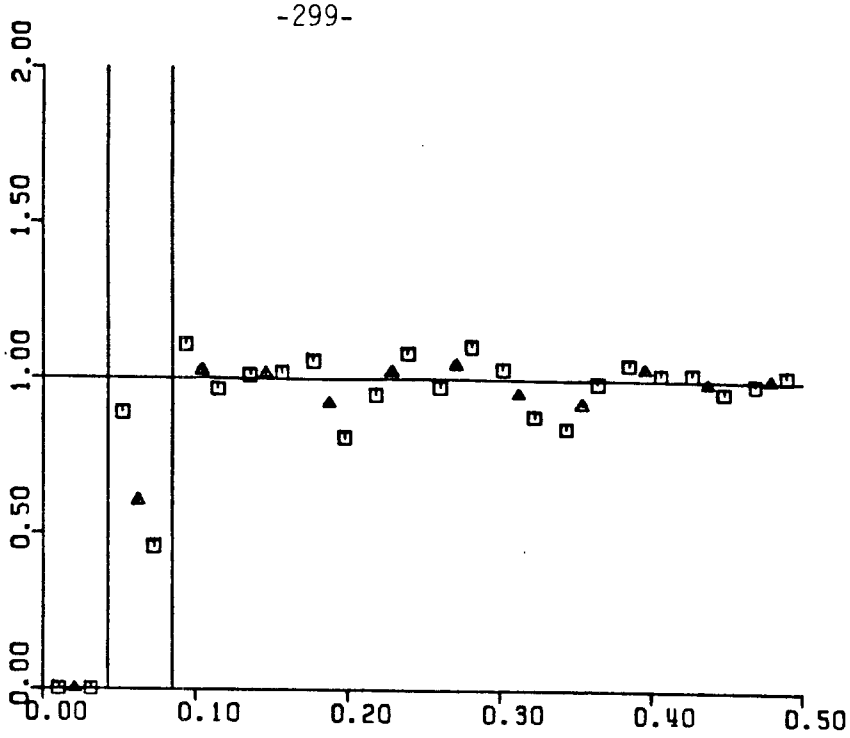
2.00
1.50
1.00
0.50
0.00
0.00
0.10
0.20
0.30
0.40
0.50

T= 5.600

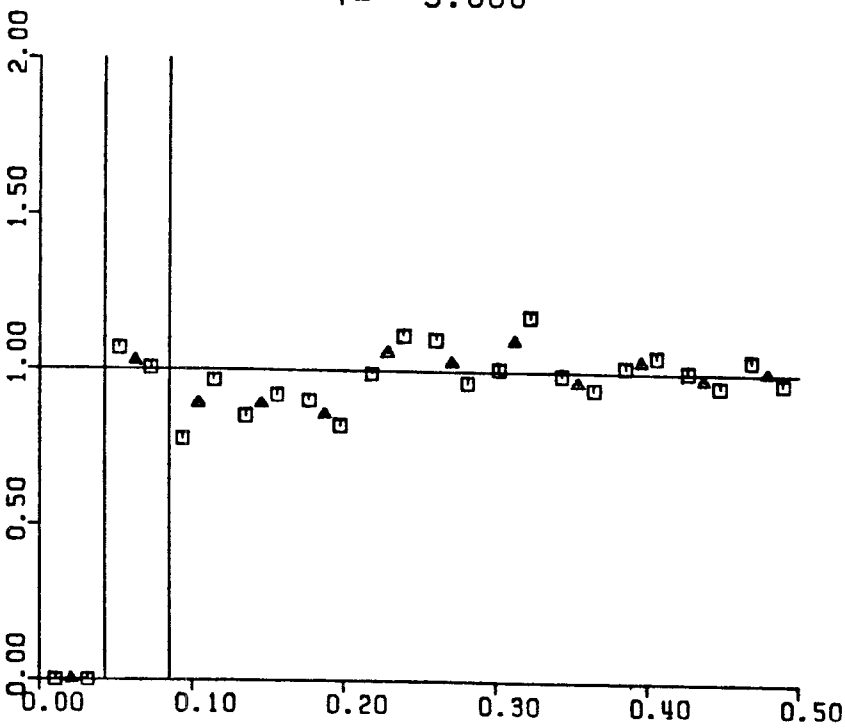
2.00
1.50
1.00
0.50
0.00
0.00
0.10
0.20
0.30
0.40
0.50

T= 6.000

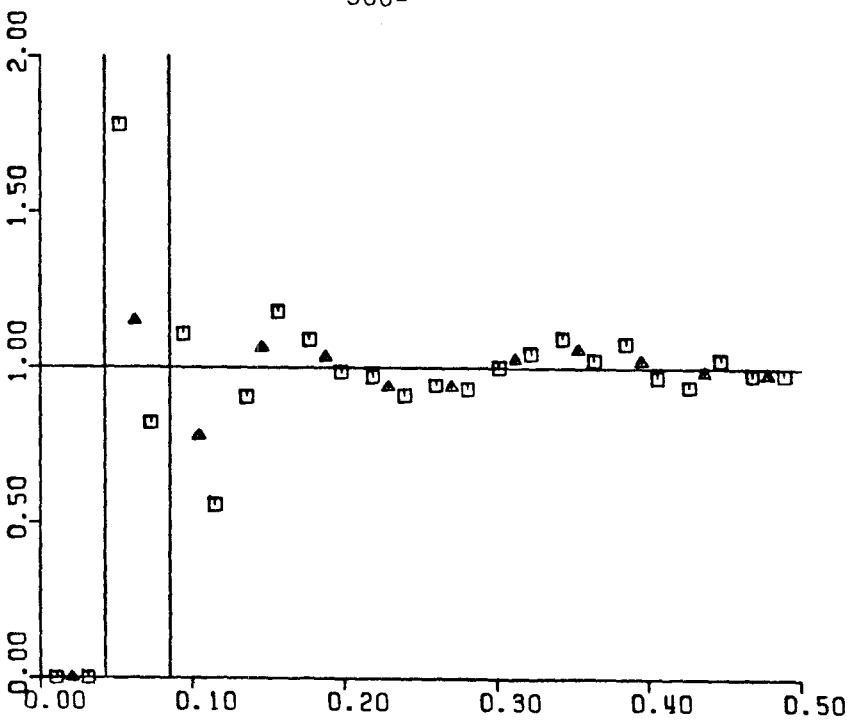
2.00
1.50
1.00
0.50
0.00
0.00
0.10
0.20
0.30
0.40
0.50

T= 6.400

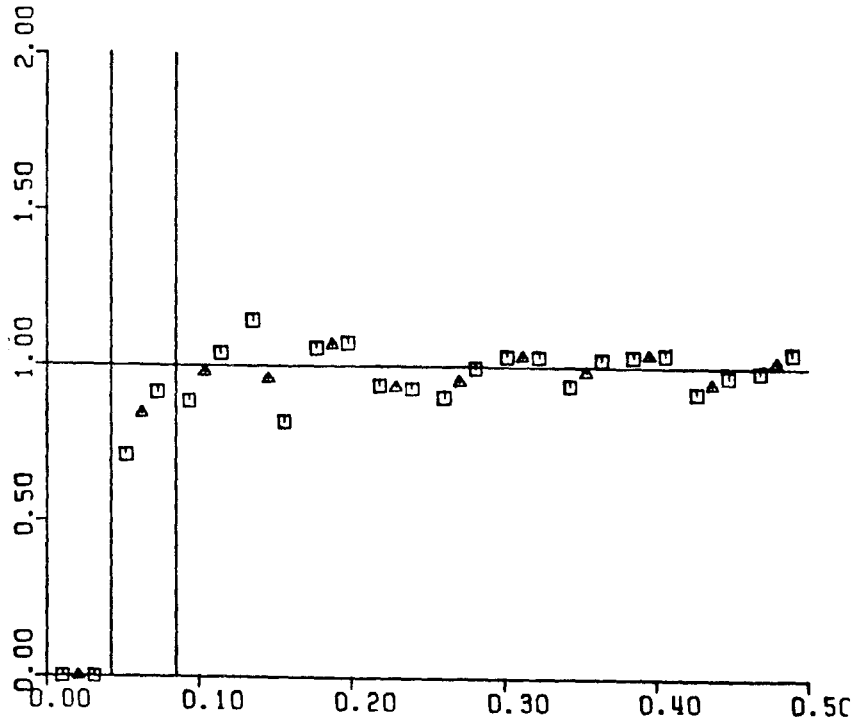
2.00
1.50
1.00
0.50
0.00
0.00
0.10
0.20
0.30
0.40
0.5C

T= 6.800

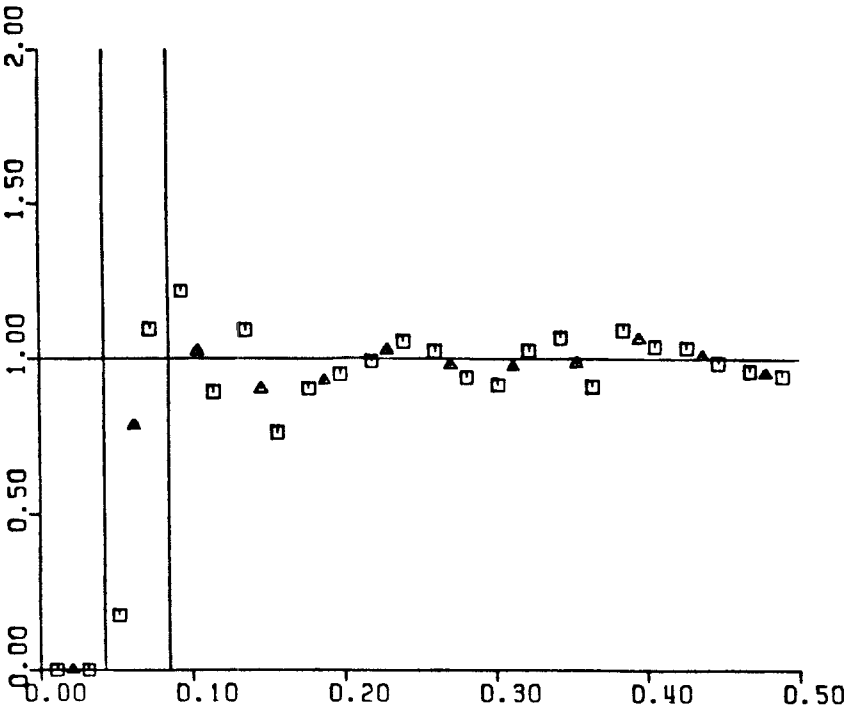
2.00
1.50
1.00
0.50
0.00
0.00
0.10
0.20
0.30
0.40
0.50

T= 7.200

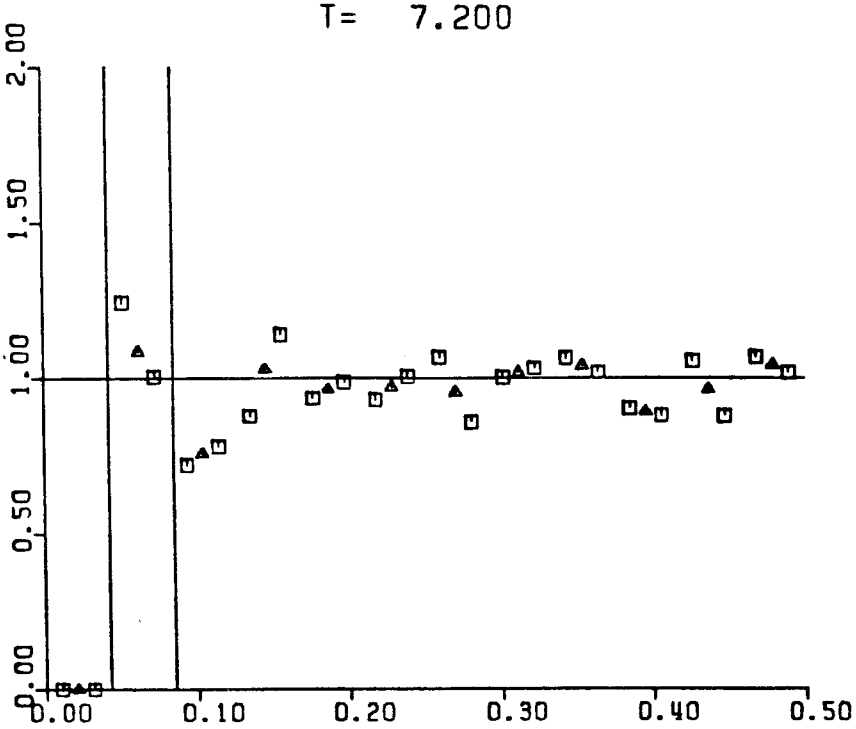
2.00
1.50
1.00
0.50
0.00
0.00
0.10
0.20
0.30
0.40
0.50

T= 7.599

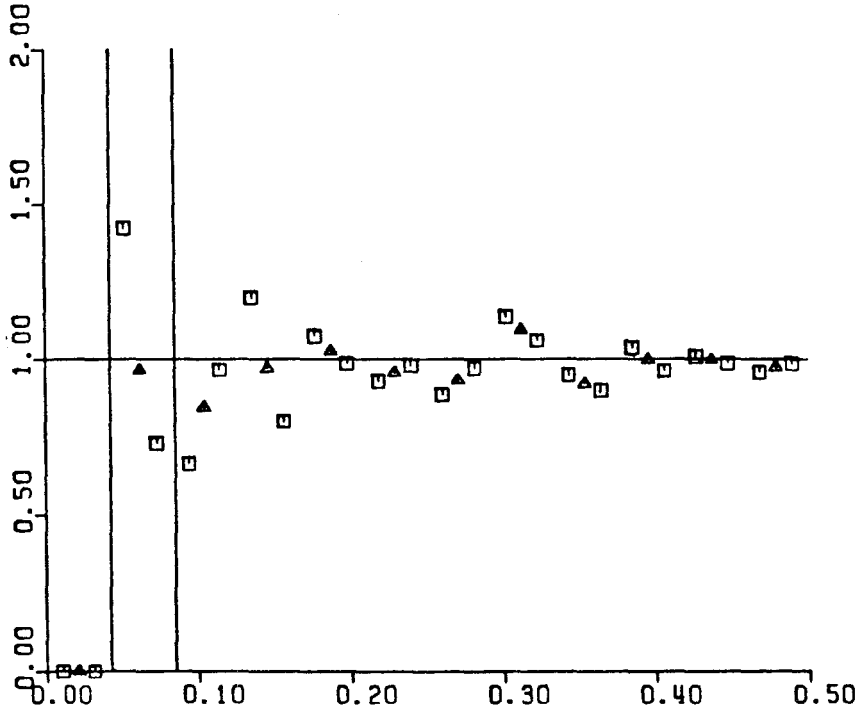


T= 7.999

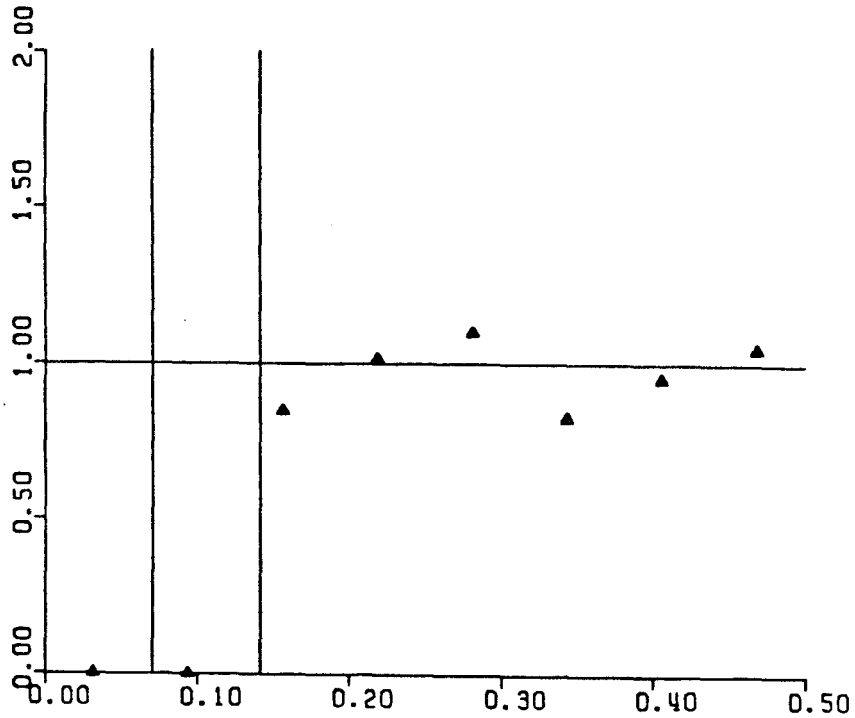


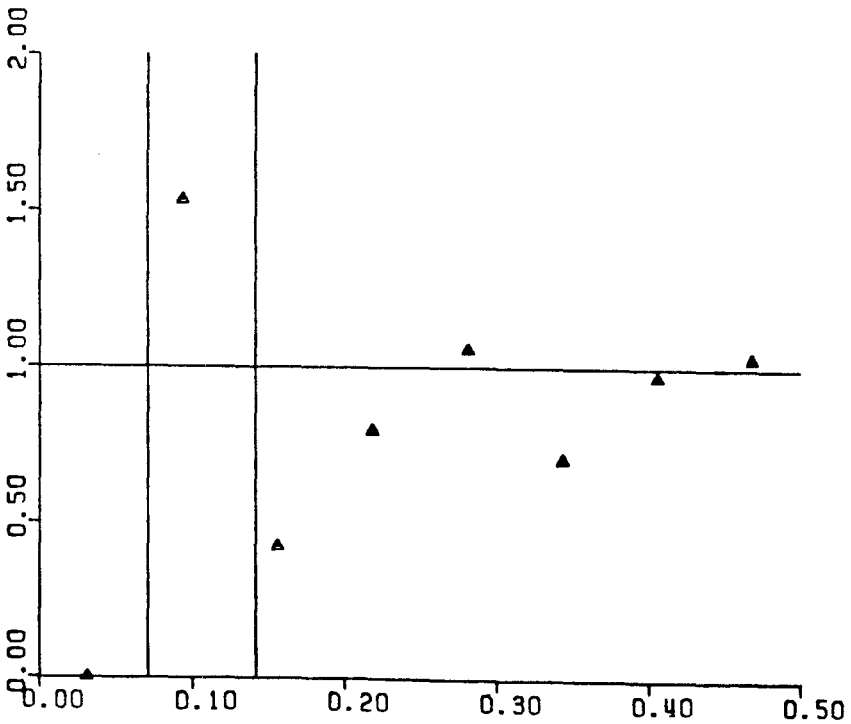


**Figure 39.** Pair-probability function for simulation run 13.

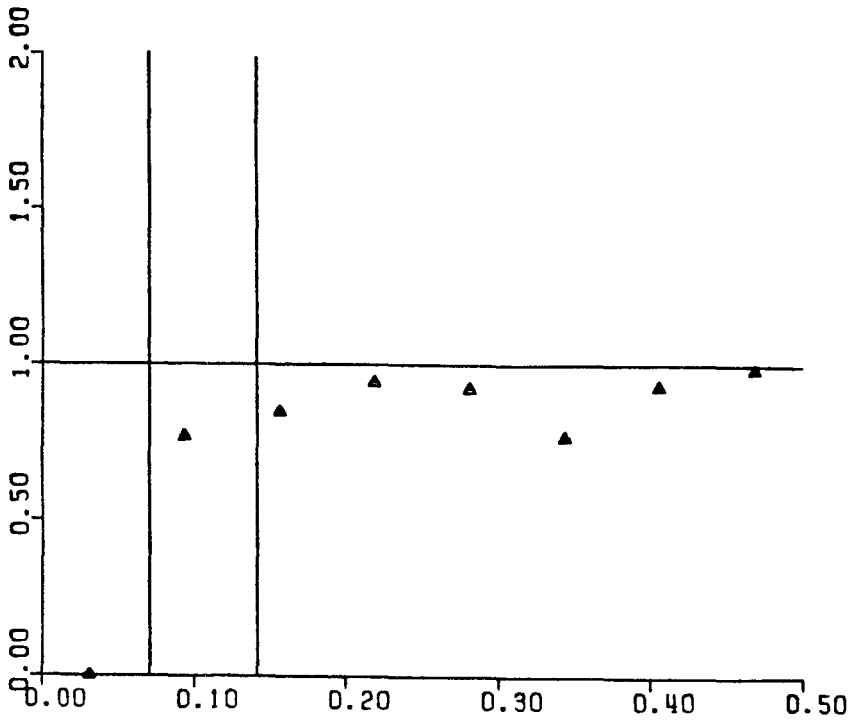
2.00
1.50
1.00
0.50
0.00
0.00
0.10
0.20
0.30
0.40
0.50

T= 0.800

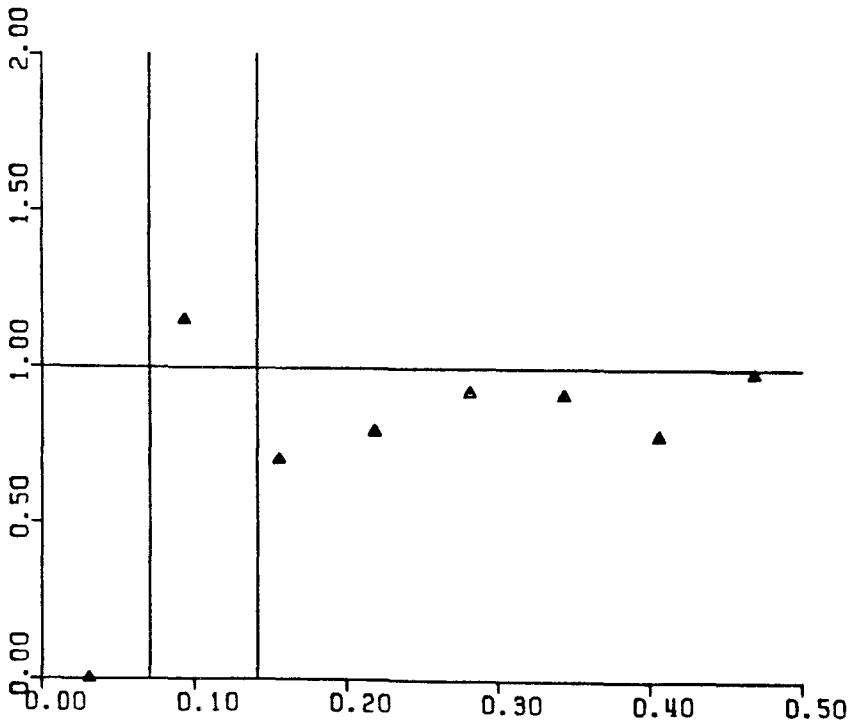
2.00
1.50
1.00
0.50
0.00
0.00
0.10
0.20
0.30
0.40
0.50

T= 1.200

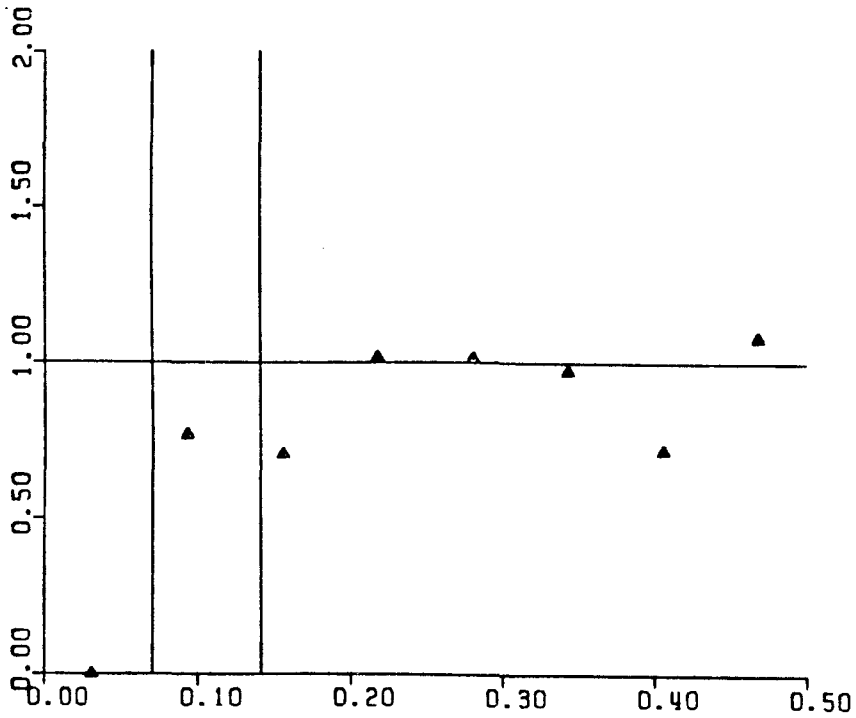
2.00
1.50
1.00
0.50
0.00
0.00
0.10
0.20
0.30
0.40
0.50

T= 1.600

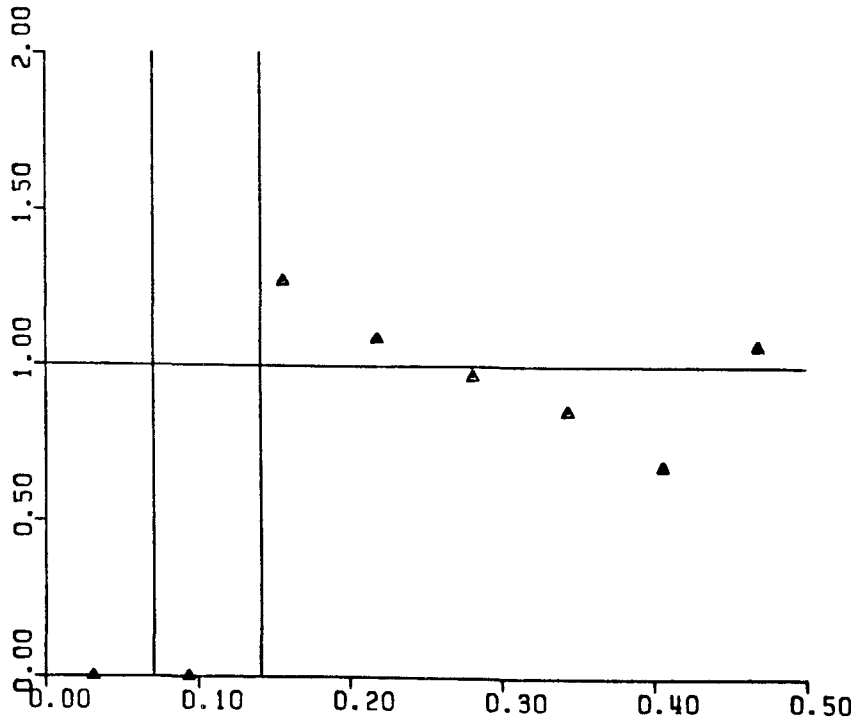
2.00
1.50
1.00
0.50
0.00
0.00
0.10
0.20
0.30
0.40
0.50

T= 2.000

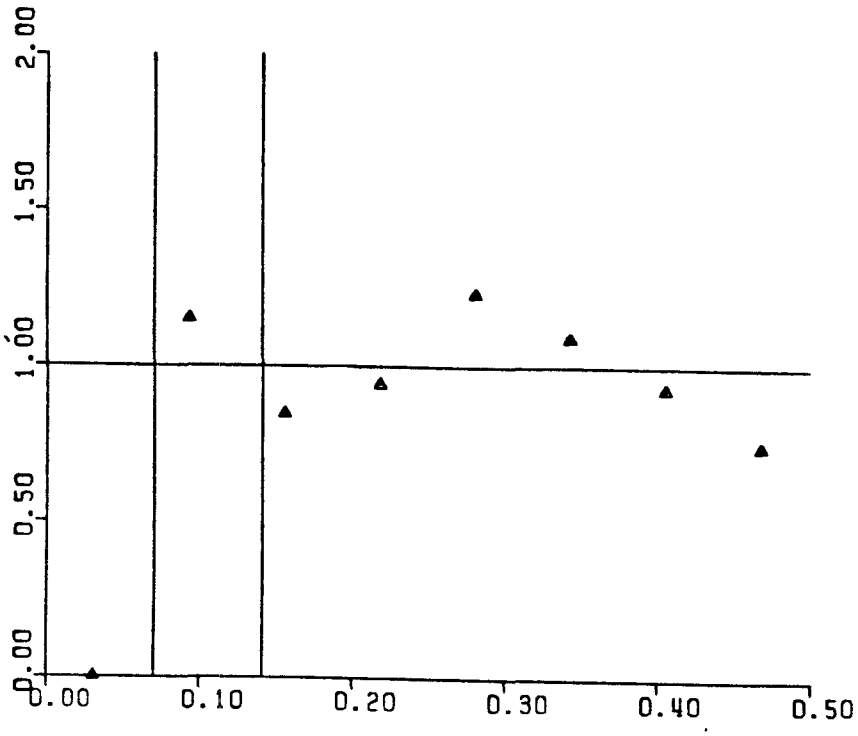
2.00
1.50
1.00
0.50
0.00
0.00
0.10
0.20
0.30
0.40
0.50

T= 2.400

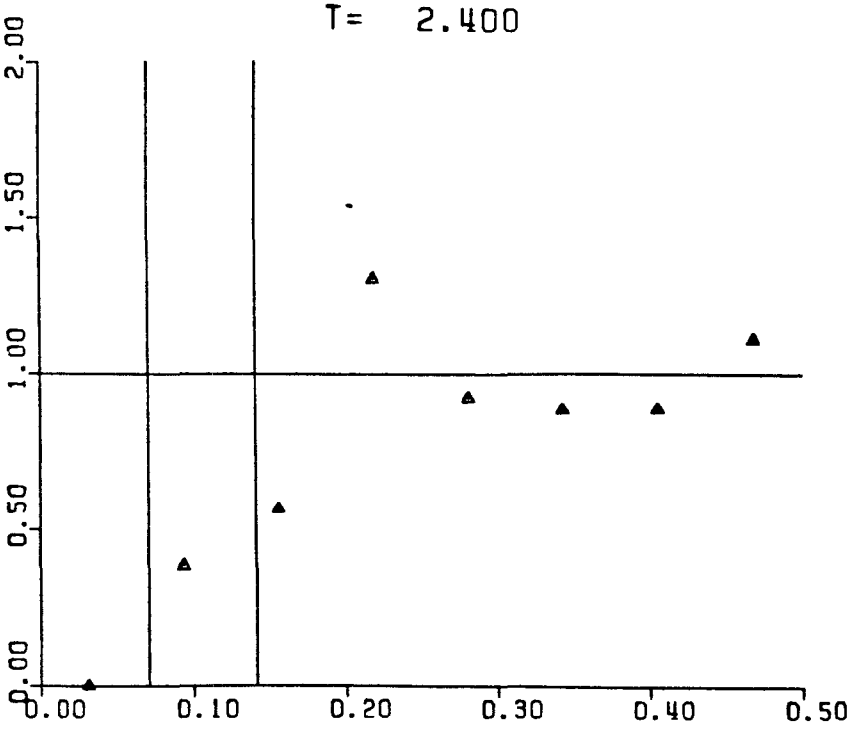
2.00
1.50
1.00
0.50
0.00
0.00
0.10
0.20
0.30
0.40
0.50

T= 2.800

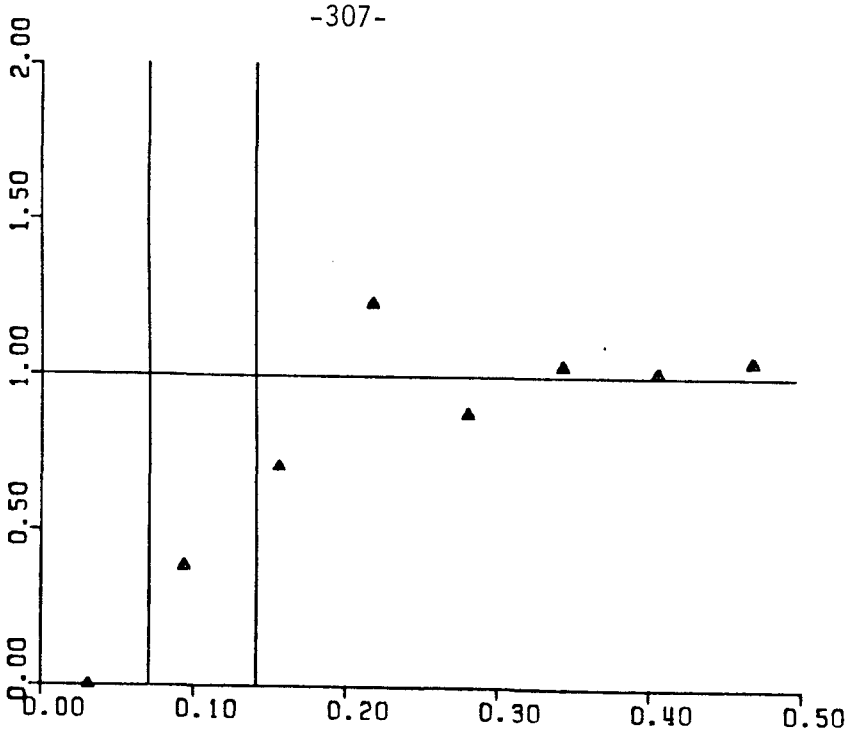
2.00
1.50
1.00
0.50
0.00
0.00
0.10
0.20
0.30
0.40
0.50

T= 3.200

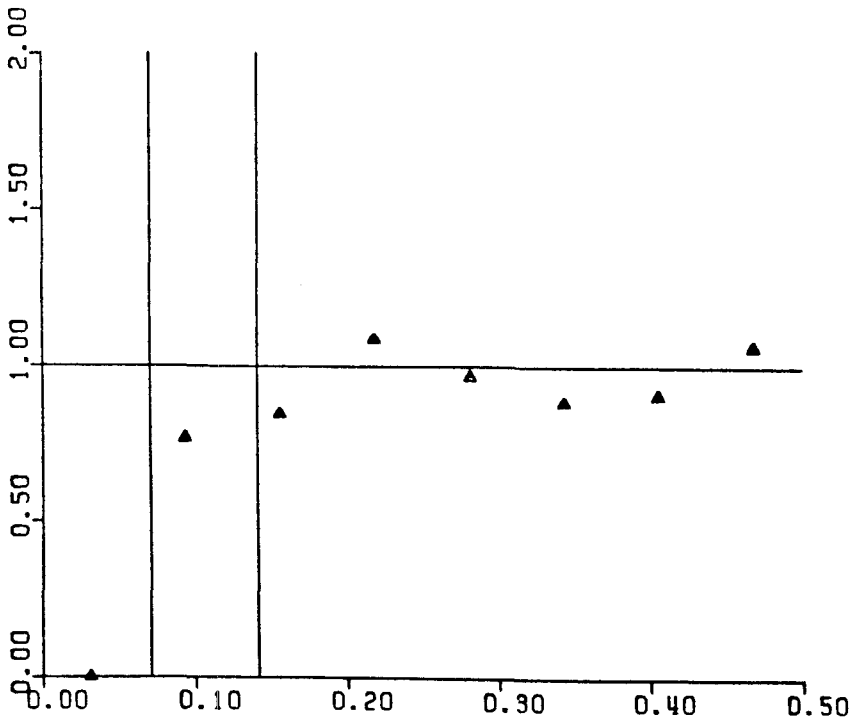
2.00
1.50
1.00
0.50
0.00
0.00
0.10
0.20
0.30
0.40
0.50

T= 3.600

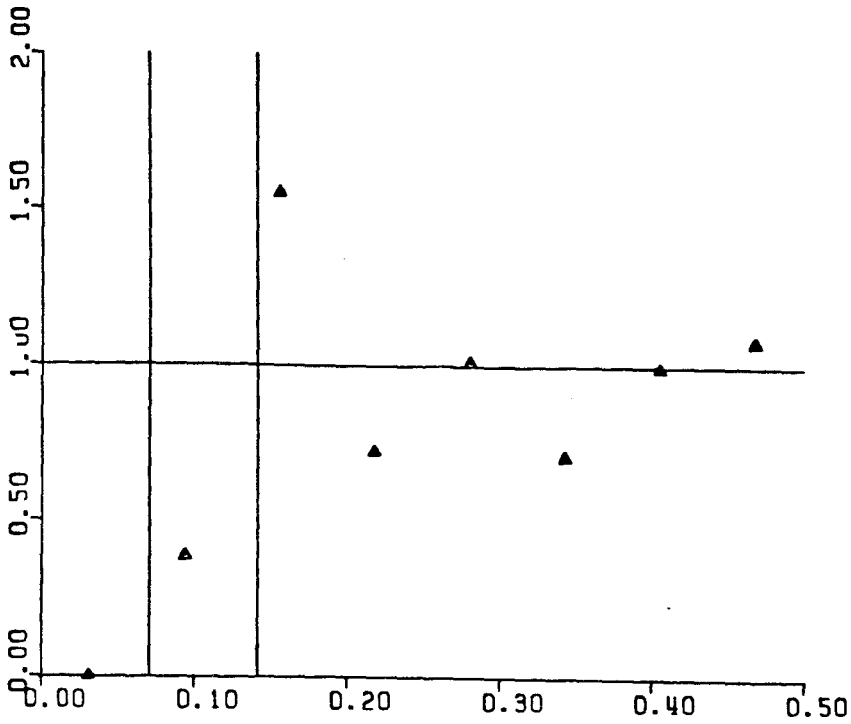
2.00
1.50
1.00
0.50
0.00
0.00
0.10
0.20
0.30
0.40
0.50

T= 4.000

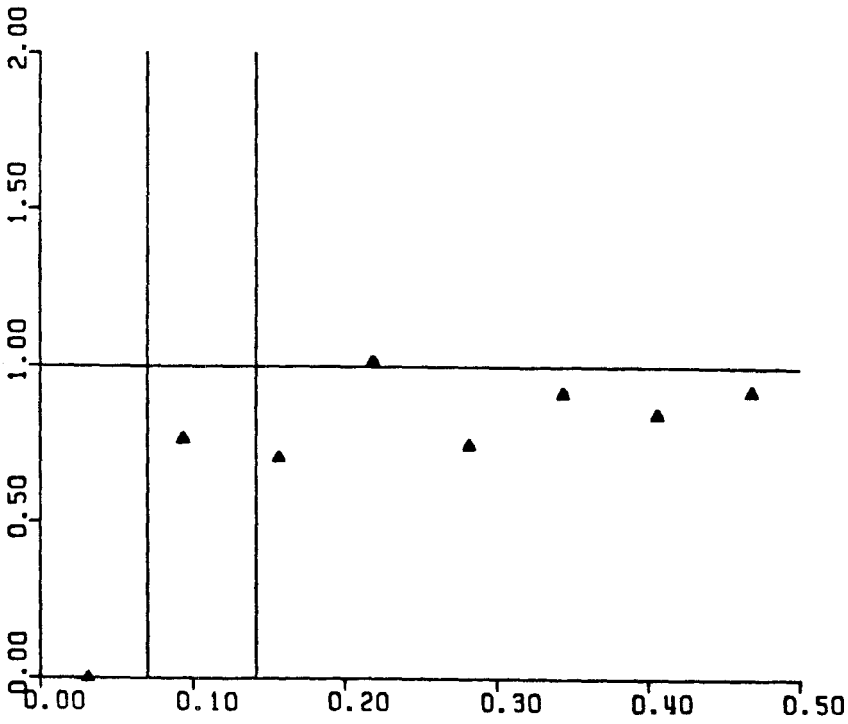
2.00
1.50
1.00
0.50
0.00
0.00
0.10
0.20
0.30
0.40
0.50

T= 4.400

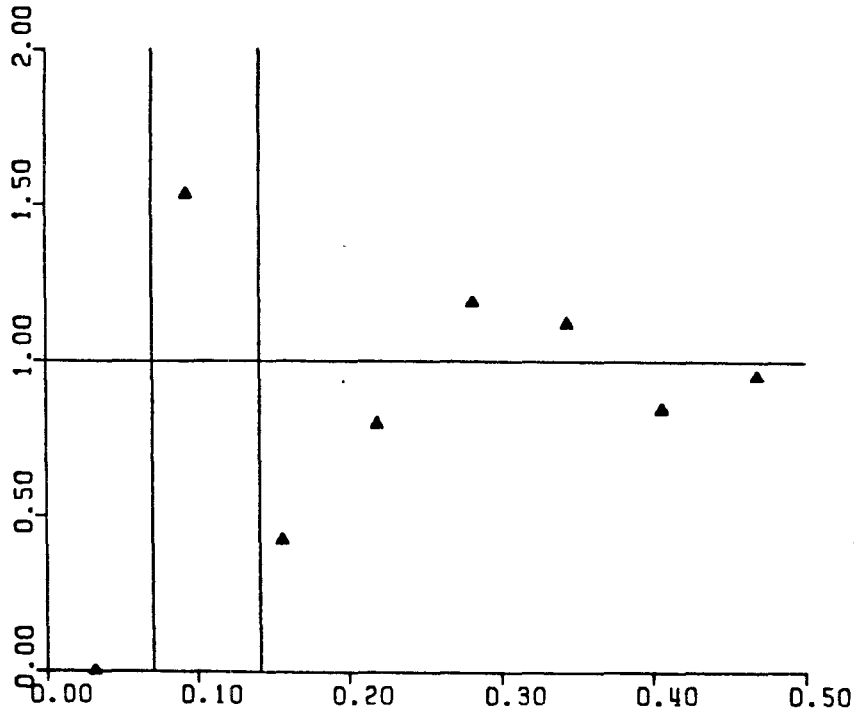
2.00
1.50
1.00
0.50
0.00
0.00
0.10
0.20
0.30
0.40
0.50

T= 4.800

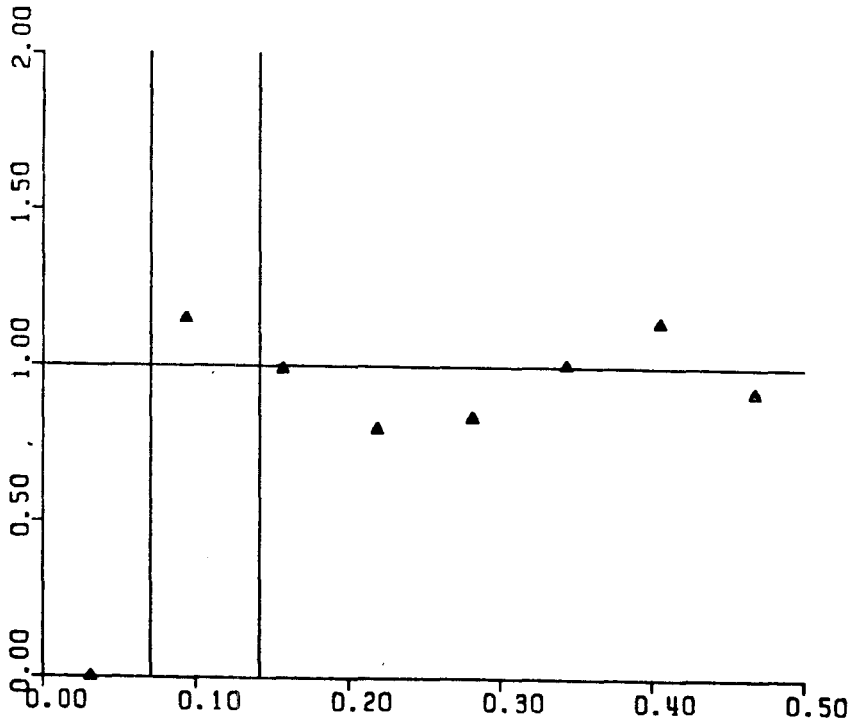
2.00
1.50
1.00
0.50
0.00
0.00
0.10
0.20
0.30
0.40
0.50

T= 5.200

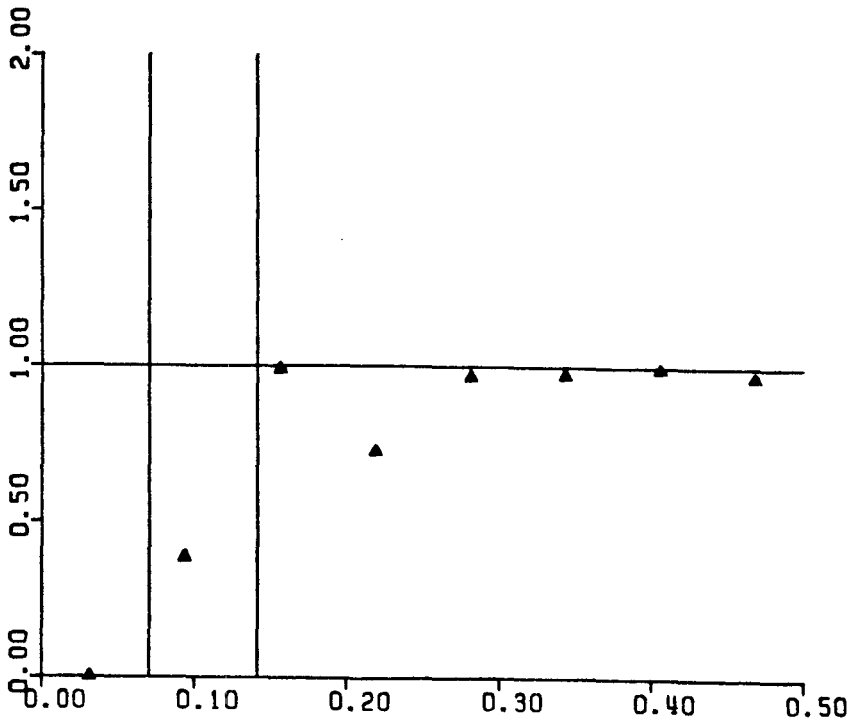
2.00
1.50
1.00
0.50
0.00
0.00
0.10
0.20
0.30
0.40
0.50

T= 5.600

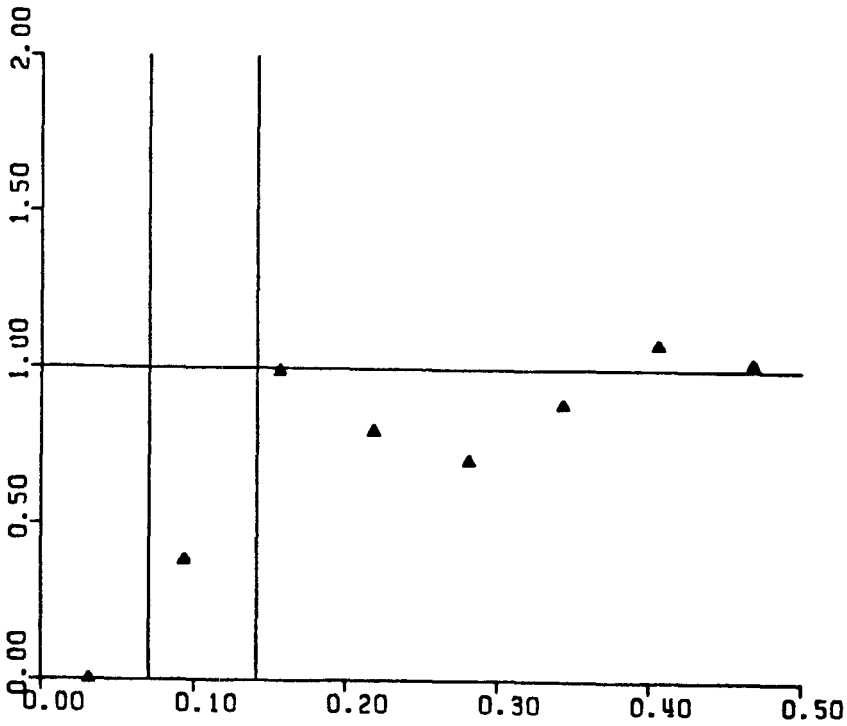
2.00
1.50
1.00
0.50
0.00
0.00
0.10
0.20
0.30
0.40
0.50

T= 6.000

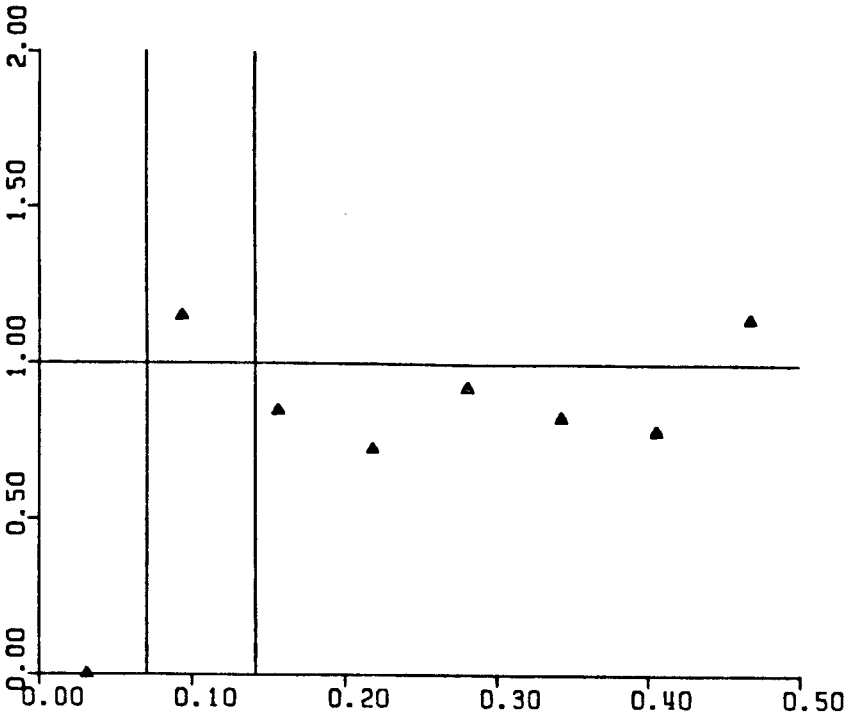
2.00
1.50
1.00
0.50
0.00
0.00
0.10
0.20
0.30
0.40
0.50

T= 6.400

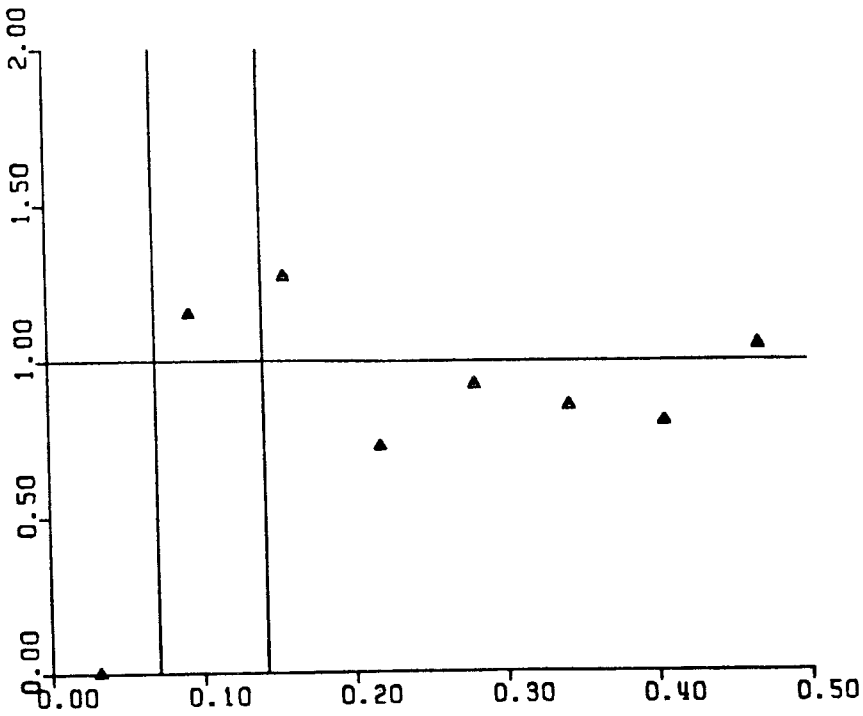
2.00
1.50
1.00
0.50
0.00
0.00
0.10
0.20
0.30
0.40
0.50

T= 6.800

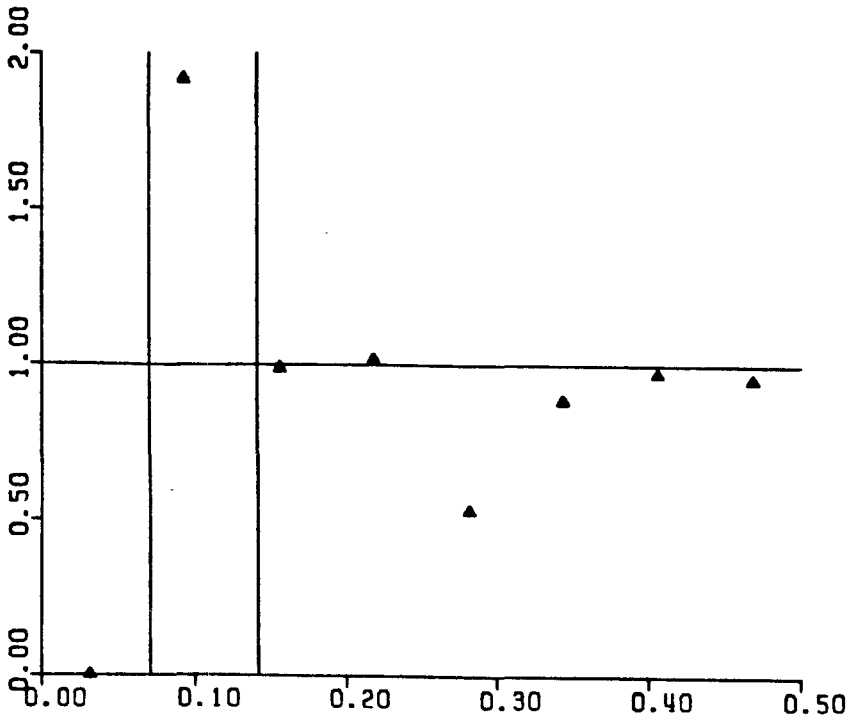
2.00
1.50
1.00
0.50
0.00
0.00
0.10
0.20
0.30
0.40
0.50

T= 7.200

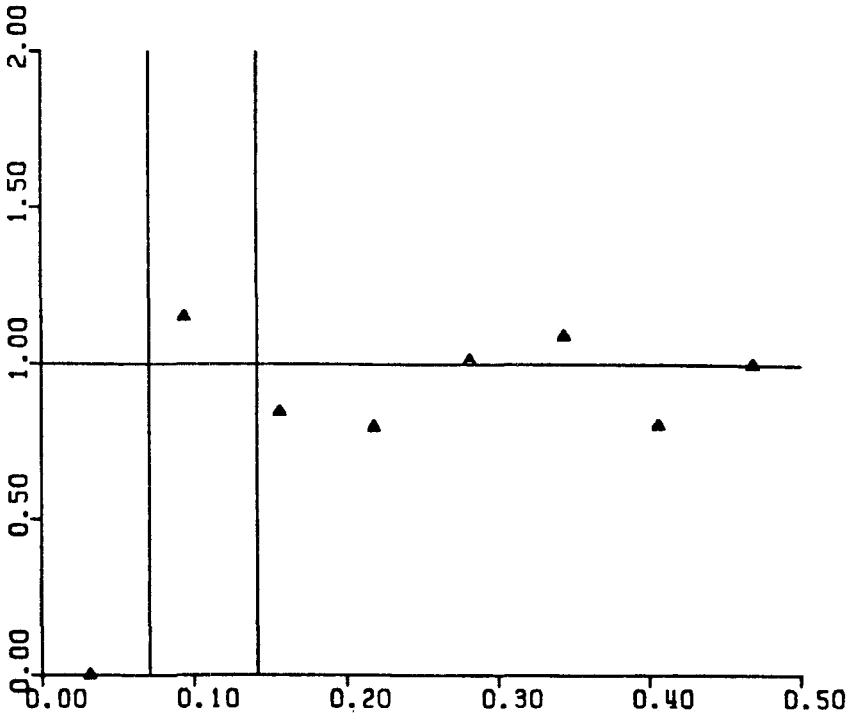
2.00
1.50
1.00
0.50
0.00
0.00
0.10
0.20
0.30
0.40
0.50

T= 7.600

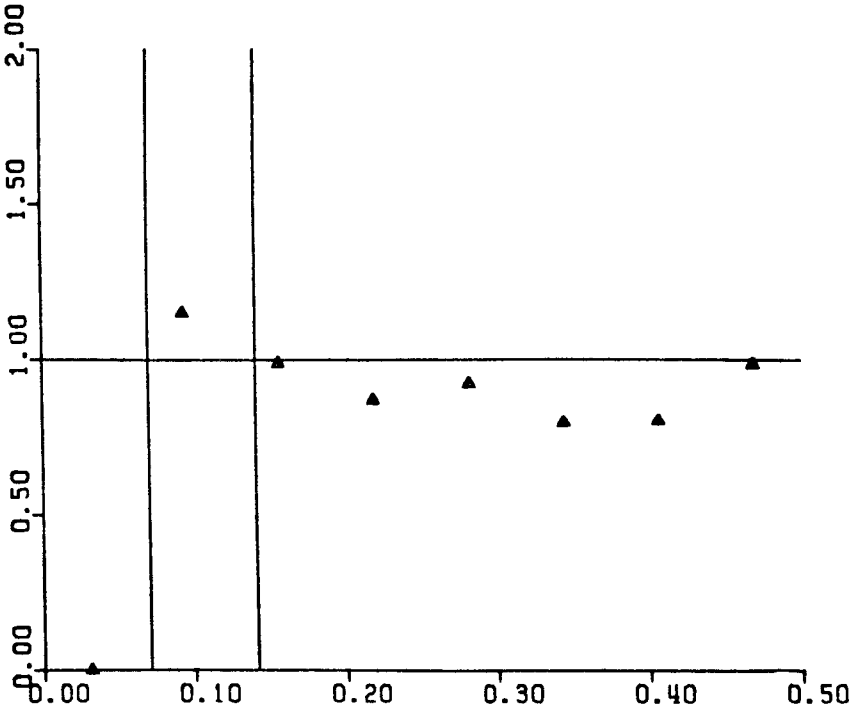


T= 8.000

**APPENDIX 5:** Ranges over which the nearfield and farfield forms of the two-particle resistance and mobility coefficients are used

As mentioned in Chapter 2, the accuracy of the available nearfield and farfield forms is different for each of the various two-particle resistance and mobility coefficients. Therefore, the ranges over which the nearfield and farfield forms are used is also different depending on the coefficient. We now list for each coefficient these ranges in terms of the separation distance $r_{\alpha\beta}$ between the particles. (The references in this appendix refer to the reference list in Chapter 2.)

$\lambda_1(r_{\alpha\beta}), \lambda_2(r_{\alpha\beta})$ (the coefficients describing the settling velocity of two particles parallel and perpendicular to the line joining their centers)–

farfield forms– $r_{\alpha\beta}/a > 8.0$

(Wakiya 1967; Happel and Brenner 1965)

nearfield forms (only $\lambda_2$)– $r_{\alpha\beta}/a < 2.0049$

(O'Neill 1969)

intermediate field results– $2.0049 < r_{\alpha\beta}/a < 8.0$

(Goldman, Cox, and Brenner 1966; Batchelor 1972)

$A(r_{\alpha\beta})$, $B(r_{\alpha\beta})$ (the coefficients describing the translational motion of the two particles in a linear flow field)–

farfield forms– $r_{\alpha\beta}/a > 2.8662$

(Batchelor and Green 1972)

nearfield forms– $r_{\alpha\beta}/a < 2.0025$

(Batchelor and Green 1972)

intermediate field results– $2.0025 < r_{\alpha\beta}/a < 2.8662$

(Batchelor and Green 1972)

The coefficients describing the forces on two particles translating parallel to the line joining their centers–

farfield forms– $r_{\alpha\beta}/a > 4.0$

(Happel and Brenner 1965)

nearfield forms– $r_{\alpha\beta}/a < 2.01$

(Arp and Mason 1977; Hansford 1970)

intermediate field results– $2.01 < r_{\alpha\beta}/a < 4.0$

(Batchelor 1976; Cooley and O'Neill 1969)

The coefficients describing the torques on two particles rotating about the axis of the line joining their centers–

farfield forms– $r_{\alpha\beta}/a > 4.0$

(Reuland, Felderhof, and Jones 1978)

touching forms– $r_{\alpha\beta}/a = 2.0$

(Takagi 1974; Majumdar 1967)

intermediate field results– $2.0 < r_{\alpha\beta}/a < 4.0$

(Jeffery 1915; Arp and Mason 1977)

The coefficients describing the forces and torques on two particles moving perpendicular to the line joining their centers–

farfield forms– $r_{\alpha\beta}/a > 7.0$

(Arp and Mason 1977; Brenner and O'Neill 1972; Brenner 1964)

nearfield forms– $r_{\alpha\beta}/a < 2.001$

(Wacholder and Sather 1974)

intermediate field results– $2.001 < r_{\alpha\beta}/a < 7.0$

(Davis 1969; O'Neill and Majumdar 1970)

The coefficients describing the forces and torques on two particles in a linear flow field–

farfield forms– $r_{\alpha\beta}/a > 10.0$

(Arp and Mason 1977; Brenner and O'Neill 1972)

nearfield forms– $r_{\alpha\beta}/a < 2.006$ for $F(r_{\alpha\beta})$; $r_{\alpha\beta}/a < 2.0006$ for $G(r_{\alpha\beta})$ and $H(r_{\alpha\beta})$ (see the notation in Arp and Mason)

(Arp and Mason 1977)

intermediate field results–all other values of $r_{\alpha\beta}$

(Arp and Mason 1977)